ELUCIDATING BIOCHEMICAL MECHANISMS OF SKP1 REGULATION BY ITS OXYGEN-DEPENDENT GLYCOSYLATION IN PROTISTS

by

DONOVAN AARON CANTRELL

(UNDER THE DIRECTION OF CHRISTOPHER M. WEST)

ABSTRACT

Skp1/Cullin1/F-Box protein (SCF) complexes represent a premier class of E3 ubiquitin ligases responsible for proteomic control by targeting proteins for degradation by the 26S proteosome. Substrate specificity is mediated by a large variety of F-box proteins (FBPs) which interact with the SCF complex via Skp1. Skp1 is utilized for oxygen sensing within the protist kingdom via oxygen-dependent glycosylation on its partially disordered C-terminal region (CTR). In the presence of oxygen, the prolyl hydroxylase PhyA hydroxylates Skp1 allowing for the attachment of a pentasaccharide by glycosyltransferases with absolute specificity for Skp1. Glycosylation of the CTR alters Skp1's FBP binding repertoire in cells and inhibits its homodimerization which may sequester it from SCF complexes. However, a biochemical understanding of these effects is needed to interpret cellular consequences. Here, we establish *in vitro* systems where the effects of glycosylation can be quantified. Utilizing sedimentation velocity experiments (SV), we demonstrate that glycosylation weakens homodimerization of Skp1 from the parasite *Toxoplasma gondii* by an order of magnitude, an effect reproduced by CTR deletion. Replacing Skp1's CTR with scrambled or poly-serine sequences indicate that amino acid composition is more important than sequence for CTR mediated homodimerization. The effects of high salt and molecular

dynamics simulations indicate the presence of an electrostatically mediated fuzzy protein interaction of Skp1's CTR that is interrupted by the glycan. Comparative studies with an unrelated protist, *Dictyostelium discoideum*, provided an example of evolutionary tuning of this mechanism. Gat1, Skp1's terminal glycosyltransferase in *Toxoplasma* is detected in the Skp1 interactome based on co-immunoprecipitation, suggesting a non-enzymatic role for Gat1. SV indicates that Gat1 forms a direct complex with Skp1 which competes with homodimerization and whose stoichiometry is dictated by glycosylation. Computational modeling suggests a mechanism whereby Gat1 utilizes Skp1's fuzzy interactions to dissociate the Skp1 homodimer, providing a second mechanism to regulate the availability of Skp1 to the SCF complex. Finally, we engineered recombinant expression systems for soluble F-box protein production for testing the effects of glycosylation on FBP binding. Overall, the studies reveal a novel mechanism for the regulation of E3(SCF) ubiquitin ligases involving titration of Skp1 availability for SCF complex formation.

INDEX WORDS: post-translational modifications, glycosylation, Skp1, *Toxoplasma gondii*, *Dictyostelium discoideum*, proteins, protein-protein interactions, ubiquitin ligase, intrinsically disordered protein, intrinsically disordered region, Cullin1, F-Box Protein, enzyme, glycosyltransferase, fuzzy protein interface, recombinant protein expression, recombinant protein production, analytical ultracentrifugation, sedimentation velocity, molecular dynamics, oxygen sensing, prolyl hydroxylation, interactome, electrostatic interactions, protein interface, exchange factor, protein purification

ELUCIDATING BIOCHEMICAL MECHANISMS OF SKP1 REGULATION BY ITS OXYGEN-DEPENDENT GLYCOSYLATION IN PROTISTS

by

DONOVAN AARON CANTRELL

B.S., Southern Illinois University, Carbondale, 2019

A Dissertation Submitted to the Graduate Faculty of The University of Georgia in Partial Fulfillment of the Requirements for the Degree

DOCTOR OF PHILOSOPHY

ATHENS, GEORGIA

2025

©2025

Donovan Aaron Cantrell

All Rights Reserved

ELUCIDATING BIOCHEMICAL MECHANISMS OF SKP1 REGULATION BY ITS OXYGEN-DEPENDENT GLYCOSYLATION IN PROTISTS

by

DONOVAN AARON CANTRELL

B.S., Southern Illinois University, Carbondale, 2019

Major Professor: Christopher Mark West

Committee: Zachary A. Wood

Adam Barb

Jeffrey L. Urbauer

Electronic Version Approved:

Ron Walcott

Vice Provost for Graduate Education and Dean of the Graduate School

The University of Georgia

August 2025

DEDICATION

I would like to dedicate my dissertation to God. I have been blessed with the mental, physical, and financial ability to pursue my academic studies to this point in my career. I have also been blessed with the presence of many people mentioned below who have contributed greatly to my ability to reach this point in my career. I would additionally like to dedicate my dissertation to all those who have supported me not just academically, but in my personal life as well. I have a lot to be grateful for regarding both the people and the opportunities I have been privileged to have in my life.

ACKNOWLEDGEMENTS

There are several people who deserve mentioning for supporting me to this point. I will start with my parents and family. My mom, Debra Cantrell-Einhorn, especially dedicated substantial time and energy to raising my siblings and me after the passing of my biological father. Her tireless efforts in supporting my educational journey from childhood to this point have been instrumental in my ability to reach my career goals. Being an educator herself, she instilled in me the importance of knowledge and education in navigating life. She spent countless hours teaching me various academic concepts and supporting me in after-school activities like scholar bowl and cross country. Considering my academic path thus far, it is obvious that these values have strongly influenced my trajectory in life. Her unwavering support in the face of the countless stressful days I undoubtedly caused her will always be appreciated.

I would also like to recognize my dad, Dennis Einhorn, who took me on and raised me as his own when he married my mother. He with my mother worked to instill a strong work ethic and set of values in me that I still carry with me today. Being a mechanic who was raised on a farm, he developed a strong get-it-done type of attitude. This was embodied by a lesson he taught me that "any person can start a job; its finishing a job that will show who you are." Additionally, when my mom was busy taking care of my other siblings, it was often my dad who would be there to support my after-school activities and take me home. Some of my fondest childhood memories interestingly involve our stops by Dairy Queen after out-of-town matches with other schools. I will be forever grateful for his choice to be there in my life while I was growing up.

I would like to thank my siblings Devon Cantrell, Dalton Cantrell, Denae Cantrell, and Dryden Einhorn for their support and the fun we've had in our various antics. They have shown their willingness to offer support in various forms in multiple instances. Whether it's simply moral support while having a few drinks, intellectual support with my car, or material support in picking me up at the airport, it has been helpful in navigating life. I would also like to thank the various friends I have had for similar contributions of support or simply helping me enjoy my journey through life. The mutual support of friends like Isaac Ludington, Derek Tucker, Kathryn Helmink, Adam Jones, and Lucas Sauerburger made college struggles a bit better. The Dungeons and Dragons campaigns Isaac, Derek, Devon, and I participated in represent some of my best college memories.

I would next like to recognize the significant contributions of my mentor Christopher West on my graduate education. He took me into his lab when the number of potential advisors that were able and willing to do the same were limited. My first experiences when coming to graduate school were overall demoralizing and left me questioning if I made the right decision to pursue a PhD. During this time, Chris not only offered me a spot in his lab, but happily contributed the time and resources needed to train me. His mentorship was instrumental in building both my confidence and competence as a researcher. He remained supportive when my experiments and projects were not going well and encouraged me to go beyond my comfort zone. This last point was instrumental in my ability to expand my skillset not just within the expertise of his lab, but within various related disciplines. His use of both positive and tactful negative feedback allowed me to better recognize what strengths I have while improving upon my weaknesses. Finally, I would like to applaud his dedication to both students and science which is inspirational for an early career scientist to see.

I would like to thank the various other professional mentors I have had, specifically Zac Wood and the rest of my dissertation committee. Zac has always been happy to offer encouragement and advice. His passion for science always made it easier to stay excited myself. He with Chris helped build my confidence as a researcher while helping me better understand my strengths and weaknesses. My committee members including Adam Barb, Jeffrey Urbauer, and previously Eva-Maria Strauch dedicated their time and energy to helping me grow as a scientist.

I would next like to thank my graduate and postdoc comrades at the bench. They have each offered their own form of mentorship and support. John Kim for example dedicated many of the first months I was in the lab to training me and helping me get my footing. Others also contributed to this effort such as Msano Mandalasi, Nathaniel Beattie, and Hanke van der Wel. I would like to thank my lab members such as John, Elisabet Gas Pascual, Msano, Megna Tiwari, Andrew Boland, Mitchell Rich, and Hanke for various forms of moral support over the years. I would also like to thank a few non-lab members for moral support as well such as Hongqi Gao, Charles-Chess, Chin Huang, Safal Shrestha, Allison Michael, and Akanksha Swarup. I would like to thank my undergraduate researcher Tania Wilson for giving me the opportunity to mentor her and for being such a great mentee to work with. I would also like to thank collaborators such as Ramona Urbauer.

Finally, I would like to thank my partner Dongeun Seo. We have been by each other's side since near the beginning of our PhD journey. She has been my biggest source of support and enjoyment during my time at UGA. We have helped each other through our many struggles and given each other reasons to laugh. In the time I have known her, she has become my best friend, and I am glad to have met her. I hope to have her in my life for a long time to come.

TABLE OF CONTENTS

Page

ACKNOWLEDGEMENTS…….v

LIST OF TABLES……...……..xv

LIST OF FIGURES……..xvi

CHAPTER

1 ROLE OF PROLYL HYDROXYLASE-DEPENDENT GLYCOSYLATION OF E3(SCF) UBIQUITIN LIGASES IN PROTISTS OXYGEN-SENSING……..….1

ABSTRACT……...2

ABBREVIATIONS……3

INTRODUCING THE SCF COMPLEX AND ITS REGULATION……..3

THE MODIFICATION PATHWAY OF SKP1……..8

The Glycoprotein Skp1……..8

Prolyl hydroxylation of Skp1……...11

Generating the core trisaccharide…….15

Completing the pentasaccharide in *Dictyostelium*……...17

Completing the pentasaccharide in *Toxoplasma*……..18

Specificity of the Skp1 Modification pathway……20

Summary of Skp1 modifications…….22

Effects of modifications on Skp1 Structure…….24

ROLES OF SKP1 MODIFICATION IN PROTIST O_2-SENSING…….28

Role of Skp1 Modification in *Dictyostelium*……...29

Role of Skp1 Modification in *Toxoplasma*……..36

BIOCHEMICAL AND STRUCTURAL CONSEQUENCES OF SKP1 MODIFICATION AND HYPOXIA……39

Dependence of Skp1 Modification on O_2……39

Role of the ubiquitin proteasome system for O_2 regulation…….41

Skp1 Isoforms……..42

Skp1 Interactions……...……..43

Physiologically Relevant FBPs……47

SUMMARY…….50

FIGURE LEGENDS……53

SUPPLEMENTAL FIGURE LEGENDS……55

REFERENCES……72

2 GLYCOSYLATION WEAKENS SKP1 HOMODIMERIZATION IN *TOXOPLASMA GONDII* BY INTERRUPTING A FUZZY INTERACTION…….97

ABSTRACT…….98

ABBREVIATIONS……..98

INTRODUCTION……...99

MATERIALS AND METHODS……...102

Generation of Skp1 Variants……..102

Purification of Skp1 Constructs…….103

Purification of Skp1 Glycosyltransferases…….104

Modification of TgSkp1…….104

Sedimentation Velocity Experiments…….106

Circular Dichroism and Thermal Melts…….107

Analysis of the TgSkp1 Dimer using All-Atom MD…….107

RESULTS……...109

TgSkp1 is a Sub-Micromolar Affinity Homodimer……...109

Glycosylation Inhibits Self-Association……....111

TgSkp1's C-Terminal Region (CTR) Contributes to Dimerization...112

Amino Acid Composition of the Skp1 C-Terminal Region is More Important than its Sequence……...113

Deleting TgSkp1's Internal Disordered Loop Weakens Dimerization……...114

Skp1's C-terminal region drives dimerization via a salt-sensitive mechanism…….115

Skp1's C-Terminal Region Participates in a Fuzzy Self-Association…….116

DISCUSSION……117

CONCLUSIONS……...……123

AUTHOR CONTRIBUTIONS……..124

FUNDING……..124

ACKNOWLEDGMENTS……124

FIGURE/TABLE LEGENDS……..…..124

SUPPLEMENTAL FIGURE LEGENDS……..129

REFERENCES……..169

3 POTENTIAL FOR THE TERMINAL SKP1 GLYCOSYLTRANSFERASE TO EXERT NON-ENZYMATIC CONTROL OF SKP1 IN *TOXOPLASMA GONDII*……178

ABSTRACT……...179

ABBREVIATIONS……179

INTRODUCTION……180

METHODS……185

Purification of Skp1 Constructs and Glycosylation of Skp1…….185

Purification of Skp1's Glycosyltransferases……..186

Sedimentation Velocity Experiments……186

Molecular Modeling of Gat1:Skp1 Complexes……188

Computational Saturation Mutagenesis……192

Skp1 Hydroxylation Assays……...193

Fbs1-Gat1 Competition Assays……194

RESULTS……...194

Gat1 Stably Binds Skp1 in a Complex whose Stoichiometry is Dependent on Skp1's Glycosylation State……194

Skp1's CTR is Likely Relatively Disordered in the Gat1:Skp1 Complex……197

Skp1 Binds Gat1 Utilizing a Core Hydrophobic Interface……200
Gat1 and Skp1 Contribute a Hybrid Ordered and Fuzzy Interface…202
Gat1 Potentially Acts as an Exchange Factor for Skp1 in a CTR Dependent Manner…….203
DISCUSSION……204
FUNDING……..208
FIGURE LEGENDS……..208
SUPPLEMENTAL FIGURE LEGENDS……..…213
REFERENCES……..265
4 ENGINEERING RECOMBINANT EXPRESSION SYSTEMS FOR SOLUBLE SCF COMPONENTS FROM PROTISTS……..….274
ABSTRACT……...275
INTRODUCTION……..…276
METHODS……278
Cloning of Purification DdSkp1A Constructs……278
Purification of Skp1 Glycosylation Enzymes and Fbs1……279
Glycosylation of DdSkp1A……279
Sedimentation Velocity Analysis of DdSkp1A Constructs……280
Building Cullin Constructs……280
Building His-MBP-FBP Constructs……...281
Expression and Solubility Screening of His-MBP-FBP Constructs..283
Solubility Screening of TgCul1 and TgGlt1……..285
Purification of His-MBP-FBP Constructs……..286

Pull Down of DdJcdI-Short-H319A……..287

RESULTS AND DISCUSSION…….288

The Skp1 Protein in Dictyostelium is Amenable to Glycostate Specific Binding Studies……..288

Engineering FBPs for Soluble Protein Expression……290

Purification of FBPs via a Two-Step Affinity Purification……292

ACKNOWLEDGMENTS…….293

FIGURE LEGENDS……..294

SUPPLEMENTAL FIGURE LEGENDS……..296

REFERENCES……..366

5 CONCLUSIONS AND FUTURE DIRECTIONS……...…371

TgSkp1 Forms a Tight, Competitive Homodimer…….372

The Skp1 Homodimer Contains a Two Component Interface……...374

Glycosylation Disrupts Skp1's Subsite-B in *Toxoplasma* Skp1……378

Stoichiometry of the Gat1:Skp1 Complex is Dictated by Skp1 Glycosylation…….380

The Gat1:Skp1 Complex Consists of a Core Hydrophobic Interface Augmented by Transient Electrostatic Contacts……381

Gat1 Acts as a Skp1 Exchange factor in a CTR Dependent Manner……...383

Dictyostelium Skp1 Homodimerization Presents Fewer Confounding Variables in Measuring Glycosylation's Effects on the Skp1-FBP interface……..385

Soluble SCF Constructs Can be Expressed and Purified from *E. coli*……..386

Future Directions in Studying the Skp1-FBP Interface…….387

Significance of the Dissertation…….389

REFERENCES……..391

LIST OF TABLES

Table 1.S1 Species with predicted Skp1 and Skp1 modification genes are classified according to phylogenetic groups…….64

Table 1.S2 Summary of known experimentally induced Skp1 mutations and predicted effects…….68

Table 1.S3 Conservation of Skp1 CTR sequences in eukaryotes…….70

Table 2.1 Predicted and observed sedimentation values for the TgSkp1 monomer and dimer species…….....133

Table 2.2 Calculated affinities of TgSkp1 isoforms…….133

Table 2.3 Energetic components for the interaction of each TgSkp1 protein region……134

LIST OF FIGURES

Figure 1.1 SCF complex and regulation……..56

Figure 1.2 Antibody specificity for Skp1 glycoforms…….57

Figure 1.3 Evolutionary tree of eukaryotic life annotated with Skp1 modification genes…...58

Figure 1.4 Skp1 modification pathways……..59

Figure 1.5 Skp1 domain diagram annotated for contacts with other proteins……60

Figure 1.6 A diagram depicting proposed regulation of Skp1 by glycosylation……..61

Figure 1.7 Protist life cycles illustrating O_2-dependences…….62

Figure 1.8 FBPs conserved among protists…….63

Figure 2.1 Structure models of *Toxoplasma* Skp1…….135

Figure 2.2 TgSkp1 isoforms and preparation of glycosylated TgSkp1……...136

Figure 2.3 Dimerization of native and glycosylated Skp1……137

Figure 2.4 Contribution of the C-terminal region (CTR) to Skp1 homodimerization…….138

Figure 2.5 Sequence and composition dependence of the CTR contribution to dimerization. ……..139

Figure 2.6 Salt sensitivity of the CTR contribution……..140

Figure 2.7 The Skp1 CTRs self-associate through an electrostatically driven fuzzy interaction.....141

Figure 2.8 Evidence supports a bipartite mechanism for Skp1 homodimerization...……...142

Figure 2.S1 c(s) Distributions over a range of TgSkp1-FL concentrations…….143

Figure 2.S2 c(s) distributions over a range of GalGlcFucGalGlcNAc-TgSkp1 concentrations. ……..144

Figure 2.S3 c(s) distributions over a range of TgSkp1ΔCTR concentrations…….145

Figure 2.S4 Thermal melting studies of TgSkp1 variants……146

Figure 2.S5 Integration ranges used to generate c(s) isotherms…….148

Figure 2.S6 c(s) distributions over a range of TgSkp1-Scrambled6 concentrations…….149

Figure 2.S7 c(s) distributions over a range of TgSkp1-Scrambled5 concentrations…….150

Figure 2.S8 c(s) distributions over a range of TgSkp1-polySer concentrations…….151

Figure 2.S9 c(s) distributions over a range of TgSkp1ΔLoop concentrations……152

Figure 2.S10 c(s) distributions over a range of TgSkp1ΔLoopΔCTR concentrations……...153

Figure 2.S11 c(s) distributions over a range of TgSkp1ΔLoop concentrations in high salt...154

Figure 2.S12 c(s) distributions over a range of TgSkp1ΔLoopΔCTR concentrations in high salt……155

Figure 2.S13 Total residue energy contributions across simulations mapped to TgSkp1 homology models……156

Figure 2.S14 Total residue energy contributions averaged across all simulations…….157

Figure 2.S15 Fuzzy CTR interactions for Simulation 2……...158

Figure 2.S16 Fuzzy CTR interactions for Simulation 3……...159

Figure 2.S17 Distances between interacting charge clusters through the MD simulations...160

Figure 2.S18 Overlaps between the dimer-mate of the Skp1 monomer and adjacent SCF components…….165

Figure 2.S19 Engineering TgSkp1 deletions…….166

Figure 2.S20 Sequences of chemically synthesized variants of TgSkp1 genes……168

Figure 3.1 Gat1's Role in Skp1 Glycosylation and Evidence for Gat1:Skp1 Interactions….218

Figure 3.2 Sedimentation Velocity Analysis of the Gat1:Skp1 Complex……219

Figure 3.3 Computational Modeling of the Gat1:Skp1 Complex……220

Figure 3.4 Energetic and Mutational Analysis of the Gat1:Skp1 Complex……..221

Figure 3.5 Examples of Interactions in the Gat1:Skp1 Complex……222

Figure 3.6 Dissociative Effects of Gat1 on Skp1 Variants……223

Figure 3.7 The Non-Enzymatic Role of Gat1 in Binding Skp1……224

Figure 3.S1 Residuals and c(s) Distributions for Gat1:Skp1 Association Experiments……225

Figure 3.S2 Residuals and c(s) Distributions for Gat1:Gly-Skp1 Association Experiments. ……..227

Figure 3.S3 Residuals and c(s) Distributions for Gat1:Skp1ΔCTR Association Experiments. ……..228

Figure 3.S4 Overlay of Distributions Utilized for Isotherms in Figure 2……231

Figure 3.S5 Alignment of TgGat1-TgSkp1 AlphaFold3 with the PuGat1 Crystal Structure. ……..232

Figure 3.S6 pLDDT Scores for the 2:1 Gat1:Skp1 Complex……...233

Figure 3.S7 Competition Assay Showing Mutually Exclusive binding of Ether Fbs1 or Gat1 to Skp1…….234

Figure 3.S8 Inhibition of PhyA in the Presence of Varying Concentrations of Gat1……..235

Figure 3.S9 Overlay of an AlphaFold2 Structure of a 2:1 Gat1:Skp1 complex with a Glycan Docked PuGat1 homodimer Structure…….236

Figure 3.S10 Per-Residue MMGBSA Scores with a Folded Skp1-CTR…….237

Figure 3.S11 Per-Residue MMGBSA Scores with a Disordered Skp1-CTR……..238

Figure 3.S12 Predicted Change in Binding Energy for Each Cluster with a Folded Skp1 CTR. ……..239

Figure 3.S13 Predicted Change in Binding Energy for Each Cluster with a Disordered Skp1 CTR…….240

Figure 3.S14 Predicted Change in Stability for Each Cluster with a Gat1 Homodimer….241

Figure 3.S15 pLDDT Scores for the 2:1 Gat1(Y18K):Skp1 Complex…….242

Figure 3.S16 pLDDT Scores for the 2:1 Gat1(A51K):Skp1 Complex……...243

Figure 3.S17 pLDDT Scores for the 2:1 Gat1(Y18K/A51K):Skp1 Complex……...244

Figure 3.S18 Distances Between Oppositely Charged Residues Between Skp1 and Gat1..245

Figure 3.S19 Residuals and c(s) Distributions for Skp1ΔCTR Homodimerization with Gat1. ……..264

Figure 4.1 SV-Isotherms of DdSkp1A Constructs……...301

Figure 4.2 Generation of Soluble FBP Constructs…….....302

Figure 4.3 Purification of FBP Constructs……..303

Figure 4.S1 Sedimentation Velocity Distributions for DdSkp1A-FL……304

Figure 4.S2 Sedimentation Velocity Distributions for Fully Glycosylated Gly-DdSkp1A-FL. ……305

Figure 4.S3 Sedimentation Velocity Distributions for DdSkp1A-ΔCTR……..306

Figure 4.S4 Sedimentation Velocity Distributions for DdSkp1A-Scrambled4…….308

Figure 4.S5 TgCul1 Solubility Screening Gels……309

Figure 4.S6 TgGlt1 Solubility Screening Gels…….311

Figure 4.S7 TgFBP Expression Screening Gels……...313

Figure 4.S8 TgFBP Solubility Screen……...314

Figure 4.S9 Expression Screen of DdFBPs……..315

Figure 4.S10 Preliminary DdJcdI Pulldown……317

Figure 4.S11 Primers Utilized in this Study…….318

Figure 4.S12 Sequences for DdSkp1A-FL and DdSkp1A-ΔCTR……..320

Figure 4.S13 Sequences for Synthesized DdSkp1A Constructs…….321

Figure 4.S14 Sequence for the Synthesized His-DdCulE + DdRbx1 Construct……...322

Figure 4.S15 Sequence for the Final His-TgCul1 + SF-TgRbx1 Construct……..325

Figure 4.S16 Sequence for the Synthesized His-TgFbxO13 + TgSkp1 Construct……...328

Figure 4.S17 Plasmid Map for the Representative His-MBP-DdFbxF Construct……...331

Figure 4.S18 FBP Sequence for DdDlrA……..335

Figure 4.S19 FBP Sequence for DdFbxD…….337

Figure 4.S20 FBP Sequence for DdFbxH…….339

Figure 4.S21 FBP Sequence for DdFbxI……..341

Figure 4.S22 FBP Sequence for DdFbxK-1…….343

Figure 4.S23 FBP Sequence for DdFbxM……345

Figure 4.S24 FBP Sequence for DdFbxN…….348

Figure 4.S25 FBP Sequence for DdJcdH…….350

Figure 4.S26 FBP Sequence for DdJcdI-Short-H319A……...352

Figure 4.S27 FBP Sequence for TgFbxO1……...353

Figure 4.S28 FBP Sequence for TgFbxO13…….355

Figure 4.S29 FBP Sequence for TgFbxO14…….357

Figure 4.S30 FBP Sequence for DdFbxA…….360

Figure 4.S31 Representative His-MBP-DdFbxN-SF Construct…….363

CHAPTER 1

ROLE OF PROLYL HYDROXYLASE-DEPENDENT GLYCOSYLATION OF E3(SCF) UBIQUITIN LIGASES IN PROTISTS OXYGEN-SENSING

Cantrell, D. A., van der Wel, H., and West, C. M. (2025) Role of prolyl hydroxylase-dependent glycosylation of E3(SCF) ubiquitin ligases in protists oxygen-sensing.
To be submitted to a peer-reviewed journal.

ABSTRACT

The Skp1/Cullin-1/F-box protein (SCF) complex is a highly conserved E3 ubiquitin ligase responsible for proteomic control throughout eukaryotes. The SCF complex polyubiquitinates substrate proteins targeting them for degradation by the 26S proteosome. SCF specificity is mediated by a wide repertoire of F-box proteins (FBPs) which link to the SCF complex via Skp1. The various components within the SCF complex facilitate a dynamic interplay of regulatory mechanisms which mediate selective proteomic control. Protists utilize an additional mode of regulation involving prolyl hydroxylation by PhyA and subsequent glycosylation of the Skp1 subunit. PhyA is evolutionarily related to the animal oxygen sensor PHD2 and serves a cellular O_2-sensing role based on genetic analysis in the social amoeba *Dictyostelium* and the pathogen *Toxoplasma*. Remarkably, the resulting hydroxyproline provides an anchor for 5 glycosyltransferase activities that assemble a linear pentasaccharide that further genetic analyses show mediates most effects of hydroxylation. Evidence suggests that Skp1 glycosylation influences the repertoire of FBPs available to SCF complexes through conformational effects on a partially intrinsically disordered region of Skp1; this is thought to directly influence the Skp1-FBP interface and reduce competitive homodimerization which sequesters Skp1 from FBPs. A direct role for SCF activity is supported by effects of glycosylation on FBP abundance and modulating effects of proteasomal inhibitors. A distribution of candidate Skp1 modification genes exists in protists, algae, and fungi in addition to widespread occurrence of a second unmodifiable Skp1 isoform. This suggests a fundamental role for proteolytic modulation of the proteome in response to oxygen availability.

ABBREVIATIONS: α-KG, α-ketoglutarate; MD, molecular dynamics; CTR, C-terminal partially disordered region of Skp1; FBP, F-box protein; SCF, complex consisting of Skp1, cullin-1, F-box protein, and Rbx1; GGFGGn-, symbol for a pentasaccharide with the sequence Gal-Gal/Glc-Fuc-Gal-GlcNAc-; GT, glycosyltransferase; Hyp, (2S,4R) hydroxyproline; jmjC, jumonji-C domain containing; KO, a gene disruption resulting in no detectable function; Ub, ubiquitin

INTRODUCING THE SCF COMPLEX AND ITS REGULATION

Skp1/Cullin-1/F-Box/RING (SCF) complexes are a major class of E3 Cullin Ring Ubiquitin Ligases (CRLs) that primarily mark proteins for degradation by the 26S proteasome **(Fig 1.1)**. These ligases typically generate linear K48-linked ubiquitin (Ub) chains that likely direct the degradation of thousands of proteins in animals [1, 2]. The SCF (or CRL1) family was originally discovered in yeast and cancer cells and has been extensively characterized in animals and higher plants. Unicellular protists have been less studied but accumulating evidence suggests that SCF complexes are also ubiquitous throughout this kingdom [3-7]. Target specificity is mediated by members of a family of F-box proteins (FBPs) that number from dozens to hundreds in different eukaryotes [8-15]. FBPs are linked through the Skp1 adaptor protein to Cullin1 (Cul1) [16, 17]; Cul1 in turn acts as a scaffold bringing the substrate into the vicinity of a Ub-charged E2 donor that is linked to Cul1 via Rbx1 [16, 18]. The Ub-E2 appears to be replaced during each cycle of Ub transfer, and subsequent Ubs are linked to the K48 of the underlying Ub though exceptions occur [19]. Poly-Ub chains are recognized by receptors that process the target in the 26S proteosome to complete the cycle [20-23]. SCF mediated protein turnover has been implicated in

a wide swath of biological processes including developmental progression [24, 25], circadian rhythm [26, 27], metabolism [12, 28-31], pathogenic virulence [32, 33], stress response [33-35], transcription regulation [36, 37], immune regulation [38-40], and the cell cycle [25, 41, 42]. Dysregulation of these SCF functions has been widely implicated in cancer progression [41, 43, 44].

To maintain effective response of the SCF complex in its diverse functions, a wide range of regulatory mechanisms must be implemented. The potential for specific targets to be polyubiquitinated will depend on the repertoire of FBPs expressed in a given cell type. Typically, potential targets do not become substrates until they are posttranslationally modified to generate a degron recognized by the substrate binding domain of the FBP. Examples include multi-phosphorylation [15, 45-63], methylation [64], acetylation [65], and glycosylation [66], and thus regulation depends on activation of those enzyme reactions. Substrate recognition sometimes depends on the presence of another protein [67, 68] or a small molecule [69, 70] to stabilize the interaction, providing another level of control. Competitive inhibition of FBP-substrate interactions have been observed under viral infection [71] and has inspired the development of synthetic FBP inhibitors [72, 73]. Finally, access of Skp1 to Cul1 might be regulated by competing interactions with its Cul1-binding interface.

SCF complexes are also regulated on a more general level. Most FBPs reside in stable complexes with Skp1, mediated by docking of its F-box domain to the C-terminal half of Skp1. While the FBP/Skp1 pair stably interacts with Cul1 of the Cul1/Rbx1 pair, this interaction is under continuous interference by competitive binding of Cand1 to Cul1. The Cand1 interaction is in turn blocked by distal neddylation of Cul1 near its Rbx1 interaction site, which is mediated by co-E3 ligase Dcn1 and the E2 Ubc12 (UBE2M) [74-78]. Nedd8 is a Ub-like protein that is susceptible to

removal by the COP9 signalosome [79], an 8-subunit enzyme that embraces one face of the assembled SCF complex [80]. After Cul1 deneddylation, Cand1 gains access to displace FBP/Skp1 subcomplexes by what has been described as a rock-and-roll mechanism progressing from initial contact near the former nedd8 site [81]. Because FBP/Skp1 subcomplexes are in excess of Cul1/Rbx1 concentrations in cells [82], this dissociative cycle is thought to ensure SCF complexes reflect the current presence of FBP/Skp1 subcomplexes. In turn, the Cand1 interaction near Rbx1 potentially primes Cul1 for Dcn1-mediated reneddylation [83]. Importantly, the action of COP9 is slowed by the presence of substrate bound to the FBP, allowing for polyubiquitination to proceed [84, 85]. Thus Cand1 has been described as an exchange factor for Skp1-FBP complexes [86-89] which favors the formation of complexes with available substrates [82, 90]. Deneddylation is thought to protect FBP/Skp1 subcomplexes lacking a substrate from autoubiquitination [84, 85], nevertheless FBP autoubiquitination can occur [31, 91-93]. This may occur through the use of a pseudosubstrate [94] or may control the abundance of predicted non-substrate receptor FBPs through a poorly understood mechanism. There may be differential effects on FBPs that vary in their direct contact with Cul1 together with Skp1 [89, 95]. This may be important considering that not all FBPs, including some with enzyme domains, contain substrate-receptor domains. Some of these appear to constitutively bind Skp1 but not Cul1, and their stability or that of their binding partners do not appear to be influenced by Cul1. For example, the yeast FBPs Rcy1 and Roy1 [96] bind Rab11 and Rab5 in a Skp1-activated manner that does not affect their abundance. There are other examples of so-called SCF-independent FBP activities [97, 98], though all may require Skp1 binding. These Skp1/FBPs may conditionally associate with Cul1/Rbx1 subcomplexes to polyubiquitinate either the FBP itself or the Rab [99, 100]. Regulation may occur via unknown factors such as compartmentalization or molecular interactions that conditionally mask the Cul1

binding site [99, 100]. Cul1 neddylation also stimulates activity of the SCF owing to conformational rearrangements of Rbx1 that promote Ub-E2 binding [101-103]. The processes described for neddylation and Cand1 may similarly regulate all CRLs [101, 104]. Another global regulation is suggested by the ability of a protein, glomulin, that interferes with E2-binding to Rbx1 [105]. The gram-negative bacterium *Yersinia pseudotuberculosis* is thought to prevent recycling of neddylated CRLs by injecting a deaminase that targets ned8 into host cells [106]. These mechanisms for global CRL regulation in metazoans and fungi may be relevant to unicellular eukaryotes.

The interaction between Skp1 and its various FBP binding partners is a less recognized point of regulation **(Fig 1.1)**. Some organisms have dozens to hundreds of Skp1 isoforms with evidence for preferential binding to specific FBPs, thus subjecting their regulation to the presence of the preferred Skp1 isoform [107-112]. However, many organisms, including humans, budding and fission yeast, and the protist pathogen *Toxoplasma gondii*, have only a single Skp1 protein. This necessitates a single Skp1 to individually bind up to 100s of FBPs through their F-box domains [8-14]. This situation sets up the possibility that Skp1 abundance might be limiting with higher affinity FBP-Skp1 interactions being prioritized. Indeed, there are examples where Skp1 availability controls FBP levels in yeast [41, 113], and cell differentiation and cancer in animals [114, 115]. Overexpression of Skp1 in *Dictyostelium* inhibits certain developmental processes [116], and amplification of identical Skp1 genes has been observed in other social amoebae; these observations suggest that availability of Skp1 is an important dimension of SCF regulation.

The heavy metal stress response of the budding yeast *Saccharomyces cerevisiae* reveals an FBP-specific example of regulating of the FBP/Skp1 interaction. In the presence of excess Cd^{2+} or other metals, the FBP Met30 dissociates from Skp1 [35, 117, 118]; this leads to its ubiquitylation

via interactions with a chaperone which specifically targets Met30 that is not bound to Skp1 [119]. This involves metal binding to the F-box domain and p97/cdc48 AAA-ATPase action. In yeast, phosphorylation of a Ser residue at the start of future helix 7 has been implicated in controlling interaction with Met30, using a phosphomimetic amino acid substitution [120, 121]. Though the same substitution reportedly did not affect SCF assembly in human cells, phosphorylation at this site enabled an apparent non-SCF role for Skp1 [120]. Phosphorylated Skp1 was involved in V-ATPase assembly, and dephosphorylation enabled SUMOylation in the CTR and that promoted binding to Sec22B to promote a specialized secretion process. Alanine scanning mutagenesis in this study revealed that point mutations in the CTR between the future helices-7 and -8 exerted selective effects on binding to different FBPs [120]. Phosphorylation was also detected when Skp1 was expressed in insect cells [122] but was not detected on DdSkp1 [123]. In plants, S-nitrosylation was mapped to a specific Cys residue that promoted assembly with an FBP and Cul1 [124]. The activity of different FBPs is modulated by oxidative changes outside of their F-box domains [125]. In another example, the interaction of the mammalian FbxL3 with Skp1 appears to require binding to its circadian rhythm protein Cry1, an interaction that is inhibited by an unknown factor [85]. Significantly, the F-box/Skp1 interface is the target of small molecule inhibitors [115, 126, 127] and Ub variants [128] that are FBP-specific, further highlighting the potential for selectivity of this interface among FBPs. Together with reports for alternative interactions of FBPs with other proteins instead of Skp1 in animal cells, the Skp1/FBP interface is a new point of regulation to be explored.

Studies in several protists have revealed a previously unknown mode of regulation involving an unusual posttranslational modification of Skp1 that also affects FBP/Skp1 interactions [129]. First discovered in the social amoeba *Dictyostelium discoideum*, Skp1 is prolyl

hydroxylated and glycosylated to generate a linear pentasaccharide in such a way as to result in altered profile of FBP/Skp1 subcomplexes in cells [14, 32, 130]. Evidence suggests this is a direct effect occurring at least in part due to alterations in Skp1's conformational ensemble to favor binding with specific FBPs [131-133]. Similar processes and effects occur in the human pathogen *Toxoplasma gondii* [13] and possibly the plant pathogen *Pythium ultimum* [3]. Glycosylation also inhibits homodimerization which, because of overlapping binding interfaces, is expected to promote the availability of Skp1 to complex with FBPs [134]. The anchorage of the glycan on a hydroxyproline, which in turn depends on O_2 and is influenced by di and tricarboxylic acid metabolites, serving as the basis for O_2-sensing. This unusual and currently novel mode of regulation exists in multiple protists, algae, and select fungi, but not animals and higher plants. This review focuses on this novel regulation of Skp1 in the context of E3(SCF)Ub ligases and O_2-sensing in general.

THE MODIFICATION PATHWAY OF SKP1

The Glycoprotein Skp1

Skp1 modification represents an unusual example of a canonical and specific glycosylation of a cytoplasmic protein [135]. Skp1 was initially discovered as a cytosolic glycoprotein, named FP21 or Fpa1, that could be metabolically labeled with [^{3}H]-fucose in growing cells of the social amoeba *Dictyostelium discoideum* [136]. FP21 could also be fucosylated with GDP-[^{3}H]-fucose in extracts of a mutant that cannot produce GDP-Fuc from GDP-Mannose [136]. The radioactive label served as a marker for its purification to homogeneity [137]. Early work was confounded by its isolation from crude cytosolic extracts in two pools, which was later attributed to involvement in different complexes [123]. Soon after, FP21 was identified as the Skp1 subunit of the SCF

complex. Early work on the glycan that characterized the product of β-elimination occurred under the assumption that the glycan was O-linked to Ser or Thr [116]. This was misleading because the Hyp-linkage is not susceptible to cleavage by β-elimination though surrounding peptide bonds were [116]. Fucose was identified as the middle sugar of a linear pentasaccharide attached to a specific hydroxylated proline residue based on mass spectrometric analysis of its tryptic peptides [137]. This Pro which is highly conserved in unicellular eukaryotes, plants and invertebrates, has been lost in vertebrates [138]. The identity of individual sugars was indicated by sequential exoglycosidase studies, together with *in vitro* reactions of the isolated glycosyltransferases (see below). *In vitro* reactions utilized radioactive sugar nucleotides and synthetic model acceptor substrates whose products were characterized by various analytical methods (see below). The core trisaccharide of Skp1's pentasaccharide was revealed to be structurally equivalent to the blood group H type 1 antigen of mammals [137]. The 4-(trans)-Hyp (or 2S,4R) hydroxyproline configuration was established using proton NMR of the peptide isolated from *in vitro* hydroxylated Skp1, using synthetic dipeptides as reference standards [139]. Confirmation of the exact linkages awaited ability to generate the full-length glycan on recombinant Skp1. This utilized co-expression of early enzymes with Skp1 in *E. coli*, followed by *ex vivo* completion of the pentasaccharide using UDP-[1-^{13}C]Gal for the final two sugars [132]. NMR was employed to establish or confirm each glycosidic linkage, and findings were partially confirmed by properties of limited amounts of the intact glycopeptide isolated from native Skp1 from cells. Methylation analysis of the glycopeptide confirmed the linear organization of the glycan [132]. Much like it was in *Dictyostelium*, glycosylation of Skp1 has been confirmed for the distantly related protist *Toxoplasma* [140, 141], and the early modification enzymes from *P. ultimum* are active *in vitro* [3]. These organisms

present a slightly divergent glycan with the 4th sugar, an α3-linked Gal, being replaced by an α3-linked Glc.

Most protist genomes possess a single Skp1 gene [142], though *D. discoideum* has 2 Skp1 genes that differ at a single unconserved position. The Ser/Ala difference may allow for differential posttranslational modification, though there is no evidence for phosphorylation and no functional differences were detected using reverse genetic approaches [116]. There does not appear to be a difference in hydroxylation/glycosylation at Pro143 between the two genetic isoforms [143]. They are similarly expressed at the mRNA and protein levels throughout the life cycle [116, 123, 143, 144], suggesting the duplication occurs more for a dosage than a functional effect. In contrast, the two isoforms in several *Phytophthora spp*. and *Fragilariopsis cylindrus* substitute the target Pro with an alternative amino acid (E or Q) and thus are not modifiable. Furthermore, the second copy in *Pythium ultimum*, which retains the Pro but has nearby differences, cannot be modified *in vitro* [3]. Other species like *Guillardia theta* and other *Pythium spp*. conserve these differences and might also have alternative forms not subject to modification [3, 123, 142, 145]. Native Skp1 with its full glycan is enriched in nuclei relative to the cytoplasm [143], similar to mammalian Skp1. Inhibiting glycosylation either by inhibiting prolyl hydroxylation or mutating the Pro to another amino acid, reduces nuclear enrichment. Allowing addition of the disaccharide is sufficient to restore nuclear enrichment [136, 146]. As for vertebrates and many protists, *Toxoplasma* contains only a single copy of Skp1. Due largely to difficulty in purifying sufficient quantities from an intracellular parasite, biochemical analysis of TgSkp1 required exogenous expression in *E. coli* [147].

The great majority of Skp1 is normally glycosylated in *Dictyostelium* and *Toxoplasma* cells maintained at ambient O_2. These Skp1 glycoforms present unique structural features as ascertained

using monospecific antibodies. Antibodies that can differentially detect most glycoforms of *Dictyostelium* Skp1 were generated by immunization with synthetic peptides and glycopeptides **(Fig 1.2)**. However, attempts to synthesize the full pentasaccharide glycopeptide or isolate it from Skp1 were unsuccessful owing to instability. Notably, greater success was achieved using outbred rabbits rather than inbred mice to generate specific antibodies [148]. These have been useful for monitoring Skp1 glycoforms *in vivo* because of their efficiency in whole cell Western blots [148, 149]. The interesting patterns of cross reactivity suggest that the epitopes might be partially conformational rather than strictly chemical. These antibodies are especially useful given that commercial antibodies against type 1 blood group H antigen and lectins have failed to recognize discrete glycoforms. This is consistent with peptides and glycopeptides favoring specific conformations, perhaps reliant on the high density of acidic residues surrounding the target Pro [148].

Prolyl hydroxylation of Skp1

Prolyl hydroxylation of Skp1 by PhyA (originally named P4H1) primes *Dictyostelium* Skp1 for glycosylation at Pro143 [116, 143, 147, 150]. PhyA was initially assayed by incubating *Dictyostelium* cytosolic extracts with recombinant Skp1 (from *E. coli*). The reaction product was detected by its ability to be labeled with [^{3}H]GlcNAc from UDP-[^{3}H]GlcNAc in the presence of Gnt1 [150]. However, activity was lost after partial purification. Bioinformatic analysis suggested that, among 5 *Dictyostelium* putative cytoplasmic prolyl hydroxylase-like sequences, the sequence later named PhyA was most similar to *C. elegans* Egl-9 and human PHD2 [138]. These enzymes had been recently recognized as the agent for O_2-control of HIFα stability as the transcriptional target of O_2-sensing in mammalian (including human) cells [138, 150]. Disruption of *phyA* blocked

Skp1 glycosylation, indicating that it was the sole Skp1 enzyme among the other predicted cytosolic prolyl hydroxylases [143, 149, 150]. Highly purified recombinant PhyA was competent to hydroxylate Skp1 but not Skp1(P143A) *in vitro*, confirming its ability to perform the function directly [116, 143, 147, 150]. A similar function was described for the homolog from *Toxoplasma gondii*, and its PhyA was capable of rescuing Skp1 hydroxylation in a *phyA*-KO strain of *Dictyostelium* [147]. Furthermore, a recombinant version of the homolog from a stramenopile protist, *Pythium ultimum*, was also active as a Skp1 prolyl hydroxylase in vitro [3]. Considerable similarities are found between DdPhyA and TgPhyA but a dramatic difference is their K_m (O_2) values [147, 151]. In contrast to DdPhyA and PHD2s, TgPhyA has its K_m below 1% O_2. Their concentration dependences on αKG were indistinguishable [147, 151], as were their sensitivities to a panel of inhibitors (unpublished observations). While the structural basis for this difference is unknown, it is clear that the enzyme can evolve to suit the needs of the organism. In this case, *Toxoplasma* traverses anaerobic environments following oral ingestion, unlike what *Dictyostelium* is thought to experience in the soil (see below).

An exhaustive phylogenetic analysis of animal PHD2, protist PhyA, and related sequences in eukaryotes and prokaryotes, indicates that animal PHDs evolved from a protist PhyA protein [152]. Biochemical, structural and physiological studies suggest that, despite modifying distinct proteins, protist PhyA and animal PHD enzymes are orthologs [152] which catalyze the formation of (2S,4R) hydroxyproline (Hyp) [139, 151]. There is a striking degree of overlap of the X-ray crystallography determined 3D structures among DdPhyA and PHDs from human and the early metazoan *Trichoplax adherens* [139, 151]. The only significant structural difference identified is the absence of a C-terminal extension in DdPhyA [139, 151]. DdPhyA and HsPHD2, like all non-heme dioxygenases depend on concentrations of its co-substrates O_2 and α-ketoglutarate (αKG or

2-oxo-glutarate), and an Fe(II) cofactor, and are supported by ascorbate [150, 151]. Significantly, their *in vitro* oxygen K_m values measured on different acceptor constructs using different methods in different labs was well above ambient oxygen concentrations. This indicates that their activity is rate-limited by O_2 consistent with roles in O_2 sensing in cells. Kinetic studies indicate similar K_m values for αKG and ascorbate, and both bind Fe(II) very tightly retaining it during purification [150, 151]. In a similar manner to PHD2, PhyA is also inhibited by several Krebs cycle intermediates such as citrate and oxaloacetate [139] and is similarly inhibited by general non-heme dioxygenase inhibitors [143, 150].

HIFα is thus far the only confirmed direct substrate of HsPHD2 [153], which conforms with Skp1 being the only direct target characterized for DdPhyA and TgPhyA. Identifying hydroxylation substrates can be challenging because of lack of facile detection methods, background owing to spontaneous oxidation, and indirect effects of genetic manipulations in cells. The interpretation that PhyA is specific for Skp1 in *Dictyostelium* and *Toxoplasma* is reinforced by related biochemical and physiological effects of mutating DdPhyA and TgPhyA and downstream glycosyltransferases including Gnt1 [13, 154]. Evidence for glycosyltransferase specificity for Skp1 is strong owing to the availability of radioactive sugar precursors that afford high sensitivity of detection. Furthermore, PhyA and Gnt1 activities are highly dependent on determinants present on the full Skp1 protein. In comparison, peptides containing the target Pro or Hyp of up to 40 amino acids in length have far lower though measurable activity [116, 139, 142]. The target Pro or Hyp is located in a partially disordered region at the C-terminus, but point mutations in the well folded N-terminal region interfere with *in vitro* activity [116, 139, 142]. Alkylation of a key internal Cys residue that is exposed after denaturation followed by spontaneous refolding, and substitution of select Cys residues with Ser have similar effects [116, 139, 142]. The

presence of PhyA in co-IPs of Skp1 from *Toxoplasma* [13], even when the great majority of Skp1 is glycosylated, is also consistent with specificity for Skp1. Furthermore, only one of the two Skp1s from *P. ultimum* is a PuPhyA-Gnt1 substrate in vitro, despite possessing the homologous Pro residue within an identical hexapeptide sequence [3]. This again points to distal determinants that are more likely to be unique to Skp1 in the cellular environment. HsPHD2, on the other hand, is reportedly highly active toward peptides containing either of the two target Pro sites in HIFα, which also occur in disordered regions [155]. Though HIFα-like sequences appear to be absent from protists, Skp1 is highly conserved in all eukaryotes, notwithstanding that vertebrate Skp1 sequences lack the critical Pro [138]. Though HsPHD2 cannot hydroxylate DdSkp1 or TgSkp1, DdPhyA and TgPhyA are quite active toward HsSkp1 in which the critical Pro is restored with an E147P replacement [116, 139, 142, 151]. In addition, HsSkp1 inhibited spontaneous αKG turnover by HsPHD2 in the absence of substrate, indicating conservation of recognition determinants despite loss of the Pro target [151]. These findings attest to a high degree of structural refinement that had occurred during protist evolution and is maintained in metazoans. The evolutionary mechanism of hypothesized target protein substitution from Skp1 to HIFα remains unexplained. It is noted that hydroxylated HIFα is recognized by the VHL substrate receptor of CRL2 which contains the Skp1 homolog elongin C. This represents a substrate shift from a Ub ligase subunit to a degron changing the proteomic impact from degradation of FBP targets to biosynthesis of HIFα targets. In some respects, activating the SCF to degrade proteins is analogous to inhibiting transcription of HIFα-dependent genes.

Generating the core trisaccharide

Gnt1 (UDP-GlcNAc: Skp1-hydroxyproline α-N-Acetyl-D-GlcNAc transferase 1) is responsible for linking the first sugar of DdSkp1's pentasaccharide to the hydroxyproline (Hyp) generated by PhyA [132, 156, 157]. Previously named Gnt51 based on its size, Gnt1 is a sugar nucleotide and Mg^{2+}-dependent glycosyltransferase (GT) that resides in the cytoplasm requiring a reducing environment for functionality. Gnt1 was purified 130,000-fold from cytosolic extracts of *Dictyostelium* based on its activity toward a preparation of mutant Skp1A-myc ectopically expressed in and purified from *Dictyostelium*. Purification was benefited by use of a novel UDP-GlcNAc affinity column and photoaffinity labeling to tag it during purification [156]. Sequencing of peptides from the purified protein identified a gene [157] whose subsequent disruption resulted in accumulation of HO-Skp1 in cells, confirming its hypothesized role. Similar findings were observed for the homolog in *Toxoplasma* [147]. In an unrelated protist from the stramenopile group, *Pythium ultimum*, the Gnt1 and PhyA sequences are expressed as a single protein that works to modify PuSkp1A to the Gn-Skp1 state [3].

Gnt1 is highly homologous to Gnt2, a Golgi resident αGlcNAcT that initiates mucin-type O-glycosylation of proteins destined to the cell surface or for secretion [138, 158]. By analogy, Gnt1 was inferred to also be a retaining glycosyltransferase, and the α-linkage was later confirmed by NMR of the isolated glycopeptide [132]. Phylogenetic analysis of Gnt1 indicates a close evolutionary relationship to several cytoplasmic, prokaryotic GT-A enzymes [157]. The prokaryotic sequences, however, lack a conserved C-terminal domain that is required for activity in eukaryotes [157]. The presence of both Gnt1 and Gnt2 or Gnt2-like glycosyltransferases in other protists indicates a likely gene duplication event before the divergence of the two enzymes [138]. Data suggest that the cytoplasmic Gnt1 is ancestral to Gnt2 [135, 157]. Gnt1 and Gnt2 were the

founding members of the CAZy GT60 family, and Gnt2 is likely ancestral to the relatively closely related Golgi-associated animal CAZy GT27 animal mucin type αGalNAc-transferases [156, 157]. GT27 glycosyltransferases likely diversified when the UDP-Gal epimerase evolved to generate UDP-GalNAc from UDP-GlcNAc [159].

Additions of the second and third monosaccharides are catalyzed by PgtA, a bifunctional di-glycosyltransferase with separate domains for the two activities. PgtA was first identified as an α-fucosyltransferase (originally FTase or FT85) toward Skp1 isolated from a *Dictyostelium* mutant unable to synthesize GDP-Fuc from GDP-Man causing accumulation of disaccharide Skp1 [145]. A survey of synthetic mono-, di- and trisaccharides used to compare mammalian fucosyltransferases associated with ABO and Lewis blood group antigens was conducted. This pointed to lacto-N-biose-1, or Galβ1,3GlcNAcβ- associated with different aglycons as an optimal acceptor. Synthetic substrates in conjunction with GDP-[^{3}H]Fuc were used to purify the activity as FT85 over 3 million-fold from cytosolic extracts of *Dictyostelium*. Although not pure by SDS-PAGE, selection of the candidate band by photoaffinity labeling with an iodinated probe provided sufficient information for cloning PgtA by PCR. When PgtA was disrupted, Skp1 surprisingly accumulated as the monoglycosylated Gn-Skp1 glycoform rather than the expected GGn-Skp1 glycoform. This led to the realization that PgtA, with an Mr of 85,000, is a di-glycosyltransferase with separate domains independently capable of mediating its β3-GalT and α2-FucT activities [160]. Domain activities were assigned using site specific mutagenesis and expression as separate domains. The α2FucT domain became the founding member of the CAZy GT74 family – unrelated to the CAZy GT10 family of α2FucTs known at the time. In comparison, the N-terminal CAZy GT2 domain, which commonly occurs in the cytoplasm of bacteria for assembly of polysaccharides slated for export to the cell surface, encodes the β3GalT activity. The result is

formation of the type 1 blood group H trisaccharide antigen structure, by convergent evolution with the mammalian glycan. As described below, this structure appears to be significant for the conformational profile of Skp1. PgtA is conserved in *Toxoplasma* and its parallel role in modifying Skp1 was confirmed by mass spectrometry analysis of Skp1 in a *pgtA*-KO strain [141]. Surprisingly, the order of the two glycosyltransferase domains is reversed compared to DdPgtA, but genomes that express the domains as separate proteins have not been detected. Interestingly, the GalT appears to be strongly inhibited by concentrations of UDP-Gal above 10 μM *in vitro* [149]. Studies using glycoform-specific Abs **(Fig 1.2)** and mass spectrometry have failed to detect significant accumulation of the mono-, di- or tri-saccharide glycoforms, suggesting that once initiated, glycosylation tends to be constitutive.

Completing the pentasaccharide in *Dictyostelium*

Addition of the final two sugars in *Dictyostelium* is catalyzed by AgtA (formerly GT78) [132]. This bifunctional enzyme contains a single catalytic domain and a series of C-terminal WD40 repeats expected to fold into a 7-bladed β-propeller domain. Both sugars are αGal residues, α3-linked to their underlying sugars [132]. AgtA was identified after purification to homogeneity from cytosolic extracts of *Dictyostelium* based on its ability to modify Fuc terminated synthetic glycans using UDP-[^{3}H]Gal [161]. Sequences of tryptic peptides from the purified protein led to the identification of the encoding gene. Its catalytic domain was the first experimentally documented glycosyltransferase in the newly formed CAZy GT77 family that initially included glycosyltransferases associated with pectin synthesis in the plant secretory pathway [142, 162]. Its role in applying the fourth sugar on Skp1 was confirmed by the finding that the trisaccharide glycoform of Skp1 accumulated when its gene was disrupted [149]. Its surprising role in also

catalyzing the addition of the fifth and final sugar resulted from mass spectrometry analysis of the product of its *in vitro* reaction with FGGn-Skp1 [163]. Interestingly, AgtA can add a single αGal residue to Fuc-terminated sugars attached to a non-protein aglycon but only adds the second αGal when the acceptor glycan is attached to Skp1. Initially, the first αGal was shown to be linked to the 3-position of Fuc based on chromatographic co-elution with standards. Other studies showed specificity for fucose that was α-linked and in the L-configuration [163]. Determination that the 5th and final Gal is also α3-linked awaited analysis of the full length Skp1 modified by AgtA with UDP-[^{13}C]Gal by NMR [132]. This corrected the prior assignment as an α1,6-linkage that had been based on recalcitrance to an α3-galactosidase [137]. This initial observation was likely because the enzyme was not pan-specific to the nature of the underlying sugar. The Skp1-AgtA interaction, mediated by its β-propeller domain, is relatively tight with an apparent affinity of about 60 nM in the presence of 50 mM NaCl [163]. A similar affinity was observed for earlier stages of Skp1 modification but it was modestly weakened upon completion of the pentasaccharide. The low K_m for FGGn-Skp1 is most consistent with AgtA binding the monomeric form of Skp1. Unlike the other enzymes, which are estimated to accumulate at low levels commensurate with catalytic roles, AgtA has been estimated to be equimolar with Skp1 in cells [162]. As described below, the intrinsic binding of AgtA to all isoforms of Skp1 is likely to impact Skp1 activity in the cell.

Completing the pentasaccharide in *Toxoplasma*

Sequence-based bioinformatics searches failed to detect a homolog of *Dictyostelium* AgtA in the *Toxoplasma* genome [141]. However, a broad search for GTs that lacked organelle targeting sequences and were phylogenetically co-distributed with TgGnt1 and TgPgtA yielded TgGlt1 and TgGat1 as candidates [164]. TgGlt1 is a CAZy family GT32 GT which is responsible for the

addition of an α-glucose to the terminal fucose of the TgSkp1 trisaccharide. NMR of the product of the *in vitro* reaction with FGGn-pNP showed α-Glc to be linked to the 3-position of Fuc, as occurs in DdSkp1. Glt1 is highly specific for the UDP-Glc substrate with minimal activity for all other tested sugar donors [164]. TgGat1 then functions to extend the resulting tetrasaccharide as indicated by genetic deletion of *gat1* resulting in accumulation of the tetrasaccharide glycoform of Skp1 [165]. Phylogenetic analysis of Gat1 evolution showed it to be closely related to glycogenin [165]. Glycogenin serves as an initiating α4GlcT for priming glycogen synthesis in yeast and metazoa, and glycogenin-like proteins, though Gat1 lacks a C-terminal glycogen synthase binding domain. Like glycogenin, Gat1 modifies Glc but in a 3- rather than 4-linkage. Interestingly, Gat1 has weak GlcT activity and glycogenin has weak GalT activity, consistent with their close evolutionary relationship. An ortholog of TgGat1 is expressed in *Pythium ultimum*, which is in the stramenopile clade of the larger SAR group in which *Toxoplasma* exists as an apicomplexan. The substrate activity profiles of its recombinantly expressed version are similar to TgGat1 including absence of the self-modification that occurs in glycogenin [165]. Both Gat1 proteins form high affinity homodimers with submicromolar K_d values like glycogenin and with an identical dimer interface. Modeling the active site confirms a preference for the Skp1 tetrasaccharide, and AlphaFold-3 modeling suggests a mechanism for Skp1 binding compatible with enzymatic processing (unpublished data). The presence of Gat1 in the Skp1 interactome of *Toxoplasma*, as assessed by co-immunoprecipitation and regardless of its modification status, was not observed for the other GTs but was for PhyA [13]. This observation invites speculation that, like the terminal glycosyltransferase of the *Dictyostelium* pathway, Gat1 has a second non-enzymatic role that affects Skp1.

Specificity of the Skp1 Modification pathway

The state of Skp1 that is a native substrate *in vivo* is unclear. Skp1 can self-associate as a homodimer with a K_d of 1-2 μM in vitro [166], similar to values for HsSkp1 [167]. This is close to the estimated Skp1 concentrations in human cell culture [82]. Remarkably, some assays indicate that the K_m for PhyA and Gnt1, toward Skp1 is in the low to sub-μM range [139, 147, 151]. Apparent μM or lower K_m values for Skp1 have also been observed for PgtA [136, 145, 149, 160], AgtA [161, 163], and Glt1 [164]. This correlation invites speculation that only the monomer is a substrate and the K_m is a function of the homodimerization K_d. In the case of AgtA, the low K_d (60 nM) and K_m observed for Skp1 has been suggested to indicate a monomeric substrate [163]. The *in vivo* concentration of free Skp1 is likely much less, however, as most will be incorporated into higher affinity complexes with FBPs [82]. Evidence shows that Skp1 is not a substrate for PhyA when bound to an FBP [139]. Also, a separate study found a K_m for PhyA that was two orders of magnitude higher [151]. The reason for the discrepancy is unknown but might be due to differences in the Skp1 isoforms and assays used. A comparison between the *in vitro* and *in vivo* substrate activities of Skp1 mutants suggests that other factors are important for the *in vivo* reaction. For example, appending an N-terminal FLAG-tag to ectopically expressed Skp1 makes it inert to hydroxylation and prevents formation of complexes with FBPs and other proteins [116]. Despite these observations analogous modifications to Skp1 do not appear to affect activity *in vitro* [139]. This applies to the Gnt1 and AgtA enzymes as well, as point mutations in Skp1's N-terminal region result in accumulation of their substrate glycoforms [137]. These mutant Skp1A pools were instrumental for use as *in vitro* substrates to purify and identify the responsible enzymes [156, 157].

A high degree of specificity of Skp1's glycosyltransferases for Skp1 has been observed. When specificity of Gnt1 was tested by supplementing *gnt1*-KO extracts with recombinant Gnt1 and UDP-[^{3}H]GlcNAc, Skp1 was the only radiolabeled protein detected [154]. Radioactive incorporation and mass spectrometry confirmed the absolute specificity of Glt1 [164] and Gat1 [165] for Skp1. Specificity for TgPgtA was shown to be cross reactive for Gn-DdSkp1 in *Dictyostelium* through specific incorporation of UDP-[^{3}H]Gal, or GDP-[^{3}H]Fuc that did not occur in *pgtA*-KO extracts [141]. PhyA [139], Gnt1 [139], PgtA [149], and AgtA [161, 163] modification of Skp1 relies heavily upon determinants in the folded region of Skp1, well beyond the target Pro and associated modifications. Similar, although less extensively tested trends have been observed for Glt1 [164] and Gat1 [165] from *Toxoplasma*. A 23-mer peptide including the target Hyp is a specific substrate for Gnt1 but has a 3000-fold higher K_m and 3-fold reduced V_{max}, consistent with the specificity determinants for PhyA [139]. Sequence comparisons of the 2 enzymes and the fusion enzyme have not revealed a basis for the shared specificities of the two enzymes. PgtA may utilize this specific Skp1 recognition for processivity by first adding a βGal to the GlcNAc of Gn-Skp1 through its N-terminal GalT domain [160]. PgtA then retains GGn-Skp1 to processively modify the βGal using the C-terminal αFucT domain, based on *in vitro* studies with UDP-[^{3}H]Gal and GDP-[^{14}C]Fuc [132, 145, 149, 160]. The role for the whole Skp1 protein in mediating processivity was reinforced by the lack of processivity for a synthetic glycopeptide substrate. In contrast to earlier activities, the FucT activity of PgtA depends primarily on recognition of the specific disaccharide linked to the polypeptide [145, 149]. The recombinantly expressed catalytic domain alone (AgtA-CAT) showed the same pattern of reactivity with the free glycans, but modified FGGn-Skp1 was no better than free FGGn-pNP [161, 163]. The addition of free recombinant C-terminal β-propeller domain strikingly activated activity toward the free glycans,

as did addition of unmodified Skp1. These findings were supported by studies indicating stable binding of AgtA to Skp1 mediated by its β-propeller domain in vitro and during purification of AgtA from cell extracts [161]. Recombinant Gat1 isolated from *E. coli* was highly active in labeling GlFGGn-Skp1 from UDP-[^{3}H]Gal with approximate K_m values for UDP-Gal and GlFGGn-Skp1 of around 5 μM [165]. These values are similar to that of TgGlt1 but 5-10 fold greater than assayed for DdAgtA. The reason for the difference is unclear but may be associated with differences in enzyme activity against monomeric or dimeric Skp1. The Skp1 homodimer K_d is expected to be about 40-fold stronger in *Toxoplasma* [134].

Summary of Skp1 modifications

Together the findings document the occurrence of a surprisingly complex O-glycosylation pathway in the cytoplasmic compartment of a wide variety of protists, algae and fungi. This is based on experimental validation of bioinformatics predictions in 3 independent protist groups. All enzymes are conventional sugar nucleotide-dependent GTs and occur as soluble proteins in cytosolic extracts from *Dictyostelium* and *Toxoplasma*. While there is no biochemical evidence for co-associating as complexes, they appear to act efficiently as we have not detected accumulation of glycoform intermediates using glycoform-specific mAbs and mass spectrometry. This suggests that once the attachment Pro is hydroxylated, glycosylation occurs rapidly to generate the full glycan. This is likely expedited by the pairing of β3GalT and α2FucT in PgtA, which from *Dictyostelium* acts processively *in vitro* [149]. Other instances exist of pairing of PhyA and Gnt1 [3] or Glt1 and Gat1 as fusion proteins **(Fig 1.3, Table 1.S1)**. AgtA is activated by binding Skp1 for the addition of the final 2 sugars [163].

The substitution of AgtA for Glt1 and Gat1 is a remarkable example of convergent evolution that may be driven by a need for the essentially the same pentasaccharide. The only difference between the two glycans is the conservative replacement of an α3Glc by an α3Gal. An interesting hypothesis is that by this transition, Gat1 was liberated to evolve into glycogenin to perform a distinct role in the cytoplasm, that of facilitating the synthesis of glycogen [13]. At present, Glt1- and Gat1-like sequences are found in the Diaphoretickes and AgtA-like sequences in the Amorpheae **(Fig 1.3, Table 1.S1, Fig 1.4)**, so it is unclear which is ancestral. In contrast, other unicellular organisms including *Acanthamoeba castellanii* and *Chlamydomonas reinhardtii* possess likely orthologs of PhyA and Gnt1, but lack any evidence for PgtA, Glt1, Gat1, and AgtA. These might be examples of intermediates that can instruct us on the role of monosaccharide modification of Skp1 that likely occurred during evolution of the full pathway. Alternatively, these examples might lead to the discovery of new cytoplasmic GTs.

An unusual feature of the Skp1 glycosylation pathway is its apparent dedication to a single protein in both *Dictyostelium* and *Toxoplasma*. This interpretation relies primarily on specificity of Skp1's GTs, as evidenced by low K_m values for Skp1 and dependence on structural features of Skp1 far from the site of glycosylation [137, 139, 143]. Failure to detect alternative substrates in GT-KO cells using biochemical complementation with highly sensitive radioactive sugars adds further support for this conclusion. In turn, the specificity of PhyA for Skp1 is reinforced by similar though not identical biochemical and physiological effects of disrupting *phyA* and *gnt1* (see below). The phenotypic differences that do occur might be due to distinct structural effects of hydroxylation and subsequent αGlcNAcylation. A second unusual feature is the finding that the non-reducing terminal GTs in both *Dictyostelium* and *Toxoplasma* exhibit unexpected affinity

toward Skp1. This is regardless of its modification status which, in *Dictyostelium*, may modulate Skp1 availability to associate with FBPs and other proteins [163].

Skp1 isoforms are good substrates for the modification enzymes whether in extracts or in recombinant form, but the optimal physical state for activity is unclear. Skp1 exists as a dimer with a ~2 μM K_d, similar to the K_m values for DdPhyA and the *Dictyostelium* GTs. This could be explained if the monomer state is the active acceptor. Skp1 hydroxylation is strongly inhibited when it is complexed with an FBP [139]. In *Dictyostelium* cells, Skp1 point variants in the BTB domain far from the modification site are poorly modified yet were invaluable as substrates for identifying Gnt1 and PhyA [137, 150, 156]. An N-terminal FLAG-tag blocks modification of ectopically expressed Skp1 despite its being a good substrate *in vitro* [116]. Thus, an unknown factor may be required in cells for Skp1 modification and function. The significance of O_2 as a rate limiting factor for PhyA activity in cells is examined below.

Effects of modifications on Skp1 Structure

Skp1 is a highly conserved, 160-180-amino acid protein that includes an N-terminal BTB domain and a partially disordered C-terminal domain in isolation **(Fig 1.5)**. Skp1 folds into a consistent canonical structure when complexed with FBPs as assessed by X-ray crystallography and cryo-EM [168-170]. The interface with the F-box domain consists of a core interaction involving helices 5, 6 and 7 (Subsite 1) and a variable interaction involving helix 8 (Subsite 2) [169]. Skp1 maintains a similar bound conformation to FBPs across phylogeny [30, 68-70, 128, 168, 171-183], except that Subsite 2 takes on a strikingly different conformation when bound to Fbs1 [178]; this does not appear to be a crystal packing artifact, consistent with an ability to accommodate divergent F-box sequences. Conformational flexibility and backbone contacts likely

underlie the ability of Skp1 to bind these various and often degenerate F-box domain sequences [184, 185].

In comparison, free Skp1 does not crystallize even upon deletion of two internal, poorly conserved disordered regions. NMR studies of DdSkp1 show that the first 120 amino acids retain the same BTB domain fold seen in complexes, but that the C-terminal ~40 aa are relatively disordered **(Fig 1.5)**. In fact, a significant entropic penalty was described which likely originates from ordering Skp1's C-terminal region upon binding the soluble mammalian FBP Fbs1 [186]. The homodimer interface overlaps with part of Subsite 1 of the F-box interface, referred to as Subsite-A **(Fig 1.5)**. Recent studies show that the partially disordered CTRs contribute a charge-based fuzzy interaction called Subsite-B [134]. This improves homodimer affinity by over an order of magnitude to an estimated K_d of 50 nM in *Toxoplasma* Skp1. Skp1's Subsite-B bears striking resemblance to other described charge-based fuzzy interactions except that it forms the only known charge-based fuzzy homodimer interface [187-190]. Glycosylation of TgSkp1, which is expected to homodimerize in the same manner, weakens the homodimer by over an order of magnitude [134]. This is nearly equivalent to removing the entire C-terminal disordered region where the glycan is anchored [134]. As described below, the structurally ordered glycan is thought to sterically interfere with the dynamic fuzzy interaction **(Fig 1.5)**. Thus Skp1's CTR has dual roles in facilitating both homodimerization and heterodimerization with FBPs. Human Skp1 was the first to be reported to form a homodimer [167], with a K_d of 1-2 μM. This value is in the range estimated for Skp1 in cultured cells [82], though Skp1 concentrations appear to be much higher in specialized cells [167]. *Dictyostelium* Skp1 also homodimerizes with a similar K_d [166]. In comparison, the ~50 nM K_d of *Toxoplasma* Skp1 homodimerization may be competitive with the only known K_d of a Skp1/FBP interaction: HsSkp1 with guinea pig Fbs1 [186]. The dynamic

nature of Skp1's fuzzy interface (Subsite-B) may facilitate exchange from the homodimer [187-190] while the well-ordered nature of the Skp1-FBP interface [169] will minimize exchange in the opposite direction. Subsite-B's dynamic nature may also facilitate hydroxylation and glycosylation in the dimer state, though the BTB domain is required for recognition by most of the enzymes. These dual roles, in addition to acceptance of post-translational modifications, presumably impose unique constraints on the sequence of the CTR, which is highly conserved throughout eukaryotes **(Table 1.S3)**. Thus, point mutations of Skp1 that have previously been inferred to selectively affect FBP interactions **(Table 1.S2)** may also influence competing homodimerization.

The impact of the glycan was assessed in more detail by NMR experiments using *Dictyostelium* GGFGGn-Skp1 labeled with [U-^{13}C]-sugars [133]. The reducing and non-reducing end sugars of the glycan exhibited rapid but correlated motions relative to the BTB domain. This was attributed to motions of the disordered peptide to which the glycan was attached [133]. Detected NOEs and inter-sugar interactions suggested by force-field and molecular dynamics (MD) analyses led to the model that the pentasaccharide has a relatively ordered structure [133, 165, 191]. This is consistent in part with prior NMR studies on the organization of the reducing end blood group H type 1 trisaccharide [192]. NMR studies of the perdeuterated dimer showed changes in 1H:15N cross peaks for Gn-Skp1 and further changes for GGFGGn-Skp1 relative to Skp1, indicating significant reorganization [133]. One consequence of αGlcNAcylation was partial induction of helix 8 seen in FBP complexes, which is predisposed to fold in this way owing to its E/R/K composition as described [193-195]. The target Pro resides at the start of future helix 8, and it is likely that its modification promotes downstream helicity [196]. Prolyl hydroxylation and αGlcNAcylation strongly favor the trans isomer of the Thr-Pro bond in model di-peptide studies analyzed by NMR [197]. This is the isomer observed in structures of unmodified Skp1 in

Skp1/FBP complexes, but the preference might influence folding of this region on a longer time scale not accessible by MD studies. Proline puckering also appears to shift dependence on hydroxylation or glycosylation state, with the Cγ-exo conformation being favored upon addition of the GlcNAc [197]. MD modeling proposed a role for the relatively rigid glycan to organize the upstream sequences that form helix 7 and the intervening loop between helices-7 and -8 in FBP complexes [132]. Interactions here are stabilized by hydrogen bonds to helix-7 and loop side chains and backbone atoms. This promotes packing of the fifth Gal in the turn represented by the junction of helix-7 with the loop. This corresponds to the region showing altered chemical shifts in NMR studies of glycosylated Skp1 [133]. MD simulations of the fully glycosylated and unmodified versions of DdSkp1 were conducted [131-133, 165]. These simulations showed that the presence of the glycan increased the average width of the pocket that docks the F-box domain of the FBP, potentially facilitating the interaction [131-133, 165]. Molecular dynamics analysis of the TgSkp1 glycan, which differs by substitution of αGal with αGlc, yielded a similar interpretation except that specific hydrogen bonds with helix-7 were of lower frequency [165]. In particular, each 4-epimer projects its -OH moiety toward the solvent, with minimal consequence on the interface with the polypeptide. There are other examples where glycosylation influences a protein's folding or conformational ensemble, though an effect of such a long glycan is unusual [196, 198-204].

Skp1's diverse conformational ensemble has been suggested to allow Skp1 to readily bind a diverse array of proteins [185]. Evidence suggests that glycosylation of Skp1's C-terminal region (CTR) influences this conformational ensemble in cells, which is likely to constrain it to be more favorable for FBP binding **(Fig 1.6)** [131-133]. It is unlikely that glycosylation influences Skp1 stability as both glycosylated and unmodified Skp1 are relatively long lived (typically 14-16 hours or up to 5 days) [116, 130, 143, 154]. There is no evidence for the glycan itself serving as a ligand

for a carbohydrate binding protein, as these proteins fail to show up in comparative Skp1 interactome studies [13, 14, 130, 205]. Overall, the effects of glycosylation are expected to favor a disorder to order shift for Skp1's C-terminal region [131-133], which is expected to lead to several consequences for Skp1's protein-protein interactions **(Fig 1.6)**. Other regions of the BTB are primarily involved in interactions with Cul1, Syp proteins, Sgt1 and Cep3, although some contacts with Cul1 also occur near the F-box interacting region. The prolyl hydroxylation, glycosylation, and phosphorylation modifications described above occur in the partially disordered CTR, which therefore would be expected to selectively affect FBP and self-interactions over the other interactions.

ROLES OF SKP1 MODIFICATION IN PROTIST O_2-SENSING

The evolutionary relationship of PhyA to animal PHD2 was an initial motivation to explore O_2-dependent behaviors in *Dictyostelium* and *Toxoplasma*, some of which are phenocopied by genetic disruption of PhyA. As detailed below, further studies indicate that Skp1 modification provides a partial molecular mechanism for O_2-sensing, though much more remains to be learned. The Skp1 modification related genes are found across unicellular organisms from algae to a range of protists to certain fungi **(Fig 1.3, Table 1.1, Table 1.S1)**. *T. gondii*, *D. discoideum*, and *P. ultimum*, protists for which modification gene activities have been documented, represent divergent clades of the eukaryotic tree of life [206]. Current genomic information suggests the genes are absent from strictly anaerobic protists and obligate multicellular eukaryotes, where PhyA is speculated to have evolved into PHD2 to modify HIFα [129]. Furthermore, the GT candidate genes are always associated with a PhyA-like gene. The model that E3(SCF) Ub ligases facilitate O_2-sensing sets a precedent for investigating O_2-sensing across the algal, protist and fungal

kingdoms where the coding genes are predicted. This perspective is not intended to exclude other potential mechanisms including heme-based O_2 sensors, which are prominent in bacteria and reviewed elsewhere [207, 208].

Role of Skp1 Modification in *Dictyostelium*

Dictyostelium discoideum is a soil based social amoeba that has been widely used as a model organism for pre-metazoan unicellular and multicellular eukaryotic life [209]. It has a well characterized asexual life cycle which is summarized in **(Fig 1.7A)**. It is a model for leukocyte chemotaxis and motility, as a reservoir for virulent bacteria, and for developmental regulation of multicellularity. *D. discoideum* spends much of its existence proliferating underground in a unicellular form by phagocytosing soil bacteria for food [210]. Upon depletion of their food source, the amoebae cooperatively aggregate using chemotaxis and intercellular adhesion mechanisms to form a multicellular slug. This slug is composed of 10-20% prestalk cells occupying the anterior end including the tip, and mainly pre-spore cells in the posterior. The slug migrates to the soil surface whereupon it will culminate to form a fruiting body composed of sacrificial stalk cells and aerial mass of spore cells. The stalk cells of the fruiting body altruistically die while the spores are dispersed to continue the life cycle upon germination as free-living amoebae in potentially more favorable locations [210].

O_2 figures in many behaviors and processes, some of which might not involve metabolic respiration per se. *Dictyostelium* is an obligate aerobe and axenic strains require >2% O_2 to proliferate in shaking culture, though can survive under anoxic conditions for long periods of time (days to a week). Single amoebae migrate toward a preferential level of O_2 (1-2%) in gradients in a process referred to as aerotaxis [211]. Evidence suggests that the response does not involve

mitochondria, nitric oxide or oxidative stress [212]. Under static conditions in nutritive medium, cells will merge into loose dynamic clusters whose sizes scale in response to changes in the local concentration of O_2 [213]. In comparison, the process of starvation induced development requires relatively higher levels of O_2 to advance to the tight aggregate stage. This is accommodated in laboratory practice by placing cells on an agar or a moist filter paper surface in the presence of a simple salts containing buffer. At an air-water interface, culmination of slugs into fruiting bodies requires a threshold of O_2 around 10%, compared to 21% at sea level [144, 214]. By analogy, early experiments in soil samples documented that slugs migrate to the soil surface suggesting attraction to O_2, although repulsion to metabolites such as NH_3 was difficult to exclude [214]. These responses to O_2 are consistent with amoebae remaining in lower O_2 regions of the soil in the unicellular state, and the multicellular slugs favoring higher O_2 environments to ensure that spores are dispersed.

Potential roles of O_2 have been further explored by restricting its availability by diffusion or physical barriers. If cells are submerged under a column of buffer, they are unable to proceed past the loose aggregate stage unless the atmosphere is held at 70-100% O_2. This appears to allow diffusion into the cell aggregates at a pace sufficient to balance consumption of O_2 by metabolism. Cells in aggregates formed in this way can differentiate with separate zones of prestalk and prespore cells reminiscent of the normal pattern in slugs [215]. A major difference is however that they are enveloped by a single layer of prestalk cells. After additional time, extensive stalk and spore differentiation ensues. When immobilized in O_2 gradients, prestalk cells are found at the higher concentration side [216]. During isometric exposure of submerged aggregates to high O_2, a pattern presents where prespore cells and spores reside in the interior, surrounded by a cortex of prestalk and stalk cells [217]. This pattern is also consistent with O_2 favoring prestalk cell

differentiation or attracting pre-differentiated prestalk cells. The differentiation of prespore cells to spores also requires high levels of ambient O_2. Similar prestalk/prespore cell polarization is observed when cells are drawn into one-dimensional arrays within a capillary tube, with the open end permitting O_2 flux [219]. Trapping developing cells between two O_2-impermeable glass slides also allows a pattern of prestalk and prespore zones to occur at the margin that is exposed to ambient O_2. In this case an opposite polarity was observed, with cells expressing a prespore marker residing at the edge of higher O_2 exposure [219]. Time-dependent rearrangements led to the suggestion that additional effects of unknown morphogens and sorting of prestalk cells to higher O_2 were involved. A related method of confining developing aggregates documented streaming of cells to a high-O_2 margin [216], consistent with slug behavior in soil studies. A second effect of higher O_2 in submerged cultures was a doubling of the ratio of prestalk to prespore cells [220]. This effect was also observed when exposing natural slugs at an air-water interface to hyperoxia. Whether these O_2-dependent effects are mediated via metabolism, associated pH changes affecting ionization of signaling molecules, reactive oxygen or nitrogen species, oxygen-binding proteins, and/or monoxygenases and dioxygenases, remains unclear. Altogether, *Dictyostelium* has many features making it an attractive model for studying mechanisms of O_2 sensing.

The discovery that *phyA*-KO *Dictyostelium* exhibited a high O_2 threshold (18-21% O_2 or more) for culmination was a recent catalyst for revisiting O_2-sensing in *Dictyostelium* [144]. The rationale was that the absence of this O_2-dependent enzyme explained why slugs were unable to culminate. This correlated with a high K_m (O_2) for isolated DdPhyA of around 40% [150], indicating sensitivity to O_2 in the ambient range. Consistent with this model, PhyA-overexpression reduced the threshold to around 5% O_2, as if compensating for reduced concentration-driven activity. The effect functions in parallel with stimulation of culmination by light, which can

partially compensate for low O_2 in culmination [144]. PhyA action lies upstream of other pathways of developmental regulation. Overexpression of the catalytic subunit of Protein Kinase A (PKA), a master regulator of development [221], partially rescued culmination under hypoxic conditions [144]. This relationship between PhyA and PKA may be related to regulation of the FBP FbxwA, which reportedly targets the PKA regulating protein RegA, a cAMP phosphodiesterase, for degradation [222]. Not only was the O_2 threshold influenced by differential PhyA activity and glycosylation, but time to culmination was also delayed in these instances [116, 144]. PhyA appears to have a signaling role because *phyA*-KO cells can be rescued by high O_2 levels, co-development in chimeras with wild-type cells, and overhead light [142, 144, 217, 223-229]; *phyA*-KO cells are additionally sensitized to the culmination inhibitor NH_3 [142, 144, 217, 223-229]. Furthermore, in chimeric mixtures with *PhyA–* strains, *PhyA+* cells preferentially sort to the anterior tip, which is thought to be the primary organizer of the slug that controls the culmination decision [230]. The numerous so-called slugger mutants that have been described might hold clues to potential mechanisms [228, 231, 232]. The O_2 checkpoint is likely activated close to the time of pre-spore and pre-stalk cell differentiation on O_2-shift experiments during development [217]. PhyA expression is observed throughout slugs and during growth and development, suggesting effects on Skp1 for other O_2-dependent processes [144]. Notably, no effect on cell proliferation has been observed in the *phyA*- or Skp1 GT-KO strains. An example of another potential O_2 sensor is the jumonji C protein and likely lysyl hydroxylase JcdI. Though a double knockout of JcdI and its paralog JcdH did not affect the O_2 threshold, its overexpression led to modestly decreased O_2 threshold, in a manner that depended on its catalytic activity but not its F-box [14]. JcdI has a K_m for oxygen of 22% indicating its activity is regulated in the physiological range of O_2 [14]. JcdI is evolutionarily related to the mammalian Jmjd6 protein [14] which acts in epigenetic regulation,

RNA splicing, and oncogenesis [233-235]. Phylogenetic analysis suggests that JmjC containing FBPs such as JcdI and JcdH represent a conserved group of protist FBPs that are ancestral to the emergence of mammalian Jmjd6 proteins [14].

If Skp1 is the primary or sole target of PhyA, then varying Skp1 levels might modulate the effects of PhyA. Significantly, the absence of PhyA did not affect Skp1 abundance [154]. Using the same culmination assay, overexpression of Skp1 in the slug, in either prespore or prestalk cells, raised the O_2 threshold which, however, could be overridden by co-overexpression of PhyA [116]. These results suggest that the role of PhyA is to activate Skp1 and, by extension, the SCF. Although similar effects of overexpression in prespore and prestalk cells was unexpected, overexpression in prespore cells might induce conversion to prestalk cells; *phyA+* (wild-type) cells migrate to the anterior end in chimeras with *phyA*-KO cells [144]. The Skp1 dosage interpretation is consistent with results indicating that Ax2, a strain lacking one Skp1 gene copy compared to Ax3, has a lower O_2 threshold for culmination [116]. Moreover, disruption of one of the two Skp1 genes in strain Ax2 led to an even lower threshold. Additionally, instituting a P143A or P143E point mutation in one of two Ax2 Skp1 genes lowered the threshold [116], while overexpression of the P143A mutant did not raise the threshold. These findings strongly support the model that PhyA signals via Skp1 for regulating culmination.

The roles for the Hyp-dependent glycosylation of Skp1 was examined using KOs of each of the GTs, which result in accumulation of the expected substrate glycoforms of Skp1 [149]. Analysis of the *Dictyostelium gnt1*-KO revealed an O_2 threshold for culmination that was closer to that of wild-type than *phyA*-KO. Because of the considerable evidence that Gnt1 is specific for Skp1, this result indicated that the effect of PhyA was specific for Skp1. Additionally, prolyl hydroxylation alone partially rescues Skp1's function in culmination. Furthermore, a double KO

with *phyA* did not increase the O_2 threshold over that of the *phyA*-KO, supporting the conclusion that the two enzymes function in the same pathway. Thus the glycosylation independent role of PhyA suggests a specific role of Hyp-isoform of Skp1 in signaling. In addition, a morphological defect in the stalk was observed for *gnt1*-KO grown on bacterial plates. Initial studies suggested that *pgtA*-KO cells, which accumulate the Gn-glycoform, were similar to *phyA*-KO cells [149]. A more extensive series of replicates, however, showed that its culmination O_2-threshold was similar to the *gnt1*-KO [154], suggesting no additional role for the first sugar. The gmd-KO and *pgtA-Noe*/*pgtA*-KO strains, which accumulate the GGn-glycoforms, had a modestly higher O_2 threshold [149], suggesting an additional role for the second sugar residue.

AgtA, which catalyzes addition of the final two sugars to the pentasaccharide, makes an unexpectedly large contribution to the O_2 threshold for culmination. Its disruption led to an increase nearly as great as loss of PhyA itself, despite the accumulation of the trisaccharide form FGGn-Skp1 [144, 149]. Complementation by overexpressing either AgtA or its N-terminal catalytic domain restored the wild-type threshold. This was surprising because the catalytic domain alone was very inefficient in catalyzing addition of the second αGal. This presumably results from its overexpression but did show that that the β-propeller domain is not required for a wild-type O_2-threshold. AgtA has unexpected characteristics as revealed by KO and overexpression studies [163]. Overexpression of AgtA on a semi-constitutive promoter mostly rescued the wild-type O_2-threshold for culmination while overexpression of an enzyme-dead point mutant did not. However, the culminants formed at 21% O_2 exhibited defective terminal differentiation. The fruiting bodies had aberrant morphologies with prespore cells that failed to differentiate into spores supported by flaccid weak stalks. Interestingly, inhibition of Skp1 modification was observed, suggesting interference by binding Skp1. This was supported by SPR evidence that AgtA binds stably with

submicromolar affinity to both its substrate glycoform (FGGn-Skp1) and unmodified Skp1 with only a twofold higher affinity (unpublished data). Consistent with binding, AgtA interfered with prolyl hydroxylation *in vitro*. The Skp1-binding activity of AgtA is salt-sensitive relative to its catalytic activity, which was used to show that binding to Skp1 was the basis for preferential activity toward FGGn-Skp1 over the small molecule substrate mimic FG-pNP. All Skp1 isoforms except the AgtA's product (GGFGGn-Skp1) can activate AgtA to modify free disaccharides but only when the β-propeller is present. This indicates that Skp1 interacts with the β-propeller domain which in turn interacts with and activates the catalytic domain. This is supported by the finding that the β-propeller domain can function in trans to activate the catalytic domain toward modifying FGGn-Skp1. The FBP Fbs1 inhibited this *in vitro* activation of AgtA activity by Skp1 toward small molecules indicating AgtA and Fbs1 bind to a shared site [163]. In addition, a *gnt1*/*agtA*-DKO essentially blocked culmination at any O_2 level. This was surprising considering that the catalytic role of AgtA depends on prior action of PhyA and underscores the significance of the binding activity of the β-propeller domain of AgtA. Together, these data raise the possibility that AgtA serves a Skp1 sequestration role. AgtA is expected to buffer Skp1 availability in cells in addition to its role as a glycosyltransferase, an effect that is deleterious when Skp1 is not activated by glycosylation.

PhyA activity was also necessary for development under submerged conditions, which relies on 70-100% atmospheric O_2 [217]. In *phyA*-KO cells, the cyst-like aggregates formed a cortical shell of stalk cells similar to the wild-type phenotype. In contrast the internal cells, which expressed prespore cell markers, failed to differentiate as spores. Spore differentiation also failed to occur in the *gnt1*- and *pgtA*-KO strains, but the *agtA*-KO strain formed variable spores with an average similar to wild type cells. Thus, assembly of the trisaccharide glycoform of Skp1 was

required for spore differentiation, which is distinct from the requirement for culmination. In addition, overexpression of either Skp1A or Skp1B under either a prestalk or prespore cell promoter, but not the Skp1(P143A) mutant that is not hydroxylated, inhibited spore differentiation. These effects parallel the findings on culmination at the air-water interface and reinforce the role of PhyA toward Skp1. Overall, the comparison of these mutants between the two conditions indicates separate checkpoints for culmination and differentiation of prespore cells into spores. Whereas failure to induce culmination serves as a block to terminal stalk and spore differentiation, once the culmination checkpoint is satisfied, spore but not stalk cell differentiation requires satisfaction of an additional checkpoint more dependent than culmination on glycosylation to the trisaccharide glycoform.

Role of Skp1 Modification in *Toxoplasma*

O_2 sensing by *Toxoplasma* had received scant if any attention prior to the discovery of its homolog of PhyA and modification of its Skp1. *Toxoplasma* is an obligate intracellular parasite of most warm-blooded animals and cannot survive outside of a host cell except as an oocyst [236, 237]. Oocysts form following sexual reproduction within the intestines of the so-called definitive host – a cat. Upon ingestion from the environment by foraging mammals or birds, sporozoites are released in the intestine and differentiate into tachyzoites in preparation for cell invasion **(Fig 1.7B)**. Intracellularly, parasites reside and proliferate within a parasitophorous vacuoles formed by interiorization of the host plasma membrane followed by subsequent remodeling. Infection of gut-associated monocytes allows dissemination throughout the body before lysing out. By the time the host mounts a sufficient immune response, the parasite has typically accumulated in regions of the brain or skeletal muscle and differentiated into a nest of slow growing bradyzoites protected by a

cyst wall [236-238]. Humans can be infected through consumption of contaminated water or meat, receiving blood or organ donations from an infected individual, or passage from a pregnant mother to her fetus [236, 237]. Up to one third of the world's population is thought to be latently infected with *Toxoplasma* [239]. Toxoplasmosis poses a serious risk to development of an unborn fetus, and to immune compromised individuals. For example, reactivation of chronic toxoplasmosis, which may occur in HIV; cancer patients; or transplant recipients, can result in debilitating injury to the brain and eyes and even death.

The life cycle of the parasite likely exposes it to a wider variation in O_2 levels than for *Dictyostelium*. This can range from anoxia in the intestine to ambient (21%) in the environment, and from <1% in cells and tissues to higher levels in the vascular space [240]. In addition to metabolic effects, these variations may signal information about the parasite's cell and tissue location. A fibroblast infection model involves cycles of invasion, proliferation and egress where O_2 can be controlled. Under these conditions growth of the parasite is either not affected (type 1) or promoted (type 2) by 0.5% O_2 compared to 21% O_2 in the atmosphere over the media [32]. In contrast, the lytic cycle of *phyA*-KO strains of either type was highly compromised at 0.5% O_2, with a relatively modest effect at 21% (ambient) O_2 [147]. While intracellular proliferation per se is slowed by low O_2, it is not known if other steps such as entry and egress are also affected. Growth on fibroblasts could be rescued by complementation under PhyA's native promoter, but not when overexpressed [32], suggesting that tuning of PhyA expression, as observed in *Dictyostelium* [116, 143], is important. Thus, the *phyA*-KO did not phenocopy low O_2. A possible explanation is that *phyA*-KO is more severe than low (0.5%) O_2, where at most half of the steady state level of Skp1 is not hydroxylated. This may be a consequence of PhyA's K_m (O_2) being quite low (~1% O_2), suggesting that sensing by PhyA is tuned to a range of O_2 where regulation of Skp1

is important. Testing the effect of lower O_2 in cell culture is impractical owing to indirect effects on the fibroblasts. Therefore, a mouse infection model was employed to examine this possibility. When introduced into mice via gavage to mimic standard infection, *phyA*-KO parasites can form an intestinal infection but are compromised in their ability to disseminate to distal tissues [32]. This was associated with a large reduction in host lethality and morbidity corresponding to compromised virulence. Possibly the *phyA*-KO parasites do not exhibit their deficiency until they exit the anaerobic niche of the gut to aerobic settings where PhyA would be activated. A significant decrease in brain cyst formation kinetics and size was also observed indicating a role of PhyA in the establishment of latent *Toxoplasma* infections. The dissemination deficit was ameliorated in *IFNγ*-KO mice suggesting that PhyA protects from this form of innate immune control. Remarkably, *phyA*-KO parasite virulence is partially rescued by supplementation with tryptophan, an amino acid that is destroyed by IFNγ through induction of indoleamine deaminase (IDO); *phyA*-KO parasites are also partially rescued in an indoleamine dioxygenase-KO mouse [32]. It is intriguing to speculate that Skp1 hydroxylation influences an FBP that regulates tryptophan availability.

By analogy to *Dictyostelium*, the current model is that TgPhyA functions only via Skp1 and that in this capacity it has an O_2-sensing function. Knocking out *gnt1*, which relies on the action of PhyA to modify Skp1, replicates the growth defect of *Toxoplasma* in fibroblast monolayers [141]. In addition and as reviewed below, *phyA*-KO and *gnt1*-KO strains exhibit similar effects on the Skp1 interactome and the abundance of select FBPs. Since radiolabeling the target(s) of exogenous Gnt1 with [^{3}H]GlcNAc identifies only Skp1 in extracts, by extension these findings support the interpretation that PhyA is also specific for Skp1 in *Toxoplasma*. There is substantial evidence that PhyA is specific for Skp1 in *Dictyostelium*, where transgenic TgPhyA is

also functional [147]. In *P. ultimum*, it is plausible that the phenotype of *phyA*-KO parasites is stronger than the lowest tested O_2 because of its absolute blockade of Skp1 hydroxylation [3]. However, exclusion of other potential PhyA targets and direct testing of its role as a functional O_2-sensor are challenging for an obligate intracellular parasite in both cell culture and animals.

Toxoplasma and other apicomplexan genomes encode a related prolyl hydroxylase homolog, PhyB [147, 152]. Though the target of *Toxoplasma* PhyB is unknown, it exhibits a K_m for O_2 above ambient, which would be complementary to the very low value for TgPhyA (<1% O_2)[147, 152, 172]. This thus potentially expands the effective range of oxygen sensing [152] for this organism, which experiences a wider range of O_2 levels in its life cycle compared to *Dictyostelium*. PhyB protects the parasite from extracellular stress by controlling protein translation elongation [152].

BIOCHEMICAL AND STRUCTURAL CONSEQUENCES OF SKP1 MODIFICATION AND HYPOXIA

Dependence of Skp1 Modification on O_2

Examples of similar outcomes from disrupting PhyA and exposure to low O_2 suggest PhyA is a mediator of hypoxia response in cells. If so, then it is predicted that the degree of Skp1 modification would correlate with increased O_2. However, *Dictyostelium* slugs maintained at 5% O_2 to inhibit culmination appear to have the majority of their Skp1 glycosylated based on gel shift analysis by Western blotting [143]. Skp1 is a long-lived protein that appears to be synthesized at a constant rate [154], and thus steady state levels reflect both history and current exposure. To assess what occurs in slug cells at the time of the culmination checkpoint, epitope-tagged Skp1 (Skp1-myc) expression was ectopically driven using promoters specific for prestalk or prespore cells

[116]. Expression was induced in tipped aggregates prior to commitment to culminate. Skp1-myc overexpression in either cell type inhibited culmination (see above) and, notably, was only weakly modified [143, 217]. Furthermore, inhibition by Skp1-myc overexpression was suppressed by co-overexpression of PhyA. The findings suggest that it may be nascent synthesized Skp1 that is functional, because expression of Skp1-myc under a constitutive promoter, allowing time for its modification, did not inhibit culmination. In another assay, development was induced in non-shaking submerged cultures where terminal differentiation under these conditions requires hyperoxia in the atmosphere above the culture. Nonglycosylated Skp1 accumulated to about 40% of the total after 24 h at 5% O_2 [143, 217]. In comparison, fibroblasts infected with *Toxoplasma* tachyzoites incubated at 0.5% O_2 accumulated substantial levels of unmodified Skp1 after 2 d [205]. The extent of accumulated unmodified Skp1 was subject to variation [13] indicating a contribution from other factors. These might include the co-substrate αKG, or other carboxylic acids that can inhibit PhyA at physiological levels [139]. In a study of extracellular *Toxoplasma*, treatment at 1% O_2 led to accumulation of low levels of unmodified Skp1 based on Western blotting which were confirmed by quantitative mass spectrometry [13].

To seek kinetic evidence that Skp1 hydroxylation is posttranslational and is rate limited by O_2, growth stage (unicellular) *Dictyostelium pgtA*-KO cells, which terminate Skp1 glycosylation at the GlcNAc-glycoform, were examined. Cells were pulse labeled with 35S-Met/Cys and at various times were immunoprecipitated with antibodies specific for unmodified Skp1 or Gn-Skp1 [154]. Skp1 modification occurred nearly as rapidly, within the time resolution of the experiment, as protein synthesis at 10%, but lagged to increasing degrees at 7.5% and 5% O_2. It is to be expected that O_2 levels within slugs would be even lower than that experienced by single cells owing to metabolic consumption. Notably, there is no evidence that hydroxylation or glycosylation

are physiologically reversible. These data can be reconciled by a model in which events regulated by O_2 are mediated by nascent Skp1 produced contemporaneously to ensure timely monitoring of changing environments. Thus, nascent Skp1 would select from available, possibly co-expressed FBPs, according to prioritization that varies according to glycosylation status. In the context of the *Dictyostelium* culmination checkpoint, a simple model would be that an FBP engages an inhibitor of culmination; hydroxylation/glycosylation of nascent Skp1 preferentially selects this FBP therefore keeping cells in the slug state until sufficient O_2 at the soil surface is available.

Role of the ubiquitin proteasome system for O_2 regulation

To address whether O_2 regulates Skp1 via the UPS, *phyA*-KO *Dictyostelium* were employed as proxy for low O_2. Wild-type and *phyA*-KO *Dictyostelium* cells were developed in the presence of a panel of proteasome inhibitors. Using the minimal concentrations that could increase an accumulation of K48-linked polyubiquitin chains based on Western blotting, *phyA*-KO mutants were partially rescued for culmination and spore formation [14]. The concentrations used had minimal effects on wild-type culmination. This is the first experimental evidence that Skp1 modification and by analogy low O_2 functions via the UPS system, though it did not confirm a role for the SCF itself. In addition, it is reviewed below that inhibition of the proteasome in *Toxoplasma* partially reverses decreased abundance of FBXO13 and FBXO14 in *phyA*-KO cells. However, Skp1 has also been reported to have roles independent of the SCF complex in yeast and metazoan [97, 98]. Examples include roles in V1/V0 assembly on endosomes and lysosomes [241-243], autophagy and secretion [120], and synaptonemal complex assembly [244]. Nevertheless, it is to be noted that Skp1 may have conditional Cul1 interactions in some instances, and interacting

proteins classified as non-FBPs might have cryptic F-box domains. This idea is reinforced by the high frequency of degeneracy in F-Box domain sequences.

Skp1 Isoforms

In addition to post-translational modifications, Skp1 is also diversified in some protists in the form of multiple coding genes. Various protists in the stramenopile, cryptomonad (possibly related to algae), heteroloboseae (Discoba), and amoebozoan lineages have second Skp1 genes whose sequences are highly similar to the primary Skp1. Within the stramenopile lineage, a group of oomycetes replaced the target Pro with a Glu residue, rendering them inert to modification. If different Skp1s preferentially associate with different FBPs, as has been shown for animals and plants that have multiple Skp1s (but not PhyA) [109], then O_2-dependent regulation will be partitioned. In the related oomycete *Pythium ultimum*, the second Skp1 (PuSkp1B) retained the target Pro but is nevertheless not modified by its own PhyA *in vitro*, contrasting with its primary Skp1A [3]. Interestingly, PuSkp1B shares characteristic nearby sequence variations with the other oomycete non-modifiable Skp1B variants, suggesting that these substitutions might control recognition by PuPhyA/Gnt1 (Phgnt). This may be significant because some of these specific substitutions also occur in the second Skp1 sequences that occur in several amoebozoan species related to *Dictyostelium discoideum* **(Table 1.S3)**. Sequence comparisons indicate that the non-modifiable Skp1s are paralogs to the modifiable form. Modifiable Skp1 represents the main lineage, which also lost its target Pro in animals and higher plants. Thus, the modifiable Skp1 appears to be ancestral in eukaryotes, but this does not resolve whether unmodified or modified Skp1 should be considered the basal state for interpreting regulation. Genes of the modification pathway are so widely distributed across protist phyla **(Fig 1.3; Table 1.S1)** that potential for

modification may also be ancestral. More sequences across phylogeny will be required to rigorously assess this. However, parsimony suggests that unmodified Skp1 is the basal state and the modifications modulate its activity, evidently selectively toward FBPs, and possibly paralogs evolved to escape regulation. Possible outcomes include increased degradation of the FBP's substrates or autodegradation of the FBP in the SCF thereby protecting the substrate. In the case of TgFbxO13 and DdJcdI, evidence favors that these FBPs are the substrates themselves, and that their F-box domains represent conditional mechanisms to control their levels.

Skp1 interactions

Broadly speaking, Skp1 can be considered as a major interaction hub with FBPs, Cul1, itself as it homodimerizes, and others at least in certain organisms. Skp1 associates with Syp proteins in a synaptonemal complex in *C. elegans* [245]; the essential cochaperone Sgt1 involved in kinetochore assembly in yeast [246]; Cep3 in the CBF3 yeast kinetochore complex [247]; Siah-interacting protein (SIP) [248, 249]; the Snrk protein kinase in plants [250]; the vacuolar ATPase in yeast [243]; and recently with the V1-subunit of the vacuolar ATPase and Sec22B in human cells associated with in autophagy and secretion [120]. With Skp1's canonical function being linking FBPs to Cul1, it remains to be determined if the interactions beyond the SCF are relevant in protists. Given that FBPs are generally insoluble *in vitro* unless complexed with Skp1 [14, 139], non-Skp1 bound FbxwD and JcdI are expected be bound to chaperones [251-253] or other factors [95, 254, 255]. However, clear candidates did not emerge using a co-pulldown approach [130]. Sgt1, an Hsp90 co-chaperone that is found throughout eukaryotes, associates with Skp1 in a manner that is compatible with binding an FBP but not Cul1 [246]. This suggests that it might be an FBP-Skp1 assembly factor. Given evidence that Skp1 has a long half-life [154], an exchange

mechanism for FBPs is expected. Here we propose that exchange may occur at the FBP/Skp1 interface, in addition to exchange at the Skp1/Cul1 interface owing to the action of Cand1.

Skp1 complexes from different modification mutants were compared by size exclusion chromatography of cytosolic fractions from *Dictyostelium* [130]. Skp1 from wild-type cells at ambient O_2, where Skp1 is mostly glycosylated, eluted primarily as a single peak. In contrast, Skp1 from *phyA*-KO cells eluted primarily at a later position, corresponding to a minor peak for glycosylated Skp1. Skp1 from the modification mutants eluted as a combination of the two peaks, with increasing modification increasing representation in the earlier peak. Thus, each step of the pathway, including prolyl hydroxylation per se, contributed to increased complex formation according to this method. The composition of these complexes was examined by proteomics analyses of anti-Skp1 and anti-Cul1 pull-downs from the wild-type and mutant strains [13, 14, 130]. Distinct profiles of binding partners were found, providing direct evidence that glycosylation impacts Skp1 activity. The representation of CulE (Cul1 ortholog) and Rbx1, and the fraction of neddylated CulE, were not affected suggesting that global SCF activity might not be affected. Complete glycosylation increased the representation of about half of the putative FBPs in the Skp1 interactome, while not detectably reducing the representation of any [13, 14, 130]. For example, the abundant FBP FbxwD was 5-fold enriched in the interactome of fully glycosylated Skp1 relative to unmodified Skp1 [14, 130]; intermediate enrichment was observed for Skp1 in the trisaccharide form. Similarly, the FBP JcdI also had increased representation in the Skp1 interactome of wild-type cells, but the effect was obscured by reduced levels of JcdI. Notably, the effect on abundance was only observed in cells developed to the slug stage and not in growing cells, indicating developmental regulation. As summarized above, the effect of the glycan on Skp1 binding to FBPs might be direct. This was based on the finding that *Dictyostelium* Gn-Skp1 and

GGFGGn-Skp1 exhibited modestly preferential binding compared to unmodified Skp1 to the uniquely soluble mammalian Fbs1 [131], and effects on Skp1 structure [130]. However, a caveat was that Fbs1 interaction with Skp1 is not naturally influenced by Skp1 hydroxylation/glycosylation in animals. While these findings do not fully explain the different complex sizes from gel filtration, increased presence of proteasomes and CSN with CulE when Skp1 is glycosylated may also contribute [130].

The interactome of Skp1 in *Toxoplasma* is similarly influenced by Skp1 glycosylation. As for *Dictyostelium*, about half of the 14 detected FBPs were enriched in Skp1 pulldowns from wild-type compared to *phyA*-KO cells [13, 205]. In contrast, Cul1 and Rbx1 were not affected suggesting that incorporation of Skp1 into SCF complexes was not affected. Closer examination of three FBPs, after their genomic loci were epitope tagged, showed that Fbxo13 (homologous with DdJcdI) and Fbxo14 were enriched because their abundance was reduced in *phyA*-KO parasites. In contrast, the level of the non-enriched FBP FbxO1 was unaffected. Importantly, the abundance of FbxO13 and FbxO14 was selectively increased in the *phyA*-KO but not wild-type cells by treatment with proteasome inhibitors. Similar effects were observed for *gnt1*-KO parasites, demonstrating that glycosylation and not hydroxylation per se was involved. Thus, it is likely that either autoubiquitination was more active when complexed with unmodified Skp1, or that they were more susceptible to other Ub ligases when not associated with Skp1. These findings were physiologically relevant, because the effect of absence of PhyA was phenocopied by incubating extracellular parasites at low (0.5%) O_2 [13, 205]; the effects of absence of PhyA and low O_2 on FbxO13 and FbxO14 levels were not additive. Interestingly, the comparison between species revealed opposite effects on abundance of the homologs DdJcdI and TgFbxo13. This suggests that other factors interact with the PhyA-dependence of FBP fate, as already inferred from the

developmental dependence of DdJcdI levels [14]. The remarkably similar dependence of select FBPs on Skp1 glycosylation between highly unrelated species emphasizes the physiological significance of a role in O_2-signaling.

The high affinity of the *Toxoplasma* Skp1 homodimer suggests a mechanism by which O_2 or other factors that regulate PhyA and the glycosyltransferases could tune the range of interacting FBPs. The availability of only a single Skp1 to interact with the dozens of FBPs that each have a distinct F-box sequence strongly implies the existence of an FBP affinity hierarchy **(Fig 1.6D)**. This is, however, challenging to demonstrate directly owing to the intrinsic insolubility of FBPs in the absence of Skp1. Weaker affinity FBPs can be expected to see greater competition from a tight Skp1 homodimer until it is weakened by glycosylation, when weaker affinity FBP/Skp1 interactions will become competitive with higher affinity FBP/Skp1 interactions. Other non-SCF proteins may enter into this competition, as suggested by the example of AgtA in *Dictyostelium*, and CRM1, STYX and chaperones in mammals [95, 254, 255] and plants [253]. *Dictyostelium* Skp1 also homodimerizes, but its substantially weaker homodimer affinity of 2.4 μM [131, 166] appears less likely to influence the FBP binding hierarchy unless there exist FBPs that bind Skp1 with lower affinity.

Progress in addressing these mechanisms must await identification of targets for the substrate receptor class of FBPs, including those with protein-protein interaction domains like WD40-repeats and LRRs. Prediction by homology has been surprisingly challenging. The SCF complex was first discovered as a regulator of the cell cycles of yeast and cancer cells [256], but this homology has not yielded obvious homologs in *Dictyostelium* and *Toxoplasma*. Most FBPs observed or predicted in *Toxoplasma* do not appear to be conserved outside of the group of coccidian apicomplexans that also modify Skp1 [13]. In fact, several appear to have strictly

coevolved with the Skp1 glycosylation pathway. An interesting concept was recently presented that FBPs have evolved primarily to process environmental signals [125]. Relative to animals whose cells reside in protected multicellular environments, unicellular protists occupy a much wider range of niches. This is exemplified by *Dictyostelium* residing in the soil and *Toxoplasma* as an obligate intracellular parasite of warm-blooded animals. This concept offers an explanation for the high degree of diversification of FBPs in unicellular organisms.

Physiologically Relevant FBPs

FBPs that are affected by PhyA have significant roles in *Dictyostelium* and *Toxoplasma*. JcdI/FbxO13 was the first FBP posited to be conserved between these two organisms. JcdI/FbxO13 and the *Dictyostelium* paralog JcdH appear to be ancestral to human JmjD6 [14], except for the presence of an F-box domain in multiple protists and higher plants. Human JmjD6 acts in epigenetic regulation, RNA splicing, and oncogenesis [233-235]. FbxO13 appears to be essential in *Toxoplasma*, but the *jcdI*/*jcdH*-double KO is tolerated in *Dictyostelium* with no apparent effect under standard conditions. However, overexpression of JcdI exerts a modest reduction on the *Dictyostelium* O_2-checkpoint for culmination independent of its F-box domain, as summarized above. This anticipates a role in human O_2-sensing, and its F-box domain in protists might regulate its abundance.

FbxwA (ChtA or FbxA) is one of the best studied *Dictyostelium* FBPs that are regulated by Skp1 glycosylation. FbxwA was discovered independently in genetic screens for altered development and cheating. Cheating occurs when a strain preferentially populates the spore lineage in chimeras with WT cells exploiting the WT strain which contributes to the sterile stalk to support the cheating spores [257, 258]. Its disruption results in arrest of development or aberrant

culmination and hypersensitivity to ammonia, with varied effects depending on editing technique and the strain background. FbxwA starts influencing cell fate during the tipped mound stage [259] and is important for the differentiation of pre-stalk cells. Higher FbxwA levels promote stalk formation and lower levels promote spore formation [257, 258]. These effects allow *fbxwA*- mutant cells to be overrepresented in the spores of chimeric fruiting bodies, yet also compromise sporulation when grown alone, similar to known cheater mutants [260]. In a related vein, *phyA*-KO cells also display a weak cheater phenotype, as they preferentially occupy the spore lineage in chimeras with *phyA*+ cells. This was interpreted to mean that cells that sense O_2 to the greatest extent migrate to the tip to control culmination. This similar phenotype suggests that PhyA supports FbxwA activity which is consistent with increased representation of FbxwA in the Skp1 interactome of *phyA*+ cells [14, 130]. Intriguingly, FbxwA has been reported to associate with CulA rather than CulE, which is the major Skp1 interactor, raising the possibility of two Cul1 homologs [222, 259, 261]. FbxwA reportedly targets RegA for degradation in an ERK2 and CulA dependent fashion [222, 259, 261]. RegA (PDE2) is a cAMP phosphodiesterase that acts with a series of other proteins in the phospho-relay network to regulate cAMP levels, PKA activity, and Ca^{2+}-signaling [230]. RegA acts to promote sporulation and development, which can explain why FbxwA disruption triggers a cheater phenotype [222, 257-259, 261]. FbxwA also influences the velocity of individual motile cells [259] which may be related to RegA's role in regulating chemotaxis [230].

The association of *Dictyostelium* FbxwD with Skp1 is also highly enhanced when it is glycosylated [14, 130]. Its overexpression in wild type *Dictyostelium* delays culmination in an F-box dependent manner almost to the extent exerted by KO of *phyA* (at ambient O_2) [130]. Overexpression, however, exerts no further delay in *phyA*-KO cells suggesting that FbxwD's effect

depends on Skp1 modification [130]. Furthermore, FbxwD overexpression blocks terminal spore cell differentiation and disorganizes stalk morphology by a mechanism that depends on Vwa1 [262]. Vwa1 is an intracellular vault protein inter-alpha-trypsin (VIT) and von Willebrand factor-A (vWFA) domain containing protein that was prominent in the FbxwD interactome. Vwa1 is highly conserved in humans but has essentially unknown functions. It is unlikely that FbxwD targets Vwa1 for degradation but the dominant negative phenotypes of truncated protein expressions indicate a role in regulating SCF complexes. This parallels a recent finding in human cells. FbxwD is also highly expressed in growing *Dictyostelium* cells and may be essential based on current inability to disrupt its gene.

In addition to JcdI, another *Dictyostelium* FBP has been recently recognized, based on its ApaG domain, to be related to FbxO3 in mammals and SKIP16 in plants **(Fig 1.8)**. ApaG domains belong to the SUKH (for Syd, US22, Knr4 homology) domain superfamily that is found in other lineages of proteins as a protein/protein interaction domain including bacterial toxins [263]. FbxoN is expressed throughout growth and development, especially in prespore cells, and is enriched in the interactome of glycosylated Skp1 [14]. These homologs target multiple mammalian and plant proteins for degradation [39, 111], some of which are conserved and therefore are potential substrate candidates for FbxoN in *Dictyostelium* development and bacterial sensing.

The roles of almost all the 17 predicted FBPs of *Toxoplasma* are similarly unknown. About half of the 14 found in its Skp1 interactome have increased representation when Skp1 is glycosylated. Several of these are found only in related apicomplexans that have the potential to modify their Skp1 proteins based on genome analysis [13]. An example is FbxO14, a cytosolic protein whose level in cells is promoted several-fold by high O_2 and Skp1 modification, evidently by reduced proteasomal degradation. This coincidence implies a role that evolved explicitly for

O_2-sensing. Conversely, FbxO1 is found in other apicomplexans lacking modification genes including *Plasmodium* (malaria) [264]. FbxO1 is a critical component of the daughter cell scaffold involved in a specialized form of parasite cytokinesis [205]. FbxO1 levels are apparently not affected by Skp1 modification during routine cell culture. FbxO13, related to *Dictyostelium* JcdI as described above, is conserved across eukaryotic phylogeny, though only protist and plant versions have F-box domains. Anther *Toxoplasma* FBP, FBXL2, associates with a perinucleolar compartment and is involved with centrosome duplication, daughter cell formation and may act as a latent guardian of stage specific gene expression [265]. FBXL2 is also preferentially enriched in the interactome of wild-type Skp1 cells, though its dependence on O_2 has not been examined. Unlike other FBPs, FBXL2 appears to be stably associated with subunits of the COP9 signalosome, suggesting that it is held in an inactive SCF complex [266, 267].

SUMMARY

Correlating all the data suggests the following model. Optimal O_2 and metabolic conditions enhance the activity of select E3 SCF Ub ligases to degrade target substrates recognized by those FBPs. This occurs by regulating the FBP/Skp1 interaction thus marking those FBPs which are preferentially eligible to enter the SCF. This occurs in addition to regulation of the selection of FBP/Skp1 complexes that may be selected based on relative abundance and depending on neddylation and Cand1. It is anticipated that FBPs that are not regulated by these conditions will depend on a separate copy of Skp1. In addition the highest affinity FBP/Skp1 pairs will be less affected. Functional analysis suggests that DdFbxA is favored by high O_2, and Skp1 interactome analysis suggests that DdFbxD, TgFbxO13, and TgFbxO14 are also favored by high O_2. In contrast, some FBPs appear to be favored by low O_2, based on normalization of phenotypes using

proteasome inhibitors, which are expected to oppose the action of the SCF. The evolutionary relationship of protist PhyA with metazoan PHD2, would be consistent with the role of HIF1α and Skp1's unmodified state respectively. Both are expected to increase protein levels via increased transcriptional activity with HIF1α and reduced protein degradation for unmodified Skp1. However, the model is provisional until target substrates and additional FBPs are identified and tracked. The confinement of Skp1 glycosylation to organisms with a largely unicellular lifestyle correlates with apparent absence of a mechanism to reverse the modification. Interestingly, the prolyl hydroxylation of HIFα is also irreversible resulting in HIFα degradation and attendant change in the proteome. Given that Skp1 appears to have a relatively long half-life, it may be that reversal is mediated simply by dilution via proliferation. Additionally, newly synthesized Skp1 may be functional in response to O_2 and metabolic regulation for contemporaneous or even newly synthesized FBPs. Precedents allow for additional complexity. For example, FBPs that lack substrates per se, or contact Cul1 in tandem with Skp1, or even bind an alternative Cul1, might be differentially regulated. The opposite effects of Skp1 modification on these homologous proteins are reflective of the complexity of SCF regulation. FBPs might be autoubiquinated when bound to Skp1, influenced by the presence of substrate, other proteins, small molecule factors, or degraded by other pathways when unmoored from Skp1.

Post-translational modifications specific for Skp1 are believed to mediate the roles of PhyA and the five dependent glycosyltransferase activities. This inference is strongly supported by inverse effects of PhyA and Skp1 abundance in *Dictyostelium*, and molecular similarities of *phyA*- and *gnt1*-KO effects in *Toxoplasma*. Though there are different outcomes for KOs of different processing enzymes in *Dictyostelium* and *Toxoplasma*, these can be rationalized in terms of differential effects. These effects may have been significant during the past evolution of the

pathway that now involves six sequentially acting enzyme activities. Of interest are Skp1s from the algae *Chlamydomonas reinhardtii*, *Volvox carteri*, and the amoebozoan *Acanthamoeba castellanii*, whose genomes lack detectable homologs of PgtA, Glt1, Gat1 and AgtA. This makes them candidates for having a minimal glycan modification, or sources of new GTs or other modification enzymes. The pairing of adjacent pathway enzymes into the same protein, sometimes acting processively, supports the idea that the pentasaccharide has evolved and achieved a favorable role. It is assembled efficiently which is consistent with lack evidence for the accumulation of processing intermediates.

Current information indicates that the effects of Skp1 modification appear to be mediated by preferential selection of FBPs via a conformational mechanism rather than as a ligand for a lectin. Given the indirect nature of much of the evidence, further structural studies on glycosylated vs. unmodified Skp1 in complexes with FBPs, are warranted. Glycosylation also tunes the affinity of *Toxoplasma* Skp1 homodimerization which is expected to compete with FBP interactions. Other evidence supports roles for the terminal GTs AgtA and Gat1 in sequestering Skp1. The occurrence of competitive high-affinity interactions together with Skp1's likely FBP affinity hierarchy may result in a shift of Skp1's FBP binding repertoire between normoxic and hypoxic conditions [13, 14, 130]. The overlapping interaction sites on Skp1 do, however, make genetic confirmation of this role *in vivo* challenging.

The importance of O_2 as an environmental cue for positional information beyond its roles in metabolism per se is a largely unexplored vista for unicellular organisms. The Skp1 modification pathway offers a molecular mechanism for certain activities in *Dictyostelium* and *Toxoplasma*, but its importance for other O_2-dependent behaviors awaits further studies. Although a role for proteasomal degradation exists, possible roles for Skp1 in non-SCF functions also cannot be

excluded. At this point in time, these findings demonstrate the value of phylogenetic comparisons. Importantly, these findings also demonstrate the utility of *Dictyostelium* for biochemical studies that originated the discovery of this novel O_2-sensing pathway as a precedent for other protists and parasites.

FIGURE LEGENDS

Figure 1.1 SCF complex and regulation. The core of the SCF complex includes the F-box protein (FBP), Skp1, Cul1, and Rbx1. The Ub-charged E2 transfers Ub to a Lys residue on the substrate bound to the FBP and is serially replaced by Ub-E2 to reiteratively build a polyUb chain that targets the substrate to the 26S-proteasome. Major general regulatory steps (in blue) include 1) priming the substrate for recognition by the FBP, 2) expression of an FBP that can recognize the substrate, 3) activation of transfer by neddylation using the E3 subunit Dcn1, 4a) deneddylation by the COP9 signalosome (CSN), 4b) which enables binding of CAND1, 4c) which evicts the FBP/Skp1 subcomplex from Cul1, and 5) homodimerization of Skp1 which competes with FBP and Cul1 binding. Protist specific regulation (in red) includes O_2-triggered hydroxylation and glycosylation that 6a) inhibits homodimerization of Skp1 (in *Toxoplasma*) and 6b) modulates FBP/Skp1 interactions, and 7) sequestration of Skp1 by AgtA (in *Dictyostelium*) and possibly Gat1 (in *Toxoplasma*). Sugar symbols and enzymes of the Skp1 modification pathway are shown for both species.

Figure 1.2 Antibody specificity for Skp1 glycoforms. Synthetic glycopeptide conjugates were used to generate mouse monoclonal (mAb) or rabbit polyclonal (pAb) antibodies. These were then used to probe a panel of mutant cell extracts that accumulated the indicated glycoforms. Panels A, C-F are from [148]; panel B is from [268]. The epitope for UOK 104 for the trisaccharide

glycoform involves the peptide because UOK 104 does not recognize the trisaccharide conjugated to other aglycons [268].

Figure 1.3 Evolutionary tree of eukaryotic life annotated with Skp1 modification genes. Locations of *Dictyostelium*, *Toxoplasma*, and *Pythium* are indicated. Adapted from [206]. See **(Table 1.S1)** for a list of species and predicted modification genes. Four species where potential Skp1 modification genes occur, *Naegleria gruberi*, *Malawimonas californiana*, *Guillardia theta* (Cryptophyte), *Emiliania huxleyi* (haptophyte), lacked sufficient genomic information to be confidently placed.

Figure 1.4 Skp1 modification pathways. Enzyme proteins, substrates, domain diagrams including CAZy GT classifications, and evolutionary origins of the protein domains are represented for **(A)** *Dictyostelium discoideum*, **(B)** *Toxoplasma gondii*, and **(C)** examples from *Pythium ultimum* and *Bigelowiella natans*.

Figure 1.5 Skp1 domain diagram annotated for contacts with other proteins. Adapted from [134]. Although not shown, interaction with V1-subunits of the V-ATPase does not compete with FBPs [120].

Figure 1.6 A diagram depicting proposed regulation of Skp1 by glycosylation. (A) The disorder to order transition, which flows to two independent modes of regulation. **(B)** Alteration of direct contacts with the FBPs (conformation ensemble). **(C)** Disruption of the fuzzy interface leading to a weaker homodimer. **(D)** An FBP affinity hierarchy showing the predicted effect on selective FBP binding. Structures represented in the figure are (PDB: 6V88) for the Skp1 homodimer and (PDB: 2P1O) for the Skp1-FBP complex.

Figure 1.7 Protist life cycles illustrating O_2-dependences. (A) *Dictyostelium discoideum*. The dashed arrow indicates the O_2-dependent culmination transition. Adapted from [7]. **(B)** Stepwise

passage of orally acquired *Toxoplasma gondii* through a human to finally differentiate as chronic slow growing cysts in the brain. Modified from [267].

Figure 1.8 FBPs conserved among protists. (A) Domain maps and phylogenetic analysis of FbxN (FbxO3 and SKP16).

SUPPLEMENTAL FIGURE LEGENDS

Table 1.S1 Species with predicted Skp1 and Skp1 modification genes are classified according to phylogenetic groups. **(A)** Summary. **(B)** Sequence identifiers. **(C)** List of species. Supports **(Fig 1.6)**.

Table 1.S2 Summary of known experimentally induced Skp1 mutations and predicted effects.

Table 1.S3 Conservation of Skp1 CTR sequences in eukaryotes. Some listings are from [3]. The modified Pro residue is marked with an asterisk. Uncertain amino acids are replaced with a question mark. To facilitate visualization of relatedness, acidic residues are in blue, basic in dark red, Gly and Pro in red, and hydrophobic in green. Positions possessing a consensus chemical characteristic are highlighted, in yellow (hydrophobic), gray (acidic), dark grey (basic), or teal (small). The bold italicized Ser39 residue in DdSkp1A is replaced by Ala in DdSkp1B, but this substitution is not observed in other sequenced cellular slime molds.

Figure 1.1

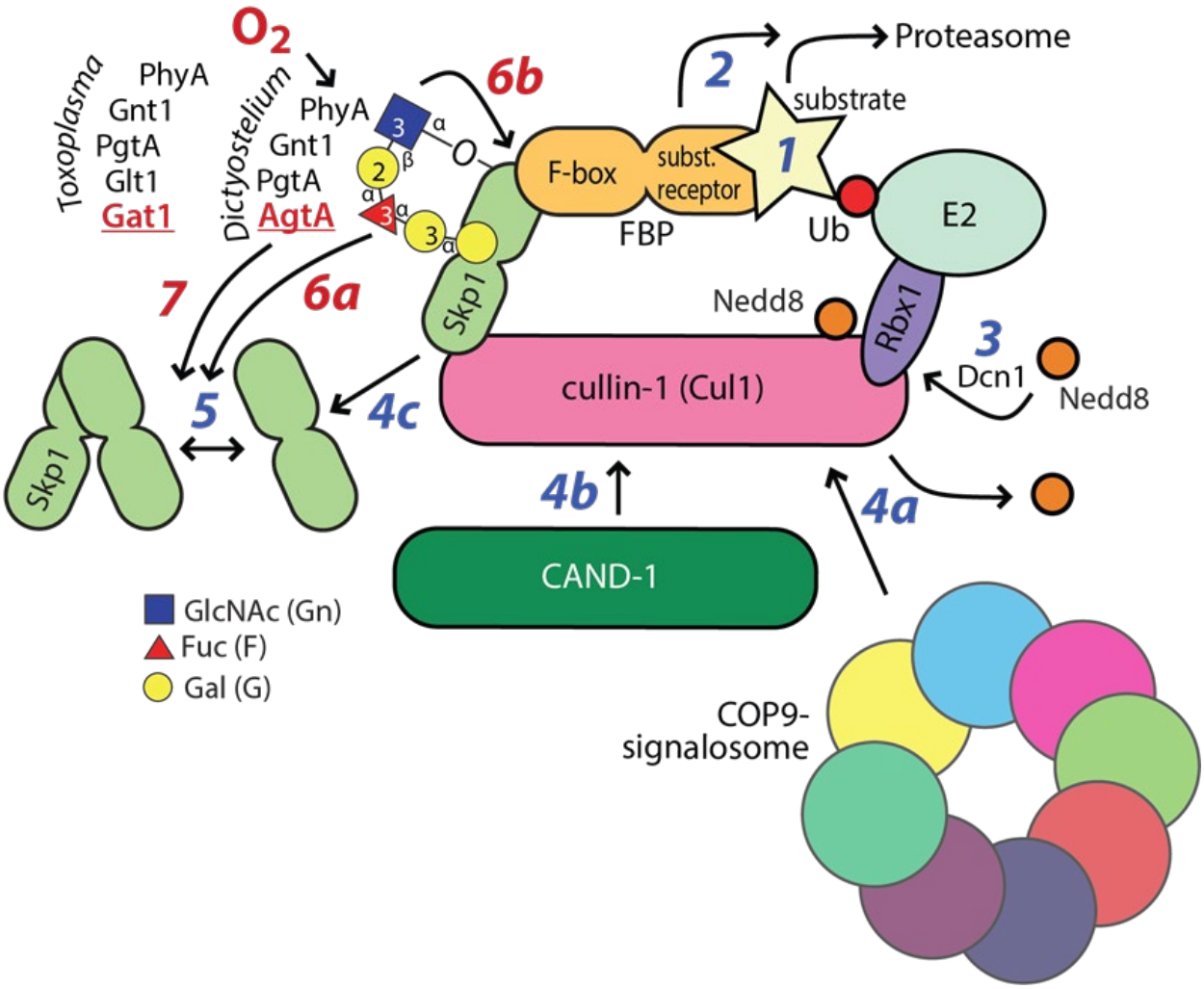

O2
Toxoplasma
PhyA
Gnt1
PgtA
Glt1
Gat1
Dictyostelium
PhyA
Gnt1
PgtA
AgtA
6b
2
Proteasome
substrate
1
F-box
subst. receptor
FBP
Ub
E2
Skp1
Nedd8
Rbx1
3
Dcn1
Nedd8
7
6a
5
4c
cullin-1 (Cul1)
Skp1
4b
4a
CAND-1
GlcNAc (Gn)
Fuc (F)
Gal (G)
COP9-
signalosome

Figure 1.2

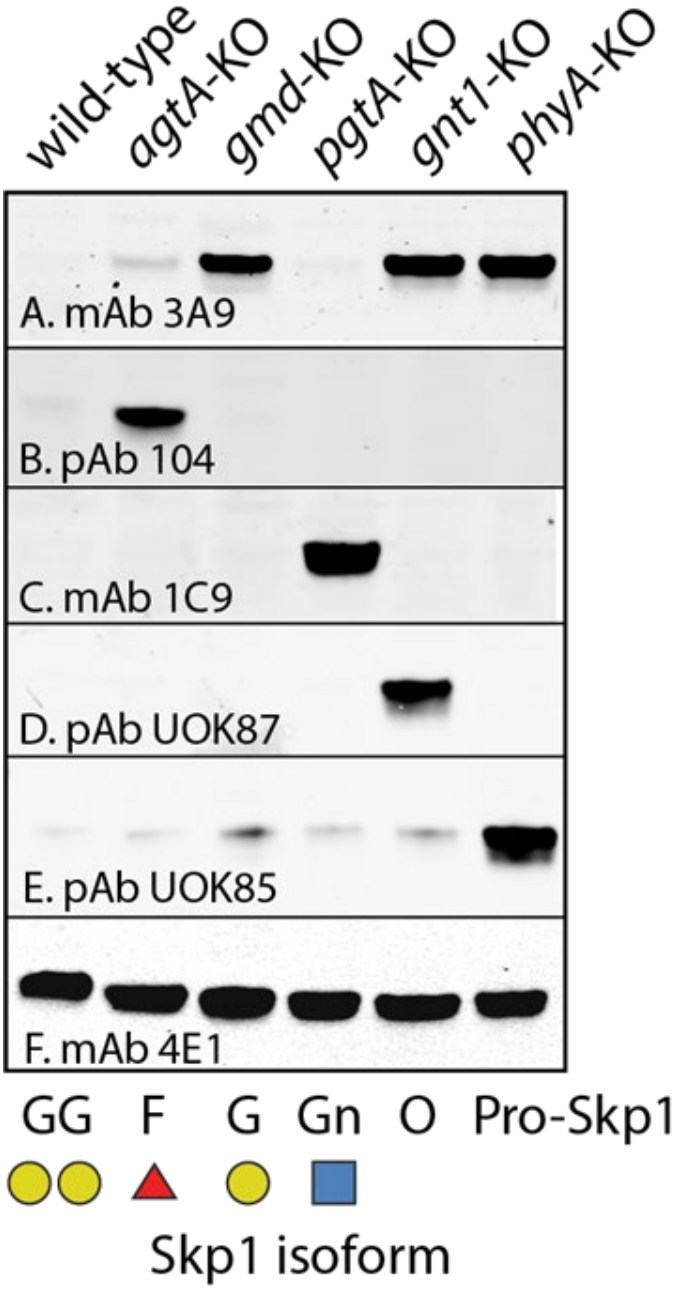

wild-type
agtA-KO
gmd-KO
pgtA-KO
gnt1-KO
phyA-KO
A. mAb 3A9
B. pAb 104
C. mAb 1C9
D. pAb UOK87
E. pAb UOK85
F. mAb 4E1
GG
F
G
Gn
O
Pro-Skp1
Skp1 isoform

Figure 1.3

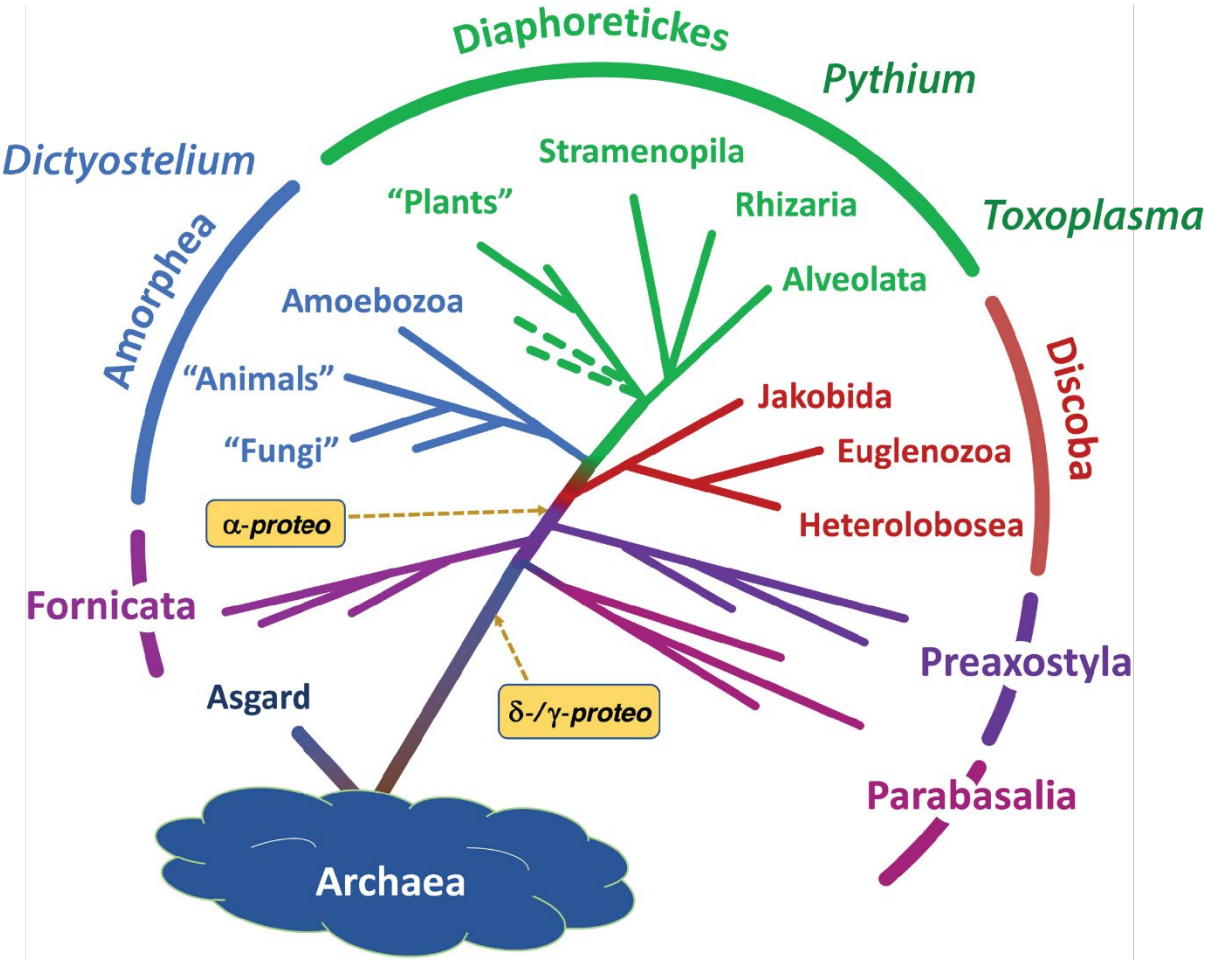

Diaphoretickes
Pythium
Dictyostelium
Stramenopila
"Plants"
Rhizaria
Toxoplasma
Amorphea
Alveolata
Amoebozoa
Discoba
"Animals"
Jakobida
"Fungi"
Euglenozoa
α-proteo
Heterolobosea
Fornicata
Preaxostyla
Asgard
δ-/γ-proteo
Parabasalia
Archaea

Figure 1.4

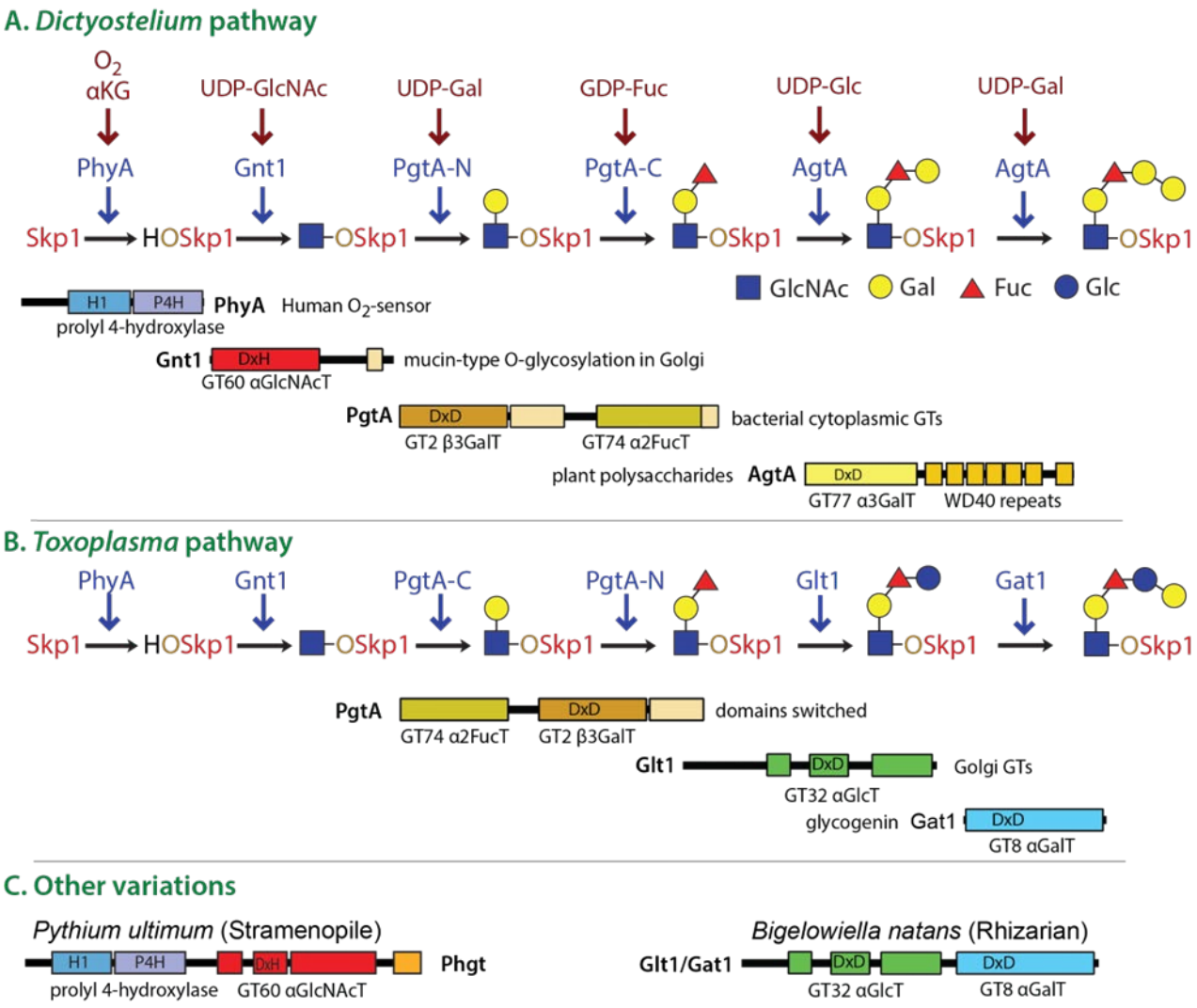

A. Dictyostelium pathway
O2
αKG
UDP-GlcNAc
UDP-Gal
GDP-Fuc
UDP-Glc
UDP-Gal
PhyA
Gnt1
PgtA-N
PgtA-C
AgtA
AgtA
Skp1
HOSkp1
OSkp1
GlcNAc
Gal
Fuc
Glc
H1
P4H
PhyA
Human O2-sensor
prolyl 4-hydroxylase
Gnt1
DxH
GT60 αGlcNAcT
mucin-type O-glycosylation in Golgi
PgtA
DxD
GT2 β3GalT
GT74 α2FucT
bacterial cytoplasmic GTs
plant polysaccharides
AgtA
DxD
GT77 α3GalT
WD40 repeats
B. Toxoplasma pathway
PhyA
Gnt1
PgtA-C
PgtA-N
Glt1
Gat1
Skp1
HOSkp1
OSkp1
PgtA
DxD
GT74 α2FucT
GT2 β3GalT
domains switched
Glt1
DxD
GT32 αGlcT
Golgi GTs
glycogenin
Gat1
DxD
GT8 αGalT
C. Other variations
Pythium ultimum (Stramenopile)
H1
P4H
DxH
Phgt
prolyl 4-hydroxylase
GT60 αGlcNAcT
Bigelowiella natans (Rhizarian)
Glt1/Gat1
DxD
DxD
GT32 αGlcT
GT8 αGalT

Figure 1.5

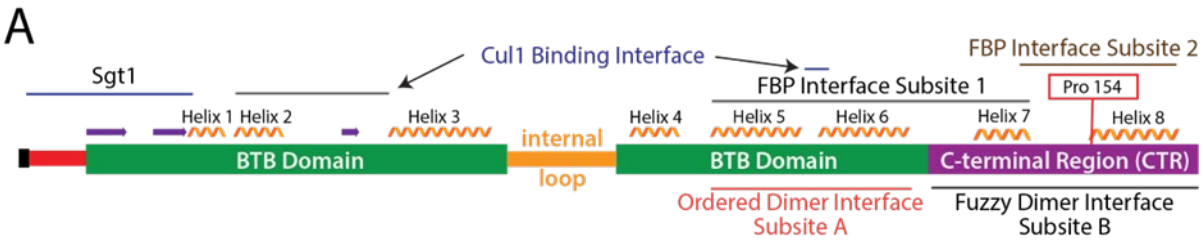

A
Sgt1
Cul1 Binding Interface
FBP Interface Subsite 2
FBP Interface Subsite 1
Pro 154
Helix 1
Helix 2
Helix 3
Helix 4
Helix 5
Helix 6
Helix 7
Helix 8
internal
loop
BTB Domain
BTB Domain
C-terminal Region (CTR)
Ordered Dimer Interface
Subsite A
Fuzzy Dimer Interface
Subsite B

Figure 1.6

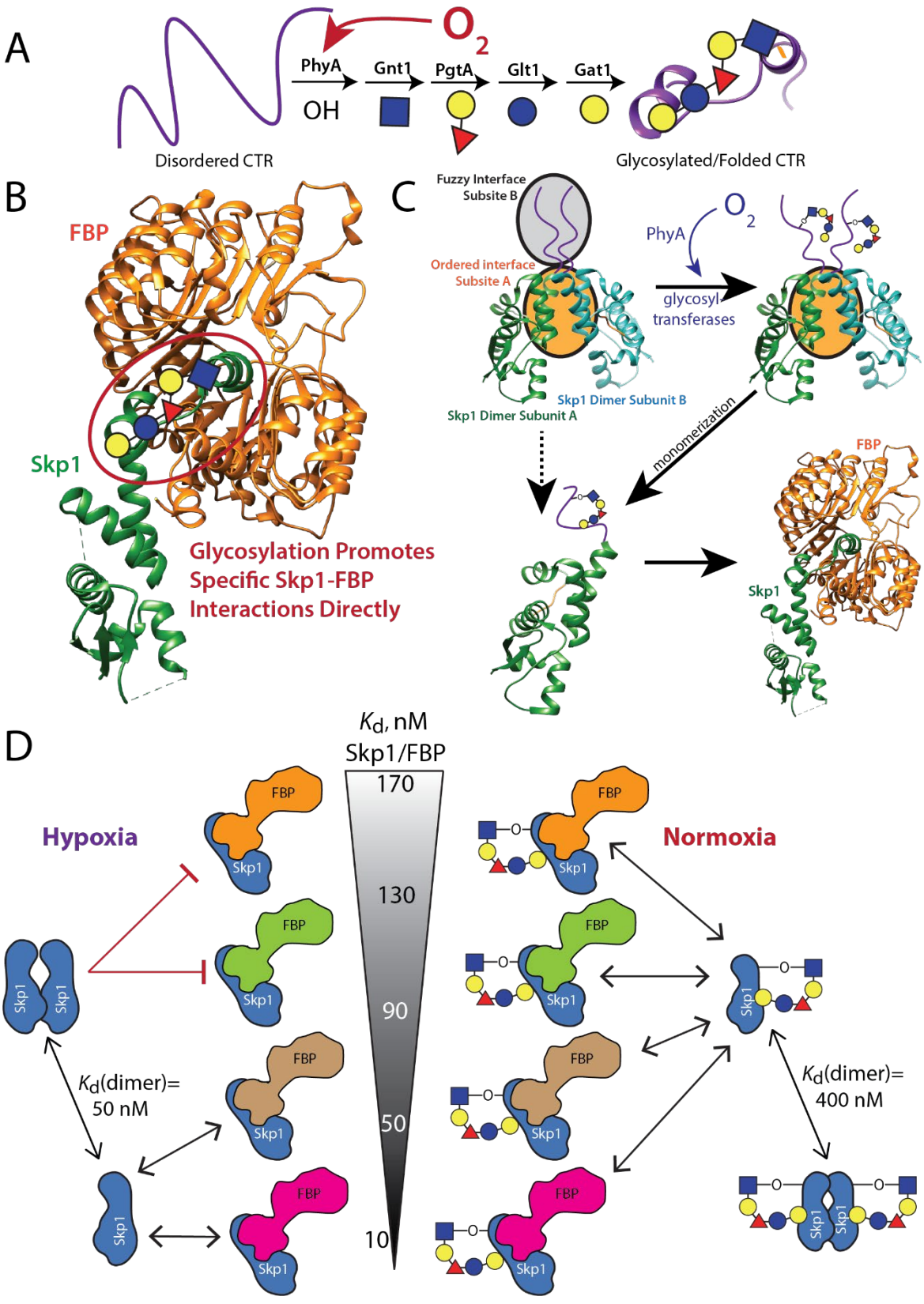

A
O2
PhyA
OH
Gnt1
PgtA
Glt1
Gat1
Disordered CTR
Glycosylated/Folded CTR
B
FBP
Skp1
Glycosylation Promotes
Specific Skp1-FBP
Interactions Directly
C
Fuzzy Interface
Subsite B
Ordered interface
Subsite A
PhyA
O2
glycosyl
transferases
Skp1 Dimer Subunit B
Skp1 Dimer Subunit A
monomerization
FBP
Skp1
D
Kd, nM
Skp1/FBP
170
130
90
50
10
Hypoxia
Normoxia
FBP
Skp1
Kd(dimer)=
50 nM
Kd(dimer)=
400 nM

Figure 1.7

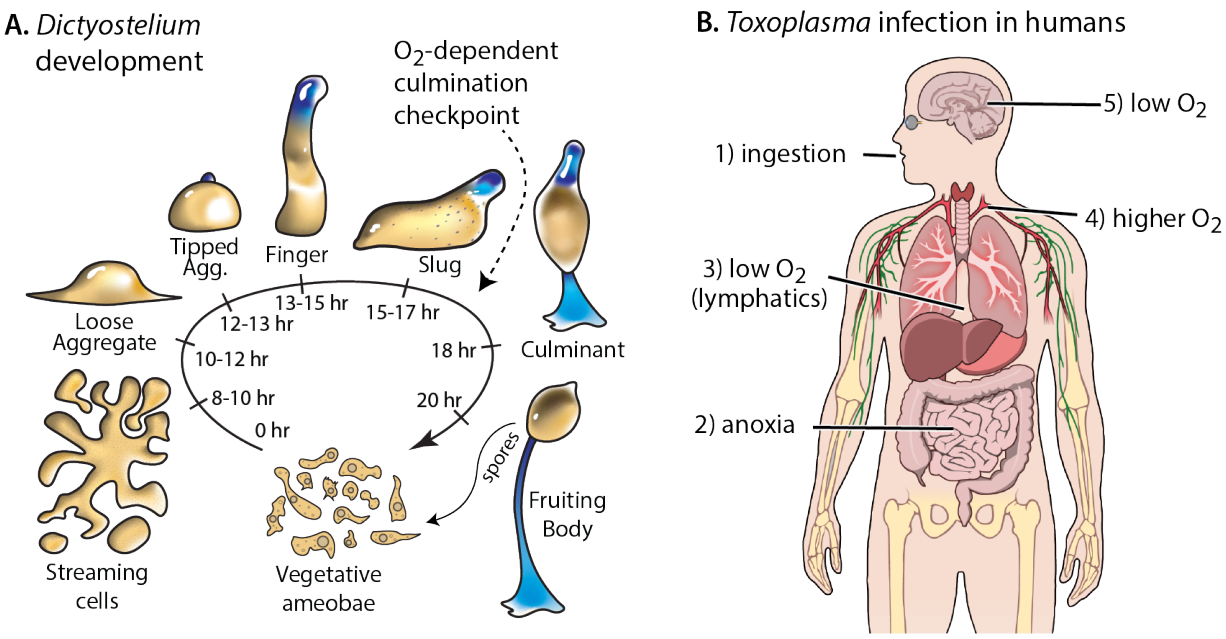

A. *Dictyostelium* development
O_2-dependent culmination checkpoint
Tipped Agg.
Finger
Slug
Loose Aggregate
12-13 hr
13-15 hr
15-17 hr
10-12 hr
18 hr
Culminant
8-10 hr
20 hr
0 hr
spores
Fruiting Body
Streaming cells
Vegetative ameobae
B. *Toxoplasma* infection in humans
1) ingestion
2) anoxia
3) low O_2 (lymphatics)
4) higher O_2
5) low O_2

Figure 1.8

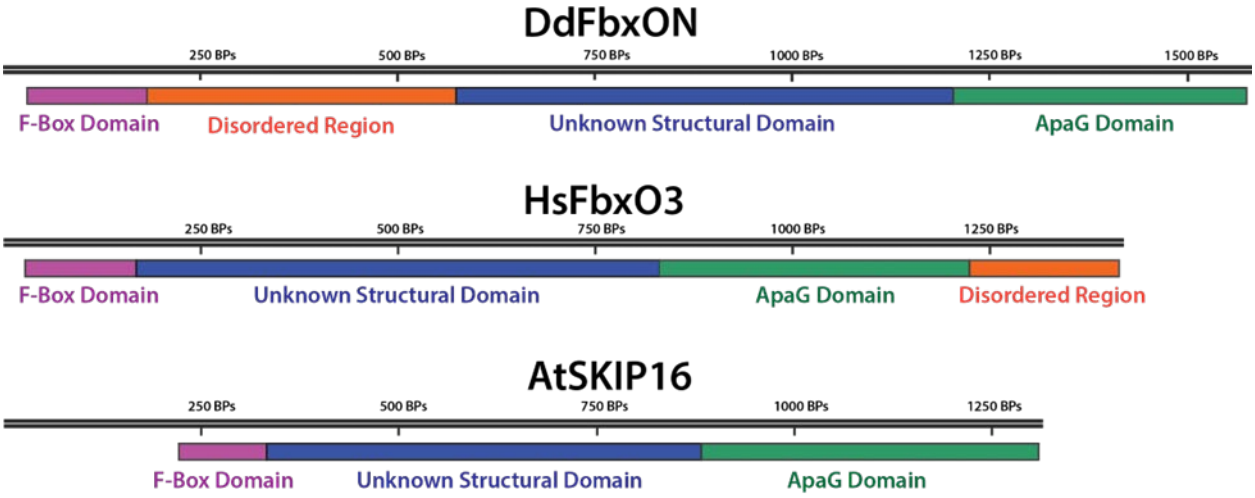

DdFbxON
250 BPs
500 BPs
750 BPs
1000 BPs
1250 BPs
1500 BPs
F-Box Domain
Disordered Region
Unknown Structural Domain
ApaG Domain
HsFbxO3
250 BPs
500 BPs
750 BPs
1000 BPs
1250 BPs
F-Box Domain
Unknown Structural Domain
ApaG Domain
Disordered Region
AtSKIP16
250 BPs
500 BPs
750 BPs
1000 BPs
1250 BPs
F-Box Domain
Unknown Structural Domain
ApaG Domain

Table 1.S1A

Kingdom	Phylum	organism	Skp1-Pro	P4H1 PhyA	Gnt1/GnT5 αGlcNAcT	FT85 = PgtA β3GalT	FT85 = PgtA α2FucT	aGalT1 = AgtA α3GalT	GT32a=glt1 αGlcT	GT8a=gat1 αGalT	phyB
Amorpheae	Amoebozoa	D. discoideum (cellular slime mold)	+(2)	+	+	+-------	-------+	+			
	Amoebozoa	D. purpureum (cellular slime mold)	+	+	+	+-------	-------+	+			
	Amoebozoa	D. fasciculatum (cellular slime mold)	++(2)	+	+	+-------	-------+	+			
	Amoebozoa	Polysphondylium pallidum (cellular slime mold)	++(2)	+	+	+-------	-------+	+			
	Amoebozoa	Acytostelium subglobosum (cellular slime mold)	++(2)	+	+	+-------	-------+	+			
	Amoebozoa	D. (aka Tieghemostelium) lacteum	+	+	+	+-------	-------+	+			
	Amoebozoa	Physarum polycephalum (acellular slime mold)	+	+	+	+-------	-------+	+			
	Amoebozoa	Acanthamoeba castellani (Neff)(soil protozoa)	+	+	+						
	Amoebozoa	Balamuthia mandrillaris (free living amoeba -> encephaliti	+	+	+						
	Fungi-Chytrids	Spizellomyces punctatus DAOM BR117 (zoospore-produ	+(2)	+-------	-------+						
	Fungi-Chytrids	Rhizoclosmatium globosum	+(3)	+-------	-------+						
	Fungi-Chytrids	Gonapodya proliferia	+(2)	+-------	-------+						
Rhizaria	Foraminifera	Reticulomyxa filosa (fresh water foraminifera)	+(4)	+	+	+	+		+-------	-------+	
	Cercozoa	Spongospora subterranea	+(3)	+	+		+			+	
	Cercozoa	Plasmodiophora brassicae (causes cabbage clubroot)	+(2)	+	+	+	+		+-------	-------+	
	Cercozoa	Bigelowiella natans CCMP2755 (chlorarachnea)	(?more	+	+	+	+		+-------	-------+	
Alveolates	Apicomplexa	Toxoplasma gondii (apicomplexan)	+(2)	+	+	+-------	-------+R		+	+	+
	Apicomplexa	Hammondia hammondi (apicomplexan)		+	+	+-------	-------+R		+	+	+
these are in	Apicomplexa	Neospora caninum (apicomplexan)	+	+	+	+-------	-------+R		+	+	+
superphylum	Apicomplexa	Sarcocystis neurona (apicomplexan)	+	+	+	+-------	-------+R		+	+	+
Alveolata	Chromerida	Vitrella brassicaformis (Vitrelliceae)	+	+	+	+-------	-------+R		+	+	+
	Chromerida	Chromera velia (Chromeraceae)	+	+	+	+-------	-------+R		+	+	+
	Ciliophora	Tetrahymena thermophila (ciliate)	+	?	+	+(?)	+(?)				+
	Ciliophora	Stylonychia lemnae (ciliate)	+	+-------	-------+	+-------	-------+R		+	+	+
	Ciliophora	Oxytricha trifallax (ciliate)	+	+-------	-------+	+-------	-------+R		+	+	
	Dinoflagellate	Karlodinium micrum (dinoflagellate)	+	+	+						
	Dinoflagellata	Karenia brevis (marine unicellar dinoflagellate; red tide)	+	+	+	+-------	-------+R			+	
	Dinoflagellata	Symbiodinium microadriaticum (dinoflagellate)	+(2)	+-------	-------+	+-------	-------+R		+	+	+
Stramenopiles	Heterokontophyta	Albugo laibachii (oomycete)	+	+-------	-------+	+-------	-------+R		+	+	
	Heterokontophyta	Pythium ultimum (oomycete)	+	+-------	-------+	+-------	-------+R		+	+	
	Heterokontophyta	Aphanomyces invadans (oomycete)	+(2)	+-------	-------+	+-------	-------+R				
	Heterokontophyta	Aphanomyces euteiches, strain: 109 (oomycete)	+(2)	+-------	-------+	+-------	-------+R		+	+	
	Heterokontophyta	Aphanomyces stellatus; strain: 57867 (oomycete)	+(2)	+-------	-------+	+-------	-------+R		+	+	
	Heterokontophyta	Saprolegnia parasitica (fish pathogen)	+	+-------	-------+						
	Heterokontophyta	Phytophtera infestans (oomycete)	+	+-------	-------+						
	Heterokontophyta	P. ramorum (oomycete)	+	+-------	-------+						
	Heterokontophyta	P. sojae (oomycete)	+	+-------	-------+						
	Heterokontophyta	Phaeodactylum tricornutum (marine pennate diatom)	+	+(2)	+						
	Heterokontophyta	Fragilariopsis cylindrus (coldwater diatom)	+	+-------	-------+						
	Heterokontophyta	Thalassiosira pseudonana (diatom)	+	+-------	-------+	+-------	-------+R		+	+	
	Heterokontophyta	Nannochloropsis gaditana (marine microalga)	+	+-------	-------+	+-------	-------+R		+	+	
	Heterokontophyta	Aureococcus anophagefferens (non-motile pelagophyte)	+		+	+-------	-------+R		+	+	
	Heterokontophyta	Ectocarpus siliculosis (brown alga)	+(2)	+-------	-------+	+-------	-------+R		+	+	
Cryptista	Cryptophyta	Guillardia theta CCMP 2712 (cryptophyte)	+	+-------	-------+	+-------	-------+R		+	+	
Haptista	Haptophyta	Emiliania huxleyi (marine haptophyte alga)	+	+-------	-------+				+		
Plantae	Charophyta	Klebsormidium nitens (green alga)	+	+-------	-------+						
	Chlorophyta	Chlamydomonas reinhardtii (chlorophyte alga)	+	+	+						
	Chlorophyta	Volvox carteri (chlorophyte alga)	+	+-------	-------+						
	Chlorophyta	Coccomyxa subellipsoidea (chlorophyte alga)	+	+-------	-------+						
	Chlorophyta	Chlorella variabilis (chlorophyte single-cell green alga)	+	+-------	-------+						
Excavates	Loukozoa	Malawimonas californiana	+	+	+						
	Percolozoa	Naegleria gruberi (amoebe flagellate, heterolobosea)	+	+-------	-------+						
Bacteria	Cyanobacteria	Trichodesmium erythraeum IMS101 (marine cyanobacterium)		+	+						
	Protobacteria	Desulvofibrio desulfuricans				+-------	-------+R				
	Firmicutes	Pelosinus sp UFO1 (Firmicutes)				+-------	-------+R				

Table 1.S1B

2023: searched also for Fuctase orthologs/2024: searched for GT8a NCBI pblast (nr database) & tblastn (wgs)
remarks 2023

* I called somewhat different ORF
* N-terminus missing, I have added
* N-terminus missing, I have added
* extracted from wgs, ** extracted from TSA database; GnT1, pgtA unsure if completely C-term, but prolly so as they come form TSA database
* extracted from WGS, contig 2961/** with exon 3 extended
* extracted from WGS (scaffold info in Balamuthia doc)
*phyA & gnt1 from esfs; some issues as of 6/'23, but fit well enough to be sure

Has a protein of 757 aa length that could also be a Skp1 (GAQ91373.1), with wrongly called introns or something. See also coccomyxa
There is also a "stand-alone phyA-ortholog: XP_042917449.1
* extracted from WGS, contig 5345
+ 2 more put Skp1's, both w/o proper P and quite bit longer: see also klebsormidium, phyA-gnt1: 1 unresolved intron/exon, but link between domains is there; could not resolve as of 4/'17
extracted from wgs: 1 unresolved intron/exon, but link between domains is there; could not resolve as of 4/'17
* extracted from wgs. Not a great overlap between wgs contigs, but it will do, as end of GT8a is on 2nd contig, GT32a C-term, GT8a N-term
* extracted from wgs. GT32a & GT8a both partials, but clear enough (8/'21).

* extracted from wgs.
ID's are for ME49 strain
* extracted from wgs.
* extracted from wgs.
Skp1, gnt1, pgtA: from VeuPath, * extracted from wgs ; pgtA: start and end on 1 supercontig (240627)

All thru VeuPath; GT8a has indicative C-term missing, so is unsure
? maybe all except Skp1 are further removed homologues. phyA not very good fit = phyB; gnt1: N-term unknown
* extracted from wgs. pgtA has 1 stopcodon in middle, that prolly/hopefully is seq error, as it is after the start of the GalTase domain
* extracted from wgs.
** from TSA database
* extracted from ESTs, **from TSA database

*C-term adjusted from genomic DNA
Decided to go with P.insidiosum (proteins found in pblast NCBI), as P.ultimum website is defunct, and it would take a lot of time to re-extract the seq from wgs from NCBI
No homologs found to GT32/GT32a, did find a GT8, but no GT8a.
* Not the best fit, but it has a proper GT8a.
* extracted from wgs. (KAF0698402.1 is same, but without very N-terminus and a different C-terminus)

* extracted from wgs.
* extracted from wgs.
2 options for phyA; no proper GnT1, unless there is alternative splicing of GnT2

* extracted from wgs.
* extracted from wgs/pgtA: some intron boundaries/loops unclear, also very C-terminus not clear
* extracted from wgs.
**N-terminus extended using wgs/* extracted from wgs
* extracted from wgs. *protein adjusted with genomic reads (from DOE for pgtA); pgtA partial, but connection between domains is there
*protein adjusted with genomic reads, * C-term is not as nice of a fit

Table S1B. Homologs of Skp1-glycosylation pathway enzymes

nd: none detected

240630

			Skp1-	P4H1	Gnt1/GnT51	FT85 = PgtA		aGalT1 = AgtA	(alternatives to AgtA) GT32a=glt1	GT8a=gat1		FbxO14 =
Kingdom	Phylum	organism	Pro	PhyA	αGlcNAcT	β3GalT	α2FucT	α3GalT	αGlcT	αGalT	phyB	TG_259880
Fungi	Chytridiomycota	Spizellomyces punctatus DAOM BR117 (zoospore-producing)	XP_016604299.1,XP_016609129.1	XP_016610870.1 (bifunctional)		nd	nd	nd	nd	nd		
	Chytridiomycota	Rhizodiosmalium globosum	ORY28377.1,ORY52288.1,ORY52280.1	ORY35251.1 (bifunctional)		nd	nd	nd	nd	nd		
	Chytridiomycota	Gonapodya prolifera	KXS21154.1,KXS18235.1	KXS09834.1 (bifunctional)		??	nd	nd	nd	nd		
Amoebozoa	cellular slime mold	Dictyostelium discoideum	DDB0191107,DDB0185043	DDB0231040	DDB0185044	DDB0191458 (bifunctional)		DDB0231341				
	cellular slime mold	D. purpureum	DPU1257391	DPU1267604	DPU1261149	DPU1266552 (bifunctional)		DPU1262408				
	cellular slime mold	D. fasciculatum	DFA1505560,DFA1594634	DFA1456752	DFA1493146	DFA1499020 (bifunctional)		DFA1492576				
	cellular slime mold	Polysphondylium pallidum (aka Heterostelium pallidum/album)	PPA1402736,PPA1286992	PPA1365136*	PPA1321980*	PPA1386612 (bifunctional)*		PPA1349878				
	cellular slime mold	Acytostelium subglobosum	XP_012748241.1,XP_012749257.1	XP_012757501.1	XP_012750718.1*	XP_012750285.1 (bifunctional)		XP_012748414.1				
	cellular slime mold	D. (aka Tieghemostelium) lacteum	KYR02280.1	KYQ98259.1	KYQ99959.1*	KYQ89972.1 (bifunctional)		KYQ88315.1				
	acellular sl. mold	Physarum polycephalum	AAL11454.1	ATCM03002566.1*	GDRG01004598.1**	GDRG01004420.1**		GDRG01004116.1**				
	amoebae	Acanthamoeba castellani (Neff)(soil protozoa)	XP_004339218.1	AHJI01002961.1*	XP_004356729.1 **		nd	nd				
	amoebae	Balamuthia mandrillaris (free living amoeba -> encephalitis)	LEOU01000239.1*	LFUI01000229.1*	LFUI01000547.1*	nd	nd	nd	nd	nd		
Excavates	Loukozoa	Malawimonas californiana	EC714007.1	EC716818.1*	EC715818.1*	nd	nd	nd	nd	nd		
	Percolozoa	Naegleria gruberi (amoebe flagellate, heterolobosea)	XP_002681295.1	ACER01000229.1 (bifunctional)		nd	nd	nd	nd	nd		
Plantae	Charophyta	Klebsormidium nitens (green alga)	GAQ80479.1	GAQ88896.1 (bifunctional)		??	nd	nd	nd	nd		
	Chlorophyta	Chlamydomonas reinhardtii (chlorophyte alga)	XP_001690964.1	XP_001702411.2 (bifunctional)		nd	nd	nd	nd	nd		
	Chlorophyta	Volvox carteri (chlorophyte alga)	XP_002947872.1	ACJH01005345.1 (bifunctional)*		nd	nd	nd	nd	nd		
	Chlorophyta	Coccomyxa subellipsoidea (chlorophyte alga)	XP_005651580.1	AGSI01000003.1		nd	nd	nd	nd	nd		
	Chlorophyta	Chlorella variabilis (chlorophyte single-cell green alga)	XP_005846142.1	ADIC01000277.1		??	nd	nd	nd	nd		
Rhizaria	Foraminifera	Reticulomyxa filosa (fresh water foraminifera)	ETO34511.1,ETO23456.1,ETO17530.1,ETO11964.1	ETO05471.1	ETO29121.1	ETO08666.1	ETO17543.1	nd	ASPP01009871.1+ASPP01005160.1*			
	Cercozoa	Spongospora subterranea	CRZ02950.1,CRZ08889.1,CRZ09429.1	OUQQ01000793.1*	OUQQ01000184.1*	OUQQ01000108.1*	OUQQ01000139.1*	nd	OUQQ01001375.1*	HACM01001251.1		
	Cercozoa	Plasmodiophora brassicae (causes cabbage clubroot)	CEP00175.1,CEO99655.1	CEO96924.1	CEO94842.1	SPQ97379.1	CEO98151.1	nd	SPQ93306.1 (bifunctional)			
	Cercozoa	Bigelowiella natans CCMP2755 (chlorarachnea)	ADNK01001322.1*	ADNK01000180.1*	ADNK01000108.1*	ADNK01000565.1*	ADNK01001148.1*	nd	ADNK01003061.1(bifunctional)*			
Alveolates	Apicomplexa	Toxoplasma gondii (apicomplexan)	XP_002369572.1	XP_002368155.1	XP_002364766.2	XP_018637080.1 (bifunctional) - R		nd	XP_018637293.1	XP_002364286.1	+	+
	Apicomplexa	Hammondia hammondi (apicomplexan)	AHJH01000967.1*	AHJH01000706.1*	AHJH01000342.1*	KEP66272.1 (bifunctional) - R		nd	KEP61959.1	AVCM01001470.1*	+	+
	Apicomplexa	Neospora caninum (apicomplexan)	XP_003879810.1	CEL67481.1	JADKZA010000043.1*	JACVML010000001.1 (bifunctional) - R*		nd	CEL66241.1	XP_003885051.1	+	+
	Apicomplexa	Sarcocystis neurona (apicomplexan)	SN3_00102155	JAQE01001214.1*	SN3_00900395	sneu_scaffold00020 (bifunctional) - R*		nd	JXWP01000004.1*	JAQE01001190.1*	+	+
	Chromerida	Vitrella brassicaformis (Vitrellaceae)	CEL99351.1	CEM16584.1	CEM00894.1	CEM00580.1 (bifunctional) - R		nd	CEM02366.1	CEM34485.1	+	
	Chromerida	Chromera velia (Chromeraceae)	Cvel_17723	Cvel_22358	Cvel_16021	Cvel_18515 (bifunctional) - R		nd	Cvel_11229	Cvel_31587??	+	
	Ciliophora	Tetrahymena thermophila (ciliate)	XP_001013810.2	?	+	+(?)	+(?)	nd		nd	+	
	Ciliophora	Stylonychia lemnae (ciliate)	CDW87582.1	CCKQ01016964.1 (bifunctional)*		CCKQ01009789.1 (bifunctional) - R*		nd	CDW75669.1	CCKQ01014997.1*	+	
	Ciliophora	Oxytricha trifallax (ciliate)	AMCR02032073.1,AMCR02017929.1*	LAEC01012911.1 (bifunctional)*		AMCR02015522.1 (bifunctional) - R*		nd	AMCR02028276.1*	AMCR02016175.1		
	Dinoflagellate	Karlodinium micrum (dinoflagellate)	ABV22203.1	HBOS01011433.1**	HBOS01025108.1**	GJRA01007463.1 (bifunctional) - R**		nd	HBOS01125818.1**	HBOS01128907.1**		
	Dinoflagellata	Karenia brevis (marine unicellar dinoflagellate; red tide)	EX970823.1*	GFLM01038132.1 (bifunctional)** - R		GFLM01013876.1 (bifunctional) - R**		nd	GFLM01080036.1**	GFLM01076699.1**		
	Dinoflagellata	Symbiodinium microadriaticum (dinoflagellate)	OLP99484.1	OLP91867.1 (bifunctional)		OLP77946.1 (bifunctional) - R		nd	OLP91655.1	OLP95499.1	+	
Stramenopiles	Heterokontophyta	Albugo laibachii (oomycete)	CCA15417.1	CCA15104.1 (bifunctional)		CCA24176.1 (bifunctional) - R		nd	CCA15666.1*	CCA19642.1		
	Heterokontophyta	Pythium insidiosum (oomycete)	KAJ0410454.1,GLD99094.1	GLD93938.1 (bifunctional)		GLE00696.1 (bifunctional) - R		nd	GLD93303.1	GLD96843.1		
	Heterokontophyta	Aphanomyces invadans (oomycete)	XP_008862889.1,XP_008863352.1	XP_008861890.1 (bifunctional)		XP_008876626.1 (bifunctional) - R		nd	nd	nd		
	Heterokontophyta	Aphanomyces euteiches, strain 109 (oomycete)	KAF0742109.1,KAI9129911.1	KAI9117365.1 (bifunctional)		KAI9100369.1 (bifunctional) - R		nd	KAI9115719.1*	KAI9126279.1		
	Heterokontophyta	Aphanomyces stellatus, strain 57867 (oomycete)	KAF0711835.1,KAF0687148.1	KAF0697729.1 (bifunctional)		KAF0693435.1 (bifunctional) - R		nd	VJMH01005242.1*	KAF0701185.1		
	Heterokontophyta	Saprolegnia parasitica (fish pathogen)	XP_012199320.1	XP_012205068.1 (bifunctional)		nd	nd	nd	nd	nd		
	Heterokontophyta	Phytophtora infestans (oomycete)	XP_002907933.1	KAI9989760.1 (bifunctional)		nd	nd	nd	nd	nd		
	Heterokontophyta	P. ramorum (oomycete)	KAH7484375.1	RYEP01000711.1 (bifunctional)*		nd	nd	nd	nd	nd		
	Heterokontophyta	P. sojae (oomycete)	XP_009526241.1	JAQQXX010000003.1 (bifunctional)*		nd	nd	nd	nd	nd		
	Heterokontophyta	Phaeodactylum tricornutum (marine pennate diatom)	XP_002176583.1	002179961.1,XP_002185943.1		nd	nd	nd	??	nd		
	Heterokontophyta	Fragilariopsis cylindrus (coldwater diatom)	OEU09899.1	OEU17087.1 (bifunctional)		nd	nd	nd	nd	nd		
	Heterokontophyta	Thalassiosira pseudonana (diatom)	XP_002294707.1,XP_002294049.1	XP_002289778.1 (bifunctional)		XP_002289426.1 (bifunctional) - R		nd	AAFD02000025.1*	XP_002291959.1		
	Heterokontophyta	Nannochloropsis gaditana (marine microalga)	AFGN01000656.1*	PEIC01000030.1 (bifunctional)*		PEIC01000025.1 (bifunctional) - R*		nd	AZIL01000121.1*	EWM28655.1		
	Heterokontophyta	Aureococcus anophagefferens (non-motile pelagophyte)	XP_009033202.1	ACJI01001205.1 (bifunctional)*		ACJI01000013.1 (bifunctional) - R*		nd	ACJI01001297.1*	KAH8059780.1		
	Heterokontophyta	Ectocarpus siliculosus (brown alga, Phaeophyceae)	CBJ48672.1,CBJ48849.1	CBJ30213.1 (bifunctional)		CBJ28669.1 (bifunctional) - R**		nd	CABU01001450.1+CABU01012819.1*	CBJ26265.1		
Cryptista	Cryptophyta	Guillardia theta CCMP 2712 (cryptophyte)	XP_005840806.1,XP_005838866.1	XP_005832372.1 (bifunctional)*		AEIE01001242.1+AEIE01001241.1 (bifunctional) - R**		nd	XP_005830157.1	XP_005838363.1(partial)		
Haptista	Haptophyta	Emiliania huxleyi (marine haptophyte alga)	XP_005781634.1	XP_005760621.1 (bifunctional)*		nd	nd	nd	XP_005784592.1?questionable	nd		

Ultimately use simple grouped annotation * from wgs ** protein seq adjusted with wgs data

1 imperfect
2 incomplete
3 speculative

slimemolds Dictybase, sacgb leibniz-fli de (Physarum

NCBI pblast protein nr expect 1
tblastn wgs expect 1
VeuPath expect 1

No signal peptide, signal anchor
presence of indicative motifs

Table 1.S1C

Species	Genus	Family	Order	Class	Phylum(division)	unranked	Superphylum	unranked	Kingdom	unranked	Domain
Dictyostelium discoideum (cellular slime mold)	Dictyostelium	Dictyostelidae	Dictyostelida	Dictyostelia	Mycetozoa (retired)			Amoebozoa	-		Eukaryota
D. purpureum (cellular slime mold)	Dictyostelium	Dictyostelidae	Dictyostelida	Dictyostelia	Mycetozoa (retired)			Amoebozoa			Eukaryota
D. lacustrium (cellular slime mold)	Dictyostelium	Dictyostelidae	Dictyostelida	Dictyostelia	Mycetozoa (retired)			Amoebozoa			Eukaryota
Polysphondylium pallidum (cellular slime mold)	Polysphondylium	Dictyostelidae	Dictyostelida	Dictyostelia	Mycetozoa (retired)			Amoebozoa			Eukaryota
Acytostelium subglobosum (cellular slime mold)	Acytostelium	Dictyostelidae	Dictyostelida	Dictyostelia	Mycetozoa (retired)			Amoebozoa			Eukaryota
Tieghemostelium lacteum	Tieghemostelium	Raperosteliaceae	Dictyostelida	Dictyostelia	Mycetozoa (retired)			Amoebozoa			Eukaryota
Physarum polycephalum (acellular slime mold)	Physarum	Physaraceae	Physarales	Myxogastria	Mycetozoa (retired)			Amoebozoa			Eukaryota
Acanthamoeba castellanii (Neff) soil protozoa)	Acanthamoeba	Acanthamoebidae	Centramoebida			Discosea		Amoebozoa			Eukaryota
Balamuthia mandillaris (free living amoeba -> encephalitis)	Balamuthia	Balamuthiidae	Centramoebida			Discosea		Amoebozoa			Eukaryota
Sozellomycon perchlora DAOM 89117 (zoospore-producing)	Sozellomycon	-	Spizellomycetales	Chytridiomycetes	Chytridiomycota				Fungi	Opisthokonta Unikonta	Eukaryota
Rhizoclosmatium globosum	Rhizoclosmatium	Chytriomycetaceae	Chytridiales	Chytridiomycetes	Chytridiomycota				Fungi	Opisthokonta Unikonta	Eukaryota
Gonapodya prolifera	Gonapodya	Gonapodyaceae	Monoblepharidales	Monoblepharidomycetes	Chytridiomycota				Fungi	Opisthokonta Unikonta	Eukaryota
Reticulomyxa filosa (fresh water foraminifera)	Reticulomyxa	-	Incertae sedis	-	Foraminifera	Rhizaria		SAR			Eukaryota
Spongospora subterranea	Spongospora	Plasmodiophoraceae	Plasmodiophorales	Phytomyxea	Cercozoa	Rhizaria		SAR			Eukaryota
Plasmodiophora brassicae (causes cabbage clubroot)	Plasmodiophora	Plasmodiophoraceae	Plasmodiophorales	Phytomyxea	Cercozoa	Rhizaria		SAR			Eukaryota
Bigelowiella natans CCMP2755 (chlorarachniea)	Bigelowiella	Chlorarachniaceae	Chlorarachniales	Chlorarachniophyceae	Cercozoa	Rhizaria		SAR			Eukaryota
Toxoplasma gondii (apicomplexan)	Toxoplasma	Sarcocystidae	Eucoccidiorida	Conoidasida	Apicomplexa	Alveolata		SAR			Eukaryota
Hammondia hammondi (apicomplexan)	Hammondia	Sarcocystidae	Eucoccidiorida	Conoidasida	Apicomplexa	Alveolata		SAR			Eukaryota
Neospora caninum (apicomplexan)	Neospora	Sarcocystidae	Eucoccidiorida	Conoidasida	Apicomplexa	Alveolata		SAR			Eukaryota
Sarcocystis neurona (apicomplexan)	Sarcocystis	Sarcocystidae	Eucoccidiorida	Conoidasida	Apicomplexa	Alveolata		SAR			Eukaryota
Vitrella brassicaformis (Vitrellaceae)	Vitrella	Vitrellaceae	-	-	Chromerida	Alveolata		SAR			Eukaryota
Chromera velia (Chromeraceae)	Chromera	Chromeraceae	-	-	Chromerida	Alveolata		SAR			Eukaryota
Tetrahymena thermophila (ciliate)	Tetrahymena	Tetrahymenidae	Hymenostomatida	Oligohymenophorea	Ciliophora	Alveolata	-	SAR			Eukaryota
Stentor coeruleus (ciliate)	Stentor	Stentoridae	Heterotrichida	Heterotrichea	Ciliophora	Alveolata	-	SAR			Eukaryota
Stylonychia lemnae (ciliate)	Stylonychia	Oxytrichidae	Sporadotrichida	Spirotrichea	Ciliophora	Alveolata	-	SAR			Eukaryota
Oxytricha trifallax (ciliate)	Oxytricha	Oxytrichidae	Sporadotrichida	Spirotrichea	Ciliophora	Alveolata	-	SAR			Eukaryota
Karlodinium micrum (dinoflagellate)	Karlodinium	-	-	Dinophyceae	Dinoflagellata	Alveolata	-	SAR			Eukaryota
Karenia brevis (marine unicellar dinoflagellate, red tide)	Karenia	Kareniaceae	Gymnodiniales	Dinophyceae	Dinoflagellata	Alveolata	-	SAR			Eukaryota
Perkinsus marinus & olseni (diarrhoea, infects molluscs)	Perkinsus	Perkinsidae	Perkinsida	Perkinsea	Perkinsozoa	Alveolata	-	SAR			Eukaryota
Symbiodinium microadriaticum (dinoflagellate)	Symbiodinium	Symbiodiniaceae	Suessiales	Dinophyceae	Dinoflagellata	Alveolata	-	SAR			Eukaryota
Albugo laibachii (oomycete)	Albugo	Albuginaceae	Peronosporales	Oomycetes	Heterokontophyta			Heterokonta			Eukaryota
Pythium ultimum (oomycete)	Pythium	Pythiaceae	Peronosporales	Oomycetes	Heterokontophyta			Heterokonta			Eukaryota
Aphanomyces invadans (oomycete)	Aphanomyces	Leptolegniaceae	Saprolegniales	Oomycetes				Heterokonta			Eukaryota
Aphanomyces euteiches, strain 199 (oomycete)	Aphanomyces	Leptolegniaceae	Saprolegniales	Oomycetes				Heterokonta			Eukaryota
Aphanomyces stellatus, strain 57667 (oomycete)	Aphanomyces	Leptolegniaceae	Saprolegniales	Oomycetes				Heterokonta			Eukaryota
Saprolegnia parasitica (fish pathogen)	Saprolegnia	Saprolegniaceae	Saprolegniales	Oomycetes				Heterokonta			Eukaryota
Phytophthora infestans (oomycete)	Phytophtera	Pythiaceae	Pythiales	Oomycetes	Heterokontophyta			Heterokonta			Eukaryota
Phytophthora ramorum (oomycete)	Phytophtera	Pythiaceae	Pythiales	Oomycetes				Heterokonta			Eukaryota
P. sojae (oomycete)	Phytophtera	Pythiaceae	Pythiales	Oomycetes				Heterokonta			Eukaryota
Phaeodactylum tricornutum (marine pennate diatom)	Phaeodactylum	Phaeodactylaceae	Naviculales	Bacillariophyceae	Bacillariophyta	Bacillariophyta	SAR	Heterokonta	Chromista		Eukaryota
Fragilariopsis cylindrus (coldwater diatom)	Fragilariopsis	Bacillariaceae	Bacillariales	Bacillariophyceae	Bacillariophyta	Bacillariophyta	SAR	Heterokonta	Chromista		Eukaryota
Thalassiosira pseudonana (diatom)	Thalassiosira	Thalassiosiraceae	Thalassiosirales	Mediophyceae	Bacillariophyta	Bacillariophyta	SAR	Heterokonta	Chromista		Eukaryota
Nannochloropsis gaditana (marine microalga)	Nannochloropsis	Eustigmataceae	Eustigmatales	Eustigmatophyceae	Ochrophyta		SAR	Heterokonta	Chromista		Eukaryota
Aureococcus anophagefferens (non-motile pelagophyte)	Aureococcus	Pelagomonadaceae	Pelagomonadales	Pelagophyceae	Ochrophyta		SAR	Heterokonta	Chromista		Eukaryota
Ectocarpus siliculosus (brown alga)	Ectocarpus	Ectocarpaceae	Ectocarpales	Phaeophyceae	Ochrophyta		SAR	Heterokonta	Chromista		Eukaryota
Guillardia theta CCMP 2712 (cryptophyte)	Guillardia	Geminigeraceae	Pyrenomonadales	Cryptophyceae	Cryptophyta				Chromista		Eukaryota
Emiliania huxleyi (marine haptophyte alga)	Emiliania	Noelaerhabdaceae	Isochrysidales	Pyrenomonadophyceae	Haptophyta		-	Haptophyta	Chromista	Diaphoretickes	Eukaryota
Klebsormidium nitens (green alga)	Klebsormidium	Klebsormidiaceae	Klebsormidiales	Klebsormidiophyceae	Chlorophyta	Streptophyta	-	Viridiplantae	Plantae		Eukaryota
Chlamydomonas reinhardtii (chlorophyte alga)	Chlamydomonas	Chlamydomonadaceae	Chlamydomonadales	Chlorophyceae	Chlorophyta		-	Viridiplantae	Plantae		Eukaryota
Volvox carteri (chlorophyte alga)	Volvox	Volvocaceae	Volvocales	Chlorophyceae	Chlorophyta		-	Viridiplantae	Plantae		Eukaryota
Coccomyxa subellipsoidea (chlorophyte alga)	Coccomyxa	Coccomyxaceae	Chlorococcales	Chlorophyceae	Chlorophyta		-	Viridiplantae	Plantae		Eukaryota
Chlorella variabilis (chlorophyte single-cell green alga)	Chlorella	Chlorellaceae	Chlorellales	Trebouxiophyceae	Chlorophyta		-	Viridiplantae	Plantae		Eukaryota
Malawimonas californiana	Malawimonas	Malawimonadidae	Malawimonadida	Malawimonadea	Neokonta	Excavata	-		-		Eukaryota
Naegleria gruberi (amoeba flagellate, heterokonea)	Naegleria	Vahlkampfiidae	Schizopyrenida	Heterolobosea	Percolozoa	Excavata	-		-		Eukaryota
Trichodesmium erythraeum MS101 (marine cyanobacterium)	Trichodesmium	Microcoleaceae	Oscillatoriales	Cyanophyceae	Cyanobacteria				Bacteria		Prokaryota
Desulfotalea psychrophila	Desulfotalea	Desulfobacteraceae	Desulfobacterales	Deltaproteobacteria	Proteobacteria				Bacteria		Prokaryota
Pelagibacter sp. UFO1 (Finniculla)	Pelagibacter	Pelagibacteraceae	Rickettsiales	Alphaproteobacteria	Proteobacteria				Bacteria		Prokaryota

Figure 1.S2

Mutation	species	sequence	Dd position	effect (ref.)
Skp1-12	Sc	L8G	L6	G1-, G2-arrest (2)
Skp1-1	Sc	E129G	P94	ts-growth (1)
Skp1-2	Sc	M130V, F176S	T95, F141	ts-growth (1)
Skp1-4	Sc	L146S	L111	ts-G2-arrest, chrom. mis-segreg. (1)
Skp1-11	Sc	G160R, R167K	G125, R132	ts-G1-arrest (2)
Skp1-3	Sc	I172N	I137	ts-G1/S-arrest (1)
	Sc	~~N108Y~~ N139Y	N104	blocks Rav1 binding (4)
	Sc	S162D	T127	weakened interaction with Met30 (5)
Skp1-A2	Sp	V102A	I100	ts-F-box interface (3)
Skp1-A7	Sp	I110T	I108	ts-selective effects on F-box binding (3)
Skp1-A3	Sp	L113F	L111	ts-core: may disrupt folding (3)
Skp1-A1	Sp	+QFVASCV[a]	C-term	ts-F-box contact? (3)
Skp1-A8	Sp	+SFVASCV[a]	C-term	ts-F-box contact? (3)
Skp1A1	Dd	I34T,D71G		incomplete glycosylation (6)
Skp1A2	Dd	K53A,V54S,L55S		incomplete glycosylation (6)
Skp1A4	Dd	H60Y,H62V		(Daniel Lin)
Flag-Skp1	Dd	+N-term FLAG		no hydroxylation, no interactome (7,8)
FLAG**Δ**-Skp1	Dd	+N-term S		(Liu, Schofield)
His10-Skp1A	Dd	+N-term His10		
Skp1(F97E)	Dd		F97	dimerization inhib (9)
Skp1A3	Dd		P143A	O_2-sensing (6)
Skp1A3a	Dd		P143E	O_2-sensing (6)
ΔN-Skp1	Tg	-5N-term aa		
Flag-SKP1	Hs	K142R	K138	(10)
Flag-SKP1	Hs	K163R	K159	(10)
Flag-SKP1	Hs	RR (K142R/K163R)	K138/K159	(10)
Flag-SKP1	Hs	T131A	T127	(10)
Flag-SKP1	Hs	T131D	T127	(10)
Flag-SKP1	Hs	T131E	T127	(10)
Flag-SKP1	Hs	97-101-5A	93-97	weak Cul1 binding (10)
Flag-SKP1	Hs	113-117-5A	109-113	no Skp2, Cul1 binding (10)
Flag-SKP1	Hs	120-124-5A	116-120	ok for Cul1, Skp2 (10)
Flag-SKP1	Hs	138-142-5A	134-138	negligible Skp2, Cul1 binding (10)
Flag-SKP1	Hs	138-141-4A	134-138	neglibible Cul1, no FBPs (10)
Flag-SKP1	Hs	T138A	I134	ok for Cul1, all FBPs (10)
Flag-SKP1	Hs	F139A	F135	reduced Cul1 and all FBPs, except no cyclinF (10)
Flag-SKP1	Hs	N140A	N136	ok for Cul1, all FBPs (10)
Flag-SKP1	Hs	I141A	I137	reduced Cul1 and all FBPs, except no cyclinF/Skp2/FBH1 (10)
Flag-SKP1	Hs	K142A	K138	ok for Cul1, all FBPs (10)
Flag-SKP1	Hs	F139A/I141A/K142A	135/137/138	reduced Cul1, no FBPs (10)
Flag-SKP1	Hs	F139A/I141A	135/137	reduced Cul1, no FBPs (10)
Flag-SKP1	Hs	F139A/K142A	135/138	ok for Cul1, low for FBPs except no cyclinF (10)
Flag-SKP1	Hs	I141A/K142A	137/138	ok for Cul1, low for FBPs except no Skp2/FBH1 (10)

[a] C-terminal extension

Sc=*Saccharomyces cerevisiae* (budding yeast), Sp=*Schizosaccharomyces pombe* (fission yeast); Dd=*Dictyostelium discoideum*

ts=temperature-sensitive

1. Connelly C, Hieter P. (1996) Budding yeast SKP1 encodes an evolutionarily conserved kinetochore protein required for cell cycle progression. Cell 86:275-285.

2. Bai C, Sen P, Hofmann K, Ma L, Goebl M, Harper JW, Elledge SJ. (1996) . Cell 86:263-274.

3. Lehmann A, Katayama S, Harrison C, Dhut S, Kitamura K, McDonald N, Toda T. (2004) Molecular interactions of fission yeast Skp1 and its role in the DNA damage checkpoint. Genes Cells 9:367-382.

4. E. J. Brace, Leah P. Parkinson, and Robert S. Fuller (2006) Skp1p Regulates Soi3p/Rav1p Association with Endosomal Membranes but Is Not Required for Vacuolar ATPase Assembly. EUKARYOTIC CELL, 5:2104–2113

5. P. Beltrao, V. Albanèse, L.R. Kenner, D.L. Swaney, A. Burlingame, J. Villén, W.A. Lim, J.S. Fraser, J. Frydman, N.J. Krogan, Systematic functional prioritization of protein posttranslational modifications, Cell 150 (2012) 413-425.

6. Sassi S, Sweetinburgh M, Erogul J, Zhang P, Teng-Umnuay P, West CM. Analysis of Skp1 glycosylation and nuclear enrichment in *Dictyostelium*. Glycobiology. 2001 11:283-95; Wang ZA, Singh D, van der Wel H, West CM. Prolyl hydroxylation- and glycosylation-dependent functions of Skp1 in O_2-regulated development of *Dictyostelium*. Dev Biol. 2011 349:283-95.

7. Wang, Z.A., D. Singh, H. van der Wel & C.M. West (2011) Prolyl hydroxylation- and glycosylation-dependent functions of Skp1 in O_2-regulated development of *Dictyostelium*. *Dev. Biol.* **349**:283-295.

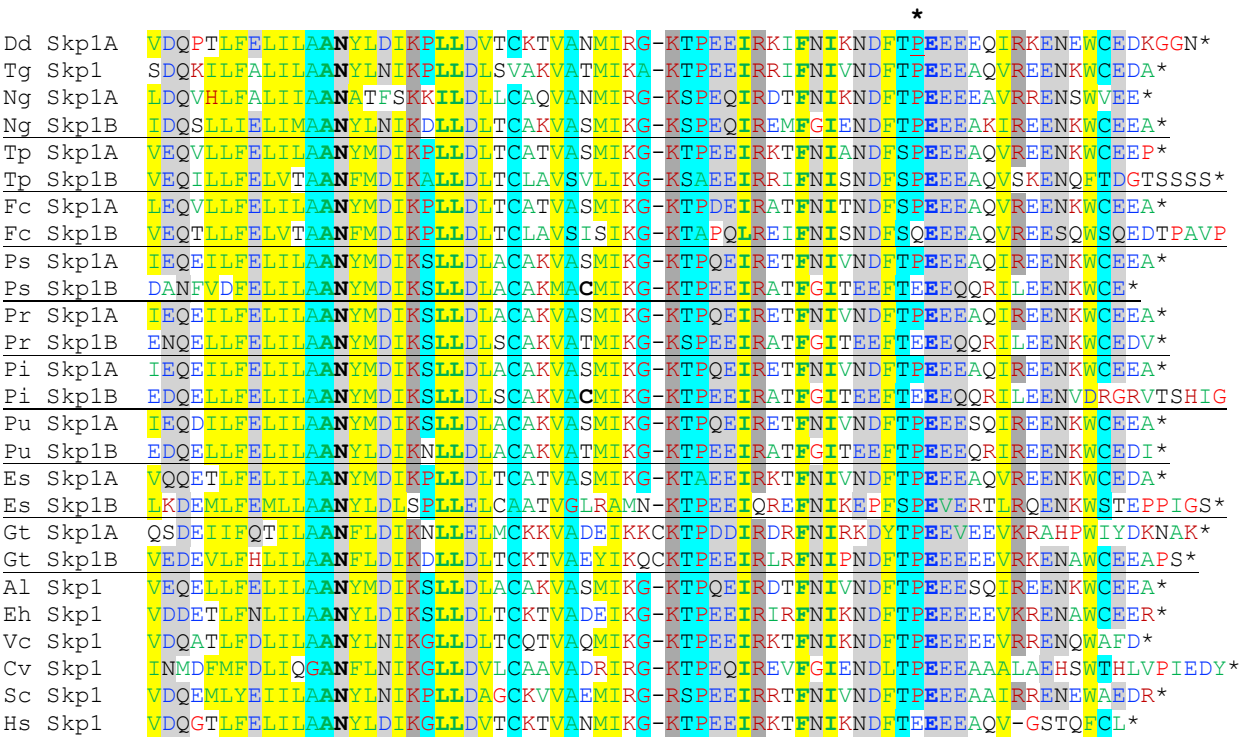
8. Sheikh, M.O., Y Xu, H. van der Wel, P. Walden, S.D. Hartson & C.M. West (2015) Glycosylation of Skp1 promotes formation of Skp1/Cullin-1/F-box protein complexes in *Dictyostelium*. *Mol. Cell. Proteomics* 14:66-80

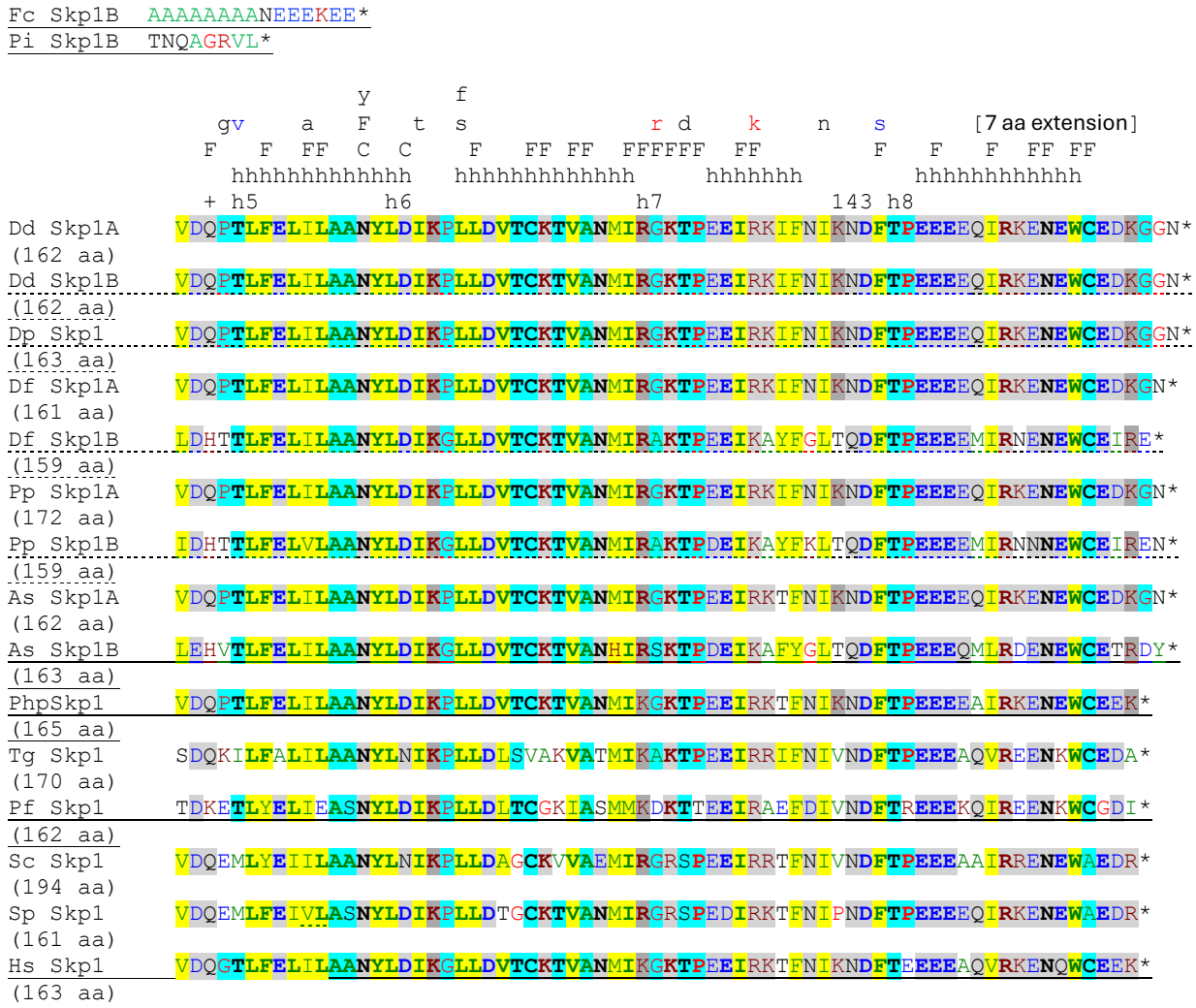
9. Kim HW, Eletsky A, Gonzalez KJ, van der Wel H, Eva-Maria Strauch EM, Prestegard JM, West CM (2020) Skp1 Dimerization Conceals Its F-Box Protein Binding Site. *Biochemistry* 59:1527-1536

10. Li, J., Krause, G. J., Gui, Q., Kaushik, S., Rona, G., Zhang, Q., Liang, F.-X., Dhabaria, A., Anerillas, C., Martindale, J. L., Vasilyev, N., Askenazi, M., Ueberheide, B., Nudler, E., Gorospe, M., Cuervo, A. M., and Pagano, M. (2023) A noncanonical function of SKP1 regulates the switch between autophagy and unconventional secretion, Science Advances 9, eadh1134.

Table 1.S3

Dd Skp1A	*Dictyostelium discoideum*	amoebozoa/mycetozoa	NCBI, AAA67888.1
Tg Skp1	*Toxoplasma gondii*	alveolate/apicomplexa	ToxoDB, TGARI_207680
Ng Skp1A	*Naegleria gruberi* scaffold 5: 131842-132718	excavate/percolozoa	DOE, version 1.0, 2/2009: in
Ng Skp1B	*N. gruberi*		NCBI, XP_002681295.1
Tp Skp1A	*Thalassiosira pseudonana* 38460	stramenopile/diatom	NCBI, XP_002294707.1
Tp Skp1B	*T. pseudonana* 10077		NCBI, XP_002294049.1
Fc Skp1A	*Fragilariopsis cylindrus* 212070	stramenopile/diatom	NCBI, OEU09899.1
Fc Skp1B	*F. cylindrus* 213790		NCBI, OEU16705.1
Ps Skp1A	*Phytophthora sojae* 108319	stramenopile/oomycete	NCBI, XP_009526241.1
Ps Skp1B	*P. sojae* 108223		NCBI, XP_009532045.1
Pr Skp1A	*Phytophthora ramorum* 71411 71411|fgenesh1_pm.C_scaffold_18000002, 6/2007	stramenopile/oomycete	DOE,
Pr Skp1B	*P. ramorum* 71622 71622|fgenesh1_pm.C_scaffold_32000004, 6/2007		DOE,
Pi Skp1A	*Phytophthora infestans* 01260.1	stramenopile/oomycete	NCBI, XP_002907933.1
Pi Skp1B	*P. infestans* 15216.1		NCBI, XP_002898672.1
Pu Skp1A	*Pythium ultimum* www.pythiumdb.org	stramenopile/oomycete	PYU1_T013675,
Pu Skp1B	*P. ultimum* www.pythiumdb.org, EST data NCBI		PYU1_T011629,
Es Skp1A	*Ectocarpus siliculosus*	heterokontophyta/brown alga	NCBI, CBJ48672.1
Es Skp1B	*E. siliculosus*		NCBI, CBJ48849.1
Gt Skp1A	*Guillardia theta CCMP2712*	cryptophyta/cryptomonad	NCBI, XP_005838866.1
Gt Skp1B	*G. theta CCMP2712*		NCBI, XP_005840806.1
Al Skp1	*Albugo laibachii*	stramenopile/oomycete	NCBI, CCA15417.1
Eh Skp1	*Emiliania huxleyi*	haptophyte/phytoplankton	NCBI, XP_005781634.1
Vc Skp1	*Volvox carteri*	cryptophyta/green alga	NCBI, XP_002947872.1
Cv Skp1	*Chlorella virus* PBCV-1	virus	NCBI, NP_048387.1
Sc Skp1	*Saccharomyces cerevisiae*	yeast	NCBI, NP_010615.3
Hs Skp1	Homo sapiens OCP2	human	NCBI, NP_008861.2





* Dd Skp1A and Skp1B genes are also known as *fpaA* and *fpaB*.

Dd – *Dictyostelium discoideum*
Dp – *D. purpureum*
Df – *D. fasciculatum*
Pp – *Polysphondylium pallidum*
As – *Acytostelium subglobosum*
Php – *Physarum polycephalum* (acellular slime mold)
Tg – *Toxoplasma gondii* (apicomplexan)
Pf – *Plasmodium falciparum* (apicomplexan)
Sc – *Saccharomyces cerevisiae* (budding yeast)
Sp – *Schizosaccharomyces pombe* (fission yeast)
Hs – *Homo sapi*

REFERENCES

(1) Soucy, T. A., Smith, P. G., Milhollen, M. A., Berger, A. J., Gavin, J. M., Adhikari, S., Brownell, J. E., Burke, K. E., Cardin, D. P., Critchley, S., Cullis, C. A., Doucette, A., Garnsey, J. J., Gaulin, J. L., Gershman, R. E., Lublinsky, A. R., McDonald, A., Mizutani, H., Narayanan, U., Olhava, E. J., Peluso, S., Rezaei, M., Sintchak, M. D., Talreja, T., Thomas, M. P., Traore, T., Vyskocil, S., Weatherhead, G. S., Yu, J., Zhang, J., Dick, L. R., Claiborne, C. F., Rolfe, M., Bolen, J. B., and Langston, S. P. (2009) An inhibitor of NEDD8-activating enzyme as a new approach to treat cancer, Nature 458, 732-736.

(2) Sarikas, A., Hartmann, T., and Pan, Z.-Q. (2011) The cullin protein family, Genome Biology 12, 220.

(3) van der Wel, H., Gas-Pascual, E., and West, C. M. (2019) Skp1 isoforms are differentially modified by a dual function prolyl 4-hydroxylase/N-acety lglucosaminyltransferase in a plant pathogen, Glycobiology 29, 705-714.

(4) Rizvi, Z., Reddy, G. S., Gorde, S. M., Pundir, P., Das, D., and Sijwali, P. S. (2024) *Plasmodium falciparum* contains functional SCF and CRL4 ubiquitin E3 ligases, and CRL4 is critical for cell division and membrane integrity, PLOS Pathogens 20, e1012045.

(5) Rojas, F., Koszela, J., Búa, J., Llorente, B., Burchmore, R., Auer, M., Mottram, J. C., and Téllez-Iñón, M. T. (2017) The ubiquitin-conjugating enzyme CDC34 is essential for cytokinesis in contrast to putative subunits of a SCF complex in *Trypanosoma brucei*, PLOS Neglected Tropical Diseases 11, e0005626.

(6) Silmon de Monerri, Natalie C., Yakubu, Rama R., Chen, Allan L., Bradley, Peter J., Nieves, E., Weiss, Louis M., and Kim, K. (2015) The Ubiquitin Proteome of *Toxoplasma gondii* Reveals Roles for Protein Ubiquitination in Cell-Cycle Transitions, Cell Host & Microbe 18, 621-633.

(7) Kim, W. D., Mathavarajah, S., and Huber, R. J. (2022) The Cellular and Developmental Roles of Cullins, Neddylation, and the COP9 Signalosome in *Dictyostelium discoideum*, Frontiers in Physiology 13.

(8) Winston, J. T., Koepp, D. M., Zhu, C., Elledge, S. J., and Harper, J. W. (1999) A family of mammalian F-box proteins, Current Biology 9, 1180-S1183.

(9) Hua, Z., Zou, C., Shiu, S.-H., and Vierstra, R. D. (2011) Phylogenetic Comparison of F-Box (FBX) Gene Superfamily within the Plant Kingdom Reveals Divergent Evolutionary Histories Indicative of Genomic Drift, PLOS ONE 6, e16219.

(10) Lee, J. E., Sweredoski, M. J., Graham, R. L. J., Kolawa, N. J., Smith, G. T., Hess, S., and Deshaies, R. J. (2011) The Steady-State Repertoire of Human SCF Ubiquitin Ligase Complexes Does Not Require Ongoing Nedd8 Conjugation, Molecular & Cellular Proteomics 10, M110.006460.

(11) Finley, D., Ulrich, H. D., Sommer, T., and Kaiser, P. (2012) The Ubiquitin–Proteasome System of *Saccharomyces cerevisiae*, Genetics 192, 319-360.

(12) Sarikaya Bayram, Ö., Bayram, Ö., Karahoda, B., Meister, C., Köhler, A. M., Thieme, S., Elramli, N., Frawley, D., McGowan, J., Fitzpatrick, D. A., Schmitt, K., de Assis, L. J., Valerius, O., Goldman, G. H., and Braus, G. H. (2022) F-box receptor mediated control of substrate stability and subcellular location organizes cellular development of *Aspergillus nidulans*, PLOS Genetics 18, e1010502.

(13) Mandalasi, M. N., Gas-Pascual, E., Baptista, C. G., Deng, B., van der Wel, H., Kruijtzer, J. A. W., Boons, G.-J., Blader, I. J., and West, C. M. (2024) Oxygen-dependent regulation of F-box proteins in *Toxoplasma gondii* is mediated by Skp1 glycosylation, Journal of Biological Chemistry 300, 107801.

(14) Boland, A. W., Gas-Pascual, E., Nottingham, B. L., van der Wel, H., Daniel, N. G., Sheikh, M. O., Schafer, C. M., and West, C. M. (2022) Oxygen-dependent regulation of E3(SCF)ubiquitin ligases and a Skp1-associated JmjD6 homolog in development of the social amoeba *Dictyostelium*, Journal of Biological Chemistry 298, 102305.

(15) Skowyra, D., Craig, K. L., Tyers, M., Elledge, S. J., and Harper, J. W. (1997) F-Box Proteins Are Receptors that Recruit Phosphorylated Substrates to the SCF Ubiquitin-Ligase Complex, Cell 91, 209-219.

(16) Zheng, N., Schulman, B. A., Song, L., Miller, J. J., Jeffrey, P. D., Wang, P., Chu, C., Koepp, D. M., Elledge, S. J., Pagano, M., Conaway, R. C., Conaway, J. W., Harper, J. W., and Pavletich, N. P. (2002) Structure of the Cul1–Rbx1–Skp1–F box^{Skp2} SCF ubiquitin ligase complex, Nature 416, 703-709.

(17) Bai, C., Sen, P., Hofmann, K., Ma, L., Goebl, M., Harper, J. W., and Elledge, S. J. (1996) SKP1 Connects Cell Cycle Regulators to the Ubiquitin Proteolysis Machinery through a Novel Motif, the F-Box, Cell 86, 263-274.

(18) Patton, E. E., Willems Ar Fau - Sa, D., Sa D Fau - Kuras, L., Kuras L Fau - Thomas, D., Thomas D Fau - Craig, K. L., Craig Kl Fau - Tyers, M., and Tyers, M. (1998) Cdc53 is a scaffold protein for multiple Cdc34/Skp1/F-box proteincomplexes that regulate cell division and methionine biosynthesis in yeast, Genes & Development 12, 692-705.

(19) Zhang, Q., Karnak, D., Tan, M., Lawrence, T. S., Morgan, M. A., and Sun, Y. (2016) FBXW7 Facilitates Nonhomologous End-Joining via K63-Linked Polyubiquitylation of XRCC4, Molecular Cell 61, 419-433.

(20) Pierce, N. W., Kleiger, G., Shan, S.-o., and Deshaies, R. J. (2009) Detection of sequential polyubiquitylation on a millisecond timescale, Nature 462, 615-619.

(21) Ciechanover, A., Heller, H., Elias, S., Haas, A. L., and Hershko, A. (1980) ATP-dependent conjugation of reticulocyte proteins with the polypeptide required for protein degradation, Proceedings of the National Academy of Sciences 77, 1365-1368.

(22) Hershko, A., Ciechanover, A., Heller, H., Haas, A. L., and Rose, I. A. (1980) Proposed role of ATP in protein breakdown: conjugation of protein with multiple chains of the polypeptide of ATP-dependent proteolysis, Proceedings of the National Academy of Sciences 77, 1783-1786.

(23) Grice, G. L., and Nathan, J. A. (2016) The recognition of ubiquitinated proteins by the proteasome, Cellular and Molecular Life Sciences 73, 3497-3506.

(24) Rayon, T., Stamataki, D., Perez-Carrasco, R., Garcia-Perez, L., Barrington, C., Melchionda, M., Exelby, K., Lazaro, J., Tybulewicz, V. L. J., Fisher, E. M. C., and Briscoe, J. (2020) Species-specific pace of development is associated with differences in protein stability, Science 369, eaba7667.

(25) Xie, J., Jin, Y., and Wang, G. (2019) The role of SCF ubiquitin-ligase complex at the beginning of life, Reproductive Biology and Endocrinology 17, 101.

(26) He, Q., Cheng, P., Yang, Y., He, Q., Yu, H., and Liu, Y. (2003) FWD1-mediated degradation of FREQUENCY in *Neurospora* establishes a conserved mechanism for circadian clock regulation, The EMBO Journal 22, 4421-4430-4430.

(27) Wegner, S., Belle, M. D. C., Hughes, A. T. L., Diekman, C. O., and Piggins, H. D. (2017) Delayed Cryptochrome Degradation Asymmetrically Alters the Daily Rhythm in Suprachiasmatic Clock Neuron Excitability, The Journal of Neuroscience 37, 7824.

(28) de Assis Leandro, J., Ulas, M., Ries Laure Nicolas, A., El Ramli Nadia Ali, M., Sarikaya-Bayram, O., Braus Gerhard, H., Bayram, O., and Goldman Gustavo, H. (2018) Regulation of *Aspergillus nidulans* CreA-Mediated Catabolite Repression by the F-Box Proteins Fbx23 and Fbx47, mBio 9, 10.1128/mbio.00840-00818.

(29) Lauinger, L., and Kaiser, P. (2021) Sensing and Signaling of Methionine Metabolism, In Metabolites.

(30) Wang, H., Shi, H., Rajan, M., Canarie, E. R., Hong, S., Simoneschi, D., Pagano, M., Bush, M. F., Stoll, S., Leibold, E. A., and Zheng, N. (2020) FBXL5 Regulates IRP2 Stability in Iron Homeostasis via an Oxygen-Responsive [2Fe2S] Cluster, Molecular Cell 78, 31-41.e35.

(31) Salahudeen, A. A., Thompson, J. W., Ruiz, J. C., Ma, H.-W., Kinch, L. N., Li, Q., Grishin, N. V., and Bruick, R. K. (2009) An E3 Ligase Possessing an Iron-Responsive Hemerythrin Domain Is a Regulator of Iron Homeostasis, Science 326, 722-726.

(32) Cordonnier, C., Mandalasi, M., Gigley, J., Wohlfert, E. A., West, C. M., and Blader, I. J. (2024) The *Toxoplasma* oxygen-sensing protein, TgPhyA, is required for resistance to interferon gamma-mediated nutritional immunity in mice, PLOS Biology 22, e3002690.

(33) Jöhnk, B., Bayram, Ö., Abelmann, A., Heinekamp, T., Mattern, D. J., Brakhage, A. A., Jacobsen, I. D., Valerius, O., and Braus, G. H. (2016) SCF Ubiquitin Ligase F-box Protein Fbx15 Controls Nuclear Co-repressor Localization, Stress Response and Virulence of the Human Pathogen *Aspergillus fumigatus*, PLOS Pathogens 12, e1005899.

(34) Yen, J. L., Su, N.-Y., and Kaiser, P. (2005) The Yeast Ubiquitin Ligase SCF^{Met30} Regulates Heavy Metal Response, Molecular Biology of the Cell 16, 1872-1882.

(35) Barbey, R., Baudouin-Cornu, P., Lee, T. A., Rouillon, A., Zarzov, P., Tyers, M., and Thomas, D. (2005) Inducible dissociation of SCF^{Met30} ubiquitin ligase mediates a rapid transcriptional response to cadmium, The EMBO Journal 24, 521-532-532.

(36) Liu, Z., Ma, K., Zhang, P., Zhang, S., Song, X., and Qin, Y. (2025) F-box protein Fbx23 acts as a transcriptional coactivator to recognize and activate transcription factor Ace1, PLOS Genetics 21, e1011539.

(37) Chae, E., Tan, Q. K. G., Hill, T. A., and Irish, V. F. (2008) An *Arabidopsis* F-box protein acts as a transcriptional co-factor to regulate floral development, Development 135, 1235-1245.

(38) Lou, Y., Han, M., Song, Y., Zhong, J., Zhang, W., Chen, Y. H., and Wang, H. (2020) The SCFβ-TrCP E3 Ubiquitin Ligase Regulates Immune Receptor Signaling by Targeting the Negative Regulatory Protein TIPE2, The Journal of Immunology 204, 2122-2132.

(39) Zhang, Z., Bao, Z., Gao, P., Yao, J., Wang, P., and Chai, D. (2022) Diverse Roles of F-Box Protein 3 in Regulation of Various Cellular Functions, Frontiers in Cell and Developmental Biology 9.

(40) Das, A., Wang, X., Wei, J., Hoji, A., Coon, T. A., Popescu, I., Brown, M., Frizzell, S., Iasella, C. J., Noda, K., Sembrat, J. C., Devonshire, K., Hannan, S. J., Snyder, M. E., Pilewski, J. M., Sanchez, P. G., Chandra, D., Mallampalli, R. K., Alder, J. K., Chen, B. B., and McDyer, J. F. (2022) Cross-Regulation of F-Box Protein FBXL2 with T-bet and TNF-α during Acute and Chronic Lung Allograft Rejection, The Journal of Immunology 209, 1788-1795.

(41) William, J. N. G., Dhar, R., Gundamaraju, R., Sahoo, O. S., Pethusamy, K., Raj, A. F. P. A. M., Ramasamy, S., Alqahtani, M. S., Abbas, M., and Karmakar, S. (2024) SKping cell cycle regulation: role of ubiquitin ligase SKP2 in hematological malignancies, Frontiers in Oncology 14.

(42) Bosu, D. R., and Kipreos, E. T. (2008) Cullin-RING ubiquitin ligases: global regulation and activation cycles, Cell Division 3, 7.

(43) Wang, Z., Liu, P., Inuzuka, H., and Wei, W. (2014) Roles of F-box proteins in cancer, Nature Reviews Cancer 14, 233-247.

(44) Tekcham, D. S., Chen, D., Liu, Y., Ling, T., Zhang, Y., Chen, H., Wang, W., Otkur, W., Qi, H., Xia, T., Liu, X., Piao, H.-l., and Liu, H. (2020) F-box proteins and cancer: an update from functional and regulatory mechanism to therapeutic clinical prospects, Theranostics 10, 4150-4167.

(45) Ye, X., Nalepa, G., Welcker, M., Kessler, B. M., Spooner, E., Qin, J., Elledge, S. J., Clurman, B. E., and Harper, J. W. (2004) Recognition of Phosphodegron Motifs in Human Cyclin E by the SCF^{Fbw7} Ubiquitin Ligase, Journal of Biological Chemistry 279, 50110-50119.

(46) Welcker, M., Singer, J., Loeb, K. R., Grim, J., Bloecher, A., Gurien-West, M., Clurman, B. E., and Roberts, J. M. (2003) Multisite Phosphorylation by Cdk2 and GSK3 Controls Cyclin E Degradation, Molecular Cell 12, 381-392.

(47) Koepp, D. M., Schaefer, L. K., Ye, X., Keyomarsi, K., Chu, C., Harper, J. W., and Elledge, S. J. (2001) Phosphorylation-Dependent Ubiquitination of Cyclin E by the SCF^{Fbw7} Ubiquitin Ligase, Science 294, 173-177.

(48) Strohmaier, H., Spruck, C. H., Kaiser, P., Won, K.-A., Sangfelt, O., and Reed, S. I. (2001) Human F-box protein hCdc4 targets cyclin E for proteolysis and is mutated in a breast cancer cell line, Nature 413, 316-322.

(49) Shao, W., Zumer, K., Fujinaga, K., and Peterlin, B. M. (2016) FBXO3 Protein Promotes Ubiquitylation and Transcriptional Activity of AIRE (Autoimmune Regulator), Journal of Biological Chemistry 291, 17953-17963.

(50) Ren, H., Koo, J., Guan, B., Yue, P., Deng, X., Chen, M., Khuri, F. R., and Sun, S.-Y. (2013) The E3 ubiquitin ligases β-TrCP and FBXW7 cooperatively mediates GSK3-dependent Mcl-1 degradation induced by the Akt inhibitor API-1, resulting in apoptosis, Molecular Cancer 12, 146.

(51) Wertz, I. E., Kusam, S., Lam, C., Okamoto, T., Sandoval, W., Anderson, D. J., Helgason, E., Ernst, J. A., Eby, M., Liu, J., Belmont, L. D., Kaminker, J. S., O'Rourke, K. M., Pujara, K., Kohli, P. B., Johnson, A. R., Chiu, M. L., Lill, J. R., Jackson, P. K., Fairbrother, W. J., Seshagiri, S., Ludlam, M. J. C., Leong, K. G., Dueber, E. C., Maecker, H., Huang, D. C. S., and Dixit, V. M. (2011) Sensitivity to antitubulin chemotherapeutics is regulated by MCL1 and FBW7, Nature 471, 110-114.

(52) Inuzuka, H., Shaik, S., Onoyama, I., Gao, D., Tseng, A., Maser, R. S., Zhai, B., Wan, L., Gutierrez, A., Lau, A. W., Xiao, Y., Christie, A. L., Aster, J., Settleman, J., Gygi, S. P., Kung, A. L., Look, T., Nakayama, K. I., DePinho, R. A., and Wei, W. (2011) SCF^{FBW7} regulates cellular apoptosis by targeting MCL1 for ubiquitylation and destruction, Nature 471, 104-109.

(53) Welcker, M., Orian, A., Jin, J., Grim, J. A., Harper, J. W., Eisenman, R. N., and Clurman, B. E. (2004) The Fbw7 tumor suppressor regulates glycogen synthase kinase 3 phosphorylation-dependent c-Myc protein degradation, Proceedings of the National Academy of Sciences 101, 9085-9090.

(54) Sears, R., Nuckolls F Fau - Haura, E., Haura E Fau - Taya, Y., Taya Y Fau - Tamai, K., Tamai K Fau - Nevins, J. R., and Nevins, J. R. (2000) Multiple Ras-dependent phosphorylation pathways regulate Myc protein stability.

(55) Kwon, Y.-W., Kim, I.-J., Wu, D., Lu, J., Stock, W. A., Jr., Liu, Y., Huang, Y., Kang, H. C., DelRosario, R., Jen, K.-Y., Perez-Losada, J., Wei, G., Balmain, A., and Mao, J.-H. (2012) Pten Regulates Aurora-A and Cooperates with Fbxw7 in Modulating Radiation-Induced Tumor Development, Molecular Cancer Research 10, 834-844.

(56) Jin, X., Yang, C., Fan, P., Xiao, J., Zhang, W., Zhan, S., Liu, T., Wang, D., and Wu, H. (2017) CDK5/FBW7-dependent ubiquitination and degradation of EZH2 inhibits pancreatic cancer cell migration and invasion, Journal of Biological Chemistry 292, 6269-6280.

(57) Fryer, C. J., White, J. B., and Jones, K. A. (2004) Mastermind Recruits CycC:CDK8 to Phosphorylate the Notch ICD and Coordinate Activation with Turnover, Molecular Cell 16, 509-520.

(58) Nateri, A. S., Riera-Sans, L., Costa, C. D., and Behrens, A. (2004) The Ubiquitin Ligase SCF^{Fbw7} Antagonizes Apoptotic JNK Signaling, Science 303, 1374-1378.

(59) Arabi, A., Ullah, K., Branca, R. M. M., Johansson, J., Bandarra, D., Haneklaus, M., Fu, J., Ariës, I., Nilsson, P., Den Boer, M. L., Pokrovskaja, K., Grandér, D., Xiao, G., Rocha, S., Lehtiö, J., and Sangfelt, O. (2012) Proteomic screen reveals Fbw7 as a modulator of the NF-κB pathway, Nature Communications 3, 976.

(60) Fukushima, H., Matsumoto, A., Inuzuka, H., Zhai, B., Lau, Alan W., Wan, L., Gao, D., Shaik, S., Yuan, M., Gygi, Steven P., Jimi, E., Asara, John M., Nakayama, K., Nakayama, Keiichi I., and Wei, W. (2012) SCF^{Fbw7} Modulates the NFκB Signaling Pathway by Targeting NFκB2 for Ubiquitination and Destruction, Cell Reports 1, 434-443.

(61) Xu, S., Abbasian, M., Patel, P., Jensen-Pergakes, K., Lombardo, C. R., Cathers, B. E., Xie, W., Mercurio, F., Pagano, M., Giegel, D., and Cox, S. (2007) Substrate Recognition and Ubiquitination of $SCF^{Skp2/Cks1}$ Ubiquitin-Protein Isopeptide Ligase, Journal of Biological Chemistry 282, 15462-15470.

(62) Malonia, S. K., Dutta, P., Santra, M. K., and Green, M. R. (2015) F-box protein FBXO31 directs degradation of MDM2 to facilitate p53-mediated growth arrest following genotoxic stress, Proceedings of the National Academy of Sciences 112, 8632-8637.

(63) Kõivomägi, M., Valk, E., Venta, R., Iofik, A., Lepiku, M., Balog, E. R. M., Rubin, S. M., Morgan, D. O., and Loog, M. (2011) Cascades of multisite phosphorylation control Sic1 destruction at the onset of S phase, Nature 480, 128-131.

(64) Johmura, Y., Sun, J., Kitagawa, K., Nakanishi, K., Kuno, T., Naiki-Ito, A., Sawada, Y., Miyamoto, T., Okabe, A., Aburatani, H., Li, S., Miyoshi, I., Takahashi, S., Kitagawa, M., and

Nakanishi, M. (2016) SCF^{Fbxo22}-KDM4A targets methylated p53 for degradation and regulates senescence, Nature Communications 7, 10574.

(65) Lai, Y., Li, J., Li, X., and Zou, C. (2017) Lipopolysaccharide modulates p300 and Sirt1 to promote PRMT1 stability via an SCF^{Fbxl17}-recognized acetyldegron, Journal of Cell Science 130, 3578-3587.

(66) Yoshida, Y., Mizushima, T., and Tanaka, K. (2019) Sugar-Recognizing Ubiquitin Ligases: Action Mechanisms and Physiology, Frontiers in Physiology 10.

(67) Baek, H.-J., Yoon, J.-H., Ann, E.-J., Kim, M.-Y., Ahn, J.-S., Kim, S.-H., Jo, E.-H., Lee, H.-J., and Park, H.-S. (2015) Alpha-synuclein negatively regulates Notch1 intracellular domain protein stability through promoting interaction with Fbw7, Neuroscience Letters 600, 6-11.

(68) Hao, B., Zheng, N., Schulman, B. A., Wu, G., Miller, J. J., Pagano, M., and Pavletich, N. P. (2005) Structural Basis of the Cks1-Dependent Recognition of $p27^{Kip1}$ by the SCF^{Skp2} Ubiquitin Ligase, Molecular Cell 20, 9-19.

(69) Tan, X., Calderon-Villalobos, L. I. A., Sharon, M., Zheng, C., Robinson, C. V., Estelle, M., and Zheng, N. (2007) Mechanism of auxin perception by the TIR1 ubiquitin ligase, Nature 446, 640-645.

(70) Sheard, L. B., Tan, X., Mao, H., Withers, J., Ben-Nissan, G., Hinds, T. R., Kobayashi, Y., Hsu, F.-F., Sharon, M., Browse, J., He, S. Y., Rizo, J., Howe, G. A., and Zheng, N. (2010) Jasmonate perception by inositol-phosphate-potentiated COI1–JAZ co-receptor, Nature 468, 400-405.

(71) Lan, K., Verma, S. C., Murakami, M., Bajaj, B., Kaul, R., and Robertson, E. S. (2007) Kaposi's sarcoma herpesvirus-encoded latency-associated nuclear antigen stabilizes intracellular activated Notch by targeting the Sel10 protein, Proceedings of the National Academy of Sciences 104, 16287-16292.

(72) Mallampalli, R. K., Coon, T. A., Glasser, J. R., Wang, C., Dunn, S. R., Weathington, N. M., Zhao, J., Zou, C., Zhao, Y., and Chen, B. B. (2013) Targeting F Box Protein Fbxo3 To Control Cytokine-Driven Inflammation, The Journal of Immunology 191, 5247-5255.

(73) Naseem, Y., Zhang, C., Zhou, X., Dong, J., Xie, J., Zhang, H., Agboyibor, C., Bi, Y., and Liu, H. (2023) Inhibitors Targeting the F-BOX Proteins, Cell Biochemistry and Biophysics 81, 577-597.

(74) Kim, A. Y., Bommeljé, C. C., Lee, B. E., Yonekawa, Y., Choi, L., Morris, L. G., Huang, G., Kaufman, A., Ryan, R. J. H., Hao, B., Ramanathan, Y., and Singh, B. (2008) SCCRO (DCUN1D1) Is an Essential Component of the E3 Complex for Neddylation, Journal of Biological Chemistry 283, 33211-33220.

(75) Kurz, T., Chou, Y.-C., Willems, A. R., Meyer-Schaller, N., Hecht, M.-L., Tyers, M., Peter, M., and Sicheri, F. (2008) Dcn1 Functions as a Scaffold-Type E3 Ligase for Cullin Neddylation, Molecular Cell 29, 23-35.

(76) Scott, D. C., Monda, J. K., Grace, C. R. R., Duda, D. M., Kriwacki, R. W., Kurz, T., and Schulman, B. A. (2010) A Dual E3 Mechanism for Rub1 Ligation to Cdc53, Molecular Cell 39, 784-796.

(77) Zhou, H., Lu, J., Liu, L., Bernard, D., Yang, C.-Y., Fernandez-Salas, E., Chinnaswamy, K., Layton, S., Stuckey, J., Yu, Q., Zhou, W., Pan, Z., Sun, Y., and Wang, S. (2017) A potent small-molecule inhibitor of the DCN1-UBC12 interaction that selectively blocks cullin 3 neddylation, Nature Communications 8, 1150.

(78) Scott, Daniel C., Sviderskiy, Vladislav O., Monda, Julie K., Lydeard, John R., Cho, Shein E., Harper, J. W., and Schulman, Brenda A. (2014) Structure of a RING E3 Trapped in Action Reveals Ligation Mechanism for the Ubiquitin-like Protein NEDD8, Cell 157, 1671-1684.

(79) Mosadeghi, R., Reichermeier, K. M., Winkler, M., Schreiber, A., Reitsma, J. M., Zhang, Y., Stengel, F., Cao, J., Kim, M., Sweredoski, M. J., Hess, S., Leitner, A., Aebersold, R., Peter, M., Deshaies, R. J., and Enchev, R. I. (2016) Structural and kinetic analysis of the COP9-Signalosome activation and the cullin-RING ubiquitin ligase deneddylation cycle, eLife 5, e12102.

(80) Cavadini, S., Fischer, E. S., Bunker, R. D., Potenza, A., Lingaraju, G. M., Goldie, K. N., Mohamed, W. I., Faty, M., Petzold, G., Beckwith, R. E. J., Tichkule, R. B., Hassiepen, U., Abdulrahman, W., Pantelic, R. S., Matsumoto, S., Sugasawa, K., Stahlberg, H., and Thomä, N. H. (2016) Cullin–RING ubiquitin E3 ligase regulation by the COP9 signalosome, Nature 531, 598-603.

(81) Baek, K., Scott, D. C., Henneberg, L. T., King, M. T., Mann, M., and Schulman, B. A. (2023) Systemwide disassembly and assembly of SCF ubiquitin ligase complexes, Cell 186, 1895-1911.e1821.

(82) Reitsma, J. M., Liu, X., Reichermeier, K. M., Moradian, A., Sweredoski, M. J., Hess, S., and Deshaies, R. J. (2017) Composition and Regulation of the Cellular Repertoire of SCF Ubiquitin Ligases, Cell 171, 1326-1339.e1314.

(83) Shaaban, M., Clapperton, J. A., Ding, S., Kunzelmann, S., Mäeots, M.-E., Maslen, S. L., Skehel, J. M., and Enchev, R. I. (2023) Structural and mechanistic insights into the CAND1-mediated SCF substrate receptor exchange, Molecular Cell 83, 2332-2346.e2338.

(84) Bornstein, G., Ganoth, D., and Hershko, A. (2006) Regulation of neddylation and deneddylation of cullin1 in SCF^{Skp2} ubiquitin ligase by F-box protein and substrate, Proceedings of the National Academy of Sciences 103, 11515-11520.

(85) Yumimoto, K., Muneoka, T., Tsuboi, T., and Nakayama, K. I. (2013) Substrate Binding Promotes Formation of the Skp1-Cul1-Fbxl3 (SCF^{Fbxl3}) Protein Complex, Journal of Biological Chemistry 288, 32766-32776.

(86) Pierce, Nathan W., Lee, J. E., Liu, X., Sweredoski, Michael J., Graham, Robert L. J., Larimore, Elizabeth A., Rome, M., Zheng, N., Clurman, Bruce E., Hess, S., Shan, S.-o., and Deshaies, Raymond J. (2013) Cand1 Promotes Assembly of New SCF Complexes through Dynamic Exchange of F Box Proteins, Cell 153, 206-215.

(87) Zemla, A., Thomas, Y., Kedziora, S., Knebel, A., Wood, N. T., Rabut, G., and Kurz, T. (2013) CSN- and CAND1-dependent remodeling of the budding yeast SCF complex, Nature Communications 4, 1641.

(88) Wu, S., Zhu, W., Nhan, T., Toth, J. I., Petroski, M. D., and Wolf, D. A. (2013) CAND1 controls *in vivo* dynamics of the cullin 1-RING ubiquitin ligase repertoire, Nature Communications 4, 1642.

(89) Schmidt, M. W., McQuary, P. R., Wee, S., Hofmann, K., and Wolf, D. A. (2009) F-Box-Directed CRL Complex Assembly and Regulation by the CSN and CAND1, Molecular Cell 35, 586-597.

(90) Gorelik, M., and Sidhu, S. S. (2018) Regulation of SCF E3 ligase activity by Cand1, Biotarget 2.

(91) Galan, J.-M., and Peter, M. (1999) Ubiquitin-dependent degradation of multiple F-box proteins by an autocatalytic mechanism, Proceedings of the National Academy of Sciences 96, 9124-9129.

(92) Zhou, P., and Howley, P. M. (1998) Ubiquitination and Degradation of the Substrate Recognition Subunits of SCF Ubiquitin–Protein Ligases, Molecular Cell 2, 571-580.

(93) Cope, G. A., and Deshaies, R. J. (2006) Targeted silencing of Jab1/Csn5 in human cells downregulates SCF activity through reduction of F-box protein levels, BMC Biochemistry 7, 1.

(94) Lan, H., Tan, M., Zhang, Q., Yang, F., Wang, S., Li, H., Xiong, X., and Sun, Y. (2019) LSD1 destabilizes FBXW7 and abrogates FBXW7 functions independent of its demethylase activity, Proceedings of the National Academy of Sciences 116, 12311-12320.

(95) Yu, H., Zhang, Y., Moss, B. L., Bargmann, B. O. R., Wang, R., Prigge, M., Nemhauser, J. L., and Estelle, M. (2015) Untethering the TIR1 auxin receptor from the SCF complex increases its stability and inhibits auxin response, Nature Plants 1, 14030.

(96) Liu, Y., Nakatsukasa, K., Kotera, M., Kanada, A., Nishimura, T., Kishi, T., Mimura, S., and Kamura, T. (2011) Non–SCF-type F-box protein Roy1/Ymr258c interacts with a Rab5-like GTPase Ypt52 and inhibits Ypt52 function, Molecular Biology of the Cell 22, 1575-1584.

(97) Hermand, D. (2006) F-box proteins: more than baits for the SCF?, Cell Division 1, 30.

(98) Nelson, D. E., Randle, S. J., and Laman, H. (2013) Beyond ubiquitination: the atypical functions of Fbxo7 and other F-box proteins, Open Biology 3, 130131.

(99) Blondel, M., Galan, J. M., Chi, Y., Lafourcade, C., Longaretti, C., Deshaies, R. J., and Peter, M. (2000) Nuclear-specific degradation of Far1 is controlled by the localization of the F-box protein Cdc4, The EMBO Journal 19, 6085-6097-6097.

(100) Lin, H.-K., Wang, G., Chen, Z., Teruya-Feldstein, J., Liu, Y., Chan, C.-H., Yang, W.-L., Erdjument-Bromage, H., Nakayama, K. I., Nimer, S., Tempst, P., and Pandolfi, P. P. (2009) Phosphorylation-dependent regulation of cytosolic localization and oncogenic function of Skp2 by Akt/PKB, Nature Cell Biology 11, 420-432.

(101) Duda, D. M., Borg, L. A., Scott, D. C., Hunt, H. W., Hammel, M., and Schulman, B. A. (2008) Structural Insights into NEDD8 Activation of Cullin-RING Ligases: Conformational Control of Conjugation, Cell 134, 995-1006.

(102) Saha, A., and Deshaies, R. J. (2008) Multimodal Activation of the Ubiquitin Ligase SCF by Nedd8 Conjugation, Molecular Cell 32, 21-31.

(103) Yamoah, K., Oashi, T., Sarikas, A., Gazdoiu, S., Osman, R., and Pan, Z.-Q. (2008) Autoinhibitory regulation of SCF-mediated ubiquitination by human cullin 1's C-terminal tail, Proceedings of the National Academy of Sciences 105, 12230-12235.

(104) Jones, J., Wu, K., Yang, Y., Guerrero, C., Nillegoda, N., Pan, Z.-Q., and Huang, L. (2008) A Targeted Proteomic Analysis of the Ubiquitin-Like Modifier Nedd8 and Associated Proteins, Journal of Proteome Research 7, 1274-1287.

(105) Duda, David M., Olszewski, Jennifer L., Tron, Adriana E., Hammel, M., Lambert, Lester J., Waddell, M. B., Mittag, T., DeCaprio, James A., and Schulman, Brenda A. (2012) Structure of a Glomulin-RBX1-CUL1 Complex: Inhibition of a RING E3 Ligase through Masking of Its E2-Binding Surface, Molecular Cell 47, 371-382.

(106) Crow, A., Hughes, R. K., Taieb, F., Oswald, E., and Banfield, M. J. (2012) The molecular basis of ubiquitin-like protein NEDD8 deamidation by the bacterial effector protein Cif, Proceedings of the National Academy of Sciences 109, E1830-E1838.

(107) Kong, H., Leebens-Mack, J., Ni, W., dePamphilis, C. W., and Ma, H. (2004) Highly Heterogeneous Rates of Evolution in the SKP1 Gene Family in Plants and Animals: Functional and Evolutionary Implications, Molecular Biology and Evolution 21, 117-128.

(108) Yamanaka, A., Yada, M., Imaki, H., Koga, M., Ohshima, Y., and Nakayama, K.-I. (2002) Multiple Skp1-Related Proteins in *Caenorhabditis elegans*: Diverse Patterns of Interaction with Cullins and F-Box Proteins, Current Biology 12, 267-275.

(109) Risseeuw, E. P., Daskalchuk, T. E., Banks, T. W., Liu, E., Cotelesage, J., Hellmann, H., Estelle, M., Somers, D. E., and Crosby, W. L. (2003) Protein interaction analysis of SCF ubiquitin E3 ligase subunits from *Arabidopsis*, The Plant Journal 34, 753-767.

(110) Gagne, J. M., Downes, B. P., Shiu, S.-H., Durski, A. M., and Vierstra, R. D. (2002) The F-box subunit of the SCF E3 complex is encoded by a diverse superfamily of genes in *Arabidopsis*, Proceedings of the National Academy of Sciences 99, 11519-11524.

(111) *Arabidopsis* Interactome Mapping, C., Dreze, M., Carvunis, A.-R., Charloteaux, B., Galli, M., Pevzner, S. J., Tasan, M., Ahn, Y.-Y., Balumuri, P., Barabási, A.-L., Bautista, V., Braun, P., Byrdsong, D., Chen, H., Chesnut, J. D., Cusick, M. E., Dangl, J. L., de los Reyes, C., Dricot, A., Duarte, M., Ecker, J. R., Fan, C., Gai, L., Gebreab, F., Ghoshal, G., Gilles, P., Gutierrez, B. J., Hao, T., Hill, D. E., Kim, C. J., Kim, R. C., Lurin, C., MacWilliams, A., Matrubutham, U., Milenkovic, T., Mirchandani, J., Monachello, D., Moore, J., Mukhtar, M. S., Olivares, E., Patnaik, S., Poulin, M. M., Przulj, N., Quan, R., Rabello, S., Ramaswamy, G., Reichert, P., Rietman, E. A., Rolland, T., Romero, V., Roth, F. P., Santhanam, B., Schmitz, R. J., Shinn, P., Spooner, W., Stein, J., Swamilingiah, G. M., Tam, S., Vandenhaute, J., Vidal, M., Waaijers, S., Ware, D., Weiner, E. M., Wu, S., and Yazaki, J. (2011) Evidence for Network Evolution in an *Arabidopsis* Interactome Map, Science 333, 601-607.

(112) Pasha, A., Subramaniam, S., Cleary, A., Chen, X., Berardini, T., Farmer, A., Town, C., and Provart, N. (2020) Araport Lives: An Updated Framework for *Arabidopsis* Bioinformatics, The Plant Cell 32, 2683-2686.

(113) Mathias, N., Johnson, S., Byers, B., and Goebl, M. (1999) The Abundance of Cell Cycle Regulatory Protein Cdc4p Is Controlled by Interactions between Its F Box and Skp1p, Molecular and Cellular Biology 19, 1759-1767.

(114) Lu, S., Xiong, W., Yi, J., Liu, S., and Zhang, F. (2025) S-phase kinase-associated protein 1 inhibits orbital fibroblasts adipogenesis to improve thyroid-associated ophthalmopathy (TAO), Biochimica et Biophysica Acta (BBA) - Molecular Cell Research 1872, 119937.

(115) Liu, Y.-Q., Wang, X.-L., Cheng, X., Lu, Y.-Z., Wang, G.-Z., Li, X.-C., Zhang, J., Wen, Z.-S., Huang, Z.-L., Gao, Q.-L., Yang, L.-N., Cheng, Y.-X., Tao, S.-C., Liu, J., and Zhou, G.-B. (2015) Skp1 in lung cancer: clinical significance and therapeutic efficacy of its small molecule inhibitors, Oncotarget; Vol 6, No 33.

(116) Wang, Z. A., Singh, D., van der Wel, H., and West, C. M. (2011) Prolyl hydroxylation- and glycosylation-dependent functions of Skp1 in O_2-regulated development of *Dictyostelium*, Developmental Biology 349, 283-295.

(117) Lauinger, L., Flick, K., Yen, J. L., Mathur, R., and Kaiser, P. (2020) Cdc48 cofactor Shp1 regulates signal-induced SCF^{Met30} disassembly, Proceedings of the National Academy of Sciences 117, 21319-21327.

(118) Yen, James L., Flick, K., Papagiannis, Christie V., Mathur, R., Tyrrell, A., Ouni, I., Kaake, Robyn M., Huang, L., and Kaiser, P. (2012) Signal-Induced Disassembly of the SCF Ubiquitin Ligase Complex by Cdc48/p97, Molecular Cell 48, 288-297.

(119) Mathur, R., Yen, J. L., and Kaiser, P. (2015) Skp1 Independent Function of Cdc53/Cul1 in F-box Protein Homeostasis, PLOS Genetics 11, e1005727.

(120) Li, J., Krause, G. J., Gui, Q., Kaushik, S., Rona, G., Zhang, Q., Liang, F.-X., Dhabaria, A., Anerillas, C., Martindale, J. L., Vasilyev, N., Askenazi, M., Ueberheide, B., Nudler, E., Gorospe, M., Cuervo, A. M., and Pagano, M. A noncanonical function of SKP1 regulates the switch between autophagy and unconventional secretion, Science Advances 9, eadh1134.

(121) Beltrao, P., Albanèse, V., Kenner, Lillian R., Swaney, Danielle L., Burlingame, A., Villén, J., Lim, Wendell A., Fraser, James S., Frydman, J., and Krogan, Nevan J. (2012) Systematic Functional Prioritization of Protein Posttranslational Modifications, Cell 150, 413-425.

(122) Kaplan, K. B., Hyman, A. A., and Sorger, P. K. (1997) Regulating the Yeast Kinetochore by Ubiquitin-Dependent Degradation and Skp1p-Mediated Phosphorylation, Cell 91, 491-500.

(123) West, C. M., Kozarov, E., and Teng-umnuay, P. (1997) The cytosolic glycoprotein FP21 of *Dictyostelium discoideum* is encoded by two genes resulting in a polymorphism at a single amino acid position1The fpa1- and fpa2-associated gene sequences of this report have accession numbers of U73685 and U73686.1, Gene 200, 1-10.

(124) Iglesias, M. J., Terrile, M. C., Correa-Aragunde, N., Colman, S. L., Izquierdo-Álvarez, A., Fiol, D. F., París, R., Sánchez-López, N., Marina, A., Calderón Villalobos, L. I. A., Estelle, M., Lamattina, L., Martínez-Ruiz, A., and Casalongué, C. A. (2018) Regulation of SCF^{TIR1}/AFBs E3 ligase assembly by S-nitrosylation of *Arabidopsis* SKP1-like1 impacts on auxin signaling, Redox Biology 18, 200-210.

(125) Hwang, J., Lauinger, L., and Kaiser, P. A.-O. (2025) Distinct Stress Regulators in the CRL Family: Emerging Roles of F-Box Proteins: Cullin-RING Ligases and Stress-Sensing.

(126) Aghajan, M., Jonai, N., Flick, K., Fu, F., Luo, M., Cai, X., Ouni, I., Pierce, N., Tang, X., Lomenick, B., Damoiseaux, R., Hao, R., del Moral, P. M., Verma, R., Li, Y., Li, C., Houk, K. N., Jung, M. E., Zheng, N., Huang, L., Deshaies, R. J., Kaiser, P., and Huang, J. (2010) Chemical genetics screen for enhancers of rapamycin identifies a specific inhibitor of an SCF family E3 ubiquitin ligase, Nature Biotechnology 28, 738-742.

(127) Chan, C.-H., Morrow, John K., Li, C.-F., Gao, Y., Jin, G., Moten, A., Stagg, Loren J., Ladbury, John E., Cai, Z., Xu, D., Logothetis, Christopher J., Hung, M.-C., Zhang, S., and Lin, H.-K. (2013) Pharmacological Inactivation of Skp2 SCF Ubiquitin Ligase Restricts Cancer Stem Cell Traits and Cancer Progression, Cell 154, 556-568.

(128) Gorelik, M., Manczyk, N., Pavlenco, A., Kurinov, I., Sidhu, S. S., and Sicheri, F. (2018) A Structure-Based Strategy for Engineering Selective Ubiquitin Variant Inhibitors of Skp1-Cul1-F-Box Ubiquitin Ligases, Structure 26, 1226-1236.e1223.

(129) West, C. M., and Blader, I. J. (2015) Oxygen sensing by protozoans: how they catch their breath, Current Opinion in Microbiology 26, 41-47.

(130) Sheikh, M. O., Xu, Y., van der Wel, H., Walden, P., Hartson, S. D., and West, C. M. (2015) Glycosylation of Skp1 Promotes Formation of Skp1–Cullin-1–F-box Protein Complexes in *Dictyostelium*, Molecular & Cellular Proteomics 14, 66-80.

(131) Sheikh, M. O., Schafer, C. M., Powell, J. T., Rodgers, K. K., Mooers, B. H. M., and West, C. M. (2014) Glycosylation of Skp1 Affects Its Conformation and Promotes Binding to a Model F-Box Protein, Biochemistry 53, 1657-1669.

(132) Sheikh, M. O., Thieker, D., Chalmers, G., Schafer, C. M., Ishihara, M., Azadi, P., Woods, R. J., Glushka, J. N., Bendiak, B., Prestegard, J. H., and West, C. M. (2017) O_2 sensing–associated glycosylation exposes the F-box–combining site of the *Dictyostelium* Skp1 subunit in E3 ubiquitin ligases, Journal of Biological Chemistry 292, 18897-18915.

(133) Xu, X., Eletsky, A., Sheikh, M. O., Prestegard, J. H., and West, C. M. (2018) Glycosylation Promotes the Random Coil to Helix Transition in a Region of a Protist Skp1 Associated with F-Box Binding, Biochemistry 57, 511-515.

(134) Cantrell, D. A., Urbauer, R. J. B., Kim, H. W., Woods, R. J., Urbauer, J. L., Wood, Z. A., and West, C. M. (2025) Glycosylation Weakens Skp1 Homodimerization in *Toxoplasma gondii* by Interrupting a Fuzzy Interaction, Biochemistry 64(10):2262-2279.

(135) West, C. M. (2003) Evolutionary and functional implications of the complex glycosylation of Skp1, a cytoplasmic/nuclear glycoprotein associated with polyubiquitination, Cellular and Molecular Life Sciences CMLS 60, 229-240.

(136) Gonzalez-Yanes, B., Cicero, J. M., Brown, R. D., and West, C. M. (1992) Characterization of a cytosolic fucosylation pathway in *Dictyostelium*, Journal of Biological Chemistry 267, 9595-9605.

(137) Teng-umnuay, P., Morris, H. R., Dell, A., Panico, M., Paxton, T., and West, C. M. (1998) The Cytoplasmic F-box Binding Protein SKP1 Contains a Novel Pentasaccharide Linked to Hydroxyproline in *Dictyostelium*, Journal of Biological Chemistry 273, 18242-18249.

(138) West, C. M., van der Wel, H., Sassi, S., and Gaucher, E. A. (2004) Cytoplasmic glycosylation of protein-hydroxyproline and its relationship to other glycosylation pathways, Biochimica et Biophysica Acta (BBA) - General Subjects 1673, 29-44.

(139) van der Wel, H., Johnson, J. M., Xu, Y., Karunaratne, C. V., Wilson, K. D., Vohra, Y., Boons, G.-J., Taylor, C. M., Bendiak, B., and West, C. M. (2011) Requirements for Skp1 Processing by

Cytosolic Prolyl 4(trans)-Hydroxylase and α-N-Acetylglucosaminyltransferase Enzymes Involved in O_2 Signaling in *Dictyostelium*, Biochemistry 50, 1700-1713.

(140) West, C. M., van der Wel, H., and Blader, I. J. (2006) Detection of Cytoplasmic Glycosylation Associated with Hydroxyproline, In Methods in Enzymology, pp 389-404, Academic Press.

(141) Rahman, K., Zhao, P., Mandalasi, M., van der Wel, H., Wells, L., Blader, I. J., and West, C. M. (2016) The E3 Ubiquitin Ligase Adaptor Protein Skp1 Is Glycosylated by an Evolutionarily Conserved Pathway That Regulates Protist Growth and Development, Journal of Biological Chemistry 291, 4268-4280.

(142) West, C. M., Wang, Z. A., and van der Wel, H. (2010) A cytoplasmic prolyl hydroxylation and glycosylation pathway modifies Skp1 and regulates O_2-dependent development in *Dictyostelium*, Biochimica et Biophysica Acta (BBA) - General Subjects 1800, 160-171.

(143) Sassi, S., Sweetinburgh, M., Erogul, J., Zhang, P., Teng-umnuay, P., and West, C. M. (2001) Analysis of Skp1 glycosylation and nuclear enrichment in *Dictyostelium*, Glycobiology 11, 283-295.

(144) West, C. M., van der Wel, H., and Wang, Z. A. (2007) Prolyl 4-hydroxylase-1 mediates O_2 signaling during development of *Dictyostelium*, Development 134, 3349-3358.

(145) West, C. M., Scott-Ward, T., Teng-umnuay, P., van der Wel, H., Kozarov, E., and Huynh, A. (1996) Purification and Characterization of an α1,2-L-Fucosyltransferase, Which Modifies the Cytosolic Protein FP21, from the Cytosol of *Dictyostelium*, Journal of Biological Chemistry 271, 12024-12035.

(146) Kozarov, E., van der Wel, H., Field, M., Gritzali, M., Brown, R. D., and West, C. M. (1995) Characterization of FP21, a Cytosolic Glycoprotein from *Dictyostelium*, Journal of Biological Chemistry 270, 3022-3030.

(147) Xu, Y., Brown, K. M., Wang, Z. A., van der Wel, H., Teygong, C., Zhang, D., Blader, I. J., and West, C. M. (2012) The Skp1 Protein from *Toxoplasma* Is Modified by a Cytoplasmic Prolyl 4-Hydroxylase Associated with Oxygen Sensing in the Social Amoeba *Dictyostelium*, Journal of Biological Chemistry 287, 25098-25110.

(148) West, C. M., van der Wel, H., Chinoy, Z., Boons, G.-J., Gauthier, T. J., Taylor, C. M., and Xu, Y. (2015) Generating Isoform-Specific Antibodies: Lessons from Nucleocytoplasmic Glycoprotein Skp1, In Glycoscience: Biology and Medicine (Taniguchi, N., and Endo, T., and Hart, G. W., and Seeberger, P. H., and Wong, C.-H., Eds.), pp 927-934, Springer Japan, Tokyo.

(149) Wang, Z. A., van der Wel, H., Vohra, Y., Buskas, T., Boons, G.-J., and West, C. M. (2009) Role of a Cytoplasmic Dual-function Glycosyltransferase in O_2 Regulation of Development in *Dictyostelium*, Journal of Biological Chemistry 284, 28896-28904.

(150) van der Wel, H., Ercan, A., and West, C. M. (2005) The Skp1 Prolyl Hydroxylase from *Dictyostelium* Is Related to the Hypoxia-inducible Factor-α Class of Animal Prolyl 4-Hydroxylases, Journal of Biological Chemistry 280, 14645-14655.

(151) Liu, T., Abboud, M. I., Chowdhury, R., Tumber, A., Hardy, A. P., Lippl, K., Lohans, C. T., Pires, E., Wickens, J., McDonough, M. A., West, C. M., and Schofield, C. J. (2020) Biochemical and biophysical analyses of hypoxia sensing prolyl hydroxylases from *Dictyostelium discoideum* and *Toxoplasma gondii*, Journal of Biological Chemistry 295, 16545-16561.

(152) Florimond, C., Cordonnier, C., Taujale, R., van der Wel, H., Kannan, N., West Christopher, M., and Blader Ira, J. (2019) A *Toxoplasma* Prolyl Hydroxylase Mediates Oxygen Stress Responses by Regulating Translation Elongation, mBio 10, 10.1128/mbio.00234-00219.

(153) Cockman, M. E., Lippl, K., Tian, Y.-M., Pegg, H. B., Figg, W. D. J., Abboud, M. I., Heilig, R., Fischer, R., Myllyharju, J., Schofield, C. J., and Ratcliffe, P. J. (2019) Lack of activity of recombinant HIF prolyl hydroxylases (PHDs) on reported non-HIF substrates, eLife 8, e46490.

(154) Zhang, D., van der Wel, H., Johnson, J. M., and West, C. M. (2012) Skp1 Prolyl 4-Hydroxylase of *Dictyostelium* Mediates Glycosylation-independent and -dependent Responses to O_2 without Affecting Skp1 Stability, Journal of Biological Chemistry 287, 2006-2016.

(155) Koivunen, P., Hirsilä, M., Kivirikko, K. I., and Myllyharju, J. (2006) The Length of Peptide Substrates Has a Marked Effect on Hydroxylation by the Hypoxia-inducible Factor Prolyl 4-Hydroxylases, Journal of Biological Chemistry 281, 28712-28720.

(156) Teng-umnuay, P., van der Wel, H., and West, C. M. (1999) Identification of a UDP-GlcNAc: Skp1-Hydroxyproline GlcNAc-transferase in the Cytoplasm of *Dictyostelium*, Journal of Biological Chemistry 274, 36392-36402.

(157) van der Wel, H., Morris, H. R., Panico, M., Paxton, T., Dell, A., Kaplan, L., and West, C. M. (2002) Molecular Cloning and Expression of a UDP-N-acetylglucosamine (GlcNAc): Hydroxyproline Polypeptide GlcNAc-transferase That Modifies Skp1 in the Cytoplasm of *Dictyostelium*, Journal of Biological Chemistry 277, 46328-46337.

(158) Wang, F., Metcalf, T., van der Wel, H., and West, C. M. (2003) Initiation of Mucin-type O-Glycosylation in *Dictyostelium* Is Homologous to the Corresponding Step in Animals and Is Important for Spore Coat Function, Journal of Biological Chemistry 278, 51395-51407.

(159) Roper, J. R., and Ferguson, M. A. J. (2003) Cloning and characterisation of the UDP-glucose 4′-epimerase of *Trypanosoma cruzi*, Molecular and Biochemical Parasitology 132, 47-53.

(160) van der Wel, H., Fisher, S. Z., and West, C. M. (2002) A Bifunctional Diglycosyltransferase Forms the Fucα1,2Galβ1,3-Disaccharide on Skp1 in the Cytoplasm of *Dictyostelium*, Journal of Biological Chemistry 277, 46527-46534.

(161) Ketcham, C., Wang, F., Fisher, S. Z., Ercan, A., van der Wel, H., Locke, R. D., Sirajud-Doulah, K., Matta, K. L., and West, C. M. (2004) Specificity of a Soluble UDP-Galactose:Fucoside α1,3-Galactosyltransferase That Modifies the Cytoplasmic Glycoprotein Skp1 in *Dictyostelium*, Journal of Biological Chemistry 279, 29050-29059.

(162) Ercan, A., Panico, M., Sutton-Smith, M., Dell, A., Morris, H. R., Matta, K. L., Gay, D. F., and West, C. M. (2006) Molecular Characterization of a Novel UDP-galactose:Fucoside α3-Galactosyltransferase That Modifies Skp1 in the Cytoplasm of *Dictyostelium*, Journal of Biological Chemistry 281, 12713-12721.

(163) Schafer, C. M., Sheikh, M. O., Zhang, D., and West, C. M. (2014) Novel Regulation of Skp1 by the *Dictyostelium* AgtA α-Galactosyltransferase Involves the Skp1-binding Activity of Its WD40 Repeat Domain, Journal of Biological Chemistry 289, 9076-9088.

(164) Rahman, K., Mandalasi, M., Zhao, P., Sheikh, M. O., Taujale, R., Kim, H. W., van der Wel, H., Matta, K., Kannan, N., Glushka, J. N., Wells, L., and West, C. M. (2017) Characterization of a cytoplasmic glucosyltransferase that extends the core trisaccharide of the *Toxoplasma* Skp1 E3 ubiquitin ligase subunit, Journal of Biological Chemistry 292, 18644-18659.

(165) Mandalasi, M., Kim, H. W., Thieker, D., Sheikh, M. O., Gas-Pascual, E., Rahman, K., Zhao, P., Daniel, N. G., van der Wel, H., Ichikawa, H. T., Glushka, J. N., Wells, L., Woods, R. J., Wood, Z. A., and West, C. M. (2020) A terminal α3-galactose modification regulates an E3 ubiquitin ligase subunit in *Toxoplasma gondii*, Journal of Biological Chemistry 295, 9223-9243.

(166) Kim, H. W., Eletsky, A., Gonzalez, K. J., van der Wel, H., Strauch, E.-M., Prestegard, J. H., and West, C. M. (2020) Skp1 Dimerization Conceals Its F-Box Protein Binding Site, Biochemistry 59, 1527-1536.

(167) Henzl, M. T., Thalmann, I., and Thalmann, R. (1998) OCP2 exists as a dimer in the organ of Corti, Hearing Research 126, 37-46.

(168) Hopf, L. V. M., Baek, K., Klügel, M., von Gronau, S., Xiong, Y., and Schulman, B. A. (2022) Structure of CRL7FBXW8 reveals coupling with CUL1–RBX1/ROC1 for multi-cullin-RING E3-catalyzed ubiquitin ligation, Nature Structural & Molecular Biology 29, 854-862.

(169) Schulman, B. A., Carrano, A. C., Jeffrey, P. D., Bowen, Z., Kinnucan, E. R. E., Finnin, M. S., Elledge, S. J., Harper, J. W., Pagano, M., and Pavletich, N. P. (2000) Insights into SCF ubiquitin ligases from the structure of the Skp1–Skp2 complex, Nature 408, 381-386.

(170) Horn-Ghetko, D., Krist, D. T., Prabu, J. R., Baek, K., Mulder, M. P. C., Klügel, M., Scott, D. C., Ovaa, H., Kleiger, G., and Schulman, B. A. (2021) Ubiquitin ligation to F-box protein targets by SCF–RBR E3–E3 super-assembly, Nature 590, 671-676.

(171) Wong, K., Perpich, J. D., Kozlov, G., Cygler, M., Abu Kwaik, Y., and Gehring, K. (2017) Structural Mimicry by a Bacterial F Box Effector Hijacks the Host Ubiquitin-Proteasome System, Structure 25, 376-383.

(172) Kumanomidou, T., Nishio, K., Takagi, K., Nakagawa, T., Suzuki, A., Yamane, T., Tokunaga, F., Iwai, K., Murakami, A., Yoshida, Y., Tanaka, K., and Mizushima, T. (2015) The Structural Differences between a Glycoprotein Specific F-Box Protein Fbs1 and Its Homologous Protein FBG3, PLOS ONE 10, e0140366.

(173) Kuchay, S., Wang, H., Marzio, A., Jain, K., Homer, H., Fehrenbacher, N., Philips, M. R., Zheng, N., and Pagano, M. (2019) GGTase3 is a newly identified geranylgeranyltransferase targeting a ubiquitin ligase, Nature Structural & Molecular Biology 26, 628-636.

(174) Xing, W., Busino, L., Hinds, T. R., Marionni, S. T., Saifee, N. H., Bush, M. F., Pagano, M., and Zheng, N. (2013) SCF^{FBXL3} ubiquitin ligase targets cryptochromes at their cofactor pocket, Nature 496, 64-68.

(175) Li, Y., and Hao, B. (2010) Structural Basis of Dimerization-dependent Ubiquitination by the SCFFbx4 Ubiquitin Ligase, Journal of Biological Chemistry 285, 13896-13906.

(176) Wong, Sarah J., Gearhart, Micah D., Taylor, Alexander B., Nanyes, David R., Ha, Daniel J., Robinson, Angela K., Artigas, Jason A., Lee, Oliver J., Demeler, B., Hart, P. J., Bardwell, Vivian J., and Kim, Chongwoo A. (2016) KDM2B Recruitment of the Polycomb Group Complex, PRC1.1, Requires Cooperation between PCGF1 and BCORL1, Structure 24, 1795-1801.

(177) Mena, E. L., Jevtić, P., Greber, B. J., Gee, C. L., Lew, B. G., Akopian, D., Nogales, E., Kuriyan, J., and Rape, M. (2020) Structural basis for dimerization quality control, Nature 586, 452-456.

(178) Mizushima, T., Yoshida, Y., Kumanomidou, T., Hasegawa, Y., Suzuki, A., Yamane, T., and Tanaka, K. (2007) Structural basis for the selection of glycosylated substrates by SCF^{Fbs1} ubiquitin ligase, Proceedings of the National Academy of Sciences 104, 5777-5781.

(179) Li, Y., Jin, K., Bunker, E., Zhang, X., Luo, X., Liu, X., and Hao, B. (2018) Structural basis of the phosphorylation-independent recognition of cyclin D1 by the SCF^{FBXO31} ubiquitin ligase, Proceedings of the National Academy of Sciences 115, 319-324.

(180) Simonetta, K. R., Taygerly, J., Boyle, K., Basham, S. E., Padovani, C., Lou, Y., Cummins, T. J., Yung, S. L., von Soly, S. K., Kayser, F., Kuriyan, J., Rape, M., Cardozo, M., Gallop, M. A., Bence, N. F., Barsanti, P. A., and Saha, A. (2019) Prospective discovery of small molecule enhancers of an E3 ligase-substrate interaction, Nature Communications 10, 1402.

(181) Hao, B., Oehlmann, S., Sowa, M. E., Harper, J. W., and Pavletich, N. P. (2007) Structure of a Fbw7-Skp1-Cyclin E Complex: Multisite-Phosphorylated Substrate Recognition by SCF Ubiquitin Ligases, Molecular Cell 26, 131-143.

(182) Shabek, N., Ticchiarelli, F., Mao, H., Hinds, T. R., Leyser, O., and Zheng, N. (2018) Structural plasticity of D3–D14 ubiquitin ligase in strigolactone signalling, Nature 563, 652-656.

(183) Nishio, K., Kawarasaki, T., Sugiura, Y., Matsumoto, S., Konoshima, A., Takano, Y., Hayashi, M., Okumura, F., Kamura, T., Mizushima, T., and Nakatsukasa, K. Defective import of mitochondrial metabolic enzyme elicits ectopic metabolic stress, Science Advances 9, eadf1956.

(184) Chandra Dantu, S., Nathubhai Kachariya, N., and Kumar, A. (2016) Molecular dynamics simulations elucidate the mode of protein recognition by Skp1 and the F-box domain in the SCF complex, Proteins: Structure, Function, and Bioinformatics 84, 159-171.

(185) Bhattacharya, A., Shukla, V. K., Kachariya, N., Preeti, Sehrawat, P., and Kumar, A. (2022) Disorder in the Human Skp1 Structure is the Key to its Adaptability to Bind Many Different Proteins in the SCF Complex Assembly, Journal of Molecular Biology 434, 167830.

(186) Tan, A., Tanner, J. J., and Henzl, M. T. (2008) Energetics of OCP1–OCP2 complex formation, Biophysical Chemistry 134, 64-71.

(187) Williamson, M. P. (2023) Protein Binding: A Fuzzy Concept, Life (Basel), 13(4), 855.

(188) Borgia, A., Borgia, M. B., Bugge, K., Kissling, V. M., Heidarsson, P. O., Fernandes, C. B., Sottini, A., Soranno, A., Buholzer, K. J., Nettels, D., Kragelund, B. B., Best, R. B., and Schuler, B. (2018) Extreme disorder in an ultrahigh-affinity protein complex, Nature 555, 61-66.

(189) Sottini, A., Borgia, A., Borgia, M. B., Bugge, K., Nettels, D., Chowdhury, A., Heidarsson, P. O., Zosel, F., Best, R. B., Kragelund, B. B., and Schuler, B. (2020) Polyelectrolyte interactions enable rapid association and dissociation in high-affinity disordered protein complexes, Nature Communications 11, 5736.

(190) Heidarsson, P. O., Mercadante, D., Sottini, A., Nettels, D., Borgia, M. B., Borgia, A., Kilic, S., Fierz, B., Best, R. B., and Schuler, B. (2022) Release of linker histone from the nucleosome driven by polyelectrolyte competition with a disordered protein, Nature Chemistry 14, 224-231.

(191) Sheikh, M. O., Thieker, D., Chalmers, G., Schafer, C. M., Ishihara, M., Azadi, P., Woods, R. J., Glushka, J. N., Bendiak, B., Prestegard, J. H., and West, C. M. (2017) O_2 sensing associated glycosylation exposes the F-box combining site of the *Dictyostelium* Skp1 subunit in E3 ubiquitin ligases, Journal of Biological Chemistry 292, 18897-18915.

(192) Almond, A., Petersen, B. O., and Duus, J. Ø. (2004) Oligosaccharides Implicated in Recognition Are Predicted to Have Relatively Ordered Structures, Biochemistry 43, 5853-5863.

(193) Sommese, R. F., Sivaramakrishnan, S., Baldwin, R. L., and Spudich, J. A. (2010) Helicity of short E-R/K peptides, Protein Science 19, 2001-2005.

(194) Sivaramakrishnan, S., Spink, B. J., Sim, A. Y. L., Doniach, S., and Spudich, J. A. (2008) Dynamic charge interactions create surprising rigidity in the ER/K α-helical protein motif, Proceedings of the National Academy of Sciences 105, 13356-13361.

(195) Swanson, C. J., and Sivaramakrishnan, S. (2014) Harnessing the Unique Structural Properties of Isolated α-Helices, Journal of Biological Chemistry 289, 25460-25467.

(196) Elbaum, M. B., and Zondlo, N. J. (2014) OGlcNAcylation and Phosphorylation Have Similar Structural Effects in α-Helices: Post-Translational Modifications as Inducible Start and Stop Signals in α-Helices, with Greater Structural Effects on Threonine Modification, Biochemistry 53, 2242-2260.

(197) Karunaratne, C. V., Weldeghiorghis, T. K., West, C. M., and Taylor, C. M. (2014) Conformational Changes Associated with Post-Translational Modifications of Pro143 in Skp1 of *Dictyostelium*—A Dipeptide Model System, Journal of the American Chemical Society 136, 15170-15175.

(198) Shental-Bechor, D., and Levy, Y. (2008) Effect of glycosylation on protein folding: A close look at thermodynamic stabilization, Proceedings of the National Academy of Sciences 105, 8256-8261.

(199) Chaffey, P. K., Guan, X., Chen, C., Ruan, Y., Wang, X., Tran, A. H., Koelsch, T. N., Cui, Q., Feng, Y., and Tan, Z. (2017) Structural Insight into the Stabilizing Effect of O-Glycosylation, Biochemistry 56, 2897-2906.

(200) Luca, V. C., Jude, K. M., Pierce, N. W., Nachury, M. V., Fischer, S., and Garcia, K. C. (2015) Structural basis for Notch1 engagement of Delta-like 4, Science 347, 847-853.

(201) Brister, M. A., Pandey, A. K., Bielska, A. A., and Zondlo, N. J. (2014) OGlcNAcylation and Phosphorylation Have Opposing Structural Effects in tau: Phosphothreonine Induces Particular Conformational Order, Journal of the American Chemical Society 136, 3803-3816.

(202) Hanson, S. R., Culyba, E. K., Hsu, T.-L., Wong, C.-H., Kelly, J. W., and Powers, E. T. (2009) The core trisaccharide of an N-linked glycoprotein intrinsically accelerates folding and enhances stability, Proceedings of the National Academy of Sciences 106, 3131-3136.

(203) Chen, Y.-X., Du, J.-T., Zhou, L.-X., Liu, X.-H., Zhao, Y.-F., Nakanishi, H., and Li, Y.-M. (2006) Alternative O-GlcNAcylation/O-Phosphorylation of Ser16 Induce Different Conformational Disturbances to the N Terminus of Murine Estrogen Receptor β, Chemistry & Biology 13, 937-944.

(204) West, C. M., and Kim, H. W. (2019) Nucleocytoplasmic O-glycosylation in protists, Current Opinion in Structural Biology 56, 204-212.

(205) Baptista, C. G., Lis, A., Deng, B., Gas-Pascual, E., Dittmar, A., Sigurdson, W., West, C. M., and Blader, I. J. (2019) *Toxoplasma* F-box protein 1 is required for daughter cell scaffold function during parasite replication, PLOS Pathogens 15, e1007946.

(206) Al Jewari, C., and Baldauf, S. L. (2023) An excavate root for the eukaryote tree of life, Science Advances 9, eade4973.

(207) Sousa, E. H. S., and Gilles-Gonzalez, M.-A. (2017) Chapter Five - Haem-Based Sensors of O_2: Lessons and Perspectives, In Advances in Microbial Physiology (Poole, R. K., Ed.), pp 235-257, Academic Press.

(208) Gondim, A. C., Guimarães, W. G., and Sousa, E. H. (2022) Heme-Based Gas Sensors in Nature and Their Chemical and Biotechnological Applications, In BioChem, pp 43-63.

(209) Huber, R. J., Williams, R. S. B., and Müller-Taubenberger, A. (2022) Editorial: *Dictyostelium*: A Tractable Cell and Developmental Model in Biomedical Research, Frontiers in Cell and Developmental Biology 10.

(210) Dunn, J. D., Bosmani, C., Barisch, C., Raykov, L., Lefrançois, L. H., Cardenal-Muñoz, E., López-Jiménez, A. T., and Soldati, T. (2018) Eat Prey, Live: *Dictyostelium discoideum* As a Model for Cell-Autonomous Defenses, Frontiers in Immunology 8.

(211) Cochet-Escartin, O., Demircigil, M., Hirose, S., Allais, B., Gonzalo, P., Mikaelian, I., Funamoto, K., Anjard, C., Calvez, V., and Rieu, J.-P. (2021) Hypoxia triggers collective aerotactic migration in *Dictyostelium discoideum*, eLife 10, e64731.

(212) Hirose, S., Hesnard, J., Ghazi, N., Roussel, D., Voituron, Y., Cochet-Escartin, O., Rieu, J.-P., Anjard, C., and Funamoto, K. (2023) The aerotaxis of *Dictyostelium discoideum* is independent of mitochondria, nitric oxide and oxidative stress, Frontiers in Cell and Developmental Biology Volume 11 - 2023.

(213) Carrère, A., d'Alessandro, J., Cochet-Escartin, O., Hesnard, J., Ghazi, N., Rivière, C., Anjard, C., Detcheverry, F., and Rieu, J. P. (2023) Microphase separation of living cells, Nature Communications 14, 796.

(214) Sandonà, D., Gastaldello, S., Rizzuto, R., and Bisson, R. (1995) Expression of Cytochrome c Oxidase during Growth and Development of *Dictyostelium*, Journal of Biological Chemistry 270, 5587-5593.

(215) Sternfeld, J., and Bonner, J. T. (1977) Cell differentiation in *Dictyostelium* under submerged conditions, Proceedings of the National Academy of Sciences 74, 268-271.

(216) Sternfeld, J., and David, C. N. (1981) Oxygen gradients cause pattern orientation in *Dictyostelium* cell clumps, Journal of Cell Science 50, 9-17.

(217) Xu, Y., Wang, Z. A., Green, R. S., and West, C. M. (2012) Role of the Skp1 prolyl-hydroxylation/glycosylation pathway in oxygen dependent submerged development of *Dictyostelium*, BMC Developmental Biology 12, 31.

(218) Bonner, J. T., Compton, K. B., Cox, E. C., Fey, P., and Gregg, K. Y. (1995) Development in one dimension: the rapid differentiation of *Dictyostelium discoideum* in glass capillaries, Proceedings of the National Academy of Sciences 92, 8249-8253.

(219) Hirano, T., Sawai, S., Sawada, Y., and Maeda, Y. (2000) Rapid patterning in 2-D cultures of *Dictyostelium* cells and its relationship to zonal differentiation, Development, Growth & Differentiation 42, 551-560.

(220) Sternfeld, J. (1988) Proportion regulation in *Dictyostelium* is altered by oxygen, Differentiation 37, 173-179.

(221) Chen, Z.-H., Singh, R., Cole, C., Lawal, H. M., Schilde, C., Febrer, M., Barton, G. J., and Schaap, P. (2017) Adenylate cyclase A acting on PKA mediates induction of stalk formation by cyclic diguanylate at the *Dictyostelium* organizer, Proceedings of the National Academy of Sciences 114, 516-521.

(222) Mohanty, S., Lee, S., Yadava, N., Dealy, M. J., Johnson, R. S., and Firtel, R. A. (2001) Regulated protein degradation controls PKA function and cell-type differentiation in *Dictyostelium*, Genes & Development 15, 1435-1448.

(223) West, C. M., and Erdos, G. W. (1988) The expression of glycoproteins in the extracellular matrix of the cellular slime mold *Dictyostelium discoideum*, Cell Differentiation 23, 1-16.

(224) Bonner, J. T., and Lamont, D. S. (2005) Behavior of cellular slime molds in the soil, Mycologia 97, 178-184.

(225) Kirsten, J. H., Xiong, Y., Dunbar, A. J., Rai, M., and Singleton, C. K. (2005) Ammonium transporter C of *Dictyostelium discoideum* is required for correct prestalk gene expression and for regulating the choice between slug migration and culmination, Developmental Biology 287, 146-156.

(226) Yoshino, R., Morio, T., Yamada, Y., Kuwayama, H., Sameshima, M., Tanaka, Y., Sesaki, H., and Iijima, M. (2007) Regulation of Ammonia Homeostasis by the Ammonium Transporter AmtA in *Dictyostelium discoideum*, Eukaryotic Cell 6, 2419-2428.

(227) Schindler, J., and Sussman, M. (1977) Ammonia determines the choice of morphogenetic pathways in *Dictyostelium discoideum*, Journal of Molecular Biology 116, 161-169.

(228) Singleton, C. K., Zinda, M. J., Mykytka, B., and Yang, P. (1998) The Histidine Kinase dhkC Regulates the Choice between Migrating Slugs and Terminal Differentiation in *Dictyostelium discoideum*, Developmental Biology 203, 345-357.

(229) Siegert, F., and Weijer, C. J. (1992) Three-dimensional scroll waves organize *Dictyostelium* slugs, Proceedings of the National Academy of Sciences 89, 6433-6437.

(230) Loomis, W. F. (2015) Genetic control of morphogenesis in *Dictyostelium*, Developmental Biology 402, 146-161.

(231) Newell, P. C., and Ross, F. M. (1982) Genetic Analysis of the Slug Stage of *Dictyostelium discoideum*, Microbiology 128, 1639-1652.

(232) Smith, T. S., Pineda, J. M., Donaghy, A. C., and Damer, C. K. (2010) Copine A plays a role in the differentiation of stalk cells and the initiation of culmination in *Dictyostelium* development, BMC Developmental Biology 10, 59.

(233) Wong, M., Sun, Y., Xi, Z., Milazzo, G., Poulos, R. C., Bartenhagen, C., Bell, J. L., Mayoh, C., Ho, N., Tee, A. E., Chen, X., Li, Y., Ciaccio, R., Liu, P. Y., Jiang, C. C., Lan, Q., Jayatilleke, N., Cheung, B. B., Haber, M., Norris, M. D., Zhang, X. D., Marshall, G. M., Wang, J. Y., Hüttelmaier, S., Fischer, M., Wong, J. W. H., Xu, H., Perini, G., Dong, Q., George, R. E., and Liu, T. (2019) JMJD6 is a tumorigenic factor and therapeutic target in neuroblastoma, Nature Communications 10, 3319.

(234) Mantri, M., Krojer, T., Bagg, E. A., Webby, C. J., Butler, D. S., Kochan, G., Kavanagh, K. L., Oppermann, U., McDonough, M. A., and Schofield, C. J. (2010) Crystal Structure of the 2-Oxoglutarate- and Fe(II)-Dependent Lysyl Hydroxylase JMJD6, Journal of Molecular Biology 401, 211-222.

(235) Böttger, A., Islam, M. S., Chowdhury, R., Schofield, Christopher J., and Wolf, A. (2015) The oxygenase Jmjd6–a case study in conflicting assignments, Biochemical Journal 468, 191-202.

(236) Attias, M., Teixeira, D. E., Benchimol, M., Vommaro, R. C., Crepaldi, P. H., and De Souza, W. (2020) The life-cycle of *Toxoplasma gondii* reviewed using animations, Parasites & Vectors 13, 588.

(237) Centers for Disease Control and Prevention (CDC). *Toxoplasmosis*. In *Parasites*; Centers for Disease Control and Prevention: Atlanta, GA, 2024.
https://www.cdc.gov/parasites/toxoplasmosis/

(238) Skariah, S., McIntyre, M. K., and Mordue, D. G. (2010) *Toxoplasma gondii*: determinants of tachyzoite to bradyzoite conversion, Parasitology Research 107, 253-260.

(239) Molan, A., Nosaka, K., Hunter, M., and Wang, W. (2019) Global status of *Toxoplasma gondii* infection: systematic review and prevalence snapshots, Trop Biomed.;36(4), 898-925.

(240) Nahid, D. S., Coffey, K. A., Bei, A. K., and Cordy, R. J. (2024) Understanding the significance of oxygen tension on the biology of *Plasmodium falciparum* blood stages: From the human body to the laboratory, PLOS Pathogens 20, e1012514.

(241) Smardon, A. M., Nasab, N. D., Tarsio, M., Diakov, T. T., and Kane, P. M. (2015) Molecular Interactions and Cellular Itinerary of the Yeast RAVE (Regulator of the H+-ATPase of Vacuolar and Endosomal Membranes) Complex, Journal of Biological Chemistry 290, 27511-27523.

(242) Brace, E. J., Parkinson Leah, P., and Fuller Robert, S. (2006) Skp1p Regulates Soi3p/Rav1p Association with Endosomal Membranes but Is Not Required for Vacuolar ATPase Assembly, Eukaryotic Cell 5, 2104-2113.

(243) Seol, J. H., Shevchenko, A., Shevchenko, A., and Deshaies, R. J. (2001) Skp1 forms multiple protein complexes, including RAVE, a regulator of V-ATPase assembly, Nature Cell Biology 3, 384-391.

(244) Kursel, L. E., Goktepe, K., and Rog, O. (2024) The structural role of Skp1 in the synaptonemal complex is conserved in nematodes, Genetics 228, iyae153.

(245) Blundon, J. M., Cesar, B. I., Bae, J. W., Čavka, I., Haversat, J., Ries, J., Köhler, S., and Kim, Y. (2024) Skp1 proteins are structural components of the synaptonemal complex in *C. elegans*, Science Advances 10, eadl4876.

(246) Willhoft, O., Kerr, R., Patel, D., Zhang, W., Al-Jassar, C., Daviter, T., Millson, S. H., Thalassinos, K., and Vaughan, C. K. (2017) The crystal structure of the Sgt1-Skp1 complex: the link between Hsp90 and both SCF E3 ubiquitin ligases and kinetochores, Scientific Reports 7, 41626.

(247) Leber, V., Nans, A., and Singleton, M. R. (2018) Structural basis for assembly of the CBF3 kinetochore complex, The EMBO Journal 37, 269-281-281.

(248) Santelli, E., Leone, M., Li, C., Fukushima, T., Preece, N. E., Olson, A. J., Ely, K. R., Reed, J. C., Pellecchia, M., Liddington, R. C., and Matsuzawa, S.-i. (2005) Structural Analysis of Siah1-Siah-interacting Protein Interactions and Insights into the Assembly of an E3 Ligase Multiprotein Complex, Journal of Biological Chemistry 280, 34278-34287.

(249) Bhattacharya, S., Lee, Y.-T., Michowski, W., Jastrzebska, B., Filipek, A., Kuznicki, J., and Chazin, W. J. (2005) The Modular Structure of SIP Facilitates Its Role in Stabilizing Multiprotein Assemblies, Biochemistry 44, 9462-9471.

(250) Farrás, R., Ferrando, A., Jásik, J., Kleinow, T., Ökrész, L., Tiburcio, A., Salchert, K., del Pozo, C., Schell, J., and Koncz, C. (2001) SKP1–SnRK protein kinase interactions mediate proteasomal binding of a plant SCF ubiquitin ligase, The EMBO Journal 20, 2742-2756-2756.

(251) Melville, M. W., McClellan, A. J., Meyer, A. S., Darveau, A., and Frydman, J. (2003) The Hsp70 and TRiC/CCT Chaperone Systems Cooperate *In Vivo* To Assemble the Von Hippel-Lindau Tumor Suppressor Complex, Molecular and Cellular Biology 23, 3141-3151.

(252) Yam, A. Y., Xia, Y., Lin, H.-T. J., Burlingame, A., Gerstein, M., and Frydman, J. (2008) Defining the TRiC/CCT interactome links chaperonin function to stabilization of newly made proteins with complex topologies, Nature Structural & Molecular Biology 15, 1255-1262.

(253) Wang, R., Zhang, Y., Kieffer, M., Yu, H., Kepinski, S., and Estelle, M. (2016) HSP90 regulates temperature-dependent seedling growth in *Arabidopsis* by stabilizing the auxin co-receptor F-box protein TIR1, Nature Communications 7, 10269.

(254) Nelson, D. E., and Laman, H. (2011) A Competitive Binding Mechanism between Skp1 and Exportin 1 (CRM1) Controls the Localization of a Subset of F-box Proteins, Journal of Biological Chemistry 286, 19804-19815.

(255) Reiterer, V., Figueras-Puig, C., Le Guerroue, F., Confalonieri, S., Vecchi, M., Jalapothu, D., Kanse, S. M., Deshaies, R. J., Di Fiore, P. P., Behrends, C., and Farhan, H. (2017) The pseudophosphatase STYX targets the F-box of FBXW7 and inhibits SCF^{FBXW7} function, The EMBO Journal 36, 260-273-273.

(256) Willems, A. R., Schwab, M., and Tyers, M. (2004) A hitchhiker's guide to the cullin ubiquitin ligases: SCF and its kin, Biochimica et Biophysica Acta (BBA) - Molecular Cell Research 1695, 133-170.

(257) Ennis, H. L., Dao, D. N., Pukatzki, S. U., and Kessin, R. H. (2000) *Dictyostelium* amoebae lacking an F-box protein form spores rather than stalk in chimeras with wild type, Proceedings of the National Academy of Sciences 97, 3292-3297.

(258) Nelson, M. K., Clark, A., Abe, T., Nomura, A., Yadava, N., Funair, C. J., Jermyn, K. A., Mohanty, S., Firtel, R. A., and Williams, J. G. (2000) An F-Box/WD40 Repeat-Containing Protein Important for *Dictyostelium* Cell-Type Proportioning, Slug Behaviour, and Culmination, Developmental Biology 224, 42-59.

(259) Ennis, H. L., Dao, D. N., Wu, M. Y., and Kessin, R. H. (2003) Mutation of the *Dictyostelium* fbxA Gene Affects Cell-Fate Decisions and Spatial Patterning, Protist 154, 419-429.

(260) Wolf, Jason B., Howie, Jennifer A., Parkinson, K., Gruenheit, N., Melo, D., Rozen, D., and Thompson, Christopher R. L. (2015) Fitness Trade-offs Result in the Illusion of Social Success, Current Biology 25, 1086-1090.

(261) Tekinay, T., Ennis Herbert, L., Wu Mary, Y., Nelson, M., Kessin Richard, H., and Ratner David, I. (2003) Genetic Interactions of the E3 Ubiquitin Ligase Component FbxA with Cyclic AMP Metabolism and a Histidine Kinase Signaling Pathway during *Dictyostelium discoideum* Development, Eukaryotic Cell 2, 618-626.

(262) Boland, A. W., Gas-Pascual, E., van der Wel, H., Kim, H. W., and West, C. M. (2023) Synergy between a cytoplasmic vWFA/VIT protein and a WD40-repeat F-box protein controls development in *Dictyostelium*, Frontiers in Cell and Developmental Biology 11.

(263) Zhang, D., Iyer, L. M., and Aravind, L. (2011) A novel immunity system for bacterial nucleic acid degrading toxins and its recruitment in various eukaryotic and DNA viral systems, Nucleic Acids Research 39, 4532-4552.

(264) Sreenivasamurthy, S. K., Baptista, C. G., West, C. M., Blader, I. J., and Dvorin, J. D. (2025) PfFBXO1 is essential for inner membrane complex formation in *Plasmodium falciparum* during both asexual and transmission stages, Communications Biology 8, 190.

(265) Baptista, C. G., Hosking, S., Gas-Pascual, E., Ciampossine, L., Abel, S., Hakimi, M.-A., Jeffers, V., Le Roch, K., West, C. M., and Blader, I. J. (2024) The *Toxoplasma gondii* F-Box Protein L2 Functions as a Repressor of Stage Specific Gene Expression, PLOS Pathogens 20, e1012269.

(266) Emberley, E. D., Mosadeghi, R., and Deshaies, R. J. (2012) Deconjugation of Nedd8 from Cul1 Is Directly Regulated by Skp1-F-box and Substrate, and the COP9 Signalosome Inhibits Deneddylated SCF by a Noncatalytic Mechanism, Journal of Biological Chemistry 287, 29679-29689.

(267) Schulze-Niemand, E., and Naumann, M. (2023) The COP9 signalosome: A versatile regulatory hub of Cullin-RING ligases, Trends in Biochemical Sciences 48, 82-95.

(268) Chinoy, Z. S., Schafer, C. M., West, C. M., and Boons, G.-J. (2015) Chemical Synthesis of a Glycopeptide Derived from Skp1 for Probing Protein Specific Glycosylation, Chemistry – A European Journal 21, 11779-11787.

(267) NIAID Visual & Medical Arts. (10/7/2024). Human Anatomy. NIAID NIH BIOART Source. bioart.niaid.nih.gov/bioart/519

CHAPTER 2

GLYCOSYLATION WEAKENS SKP1 HOMODIMERIZATION IN *TOXOPLASMA GONDII* BY INTERRUPTING A FUZZY INTERACTION

Cantrell, D. A., Urbauer, R. J. B., Kim, H. W., Woods, R. J., Urbauer, J. L., Wood, Z. A., and West, C. M. (2025) Glycosylation Weakens Skp1 Homodimerization in *Toxoplasma gondii* by Interrupting a Fuzzy Interaction, Biochemistry 64(10):2262-2279.
Reprinted here with permission of publisher.

ABSTRACT

Skp1/Cullin1/F-Box protein (SCF) complexes represent a major class of E3 ubiquitin ligases responsible for proteomic control throughout eukaryotes. Target specificity is mediated by a large set of F-box proteins (FBPs) whose F-box domains interact with Skp1 in a conserved, well-organized fashion. In the social amoeba *Dictyostelium*, Skp1 is regulated by oxygen-dependent glycosylation which alters Skp1's FBP interactome and inhibits homodimerization that is mediated in part by an ordered interface which overlaps with that of FBPs. Based on sedimentation velocity experiments, Skp1 from the intracellular pathogen *Toxoplasma gondii* exhibits a homodimerization K_d comparable to that of a previously measured FBP/Skp1 interaction. Glycosylation of Skp1's disordered C-terminal region (CTR) distal to the ordered homodimer interface significantly weakens Skp1 homodimerization, an effect reproduced by CTR deletion. Replacement with a randomized CTR sequence retains high affinity excluding an extension of the ordered dimer interface. Substitution by poly-serine weakens the homodimer to a degree equal to its deletion, indicating a composition dependent effect. The contribution of the CTR to Skp1 homodimerization is canceled by high salt consistent with an electrostatic mechanism. All-atom molecular dynamics simulations suggest that the CTR promotes homodimerization via charge cluster interactions. Taken together, the data indicate that glycosylation weakens homodimerization by disrupting a C-terminal fuzzy interaction that functions in tandem with the ordered dimer interface, thereby freeing Skp1 for FBP binding. Thus, the CTR contributes to Skp1/Skp1 and Skp1/FBP interactions via independent mechanisms that are each influenced by O_2, indicating multiple constraints on the evolution of its sequence.

ABBREVIATIONS: AUC, analytical ultracentrifugation; CD, circular dichroism; CTR, C-terminal region; DdSkp1, Skp1 from *Dictyostelium discoideum*; GGlFGGn-

Skp1, fully glycosylated Skp1, with a GalGlcFucGalGlcNAc-glycan at Hyp154; MALDI-TOF-MS, matrix assisted laser desorption ionization time-of-flight mass spectrometry; MD, molecular dynamics; Skp1-FL, full-length Skp1 with a Ser-Met extension N-terminal to the normal Ser N-terminus, TgSkp1, Skp1 from *Toxoplasma gondii*

INTRODUCTION

The local concentrations of O_2 that surround cells provide important information regarding metabolic potential, oxidative risks, and positional information [1]. In particular, the sensing of O_2 gradients can assist free-living protists to seek optimal niches, pathogenic protists to home to favorable locations, and individual cells of multicellular organisms to form patterns [2]. As a specific example, the apicomplexan pathogen *Toxoplasma gondii*, upon oral ingestion, navigates a complex trajectory from its entry via the alimentary canal to achieve chronic and latent infections in distant target tissues, and gradients of O_2 concentrations are likely to provide guidance. *Toxoplasma gondii* is an obligate intracellular parasite and the causative agent for Toxoplasmosis [3]. Infection poses a major threat to the fetus of previously unexposed pregnant women, and for immune compromised individuals poses a serious risk of debilitating injury of the brain and eyes. Following progression from an initial acute infection, healthy individuals progress to a chronic phase owing to immune control. An estimated 11% of the United States population over the age of 6 is thought to be latently infected with *Toxoplasma gondii*, and the frequency approaches 80% in some Western countries. Persistent latent infections mean that once individuals become infected, they are at risk of significant life-threatening disease if they become immune compromised later

in life. This threat is exacerbated by limited treatment options for clearing persistent *Toxoplasma* infections forcing immune compromised individuals to undergo treatment for life [3].

A conserved prolyl hydroxylase, from which human PHD2 likely evolved [4], has been implicated in O_2-sensing in the social soil amoeba *Dictyostelium discoideum*, an unrelated protist that is more closely related to metazoans. By using O_2 as a co-substrate, PhyA regulates the O_2 checkpoint for a process called culmination, when multicellular *Dictyostelium* slugs commit to converting into sessile fruiting bodies after migration to the O_2-rich surface of the soil [2,5,6]. The *Toxoplasma* ortholog regulates fitness in cell culture [7] and dissemination from the gut in a mouse infection model [8]. In both organisms, PhyA specifically modifies a conserved Pro residue of Skp1, a subunit of the SCF (Skp1/cullin-1/F-box protein/Rbx1) class of E3 ubiquitin ligases that generate poly-ubiquitin tags that target proteins for proteasomal degradation. Target protein specificity is mediated by dozens (or more) of F-box proteins (FBPs) serving as substrate receptors and, in some cases, the generation of degron-inducing posttranslational modifications of the protein target [9].

The mechanism of PhyA's action is unclear, but several clues have emerged. In both organisms, the enzyme modulates the FBP interactome of Skp1 [10-12] and is associated with differential abundance of select FBPs by a mechanism that appears to involve their degradation [12]. Another clue is that hydroxylation inhibits the homodimerization of *Dictyostelium* Skp1 [13], which is competitive with FBP-Skp1 interactions [14]. Other evidence for the significance of dimerization comes from recent studies in nematode worms, where Skp1 paralogs are specialized for an essential non-SCF role in meiotic synaptonemic complexes that require their homodimerization [15,16]. The action of PhyA enables the posttranslational assembly on the resulting hydroxyproline (Hyp) of a defined linear pentasaccharide of almost identical sequence

on Skp1 from both organisms as a result in part of convergent evolution [2]. Genetic evidence indicates that glycosylation mediates the action of PhyA [10,11], leading us to further investigate the mechanism by which the oligosaccharide influences the structural and biochemical properties of Skp1.

Skp1 is highly conserved throughout eukaryotic phylogeny, but its post-translational hydroxylation and glycosylation appears to be confined to the protist domain of life [17]. Crystallographic evidence from complexes with FBPs from animals, yeast and plants reveals four C-terminal α-helices that comprise subsite-1 and subsite-2 of the interface with F-box domains [18], and an upstream N-terminal region that docks to the cullin-1 scaffold **(Figure 2.1A)**. Cul1 in turn links to the Ub-charged E2 via the RING-protein Rbx1 [19] to complete the horseshoe-shaped SCF Ub-ligase with the target docked at its open end. The Hyp-linked glycan, which is located at the start of the final C-terminal helix-8 that comprises subsite-2, is expected to reside on the backside of the F-box interface. In its free form, NMR and AUC studies show that both mammalian and *Dictyostelium* Skp1 exist as a homodimer with a K_d in the 1-2.5 μM range [14,20,21]. Detailed studies of DdSkp1 reveal that its individual monomers fold in a similar manner to that seen in complexes with FBPs up through α-helix-6. However, the downstream region that can fold as α-helices-7 and -8 with FBPs is partially disordered, and the organization of this C-terminal region (CTR) is influenced by O_2-dependent glycosylation [13,14,21]. A truncated version lacking the CTR retains the ability to homodimerize, with an interface that involves α-helices-5 and -6 and therefore competes with F-box binding. The semiparallel orientation of the dimer-mates would orient the missing C-termini in juxtaposition with one another. Because of its intrinsic disorder in the homodimer, we hypothesized that the CTR contributes to homodimerization by a mechanism different from that used to bind FBPs and distinctly modulated by glycosylation.

To confirm Skp1's homodimerization and the influence of its glycan, we turned our attention from *Dictyostelium* to *Toxoplasma* Skp1 and at the same time quantified the role of the CTR and its glycosylation. Like DdSkp1, truncated TgSkp1 lacking the CTR homodimerizes with a μM K_d. Significantly, the presence of the CTR contributes over an estimated order of magnitude decrease in the K_d rendering it potentially competitive with FBP binding [22]. Our further biochemical studies characterized a contribution of the CTR to homodimerization based on criteria predicted for a charge-based fuzzy interaction [23-25], which was supported by all-atom molecular dynamics (MD) simulations, and we quantified the inhibitory role of the glycan. We propose that O_2-dependent glycosylation of Skp1 interferes with the charge-based fuzzy interaction thereby providing a facile mechanism to increase the availability of monomeric Skp1 for its physiological role in SCF complex formation.

MATERIALS AND METHODS

Generation of Skp1 Variants.

Full-length His_6-TgSkp1 (UniProt A0A0F7UNE6) was expressed from pNIC28-HisTEVTgSkp1 as previously described [26]. Staggered primers were designed to delete the CTR or replace the internal loop **(Figure 2.S19)** using PCR reactions with GXL-Prime STAR polymerase (TaKaRa) or SuperFi Platinum polymerase (Thermo-Fisher). Clones were screened by colony PCR utilizing primers specific for the pNIC28 plasmid **(Figure 2.S19)**. Positive clones were sequenced utilizing full plasmid nanopore sequencing or Sanger Sequencing initiating from both directions.

The sequence for TgSkp1's C-terminal region (CTR) was randomized 6 times using the Hanging Hyena word scrambler [27]. Scrambled sequences were appended to the TgSkp1-ΔCTR

sequence and analyzed at the NetSurfP-2.0 server to evaluate propensity to form ordered secondary structure [28]. Two sequences least likely to form ordered secondary structure were codon optimized and synthesized by GenScript in the pNIC28 plasmid **(Figure 2.S20)** [29]. Similarly, the poly-Ser TgSkp1 variant was created by replacing the CTR coding region with Ser codons.

Purification of Skp1 Constructs.

The Skp1 expression constructs were transformed into ER2566 strain *E. coli* for protein production. Clones were grown in Terrific Broth at 37°C in the presence of 50 µg/ml kanamycin [29]. After reaching an OD_{600} of 1.0, cultures were shifted to 18°C for 30 min and then induced by addition of IPTG to 500 µM for 16-18 h. Cells were recovered by centrifugation and frozen at -80°C.

Pellets were resuspended in Lysis Buffer (50 mM Na/K phosphate (pH 7.4), 300 mM NaCl, 5 mM benzamidine, 10 µg/ml leupeptin, 10 µg/ml aprotinin, and 0.5 µg/ml pepstatin A) or Super Lysis Buffer (100 mM Na/K phosphate (pH 7.4), 150 mM NaCl, 0.5 M D-sorbitol, 1 M glycine betaine, 0.7 M trehalose, 5 mM benzamidine, 10 µg/ml leupeptin, 10 µg/ml aprotinin, and 0.5 µg/ml pepstatin A). Suspended pellets were lysed using 3 passes through a French Pressure cell before centrifugation at 27,000 × g for 40 min. Supernatants were further clarified by spinning at 100,000 × g for 70 min before loading onto a 5 ml Talon column (TaKaRa). The column was washed with 50 ml each of Wash Buffer (50 mM Na/K phosphate (pH 7.4), 300 mM NaCl), High Salt Buffer (50 mM Na/K phosphate (pH 7.4), 1 M NaCl), Glycerol Buffer (50 mM Na/K phosphate (pH 7.4), 300 mM NaCl, 10% (v/v) glycerol), and Wash Buffer. Bound protein was then eluted with Elution Buffer (50 mM Na/K phosphate (pH 7.4), 300 mM NaCl, 300 mM imidazole (pH 7.4)). Eluted proteins were immediately dialyzed into 50 mM Tris-HCl (pH 7.4), 150 mM

NaCl, 0.1 mM EDTA (pH 8.0) before being dialyzed into 50 mM Tris-HCl (pH 7.4), 150 mM NaCl, 1 mM DTT. TEV protease cleavage was performed as previously described [26], and after 2 consecutive dialysis steps against Wash Buffer, samples were passed over a second 5 ml Talon Column, concentrated to 50 mg/ml by centrifugal ultrafiltration, divided into 0.5 ml aliquots, and frozen in liquid nitrogen for later use. Protein properties including extinction coefficients used in quantifying the constructs were calculated using the ProtParam ExPASy server [30]. Skp1 constructs prepared in this way yielded greater than 20 mg/l.

Purification of Skp1 Glycosyltransferases.

TgGlt1 and DdPgtA were purified as previously described [31,32]. TgGat1 was expressed with an autoinduction method utilizing lactose allowing for slow expression [33,34]. *E. coli* Gold cells containing pET15-His-TEV-GT8a(Gat1) [33,34] were grown to confluence in 200 ml of Luria Broth starter culture supplemented with 100 µg/ml ampicillin for ~16 h. 50 ml of the starter culture was used to inoculate 1 l of Autoinduction medium (3 g/l KH_2PO_4, 6 g/l Na_2HPO_4 (pH 7.2), 20 g/l Tryptone, 5 g/l Bacto yeast extract, 5 g/l NaCl, 100 µg/ml ampicillin, 0.52 g/l D-glucose, 2.1 g/l lactose, 0.6% (v/v) glycerol). Cultures were grown at 37°C for 2 h before shifting to 18°C for 46 additional h. Cells were pelleted by centrifugation at 5,000 × g for 10 min and frozen at -80°C until purification as described above for Skp1. TgGat1 was typically recovered at >20 mg/l of culture.

Modification of TgSkp1.

Gn-TgSkp1 was purified as above, and its modification confirmed using MALDI-TOF-MS. For analysis, samples were desalted, spotted on a plate with sinapinic acid using the sandwich

method, air dried, and analyzed in an ABI MALDI-TOF MS operated in linear positive ion mode. Gn-TgSkp1 (0.12 mg/ml) was incubated for 16 h at room temperature with 5 µg/ml DdPgtA in 24 µM UDP-Gal (4-fold excess over TgSkp1), 42 µM GDP-Fuc (7-fold excess over TgSkp1), 10 µg/ml leupeptin, 10 µg/ml aprotinin, 10 mM $MgCl_2$, 2 mM $MnCl_2$, 0.1% (v/v) Tween-20, 50 mM Tris-HCl (pH 7.4), 5 mM DTT, 120 mM NaCl, and 0.12 U/ml Shrimp alkaline phosphatase, with modification monitored using MALDI-TOF-MS. The reaction mixture was loaded onto a 1-ml Ni-Sepharose column (GE Healthcare), which was then washed with 50 mM Na/K phosphate (pH 7.5), 300 mM NaCl, 20 mM imidazole, and eluted with 50 mM Na/K phosphate (pH 7.5), 300 mM NaCl, 500 mM imidazole. Skp1 was concentrated to 3 mg/ml and buffer exchanged into 50 mM HEPES-NaOH (pH 8.0) using a 10k-Da cutoff centrifugal ultrafiltration device. FGGn-TgSkp1 (0.77 mg/ml) was incubated for 16 h at 37°C with 0.05 mg/ml TgGlt1, 280 µM UDP-Glc (8-fold excess over Skp1), 10 µg/ml leupeptin, 10 µg/ml aprotinin, 2 mM $MgCl_2$, 2 mM $MnCl_2$, 50 mM HEPES-NaOH (pH 8.0), 5 mM DTT, and 2.4 U/ml Shrimp Alkaline Phosphatase. After confirmation of conversion to GlFGGn-TgSkp1 by MALDI-TOF-MS, the sample was buffer exchanged using a 10-kDa cutoff centrifugal ultrafiltration device to 50 mM HEPES-NaOH (pH 7.0), concentrated to 2 mg/ml, incubated at 35 µM (0.7mg/ml) with 1.75 µM (0.07 mg/ml) TgGat1, 140 µM UDP-Gal (4-fold excess over Skp1), 10 µg/ml aprotinin, 10 µg/ml leupeptin, 2 mM $MnCl_2$, 2 mM $MgCl_2$, 0.2% Tween20, 50 mM HEPES-NaOH (pH 7.0), 5 mM DTT, and 0.1 U/ml Shrimp Alkaline Phosphatase for 16 h at 37°C, and checked using MALDI-TOF-MS to confirm complete conversion to GGlFGGn-TgSkp1. TEV cleavage occurred concurrently with the TgGlt1 and TgGat1 reactions on account of inadvertent contamination from TEV-treatment of Glt1. The sample was then purified over a 5-ml HiTrap Q HP ion exchange column (Cytiva) followed by a Superdex 75 (16/600) preparative gel filtration column (Cytiva) into 50 mM K phosphate (pH 7.4),

25 mM KCl, and checked for purity using MALDI-TOF-MS and SDS-PAGE **(Figures 2.2B,C)**. SDS-PAGE was performed using InVitrogen NuPage preformed 4-12% SDS-PAGE gels in MES buffer, and gels were stained in Coomassie Brilliant Blue.

Sedimentation Velocity Experiments.

Skp1 aliquots were thawed at room temperature, supplemented with 1 mM Na EDTA (pH 8.0), and 450 µl was re-run on a Superdex 75 (16/600) column in freshly degassed 50 mM K phosphate (pH 7.4), 25 mM KCl. The peak fraction was serially diluted in the same buffer, and aliquots were loaded into 12 mm double-sector Epon centerpieces with quartz windows before equilibration for 2 h at 20°C. Samples were centrifuged on a Beckman Optima XLA Analytical Ultracentrifuge at 50,000 RPM at 20°C, and absorbance measurements were collected at 215 nm, 230 nm, 280 nm, or 295 nm (depending on the concentration) with a 0.003 cm step size. Buffer and protein parameters were calculated using SenNTerp and c(s) distributions were modeled using SedFit [36,37]. Data were modeled as a continuous c(s) distribution and fitted using baseline, meniscus, frictional coefficient, and noise parameters. Distributions were overlayed in Gussi and the region corresponding to the monomer and dimer species were integrated to determine the average S_w position of each distribution [38]. These values were plotted in SedPhat where a Monomer-Dimer self-association model was utilized to derive the affinity of each Skp1 construct [39]. Predicted S_w values for the monomer and dimer species were obtained using HYDROPRO40 using models generated using Modeler [41], SwissModel [42], or MD simulations utilizing DdSkp1ΔloopΔCTR (PDB: 6V88) as the template.

Circular Dichroism and Thermal Melts.

Skp1 was dialyzed overnight against degassed 20 mM K phosphate (pH 7.5), 10 mM KCl, 1 mM DTT, and diluted to 5-13 μM based on A_{280} in a UV-Vis spectrophotometer. Thermal stabilities were assessed by measuring temperature induced unfolding. Unfolding was followed using circular dichroism (CD) by monitoring the ellipticity at 222 nm at 1 °C intervals as the proteins were heated from 20 °C to 90 °C at a rate of 1 °C per min. Refolding (90 °C to 20 °C) was followed in the same manner. Far UV CD spectra were acquired at 20 °C before unfolding, at 90 °C, and again at 20 °C upon refolding. Data were collected from 260 nm to 190 nm in 1 nm increments with a scan rate of 100 nm/min, with four spectra averaged to give a final spectrum. CD measurements were performed using a Jasco J-715 spectropolarimeter with a Peltier temperature controller and a cuvette with a 1 mm path length. Thermal unfolding experiments were performed 2-3 times for each of the five protein constructs. As described previously [43], the fractions of folded and unfolded states were determined at each temperature and the Gibbs-Helmholtz equation was used to describe the thermodynamics as a function of temperature. For all proteins the heat capacity was assumed to be equal to zero. Data fitting employed the Levenberg-Marquardt algorithm as implemented in the Kaleidagraph44 general curve fit utility.

Analysis of the TgSkp1 Dimer using All-Atom MD.

Starting molecular coordinates for the TgSkp1 dimers were generated using the Modeler homology modeling software [41]. The lowest energy conformer of the solution NMR structure of DdSkp1AΔloopΔCTR (PDB: 6V88) was used as a template. Due to this construct lacking either the internal loop or CTR, these segments were modeled in the extended conformation. Six homology models were generated with their disordered segments in an extended conformation,

and three were chosen based on their stability during preliminary MD simulations for further analysis. MD simulations were performed with the pmemd.cuda version of AMBER22.3 [45]. Amino acid residues were parameterized with the ff14SB force field [46]. The system was built in a truncated octahedral box with a 15 Å distance from the solute to the end of the unit cell, neutralized with Na^+, and solvated using TIP3P water [47,48]. Electrostatic interactions were simulated using the particle mesh-Ewald algorithm with a non-bonded cut-off of 8 Å [49]. SHAKE was used to constrain hydrogen-containing bonds allowing for a step size of 2 fs. Solvent minimization was conducted over 100,000 cycles with steepest descent being used for 500 cycles with conjugate gradient being used for the remaining cycles with solute being restrained with 100 kcal/mol $Å^2$. Total system minimization was conducted over 100,000 cycles with steepest descent being used for 500 cycles with conjugate gradient being used for the remaining cycles. The system was heated to 300 K under NVT (constant particle number, volume, and temperature) conditions over 60 ns before being held steady at 300 K for an additional 10 ns. Conditions were then changed to NPT (constant particle number, pressure, and temperature) and the system was equilibrated for 140 ns before a 1 μs production phase.

Every 0.5 ns frame of the production phase was utilized for MMGBSA calculations with the mmpbsa.py script [50]. Chain A was treated as the receptor and Chain B as the ligand. An igb of 2 was utilized while an idecomp of 3 was used to generate pairwise interaction energies and an idecomp of 1 was used to generate per residue total interaction energies. Total per residue interaction energies were averaged across all three simulations and between dimer mates for a total of six molecules. Pairwise interaction energies were organized into matrixes and the portion of the matrix corresponding to the interaction of Chain A with Chain B was extracted. Interaction energies associated with each interaction (BTB/BTB; BTB/C-term; C-term/C-term) were added

using the matrix and the total value was divided by two to normalize for each dimer mate. The interactions between oppositely charged CTR residues showing interaction energies greater than -1 kCal/mol in magnitude were further analyzed to observe association and dissociation of charged groups. Atoms used to represent these groups were CZ for Arg, NZ for Lys, CD for Glu, and CG for Asp.

Cluster analysis was carried out using the MD Ensemble Cluster analysis tool in UCSF Chimera [51] which groups frames in the production run into groups of similar structures or ensemble clusters and selects a representative structure as previously described [52]. Three 1 μs simulations were compiled and one frame every 10 ns was loaded for analysis. This resulted in 300 total frames being analyzed with the identification of 25 total clusters. The representative structure/frame from each cluster was then analyzed using HYDROPRO [40] and the s-value was obtained by a weighted average based on the number of frames in each cluster.

RESULTS

TgSkp1 is a Sub-Micromolar Affinity Homodimer.

Throughout eukaryotic phylogeny, Skp1 consists of a globular BTB/POZ (BTB for BR-C, ttk and bab or POZ for Pox virus and Zinc finger) domain with an internal loop, and a C-terminal region (CTR) where, in many Protists, Pro hydroxylation and glycosylation occurs **(Figure 2.1A)** [14,17]. In 20 structures of Skp1 with FBPs from humans, plants, and yeast [53-55], Skp1 adopts the fold represented in **(Figure 2.1C)**, in which the CTR typically organizes as a pair of α-helices, helix-7 and helix-8 separated by a loop. In only one known FBP-Skp1 complex (Fbs1) does the prospective α-helix-8 appear to fail to fold in this way [56]. α-helices-5-7 form a bundle that represents the core interface with the F-box, referred to as subsite-1, and α-helix-8 contributes the

so-called variable interface [18] referred to here as subsite-2 **(Figures 2.1A,C)**. In contrast, free mammalian and *Dictyostelium* Skp1s form soluble homodimers [14,20]. The NMR structure of a truncated version of DdSkp1 lacking the CTR and having its internal loop replaced with GGSG also formed a stable homodimer [14]. The BTB/POZ domain was organized essentially identically to its fold in complexes with FBPs **(Figure 2.1D)**. The interface involved α-helices-5 and -6, which also contribute to the subsite-1 contact surface with FBPs. This predominantly hydrophobic interface is referred to as the ordered interface or subsite-A with respect to self-dimerization. The CTRs were found to be disordered [21], and **(Figure 2.1D)** illustrates the juxtaposition of the CTRs, which were absent from the construct, as imposed by the ordered homodimer interface. The high level of sequence conservation of TgSkp1 **(Figure 2.1E)** indicates that it will adopt similar conformations as for these examples. Under normoxic conditions, PhyA hydroxylates Skp1 on a conserved proline (Pro154 in TgSkp1), which anchors the canonical O-linked glycan **(Figure 2.1B)** [57]. The contribution of the CTR to homodimerization and the influence of glycosylation are the subject of this report.

TgSkp1 was recombinantly expressed in *E. coli* and purified essentially to homogeneity based on SDS-PAGE **(Figure 2.2A)**. The recombinant protein lacked detectable post-translational modifications based on intact protein mass spectrometry but was extended by a SerMet-stub preceding the normally processed Ser N-terminus after proteolytic removal of the His_6-tag. Using sedimentation velocity analysis in an analytical ultracentrifuge to assess self-interaction **(Figure 2.S1)**, 50 μM full-length TgSkp1 (TgSkp1-FL) exhibited a sedimentation coefficient (S) of 2.7, in good agreement with the predicted value using cluster analysis of MD simulations **(Figure 2.3A, Table 2.1)**. The conclusion that this peak represents a dimer species is reinforced by a matching dimer position with the similarly sized and structured DdSkp1 and TgSkp1 constructs where a

monomer-dimer equilibrium was observable **(Table 2.1)** [14]. At the lowest concentration that could be accurately monitored by absorbance at 215 nm, 300 nM TgSkp1-FL remained largely dimeric **(Figure 2.3A)**. Peak broadening and a slightly reduced s-value (to 2.5) indicated partial but apparent rapidly equilibrating dissociation. Modeling the sedimentation of the monomer subunit using Hydropro yields a sedimentation value of 1.4-1.5, though comparison with other full-length variants indicates a sedimentation coefficient of 1.6. By estimating the degree of dissociation at 300 nM to be ~18% based on these values and assuming non-cooperative binding, a K_d of approximately 50 nM is inferred.

Glycosylation Inhibits Self-Association.

To characterize the effect of the glycan, TgSkp1-FL was co-expressed in *E. coli* with TgPhyA and DdGnt1 which resulted in a near homogeneous preparation of Gn-TgSkp1-FL **(Figures 2.2A,C)**. The glycan was completed *ex vivo* with recombinant DdPgtA, TgGlt1, and TgGat1, resulting in highly purified GGlFGGn-TgSkp1 modified with the full-length linear pentasaccharide as assessed by MALDI-TOF mass spectrometry **(Figures 2.2A-D)**. 300 nM GGlFGGn-TgSkp1 sedimented with an s-value of 1.9 **(Figures 2.3B)**, midway between the predicted s-values of the monomer and dimer states, suggesting that at this concentration GGlFGGn-TgSkp1 exists in a rapid equilibrium on the time scale of the experiment. The s-value gradually increased at higher concentrations reaching 2.7 at 28 μM indicative of the dimer species, with only a minor peak observed at an s-value of 1.7, slightly higher than expected for the monomer state **(Figures 2.3B, Table 2.1)**. A concentration series of c(s) distributions **(Figures 2.S2)** were deconvolved into monomer and dimer contributions and plotted as an isotherm to determine the K_d **(Figure 2.3C)**. The calculated K_d of 400 nM **(Figure 2.3D)** indicates a substantial

weakening of homodimerization due to glycosylation, as summarized in **(Table 2.2)**. Given the location of the glycan near the middle of the CTR, we next turned to examining its role in dimerization.

TgSkp1's C-Terminal Region (CTR) Contributes to Dimerization.

NMR studies previously indicated that the CTR of free dimeric DdSkp1 exists in a partially disordered state [21], which was consistent with ITC studies suggesting that complexing of human Skp1 with an FBP caused a relatively large disorder to order transition [22]. The role of the CTR was first assessed by its truncation at 3 residues past the C-terminus of α-helix-6 **(Figure 2.4A)**, by analogy to that of DdSkp1ΔCTR. The similar circular dichroism spectra recorded for the FL and ΔCTR variants **(Figure 2.4B)** are consistent with a lack of stable secondary structure in Skp1's CTR, and the decreased % unordered content **(Fig 2.S4K)** supports this interpretation. In addition, thermal denaturation experiments indicated a single transition in which the Skp1 constructs had minimal differences in T_m, 61.3±0.4°C for TgSkp1-FL and 60.2±0.2°C for TgSkp1ΔCTR **(Figure 2.S4A-D)**, consistent with TgSkp1ΔCTR being properly folded. 300 nM TgSkp1ΔCTR sedimented with a predominant species at S=1.5, close to the monomer position predicted by Hydropro **(Figure 2.4C, Table 2.1)**. At the highest concentration tested (220 μM), TgSkp1ΔCTR sedimented at 2.4, closely matching the S=2.5 value predicted for the TgSkp1ΔCTR dimer **(Figures 2.4C,E)**. An isotherm generated using the weighted s-values for the monomer and dimer positions yielded a K_d of 900 nM for TgSkp1ΔCTR **(Figures 2.4D,E, 2.S3)**. This represents an 18-fold decrease in affinity relative to the estimated K_d for TgSkp1-FL, or an expected energetic cost of ~1.7 kcal/mol. This is unlikely to be due to an entropic effect of the loss of the 34 amino acids per se, because replacement with an uncharged polySer chain failed to strengthen the

homodimer **(Figures 2.5E, 2.S8, Table 2.1)**. The simplest interpretation for the inhibitory effect of glycosylation is that it disrupts the contribution of the CTR to homodimerization.

Amino Acid Composition of the Skp1 C-Terminal Region is More Important than its Sequence.

To probe the mechanism by which TgSkp1's CTR could drive dimerization, its sequence was first scrambled **(Figure 2.5A)**. A series of scrambled sequences appended to the C-terminus of Skp1's BTB domain were submitted to NetSurfP-2.0 to predict their propensity to form disordered coils or secondary structure **(Figure 2.5B)**. Two top sequences were chosen based on minimal predicted secondary structure and high likelihood for disorder. As for the TgSkp1-FL and ΔCTR constructs, thermal denaturation experiments with these scrambled variants as well as the polySer construct showed a single transition with minimal differences in thermal stability **(Figure 2.S4)**. Sedimentation velocity experiments on The TgSkp1-Scrambled6 variant had % unordered content comparable to TgSkp1-FL based on CD **(Figure 2.S4K)** and formed a high affinity homodimer with an apparent affinity similar to the native sequence **(Figures 2.5C, 2.S6)**. The lack of sequence specificity suggested that the CTR drives dimerization while in a disordered state. This was reinforced by nearly identical sedimentation velocities of the native and Scrambled-6 proteins consistent with similar overall structures **(Table 2.1)**. A degree of sequence dependence was however observed for the TgSkp1-Scrambled5 variant. An S_w isotherm modeled a K_d of 200 nM **(Figures 2.5D, 2.S5A, 2.S7)**, intermediate between values for TgSkp1-FL and TgSkp1ΔCTR. A mild to moderate sequence dependence has been observed elsewhere for the electrostatic association of proteins [58-62], indicating that charge distribution can play a major role in association and, as discussed below, the Scrambled5 sequence lacks directly paired positively

charged residues found in the FL and Scrambled6 sequences. The nearly identical sedimentation velocities of the native, the two scrambled, and the polySer dimer constructs **(Table 2.1)** largely exclude a difference in 3-dimensional structure, and their near identical T_m values indicate minimal disruption of structure or stability **(Figure 2.S4)**. However, CD studies noted increased % unordered in the Scrambled5 and polySer constructs at the expense of α-helix content which, interpreted against all the other data, might reflect challenges faced in modeling CD data of proteins with unique structural properties [63]. These findings, paired with the negligible contribution of a poly-Ser replacement **(Figure 2.5E, Table 2.1)**, are inconsistent with a length dependent mechanism, which excludes an entropic tuning model [64] for how Skp1's CTR drives dimerization. Taken together, these data indicate that the CTR drives dimerization through an amino acid composition dependent mechanism which, considering the high proportion of charged (44%) and polar (18%) amino acids and low proportion of hydrophobic amino acids (26%), might involve an electrostatically driven interaction.

Deleting TgSkp1's Internal Disordered Loop Weakens Dimerization.

DdSkp1 contains an internal intrinsically disordered loop based on sequence prediction and NMR analysis [21]. This 16-amino acid loop has been often replaced by a short linker peptide (GGSG) to facilitate crystallization of complexes with FBPs [14,18,55,65] and was similarly replaced in the DdSkp1 homodimer NMR structure study to reduce size. However, preliminary studies suggested that restoration of this internal loop promoted dimerization (data not shown) of the F97E mutant of DdSkp1 [14]. Thus, the significance of the internal loop for TgSkp1 was tested by replacement with GGSG **(Figure 2.6A)**. Although TgSkp1-Δloop still formed a relatively tight

homodimer, its K_d increased to 200 nM, near the lower limit of detection with our system **(Figures 2.6B, 2.S5C, 2.S9)**.

Deletion of Skp1's CTR against the Δloop background revealed, as expected, a weakened affinity compared to TgSkp1Δloop **(Figures 2.6D,E)**. Integration of the c(s) distributions yielded a K_d of 2.4 μM **(Figures 2.6E, 2.S5E, 2.S10)**, or about a 10-fold loss of affinity relative to TgSkp1ΔloopΔCTR, indicating an energetic contribution from the CTR of about 1.36 kCal/mol that was comparable to the difference between the TgSkp1-FL and TgSkp1ΔCTR homodimers. Shortening the loop enabled comparison of affinities without the extrapolations required for the higher affinity interactions.

Skp1's C-terminal region drives dimerization via a salt-sensitive mechanism.

We then examined a potential role for electrostatics in the positive contribution of Skp1's CTR to dimerization by raising the ionic strength of the solution to a value shown to interfere with electrostatic interactions in other examples [58,59,66,67]. AUC experiments up to this point had utilized a buffer containing 50 mM K/Phosphate and 25 mM KCl at pH 7.4. This yields an ionic strength of about 140 mM within the physiological range expected for mammalian cells [68]. At 600 mM KCl (high salt; ionic strength of 710 mM), a sedimentation velocity isotherm for TgSkp1Δloop showed a substantial increase in K_d from ~200 nM to 8.5 μM **(Figures 2.6B,C, 2.S5D, 2.S11)**. In contrast, the affinity of TgSkp1ΔloopΔCTR dimerization was hardly affected **(Figures 2.6E,F, 2.S12, 2.S5F)**, changing from a K_d of 2.4 μM at normal ionic strength to 1.9 μM at high salt, indicating a minimal electrostatic contribution from the remaining subsite-A. This was not unexpected as TgSkp1's ordered dimer interface, whose sequence is similar to that of DdSkp1 **(Figure 2.1)** [14], has a primarily hydrophobic character. An effort to test the effect of high salt on

TgSkp1-FL was confounded by higher order aggregation at an s-value of 3.8-3.9 that was only observed at ≥100 μM for TgSkp1-FL, preventing assessment of CTR-Loop interactions to homodimerization. Inhibition of TgSkp1Δloop homodimerization by high salt can be attributed to an effect on the CTR and applies another constraint on the nature of the interaction: that it is dominated by polar and electrostatic forces in addition to being dynamic.

Skp1's C-Terminal Region Participates in a Fuzzy Self-Association.

To investigate how high salt inhibits dimerization, we utilized all-atom MD simulations with explicit water. The Modeler homology modeling software was used to generate full-length models of the TgSkp1 dimer using the DdSkp1AΔloopΔCTR homodimer as the template. Unlike previous studies where the starting conformations were borrowed from the FBP bound state [34,69], separate extended conformations for the disordered protein segments based on more recent data [21] were modeled to reduce bias. Over the course of the first 140 ns, the CTRs were found to entangle into varied and dynamic conformations that are referred to as collapsed. Following this transition, a 1-μs production run was used for energetic analysis through MM-GBSA. **(Figure 2.7)** summarizes results from the first of 3 simulations. Assessment of total per-residue energetic contributions highlighted both the ordered dimer interface and a second electrostatically driven interface, subsites-A and -B respectively **(Figures 2.7A, 2.S13, 2.S14)**. The strong ordered dimer interface matches closely with that previously characterized for DdSkp1A by NMR, with major contributions from F108 (F97 in DdSkp1), I134 (I123), and L112 (L101).

Each subunit's CTR largely contributed to dimerization via direct interactions with the CTR of the opposite dimer subunit, however some contribution of CTR-BTB interactions were also observed **(Table 2.3)**. Productive CTR-CTR contacts were observable across the length of all

three simulations **(Figure 2.S17)**. The bound states for CTR interactions were conformationally diverse with residence times primarily in the sub-5 ns range **(Figures 2.7B, 2.S15A, 2.S16A, 2.S17)**. Qualitative analysis indicated contributions from both proximal and distal CTR-CTR conformations. Favorable interactions were largely centered around consecutive positively or negatively charged residues, or charge clusters. Interaction of opposite charges was observed through both direct residue-residue contacts and interaction of each residue's hydration shell **(Figure 2.7C, 2.S15B, 2.S16B)**. For comparison, these direct interactions and kinetics closely resemble the association of residues observed in all atom MD simulations of ProTα and H1 phase separation events [70]. Although all positively charged residues participated in favorable electrostatic interactions, the bulk of favorable interaction energy contributed by positively charged residues came from the paired R143-R144 charge cluster **(Figures 2.7A, 2.S14)**. This is in line with data from the scrambled variants as the weaker TgSkp1-Scrambled5 dimer lacks directly paired positively charged residues like the Scrambled6 and wild-type examples **(Figures 2.5B, 2.1E)**. The majority of negatively charged residues rendered a net weakening effect on dimerization **(Figures 2.7A, 2.S14)**. This is likely due to the repulsive effects of the net negative charge of TgSkp1 and its CTR, where acidic outnumber basic residues by a 10:5 ratio resulting in fewer favorable binding states. The ability to form favorable binding states despite the identical charge of each subunit likely lies in the solvent's electrostatic screening of distant charges (>8 Å) modeled here using the particle mesh-Ewald algorithm [49].

DISCUSSION

Here we propose a role for a dynamic, charge based, fuzzy interaction between identical sequences, that acts in concert with a second ordered site to define the full homodimer interface of

Skp1. The contribution of the disordered CTR to homodimer affinity was substantial in terms of affinity measured using AUC. A decrease in K_d from 900 nM for TgSkp1ΔCTR, which folds well **(Figures 2.4B, 2.S4)**, to an estimated 50 nM for full length TgSkp1 was observed. Remarkably, a randomly scrambled sequence of the CTR served nearly as well, lowering the apparent affinity to a similar value as full length TgSkp1. However, lesser success was achieved with another scrambled sequence and an equal length polySer sequence rendered no improvement.

Studies on TgSkp1Δloop, which replaces 12 internal-disordered amino acids with a GGSG tetrapeptide, established a contribution by this region based on an increase of the K_d to 200 nM. Deletion of the CTR in this construct (TgSkp1ΔloopΔCTR) raised the K_d to 2400 nM. This confirms the contribution of the CTR where all K_d values rose to within the range that can be directly measured by absorbance in the AUC. The results also showed that the contribution of the CTR was at least partly independent of the internal disordered loop. By raising the ionic strength of the solution, the contribution of the CTR to affinity was abolished while having a minimal effect on the ordered interaction site. This is consistent with the predominantly hydrophobic nature of Skp1's ordered homodimer interface (subsite-A) and is the basis for concluding that the CTR-CTR interaction serves as subsite-B **(Figure 2.8)**.

Modeling with all-atom MD utilizing explicit water provided support for frequent, transient and varying interactions between oppositely charged residues across the two CTRs, whose proximity is dictated by the ordered interface. Energy calculations showed enhanced contributions between clustered charge regions and, in some instances, neighboring hydrophobic contacts. This corresponds to a definition of charge-based fuzzy protein interactions consisting of electrostatically facilitated protein-protein interactions mediated by an ensemble of bound conformations [23-25]. This contrasts with hydrophobically facilitated fuzzy protein interactions

such as those made by Gcn4 where many weak hydrophobic contacts mediate binding [72]. The different contributions of the replacement CTR sequences to homodimer affinity is consistent with a fuzzy interaction. In contrast to the native and Scrambled6 sequences, the less effective Scarmbled5 sequence lacked directly paired positively charged residues, which have been shown to influence the properties of biomolecular condensates [59,60,73,74]. The inertness of the poly-Ser replacement is consistent with the importance of coulombic interactions rather than entropy being a driving force.

Charge-based fuzzy protein interactions are an interesting recent development in understanding the functions of intrinsically disordered proteins and protein segments and can be mechanistically related to liquid-liquid phase separation [66]. The paradigm of charge based fuzzy interactions of disordered proteins has mostly been applied to the association of two oppositely charged regions with lesser contributions from charge distribution [58,66]. This can allow collapse of extended protein segments into a population of dynamically interconverting conformers, resulting in an increase in conformational entropy [58]. Reliance of the conformational collapse on polar and ionic interactions makes these fuzzy protein interactions particularly sensitive to salt concentration, as observed here. Despite the term ‘fuzzy interaction’ being more typically applied to the interaction of dissimilar sequences, here we propose that this term can also apply to the homodimerization of two identical intrinsically disordered segments and not depend on net charge differences to be a primary driving factor.

The utilization of the same sequence for two independent binding mechanisms, i.e., to FBPs and to itself, imposes critical constraints on the nature and evolution of both. It is proposed here that the fuzzy component for homodimerization has characteristics that are highly suitable for this dual activity. The interface with FBPs is striking in its high expected affinity toward all of the

dozens or more of predicted FBPs in organisms with a single Skp1, despite the low sequence identity of their F-box domains. Crystallographic studies highlight the involvement of α-helices 5-7 as part of the core interaction, termed subsite-1 here, and α-helix-8, as contributing a dispensable variable interaction, here termed subsite-2 **(Figure 2.8)**. While subsite-1 is sufficient for binding, the inclusion of subsite-2 increases the half-life of the complex from hours to days for human Skp1 [18]. Whereas subsite-A of self-interaction involves α-helices 5-6 (which bear no resemblance to F-box sequences), subsite-B involves the CTR, which remains disordered as a fuzzy interaction. The relaxed sequence specificity of the fuzzy interaction is predicted to have been compatible with evolutionary optimization of binding of the CTR to F-box domains. Furthermore, the different binding mechanisms between FBPs and self may allow for differential evolutionary tuning of the strength of the homodimer. For example, charged residues are important for fuzzy interactions but typically less conserved and less important for the formation of ordered dimer interfaces such as for FBP/Skp1 interactions. The identity of positive charge residues has also been observed to alter dynamic interactions with Arg residues contributing disproportionately to these interactions compared to Lys residues [75-81]. Evolutionary variation of charged residues within the Skp1 CTR may therefore offer a selective way to influence the strength of the Skp1 homodimer. This may explain differences in Skp1 homodimerization affinities in different organisms [14,20] that may be independent of FBP/Skp1 interactions. Additionally, alteration of charges through phosphorylation has been shown to alter the propensity for liquid-liquid phase separation [74]. The previously observed phosphorylation of the CTR of yeast Skp1 [82] may, therefore, influence its homodimerization too.

The presence of a fuzzy component to the homodimer interface may facilitate kinetic exchange between the homodimer, FBPs, and Skp1's modification enzymes. Charge-based fuzzy

interactions can drive higher on and off rates for dimer subunits [25,66,83,84] and, in the case of Skp1, may provide an opportunity for invasion of the F-box domain. Once bound, the F-box binding interface will involve α-helices-5 and -6 that contribute to the ordered homodimerization subsite-A. The CTR of the fuzzy homodimerization subsite-B almost always folds into an α-helix pair, with helix-8 overlapping with the previously described subsite-2 of the FBP interface [18]. The fully ordered interaction of the CTR with FBPs may be less susceptible to dissociation. Fuzzy interactions are thought to be more receptive to post translational modifications [25,66,83,84], which in the case of Skp1 might facilitate O_2-sensing via more ready access to the CTR by PhyA and the glycosyltransferases, whose actions are inhibited in complexes with FBPs [35].

Glycosylation of Skp1's CTR resulted in a significant weakening of the Skp1 homodimer by over an estimated order of magnitude, mirroring the effect of deleting Skp1's CTR. The simplest interpretation is that glycosylation negates the CTR's contribution to homodimerization. Previous studies of both TgSkp1 and DdSkp1 suggested that the glycan has a relatively ordered structure that associates with and therefore partially orders the region of α-helix-7 and the connecting loop to the start of the α-helix-8 region [21,34,69]. This interaction would interfere with the dynamic contacts of charge clusters that form the basis of the fuzzy interaction and deserves future analysis.

The estimated 50 nM K_d value that describes the homodimer interaction of unmodified Skp1 implies that the vast majority of Skp1, estimated in mammalian cells to be 1-2 μM [85], will be in the dimer state. However, a substantial fraction of Skp1 will be complexed at a 1:1 ratio with FBPs, which for a single example has been characterized to have a K_d of ~25 nM [22]. Since the interaction sites for FBPs and Cul1 overlap with the Skp1 homodimer interface **(Figure 2.S18)**, most free Skp1 will be sequestered from the SCF complex. Under normoxic conditions, hydroxylation and subsequent glycosylation of Skp1's CTR will disrupt the fuzzy dimerization

interface resulting in less sequestration of Skp1 into the homodimer species. Under hypoxic conditions the fuzzy interface will remain intact driving greater sequestration of Skp1 into the homodimer species **(Figure 2.8)**. This would theoretically result in a reduced polyubiquitination activity for substrates of FBPs reliant on the SCF complex especially for lower affinity FBP/Skp1 species. This parallels the role of animal PHD2 where reduced polyubiquitination of HIF1α results in the activation of the hypoxic response [86].

The varied sequences of FBPs that associate with the single Skp1 suggests the existence of an affinity hierarchy. A consequence of the destabilizing effect of glycosylation might be to reduce the significance of FBP preferences. For example, weakening of the Skp1 homodimer will exert a stronger associative effect on relatively weak FBP/Skp1 interactions while having a relatively minimal effect for high affinity FBPs that already had an advantage. This effect can also be extended to include a concentration hierarchy where higher abundance FBPs will be able to more effectively outcompete a high affinity Skp1 homodimer. This would allow variations in FBP transcription to influence the tuning of FBP/Skp1 interactions by homodimer sequestration that is in turn responsive to physiological O_2 levels.

It has been previously estimated that 40% of proteins encoded in the human genome have an intrinsically disordered protein segment greater than 30 residues in length [87-90]. Many of these participate in liquid-liquid phase separation [71], fuzzy protein interactions [71], chaperoning [91], altering internal protein dynamics [92,93], and tuning protein function through entropic force generation [64], though most have no known function. Here, we suggest that our interpretation that a fuzzy interface consisting of identical charge-rich sequences can promote homodimerization offers a new functional dimension for interactions of intrinsically disordered regions.

CONCLUSIONS

Quantitative measurements of the homodimerization K_d of Skp1 from the protozoan parasite *Toxoplasma gondii*, using analytical ultracentrifugation, emphasize its potential impact on the activities of E3(SCF) ubiquitin ligases in cells. The relatively high (multi-nM) affinity of its self-interaction is likely to compete with the formation of Skp1/FBP subcomplexes by a sequestration mechanism. Both interfaces are bipartite consisting of a stably folded Skp1 domain and the CTR. Whereas the CTR folds into a stereotyped pair of α-helices when bound to FBPs, it participates in a largely charged-based fuzzy interaction involving ensembles of conformations in the homodimer. Fuzzy interactions have been implicated in formation of biomolecular condensates but have rarely been invoked for homodimerization. Thus the CTR contributes substantial affinity to the homodimer but its intrinsically dynamic nature is predicted to also help enable exchange with FBPs. The weakening of the CTR/CTR interaction by O_2-dependent glycosylation, which may impose local order to the CTR, suggests that sequestration of Skp1 from FBPs is regulated in cells. Previous studies suggested that the glycan also promotes favorable conformations for binding FBPs. The alternative organization of the CTR in the different complexes imposes unusual constraints on the evolution of its sequence, which is remarkably well conserved across eukaryotic evolution. Although glycosylation appears to be confined to the protist kingdom and pathogenic fungi, homodimerization of Skp1 and its regulation by other mechanisms is likely to be a widespread mechanism to influence the activities of the SCF family of E3 ubiquitin ligases.

AUTHOR CONTRIBUTIONS

DAC, RJBU and HWK preformed the experiments; DAC, RJW, JLU, ZAW and CMW conceptualized the study; DAC wrote the first draft; all authors edited and approved the manuscript.

FUNDING

This work was supported by NIH grant 1R01-AI169849 to CMW, and Human Frontiers in Science grant RGP0051 to CMW. Molecular graphics and analyses performed with UCSF Chimera, developed by the Resource for Biocomputing, Visualization, and Informatics at the University of California, San Francisco, with support from NIH P41-GM103311.

ACKNOWLEDGMENTS

We are grateful to Hanke van der Wel for her technical guidance and for providing reagents for this study. Xiacong Wang provided invaluable advice for the use of MMGBSA.

FIGURE/TABLE LEGENDS

Table 2.1 Predicted and observed sedimentation values for the TgSkp1 monomer and dimer species. Expected sedimentation values were predicted using Hydropro and either homology models (HM) for TgSkp1ΔCTR, TgSkp1-FL, or representative MD structures of TgSkp1-FL. Observed sedimentation values were taken from the maximum and minimum positions of each c(s) isotherm or from the dimer positions of the highest concentration (TgSkp1-FL, TgSkp1-Scrambled6).

Table 2.2 Calculated affinities of TgSkp1 isoforms

* indicates calculation by extrapolation

Table 2.3 Energetic components for the interaction of each TgSkp1 protein region. Pairwise interaction energy components between TgSkp1 regions are derived from the MD simulations and given in kcal/mol. The association between each subunit's BTB region is primarily contributed by Skp1's ordered dimer interface (subsite-A). The association of each subunit's CTR with both the BTB and CTR region of the opposite subunit indicates Skp1's fuzzy interface. The CTR-CTR and BTB-BTB rows represent each respective single interaction. The CTR-BTB row represents the sum of intermolecular interactions between the CTRs and BTB domains of each subunit.

Figure 2.1 Structure models of *Toxoplasma* Skp1. (A) Domain diagram for TgSkp1 (UniProt A0A0F7UNE6). Secondary structures, intermolecular contact sites, and the glycosylation site at Pro154 are indicated above. Skp1 consists of an N-terminal SerMet (black) extension remaining from removal of a His_6-tag, a disordered segment of N-terminal amino acids (red), a globular BTB domain (green), an intervening disordered internal loop (orange), and a C-terminal region (CTR) which is disordered when not bound to an FBP (purple). The homodimer subsites are indicated below. **(B)** Glycosylation pathway responsible for the canonical, linear glycosylation of TgSkp1 initiated by the O_2-dependent prolyl-4 hydroxylase PhyA. **(C)** Homology model for TgSkp1 bound to an FBP. Color coding is as in panel A. α-helixes-5, -6, and -7, which contribute to subsite 1, and α-helix 8 which contributes to subsite 2, are depicted. Amino acids at the homodimer interface are shown in yellow as sticks. **(D)** Previously determined structure of the truncated DdSkp1 homodimer (PDB ID: 6V88), with the location of the missing CTR arbitrarily represented in extended form. **(E)** Alignment of the C-terminal TgSkp1 sequence associated with FBP and self-binding (i.e., contributing to helixes 5-8 in complexes with FBPs) with corresponding regions from

Skp1s across phylogeny. Amino acids are colored according to their chemical class, in bold if extensively conserved, and highlighted if the chemical class is highly conserved across phylogeny. Key to species: Hs, *Homo sapiens*; At, *Arabidopsis thaliana*; Sc, *Saccharomyces cerevisiae*; Pu, *Pythium ultimum*.

Figure 2.2 TgSkp1 isoforms and preparation of glycosylated TgSkp1. (A) Coomassie Brilliant Blue gel stained SDS-PAGE gels loaded with 3 μg protein each. **(B)** Same for fully glycosylated TgSkp1. Lanes excerpted from the same gel are denoted by dashed lines. **(C)** Alignment of MALDI-TOF mass spectra demonstrating sequential conversion between each glycoform in untagged TgSkp1. **(D)** Schematic for generating glycosylated TgSkp1.

Figure 2.3 Dimerization of native and glycosylated Skp1. (A) c(s) distributions from sedimentation velocity AUC experiments with TgSkp1-FL at 50 μM (blue) and 300 nM (orange). The dashed lines represent the predicted s-values for monomeric TgSkp1-FL as predicted by modeler (HM, purple) and the dimer as predicted by MD cluster analysis (green). **(B)** c(s) distributions of GGlFGGn-TgSkp1. **(C)** c(s) distributions across a concentration range (color coordinated with panel **(D)** values) of GGlFGGn-TgSkp1. **(D)** An S_w isotherm derived from integration of the color coordinated data in panel C was used to derive the homodimerization K_d value for GGlFGGn-TgSkp1. Deviations of measured values from the fitted curve are plotted in the bottom panel as residuals. Supporting c(s) distributions are in **(Figures 2.S1, 2.S2)**.

Figure 2.4 Contribution of the C-terminal region (CTR) to Skp1 homodimerization. (A) Domain diagrams of TgSkp1-FL and the TgSkp1ΔCTR variants. **(B)** Circular dichroism spectra of the TgSkp1-FL and TgSkp1ΔCTR constructs. **(C)** c(s) distributions from sedimentation velocity experiments of TgSkp1ΔCTR at two concentrations, as in **(Figures 2.3A,B)**. **(D)** c(s) distributions

over a range of concentrations to generate the S_w isotherm in panel **(E)**. **(E)** S_w isotherm with residuals, as in **(Figure 2.3D)**. Supporting c(s) distributions are in **(Figure 2.S3)**.

Figure 2.5 Sequence and composition dependence of the CTR contribution to dimerization. **(A)** Domain diagrams for TgSkp1-FL and CTR sequence variants. **(B)** Native and scrambled CTR sequences are shown with NetSurfP-2.0 predictions for solvent exposure (red=likely, blue=unlikely), secondary structure (orange), and disorder (grey bar thickness). **(C)** c(s) distributions for TgSkp1-FL (orange), TgSkp1ΔCTR (green), and TgSkp1-Scrambled6 (blue). **(D)** S_w isotherm for TgSkp1-Scrambled5, with residuals at the bottom. **(E)** S_w isotherm for TgSkp1-polySer, as in panel **(D)**. See **(Figures 2.S5-2.S8)** for supporting c(s) distributions.

Figure 2.6 Salt sensitivity of the CTR contribution. (A) Domain diagram for TgSkp1Δloop. **(B)** S_w isotherm was used to determine the homodimerization affinity using the standard buffer (25 mM KCl, 50 mM K/H PO4 (pH 7.4)). The K_d was estimated using an isotherm modeled by integrating the monomer and dimer positions of Skp1 based on data shown in **(Figure 2.S5)**. **(C)** Same as panel **(B)** except for the presence of 600 mM KCl (high salt). **(D)** Domain diagram for TgSkp1ΔloopΔCTR. **(E, F)** S_w isotherms used to determine the homodimerization affinity in standard buffer **(E)** or high salt buffer **(F)** for TgSkp1ΔLoopΔCTR. Deviations of measured values from the fitted curves are plotted in the bottom panels as residuals. See **(Figures 2.S5, 2.9-2.12)** for supporting c(s) distributions.

Figure 2.7 The Skp1 CTRs self-associate through an electrostatically driven fuzzy interaction. (A) In tabular form, energetic contributions for residues corresponding to subsites A and B are shown. Residues previously shown as part of the dimer interface are highlighted in light green. In the CTR (subsite B) positively charged residues are highlighted in light blue, negatively charged residues in light pink, and aromatic residues in yellow. **(B)** An interaction energy matrix

or heat map for the pairwise interaction energies of each CTR residue from Simulation 1. Residue labels corresponding to Chain A are colored blue while residue labels corresponding to Chain B are colored magenta. Pairwise energies representing the interaction of oppositely charged residues are boxed in black while energies representing the interaction of identically charged residues are boxed in red. Individual residue contributions were calculated by adding all CTR pairwise interactions and dividing by two. **(C)** An example of direct and indirect interactions of oppositely charged residues, annotated with atom distances. Positive residues are colored in cyan while negative residues are colored in orange. Residue labels corresponding to Chain A are colored blue while residue labels corresponding to Chain B are colored magenta. Chain A is light blue while Chain B is plum. **(D)** Directly interacting residues are shown as sticks with their van der Waals surfaces, with chains colored as in panel **(C)**. See **(Figures 2.S15, 2.S16)** for Simulations 2 and 3.

Figure 2.8 Evidence supports a bipartite mechanism for Skp1 homodimerization. Subsite A includes the stably ordered α-helices-5 and -6, and subsite B includes the intrinsically disordered CTR. Subsite A buries ~750 $Å^2$ of predominantly hydrophobic surface, whereas subsite B involves a fuzzy interaction characterized primarily by dynamic electrostatic interactions that are hindered by the glycan. The dynamic nature of the CTR may facilitate access to the post-translational modification enzymes and exchange of a Skp1 monomer for an FBP, and O_2-dependent glycosylation is expected to promote accessibility of monomeric Skp1 to F-box proteins (FBPs), as represented by the solid vs. dashed vertical or diagonal arrows. Individual DdSkp1 subunits are from PDB ID: 6V88 while the Skp1-FBP interaction is from PDB ID: 2P1O (Skp1-like protein 1A and Tir1 from *A. thaliana*).

SUPPLEMENTAL FIGURE LEGENDS

Figure 2.S1 c(s) Distributions over a range of TgSkp1-FL concentrations. Samples were monitored at the indicated wavelengths. Buffer components were identical for all standard runs (50 mM KPhosphate (pH 7.4), 25 mM KCl), with an ionic strength of ~150 mM. Predicted s-values for the monomer as predicted by homology modeling (purple) and the dimer as predicted by MD Cluster analysis (brown) are shown. The data support **(Figure 2.3)**.

Figure 2.S2 c(s) distributions over a range of GalGlcFucGalGlcNAc-TgSkp1 concentrations. Studies were performed as in **(Figure 2.S1)**. The replicate distribution of 330 nM GalGlcFucGalGlcNAc-TgSkp1 boxed in red more clearly shows the monomer and dimer species but was not used in generating the S_w isotherm. The data support **(Figure 2.3)**.

Figure 2.S3 c(s) distributions over a range of TgSkp1ΔCTR concentrations. Studies were performed as in **(Figure 2.S1)** except that homology modeling was used to predict the monomer (purple) and dimer (green) s-values. The data support **(Figure 2.4)**.

Figure 2.S4 Thermal melting studies of TgSkp1 variants. Forward (black) and reverse (red) thermal melts for TgSkp1-FL **(A)**, TgSkp1-ΔCTR **(C)**, TgSkp1-Scrambled6 **(E)**, TgSkp1-Scrambled5 **(G)**, and TgSkp1-PolySer **(I)** were modeled to the Gibbs-Helmholtz equation, with Tm and ΔH values indicated. CD spectra for the beginning (black), max temperature (blue), and end (red) of each thermal melt for TgSkp1-FL **(B)**, TgSkp1-ΔC-term **(D)**, TgSkp1-Scrambled6 **(F)**, TgSkp1-Scrambled5 **(H)**, and TgSkp1-PolySer **(J)** are shown, and their secondary structure contents were modeled **(K)**.

Figure 2.S5 Integration ranges used to generate c(s) isotherms. (A-F) Distributions and integration ranges are shown for the indicated constructs at the indicated salt concentrations.

Figure 2.S6 c(s) distributions over a range of TgSkp1-Scrambled6 concentrations. Studies were performed as described in **(Figure 2.S1)**. The data support **(Figure 2.5)**.

Figure 2.S7 c(s) distributions over a range of TgSkp1-Scrambled5 concentrations. Studies were performed as in **(Figure 2.S1)**. The data support **(Figure 2.5)**.

Figure 2.S8 c(s) distributions over a range of TgSkp1-polySer concentrations. Studies were performed as in **(Figure 2.S1)**. The data support **(Figure 2.5)**.

Figure 2.S9 c(s) distributions over a range of TgSkp1ΔLoop concentrations. Studies were performed as in **(Figure 2.S1)**. The data support **(Figure 2.6)**.

Figure 2.S10 c(s) distributions over a range of TgSkp1ΔLoopΔCTR concentrations. Studies were performed as in **(Figure 2.S3)**. The data support **(Figure 2.6)**.

Figure 2.S11 c(s) distributions over a range of TgSkp1ΔLoop concentrations in high salt. Studies were performed as in **(Figure 2.S1)**, except that buffer components were 50 mM K phosphate (pH 7.4), 600 mM KCl, with an ionic strength of ~730 mM. The data support **(Figure 2.6)**.

Figure 2.S12 c(s) distributions over a range of TgSkp1ΔLoopΔCTR concentrations in high salt. Studies were performed as in **(Figure 2.S11)**, except that homology modeling was used to predict the monomer (purple) and dimer (green) s-values. The data support **(Figure 2.6)**.

Figure 2.S13 Total residue energy contributions across simulations mapped to TgSkp1 homology models. Total per residue energies for each simulation were mapped to their respective homology models. These energies were averaged together to yield the averaged per residue interaction energies and mapped to the starting homology model for simulation 1.

Figure 2.S14 Total residue energy contributions averaged across all simulations. In tabular form, residues corresponding to subsite-A of the dimer interface are highlighted in light green. In

the CTR, subsite B, positively charged residues are highlighted in light blue, negatively charged residues in light pink, and aromatic residues in yellow. These findings relate to **(Figures 2.7, 2.S15, 2.S16)**.

Figure 2.S15 Fuzzy CTR interactions for Simulation 2. (A) Interaction energy matrix showing the pairwise interaction energies for each Skp1 CTR residue. **(B)** Examples of direct and indirect interactions of oppositely charged residues shown through atom distances. **(C)** Directly interacting residues are shown as sticks with their Van der Waals surfaces. See **(Figure 2.7)** for explanation.

Figure 2.S16 Fuzzy CTR interactions for Simulation 3. (A) Interaction energy matrix showing the pairwise interaction energies for each Skp1 CTR residue. **(B)** Examples of direct and indirect interactions of oppositely charged residues shown through atom distances. **(C)** Directly interacting residues are shown as sticks with their Van der Waals surfaces. See **(Figure 2.7)** for explanation.

Figure 2.S17 Distances between interacting charge clusters through the MD simulations. Distances are shown for the interactions of oppositely charged residues indicated to have an interaction energy of <–1 kcal/mol across all three simulations. Distances within 8 Å are highlighted in a yellow box. Residues are color coded as above.

Figure 2.S18 Overlaps between the dimer-mate of the Skp1 monomer and adjacent SCF components. Backbone atom overlays of SCF components (from a Cul1/Rbx1/Skp1/F-box(Skp2); PDB: 1LDK) and the Skp1 homodimer (PDB: 6V88). The representative SCF complex contains Skp1 (green), FBP(Skp2, magenta), and Cullin1 (blue). The Skp1 homodimer contains two subunits with one (light grey) overlaying well with the SCF bound form of Skp1 and the other (dark grey) sterically clashing with both Skp2 and Cul1. Four poses are represented **(A-D)**.

Figure 2.S19 Engineering TgSkp1 deletions. (A) Primer pairs used to delete the C-Terminal Region (CTR), the internal loop, or both (starting with the internal loop) of TgSkp1 (UniProt

A0A0F7UNE6). Clones were screened by colony PCR utilizing flanking primers annealing with the pNIC28 plasmid backbone. **(B)** Sequence of the pNIC28-TgSkp1-FL parental plasmid utilized for deletions. The coding region of the original plasmid is underlined in black with amino acids above in bold black. The TEV-cleavage motif is highlighted in yellow with the cut site in teal. Primers are shown in red with annealing residues capitalized. The resulting deletions are indicated below each site in blue. Residues are numbered relative to the native start site (Met).

Figure 2.S20 Sequences of chemically synthesized variants of TgSkp1 genes. The pNIC28-TgSkp1 plasmid served as the plasmid backbone for gene synthesis products and its sequence (underlined) and translation of the open reading frame (bold) are shown in black. The TEV-cleavage motif is highlighted in yellow with the cut site in teal. The alternative C-terminal regions (CTRs) are represented as different colors. Amino acid residues are numbered relative to the native Met start site.

Table 2.1

Expected from Hydropro	S, Monomer	S, Dimer
TgSkp1-FL (MD)	NA	2.7
TgSkp1-FL (HM)	1.4 - 1.5	2.1 - 2.3
TgSkp1ΔCTR (HM)	1.5 - 1.6	2.3 - 2.5
Experimental/Observed		
TgSkp1-FL	NA	2.7
TgSkp1ΔCTR	1.4	2.6
TgSkp1-polySer	1.6	2.8
TgSkp1-Scrambled5	1.6	2.8
TgSkp1-Scrambled6	NA	2.7
TgSkp1Δloop	2	2.6
TgSkp1Δloop, high salt	2.3	2.9
TgSkp1ΔloopΔCTR	1.5	2.4
TgSkp1ΔloopΔCTR, high salt	1.8	2.4
GGlFGGn-TgSkp1	1.5	2.8

Table 2.2

Construct	K_d
TgSkp1-FL	~50 nM*
TgSkp1ΔCTR	900 nM
TgSkp1-polySer	900 nM
TgSkp1-Scrambled5	200 nM*
TgSkp1-Scrambled6	~50 nM*
TgSkp1Δloop	200 nM*
TgSkp1Δloop, high salt	8500 nM
TgSkp1ΔloopΔCTR	2400 nM
TgSkp1ΔloopΔCTR, high salt	1900 nM
GGlFGGn-TgSkp1	400 nM

Table 2.3

	Electrostatic	Polar Solvation	Non-Polar Solvation	van der Waals	Total	Average Deviation
(CTR) (BTB)	160	-160	-6.3	-8.4	-23	±4.9
(CTR) (CTR)	39	-51	-7.9	-10	-30	±8.0
(BTB) (BTB)	130	-140	-14	-21	-42	±2.5
				Total Energy	-96	±12

Figure 2.1

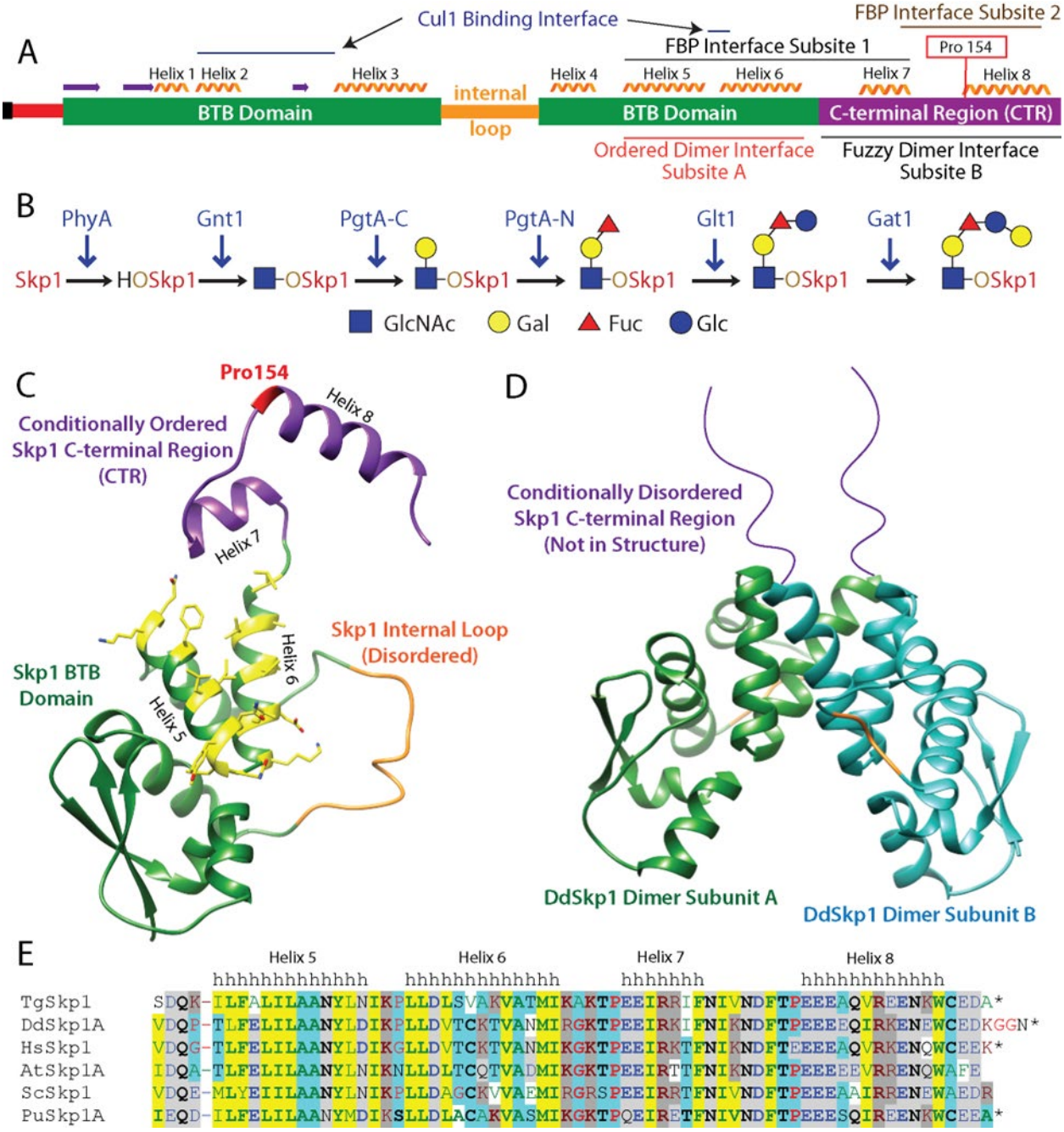

A
Cul1 Binding Interface
FBP Interface Subsite 2
FBP Interface Subsite 1
Pro 154
Helix 1
Helix 2
Helix 3
Helix 4
Helix 5
Helix 6
Helix 7
Helix 8
BTB Domain
internal loop
BTB Domain
C-terminal Region (CTR)
Ordered Dimer Interface Subsite A
Fuzzy Dimer Interface Subsite B
B
PhyA
Gnt1
PgtA-C
PgtA-N
Glt1
Gat1
Skp1
HOSkp1
OSkp1
GlcNAc
Gal
Fuc
Glc
C
Pro154
Helix 8
Conditionally Ordered Skp1 C-terminal Region (CTR)
Helix 7
Skp1 Internal Loop (Disordered)
Skp1 BTB Domain
Helix 6
Helix 5
D
Conditionally Disordered Skp1 C-terminal Region (Not in Structure)
DdSkp1 Dimer Subunit A
DdSkp1 Dimer Subunit B
E
Helix 5
Helix 6
Helix 7
Helix 8
TgSkp1
DdSkp1A
HsSkp1
AtSkp1A
ScSkp1
PuSkp1A

Figure 2.2

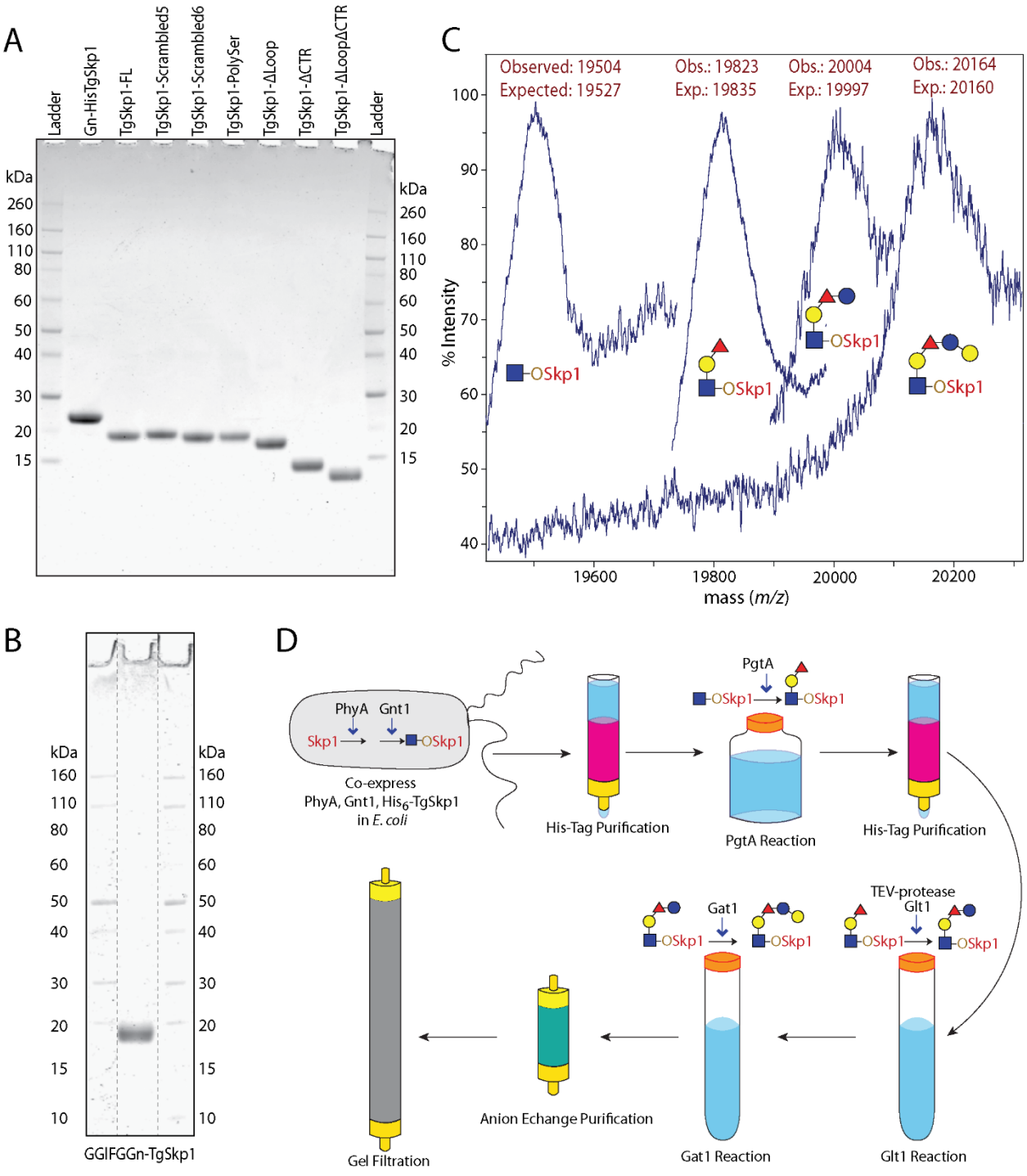

A
Ladder
Gn-HisTgSkp1
TgSkp1-FL
TgSkp1-Scrambled5
TgSkp1-Scrambled6
TgSkp1-PolySer
TgSkp1-ΔLoop
TgSkp1-ΔCTR
TgSkp1-ΔLoopΔCTR
Ladder
kDa
260
160
110
80
60
50
40
30
20
15
C
Observed: 19504
Expected: 19527
Obs.: 19823
Exp.: 19835
Obs.: 20004
Exp.: 19997
Obs.: 20164
Exp.: 20160
% Intensity
mass (m/z)
OSkp1
B
GGlFGGn-TgSkp1
D
PhyA
Gnt1
Skp1
OSkp1
Co-express
PhyA, Gnt1, His6-TgSkp1
in E. coli
His-Tag Purification
PgtA
PgtA Reaction
His-Tag Purification
TEV-protease
Glt1
Gat1
Glt1 Reaction
Gat1 Reaction
Anion Echange Purification
Gel Filtration

Figure 2.3

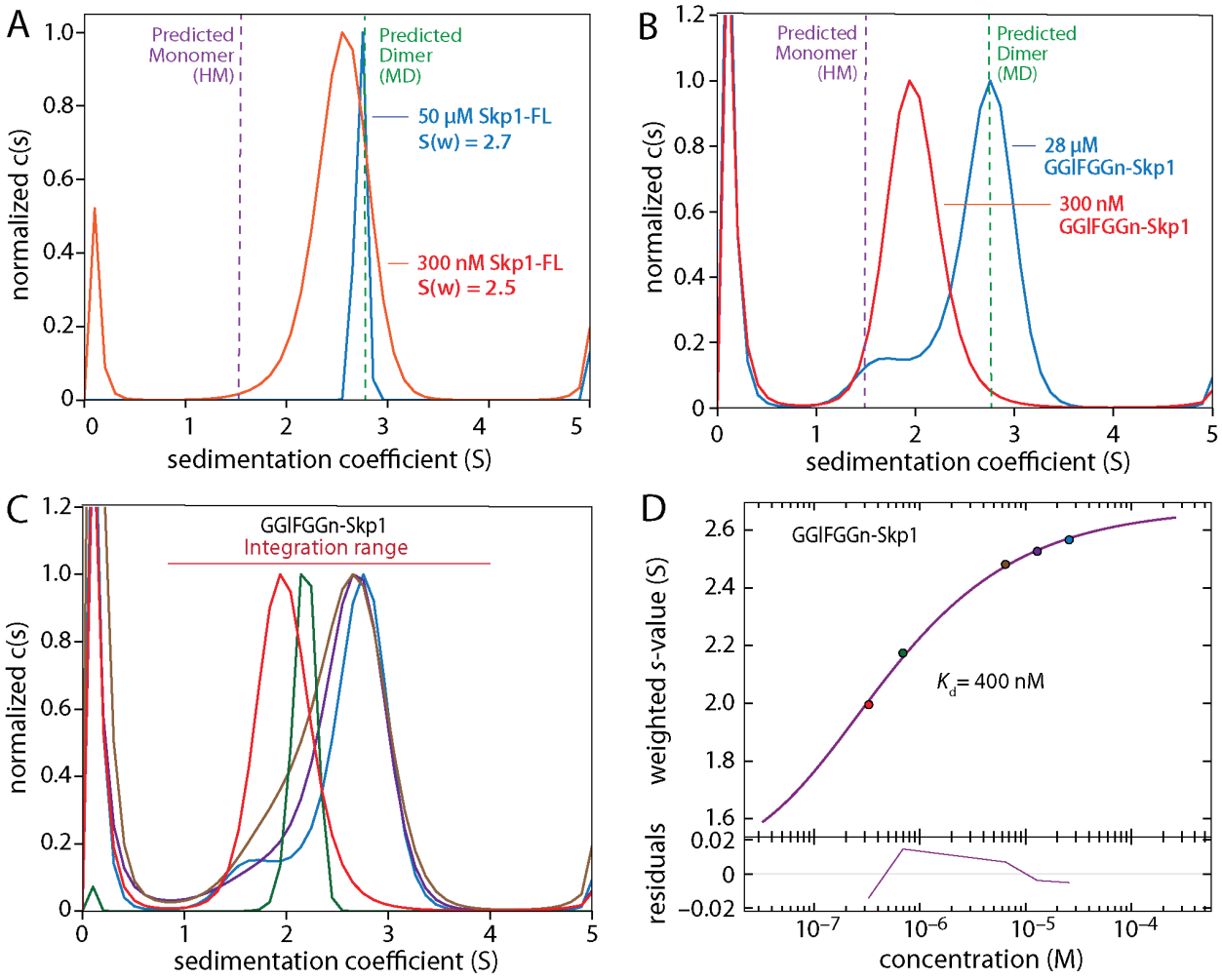

A
Predicted Monomer (HM)
Predicted Dimer (MD)
50 µM Skp1-FL
S(w) = 2.7
300 nM Skp1-FL
S(w) = 2.5
normalized c(s)
sedimentation coefficient (S)
B
Predicted Monomer (HM)
Predicted Dimer (MD)
28 µM GGlFGGn-Skp1
300 nM GGlFGGn-Skp1
normalized c(s)
sedimentation coefficient (S)
C
GGlFGGn-Skp1
Integration range
normalized c(s)
sedimentation coefficient (S)
D
GGlFGGn-Skp1
K_d = 400 nM
weighted s-value (S)
residuals
concentration (M)

Figure 2.4

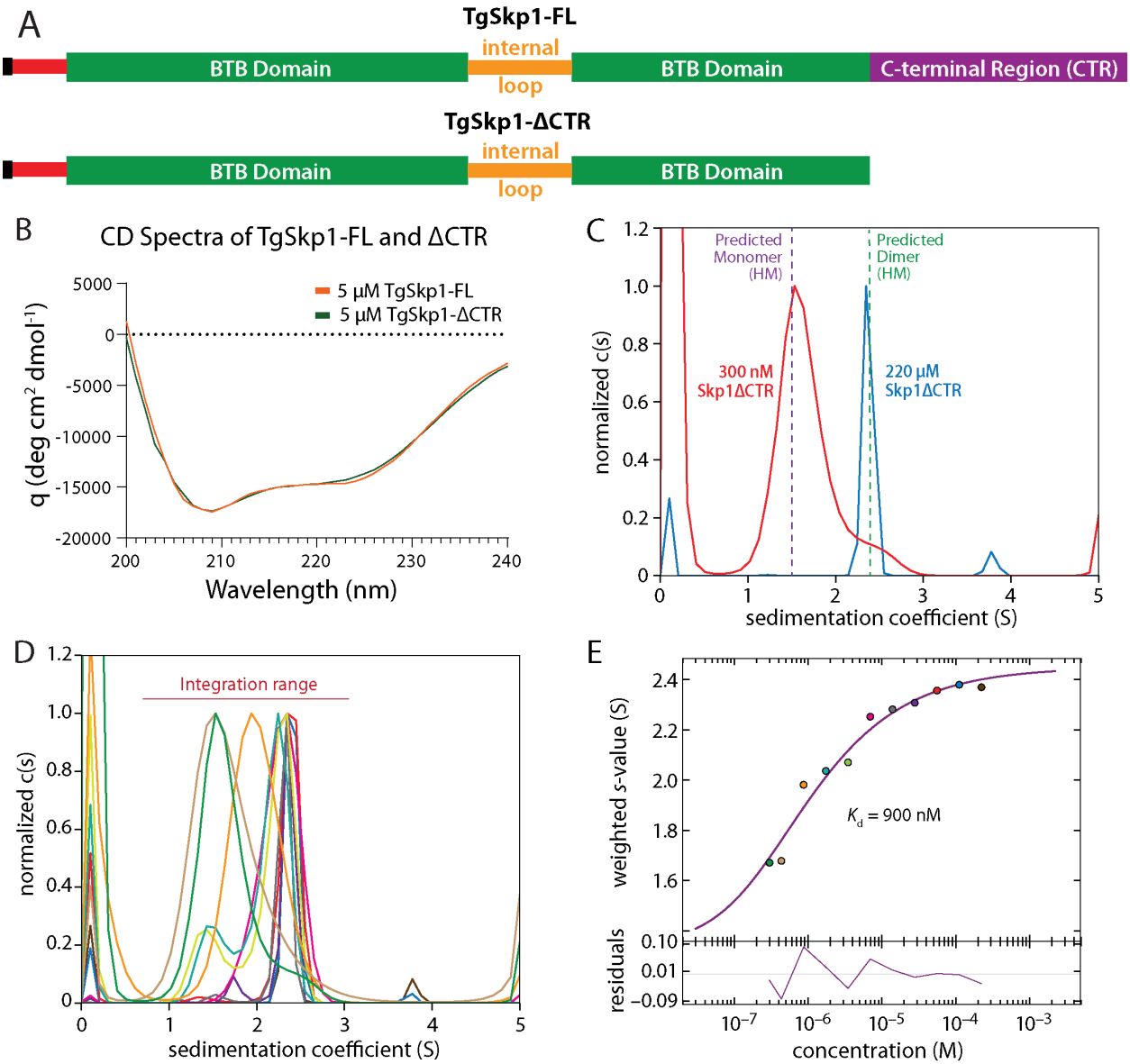

A
TgSkp1-FL
internal loop
BTB Domain
BTB Domain
C-terminal Region (CTR)
TgSkp1-ΔCTR
internal loop
BTB Domain
BTB Domain
B
CD Spectra of TgSkp1-FL and ΔCTR
5 μM TgSkp1-FL
5 μM TgSkp1-ΔCTR
q (deg cm² dmol⁻¹)
Wavelength (nm)
C
Predicted Monomer (HM)
Predicted Dimer (HM)
300 nM Skp1ΔCTR
220 μM Skp1ΔCTR
normalized c(s)
sedimentation coefficient (S)
D
Integration range
normalized c(s)
sedimentation coefficient (S)
E
weighted s-value (S)
K_d = 900 nM
residuals
concentration (M)

Figure 2.5

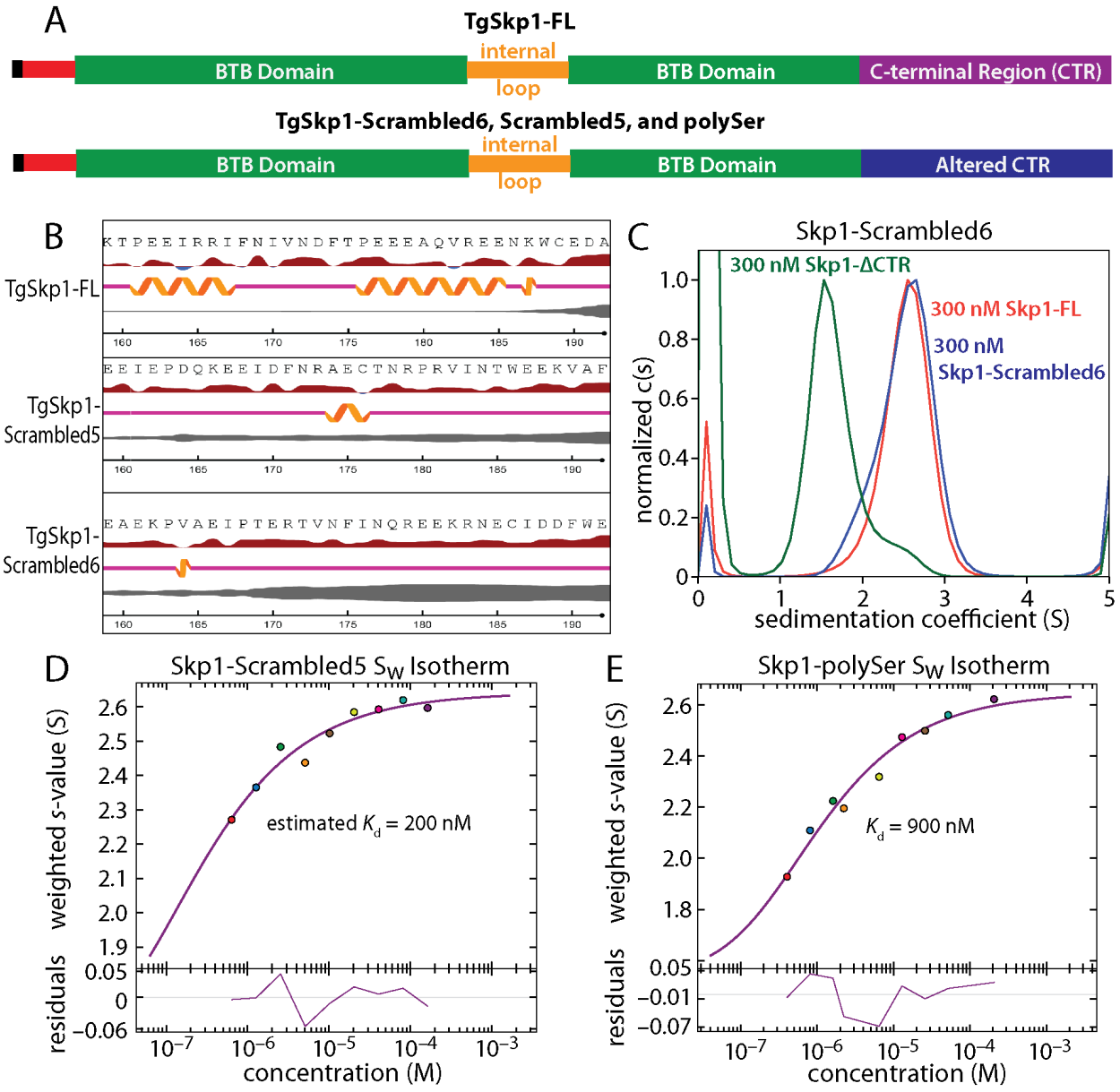

A
TgSkp1-FL
BTB Domain
internal loop
BTB Domain
C-terminal Region (CTR)
TgSkp1-Scrambled6, Scrambled5, and polySer
BTB Domain
internal loop
BTB Domain
Altered CTR
B
TgSkp1-FL
TgSkp1-Scrambled5
TgSkp1-Scrambled6
C
Skp1-Scrambled6
300 nM Skp1-ΔCTR
300 nM Skp1-FL
300 nM Skp1-Scrambled6
normalized c(s)
sedimentation coefficient (S)
D
Skp1-Scrambled5 S_W Isotherm
estimated K_d = 200 nM
weighted s-value (S)
residuals
concentration (M)
E
Skp1-polySer S_W Isotherm
K_d = 900 nM
weighted s-value (S)
residuals
concentration (M)

Figure 2.6

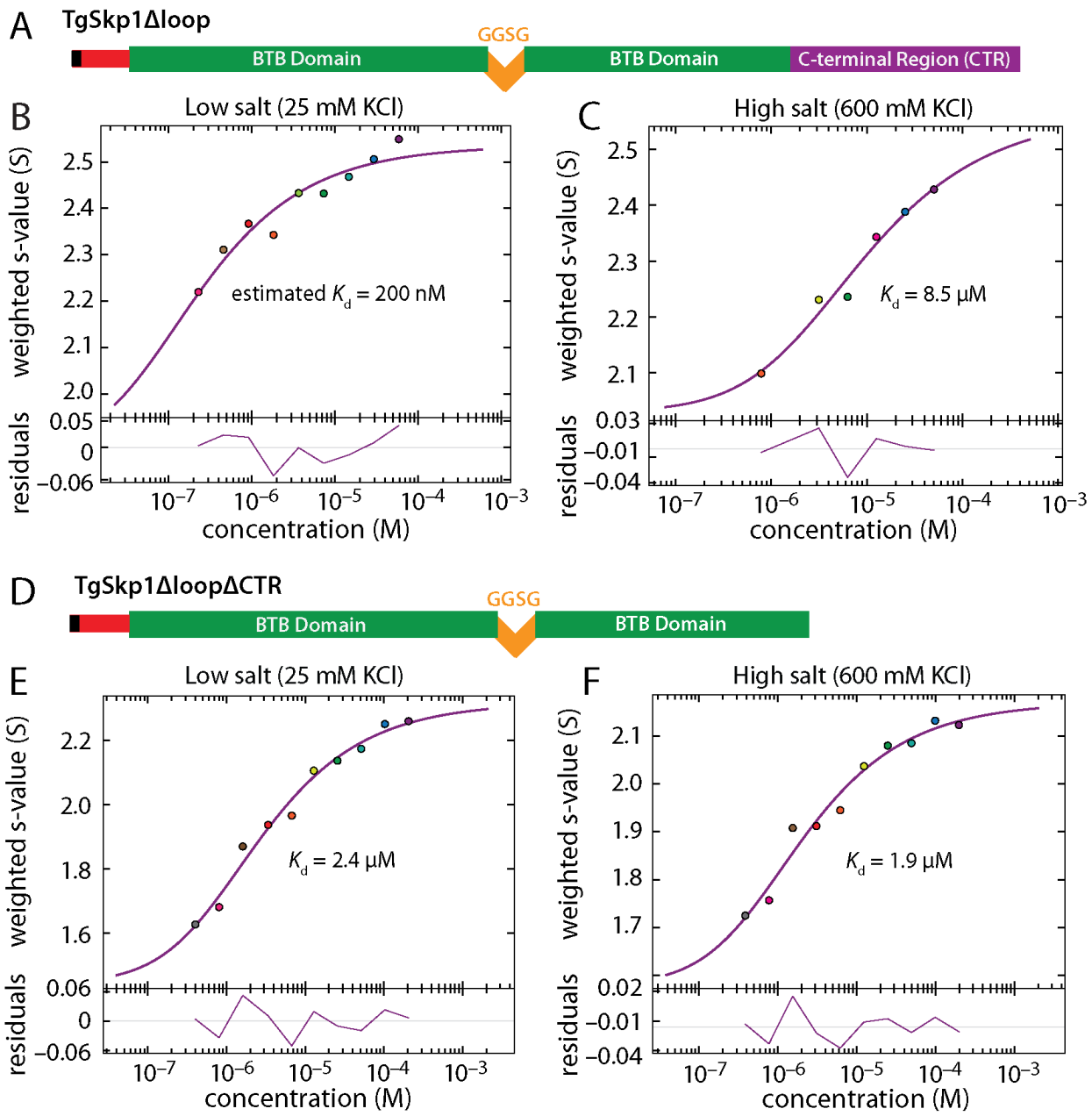

A
TgSkp1Δloop
GGSG
BTB Domain
BTB Domain
C-terminal Region (CTR)
B
Low salt (25 mM KCl)
weighted s-value (S)
residuals
estimated K_d = 200 nM
concentration (M)
C
High salt (600 mM KCl)
K_d = 8.5 μM
D
TgSkp1ΔloopΔCTR
E
Low salt (25 mM KCl)
K_d = 2.4 μM
F
High salt (600 mM KCl)
K_d = 1.9 μM

Figure 2.7

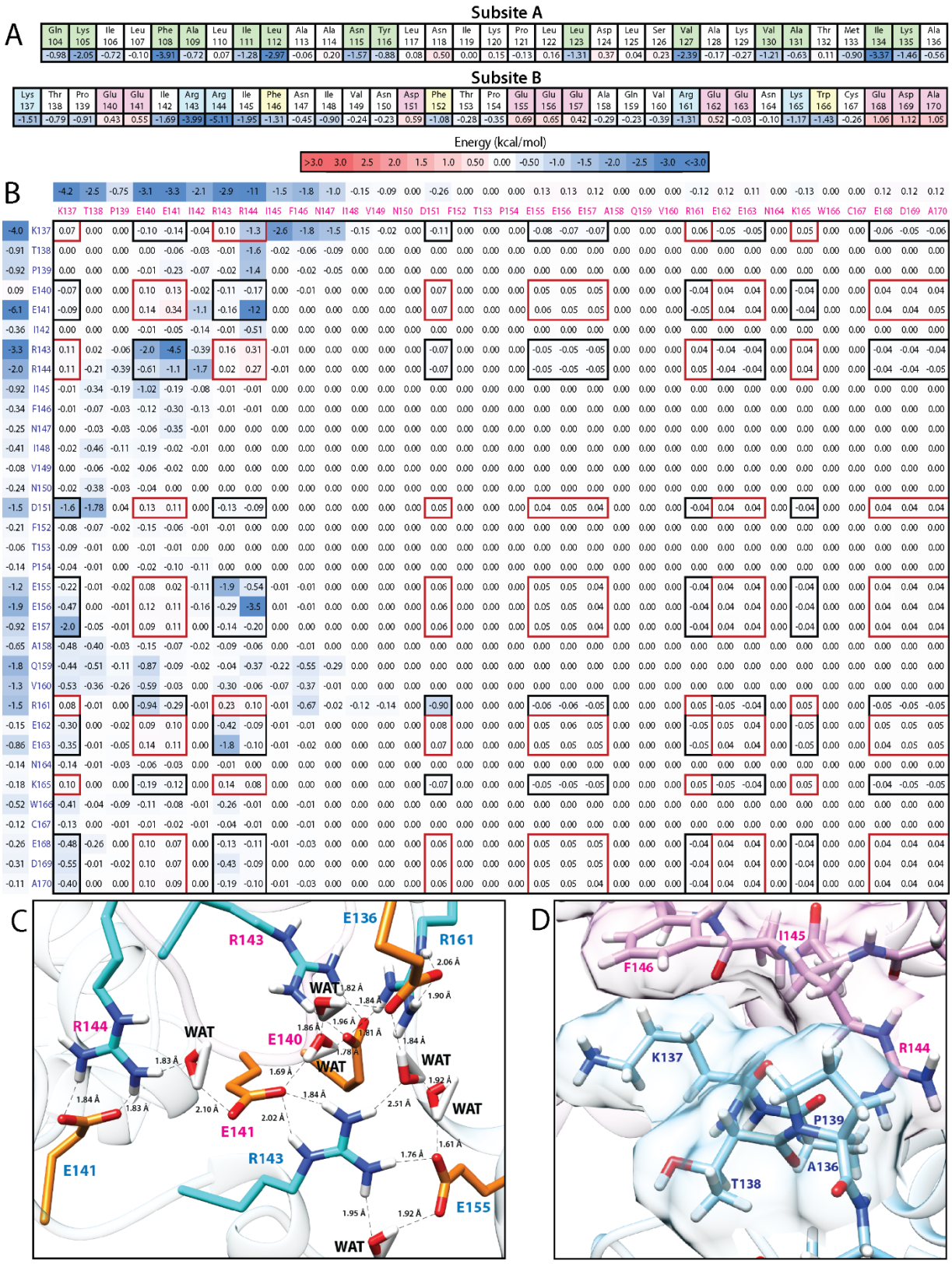

A
Subsite A
Gln 104 Lys 105 Ile 106 Leu 107 Phe 108 Ala 109 Leu 110 Ile 111 Leu 112 Ala 113 Ala 114 Asn 115 Tyr 116 Leu 117 Asn 118 Ile 119 Lys 120 Pro 121 Leu 122 Leu 123 Asp 124 Leu 125 Ser 126 Val 127 Ala 128 Lys 129 Val 130 Ala 131 Thr 132 Met 133 Ile 134 Lys 135 Ala 136
-0.98 -2.05 -0.72 -0.10 -3.91 -0.72 0.07 -1.28 -2.97 -0.06 0.20 -1.57 -0.88 0.08 0.50 0.00 0.15 -0.13 0.16 -1.31 0.37 0.04 0.23 -2.39 -0.17 -0.27 -1.21 -0.63 0.11 -0.90 -3.37 -1.46 -0.56
Subsite B
Lys 137 Thr 138 Pro 139 Glu 140 Glu 141 Ile 142 Arg 143 Arg 144 Ile 145 Phe 146 Asn 147 Ile 148 Val 149 Asn 150 Asp 151 Phe 152 Thr 153 Pro 154 Glu 155 Glu 156 Glu 157 Ala 158 Gln 159 Val 160 Arg 161 Glu 162 Glu 163 Asn 164 Lys 165 Trp 166 Cys 167 Glu 168 Asp 169 Ala 170
-1.51 -0.79 -0.91 0.43 0.55 -1.69 -3.99 -5.11 -1.95 -1.31 -0.45 -0.90 -0.24 -0.23 0.59 -1.08 -0.28 -0.35 0.69 0.65 0.42 -0.29 -0.23 -0.39 -1.31 0.52 -0.03 -0.10 -1.17 -1.43 -0.26 1.06 1.12 1.05
Energy (kcal/mol)
>3.0 3.0 2.5 2.0 1.5 1.0 0.50 0.00 -0.50 -1.0 -1.5 -2.0 -2.5 -3.0 <-3.0
B
C
R143
E136
R161
WAT
R144
WAT
E140
WAT
WAT
WAT
E141
E141
R143
E155
WAT
D
I145
F146
R144
K137
P139
A136
T138

Figure 2.8

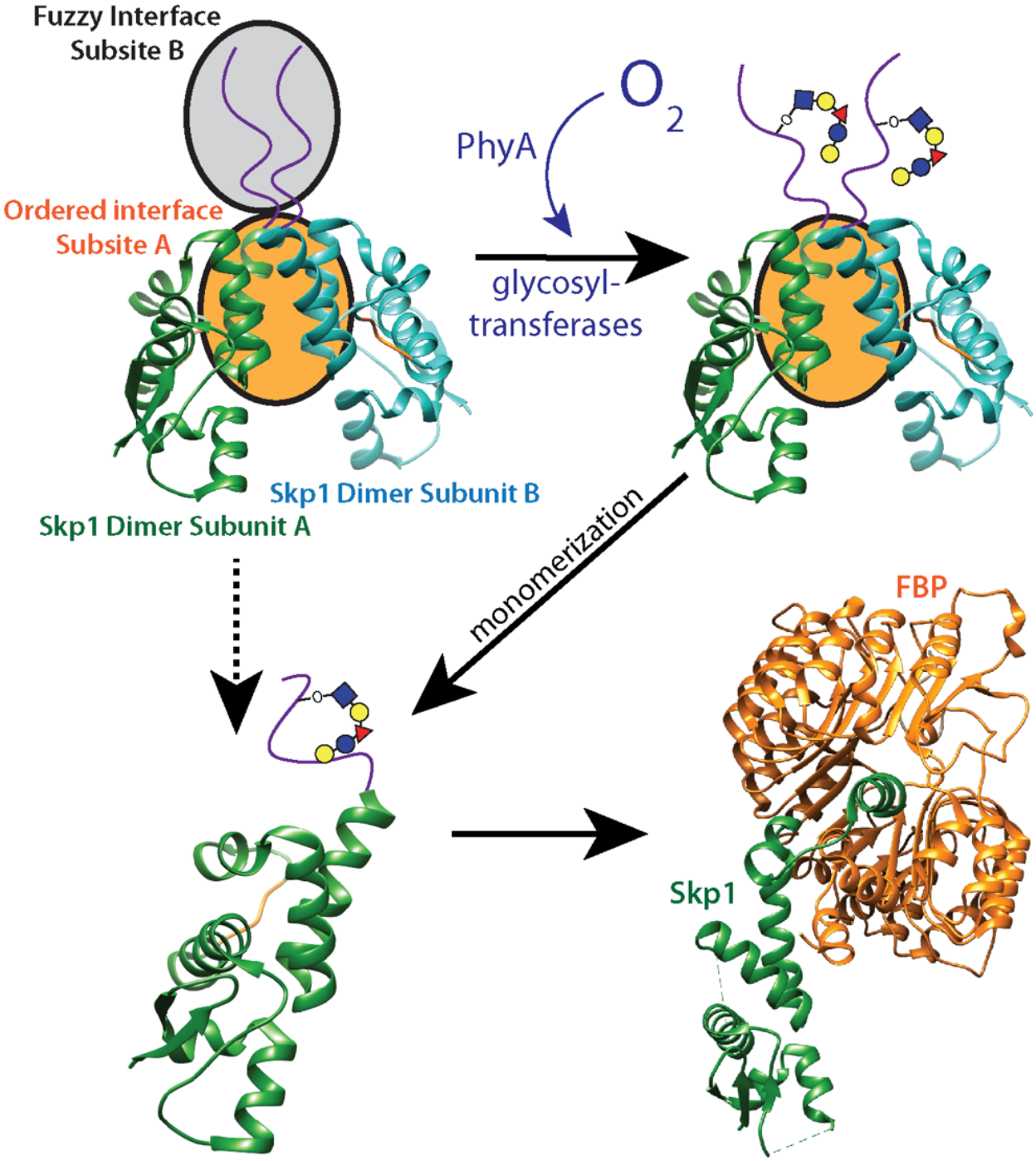

Fuzzy Interface
Subsite B
Ordered interface
Subsite A
PhyA
O_2
glycosyl-
transferases
Skp1 Dimer Subunit B
Skp1 Dimer Subunit A
monomerization
FBP
Skp1

Figure 2.S1

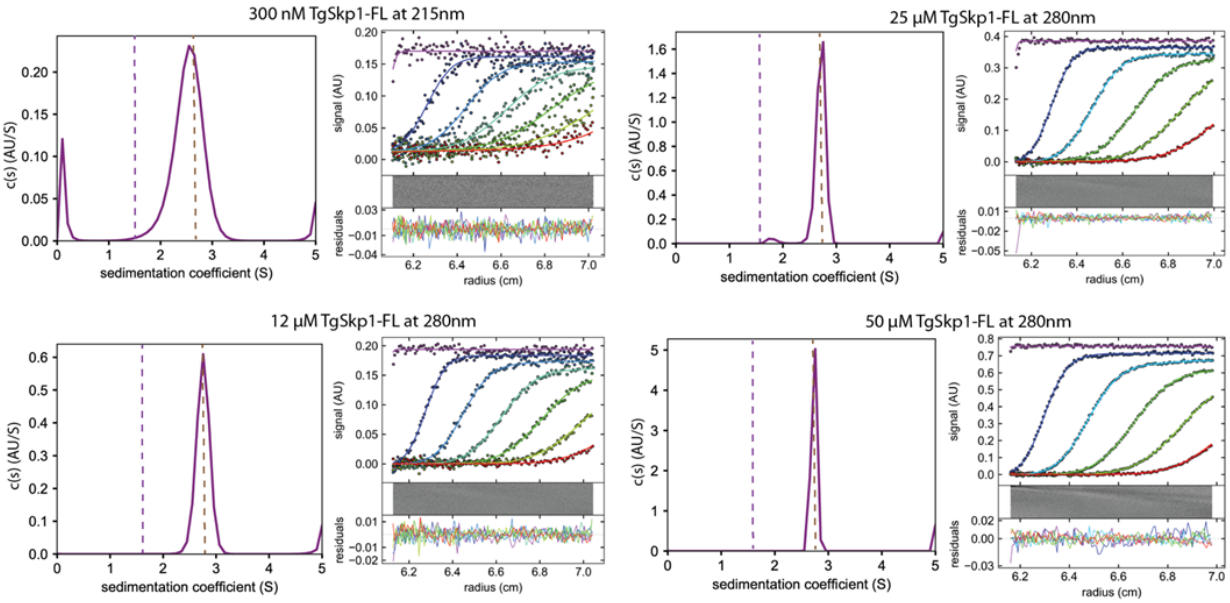

300 nM TgSkp1-FL at 215nm
25 μM TgSkp1-FL at 280nm
12 μM TgSkp1-FL at 280nm
50 μM TgSkp1-FL at 280nm
c(s) (AU/S)
sedimentation coefficient (S)
signal (AU)
residuals
radius (cm)

Figure 2.S2

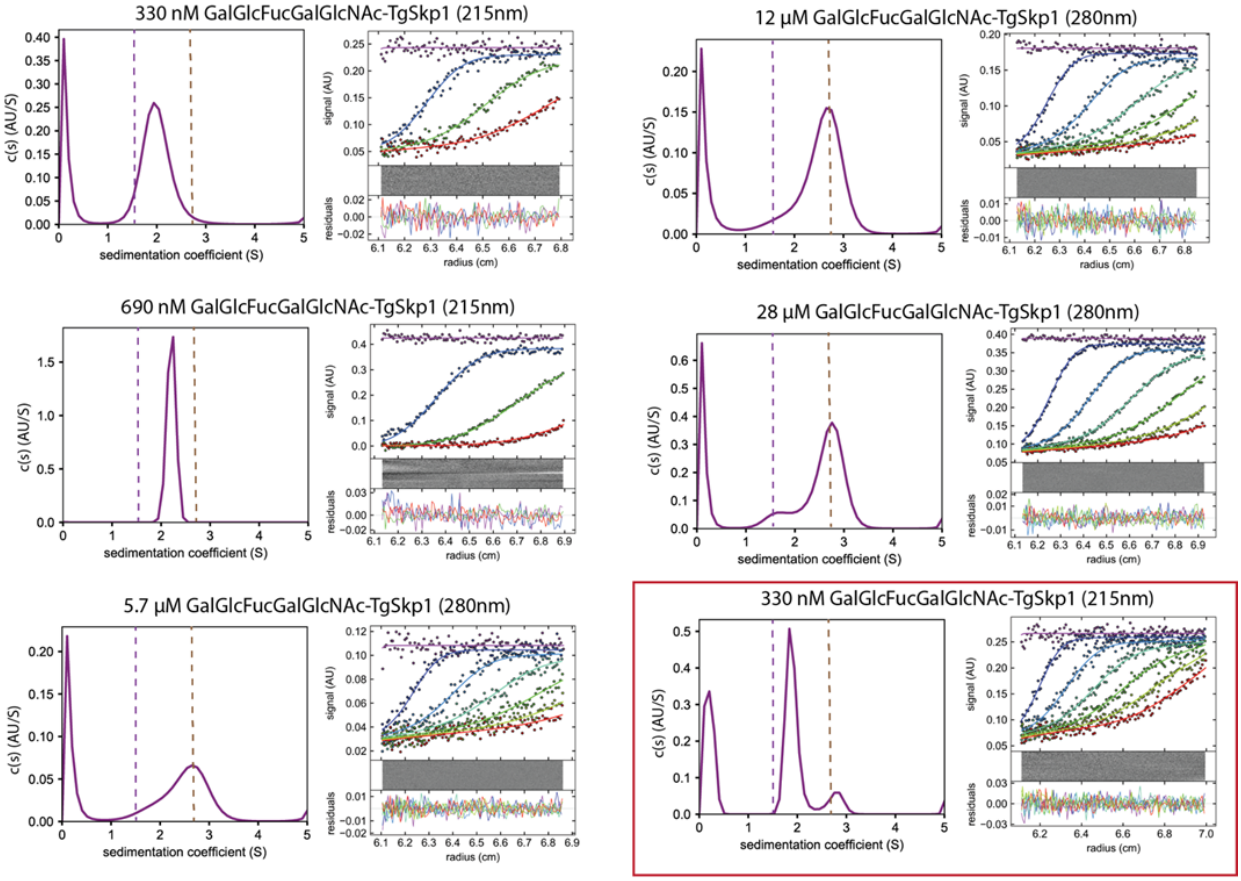

330 nM GalGlcFucGalGlcNAc-TgSkp1 (215nm)
12 μM GalGlcFucGalGlcNAc-TgSkp1 (280nm)
690 nM GalGlcFucGalGlcNAc-TgSkp1 (215nm)
28 μM GalGlcFucGalGlcNAc-TgSkp1 (280nm)
5.7 μM GalGlcFucGalGlcNAc-TgSkp1 (280nm)
330 nM GalGlcFucGalGlcNAc-TgSkp1 (215nm)
c(s) (AU/S)
sedimentation coefficient (S)
signal (AU)
residuals
radius (cm)

Figure 2.S3

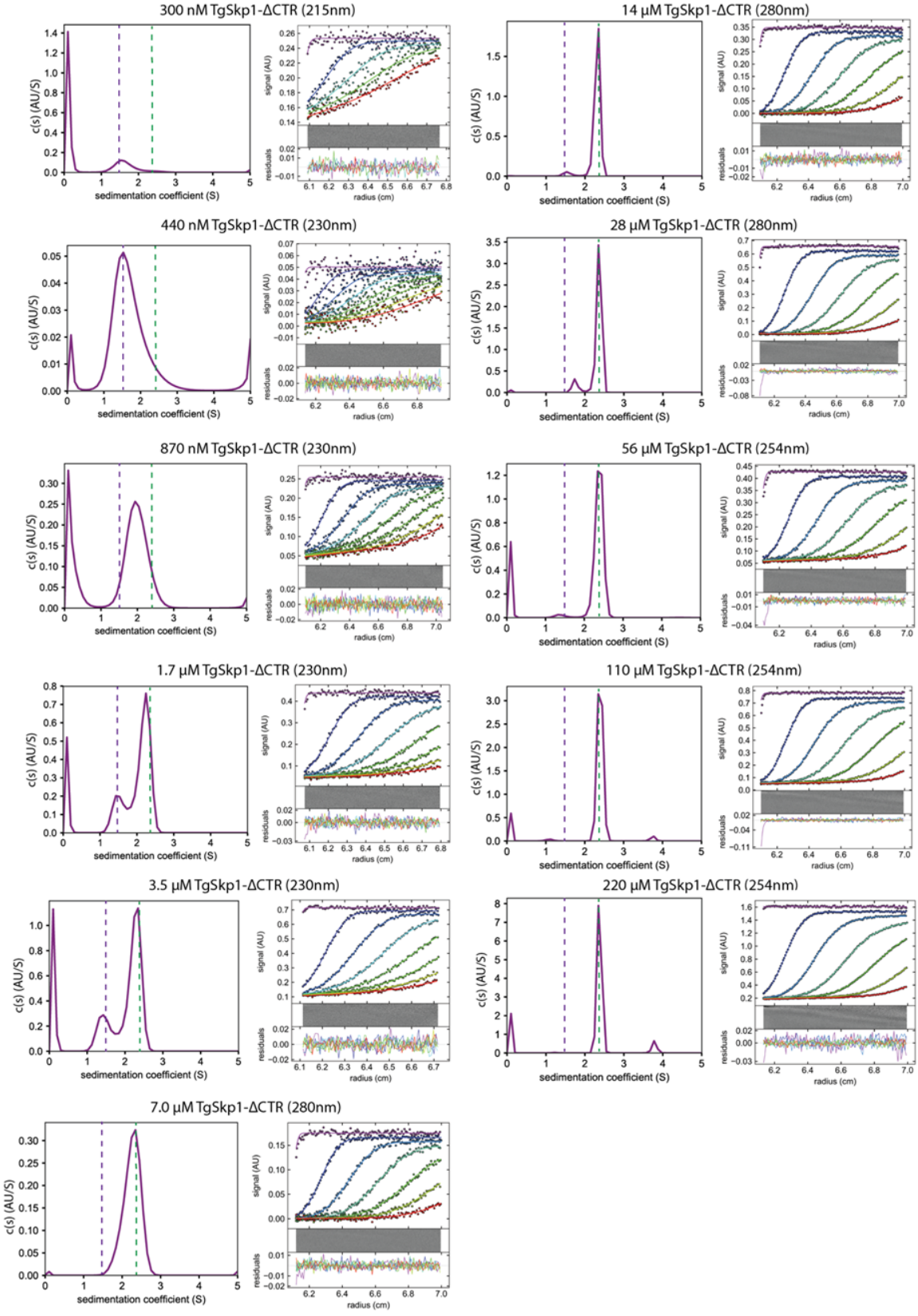
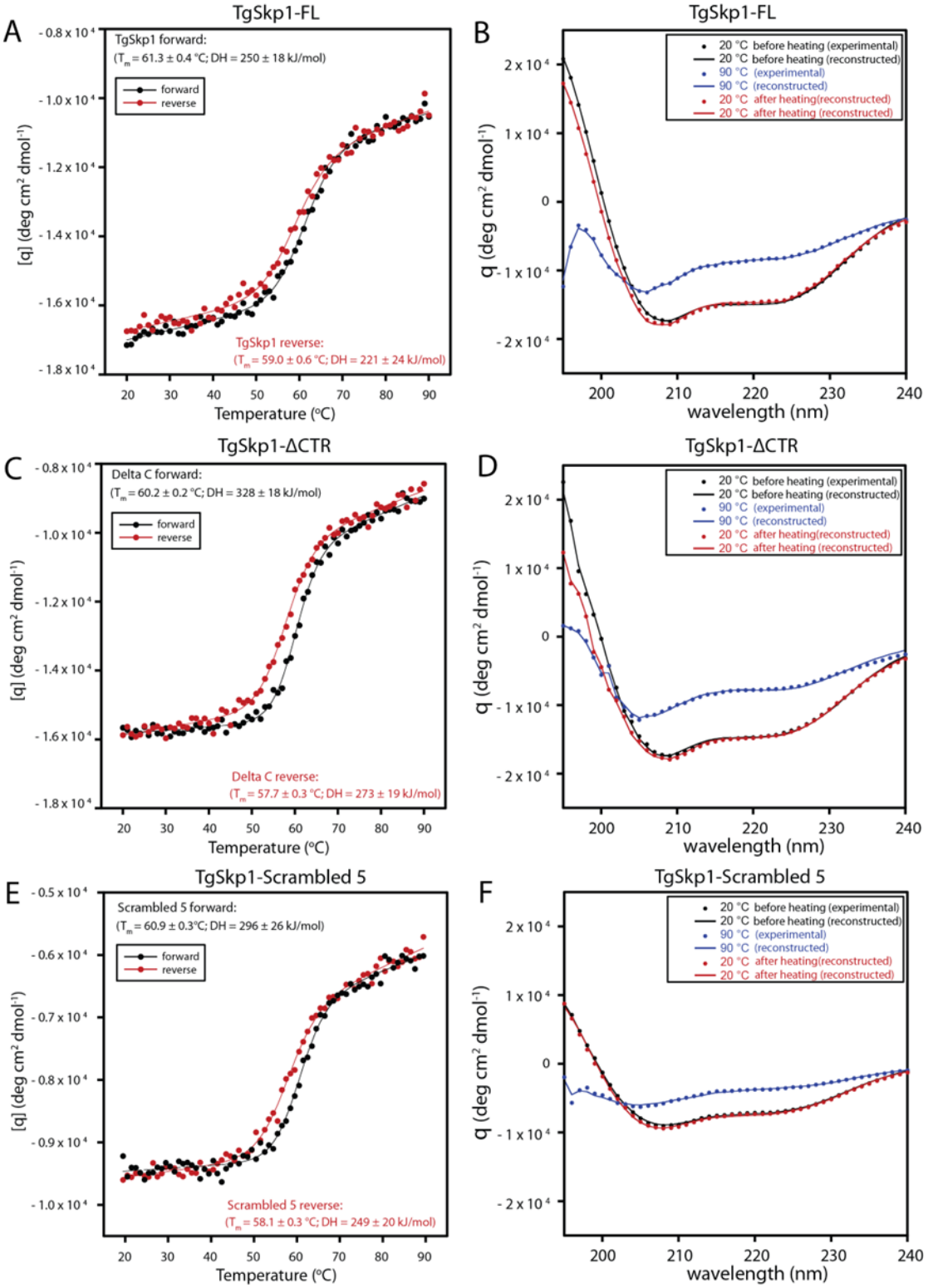
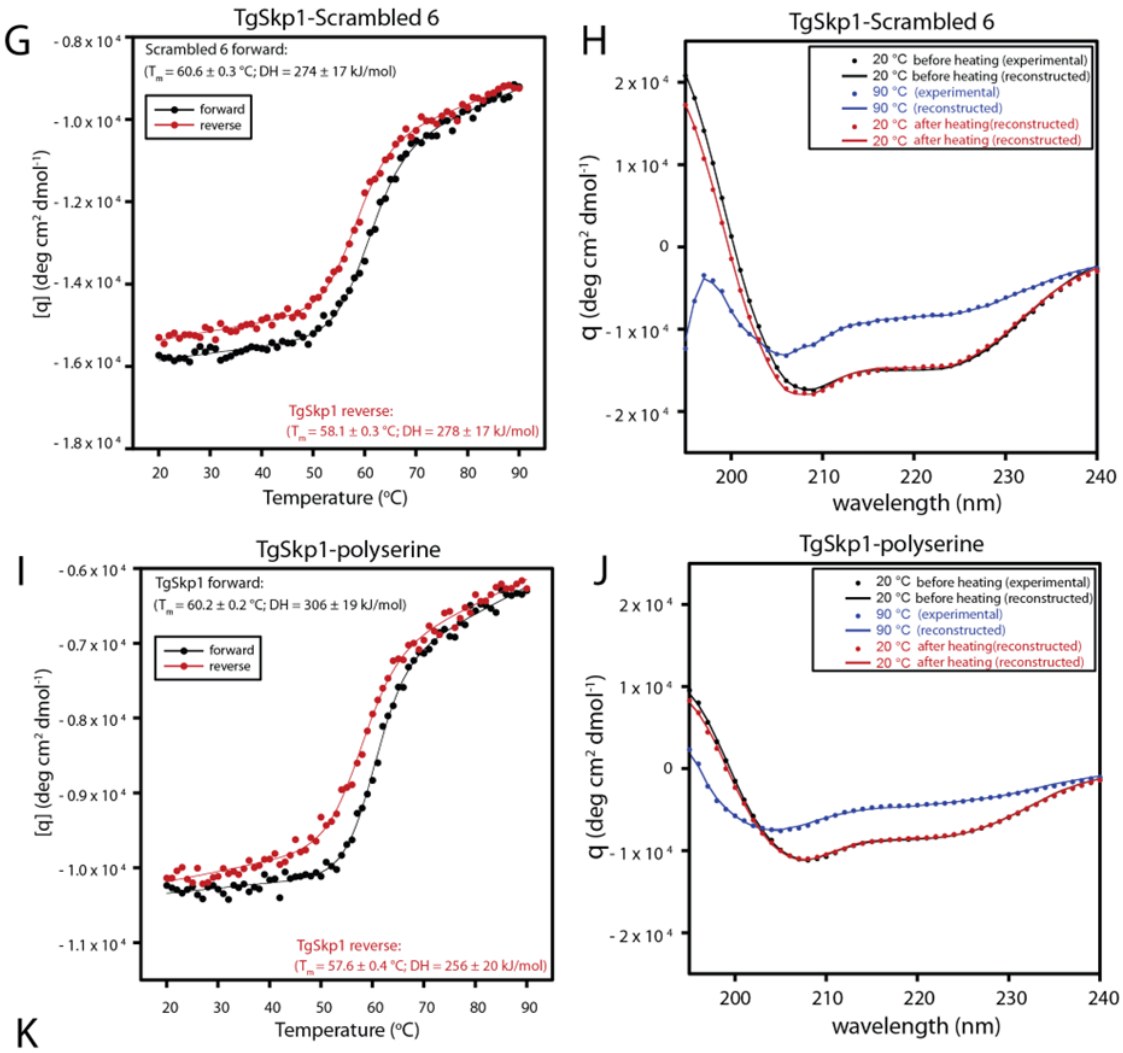

300 nM TgSkp1-ΔCTR (215nm)
14 μM TgSkp1-ΔCTR (280nm)
440 nM TgSkp1-ΔCTR (230nm)
28 μM TgSkp1-ΔCTR (280nm)
870 nM TgSkp1-ΔCTR (230nm)
56 μM TgSkp1-ΔCTR (254nm)
1.7 μM TgSkp1-ΔCTR (230nm)
110 μM TgSkp1-ΔCTR (254nm)
3.5 μM TgSkp1-ΔCTR (230nm)
220 μM TgSkp1-ΔCTR (254nm)
7.0 μM TgSkp1-ΔCTR (280nm)
c(s) (AU/S)
sedimentation coefficient (S)
signal (AU)
residuals
radius (cm)

Figure 2.S4


A
TgSkp1-FL
TgSkp1 forward:
(Tm = 61.3 ± 0.4 °C; DH = 250 ± 18 kJ/mol)
forward
reverse
TgSkp1 reverse:
(Tm = 59.0 ± 0.6 °C; DH = 221 ± 24 kJ/mol)
[q] (deg cm2 dmol-1)
Temperature (°C)
B
TgSkp1-FL
20 °C before heating (experimental)
20 °C before heating (reconstructed)
90 °C (experimental)
90 °C (reconstructed)
20 °C after heating(reconstructed)
20 °C after heating (reconstructed)
q (deg cm2 dmol-1)
wavelength (nm)
C
TgSkp1-ΔCTR
Delta C forward:
(Tm = 60.2 ± 0.2 °C; DH = 328 ± 18 kJ/mol)
forward
reverse
Delta C reverse:
(Tm = 57.7 ± 0.3 °C; DH = 273 ± 19 kJ/mol)
[q] (deg cm2 dmol-1)
Temperature (°C)
D
TgSkp1-ΔCTR
20 °C before heating (experimental)
20 °C before heating (reconstructed)
90 °C (experimental)
90 °C (reconstructed)
20 °C after heating(reconstructed)
20 °C after heating (reconstructed)
q (deg cm2 dmol-1)
wavelength (nm)
E
TgSkp1-Scrambled 5
Scrambled 5 forward:
(Tm = 60.9 ± 0.3°C; DH = 296 ± 26 kJ/mol)
forward
reverse
Scrambled 5 reverse:
(Tm = 58.1 ± 0.3 °C; DH = 249 ± 20 kJ/mol)
[q] (deg cm2 dmol-1)
Temperature (°C)
F
TgSkp1-Scrambled 5
20 °C before heating (experimental)
20 °C before heating (reconstructed)
90 °C (experimental)
90 °C (reconstructed)
20 °C after heating(reconstructed)
20 °C after heating (reconstructed)
q (deg cm2 dmol-1)
wavelength (nm)



K

Sample	α-helix (%)	β-strand (%)	β-turns (%)	Unordered (%)
TgSkp1-FL (before 20 °C)	52	7	14	27
TgSkp1-FL (90 °C)	38	21	14	28
TgSkp1-FL (after 20 °C)	56	7	13	23
TgSkp1-ΔC terminus (before 20 °C)	57	10	12	19
TgSkp1-ΔC terminus (90 °C)	35	11	16	38
TgSkp1-ΔC terminus (after 20 °C)	56	10	14	21
TgSkp1-Scrambled 6 (before 20 °C)	49	10	14	28
TgSkp1-Scrambled 6 (90 °C)	16	13	13	58
TgSkp1-Scrambled 6 (after 20 °C)	50	9	17	24
TgSkp1-Scrambled 5 (before 20 °C)	22	23	20	35
TgSkp1-Scrambled 5 (90 °C)	5	28	18	47
TgSkp1-Scrambled 5 (after 20 °C)	25	19	28	36
TgSkp1-polyserine (before 20 °C)	32	13	18	37
TgSkp1-polyserine (90 °C)	7	29	27	46
TgSkp1-polyserine (after 20 °C)	32	11	16	41

Figure 2.S5

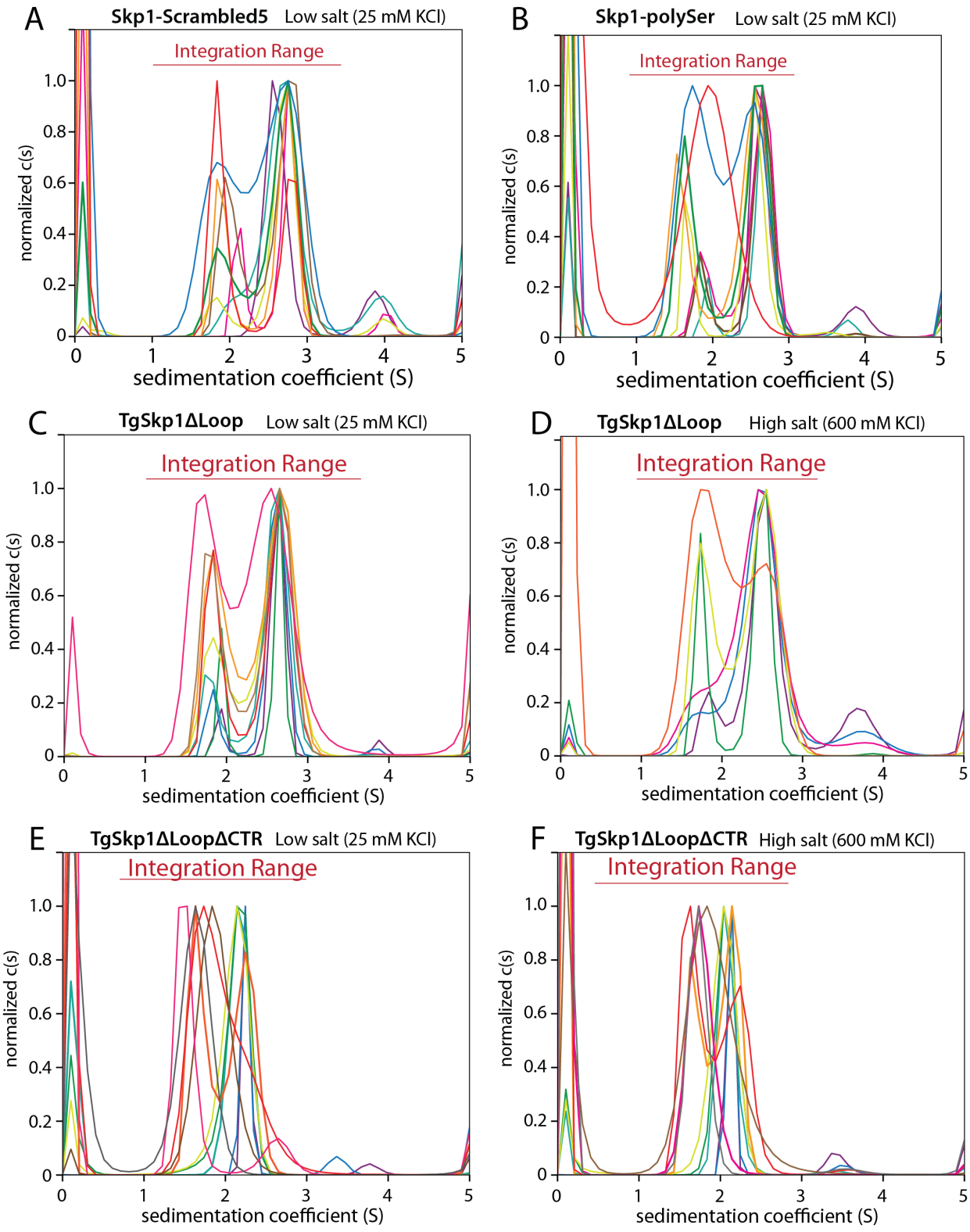

A
Skp1-Scrambled5 Low salt (25 mM KCl)
Integration Range
normalized c(s)
sedimentation coefficient (S)
B
Skp1-polySer Low salt (25 mM KCl)
Integration Range
normalized c(s)
sedimentation coefficient (S)
C
TgSkp1ΔLoop Low salt (25 mM KCl)
Integration Range
normalized c(s)
sedimentation coefficient (S)
D
TgSkp1ΔLoop High salt (600 mM KCl)
Integration Range
normalized c(s)
sedimentation coefficient (S)
E
TgSkp1ΔLoopΔCTR Low salt (25 mM KCl)
Integration Range
normalized c(s)
sedimentation coefficient (S)
F
TgSkp1ΔLoopΔCTR High salt (600 mM KCl)
Integration Range
normalized c(s)
sedimentation coefficient (S)

Figure 2.S6

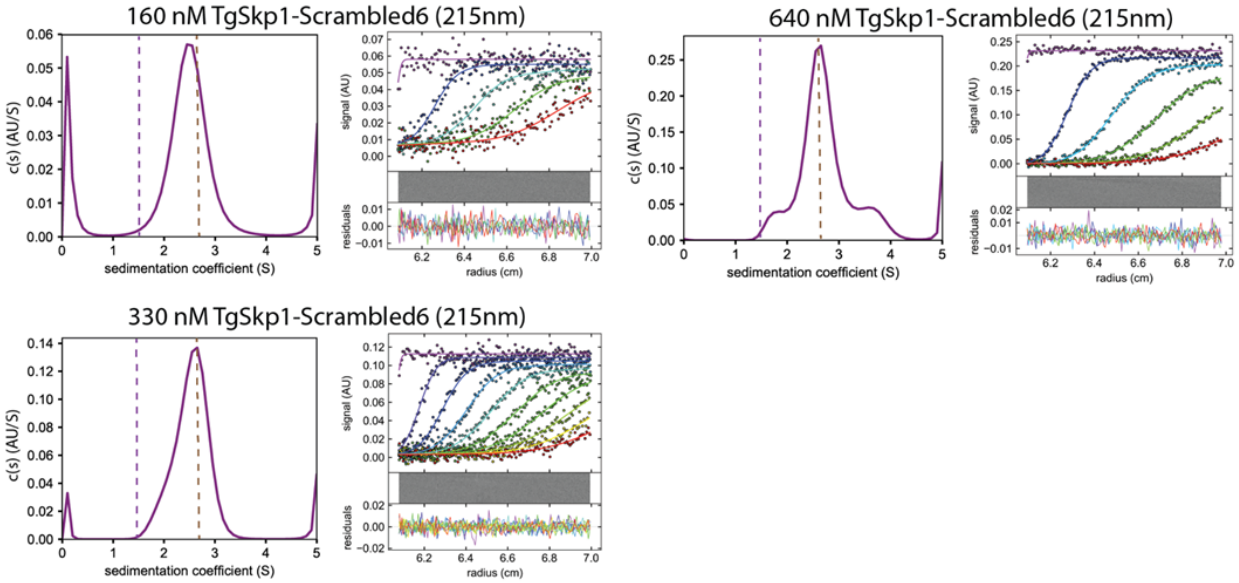

160 nM TgSkp1-Scrambled6 (215nm)
640 nM TgSkp1-Scrambled6 (215nm)
330 nM TgSkp1-Scrambled6 (215nm)
c(s) (AU/S)
sedimentation coefficient (S)
signal (AU)
residuals
radius (cm)

Figure 2.S7

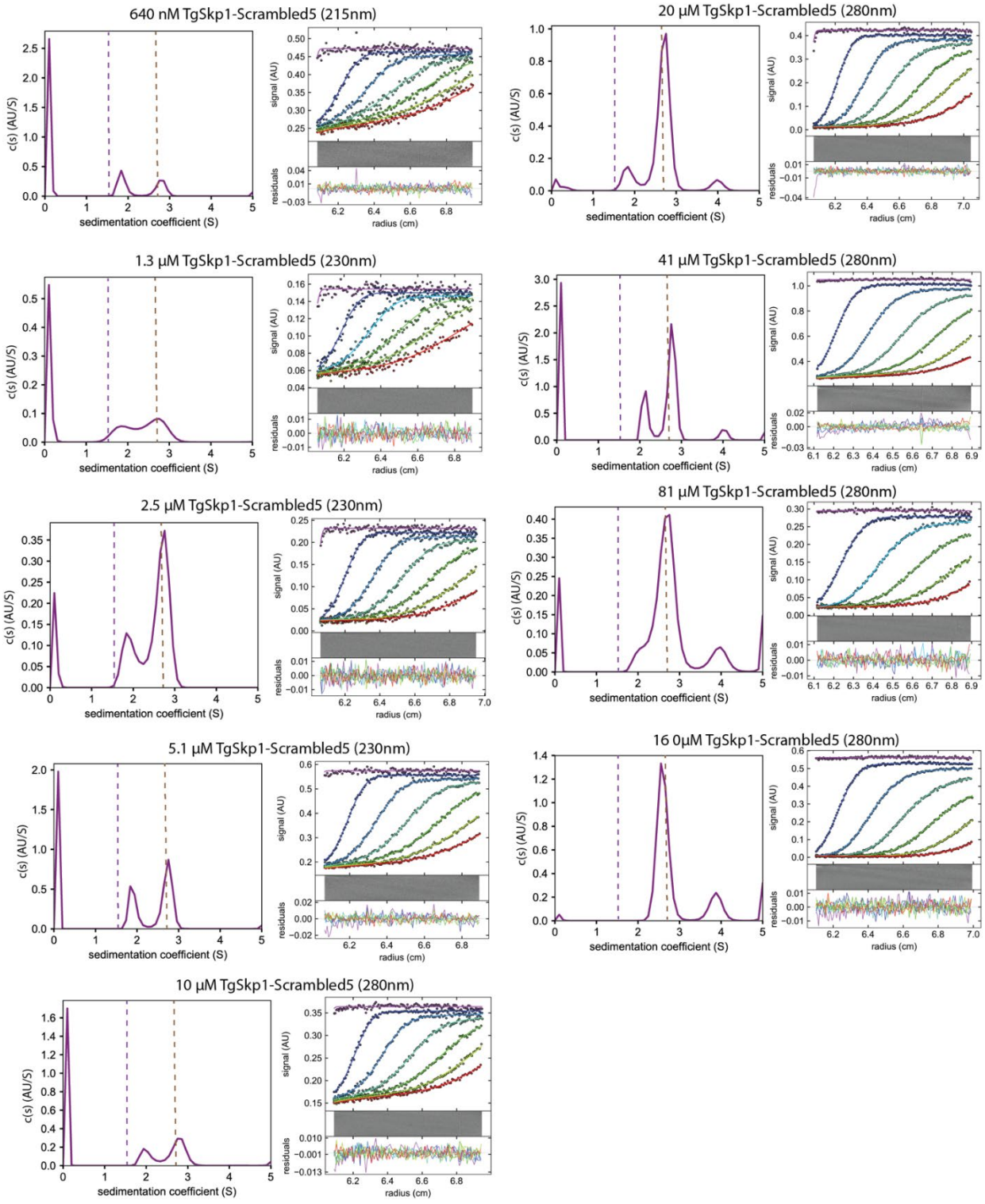

640 nM TgSkp1-Scrambled5 (215nm)
20 μM TgSkp1-Scrambled5 (280nm)
1.3 μM TgSkp1-Scrambled5 (230nm)
41 μM TgSkp1-Scrambled5 (280nm)
2.5 μM TgSkp1-Scrambled5 (230nm)
81 μM TgSkp1-Scrambled5 (280nm)
5.1 μM TgSkp1-Scrambled5 (230nm)
16 0μM TgSkp1-Scrambled5 (280nm)
10 μM TgSkp1-Scrambled5 (280nm)
c(s) (AU/S)
sedimentation coefficient (S)
signal (AU)
residuals
radius (cm)

Figure 2.S8

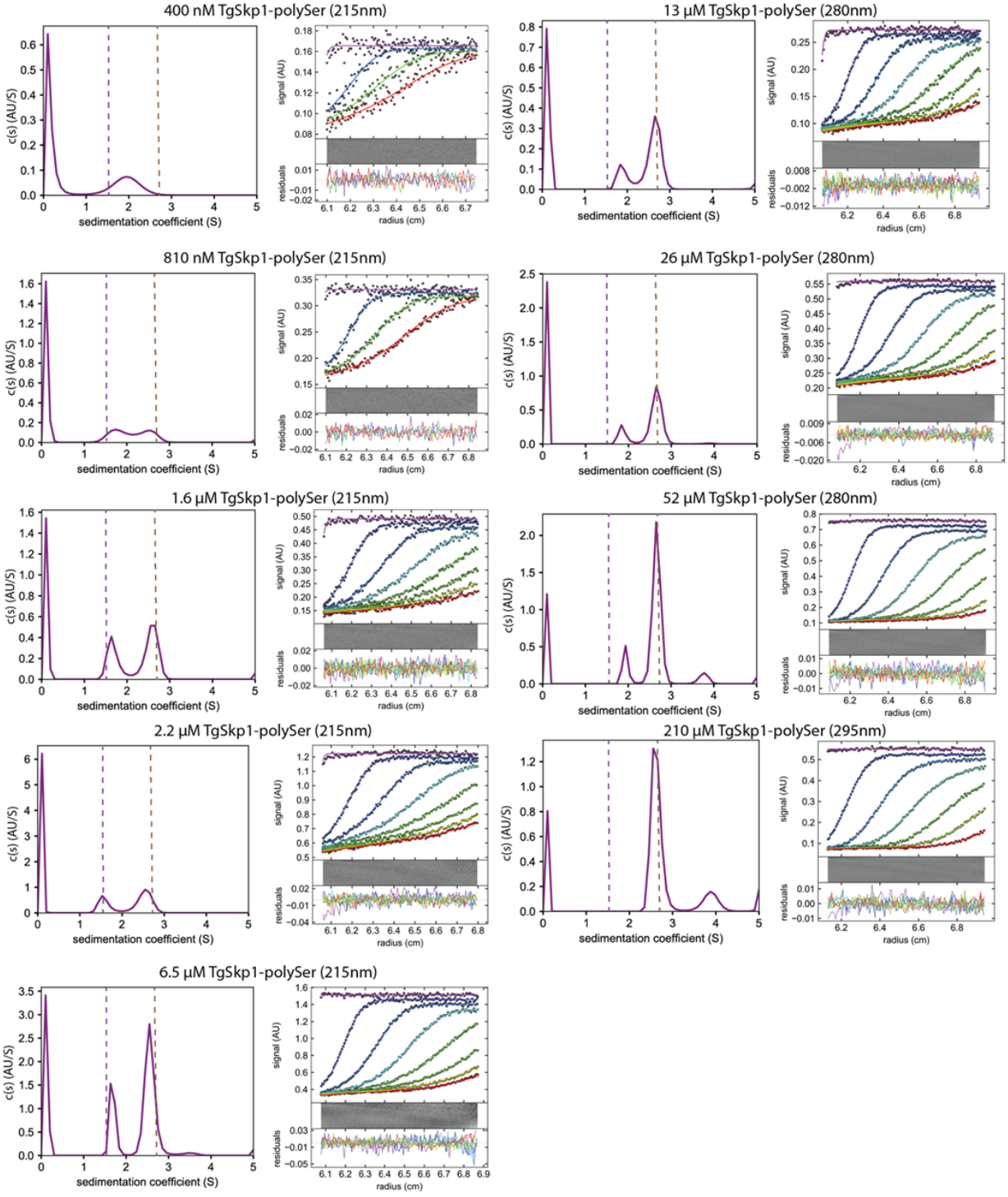

400 nM TgSkp1-polySer (215nm)
13 µM TgSkp1-polySer (280nm)
810 nM TgSkp1-polySer (215nm)
26 µM TgSkp1-polySer (280nm)
1.6 µM TgSkp1-polySer (215nm)
52 µM TgSkp1-polySer (280nm)
2.2 µM TgSkp1-polySer (215nm)
210 µM TgSkp1-polySer (295nm)
6.5 µM TgSkp1-polySer (215nm)
c(s) (AU/S)
sedimentation coefficient (S)
signal (AU)
residuals
radius (cm)

Figure 2.S9

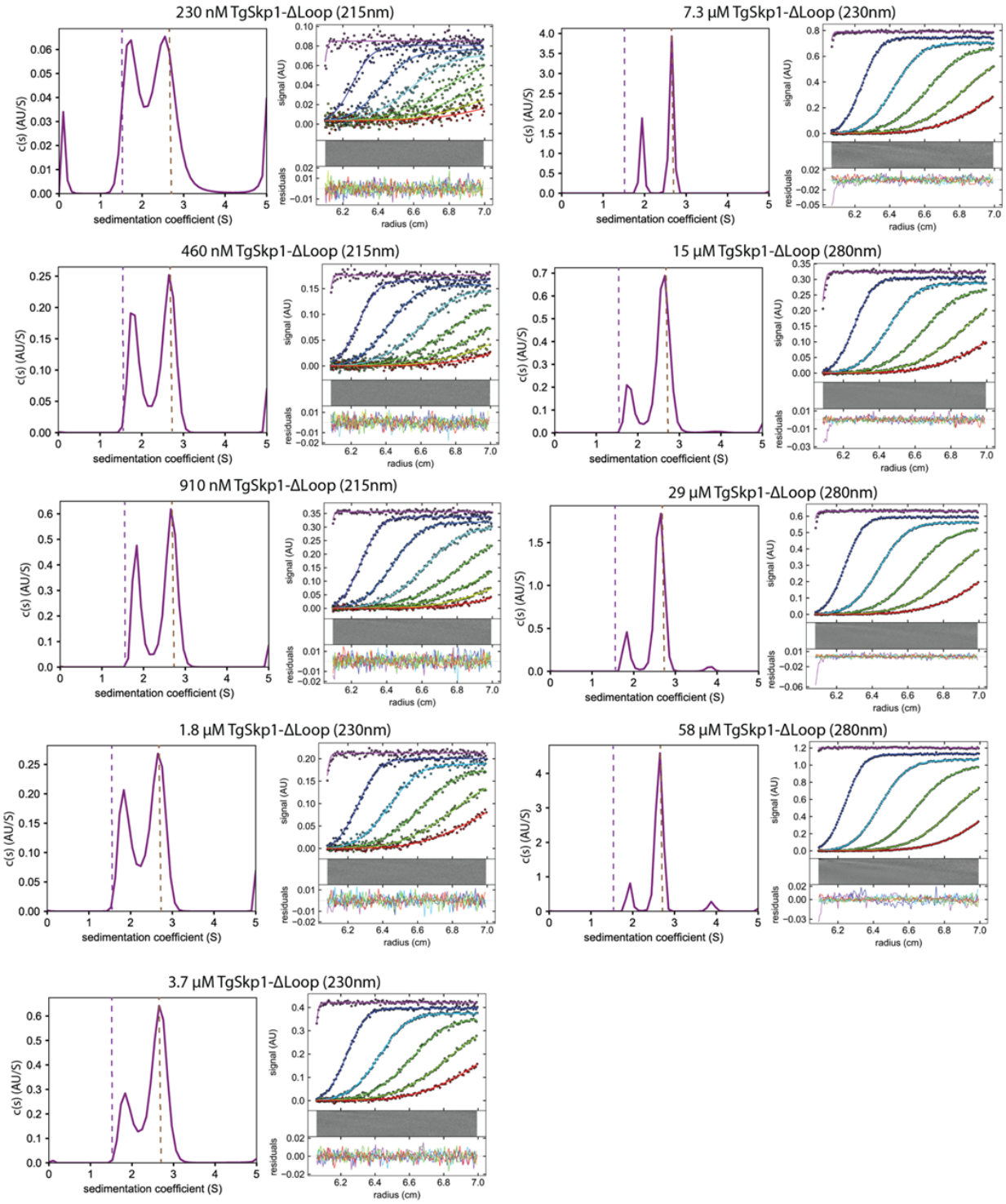

230 nM TgSkp1-ΔLoop (215nm)
7.3 μM TgSkp1-ΔLoop (230nm)
460 nM TgSkp1-ΔLoop (215nm)
15 μM TgSkp1-ΔLoop (280nm)
910 nM TgSkp1-ΔLoop (215nm)
29 μM TgSkp1-ΔLoop (280nm)
1.8 μM TgSkp1-ΔLoop (230nm)
58 μM TgSkp1-ΔLoop (280nm)
3.7 μM TgSkp1-ΔLoop (230nm)
c(s) (AU/S)
sedimentation coefficient (S)
signal (AU)
residuals
radius (cm)

Figure 2.S10

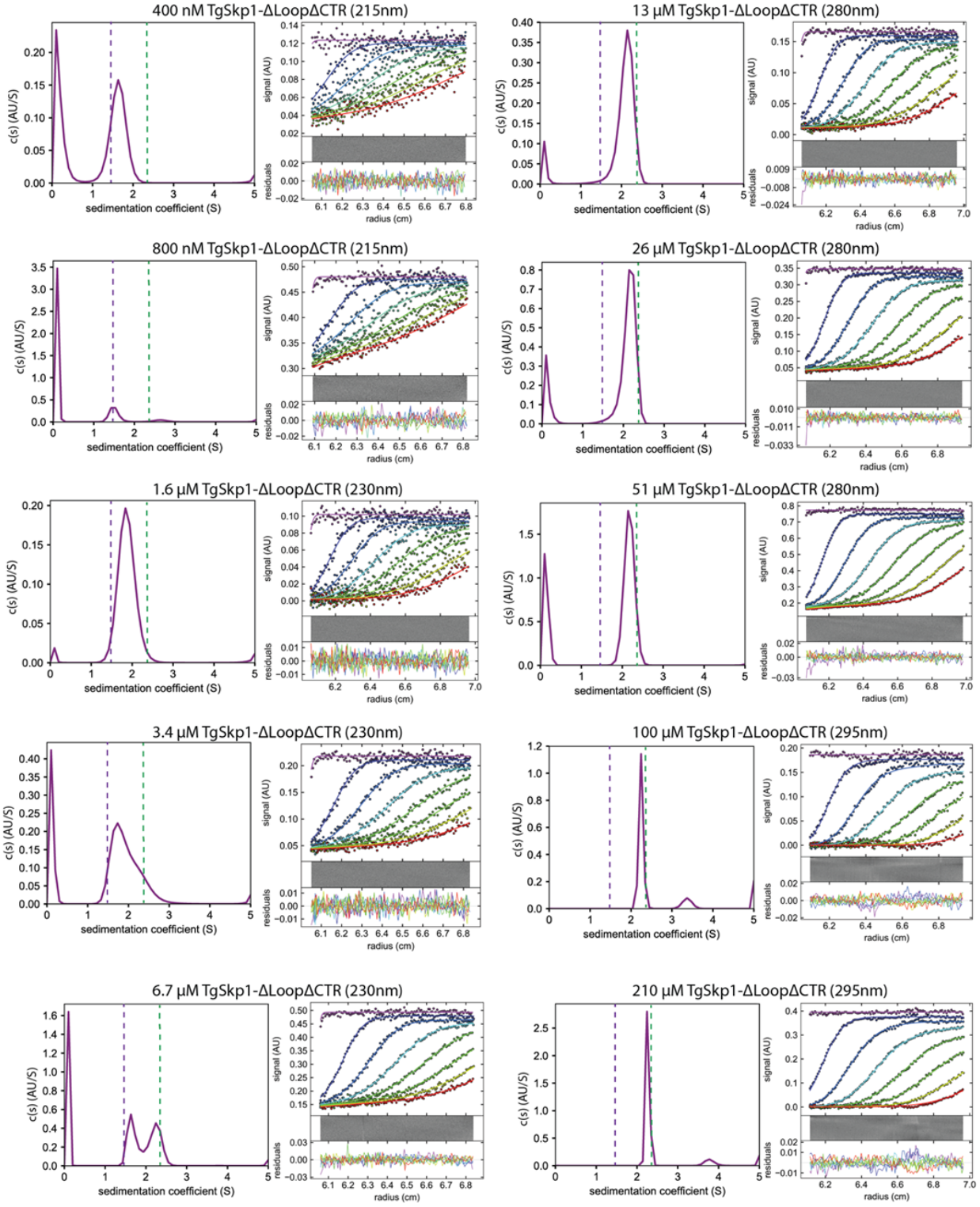

400 nM TgSkp1-ΔLoopΔCTR (215nm)
13 μM TgSkp1-ΔLoopΔCTR (280nm)
800 nM TgSkp1-ΔLoopΔCTR (215nm)
26 μM TgSkp1-ΔLoopΔCTR (280nm)
1.6 μM TgSkp1-ΔLoopΔCTR (230nm)
51 μM TgSkp1-ΔLoopΔCTR (280nm)
3.4 μM TgSkp1-ΔLoopΔCTR (230nm)
100 μM TgSkp1-ΔLoopΔCTR (295nm)
6.7 μM TgSkp1-ΔLoopΔCTR (230nm)
210 μM TgSkp1-ΔLoopΔCTR (295nm)
c(s) (AU/S)
sedimentation coefficient (S)
signal (AU)
residuals
radius (cm)

Figure 2.S11

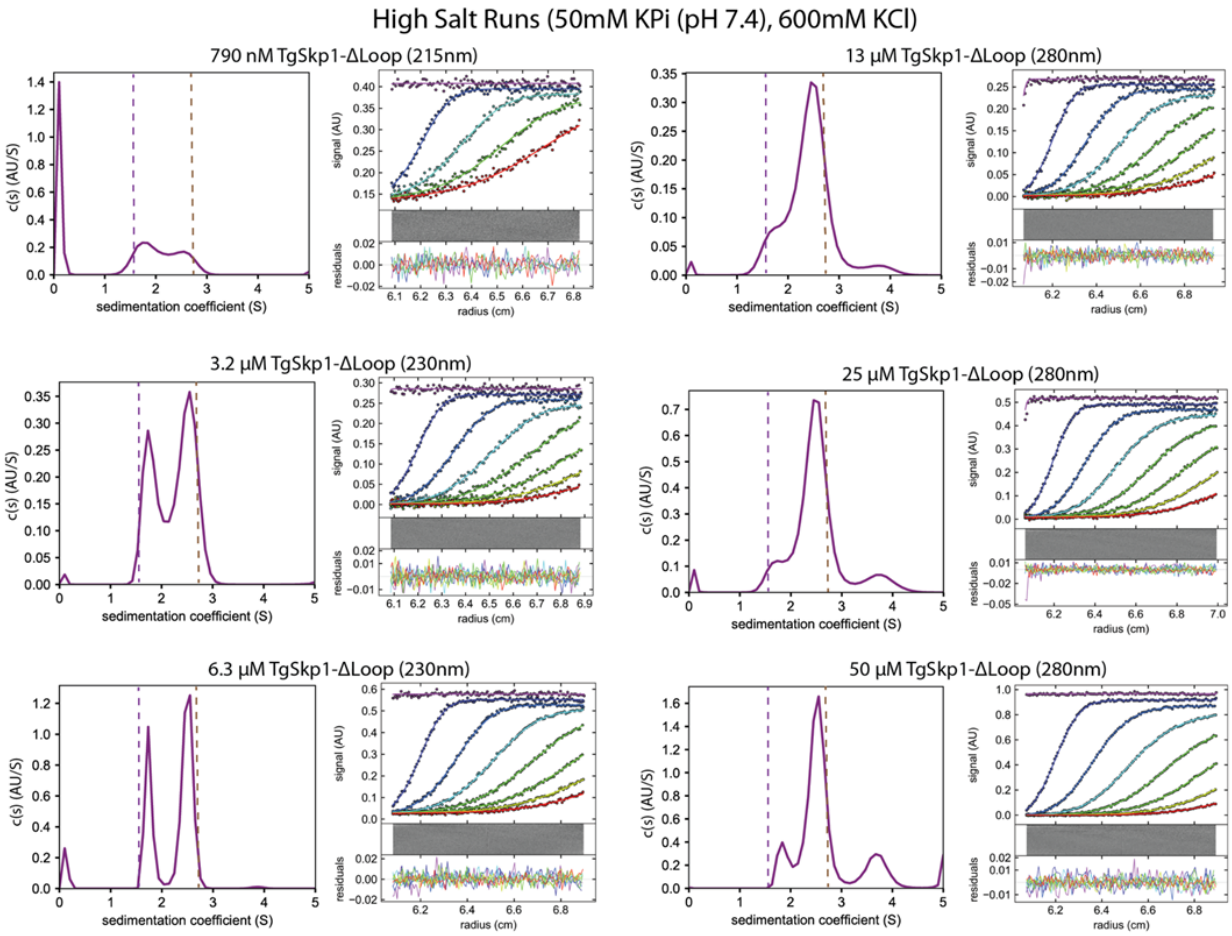

High Salt Runs (50mM KPi (pH 7.4), 600mM KCl)
790 nM TgSkp1-ΔLoop (215nm)
13 μM TgSkp1-ΔLoop (280nm)
3.2 μM TgSkp1-ΔLoop (230nm)
25 μM TgSkp1-ΔLoop (280nm)
6.3 μM TgSkp1-ΔLoop (230nm)
50 μM TgSkp1-ΔLoop (280nm)
c(s) (AU/S)
sedimentation coefficient (S)
signal (AU)
residuals
radius (cm)

Figure 2.S12

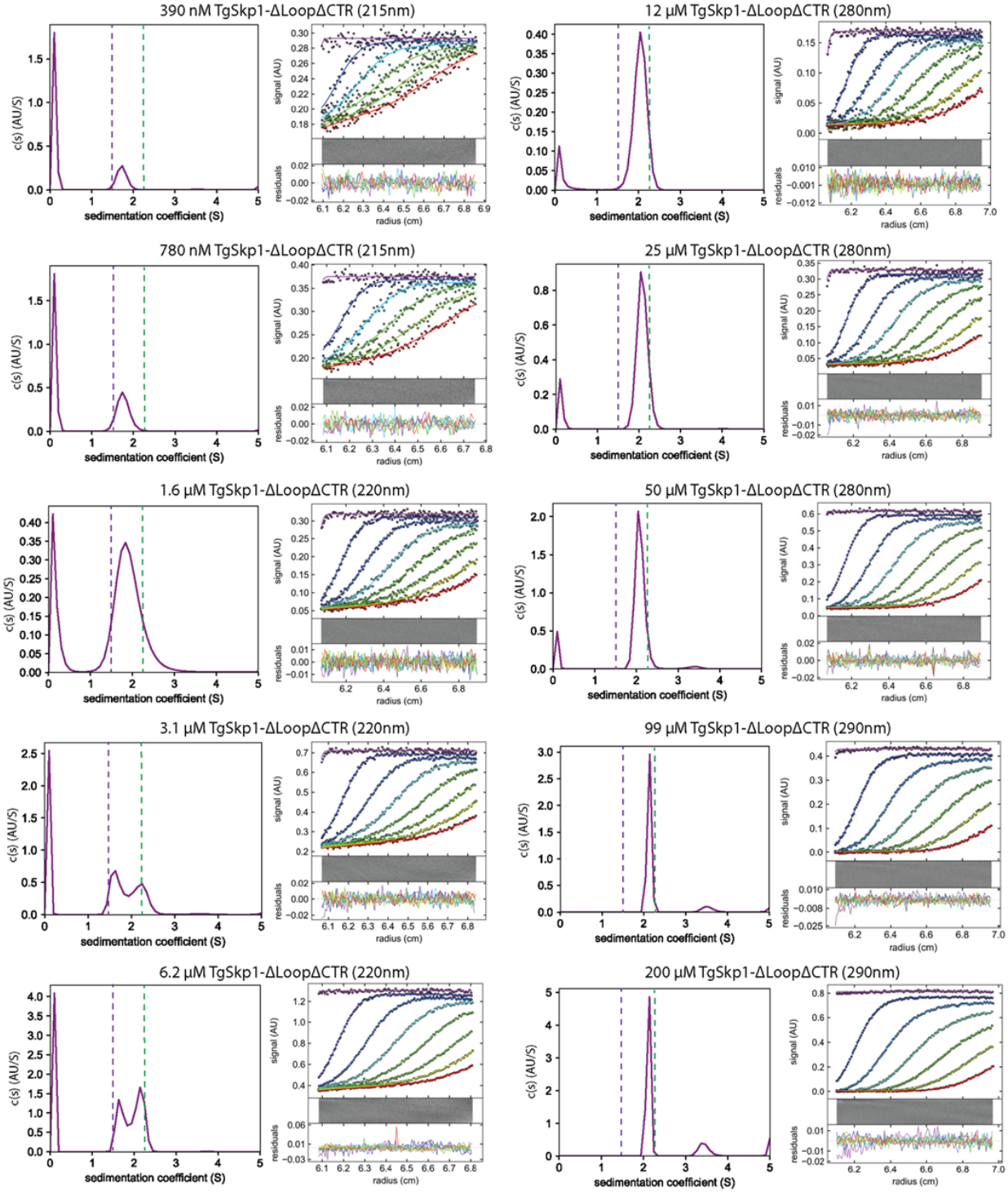

390 nM TgSkp1-ΔLoopΔCTR (215nm)
12 μM TgSkp1-ΔLoopΔCTR (280nm)
780 nM TgSkp1-ΔLoopΔCTR (215nm)
25 μM TgSkp1-ΔLoopΔCTR (280nm)
1.6 μM TgSkp1-ΔLoopΔCTR (220nm)
50 μM TgSkp1-ΔLoopΔCTR (280nm)
3.1 μM TgSkp1-ΔLoopΔCTR (220nm)
99 μM TgSkp1-ΔLoopΔCTR (290nm)
6.2 μM TgSkp1-ΔLoopΔCTR (220nm)
200 μM TgSkp1-ΔLoopΔCTR (290nm)
c(s) (AU/S)
sedimentation coefficient (S)
signal (AU)
residuals
radius (cm)

Figure 2.S13

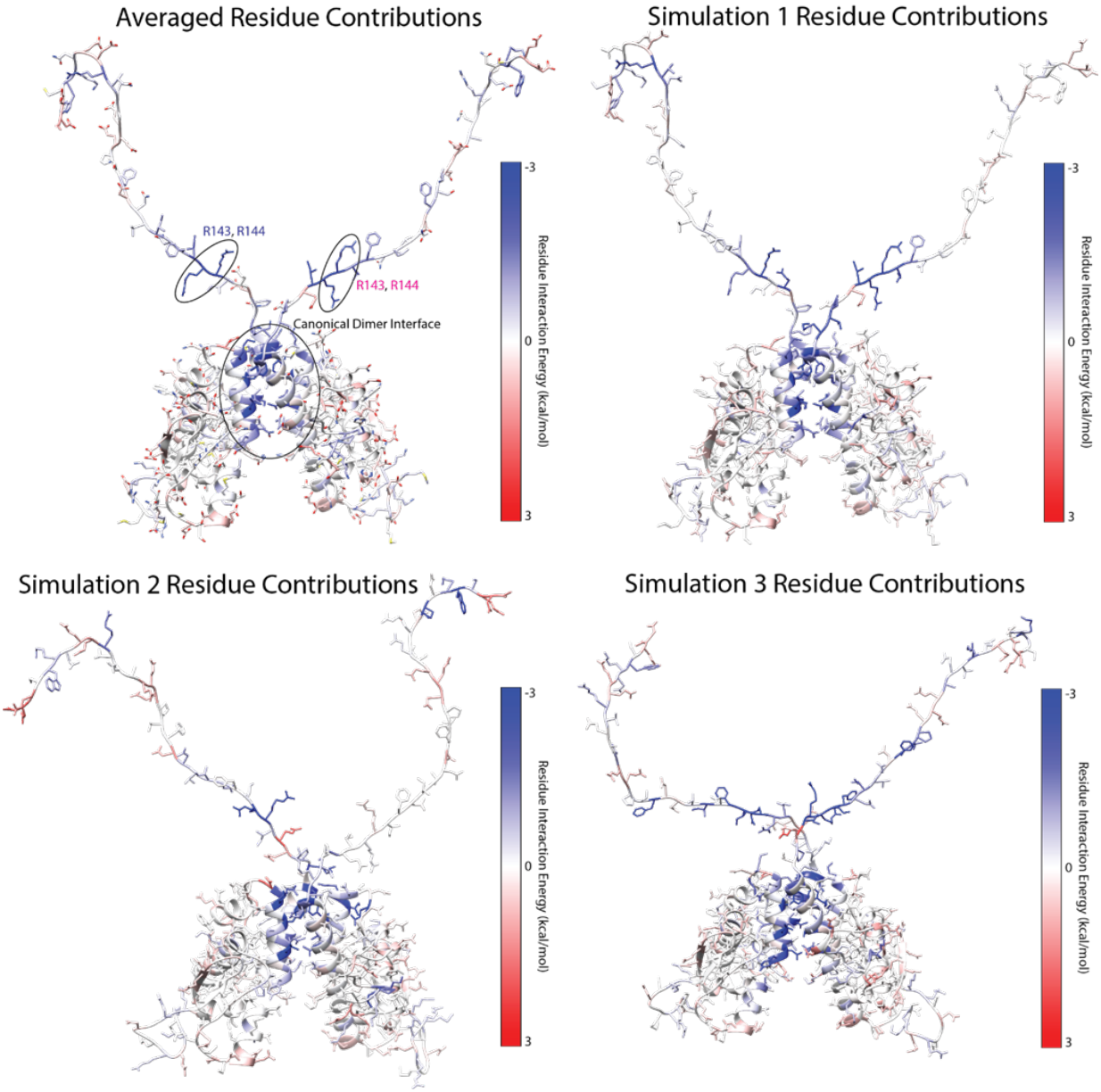

Averaged Residue Contributions
R143, R144
R143, R144
Canonical Dimer Interface
-3
0
3
Residue Interaction Energy (kcal/mol)
Simulation 1 Residue Contributions
-3
0
3
Residue Interaction Energy (kcal/mol)
Simulation 2 Residue Contributions
-3
0
3
Residue Interaction Energy (kcal/mol)
Simulation 3 Residue Contributions
-3
0
3
Residue Interaction Energy (kcal/mol)

Figure 2.S14

Dimer interface subsite-A

CTR Basic Residues

CTR Acidic Residues

CTR Aromatic Residues

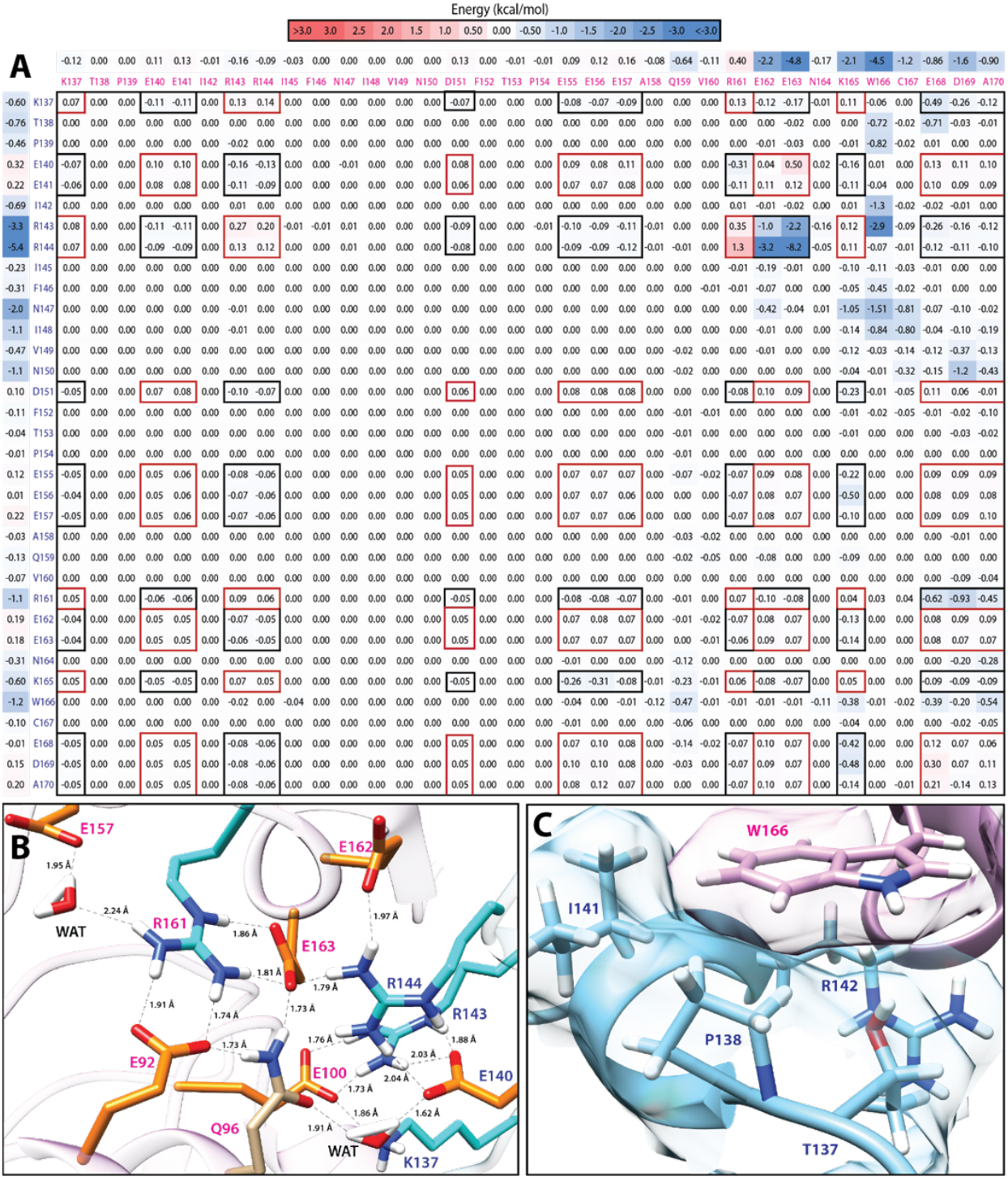
Residue	Energy
M1	-0.63
S2	0.00
K3	-0.62
E4	0.61
R5	-0.64
M6	0.00
G7	0.00
D8	0.61
A9	0.00
R10	-0.62
K11	-0.63
V12	0.01
T13	0.01
L14	0.02
V15	0.02
S16	0.05
Q17	0.11
E18	0.76
G19	0.01
D20	0.71
E21	0.65
F22	-0.01
D23	0.64
V24	0.00
D25	0.67
I26	0.01
E27	0.74
V28	0.03
A29	0.03
S30	0.06
M31	0.07
S32	-0.01
A33	0.03
L34	-0.32
I35	-0.02
K36	-0.70
T37	0.03
M38	-0.11
V39	0.00
E40	0.77
E41	0.75
D42	0.67
S43	0.00

Residue	Energy
D44	0.62
C45	0.00
Q46	0.01
E47	0.66
S48	0.03
I49	-0.05
P50	-0.02
L51	0.07
P52	-0.33
N53	-0.09
V54	0.01
D55	0.59
T56	-0.01
C57	-0.07
I58	-0.03
L59	-0.01
K60	-0.61
K61	-0.36
I62	0.02
I63	-0.01
E64	0.75
Y65	-0.01
C66	-0.01
E67	0.68
H68	0.01
H69	0.03
H70	0.01
N71	0.00
N72	0.02
P73	0.02
P74	0.00
E75	0.92
E76	1.0
P78	0.00
K79	-0.82
P80	-0.67
L81	-0.98
K82	-1.0
S83	-0.05
S84	-0.19
N85	-0.44
L86	-1.1
A87	-0.47

Residue	Energy
E88	0.89
V89	-0.22
V90	-0.09
S91	-0.06
E92	0.76
W93	0.01
D94	0.87
Y95	-0.05
Q96	0.06
F97	0.01
I98	0.00
N99	0.11
E100	-0.40
N101	0.17
S102	-0.21
D103	0.82
Q104	-0.98
K105	-2.1
I106	-0.72
L107	-0.10
F108	-3.9
A109	-0.72
L110	0.07
I111	-1.3
L112	-3.0
A113	-0.06
A114	0.20
N115	-1.6
Y116	-0.88
L117	0.08
N118	0.50
I119	0.00
K120	0.15
P121	-0.13
L122	0.16
L123	-1.3
D124	0.37
L125	0.04
S126	0.23
V127	-2
A128	-0.17
K129	-0.27
V130	-1.2

Residue	Energy
A131	-0.63
T132	0.11
M133	-0.90
I134	-3.4
K135	-1.5
A136	-0.56
K137	-1.5
T138	-0.79
P139	-0.91
E140	0.43
E141	0.55
I142	-1.7
R143	-4.0
R144	-5.1
I145	-1.9
F146	-1.3
N147	-0.45
I148	-0.90
V149	-0.24
N150	-0.23
D151	0.59
F152	-1.1
T153	-0.28
P154	-0.35
E155	0.69
E156	0.65
E157	0.42
A158	-0.29
Q159	-0.23
V160	-0.39
R161	-1.3
E162	0.52
E163	-0.03
N164	-0.10
K165	-1.2
W166	-1.4
C167	-0.26
E168	1.1
D169	1.1
A170	1.0

Figure 2.S15



		K137	T138	P139	E140	E141	I142	R143	R144	I145	F146	N147	I148	V149	N150	D151	F152	T153	P154	E155	E156	E157	A158	Q159	V160	R161	E162	E163	N164	K165	W166	C167	E168	D169	A170
-0.60	K137	0.07	0.00	0.00	-0.11	-0.11	0.00	0.13	0.14	0.00	0.00	0.00	0.00	0.00	0.00	-0.07	0.00	0.00	0.00	-0.08	-0.07	-0.09	0.00	0.00	0.00	0.13	-0.12	-0.17	-0.01	0.11	-0.06	0.00	-0.49	-0.26	-0.12
-0.76	T138	0.00	0.00	0.00	0.00	0.00	0.00	0.00	0.00	0.00	0.00	0.00	0.00	0.00	0.00	0.00	0.00	0.00	0.00	0.00	0.00	0.00	0.00	0.00	0.00	0.00	0.00	-0.02	0.00	0.00	-0.72	-0.02	-0.71	-0.03	-0.01
-0.46	P139	0.00	0.00	0.00	0.00	0.00	0.00	-0.02	0.00	0.00	0.00	0.00	0.00	0.00	0.00	0.00	0.00	0.00	0.00	0.00	0.00	0.00	0.00	0.00	0.00	0.00	-0.01	-0.03	0.00	-0.01	-0.82	-0.02	0.01	0.00	0.00
0.32	E140	-0.07	0.00	0.00	0.10	0.10	0.00	-0.16	-0.13	0.00	0.00	-0.01	0.00	0.00	0.00	0.08	0.00	0.00	0.00	0.09	0.08	0.11	0.00	0.00	0.00	-0.31	0.04	0.50	0.02	-0.16	0.01	0.00	0.13	0.11	0.10
0.22	E141	-0.06	0.00	0.00	0.08	0.08	0.00	-0.11	-0.09	0.00	0.00	0.00	0.00	0.00	0.00	0.06	0.00	0.00	0.00	0.07	0.07	0.08	0.00	0.00	0.00	-0.11	0.11	0.12	0.00	-0.11	-0.04	0.00	0.10	0.09	0.09
-0.69	I142	0.00	0.00	0.00	0.00	0.00	0.00	0.01	0.00	0.00	0.00	0.00	0.00	0.00	0.00	0.00	0.00	0.00	0.00	0.00	0.00	0.00	0.00	0.00	0.00	0.01	-0.01	-0.02	0.00	0.01	-1.3	-0.02	-0.02	-0.01	0.00
-3.3	R143	0.08	0.00	0.00	-0.11	-0.11	0.00	0.27	0.20	-0.01	-0.01	0.01	0.00	0.00	0.00	-0.09	0.00	0.00	-0.01	-0.10	-0.09	-0.11	-0.01	0.00	0.00	0.35	-1.0	-2.2	-0.16	0.12	-2.9	-0.09	-0.26	-0.16	-0.12
-5.4	R144	0.07	0.00	0.00	-0.09	-0.09	0.00	0.13	0.12	0.00	0.00	0.01	0.00	0.00	0.00	-0.08	0.00	0.00	0.00	-0.09	-0.09	-0.12	-0.01	-0.01	0.00	1.3	-3.2	-8.2	-0.05	0.11	-0.07	-0.01	-0.12	-0.11	-0.10
-0.23	I145	0.00	0.00	0.00	0.00	0.00	0.00	0.00	0.00	0.00	0.00	0.00	0.00	0.00	0.00	0.00	0.00	0.00	0.00	0.00	0.00	0.00	0.00	0.00	0.00	-0.01	-0.19	-0.01	0.00	-0.10	-0.11	-0.03	-0.01	0.00	0.00
-0.31	F146	0.00	0.00	0.00	0.00	0.00	0.00	0.00	0.00	0.00	0.00	0.00	0.00	0.00	0.00	0.00	0.00	0.00	0.00	0.00	0.00	0.00	0.00	0.00	-0.01	-0.01	-0.07	0.00	0.00	-0.05	-0.45	-0.02	-0.01	0.00	0.00
-2.0	N147	0.00	0.00	0.00	0.00	0.00	0.00	-0.01	0.00	0.00	0.00	0.00	0.00	0.00	0.00	0.00	0.00	0.00	0.00	0.00	0.00	0.00	0.00	0.00	0.00	0.00	-0.42	-0.04	0.01	-1.05	-1.51	-0.81	-0.07	-0.10	-0.02
-1.1	I148	0.00	0.00	0.00	0.00	0.00	0.00	-0.01	0.00	0.00	0.00	0.00	0.00	0.00	0.00	0.00	0.00	0.00	0.00	0.00	0.00	0.00	0.00	0.00	0.00	0.00	-0.01	0.00	0.00	-0.14	-0.84	-0.80	-0.04	-0.10	-0.19
-0.47	V149	0.00	0.00	0.00	0.00	0.00	0.00	0.00	0.00	0.00	0.00	0.00	0.00	0.00	0.00	0.00	0.00	0.00	0.00	0.00	0.00	0.00	0.00	-0.02	0.00	0.00	-0.01	0.00	0.00	-0.12	-0.03	-0.14	-0.12	-0.37	-0.13
-1.1	N150	0.00	0.00	0.00	0.00	0.00	0.00	0.00	0.00	0.00	0.00	0.00	0.00	0.00	0.00	0.00	0.00	0.00	0.00	0.00	0.00	0.00	0.00	-0.02	0.00	0.00	0.00	0.00	0.00	-0.04	-0.01	-0.32	-0.15	-1.2	-0.43
0.10	D151	-0.05	0.00	0.00	0.07	0.08	0.00	-0.10	-0.07	0.00	0.00	0.00	0.00	0.00	0.00	0.06	0.00	0.00	0.00	0.08	0.08	0.08	0.00	0.00	0.00	-0.08	0.10	0.09	0.00	-0.23	-0.01	-0.05	0.11	0.06	-0.01
-0.11	F152	0.00	0.00	0.00	0.00	0.00	0.00	0.00	0.00	0.00	0.00	0.00	0.00	0.00	0.00	0.00	0.00	0.00	0.00	0.00	0.00	0.00	0.00	-0.01	-0.01	0.00	0.00	0.00	0.00	-0.01	-0.02	-0.05	-0.01	-0.02	-0.10
-0.04	T153	0.00	0.00	0.00	0.00	0.00	0.00	0.00	0.00	0.00	0.00	0.00	0.00	0.00	0.00	0.00	0.00	0.00	0.00	0.00	0.00	0.00	0.00	-0.01	0.00	0.00	0.00	0.00	0.00	-0.01	0.00	0.00	0.00	-0.03	-0.02
-0.01	P154	0.00	0.00	0.00	0.00	0.00	0.00	0.00	0.00	0.00	0.00	0.00	0.00	0.00	0.00	0.00	0.00	0.00	0.00	0.00	0.00	0.00	0.00	-0.01	0.00	0.00	0.00	0.00	0.00	0.00	0.00	0.00	0.00	0.00	0.00
0.12	E155	-0.05	0.00	0.00	0.05	0.06	0.00	-0.08	-0.06	0.00	0.00	0.00	0.00	0.00	0.00	0.05	0.00	0.00	0.00	0.07	0.07	0.07	0.00	-0.07	-0.02	-0.07	0.09	0.08	0.00	-0.22	0.00	0.00	0.09	0.09	0.09
0.01	E156	-0.04	0.00	0.00	0.05	0.06	0.00	-0.07	-0.06	0.00	0.00	0.00	0.00	0.00	0.00	0.05	0.00	0.00	0.00	0.07	0.07	0.06	0.00	0.00	0.00	-0.07	0.08	0.07	0.00	-0.50	0.00	0.00	0.08	0.09	0.08
0.22	E157	-0.05	0.00	0.00	0.05	0.06	0.00	-0.07	-0.06	0.00	0.00	0.00	0.00	0.00	0.00	0.05	0.00	0.00	0.00	0.07	0.07	0.06	0.00	0.00	0.00	-0.07	0.08	0.07	0.00	-0.10	0.00	0.00	0.09	0.09	0.10
-0.03	A158	0.00	0.00	0.00	0.00	0.00	0.00	0.00	0.00	0.00	0.00	0.00	0.00	0.00	0.00	0.00	0.00	0.00	0.00	0.00	0.00	0.00	0.00	-0.03	-0.02	0.00	0.00	0.00	0.00	0.00	0.00	0.00	0.00	-0.01	0.00
-0.13	Q159	0.00	0.00	0.00	0.00	0.00	0.00	0.00	0.00	0.00	0.00	0.00	0.00	0.00	0.00	0.00	0.00	0.00	0.00	0.00	0.00	0.00	0.00	-0.02	-0.05	0.00	-0.08	0.00	0.00	-0.09	0.00	0.00	0.00	0.00	0.00
-0.07	V160	0.00	0.00	0.00	0.00	0.00	0.00	0.00	0.00	0.00	0.00	0.00	0.00	0.00	0.00	0.00	0.00	0.00	0.00	0.00	0.00	0.00	0.00	0.00	0.00	0.00	0.00	0.00	0.00	0.00	0.00	0.00	0.00	-0.09	-0.04
-1.1	R161	0.05	0.00	0.00	-0.06	-0.06	0.00	0.09	0.06	0.00	0.00	0.00	0.00	0.00	0.00	-0.05	0.00	0.00	0.00	-0.08	-0.08	-0.07	0.00	-0.01	0.00	0.07	-0.10	-0.08	0.00	0.04	0.03	0.04	-0.62	-0.93	-0.45
0.19	E162	-0.04	0.00	0.00	0.05	0.05	0.00	-0.07	-0.05	0.00	0.00	0.00	0.00	0.00	0.00	0.05	0.00	0.00	0.00	0.07	0.08	0.07	0.00	-0.01	-0.02	-0.07	0.08	0.07	0.00	-0.13	0.00	0.00	0.08	0.09	0.09
0.18	E163	-0.04	0.00	0.00	0.05	0.05	0.00	-0.06	-0.05	0.00	0.00	0.00	0.00	0.00	0.00	0.05	0.00	0.00	0.00	0.07	0.07	0.07	0.00	0.00	-0.01	-0.06	0.09	0.07	0.00	-0.14	0.00	0.00	0.08	0.07	0.07
-0.31	N164	0.00	0.00	0.00	0.00	0.00	0.00	0.00	0.00	0.00	0.00	0.00	0.00	0.00	0.00	0.00	0.00	0.00	0.00	-0.01	0.00	0.00	0.00	-0.12	0.00	0.00	0.00	0.00	0.00	0.00	0.00	0.00	0.00	-0.20	-0.28
-0.60	K165	0.05	0.00	0.00	-0.05	-0.05	0.00	0.07	0.05	0.00	0.00	0.00	0.00	0.00	0.00	-0.05	0.00	0.00	0.00	-0.26	-0.31	-0.08	-0.01	-0.23	-0.01	0.06	-0.08	-0.07	0.00	0.05	0.00	0.00	-0.09	-0.09	-0.09
-1.2	W166	0.00	0.00	0.00	0.00	0.00	0.00	-0.02	0.00	-0.04	0.00	0.00	0.00	0.00	0.00	0.00	0.00	0.00	0.00	-0.04	0.00	-0.01	-0.12	-0.47	-0.01	-0.01	-0.01	-0.01	-0.11	-0.38	-0.01	-0.02	-0.39	-0.20	-0.54
-0.10	C167	0.00	0.00	0.00	0.00	0.00	0.00	0.00	0.00	0.00	0.00	0.00	0.00	0.00	0.00	0.00	0.00	0.00	0.00	-0.01	0.00	0.00	0.00	-0.06	0.00	0.00	0.00	0.00	0.00	-0.04	0.00	0.00	0.00	-0.02	-0.05
-0.01	E168	-0.05	0.00	0.00	0.05	0.05	0.00	-0.08	-0.06	0.00	0.00	0.00	0.00	0.00	0.00	0.05	0.00	0.00	0.00	0.07	0.10	0.08	0.00	-0.14	-0.02	-0.07	0.10	0.07	0.00	-0.42	0.00	0.00	0.12	0.07	0.06
0.15	D169	-0.05	0.00	0.00	0.05	0.05	0.00	-0.08	-0.06	0.00	0.00	0.00	0.00	0.00	0.00	0.05	0.00	0.00	0.00	0.10	0.10	0.08	0.00	-0.03	0.00	-0.07	0.09	0.07	0.00	-0.48	0.00	0.00	0.30	0.07	0.11
0.20	A170	-0.05	0.00	0.00	0.05	0.05	0.00	-0.08	-0.06	0.00	0.00	0.00	0.00	0.00	0.00	0.05	0.00	0.00	0.00	0.08	0.12	0.07	0.00	0.00	0.00	-0.07	0.10	0.07	0.00	-0.14	0.00	-0.01	0.21	-0.14	0.13

Figure 2.S16

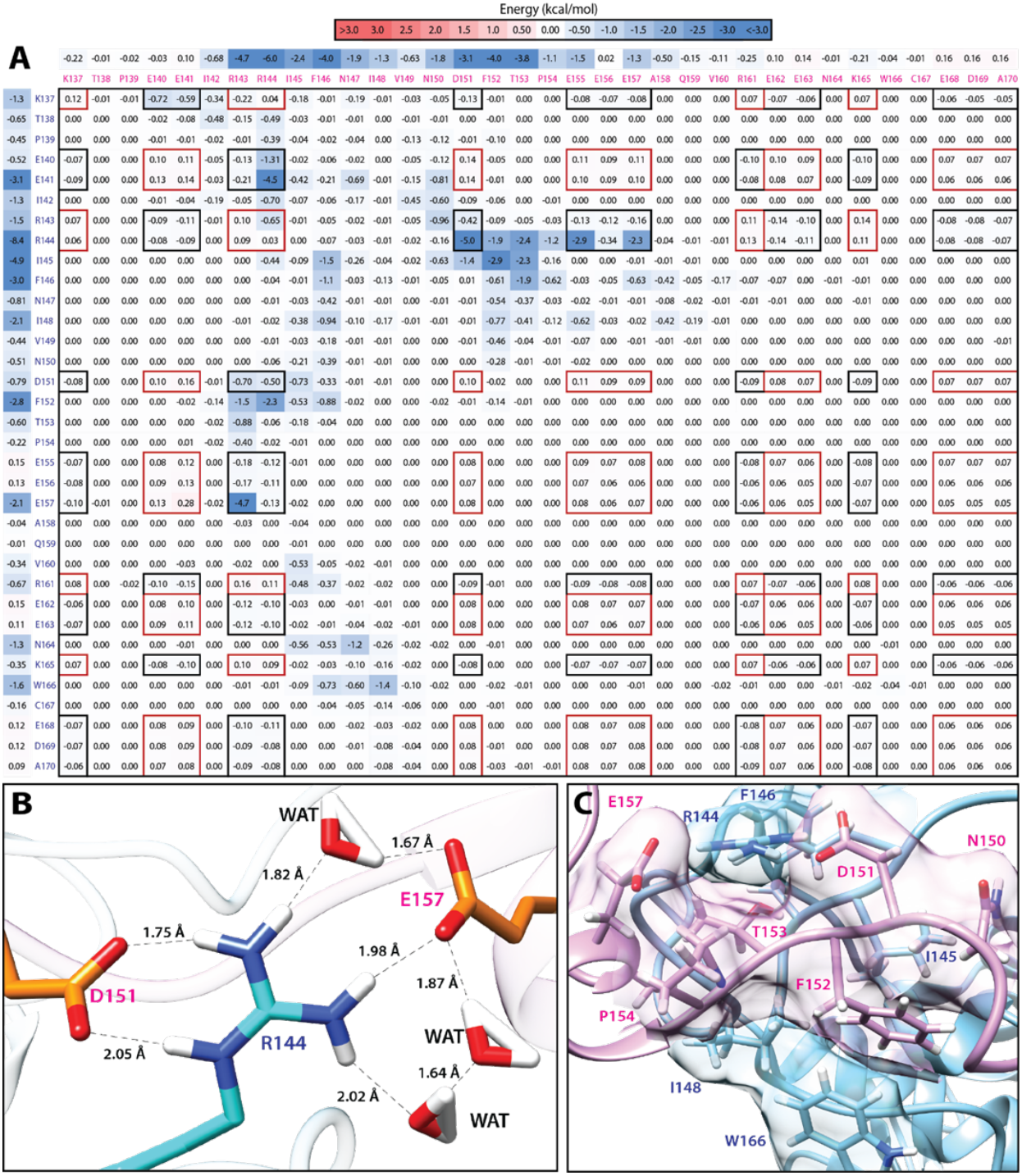
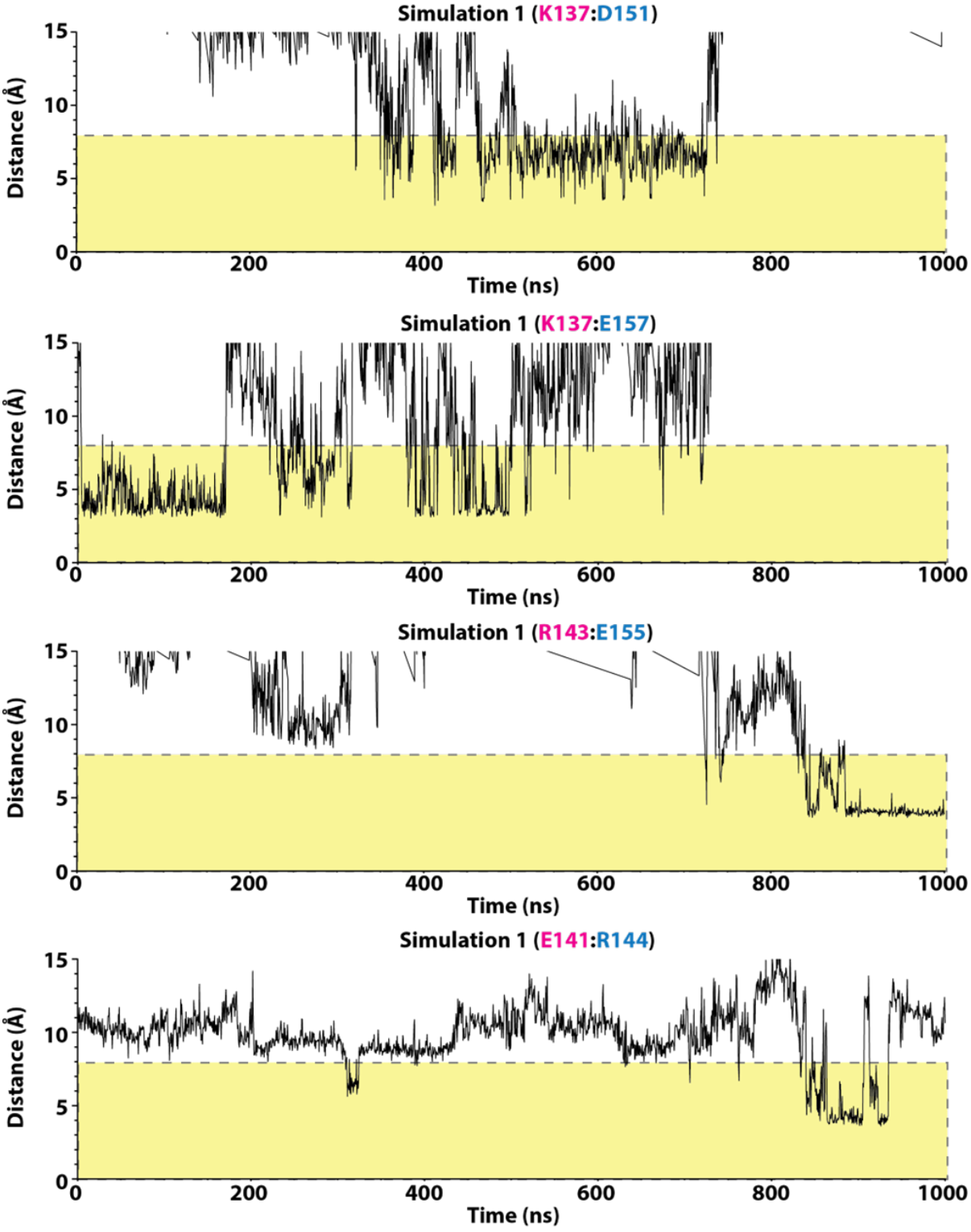
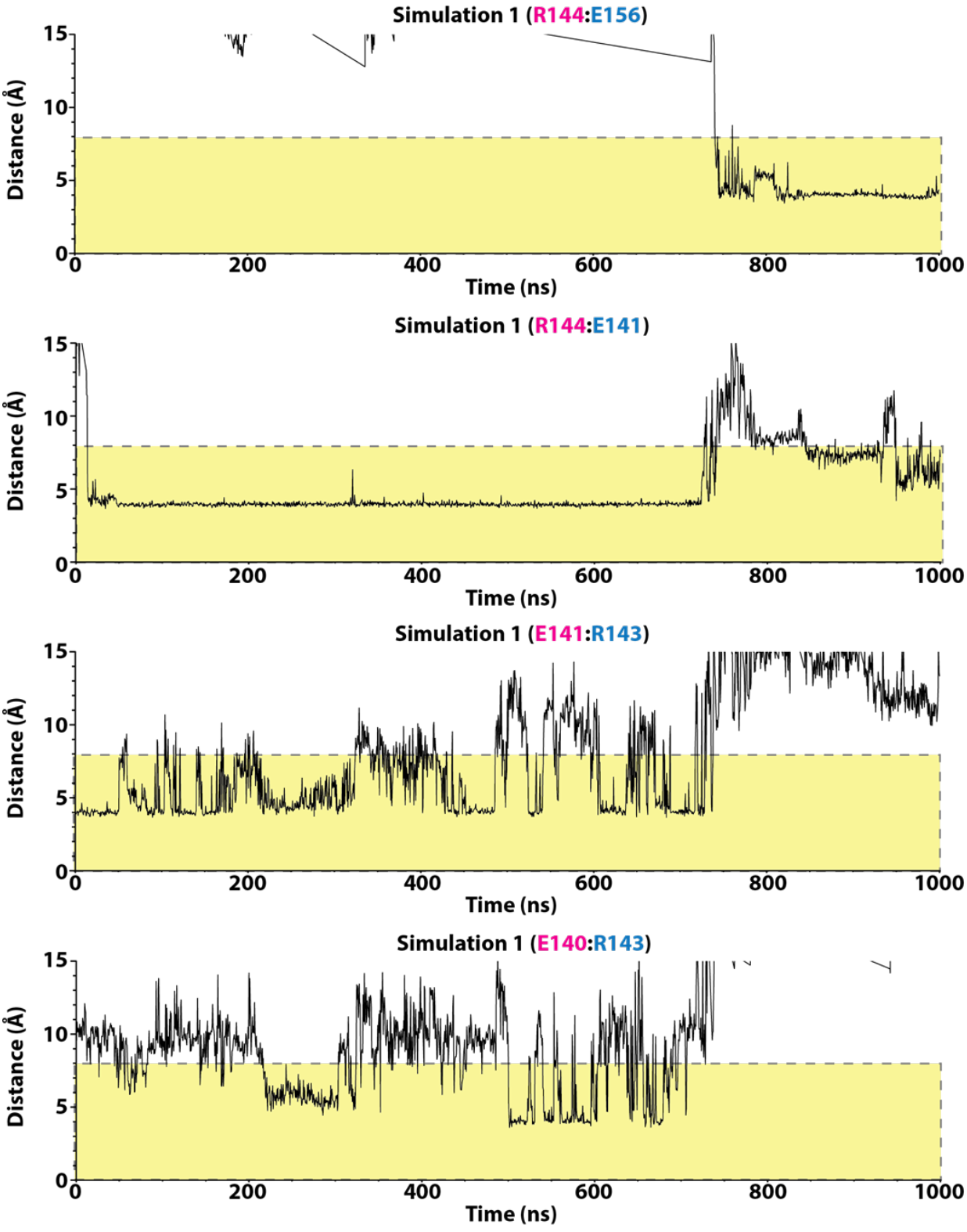
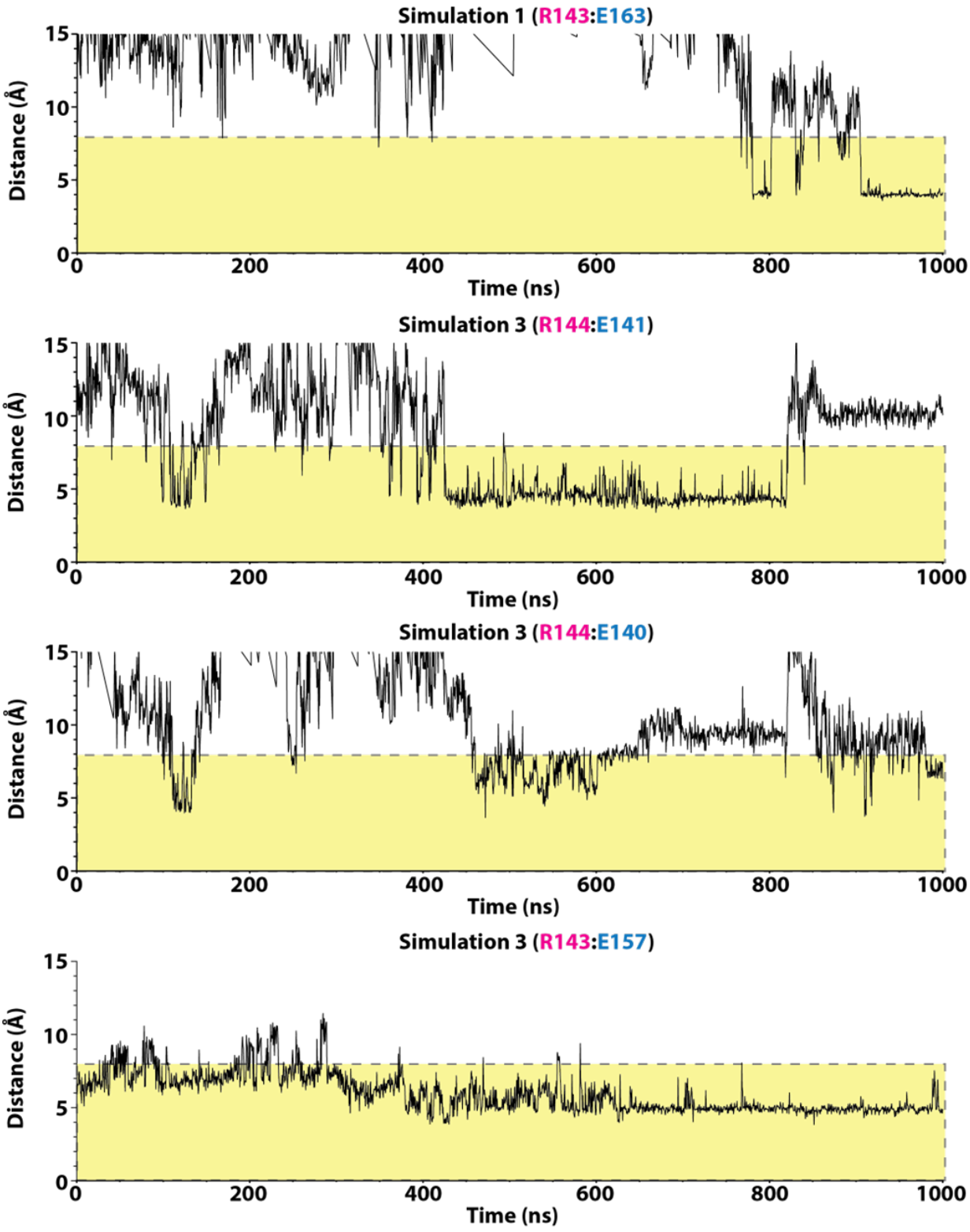
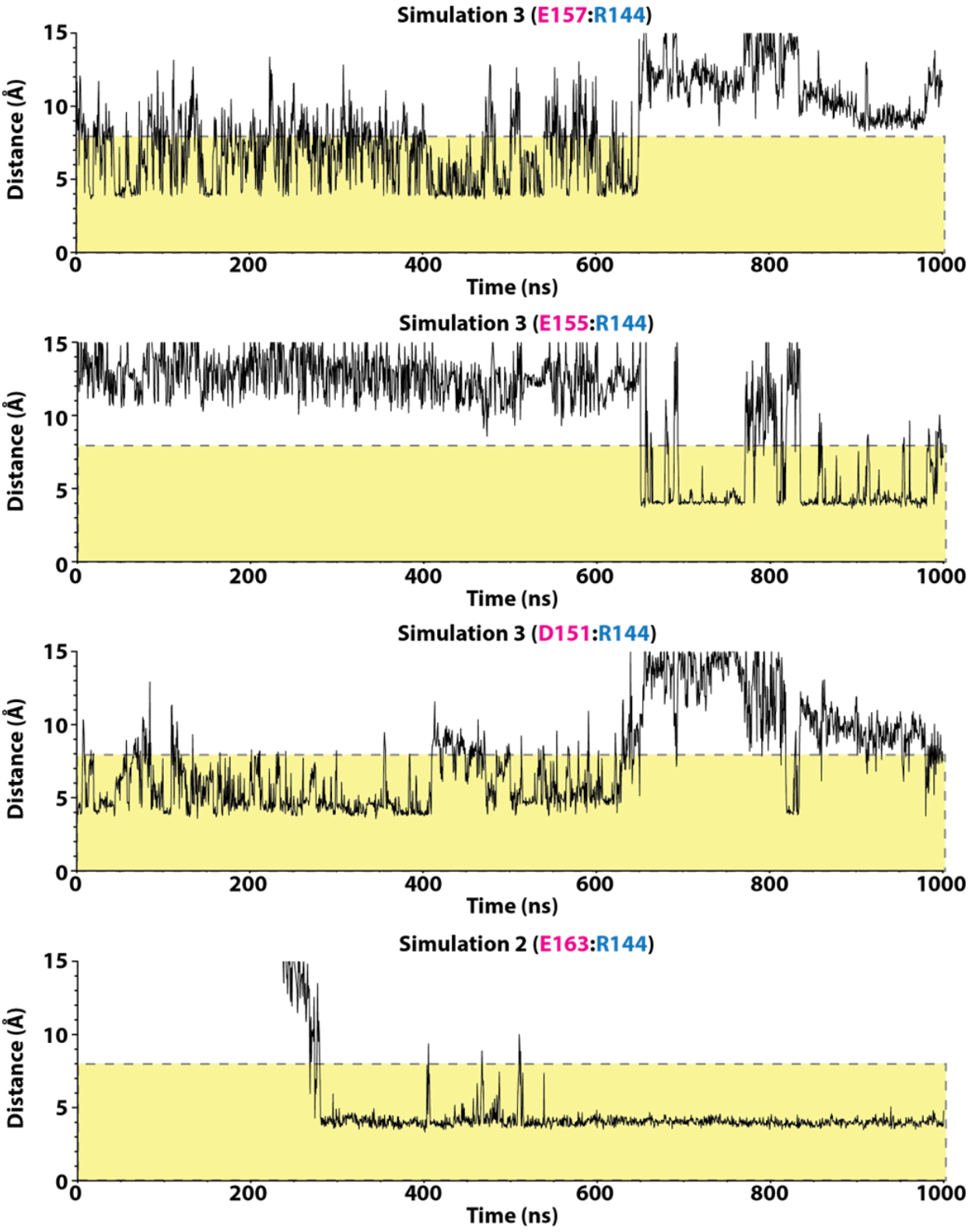

Energy (kcal/mol)
>3.0 3.0 2.5 2.0 1.5 1.0 0.50 0.00 -0.50 -1.0 -1.5 -2.0 -2.5 -3.0 <-3.0
A
K137 T138 P139 E140 E141 I142 R143 R144 I145 F146 N147 I148 V149 N150 D151 F152 T153 P154 E155 E156 E157 A158 Q159 V160 R161 E162 E163 N164 K165 W166 C167 E168 D169 A170
K137 T138 P139 E140 E141 I142 R143 R144 I145 F146 N147 I148 V149 N150 D151 F152 T153 P154 E155 E156 E157 A158 Q159 V160 R161 E162 E163 N164 K165 W166 C167 E168 D169 A170
B
WAT
1.67 Å
1.82 Å
E157
1.75 Å
1.98 Å
1.87 Å
D151
R144
WAT
2.05 Å
1.64 Å
2.02 Å
WAT
C
E157
R144
F146
N150
D151
T153
I145
F152
P154
I148
W166

Figure 2.S17


Simulation 1 (K137:D151)
Distance (Å)
Time (ns)
Simulation 1 (K137:E157)
Distance (Å)
Time (ns)
Simulation 1 (R143:E155)
Distance (Å)
Time (ns)
Simulation 1 (E141:R144)
Distance (Å)
Time (ns)


Simulation 1 (R144:E156)
Distance (Å)
Time (ns)
Simulation 1 (R144:E141)
Distance (Å)
Time (ns)
Simulation 1 (E141:R143)
Distance (Å)
Time (ns)
Simulation 1 (E140:R143)
Distance (Å)
Time (ns)


Simulation 1 (R143:E163)
Distance (Å)
Time (ns)
Simulation 3 (R144:E141)
Distance (Å)
Time (ns)
Simulation 3 (R144:E140)
Distance (Å)
Time (ns)
Simulation 3 (R143:E157)
Distance (Å)
Time (ns)


Simulation 3 (E157:R144)
Distance (Å)
Time (ns)
Simulation 3 (E155:R144)
Distance (Å)
Time (ns)
Simulation 3 (D151:R144)
Distance (Å)
Time (ns)
Simulation 2 (E163:R144)
Distance (Å)
Time (ns)

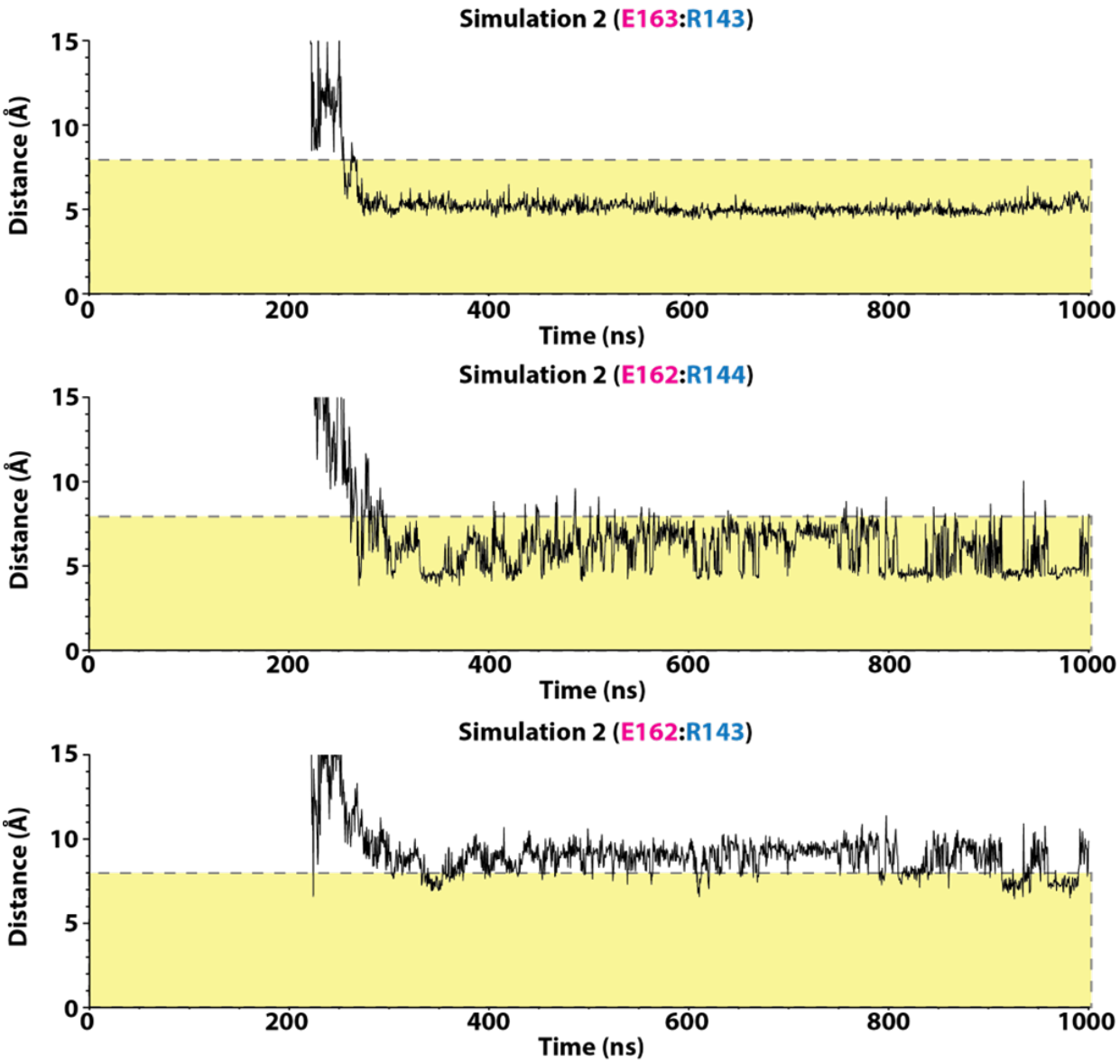

Simulation 2 (E163:R143)
Distance (Å)
Time (ns)
Simulation 2 (E162:R144)
Distance (Å)
Time (ns)
Simulation 2 (E162:R143)
Distance (Å)
Time (ns)

Figure 2.S18

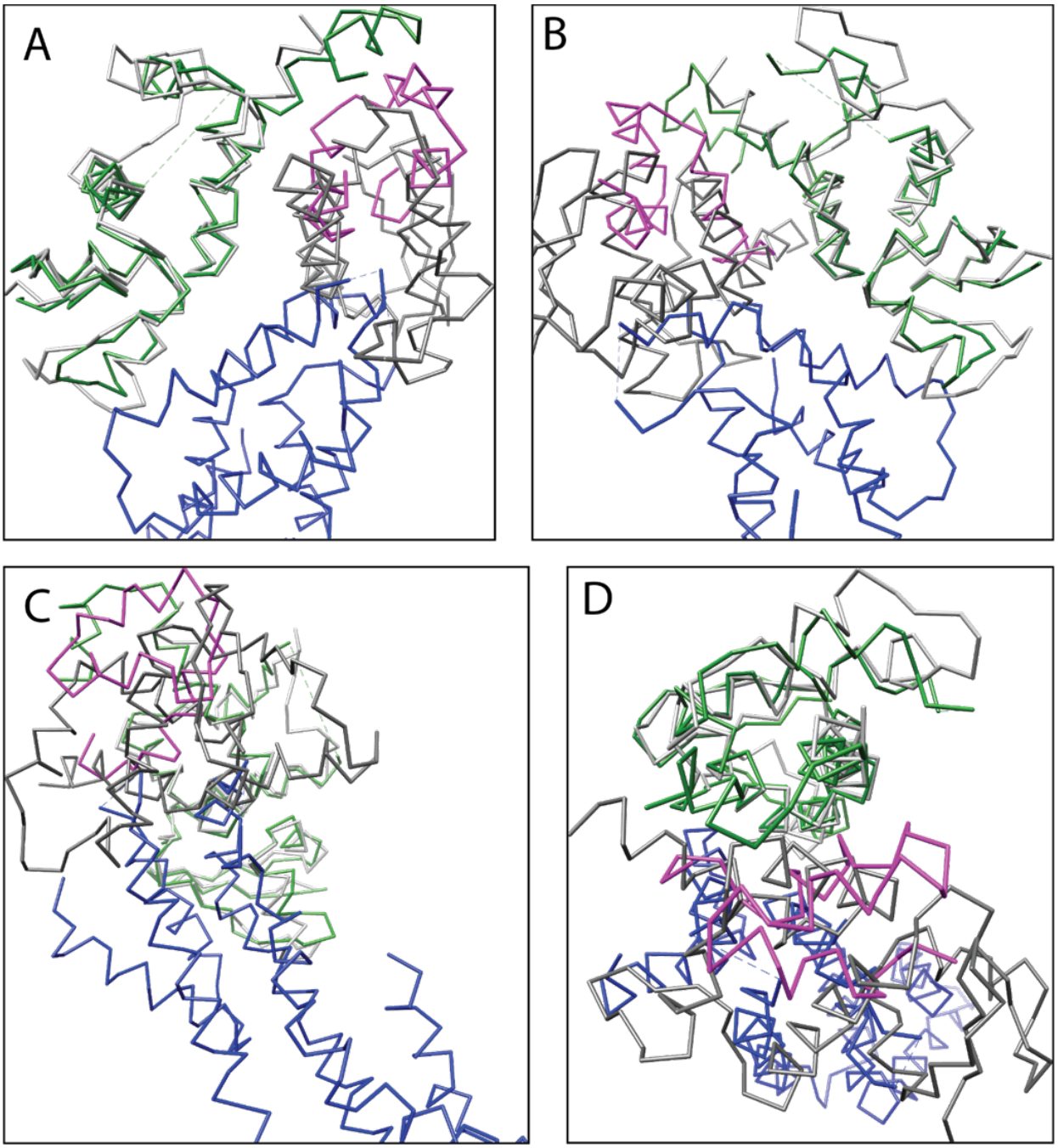


Figure 2.S19

A.

Primer	Sequence
TgSkp1_ΔCTR-F	5′-gatcaaagccTGACAGTAAAGGTGGATACGGATCCG
TgSkp1_ΔCTR-R	5′-tttactgtcaGGCTTTGATCATTGTCGCCACTTTC
TgSkp1_ΔLoop-F	5′-aacaacccaggtggttccggaCTTGCTGAAGTGGTCAGCGAGTG
TgSkp1_ΔLoop-R	5′-ttcagcaagtccggaaccaccTGGGTTGTTGTGGTGATGTTCAC
pNIC28_Screening-F	5′-CGGGGCCTGCCACCATACCCACG
pNIC28_Screening-R	5′-GTGGTGGTGGTGGTGCTCGAGTGCGG

B.

>pNIC28-HisTEVTgSkp1-FL

GCCACGGGGCCTGCCACCATACCCACGCCGAAACAAGCGCTCATGAGCCCGAAGTGGCGA
5′-CGGGGCCTGCCACCATACCCACG
pNIC28_Screening-F

GCCCGATCTTCCCCATCGGTGATGTCGGCGATATAGGCGCCAGCAACCGCACCTGTGGCG
CCGGTGATGCCGGCCACGATGCGTCCGGCGTAGAGGATCGAGATCTCGATCCCGCGAAAT

M H H H H H H S S G V

TGTTTAACTTTAAGAAGGAGATATACATATGCACCATCATCATCATCATTCTTCTGGTGT

D L G T E N L Y F Q><S M S K E R M G D A A9

AGATCTGGGTACCGAGAACCTGTACTTCCAATCCATGTCAAAAGAAAGAATGGGAGATGC TEV Site

R K V T L V S Q E G D E F D V D I E V A A29

CCGGAAGGTCACTCTCGTCTCGCAAGAGGGAGACGAGTTTGATGTTGACATCGAGGTCGC

S M S A L I K T M V E E D S D C Q E S I I49

CTCCATGAGTGCGTTGATAAAGACAATGGTGGAAGAAGACAGCGACTGCCAAGAGAGCAT

P L P N V D T C I L K K I I E Y C E H H H69

TCCTCTTCCCAACGTGGATACATGCATTCTGAAGAAAATCATCGAGTATTGTGAACATCA
CACTTGTAGT TgSkp1_ΔLoop-R

H N N P P E E I P K P L K S S N L A E V V89

CCACAACAACCCACCCGAAGAAATCCCCAAGCCTCTAAAGTCGTCCAACCTTGCTGAAGT
GGTGTTGTTGGGTccaccaaggcctgaacgactt-5′
5′-aacaacccaggtggttccggaCTTGCTGAAGT TgSkp1_ΔLoop-F

H N N P - - - - - - - - - G G S G L A E V ΔLoop

CCACAACAACCCA----------GGTGGTTCCGGACTTGCTGAAGT or **ΔLoopΔCTR**

V S E W D Y Q F I N E N S D Q K I L F A A109

GGTCAGCGAGTGGGACTACCAATTCATCAACGAAAACAGCGACCAGAAGATTTTGTTTGC
GGTCAGCGAGTG

L I L A A N Y L N I K P L L D L S V A K K129

TTTGATTTTGGCGGCTAACTACCTCAACATCAAGCCGCTGCTGGATCTGAGCGTCGCGAA
CTT TgSkp1_ΔCTR-R

V A T M I K A K T P E E I R R I F N I V V149

AGTGGCGACAATGATCAAAGCCAAGACGCCGGAAGAAATCCGACGCATTTTCAACATCGT
TCACCGCTGTTACTAGTTTCGGactgtcattt-5′

V A T M I K A - - - - - - - - - - - - - - **ΔCTR**
AGTGGCGACAATGATCAAAGCC---------- or **ΔLoopΔCTR**

N D F T P E E E A Q V R E E N K W C E D **D169**
CAATGACTTCACTCCTGAGGAAGAAGCTCAGGTGCGCGAGGAGAACAAGTGGTGCGAAGA
5′-gatcaa TgSkp1_ΔCTR-F
- - - - - - - - - - - - - - - - - - - - **ΔCTR**
---------- or **ΔLoopΔCTR**

A * **A170**
TGCATGACAGTAAAGGTGGATACGGATCCGAATTCGAGCTCCGTCGACAAGCTTGCGGCC
agccTGACAGTAAAGGTGGATACGGATCCG
GG
pNIC28_Screening-R

- * **ΔCTR** or **ΔLoopΔCTR**
----TGACAGTAAAGGTGGATACGGATCCGAATTCGAGCTCCGTCGACAAGCTTGCGGCC

GCACTCGAGCACCACCACCACCACCACTGAGATCCGGCTGCTAACAAAGCCCGAAAGGAA
CGTGAGCTCGTGGTGGTGGTGGTG-5′

Figure 2.S20

>pNIC28-HisTEVTgSkp1-(PolySer; Scrambled5/Scr-5; Scrambled6/Scr-6)

```
TAATACGACTCACTATAGGGGAATTGTGAGCGGATAACAATTCCCCTCTAGAAATAATTT

                              M  H  H  H  H  H  H  S  S  G  V
TGTTTAACTTTAAGAAGGAGATATACATATGCACCATCATCATCATCATTCTTCTGGTGT

 D  L  G  T  E  N  L  Y  F  Q><S  M  S  K  E  R  M  G  D  A        A9
AGATCTGGGTACCGAGAACCTGTACTTCCAATCCATGTCAAAAGAAAGAATGGGAGATGC

 R  K  V  T  L  V  S  Q  E  G  D  E  F  D  V  D  I  E  V  A        A29
CCGGAAGGTCACTCTCGTCTCGCAAGAGGGAGACGAGTTTGATGTTGACATCGAGGTCGC

 S  M  S  A  L  I  K  T  M  V  E  E  D  S  D  C  Q  E  S  I        I49
CTCCATGAGTGCGTTGATAAAGACAATGGTGGAAGAAGACAGCGACTGCCAAGAGAGCAT

 P  L  P  N  V  D  T  C  I  L  K  K  I  I  E  Y  C  E  H  H        H69
TCCTCTTCCCAACGTGGATACATGCATTCTGAAGAAAATCATCGAGTATTGTGAACATCA

 H  N  N  P  P  E  E  I  P  K  P  L  K  S  S  N  L  A  E  V        V89
CCACAACAACCCACCCGAAGAAATCCCCAAGCCTCTAAAGTCGTCCAACCTTGCTGAAGT

 V  S  E  W  D  Y  Q  F  I  N  E  N  S  D  Q  K  I  L  F  A        A109
GGTCAGCGAGTGGGACTACCAATTCATCAACGAAAACAGCGACCAGAAGATTTTGTTTGC

 L  I  L  A  A  N  Y  L  N  I  K  P  L  L  D  L  S  V  A  K        K129
TTTGATTTTGGCGGCTAACTACCTCAACATCAAGCCGCTGCTGGACTTAAGCGTTGCTAA

 V  A  T  M  I  K  A  S  S  S  S  S  S  S  S  S  S  S  S  S        S149
AGTTGCGACCATGATTAAGGCTAGCTCCAGCTCATCTAGCTCTTCTAGCAGTTCCAGCTC        polySer
 V  A  T  M  I  K  A  E  E  I  E  P  D  Q  K  E  E  I  D  F        F149
AGTTGCCACTATGATTAAGGCGGAAGAAATTGAACCCGACCAAAAGGAAGAAATCGACTT        Scr-5
 V  A  T  M  I  K  A  E  A  E  K  P  V  A  E  I  P  T  E  R        R149
AGTTGCCACTATGATTAAGGCGGAAGCGGAGAAGCCGGTGGCTGAGATCCCGACCGAGCG        Scr-6

 S  S  S  S  S  S  S  S  S  S  S  S  S  S  S  S  S  S  S  S        S169
CTCCAGCTCCTCTTCTTCCAGCTCCAGCAGCAGCTCATCTAGCTCGTCTTCCAGCTCGTC        polySer
 N  R  A  E  C  T  N  R  P  R  V  I  N  T  W  E  E  K  V  A        A169
CAACCGGGCTGAGTGCACTAACAGACCCCGGGTCATTAACACTTGGGAAGAAAAGGTGGC        Scr-5
 T  V  N  F  I  N  Q  R  E  E  K  R  N  E  C  I  D  D  F  W        W169
CACCGTTAATTTCATCAACCAGCGTGAAGAGAAGCGCAACGAGTGCATTGATGATTTCTG        Scr-6

 S  *                                                               S170
GTCCTAAGGATCCGAATTCGAGCTCCGTCGACAAGCTTGCGGCCGCACTCGAGCACCACC        polySer
 F  *                                                               F170
GTTTTAAGGATCCGAATTCGAGCTCCGTCGACAAGCTTGCGGCCGCACTCGAGCACCACC        Scr-5
 E  *                                                               E170
GGAATAAGGATCCGAATTCGAGCTCCGTCGACAAGCTTGCGGCCGCACTCGAGCACCACC        Scr-6

ACCACCACCACTGAGATCCGGCTGCTAACAAAGCCCGAAAGGAAGCTGAGTTGGCTGCTG
CCACCGCTGAGCAATAACTAGCATAACCCCTTGGGGCCTCTAAACGGGTCTTGAGGGGTT
```

REFERENCES

(1) Li, L., Shen, S., Bickler, P., Jacobson, M. P., Wu, L. F., and Altschuler, S. J. (2023) Searching for molecular hypoxia sensors among oxygen-dependent enzymes, eLife 12, e87705.

(2) West, C. M., and Blader, I. J. (2015) Oxygen sensing by protozoans: how they catch their breath, Current Opinion in Microbiology 26, 41-47.

(3) Prevention, C. f. D. C. a. (2018) Epidemiology and risk factors, In Parasites - Toxoplasmosis (*Toxoplasma* infection), U.S. Department of Health and Human Services, Centers for Disease Control and Prevention.

(4) van der Wel, H., Ercan, A., and West, C. M. (2005) The Skp1 prolyl hydroxylase from *Dictyostelium* Is related to the Hypoxia-inducible Factor-α class of animal prolyl 4-hydroxylases, Journal of Biological Chemistry 280, 14645-14655.

(5) West, C. M., van der Wel, H., and Wang, Z. A. (2007) Prolyl 4-hydroxylase-1 mediates O_2 signaling during development of *Dictyostelium*, Development 134, 3349-3358.

(6) Xu, Y., Wang, Z. A., Green, R. S., and West, C. M. (2012) Role of the Skp1 prolyl-hydroxylation/glycosylation pathway in oxygen dependent submerged development of *Dictyostelium*, BMC Developmental Biology 12, 31.

(7) Xu, Y., Brown, K. M., Wang, Z. A., van der Wel, H., Teygong, C., Zhang, D., Blader, I. J., and West, C. M. (2012) The Skp1 protein from *Toxoplasma* Is modified by a cytoplasmic prolyl 4-hydroxylase associated with oxygen sensing in the social amoeba *Dictyostelium*, Journal of Biological Chemistry 287, 25098-25110.

(8) Cordonnier, C., Mandalasi, M., Gigley, J., Wohlfert, E. A., West, C. M., and Blader, I. J. (2024) The *Toxoplasma* oxygen-sensing protein, TgPhyA, is required for resistance to interferon gamma-mediated nutritional immunity in mice, PLOS Biology 22, e3002690.

(9) Lee, J. M., Hammarén, H. M., Savitski, M. M., and Baek, S. H. (2023) Control of protein stability by post-translational modifications, Nature Communications 14, 201.

(10) Sheikh, M. O., Xu, Y., van der Wel, H., Walden, P., Hartson, S. D., and West, C. M. (2015) Glycosylation of Skp1 promotes formation of Skp1–Cullin-1–F-box protein complexes in *Dictyostelium*, Molecular & Cellular Proteomics 14, 66-80.

(11) Boland, A. W., Gas-Pascual, E., Nottingham, B. L., van der Wel, H., Daniel, N. G., Sheikh, M. O., Schafer, C. M., and West, C. M. (2022) Oxygen-dependent regulation of E3(SCF)ubiquitin ligases and a Skp1-associated JmjD6 homolog in development of the social amoeba *Dictyostelium*, Journal of Biological Chemistry 298, 102305.

(12) Mandalasi, M., Gas-Pascual, E., Baptista, C. G., Deng, B., van der Wel, H., Kruijtzer, J., Boons, G.-J., Blader Ira, J., and West Christopher, M. (2024) Oxygen-dependent regulation of F-box proteins in *Toxoplasma gondii*, Journal of Biological Chemistry, 300(11), 107801.

(13) Sheikh, M. O., Schafer, C. M., Powell, J. T., Rodgers, K. K., Mooers, B. H. M., and West, C. M. (2014) Glycosylation of Skp1 affects its conformation and promotes binding to a model F-box protein, Biochemistry 53, 1657-1669.

(14) Kim, H. W., Eletsky, A., Gonzalez, K. J., van der Wel, H., Strauch, E.-M., Prestegard, J. H., and West, C. M. (2020) Skp1 dimerization conceals its F-box protein binding site, Biochemistry 59, 1527-1536.

(15) Blundon, J. M., Cesar, B. I., Bae, J. W., Čavka, I., Haversat, J., Ries, J., Köhler, S., and Kim, Y. (2024) Skp1 proteins are structural components of the synaptonemal complex in *C. elegans*, Science Advances 10, eadl4876.

(16) Kursel, L. E., Goktepe, K., and Rog, O. (2024) The structural role of Skp1 in the synaptonemal complex is conserved in nematodes, Genetics 228, iyae153.

(17) van der Wel, H., Gas-Pascual, E., and West, C. M. (2019) Skp1 isoforms are differentially modified by a dual function prolyl 4-hydroxylase/N-acetylglucosaminyltransferase in a plant pathogen, Glycobiology 29, 705-714.

(18) Schulman, B. A., Carrano, A. C., Jeffrey, P. D., Bowen, Z., Kinnucan, E. R. E., Finnin, M. S., Elledge, S. J., Harper, J. W., Pagano, M., and Pavletich, N. P. (2000) Insights into SCF ubiquitin ligases from the structure of the Skp1–Skp2 complex, Nature 408, 381-386.

(19) Zheng, N., Schulman, B. A., Song, L., Miller, J. J., Jeffrey, P. D., Wang, P., Chu, C., Koepp, D. M., Elledge, S. J., Pagano, M., Conaway, R. C., Conaway, J. W., Harper, J. W., and Pavletich, N. P. (2002) Structure of the Cul1–Rbx1–Skp1–F box^{Skp2} SCF ubiquitin ligase complex, Nature 416, 703-709.

(20) Henzl, M. T., Thalmann, I., and Thalmann, R. (1998) OCP2 exists as a dimer in the organ of Corti, Hearing Research 126, 37-46.

(21) Xu, X., Eletsky, A., Sheikh, M. O., Prestegard, J. H., and West, C. M. (2018) Glycosylation promotes the random coil to helix transition in a region of a protist skp1 associated with F-box binding, Biochemistry 57, 511-515.

(22) Tan, A., Tanner, J. J., and Henzl, M. T. (2008) Energetics of OCP1–OCP2 complex formation, Biophysical Chemistry 134, 64-71.

(23) Fuxreiter, M. (2024) Context-dependent, fuzzy protein interactions: Towards sequence-based insights, Current Opinion in Structural Biology 87, 102834.

(24) Sanborn, A. L., Yeh, B. T., Feigerle, J. T., Hao, C. V., Townshend, R. J. L., Lieberman Aiden, E., Dror, R. O., and Kornberg, R. D. (2021) Simple biochemical features underlie transcriptional activation domain diversity and dynamic, fuzzy binding to Mediator, eLife 10, e68068.

(25) Williamson, M. P. (2023) Protein binding: a fuzzy concept, Life (Basel) 13, 855.

(26) Liu, T., Abboud, M. I., Chowdhury, R., Tumber, A., Hardy, A. P., Lippl, K., Lohans, C. T., Pires, E., Wickens, J., McDonough, M. A., West, C. M., and Schofield, C. J. (2020) Biochemical and biophysical analyses of hypoxia sensing prolyl hydroxylases from *Dictyostelium discoideum* and *Toxoplasma gondii*, Journal of Biological Chemistry 295, 16545-16561.

(27) Hyena, H. (2022) Word Scrambler, Hanging Hyena, Web.

(28) Klausen, M. S., Jespersen, M. C., Nielsen, H., Jensen, K. K., Jurtz, V. I., Sønderby, C. K., Sommer, M. O. A., Winther, O., Nielsen, M., Petersen, B., and Marcatili, P. (2019) NetSurfP-2.0: Improved prediction of protein structural features by integrated deep learning, Proteins: Structure, Function, and Bioinformatics 87, 520-527.

(29) Savitsky, P., Bray, J., Cooper, C. D. O., Marsden, B. D., Mahajan, P., Burgess-Brown, N. A., and Gileadi, O. (2010) High-throughput production of human proteins for crystallization: The SGC experience, Journal of Structural Biology 172, 3-13.

(30) Wilkins, M. R., Gasteiger, E., Bairoch, A., Sanchez, J.-C., Williams, K. L., Appel, R. D., and Hochstrasser, D. F. (1999) Protein identification and analysis tools in the ExPASy Server, In 2-D Proteome Analysis Protocols (Link, A. J., Ed.), pp 531-552, Humana Press, Totowa, NJ.

(31) Rahman, K., Mandalasi, M., Zhao, P., Sheikh, M. O., Taujale, R., Kim, H. W., van der Wel, H., Matta, K., Kannan, N., Glushka, J. N., Wells, L., and West, C. M. (2017) Characterization of a cytoplasmic glucosyltransferase that extends the core trisaccharide of the *Toxoplasma* Skp1 E3 ubiquitin ligase subunit, Journal of Biological Chemistry 292, 18644-18659.

(32) Wang, Z. A., van der Wel, H., Vohra, Y., Buskas, T., Boons, G.-J., and West, C. M. (2009) Role of a Cytoplasmic dual-function glycosyltransferase in O_2 regulation of development in *Dictyostelium*, Journal of Biological Chemistry 284, 28896-28904.

(33) Báez-Santos Yahira, M., Mielech Anna, M., Deng, X., Baker, S., and Mesecar Andrew, D. (2014) Catalytic function and substrate specificity of the papain-like protease domain of nsp3 from the Middle East Respiratory Syndrome Coronavirus, Journal of Virology 88, 12511-12527.

(34) Mandalasi, M., Kim, H. W., Thieker, D., Sheikh, M. O., Gas-Pascual, E., Rahman, K., Zhao, P., Daniel, N. G., van der Wel, H., Ichikawa, H. T., Glushka, J. N., Wells, L., Woods, R. J., Wood, Z. A., and West, C. M. (2020) A terminal α3-galactose modification regulates an E3 ubiquitin ligase subunit in *Toxoplasma gondii*, Journal of Biological Chemistry 295, 9223-9243.

(35) van der Wel, H., Johnson, J. M., Xu, Y., Karunaratne, C. V., Wilson, K. D., Vohra, Y., Boons, G.-J., Taylor, C. M., Bendiak, B., and West, C. M. (2011) Requirements for Skp1 processing by

cytosolic prolyl 4(trans)-hydroxylase and α-N-Acetylglucosaminyltransferase enzymes involved in O_2 signaling in *Dictyostelium*, Biochemistry 50, 1700-1713.

(36) Thomas M. Laue, B. S., Teresa M. Ridgeway, S. L. Pelletier. (1992) Computer-aided interpretation of sedimentation data for proteins, In Analytical ultracentrifugation in biochemistry and polymer science (S. E. Harding, J. C. H., A. J. Rowe, Ed.), pp 90-125, Royal Society of Chemistry, Cambridge, UK.

(37) Schuck, P. (2000) Size-distribution analysis of macromolecules by sedimentation velocity ultracentrifugation and lamm equation modeling, Biophysical Journal 78, 1606-1619.

(38) Brautigam, C. A. (2015) Chapter Five - Calculations and publication-quality illustrations for analytical ultracentrifugation data, In Methods in Enzymology (Cole, J. L., Ed.), pp 109-133, Academic Press.

(39) Schuck, P. (2003) On the analysis of protein self-association by sedimentation velocity analytical ultracentrifugation, Analytical Biochemistry 320, 104-124.

(40) Ortega, A., Amorós, D., and García de la Torre, J. (2011) Prediction of hydrodynamic and other solution properties of rigid proteins from atomic- and residue-level models, Biophysical Journal 101, 892-898.

(41) Webb, B., and Sali, A. (2016) Comparative protein structure modeling using MODELLER, Current Protocols in Bioinformatics 54, 5.6.1-5.6.37.

(42) Waterhouse, A., Bertoni, M., Bienert, S., Studer, G., Tauriello, G., Gumienny, R., Heer, F. T., de Beer, T. A P., Rempfer, C., Bordoli, L., Lepore, R., and Schwede, T. (2018) SWISS-MODEL: homology modelling of protein structures and complexes, Nucleic Acids Research 46, W296-W303.

(43) Greenfield, N. J. (2006) Using circular dichroism collected as a function of temperature to determine the thermodynamics of protein unfolding and binding interactions, Nature Protocols 1, 2527-2535.

(44) C.N. Pace, B. A. S., and J.A. Thomson. (1989) Measuring the conformational stability of a protein, In Protein Structure: a practical approach (Creighton, T. E., Ed.), pp 311-330, Oxford University Press, IRL Press, Oxford.

(45) Case, D. A., Aktulga, H. M., Belfon, K., Cerutti, D. S., Cisneros, G. A., Cruzeiro, V. W. D., Forouzesh, N., Giese, T. J., Götz, A. W., Gohlke, H., Izadi, S., Kasavajhala, K., Kaymak, M. C., King, E., Kurtzman, T., Lee, T.-S., Li, P., Liu, J., Luchko, T., Luo, R., Manathunga, M., Machado, M. R., Nguyen, H. M., O'Hearn, K. A., Onufriev, A. V., Pan, F., Pantano, S., Qi, R., Rahnamoun, A., Risheh, A., Schott-Verdugo, S., Shajan, A., Swails, J., Wang, J., Wei, H., Wu, X., Wu, Y., Zhang, S., Zhao, S., Zhu, Q., Cheatham, T. E., III, Roe, D. R., Roitberg, A., Simmerling, C., York, D. M., Nagan, M. C., and Merz, K. M., Jr. (2023) AmberTools, Journal of Chemical Information and Modeling 63, 6183-6191.

(46) Maier, J. A., Martinez, C., Kasavajhala, K., Wickstrom, L., Hauser, K. E., and Simmerling, C. (2015) ff14SB: Improving the accuracy of protein side chain and backbone parameters from ff99SB, Journal of Chemical Theory and Computation 11, 3696-3713.

(47) Jorgensen, W. L., Chandrasekhar, J., Madura, J. D., Impey, R. W., and Klein, M. L. (1983) Comparison of simple potential functions for simulating liquid water, The Journal of Chemical Physics 79, 926-935.

(48) Joung, I. S., and Cheatham, T. E., III. (2008) Determination of alkali and halide monovalent ion parameters for use in explicitly solvated biomolecular simulations, The Journal of Physical Chemistry B 112, 9020-9041.

(49) Darden, T., York, D., and Pedersen, L. (1993) Particle mesh Ewald: An N·log(N) method for Ewald sums in large systems, The Journal of Chemical Physics 98, 10089-10092.

(50) Miller, B. R., III, McGee, T. D., Jr., Swails, J. M., Homeyer, N., Gohlke, H., and Roitberg, A. E. (2012) MMPBSA.py: An efficient program for end-state free energy calculations, Journal of Chemical Theory and Computation 8, 3314-3321.

(51) Pettersen, E. F., Goddard, T. D., Huang, C. C., Couch, G. S., Greenblatt, D. M., Meng, E. C., and Ferrin, T. E. (2004) UCSF Chimera—A visualization system for exploratory research and analysis, Journal of Computational Chemistry 25, 1605-1612.

(52) Kelley, L. A., Gardner, S. P., and Sutcliffe, M. J. (1996) An automated approach for clustering an ensemble of NMR-derived protein structures into conformationally related subfamilies, Protein Engineering, Design and Selection 9, 1063-1065.

(53) Simonetta, K. R., Taygerly, J., Boyle, K., Basham, S. E., Padovani, C., Lou, Y., Cummins, T. J., Yung, S. L., von Soly, S. K., Kayser, F., Kuriyan, J., Rape, M., Cardozo, M., Gallop, M. A., Bence, N. F., Barsanti, P. A., and Saha, A. (2019) Prospective discovery of small molecule enhancers of an E3 ligase-substrate interaction, Nature Communications 10, 1402.

(54) Tan, X., Calderon-Villalobos, L. I. A., Sharon, M., Zheng, C., Robinson, C. V., Estelle, M., and Zheng, N. (2007) Mechanism of auxin perception by the TIR1 ubiquitin ligase, Nature 446, 640-645.

(55) Nishio, K., Kawarasaki, T., Sugiura, Y., Matsumoto, S., Konoshima, A., Takano, Y., Hayashi, M., Okumura, F., Kamura, T., Mizushima, T., and Nakatsukasa, K. (2023) Defective import of mitochondrial metabolic enzyme elicits ectopic metabolic stress, Science Advances 9, eadf1956.

(56) Mizushima, T., Yoshida, Y., Kumanomidou, T., Hasegawa, Y., Suzuki, A., Yamane, T., and Tanaka, K. (2007) Structural basis for the selection of glycosylated substrates by SCF^{Fbs1} ubiquitin ligase, Proceedings of the National Academy of Sciences 104, 5777-5781.

(57) Rahman, K., Zhao, P., Mandalasi, M., van der Wel, H., Wells, L., Blader, I. J., and West, C. M. (2016) The E3 ubiquitin ligase adaptor protein skp1 is glycosylated by an evolutionarily conserved pathway that regulates protist growth and development, Journal of Biological Chemistry 291, 4268-4280.

(58) Hazra, M. K., and Levy, Y. (2022) Affinity of disordered protein complexes is modulated by entropy–energy reinforcement, Proceedings of the National Academy of Sciences 119, e2120456119.

(59) Yeong, V., Wang, J.-w., Horn, J. M., and Obermeyer, A. C. (2022) Intracellular phase separation of globular proteins facilitated by short cationic peptides, Nature Communications 13, 7882.

(60) Das, R. K., and Pappu, R. V. (2013) Conformations of intrinsically disordered proteins are influenced by linear sequence distributions of oppositely charged residues, Proceedings of the National Academy of Sciences 110, 13392-13397.

(61) Yu, F., and Sukenik, S. (2023) Structural preferences shape the entropic force of disordered protein ensembles, The Journal of Physical Chemistry B 127, 4235-4244.

(62) Hazra, M. K., and Levy, Y. (2020) Charge pattern affects the structure and dynamics of polyampholyte condensates, Physical Chemistry Chemical Physics 22, 19368-19375.

(63) Micsonai, A., Wien, F., Kernya, L., Lee, Y.-H., Goto, Y., Réfrégiers, M., and Kardos, J. (2015) Accurate secondary structure prediction and fold recognition for circular dichroism spectroscopy, Proceedings of the National Academy of Sciences 112, E3095-E3103.

(64) Keul, N. D., Oruganty, K., Schaper Bergman, E. T., Beattie, N. R., McDonald, W. E., Kadirvelraj, R., Gross, M. L., Phillips, R. S., Harvey, S. C., and Wood, Z. A. (2018) The entropic force generated by intrinsically disordered segments tunes protein function, Nature 563, 584-588.

(65) Orlicky, S., Tang, X., Willems, A., Tyers, M., and Sicheri, F. (2003) Structural basis for phosphodependent substrate selection and orientation by the SCF^{Cdc4} ubiquitin ligase, Cell 112, 243-256.

(66) Borgia, A., Borgia, M. B., Bugge, K., Kissling, V. M., Heidarsson, P. O., Fernandes, C. B., Sottini, A., Soranno, A., Buholzer, K. J., Nettels, D., Kragelund, B. B., Best, R. B., and Schuler, B. (2018) Extreme disorder in an ultrahigh-affinity protein complex, Nature 555, 61-66.

(67) Gestaut, D., Roh, S. H., Ma, B., Pintilie, G., Joachimiak, L. A., Leitner, A., Walzthoeni, T., Aebersold, R., Chiu, W., and Frydman, J. (2019) The chaperonin TRiC/CCT associates with prefoldin through a conserved electrostatic interface essential for cellular proteostasis, Cell 177, 751-765.e715.

(68) Liu, B., Poolman, B., and Boersma, A. J. (2017) Ionic strength sensing in living cells, ACS Chemical Biology 12, 2510-2514.

(69) Sheikh, M. O., Thieker, D., Chalmers, G., Schafer, C. M., Ishihara, M., Azadi, P., Woods, R. J., Glushka, J. N., Bendiak, B., Prestegard, J. H., and West, C. M. (2017) O_2 sensing–associated glycosylation exposes the F-box–combining site of the *Dictyostelium* Skp1 subunit in E3 ubiquitin ligases, Journal of Biological Chemistry 292, 18897-18915.

(70) Galvanetto, N., Ivanović, M. T., Chowdhury, A., Sottini, A., Nüesch, M. F., Nettels, D., Best, R. B., and Schuler, B. (2023) Extreme dynamics in a biomolecular condensate, Nature 619, 876-883.

(71) Holehouse, A. S., and Kragelund, B. B. (2024) The molecular basis for cellular function of intrinsically disordered protein regions, Nature Reviews Molecular Cell Biology 25, 187-211.

(72) Brzovic, Peter S., Heikaus, Clemens C., Kisselev, L., Vernon, R., Herbig, E., Pacheco, D., Warfield, L., Littlefield, P., Baker, D., Klevit, Rachel E., and Hahn, S. (2011) The Acidic Transcription Activator Gcn4 Binds the Mediator Subunit Gal11/Med15 Using a Simple Protein Interface Forming a Fuzzy Complex, Molecular Cell 44, 942-953.

(73) Hazra, M. K., and Levy, Y. (2021) Biophysics of phase separation of disordered proteins is governed by balance between short- and long-range Interactions, The Journal of Physical Chemistry B 125, 2202-2211.

(74) Yamazaki, H., Takagi, M., Kosako, H., Hirano, T., and Yoshimura, S. H. (2022) Cell cycle-specific phase separation regulated by protein charge blockiness, Nature Cell Biology 24, 625-632.

(75) Hong, Y., Najafi, S., Casey, T., Shea, J.-E., Han, S.-I., and Hwang, D. S. (2022) Hydrophobicity of arginine leads to reentrant liquid-liquid phase separation behaviors of arginine-rich proteins, Nature Communications 13, 7326.

(76) Vernon, R. M., Chong, P. A., Tsang, B., Kim, T. H., Bah, A., Farber, P., Lin, H., and Forman-Kay, J. D. (2018) Pi-Pi contacts are an overlooked protein feature relevant to phase separation, eLife 7, e31486.

(77) Qamar, S., Wang, G., Randle, S. J., Ruggeri, F. S., Varela, J. A., Lin, J. Q., Phillips, E. C., Miyashita, A., Williams, D., Ströhl, F., Meadows, W., Ferry, R., Dardov, V. J., Tartaglia, G. G., Farrer, L. A., Kaminski Schierle, G. S., Kaminski, C. F., Holt, C. E., Fraser, P. E., Schmitt-Ulms, G., Klenerman, D., Knowles, T., Vendruscolo, M., and St George-Hyslop, P. (2018) FUS phase separation is modulated by a molecular chaperone and methylation of arginine cation-π interactions, Cell 173, 720-734.e715.

(78) Greig, J. A., Nguyen, T. A., Lee, M., Holehouse, A. S., Posey, A. E., Pappu, R. V., and Jedd, G. (2020) Arginine-enriched mixed-charge domains provide cohesion for nuclear speckle condensation, Molecular Cell 77, 1237-1250.e1234.

(79) Schuster, B. S., Dignon, G. L., Tang, W. S., Kelley, F. M., Ranganath, A. K., Jahnke, C. N., Simpkins, A. G., Regy, R. M., Hammer, D. A., Good, M. C., and Mittal, J. (2020) Identifying sequence perturbations to an intrinsically disordered protein that determine its phase-separation behavior, Proceedings of the National Academy of Sciences 117, 11421-11431.

(80) Wang, J., Choi, J.-M., Holehouse, A. S., Lee, H. O., Zhang, X., Jahnel, M., Maharana, S., Lemaitre, R., Pozniakovsky, A., Drechsel, D., Poser, I., Pappu, R. V., Alberti, S., and Hyman, A. A. (2018) A molecular grammar governing the driving forces for phase separation of prion-like RNA binding proteins, Cell 174, 688-699.e616.

(81) Fisher, R. S., and Elbaum-Garfinkle, S. (2020) Tunable multiphase dynamics of arginine and lysine liquid condensates, Nature Communications 11, 4628.

(82) Beltrao, P., Albanèse, V., Kenner, Lillian R., Swaney, Danielle L., Burlingame, A., Villén, J., Lim, Wendell A., Fraser, James S., Frydman, J., and Krogan, Nevan J. (2012) Systematic functional prioritization of protein posttranslational modifications, Cell 150, 413-425.

(83) Sottini, A., Borgia, A., Borgia, M. B., Bugge, K., Nettels, D., Chowdhury, A., Heidarsson, P. O., Zosel, F., Best, R. B., Kragelund, B. B., and Schuler, B. (2020) Polyelectrolyte interactions enable rapid association and dissociation in high-affinity disordered protein complexes, Nature Communications 11, 5736.

(84) Heidarsson, P. O., Mercadante, D., Sottini, A., Nettels, D., Borgia, M. B., Borgia, A., Kilic, S., Fierz, B., Best, R. B., and Schuler, B. (2022) Release of linker histone from the nucleosome driven by polyelectrolyte competition with a disordered protein, Nature Chemistry 14, 224-231.

(85) Reitsma, J. M., Liu, X., Reichermeier, K. M., Moradian, A., Sweredoski, M. J., Hess, S., and Deshaies, R. J. (2017) Composition and regulation of the cellular repertoire of SCF ubiquitin ligases, Cell 171, 1326-1339.e1314.

(86) Jaakkola, P., Mole, D. R., Tian, Y.-M., Wilson, M. I., Gielbert, J., Gaskell, S. J., Kriegsheim, A. v., Hebestreit, H. F., Mukherji, M., Schofield, C. J., Maxwell, P. H., Pugh, C. W., and Ratcliffe, P. J. (2001) Targeting of HIF-α to the von Hippel-Lindau Ubiquitylation Complex by O_2-Regulated Prolyl Hydroxylation, Science 292, 468-472.

(87) Oldfield, C. J., Cheng, Y., Cortese, M. S., Brown, C. J., Uversky, V. N., and Dunker, A. K. (2005) Comparing and combining predictors of mostly disordered proteins, Biochemistry 44, 1989-2000.

(88) Uversky, V. N., and Dunker, A. K. (2010) Understanding protein non-folding, Biochimica et Biophysica Acta (BBA) - Proteins and Proteomics 1804, 1231-1264.

(89) Chouard, T. (2011) Structural biology: Breaking the protein rules, Nature 471, 151-153.

(90) Burger, V. M., Gurry, T., and Stultz, C. M. (2014) Intrinsically disordered proteins: where computation meets experiment, Polymers 6, 2684-2719.

(91) Tompa, P., and Kovacs, D. (2010) Intrinsically disordered chaperones in plants and animals, Biochemistry and Cell Biology 88, 167-174.

(92) Gurumoorthy, V., Shrestha, U. R., Zhang, Q., Pingali, S. V., Boder, E. T., Urban, V. S., Smith, J. C., Petridis, L., and O'Neill, H. (2023) Disordered domain shifts the conformational ensemble of the folded regulatory domain of the multidomain oncoprotein c-Src, Biomacromolecules 24, 714-723.

(93) Staby, L., Kemplen, K. R., Stein, A., Ploug, M., Clarke, J., Skriver, K., Heidarsson, P. O., and Kragelund, B. B. (2021) Disorder in a two-domain neuronal Ca^{2+}-binding protein regulates domain stability and dynamics using ligand mimicry, Cellular and Molecular Life Sciences 78, 2263-2278.

CHAPTER 3

POTENTIAL FOR THE TERMINAL SKP1 GLYCOSYLTRANSFERASE TO EXERT NON-ENZYMATIC CONTROL OF SKP1 IN *TOXOPLASMA GONDII*

Cantrell, D. A., Gas-Pascual, E., Mandalasi, M. N., and West, C. M. (2025) Potential for the Terminal Skp1 Glycosyltransferase to Exert Non-Enzymatic Control of Skp1 in *Toxoplasma gondii*.
To be submitted to a peer-reviewed journal.

ABSTRACT

The Skp1/Cul1/F-Box (SCF) complex is an E3 ubiquitin ligase responsible for targeting a range of proteins for degradation by the 26S proteosome. Within this complex, a variety of F-box proteins (FBPs) link to the SCF complex via the Skp1 adaptor protein allowing for differential substrate recognition. Within the intracellular parasite *Toxoplasma gondii*, Skp1 is subject to oxygen dependent regulation. Under normoxic conditions, the prolyl hydroxylase PhyA hydroxylates Skp1 priming it for modification by five Skp1 specific glycosyltransferase activities. Glycosylation plays an important role in controlling Skp1 availability by weakening the tight Skp1 homodimer and altering Skp1's FBP binding repertoire. However, the presence of the terminal Skp1 glycosyltransferase, Gat1, in the Skp1 interactome regardless of its glycosylation status is atypical for an enzyme. This behavior is reminiscent of its functional counterpart AgtA in *Dictyostelium* which exerts non-catalytic functions on Skp1. Utilizing sedimentation velocity analytical ultracentrifugation, we demonstrate that the Gat1 dimer forms a high affinity complex with Skp1 monomers with the stoichiometry dictated by its glycostate. Computational modeling indicates that Gat1 competes with the same core hydrophobic interface utilized by FBPs and the Skp1 homodimer. This interface is modulated by variable, transient interactions made by Skp1's intrinsically disordered C-terminal region (CTR) that are in turn constrained by the glycan. Remarkably, substoichiometric levels of Gat1 mediate monomerization of Skp1 in a CTR-dependent manner, indicating that Gat1 has the kinetic potential to promote Skp1 monomer availability for FBP binding in cells.

ABBREVIATIONS: CTR, partially disordered C-terminal region of Skp1; GaGlFGaGn-Skp1, notation that identifies the individual monosaccharides of the Skp1 glycan,

including galactose, glucose, fucose, N-acetylglucosamine; Gly-Skp1, abbreviated notation for fully glycosylated Skp1; GT, glycosyltransferase; KO, knock-out or inactivation of the protein coding capacity of a gene; MMGBSA, Molecular Mechanics/Generalized Born Surface Area; SV-AUC, sedimentation velocity analytical ultracentrifugation

INTRODUCTION

Toxoplasmosis is a disease characterized by both acute and chronic stages caused by the obligate intracellular protozoan parasite *Toxoplasma gondii* [1]. *Toxoplasma* infections can occur from a variety of sources including ingesting undercooked meat, handling potentially infections materials such as cat litter, or from receiving an infected person's blood. Acute progression of *Toxoplasma* infections followed by immune control leads to the development of latent infections. During latent infections, *Toxoplasma* transforms into cyst forming bradyzoites protecting them from clearance from the immune system or pharmacological treatments [2-4]. Immune compromised individuals and pregnant women are at increased risk from acute toxoplasmosis [5, 6]. When pregnant women become infected, neonatal toxoplasmosis can lead to potentially debilitating birth defects [6]. Within immune compromised individuals, acute toxoplasmosis is characterized by a potentially life-threatening infection that can be especially detrimental to the brain and eyes [5]. Acute toxoplasmosis represents the leading cause of death from foodborne illness within the United States [1]. Up to a third of the world's population is thought to be latently infected with *Toxoplasma* and this proportion approaches 80% in some western countries [7]. Once present, a latent *Toxoplasma* infection can relapse at any point into an acute infection, a state that is especially dangerous for immunocompromised individuals [1]. Due to this fact and the inability

to clear latent *Toxoplasma* through pharmaceutical means, immunocompromised individuals are forced to undergo treatment for life [1].

To effectively infect new hosts, navigate its various environments, and home into preferred host tissues, *Toxoplasma* needs to maintain effective environmental sensing [8]. A major component of environmental sensing is O_2. Within *Toxoplasma*, the prolyl hydroxylase PhyA, serves as a likely sequence ortholog of human PHD2 [8-10]. PHD2 regulates Hypoxia Inducible-1α (HIF1α) in animals and acts as a major oxygen sensing enzyme [11]. In an oral mouse infection model using a *Toxoplasma* mutant deleted for *phyA*, tissue homing and parasite virulence is severely impaired [12]. PhyA acts by hydroxylating a specific Pro residue conserved within protist Skp1 (P154 for *Toxoplasma*) allowing for the completion of a pentasaccharide [8, 10]. A primary if not sole role of Skp1 is as the adaptor subunit of the Skp1/Cul1/F-box (SCF) complex which is an E3 ubiquitin ligase partially responsible for proteomic control throughout eukaryotes [13, 14]. Skp1 acts to facilitate the attachment of a large variety of substrate binding FBPs, via Subsites 1 and 2, to Cul1 of the SCF complex [15-22]. Upon substrate recognition by the appropriate FBP and its attachment to the SCF complex the bound protein target can be polyubiquitinated [23, 24]. Polyubiquitination by canonical K48 linkages typically results in recognition and subsequent degradation by the 26S proteosome [25-28].

Skp1 hydroxylation and subsequent glycosylation exerts several effects on the SCF complex. Glycosylation has been observed to alter Skp1's FBP binding repertoire likely altering the substrate proteins being recognized and targeted for degradation [20, 21, 29]. Studies that originated in another protist that conserves this modification, the social amoeba *Dictyostelium discoideum*, suggested that the altered interactome results from changes in Skp1's conformational ensemble [30-32]. Glycosylation is expected to promote a disorder to order transition in its

partially disordered C-terminal region **(Fig 3.1B)**. This is expected to alter Skp1's FBP binding repertoire by directly influencing the Skp1-FBP interface [30-32]. The second effect would be through changes in the pool of available Skp1. The Skp1 homodimer forms a complex which is mutually exclusive with binding to FBPs [33]. Unlike the 1-2.5 μM K_d value that describes the affinity of the isolated Skp1 homodimer from mammals [34] and *Dictyostelium* [33], *T. gondii* Skp1 has a greater propensity to homodimerize with a K_d of ~50 nM [35]. This value is close to the 25 nM K_d described for a mammalian FBP-Skp1 interaction [36]. Considering their overlapping interface, these interactions may compete with one another in the cell. This high affinity homodimer is facilitated by a bipartite interface consisting of an ordered Subsite-A, and a fuzzy/disordered Subsite-B at the C-terminal region (CTR) that includes the glycosylation site [35]. Subsites A and B partially overlap with Subsites-1 and -2 of the interface with FBPs, rendering homodimerization competitive with FBP-binding. Weakening of Skp1's homodimer is believed to occur through effects on a fuzzy component of Skp1's homodimer interface [35]. The fuzzy component of Skp1's interface is expected to have implications in its ability to receive post translational modifications and exchange with other binding partners [37-40]. Glycosylation disrupts Skp1's fuzzy Subsite-B resulting in an affinity shift of the Skp1 homodimer to a K_d value of about 400 nM. By significantly weakening this tight competitive interaction [35], glycosylation may promote interactions with FBPs that are predicted to have lower affinity. Overall, glycosylation is expected to regulate the SCF complex through changes in direct protein-protein interactions and through altered sequestration of free Skp1.

The Skp1 glycan from *Toxoplasma* and *Dictyostelium* is a linear pentasaccharide that consists of core trisaccharide that is equivalent to the type 1 blood group H glycan of humans. This is followed by a peripheral disaccharide that is Galα1,3Glcα1,3- in *Toxoplasma* and

Galα1,3Galα1,3- in *Dictyostelium* **(Fig 3.1A)**. The glycosyltransferases (GTs) are distinctive in functioning in the cytoplasmic compartment of cells and evidently dedicated solely to modifying Skp1 [8]. Several of these enzymes are evolutionarily related to sugar nucleotide-dependent counterparts in the secretory pathway [41-44] while others are related to cytoplasmic GTs [45, 46]. The GTs that catalyze the assembly of the core trisaccharide are conserved between these two protists and likely encoded by many other protist genomes [47]. Addition of the last two sugar moieties on the other hand is mediated by unrelated GTs [45, 48, 49]. Nevertheless, the resulting pentasaccharides appear to be similarly structured, indicating a likely example of convergent evolution [45]. The functional ortholog of *Toxoplasma* Gat1 in *Dictyostelium*, AgtA, mediates the addition of both distal sugars, by a mechanism that is greatly enhanced by its WD40-repeat β-propeller domain [49, 50]. AgtA forms a stable complex *in vitro* with all isoforms with Skp1 except for a slightly weaker K_d for the fully glycosylated product (unpublished data). This occurs in a manner that is competitive with FBP binding [49, 50]. In cells, a double knockout (KO) of both *phyA* and *agtA* essentially blocks an O_2-dependent developmental transition that depends on Skp1 hydroxylation and glycosylation. This is unexpected because AgtA activity depends on the prior action of PhyA on Skp1. In addition, overexpression of AgtA inhibits Skp1 hydroxylation and glycosylation and this effect is strongly amplified when using a catalytically dead point mutant of AgtA. Furthermore, overexpression of mutant AgtA results in morphological defects in the formation of fruiting bodies [49]. These *in vivo* effects are potentially due to the binding action described *in vitro* and suggests a mechanism by which AgtA titrates Skp1's availability for interacting with FBPs, potentially serving as an FBP exchange factor.

Although the terminal GT in the *Toxoplasma* pathway, Gat1, is unrelated to AgtA, Gat1 consistently shows up on co-IP pull downs of Skp1 in *Toxoplasma* regardless of glycosylation

status **(Fig 3.1D)** [20, 51]. It is unusual for a GT to be bound to non-substrate glycoforms and its product, and stable interactions were not observed for the other GTs. Thus, the possibility of a phenomenon related to that in *Dictyostelium* also occurring in *Toxoplasma* was investigated. Unlike in *Dictyostelium*, a double-KO between an early enzyme gene in the pathway, in this case *phyA*, and *gat1* did not yield a noticeable phenotype in a fibroblast infection and growth assay (Mandalasi M, Gas-Pascual E, West CM, unpublished data). However, this genetic construct was created in a type 1 strain that does not efficiently differentiate, which is where the double-KO of *Dictyostelium* has a phenotype. A separate study in a type 2 strain, which efficiently differentiates into tissue cysts both in fibroblast monolayers and in mouse infection models, will be required to address this. Therefore, we focused our attention on characterizing the *in vitro* interaction between Gat1 and glycosylated or unmodified isoforms of Skp1. First, we utilized sedimentation velocity analytical ultracentrifugation (SV-AUC) to confirm the formation of a direct complex between the two proteins. Gat1 is a stable homodimer and, interestingly, a stoichiometric shift from a 2:1 to a 2:2 Gat1:Skp1 ratio occurred upon glycosylation of Skp1. AlphaFold3, followed by all atom MD simulations identified a candidate core hydrophobic interface which overlaps with Skp1's interface with FBPs and its own homodimerization interface. The interaction was supplemented by dynamic charge-based contributions from Skp1's intrinsically disordered CTR that also contributes to homodimerization and FBP binding albeit by distinct mechanisms. Despite the high affinity of the Skp1 homodimer, Gat1 thus appears to enzymatically modify only the Skp1 monomer. Furthermore, monomerization of Skp1 also occurs for unmodified Skp1 and the fully glycosylated product, Gly-Skp1, leading to the accumulation of monomeric Skp1 in solution by a substoichiometric process that depends on the CTR. We suggest that Gat1 moonlights as a Skp1

exchange factor to facilitate generation of monomeric Skp1 for complexing with FBPs, in addition to its role as a terminal GT.

METHODS

Purification of Skp1 Constructs and Glycosylation of Skp1.

Skp1 constructs were purified as previously described [35]. Briefly, constructs were expressed in the ER2566 strain of *Escherichia coli* using the pNIC28-HisTEVTgSkp1 plasmid. Clones were grown in Terrific Broth at 37°C with 50 µg/ml kanamycin present as a resistance marker. After reaching an OD_{600} of 1.0, growth temperature was shifted to 18°C for 30 min, before induction with 500 µM IPTG for 16-18h. Cells were collected by centrifugation at 5,000 g for 15 min at 4°C before being frozen at -80°C. Cells were suspended in either Lysis Buffer (50 mM Na/K Phosphate (pH 7.4), 300 mM NaCl, 5 mM benzamidine, 10 µg/ml leupeptin, 10 µg/ml aprotinin, and 0.5 µg/ml pepstatin A) or Super Lysis Buffer (100 mM Na/K Phosphate (pH 7.4), 150 mM NaCl, 500 mM D-Sorbitol, 1 M glycine betain, 700 mM trehalose, 5 mM benzamidine, 10 µg/ml leupeptin, 10 µg/ml aprotinin, and 0.5 µg/ml pepstatin A). Cells were then lysed using 3 passes through a French pressure cell. Lysates were clarified through two centrifugation steps, one at 27,000 g for 40 min at 4°C, and the next at 100,000 g for 70 min at 4°C. Clarified lysates were loaded onto a 5 ml Talon FPLC column (TaKaRa) and washed with Wash Buffer (50 Mm Na/K Phosphate (pH 7.4), 300 mM NaCl), High Salt Buffer (50 mM Na/K Phosphate (pH 7.4), 1 M NaCl), Glycerol Buffer (50 mM Na/K Phosphate (pH 7.4), 300 mM NaCl, 10% (v/v) glycerol), and Wash Buffer. Immobilized protein was eluted using Elution Buffer (50 Mm Na/K Phosphate (pH 7.4), 300 mM NaCl, 300 Mm Imidazole (pH 7.4)). Eluted proteins were dialyzed into Dialysis Buffer 1 (50 mM TRIS-HCl (pH 7.4), 150 mM NaCl, 0.1 mM EDTA (pH 8.0)) before being

dialyzed into TEV Buffer (50 mM TRIS-HCl (pH 7.4), 150 mM NaCl, 1 mM DTT). After 1 h, TEV protease cleavage was performed by adding 0.7 mg of TEV protease to ~100 mg of Skp1, mixing, and incubating at 20°C overnight. Skp1 was then dialyzed twice against Wash Buffer to remove DTT and run over a second subtractive TaKaRa 5 mL Talon Column. Skp1 was then concentrated to ~50 mg/ml by centrifugal ultrafiltration, divided into 0.5 ml aliquots, and frozen in liquid nitrogen for later use. Skp1 was glycosylated as previously described [35].

Purification of Skp1's Glycosyltransferases.

TgGlt1 and DdPgtA were purified as described previously [48, 52]. TgGat1 was purified though autoinduction as previously described [35].

Sedimentation Velocity Experiments.

Proteins were subjected to gel filtration with either an S200 or S75 (16/600) column depending on their size into AUC Buffer (50 mM K^+/H^+ phosphate (pH 7.4), 25 mM KCl). Peak fractions were taken, and dilutions were made with the same buffer. Proteins were diluted from peak fractions and mixed to appropriate concentrations. When varying either Skp1 or Gat1, the protein being varied was serially diluted from a peak fraction. The protein being held constant was diluted two-fold from a common stock with the serially diluted protein. Samples were loaded into 12 mm double-sector Epon centerpieces with quartz windows and equilibrated for 2 h at 20°C. Absorbance measurements were taken at 215 nm, 230 nm 280 nm, or 295 nm depending on the concentration with a 3 mm step size. Buffer and protein parameters were computed using SedNTerp and c(s) distributions (differential sedimentation coefficient distributions) were

modeled using SedFit [53, 54]. Data were modeled as a continuous c(s) distribution and fit using baseline, meniscus, frictional coefficient, buffer, protein, and noise parameters.

Distributions were overlaid in Gussi and regions of interest for each plot were integrated to determine the average S_w (weight-average sedimentation coefficient) position for each distribution [55]. Regions corresponding to the Skp1 monomer and dimer species were separately integrated from regions corresponding to the Gat1 homodimer and Gat1-Skp1 complexes **(Fig 3.S4)**. Plots aimed at identifying the stoichiometry of the Gat1:Skp1 complex were integrated from 3.5-6.0 corresponding to the region where the Gat1 dimer, 2:1 Gat1:Skp1, and 2:2 Gat1:Skp1 species would sediment. Average S_w positions were plotted in Prism and fit to a sigmoidal curve to determine the upper asymptote. This corresponded either to a predicted 2:1 or 2:2 complex for each Skp1 variant.

Normalized S_w values were calculated through the following means. Isotherms aimed at determining apparent affinities were integrated from 1.0-3.5 corresponding to the region where the Skp1 monomer and Skp1 dimer would sediment **(Fig 3.S4)**. These isotherms were additionally integrated from 3.5 to 6.0 corresponding to the region where the Gat1 dimer, 2:1 Gat1:Skp1 complex, and 2:2 Gat1:Skp1 complex would sediment. Extinction coefficients at 280nm for each protein subunit were predicted using ProtParam tool from ExPASy [56]. Protein quantified using UV-Vis was then serially diluted and approximate extinction coefficients were calculated for relevant wavelengths by solving for the equation ($A=cl\varepsilon$) where "A" is the absorbance at a specified wavelength, "c" is the concentration at the wavelength, "l" is the pathlength of the cuvette, and "ε" is the extinction coefficient of the protein. Values giving an absorbance close to 0.6 were preferred for the best accuracy. The approximate contribution of each species in the Gat1-Skp1 complex peak were determined by solving for the equation ($S_w = \frac{\sum_i s_i c_i \varepsilon_i}{\sum_i c_i \varepsilon_i}$) where "$s_i$" is the

sedimentation value, "c_i" is the concentration, and "ε_i" is the extinction coefficient for each species (Gat1 dimer; 2:1 Gat1:Skp1 complex; 2:2 Gat1:Skp1 complex). Known total concentrations for each subunit were used as constraints in these estimates. Free Skp1 was then calculated by subtracting the amount of complex Skp1 from the total Skp1 concentration. An OD_{280} normalized S_w value was then determined using the equation ($S_w = \frac{\sum_i s_i c_i \varepsilon_i}{\sum_i c_i \varepsilon_i}$) where "$s_i$" is the sedimentation value, "c_i" is the concentration and "ε_i" is the extinction coefficient of each species (Skp1 (1*Monomer + 2*Dimer); Gat1 dimer; 2:1 Gat1:Skp1 complex; 2:2 Gat1:Skp1 complex). Normalized S_w positions were plotted in SedPhat where a {(A+A)+(B+B) <-> A+AB+B <-> (AA)B+B <-> A+A(BB) <-> (AA)(BB); self-association A and B; macroscopic K} model was used [57]. Previously determined or estimated Skp1 homodimer affinities, an artificially low Gat1 homodimer affinity (10 nM), and previously determined sedimentation velocities were used for initial fitting. These values were held constant during initial fitting before being incrementally adjusted to yield the best fit to the data. Predicted S_w values for each species were calculated using HYDROPRO [58] using models obtained from AlphaFold3 [59] or MD cluster analysis as previously described [35].

Molecular Modeling of Gat1:Skp1 Complexes.

Initial models were generated using AlphaFold3 using the DeepMind web server [59]. Five structures were analyzed for each Skp1 isoform, which were each further refined using all atom molecular dynamics simulations. MD simulations were performed using the pmemd.cuda version of AMBER22.3 [60]. Amino acid residues were parameterized with the ff14SB force field [61] while glycan moieties were parameterized with the GLYCAM_06j-1 force field [62]. The system was built in a truncated octahedral box with a 15 Å distance from the solute to the end of the unit

cell, neutralized with Na^+, and solvated using TIP3P water [63, 64]. Electrostatic interactions were simulated using the particle mesh-Ewald algorithm with a nonbonded cutoff of 8 Å [65]. SHAKE was used to constrain hydrogen-containing bonds which allowed for a step size of 2 fs. Solvent minimization was conducted over 5,000 cycles with steepest descent followed by 5,000 cycles of conjugate gradient with solute being restrained with a 100 kcal/mol $Å^2$ energy barrier, followed by total system minimization conducted in the same manner. The system was heated to 300° K under NVT (constant particle number, volume, and temperature) conditions over 20 ns before being held steady at 300° K for an additional 10 ns. Conditions were then changed to NPT (constant particle number, pressure, and temperature) and the system was equilibrated for 270 ns. Structures were then subjected to a 1 μs production run for analysis.

AlphaFold3 generated complexes utilizing Skp1's C-Terminal Region (CTR) were split into two groups with five structures each. The first group (Folded CTR) utilized the AlphaFold3 generated structures which contained α-helixes 7 and 8 typically observed in complexes with FBPs. Due to the high probability of disorder in this region, the second group (Disordered CTR) replaced the structure of Skp1's CTR with an extended conformation using the Modeler homology modeling software [66].

Models of glycosylated Skp1 were generated using AlphaFold3 structures which utilized Skp1's CTR. First, the lowest energy state of the previously described [45] pentasaccharide from *Toxoplasma* was modeled using GLYCAM-Web [67]. Since NMR data indicated that glycosylation promotes a disorder to order transition in *Dictyostelium* Skp1's CTR [32], AlphaFold3 was utilized to generate structures of *Toxoplasma* Skp1 with TgFbxO1, TgFbxO13, and TgFbxO14. The structure with the highest average predicted Local Distance Difference Test (pLDDT) score within Skp1's CTR (TgFbxO13) was selected as the template for an ordered CTR.

The glycan was linked to this ordered CTR and the extended conformation above, according to previous modelling [31, 45] utilizing UCSF Chimera [68]. Skp1's CTR was linked to its BTB domain from the FBP bound model of Skp1 using manual PDB editing and UCSF Chimera. The positioning of Skp1's CTR was further refined in Chimera to avoid clashes. A no-glycan control was then generated by deleting the Skp1 glycan in these models and replacing the OLP (O-linked Pro) with a PRO designation.

Every 0.5 ns frame of the production phase was utilized for MMGBSA (Molecular Mechanics/Generalized Born Surface Area) which utilized the mmpbsa.py script [69]. The Skp1 protein (with the glycan if applicable) was treated as the ligand with the rest of the complex being treated as the receptor. An igb of 2 was used with an idecomp of 3 for pairwise interactions and 1 for per-residue interaction energies. Total per-residue interaction energies were averaged across all five simulations for each group. Pairwise interaction energies of electrostatic residues contributing more than -1 kCal/mol were identified and their distances were computed over the length of the production runs. Atoms representing each charge group were CZ for Arg, NZ for Lys, CD for Glu, CG for Asp, N for the N-terminal residue, and C for the C-terminal residue. Ensemble clustering has been shown to improve the reliability of protein structure analysis of dynamic proteins and complexes in several examples [35, 70]. Cluster analysis was carried out in a similar manner as previously described [35]. The MD Ensemble Cluster analysis tool was utilized in UCSF Chimera [68]. This tool groups similar structures into ensemble clusters and selects a representative structure from each cluster as previously described [71]. The top 5 representative clusters were obtained and their s-values were predicted using HYDROPRO [58]. Buried surface area was calculated using FreeSASA [72], which utilizes the Lee & Richards [73] and Shrake & Rupley [74] algorithms to calculate solvent accessible surface area (SASA). First, SASA was calculated

for the Skp1 subunit, Gat1 dimer, and the total complex obtained from each representative structure from ensemble clustering. Buried surface area of each representative structure was then calculated according to the following equation: (((Gat1 dimer SASA)+(Skp1 SASA))-(Complex SASA)=(Complex buried SASA)). This was repeated for the total buried surface area, buried hydrophobic surface area (hydrophobic residues only), and buried polar surface area (electrostatic and polar residues only). Final values from each group of simulations were obtained from the weighted average of each representative structure weighted by the number of frames in each cluster.

A variability analysis was carried out using a matrix of Cα-Cα distances. Distances for each Cα pair within the structure were obtained using cpptraj. The average distances and standard deviation for each Cα pair were computed and organized into a matrix. Standard deviations organized into a Distance Variability Matrix (DVM) represent the variability of distances between residues in a protein chain and assesses the flexibility of the predicted structure. Values for each position within these DVMs were averaged across all five simulations to give the final DVM representing the specific group of simulations. Due to potential alignment artifacts for large proteins or proteins with large intrinsically disordered regions [75], RMSF was not used to score flexibility for each residue. Instead, residues were scored utilizing the DVM for each individual simulation. The Trimmed Average/Mean of the Standard Deviation utilizing 50% of the data (TASD50) score was calculated by removing the highest and lowest 25% of values to remove biases from very close and particularly flexible residues. The mean of the remaining data was obtained to yield the TASD50 score for a particular residue. TASD50 scores from each simulation were then averaged to give the final TASD50 score for each residue within a simulation group.

Computational Saturation Mutagenesis.

Computational scanning mutagenesis (CSM) was performed as previously described for the *Dictyostelium* Skp1 homodimer [33]. The top five ensemble clusters from each group of simulations representing the 2:1 Gat1:Skp1 complex with a pre-folded and disordered CTR were used as starting structures. Non-electrostatic residues on Gat1 which contributed more than -1 kcal/mol of energy in both groups of simulations were selected for mutagenesis. Starting structures were relaxed using the "fast relax" protocol in the Rosetta software suite [76, 77]. Utilizing relaxed structures from each ensemble cluster, the designated residues were then subjected to saturation mutagenesis via the flex ddG protocol [78, 79]. This method takes advantage of the Rosetta backrub protocol to allow for more effective optimization of mutated structures [80]. The original script was adapted to mutate both subunits of the Gat1 homodimer simultaneously. The "fa_talaris2014" scoring function was utilized with the "talaris2014" weights, and default values were used for other settings. The weighted average of the three most favorable clusters for each group (Folded or Disordered) was calculated weighted by the population each cluster.

The influence of each mutation on protein stability was calculated using the ddG monomer tool in Rosetta [81]. Five simulations representing the Gat1 dimer were clustered and representative structures from the top 5 clusters were relaxed using the "fast relax" protocol as for CSM. Relaxed structures were iteratively mutated on each subunit at each targeted residue. Soft-repulsive weights were utilized for initial sidechain optimization. A full-atom maximum interaction distance of 9.0 Å was utilized. The local optimization restriction was set to "false" to allow wider optimization of the mutated protein structure. The three lowest scores from 50 replicates were averaged to give the initial stability score for each residue. These scores were then normalized against the wild-type control mutation for each residue to give the final residue score

for each cluster. The weighted average of the three lowest scoring clusters for each mutation was then divided by two, to account for each subunit, to give the final stability score for each mutation.

Skp1 Hydroxylation Assays.

Skp1 hydroxylation assays were utilized to determine if Gat1 exerts an inhibitory effect on Skp1 hydroxylation. Common Master Mix solutions were prepared for each reaction condition. Master Mix 1 (4X concentration of Skp1) contained (50 mM HEPES (pH 7.4); 400 nM TgSkp1; 10 µg/ml Leupeptin; 10 µg/ml Aprotinin; 0.25 mg/ml BSA; 5 µM $FeSO_4$; 1.5 mM α-ketoglutarate; 2 mM Ascorbate; 0.8 mg/ml Catalase; and 1 mM TCEP). Master Mix 2 (4X concentration of PhyA) contained (50 mM HEPES (pH 7.4); 10 µg/ml Leupeptin; 10 µg/ml Aprotinin; 0.25 mg/ml BSA; 5 µM $FeSO_4$; 1.5 mM α-ketoglutarate; 2 mM Ascorbate; 1 mM TCEP; and 20 nM TgPhyA). TgGat1 and control inhibitors were mixed with the Skp1 Master Mix to yield a pre-initiated mix at 75% the total volume. Reactions were initiated by rapidly mixing preincubated pre-initiation mixes with the PhyA maser mix to yield a final reaction concentration of (50 mM HEPES (pH 7.4); 100 nM TgSkp1; 5 nM TgPhyA; 10 µg/ml Leupeptin; 10 µg/ml Aprotinin; 0.25 mg/ml BSA; 5 µM $FeSO_4$; 1.5 mM α-ketoglutarate; 2 mM Ascorbate; 0.2 mg/ml Catalase; 1 mM TCEP; and an appropriate concentration of the tested inhibitors). Inhibitor concentrations were (100 nM TgGat1 (1:1); 200 nM TgGat1 (2:1); 600 nM TgGat1 (6:1); 2 µM TgGat1 (20:1); 500 µM PCA; and 500 µM Folate). Reactions were incubated for 23 min and 1.5 h and were quenched using an SDS containing gel loading buffer. A control reaction was run alongside the experimental reactions and used to measure reaction progress. Background was measured using a T0 where the SDS containing loading buffer was pre-added to the pre-initiation mix. Samples were loaded onto western blots and the presence of hydroxylated Skp1 was measured using UOK85 polyclonal

antibodies [82]. A calibration curve was established by mixing fully hydroxylated or unmodified Skp1 in varying ratios and plotting the resulting densitometry. Densitometry was calculated for each experimental condition, replicates were normalized based on their control reactions, and percent hydroxylation was calculated using the established calibration curve.

Fbs1-Gat1 Competition Assays.

Gel filtration experiments were conducted similar to what was previously described [30]. Briefly, buffers consisted of 50 mM HEPES (pH 7.4), 1.8 mM Na/K Phosphate (pH 7.4), 60 mM NaCl, and 1 mM DTT. Solutions containing 5 µM Fbs1, 10 µM Gat1, or appropriate mixtures were made followed by addition of 5 µM Skp1. Solutions were preincubated for 30 min before injecting 50 µl of solution into a Superdex 200 PC 3.2/30 column using a 100 µl loading loop on a Pharmacia SMART-System at 80 µl/min. 50 µl fractions were collected and run on a CBB or Western Blot gel. Densitometry was then used to measure the elution profile of Gat1 and Fbs1 for each relevant condition.

RESULTS

Gat1 Stably Binds Skp1 in a Complex whose Stoichiometry is Dependent on Skp1's Glycosylation State.

To characterize the nature of Gat1's association with Skp1 indicated by the co-IP pulldowns, Skp1 and Gat1 were recombinantly expressed in *E. coli* and purified to homogeneity. Using sedimentation velocity, clear peaks were observable for the individual homodimers of both Skp1-FL and Gat1 at 5 µM concentration **(Fig 3.1E)**. The lack of visible monomer species for either protein is consistent with the previously reported high affinity homodimer of each protein

[35, 45]. Upon mixing equimolar concentrations of Skp1 and Gat1, a reduction in the magnitude of the Skp1 homodimer peak was observed. This accompanies a shift in the Gat1 dimer peak to a position consistent with a 2:1 Gat1:Skp1 complex based on modeling **(Fig 3.1E)**. This indicates dissociation of the Skp1 homodimer in favor of interacting with Gat1. With an approximate 2-fold excess of Gat1, mostly complete depopulation of the Skp1 homodimer species was observed with a minimal shift in the position of the Gat1:Skp1 complex **(Fig 3.1E)**. The lack of discrete species for either the Gat1 homodimer or a 2:2 Gat1:Skp1 complex is suggestive of a relatively rapid equilibrium to the formation of a 2:1 complex on the timescale of the experiment **(Fig 3.1E)**.

Protein concentrations were then lowered to more physiological levels. Skp1-FL was held constant at 500 nM, which still allowed detection of the relatively weak Skp1 absorbance signal, while the concentration of Gat1 was varied. The region of each distribution corresponding to the Gat1 homodimer and the Gat1:Skp1 complex was then integrated to determine the saturating S_w value **(Fig 3.S4)**. As can be observed by the graph in **(Fig 3.2A)**, the S_w position for the Gat1:Skp1 complex effectively saturates at a position slightly below the 4.7 value predicted for the 2:1 Gat1:Skp1 complex. The significance of Skp1's pentasaccharide was evaluated with the same titration using fully glycosylated Skp1 (Gly-Skp1). Interestingly, the saturating S_w position for the Gat1:Skp1 species increased to a value consistent with a 2:2 Gat1:Skp1 complex **(Fig 3.2C)**. This indicates that stoichiometry of the Gat1:Skp1 complex is dictated by Skp1 glycosylation status and suggests an altered protein-protein interaction controlled by Skp1 glycosylation. Glycosylation of Skp1 was previously reported to weaken Skp1 homodimerization by disrupting a fuzzy interaction of Skp1's CTR [35]. Given this, we next determined the role of Skp1's CTR on controlling the stoichiometry of the Gat1:Skp1 complex. As shown in **(Fig 3.2E)**, Skp1-ΔCTR forms a 2:2 Gat1:Skp1 complex analogous to the behavior of Gly-Skp1. This indicates that glycosylation

controls stoichiometry through effects on the Skp1 protein itself rather than a direct lectin-like binding interaction between Gat1 and the glycan. Taken together, these data are consistent with a model where glycosylation controls Gat1 association through effects on Skp1's CTR.

We next modeled the apparent affinities of each interaction using Sedphat [57]. The range of S_w values associated with the Skp1 monomer and Skp1 dimer were integrated and used alongside the range associated with the Gat1 dimer and Gat1:Skp1 complex **(Fig 3.S4)**. These integrations were used to generate a normalized S_w value which was plotted as a function of Gat1 concentration into an isotherm. As shown in **(Fig 3.2B)**, these plots exhibit three regions of interest. The component observable at negligible Gat1 concentrations represents the Skp1 monomer-dimer equilibrium. The isotherm at this region represents the contribution of the Skp1 homodimer at this concentration (500 nM). As more Gat1 is titrated into the solution, the average S_w of the system increases consistent with both the increased representation of the Gat1 species and greater incorporation of Skp1 into the larger Gat1:Skp1 complex. The average S_w of the system peaks when the maximum amount of both Skp1 and Gat1 have been bound up by the Gat1:Skp1 complex. The position, shape, and height of this peak are determined by both the stoichiometry and affinities of this complex. Once this peak has been attained, titration of increasing Gat1 drives the average S_w toward a value representing the Gat1 homodimer. Overrepresentation of the Gat1 homodimer in this region brings down the average S_w value of the system.

The Skp1 homodimer [35] and Gat1 homodimer [45] were previously characterized to have very tight affinities. Based on these values, the S_w values for each species and complex, and the stoichiometries of the Gat1:Skp1 complexes; apparent affinities for each Gat1:Skp1 interaction were calculated. The apparent affinity of Skp1 with Gat1 was approximately 84 nM (K_d) **(Fig 3.2B)** and attempts to model the interaction as a 2:2 Gat1:Skp1 complex were unsuccessful. The

apparent affinity for the Gat1 homodimer modeled to <10 nM consistent with previous observations that Gat1 forms a very tight homodimer [45]. Interestingly, the homodimer affinity of Skp1 modeled to ~120 nM, which is more than twofold higher than previously estimated [35]. This difference may result from a strong dissociative effect of the Gat1 dimer on the Skp1 homodimer **(Fig 3.6A)**. Upon modeling a similar isotherm with Gly-Skp1, two binding events were effectively modeled with each having an apparent affinity close to 200 nM **(Fig 3.2D)**. This is weaker than the affinity seen with Skp1ΔCTR suggesting that rather than contribute to binding, Gly-Skp1's CTR slightly disfavors Gat1 binding **(Fig 3.2F)**. This may represent the loss of favorable contacts upon glycosylation, a shift toward a less favorable Skp1 conformational ensemble, entropic excluded volume effects, or a combination of effects.

Skp1's CTR is Likely Relatively Disordered in the Gat1:Skp1 Complex.

To explore the mechanism by which Skp1's CTR may control complex asymmetry, we turned to computational modeling starting with AlphaFold3. We first modeled the 2:1 Gat1:Skp1 complex observed for unmodified Skp1 **(Fig 3.3A)**. In this model Gat1 forms a homodimer which matches closely with the crystal structure solved for the highly similar Pythium Gat1 **(Fig 3.S5)**. A relatively large intervening loop is present in Gat1 relative to Pythium Gat1 [45] as a region of low confidence in AlphaFold3's pLDDT which interprets confidence in local structural features **(Fig 3.3C)**. It is also clearly visible using AlphaFold3's Predicted Alignment Error (PAE) matrix **(Fig 3.3B)**, which interprets confidence in the global structural model. This can indicate flexible or disordered regions as well as reliability of the predicted interface. A low confidence helix is predicted within this intervening loop **(Fig 3.3A,C)** which may be the result of patches of electrostatic residues. Large and especially alternating patches of electrostatic residues are known

to promote free helix formation such as with E-R/K helixes [83-86]. Skp1 is positioned with high confidence on a single subunit of the Gat1 homodimer **(Fig 3.3A-C)**. No interactions of an intact Skp1 homodimer were observed when a second Skp1 subunit was modeled. The positioning of Skp1 onto the single Gat1 subunit is likely directed by a core hydrophobic interface surrounded by both polar and electrostatic interactions **(Fig 3.4-3.5)**. This interface is also utilized by the Skp1 homodimer and offers a mechanism for incorporating a single Skp1 subunit for a first binding event. This is a necessary feature of a modeled Gat1:Skp1 complex due to a 2:1 Gat1:Skp1 complex being observed at concentrations even orders of magnitude above the Skp1 homodimer K_d [35]. Additionally, this prediction is consistent with data that Gat1 binding to Skp1 is mutually exclusive with FBP binding **(Fig 3.S7)**. Skp1 bound into a complex with Gat1 becomes recalcitrant to hydroxylation by PhyA **(Fig 3.S8)**, an effect also observed with FBPs [49, 87, 88] and *Dictyostelium* AgtA [49]. Skp1's N-terminal extension is modeled with low confidence extending into the solvent consistent with a disordered protein region **(Fig 3.3A,C)**. Skp1's internal loop is modeled with relatively low confidence but higher confidence than other typically disordered regions of the protein **(Fig 3.3A-C)**. This likely stems from the presence of two anchoring sites for this disordered protein segment as opposed to the single anchoring site for the N- and C-termini. Skp1's CTR is modeled with low confidence though folding as helixes 7 and 8 similar to complexes with FBPs was observed [89-91]. This might be the result of bias in the prediction owing to an abundance of FBP containing structures of Skp1 **(Fig 3.3A-C)** [89-91]. Given the low confidence in this region, there is a high likelihood that this portion of the protein lacks stable structure. Positioning of these helixes is also relatively inconsistent between independently generated models **(Fig 3.S6)**. Whether or not Skp1's CTR is assumed to be disordered, the positioning of Skp1 orients the CTR to face toward Gat1's active site **(Fig 3.3A, Fig 3.S9)**. This is

significant, as orientation of Skp1's CTR toward Gat1's active site would likely be necessary for efficient enzymatic activity of Gat1 for Skp1.

AlphaFold3 is capable of effectively modeling the general structure of an individual protein or protein complex but often falls short when modeling specific interactions [92-94] or intrinsically disordered regions [93-95]. Thus, we turned to all atom molecular dynamics simulations to model specific interactions within the Gat1:Skp1 complex and their dynamics. Five structures generated by AlphaFold3 were directly used to initiate independent molecular dynamics simulations termed "Folded CTR Simulations." A second group of five structures was generated where Skp1's CTR was assumed to be initially disordered termed "Disordered CTR Simulations." This was done by deleting the residues associated with Skp1's CTR and modeling them back in an extended conformation using Modeler as done previously with the Skp1 homodimer [35]. After an initial heating step, structures were subjected to refinement through a 270 ns equilibration step which allowed for structural adjustment based on Amber's force fields. Following this equilibration step, a 1 μs simulation was run and the structural and dynamic properties of the complex were analyzed. Given the relatively large size of the complexes (up to 100 kDa) and large proportion of disordered regions, a high impact from alignment artifacts can be expected from techniques such as RMSF [75]. Given this, an approach utilizing distance matrixes was selected as more appropriate for analyzing protein flexibility. To do this, we calculated and plotted the standard deviation of Cα-Cα distances into a Distance Variability Matrix **(Fig 3.3D-E)**, which showed similar dynamic behavior for both groups of simulations. The regions with high degrees of flexibility correspond well to the regions of low confidence in AlphaFold3's PAE matrix. A high degree of flexibility is observed within the internal loop of each Gat1 subunit. Additionally, high flexibility is observed within the N-terminal region, internal loop, and CTR of Skp1. Relatively low variability is observed between

the well-ordered regions of each complex subunit indicating a relatively immobile complex with stable protein-protein interfaces including with Skp1. To further analyze the mobility of individual residues, the trimmed mean of average standard deviations was calculated for all Cα-Cα distances per each atom; 50% of the total values (25% of the highest and lowest) were excluded when calculating the mean standard deviation of each residue. This reduced artifacts from both highly mobile and nearby residues to give a Trimmed Average Standard Deviation (TASD50) score for each residue. As shown in **(Fig 3.3F-H)**, the protein subunits from each group of simulations behaved similarly. Regions of high flexibility (TASD50 > 2Å) correspond well to regions of the structure with relatively low pLDDT confidence scores. Specifically, a relatively high TASD50 score for Skp1's CTR was determined for both groups of simulations supporting the model where Skp1's CTR remains highly mobile within a complex between Skp1 and Gat1.

Skp1 Binds Gat1 Utilizing a Core Hydrophobic Interface.

The Gat1:Skp1 interface buries an expansive surface area of 3380 Å2 when a disordered CTR is modeled and 3180 Å2 when a folded CTR is modeled. The buried hydrophobic surface area represents a large component of this with 2070 Å2 and 1840 Å2 for the disordered and folded CTRs, respectively. To determine which residues are likely most important for maintaining the Gat1:Skp1 complex, we turned to analysis through MMGBSA. As illustrated in **(Fig 3.4A)** and **(Fig 3.5D)**, significant contributions were observed to occur from Skp1 F108, I111, L112, N115, and Y116, which also contribute significantly to Skp1 homodimerization via Subsite-A [35]. Significant, but less consistent contributions were also observed for other residues in Subsite-A such as Q104, K105, A109, M133, and I134. Hydrophobic contacts from Skp1's N-terminal lobe, involved in Cul1 binding, included L34, T37, M38, P52, and N53 and less consistent contributions

from E41, L51, and V54. Significant, but highly conformationally dependent interactions were also observed within Skp1's CTR that is reminiscent of previously observed homo-interactions within Skp1's fuzzy Subsite-B. Importantly, many Skp1 residues identified to be most important for binding to Gat1 are also important for Skp1 homodimerization. This and our previous AUC data support two conclusions in studying the Gat1-Skp1 interaction: it is finely balanced with Skp1 homodimerization, and mutagenesis studies targeting the Skp1 side of the interface would be confounded by effects on Skp1 homodimerization.

Large (<-1 kCal/mol) energetic contributions to the interaction were observed for both simulation groups from Gat1 residues N14, Y17, Y18, S47, T48, K50, A51, Y54, W317, P320, W330, F333, and L334 **(Figs 3.4B, 3.5D)**. Less consistent but still significant interactions were made by F16, S45, Q46, Q55, R137, R139, H289, M290, Y298, S312, Q319, A321, K331, and T335. The charged residues are suspected to contribute transient protein contacts **(Fig 3.5)**. To test the role of the largely hydrophobic interface, we turned to Computational Scanning Mutagenesis (CSM) with the Rosetta software suite. The Gat1 portion of the interface was targeted due to the confounding effects of the Skp1 interface with FBP binding and Skp1 homodimerization. Residues that were consistently important in both groups of simulations (folded and disordered Skp1 CTR) were targeted for mutagenesis. The role of each mutation in influencing the Gat1:Skp1 complex was tested using the flex ddG algorithm. Mutations in simulation groups were predicted to have similar effects on the stability of the Gat1:Skp1 interface **(Fig 3.4C,D)**. The ddG Monomer algorithm was then utilized to test the influence of each mutation on the stability of Gat1 **(Fig 3.4E)**. From these datasets, the Y18K and A51K point mutations were predicted to weaken the Skp1:Gat1 interface while simultaneously preventing destabilization of Gat1 and were chosen for further analysis. Since AlphaFold3 has proven useful in predicting the effects of mutagenesis on

protein-protein complex formation [95], the PAE matrixes from each of the mutant Gat1:Skp1 structures were analyzed and showed a large decrease in the confidence of placing Skp1 in the Gat1:Skp1 complex **(Fig 3.4F-H)**. A relatively small decrease in the pLDDT score was observed for interface residues in each instance **(Figs 3.S15-3.S17)**, however the effect of proper Skp1:Gat1 folding maintained a higher degree of confidence with this metric. Additionally, the Y18K and Y18K-A51K mutants resulted in inconsistent placement of Skp1 in the Gat1:Skp1 complex **(Figs 3.S15-3.S17)**. Taken together, despite AlphaFold3 confidence metrics showing high confidence in each protein's fold, the ability to place Skp1 properly in the Gat1:Skp1 complex was substantially hindered by these point mutations. Studies to confirm the predicted effect of these point mutations are in progress.

Gat1 and Skp1 Contribute a Hybrid Ordered and Fuzzy Interface.

Skp1's CTR and Gat1's internal loop show high mobility in **(Fig 3.3)** and also exhibit a high diversity of contacts with one another and other surfaces on each protein **(Fig 3.5A,E,G)**. In all simulations a core hydrophobic and ordered interface similar to that depicted in **(Fig 3.5D)** is present. As visualized through MMGBSA, significant electrostatic based interactions are present within the Gat1:Skp1 complex **(Figs 3.S10-3.S11)**. Much of this energy is centered around clusters of positively or negatively charged residues, an effect observed in simulations of Skp1's fuzzy interface [35]. To observe the kinetics of these interactions, pairwise MMGBSA energies were calculated for each pair of oppositely charged electrostatic residues. Distances between electrostatic pairs with contributions greater than -1 kCal/mol in an individual simulation were plotted across the length of the simulation **(Fig 3.S18)**. A total of 146 examples of these electrostatic pairs were observed across all 10 simulations to give an average of 14.6 electrostatic

pairs per simulation. A strong bias was observed in favor of a starting disordered CTR with 97 electrostatic pairs versus the 49 observed with a folded CTR. This indicates that conformations accessible within "disordered CTR" simulations provided 19.4 productive contacts per simulation versus the 9.8 observed when Skp1's CTR was pre-folded. The transient formation of electrostatic interaction networks was observed in every simulation with several examples depicted in **(Fig 3.5)**. Skp1's CTR readily formed these interactions with charge clusters both on Subunit-1 **(Fig 3.5F)** and Subunit-2 **(Fig 3.5B,C)** of Gat1. Interestingly, Gat1's internal loop, including several positive charge clusters, also readily formed electrostatic interaction networks with Skp1's CTR and its BTB domain **(Figs 3.5H, 3.S10-3.S11, 3.S18)**.

Gat1 Potentially Acts as an Exchange Factor for Skp1 in a CTR Dependent Manner.

Previous studies have suggested that the high kinetic exchange of specific interactions in fuzzy protein complexes can facilitate exchange between interacting macromolecular species [37-40]. Therefore, we investigated a possible role of Gat1 in facilitating the exchange of the tight Skp1 homodimer. As shown in **(Fig 3.6A)**, a substoichiometric concentration of Gat1 is capable of weakening the Skp1 homodimer. The affinity of the full-length, unmodified construct has been previously estimated at about 50 nM [35]. Even at a 20 nM concentration of Gat1 (10 nM in terms of the dimer), a significant shift in the equilibrium of 500 nM Skp1 is observable moving a predominately dimeric Skp1 to mostly its monomeric form. This is significant considering that 500 nM is an order of magnitude above Skp1's previously estimated K_d, and more impressive considering Gat1 binds Skp1 in a strict 2:1 Gat1:Skp1 complex **(Fig 3.2A)**. A similar effect is observable with Gly-Skp1 where a shift to monomeric Skp1 is observable with the addition of 40 nM Gat1 **(Fig 3.2B)**. This is, however, less impressive than the effect observed with Skp1 due to

the much higher homodimer K_d of Gly-Skp1 of 400 nM [35], higher concentration of Gat1 used, and 2:2 stoichiometry of the Gat1:Skp1 complex **(Fig 3.2C)**. Thus, Gat1 increases the apparent K_d of the Skp1 homodimers presumably by stimulating the k_{off} rate. Considering its role in forming Skp1's fuzzy interface, we next sought to determine the role of Skp1's CTR in Skp1's Gat1 dependent monomerization. A concentration series of Skp1ΔCTR in the presence of a 1:10 ratio of Gat1:Skp1 was analyzed via sedimentation velocity **(Fig 3.6C)**. The region associated with the Skp1 monomer and dimer species were integrated and deconvoluted into monomer and dimer contributions to yield an apparent K_d of 900 nM **(Fig 3.6D)**. This matches the homodimer K_d previously determined for this construct [35] and indicates that Skp1's exchange toward the monomeric species is dependent on the presence of Skp1's CTR.

DISCUSSION

Gat1 is a soluble cytosolic glycosyltransferase that exists as a tight homodimer, like its evolutionarily related homolog glycogenin. Its substrate GlFGaGn-Skp1 is also a tight homodimer, but how their homodimer states influence catalytic addition of a Gal to generate GaGlFGaGn-Skp1 was unknown. The Skp1 protein promotes catalytic activity of Gat1 based on the finding that modification of GlFGaGn-Skp1 is >30-fold more active than when GlFGaGn- is linked to paranitrophenol [45]. We previously observed that Gat1 forms stable interactions with both unmodified (non-substrate) and fully glycosylated (product) isoforms of Skp1 *in vivo*. Direct *in vitro* complexes of Gat1 with these Skp1 isoforms and a variant lacking its CTR indicate that the *in vivo* interaction is direct. SV-AUC analysis of the Gat1:Skp1 (unmodified) complex indicated a 2:1 ratio, consistent with the Gat1 homodimer splitting the Skp1 homodimer. Computational modeling through the combined use of AlphaFold3 and all-atom MD simulations identified a

candidate core hydrophobic interface. This interface approximately involves the region of Skp1 that mediates Subsite-1 of its interaction with FBPs and Subsite-A of its self-interaction **(Fig 3.1B)**. Additionally, Gat1 leverages contacts in the Cul1 binding region of Skp1 to further enhance binding. The position of the Gat1 interface aligned the CTR of Skp1 in such a way to be compatible with insertion of its tetrasaccharide into Gat1's active site **(Fig 3.S9)**. However, in the absence of the glycan the CTR sampled a wide range of transient interactions against either Gat1 subunit. Both regions remain highly mobile regardless of whether Skp1's CTR was modeled with a folded CTR according to AlphaFold3 or in an extended conformation. The interaction between the CTR and Gat1 is reminiscent of the fuzzy interaction between the two CTRs of the Skp1 homodimer [35]. Major differences do exist in that the ordered region of Gat1 is conformationally stable, and the disordered Gat1 loop is not identical in sequence. The presence of the acceptor tetrasaccharide glycan at Hyp154, which was previously modeled into a groove in the active site [45] **(Fig 3.S9)**, would be expected to overcome this dynamic character until completed.

Upon glycosylation, the Gat1:Skp1 complex shifts from a 2:1 to a 2:2 complex **(Fig 3.2)**. Previous NMR and modeling studies showed that the full glycan imposed a greater order to the CTR [31, 32, 45]. This would be expected to limit the dynamic fuzzy-like interactions of Skp1's CTR that extended to both Gat1 subunits, as well as excluded volume effects of Skp1's CTR **(Fig 3.7A)**. There was a roughly 2-fold reduction in the number of productive electrostatic contacts observed when a folded CTR was used as a starting point for MD simulations **(Fig 3.S18)**. This indicates that a bias toward even a partially more well-ordered structure in this region would be expected to weaken an electrostatically mediated fuzzy interaction made with Gat1. Together with the weakening of the Skp1 homodimer by its glycosylation, these effects are predicted to permit both Gat1 subunits to bind separate Gly-Skp1 subunits in a symmetrical manner **(Fig 3.7B)**. This

is supported by isotherm modeling indicating that the apparent affinities of each Gat1:Skp1 interaction are roughly equivalent within a construct **(Fig 3.2)**. In contrast, the affinity of Gly-Skp1 toward Gat1 is less than that of Skp1, which may be relevant to the Skp1 exchange activity proposed below. Taken together, Skp1's CTR has an unexpectedly complex role in controlling stoichiometry of the Gat1:Skp1 complex that is in turn subject to control by its posttranslational modification.

Binding of Skp1 to Gat1 competes with its tight homodimerization and binding to FBPs, and the balance among the mutual affinities is likely to be physiologically significant. The substoichiometric effect of generating free Skp1 monomer at a concentration where Skp1 is largely dimeric informs a potential mechanism **(Fig 3.6)**. Given that the Skp1 homodimer K_d is equivalent to the ratio of rate constants k_{off}/k_{on}, and that Gat1 is unlikely to strongly influence k_{on}, Gat1 is inferred to increase k_{off}. There is a persistence of monomeric Skp1 in the SV-AUC experiments, even at 500 nM far above its ~50 nM K_d. This may indicate that this low natural K_d is achieved by relatively slow k_{on} and k_{off} rate constants when compared to other Skp1 interactions. The K_d that describes the Gat1:Skp1 interaction (84 nM) **(Fig 3.2)** is inferred to be similar to the Skp1 homodimer K_d. There are also several instances for somewhat discrete Skp1 monomer and dimer peaks **(Figs 3.S1-3.S3)**, but there is no evidence for discrete Gat1:Skp1 complex peaks in the SV-AUC studies. It is likely that its K_d is characterized by a ratio of fast k_{off} and k_{on} rate constants. This inference explains how substoichiometric Gat1 is able to control the monomer/dimer status of a 10-fold molar excess of Skp1. The encounter of Skp1 and Gat1 dimers in solution may result in an increased off rate for the Skp1 homodimer. This coupled with the fast on rate of one Skp1 subunit to the Gat1 dimer results in a free subunit of Skp1 left over from the dissociated Skp1 homodimer. This effect may be enhanced by the relatively rapid release of the bound Skp1 subunit.

If this is combined with a relatively slow reassociation of the Skp1 homodimer, this may increase the pool of monomeric Skp1 available to bind other partners such as FBPs. This effect on the Skp1 homodimer depends on the presence of its CTR **(Fig 3.6)**. Previous findings indicate that fuzzy protein interactions can facilitate the rapid exchange of binding partners in high affinity complexes and allow for the more facile addition of post translational modifications [37-40]. Once these interactions have been removed from the Skp1 homodimer, the remaining Subsite-A remains inefficient at maintaining the high affinity complex. Gat1 may leverage this property of fuzzy interactions to exchange Skp1:Skp1 fuzzy interactions with Skp1:Gat1 interactions in Skp1's CTR and thus serve as a Skp1 exchange factor. This activity will be modified for Gly-Skp1. With a K_d almost an order of magnitude greater than that of Skp1, the monomer is already more abundant. Despite this, Gat1 is still expected to drive monomerization **(Fig 3.6B)**. Gat1 additionally binds two Gly-Skp1 subunits which may have subtle contributions on the availability of Skp1 for binding FBPs which is the premier functional role of Skp1. There may be an affinity hierarchy of FBPs, each with distinct F-box sequences, for the single Skp1 which is thought to be in limiting. Subtle changes in availability should therefore have differential effects on the formation of FBP-Skp1 complexes *in vivo*.

Gat1 may act to complement or buffer the action of PhyA through non-enzymatic means **(Fig 3.7C)**. Homodimerization competes with the availability of monomers to form functional 1:1 FBP-Skp1 subcomplexes [33]. Under normoxic conditions, PhyA will efficiently hydroxylate Skp1 allowing for its glycosylation. Upon glycosylation, the Skp1 homodimer will substantially weaken to free more Skp1 for incorporation into the SCF complex [35]. Under these conditions, Gat1 may tune Skp1 availability itself through dual binding events on the Gat1 homodimer. Under hypoxic conditions, however, PhyA will not as efficiently hydroxylate Skp1 resulting in a

reduction in glycosylation. Unmodified Skp1 forms a tight homodimer that can effectively compete with FBP binding [35]. Under these conditions, Gat1 will be able to effectively access the Skp1 homodimer and act as an exchange factor to promote the formation of monomeric Skp1. This monomeric Skp1 will then be available for FBP binding allowing for sufficient SCF activity even under low oxygen conditions. This mirrors the previously proposed role for *Dictyostelium* AgtA to act as a buffer for Skp1 via a sequestration mechanism [49]. It must be considered that the balance is distinct given the considerably higher K_d (~2 μM) for the *Dictyostelium* Skp1 homodimer. Through apparent adaptations of their substrate binding activities, these two terminal yet unrelated GTs have evolved similar new secondary roles that regulate the activities of their Skp1 substrates. This posits the potential for convergent evolution of Skp1's terminal GTs to tune the sequestration of its Skp1 substrate through non-enzymatic means.

FUNDING

This research was supported by research grants to CMW from the NIH (1R01AI169849) and the Human Frontiers in Science Program (RGP0051/2021).

FIGURE LEGENDS

Figure 3.1 Gat1's Role in Skp1 Glycosylation and Evidence for Gat1:Skp1 Interactions. (A) Comparison of oxygen dependent glycosylation pathways in *Toxoplasma* and *Dictyostelium*. Modifications and utilized enzyme activities are indicated. **(B)** A domain diagram of Skp1 indicates the N-terminal disordered region (red), folded BTB domain (green), a disordered internal loop (orange), and a conditionally disordered/ordered C-terminal Region (purple). The positions of secondary structural elements are indicated. Helixes 5, 6, and 7 constitute Skp1's F-Box binding

Subsite-1 while helix 8 represents Skp1's variable F-box binding Subsite-2. Skp1 hydroxylation and glycosylation occur at the N-terminus of helix 8 which is expected to favor a disorder to order transition. This disrupts Skp1's fuzzy homodimer Subsite-B which complements Skp1's ordered homodimer Subsite-A. This is expected to favor FBP binding through both weakening a competing interaction while stabilizing conformations favorable to FBP complex formation. These interactions occur distally from binding of other Skp1 binding partners such as Cul1 and possibly Sgt1. Gat1's core hydrophobic interface is expected to leverage contacts overlapping with the Skp1 homodimer interface, Skp1-FBP interface, and Skp1-Cul1 interface. **(C)** A domain diagram of Gat1 indicates sequence components that are part of the catalytic GT-A fold or comprise a disordered internal loop. **(D)** Co-IP pull down experiments indicate stable binding of Gat1 *in vivo*. This data was previously published in [20]. Additionally, levels of Gat1 pulled down in Co-Ips are comparable to those of known FBPs. **(E)** c(s) distributions demonstrate the sedimentation profiles of 5 μM Skp1 (green), 5 μM Gat1 (brown), 5 μM Gat1 with 5 μM Skp1 (blue), and 5 μM Gat1 with 2.5 μM Skp1 (purple). Dashed lines represent the expected sedimentation of the Skp1 monomer (orange), Skp1 dimer (hot pink), Gat1 dimer in the absence of Skp1 (green), and 2:1 Gat1:Skp1 complex (black).

Figure 3.2 Sedimentation Velocity Analysis of the Gat1:Skp1 Complex. Plots showing the average S_w position for the Gat1-homodimer and Gat1:Skp1 complex peaks when 500 nM Skp1 **(A)**, Gly-Skp1 **(C)** or Skp1ΔCTR **(E)** are titrated with Gat1. The decreasing concentrations of Gat1 left to right represent increasing ratios of Skp1 to Gat1. S_w positions were fit to a sigmoidal curve and the upper asymptote was analyzed. The positions of the Gat1 homodimer (orange), 2:1 Gat1:Skp1 complex (blue), and 2:2 Gat1:Skp1 complex (green) are shown by dashed lines. The

weighted sums of S_w positions for the Skp1 monomer, Skp1 homodimer, Gat1 monomer, Gat1 homodimer, and Gat1:Skp1 complexes were plotted in Sephat and the apparent affinity of each interaction was modeled with Skp1 **(B)**, Gly-Skp1 **(D)**, and Skp1ΔCTR **(F)**. Isotherms where the Skp1 (purple) or Gat1 (blue) concentration was varied are shown. Apparent affinities for each relevant interaction were modeled and are depicted in interaction diagrams.

Figure 3.3 Computational Modeling of the Gat1:Skp1 Complex. (A) General structure of the Gat1-Skp1 complex as predicted by AlphaFold3. Skp1 (green), Gat1 Subunit 1 (blue), and Gat1 Subunit 2 (orange) are shown with the location of each active site circled in yellow. **(B)** Predicted Alignment Error (PAE) matrix for the AlphaFold3 generated Gat1-Skp1 complex. The position of each complex subunit and intrinsically disordered regions (high error scores) are shown. **(C)** Average predicted Local Distance Difference Test (pLDDT) scores for the Gat1-Skp1 complex are shown and colored by confidence. **(D)** Distance variability matrix for the group of simulations where a folded Skp1 CTR was used to start MD simulations. Cα distances are colored by the average of their standard deviations across all five simulations. **(E)** Same as **(E)** except that a disordered Skp1 CTR initiated the MD simulations. **(F-H)** Calculated TASD50 scores (Trimmed Average/Mean of the Standard Deviation utilizing 50% of the data) for each residue in Gat1 Subunit 1 **(F)**, Gat1 Subunit 2 **(G)**, and Skp1 **(H)**. The 2 Å variability cutoff for "disordered" segments is highlighted green. Values for simulations initiated with a folded (red) or a disordered (blue) CTR are shown with shading representing the standard error of the mean.

Figure 3.4 Energetic and Mutational Analysis of the Gat1:Skp1 Complex. (A) MMGBSA predicted binding energies toward Gat1 for residues in Skp1. Values for simulations starting with

a folded (red) or a disordered (blue) CTR are shown with shading representing the standard error of the mean. **(B)** Same as in **(A)** except for predicted binding energies toward Skp1 for residues in Gat1. **(C)** Predicted change in binding energy for amino acid substitutions made for significant Gat1 residues in simulations where a folded Skp1 CTR was used for starting structures. **(D)** Same as **(C)** except using simulations for which a disordered CTR was used. **(E)** Predicted changes in protein stability for mutations made against residues in Gat1. **(F-H)** PAE matrices for a 2:1 Gat1:Skp1 complex where the Gat1(Y18K) **(F)**, Gat1(A51K) **(G)**, and Gat1(Y18K/A51K) **(H)** variants are examined.

Figure 3.5 Examples of Interactions in the Gat1:Skp1 Complex. (A) A frequently occurring structure of the Gat1:Skp1 complex in Simulation 5. Subunits are colored as in **(Fig 3.3A)**, with Skp1 in green and the Gat1 subunits in blue and orange. Yellow boxes highlight regions shown in panels **(B-D)**. **(B, C)** Electrostatic interaction networks involving the Skp1 CTR. Protein backbones are shown as ribbons with Gat1 colored hot pink and Skp1 colored blue, and Skp1 residue labels are blue while Gat1 residue labels are orange. Residues from Gat1 Subunit 1 are denoted by "-A" and "-B" for Subunit 2. **(D)** A structure of the core hydrophobic interface from Simulation 3. The protein backbones are shown as ribbons with Skp1 being green and Gat1 being grey. Only consistently important (<-1 kCal/mol contribution in both simulation groups) are shown. Residues are colored by interaction energies predicted by MMGBSA in the Disordered CTR group of simulations. **(E, G)** Frequently occurring structures of the Gat1:Skp1 complex from Simulations 2 and 1 respectively. **(F, H)** Zoom-in views of electrostatic interaction networks from Simulations 2 and 1, respectively, with labels and colors as in **(B)**. **(Figure 3.S18)** documents that these examples occur at high frequency in most of the simulations.

Figure 3.6 Dissociative Effects of Gat1 on Skp1 Variants. (A) c(s) distributions for 500 nM Skp1 (blue) and 500 nM Skp1 + 20 nM Gat1 (orange). Predicted s-values for the Skp1 monomer and dimer species are shown as vertical dashed lines. **(B)** Same as in **(A)** using 500 nM Gly-Skp1 and 500 nM Gly-Skp1 + 40 nM Gat1. **(C)** Series of c(s) distributions for various concentrations of a 1:10 ratio of Gat1:Skp1ΔCTR used to generate the isotherm in **(D)**. The integration range used for the monomer and dimer species is shown with a red line. The region associated with the Gat1:Skp1 complex is shown with a purple line. **(D)** Isotherm showing the apparent homodimer affinity for Skp1ΔCTR not bound by Gat1 in the presence of a 1:10 ratio of Gat1:Skp1ΔCTR.

Figure 3.7 The Non-Enzymatic Role of Gat1 in Binding Skp1. (A) Model for the 2:1 Gat1:Skp1 complex. The Skp1 homodimer forms a two-component interface composed of a core Subsite-A and a fuzzy Subsite-B. These two interfaces exchange with similar interactions occurring in the 2:1 Gat1:Skp1 complex. A second binding event with the other Gat1 subunit is inhibited by excluded volume and competitive binding effects with the intrinsically disordered Skp1 CTR. **(B)** Model for the 2:2 Gat1: Gly-Skp1 complex. Glycosylation promotes a disorder to order transition in Skp1's CTR reducing the fuzzy interactions. The lack of fuzzy interactions between Skp1 and Gat1 allows for symmetrical binding of a second Gly-Skp1 to the other Gat1 subunit. Additionally, the Skp1 homodimer, weakened by the loss of Subsite-B, is no longer able to effectively compete with the Gat1:Skp1 complex for free Skp1. **(C)** Model for Gat1's role as a Skp1 exchange factor. PhyA acts in the presence of high oxygen to glycosylate Skp1 and weaken Skp1 homodimerization by disrupting Subsite-B. This allows for free Skp1 to be readily engaged with FBPs under high oxygen conditions. Under low oxygen conditions, Gat1 acts as an exchange factor allowing for the

formation of monomeric Skp1. This allows for the generation of a free Skp1 monomer pool even in the absence of glycosylation. This acts to partially rescue the activity of the SCF complex by offering an alternative mechanism for Skp1 incorporation.

SUPPLEMENTAL FIGURE LEGENDS

Figure 3.S1 Residuals and c(s) Distributions for Gat1:Skp1 Association Experiments. c(s) distributions and associated sedimentation data used in modeling the Association of Gat1 and Skp1.

Figure 3.S2 Residuals and c(s) Distributions for Gat1:Gly-Skp1 Association Experiments. c(s) distributions and associated sedimentation data used in modeling the association of Gat1 and Gly-Skp1.

Figure 3.S3 Residuals and c(s) Distributions for Gat1:Skp1ΔCTR Association Experiments. c(s) distributions and associated sedimentation data used in modeling the association of Gat1 and Skp1ΔCTR.

Figure 3.S4 Overlay of Distributions Utilized for Isotherms in Figure 3.2. Overlay of c(s) distributions used in modeling the association of Gat1 and Skp1 variant isotherms. The Skp1 and Complex peaks were separately integrated, normalized by extinction coefficients, and plotted into a c(s) isotherm. The integration of each complex peak with a constant Skp1 concentration was used in modeling the stoichiometry of each complex.

Figure 3.S5 Alignment of TgGat1-TgSkp1 AlphaFold3 with the PuGat1 Crystal Structure. Overlay of the top scoring 2:1 Gat1:Skp1 complex backbone trace from AlphaFold3 with that of the PuGat1 crystal structure (PDB: 6MW8).

Figure 3.S6 pLDDT Scores for the 2:1 Gat1:Skp1 Complex. Average per residue pLDDT score for each AlphaFold3 model for the 2:1 Gat1:Skp1 complex. These scores were averaged across all 5 structures generated by AlphaFold3 and plotted onto the top scoring model.

Figure 3.S7 Competition Assay Showing Mutually Exclusive binding of Ether Fbs1 or Gat1 to Skp1. (A) Competition assays between Gat1 and Fbs1 for limiting Skp1 concentrations. Mixtures containing (Gat1; Fbs1; Skp1, Gat1; Skp1, Fbs1; Skp1, Gat1, Fbs1; and Skp1) were run over an S200 size exclusion column and fractionated. **(B)** Fractions were run on Western Blots or CBB Gels, and **(C)** densitometry was used to observe the elution profiles of Gat1 and Fbs1. Both Fbs1 and Gat1 showed an earlier elution profile in the presence of Skp1. When Gat1 and Fbs1 are mixed with limiting Skp1, Fbs1 shows an elution profile matching that of when Fbs1 is mixed with Skp1 alone. In the same condition, Gat1's elution profile matches that of Gat1 in the absence of Skp1. This supports a conclusion where Gat1 is excluded from a complex with Skp1 in the presence of Fbs1 in line with a competitive binding model.

Figure 3.S8 Inhibition of PhyA in the Presence of Varying Concentrations of Gat1. (A) PhyA inhibition assays were conducted according to the following framework. Premade mixtures of Skp1 with any inhibitor (Gat1, PCA, Folate) were mixed with PhyA to start the reaction giving a final Skp1 concentration of 100 nM. Separate reaction setups were made for T0 containing SDS to confirm the absence of activity in the SDS quenching buffer. Reactions were quenched at different timepoints with SDS. Quenched reactions were western blotted, densitometry readings were obtained, and densitometry was normalized to a control reaction on the same gel. **(B)** Varying ratios of hydroxylated and unmodified Skp1 at 100 nM were run on a western blot and the observed densitometry was plotted onto a calibration curve shown in **(C)**. **(D)** Percent hydroxylation for

reactions quenched at 23 min were plotted to show the effect of Gat1 on Skp1's hydroxylation efficiency. **(E)** Gels used to calculate hydroxylation efficiency under each condition.

Figure 3.S9 Overlay of an AlphaFold2 Structure of a 2:1 Gat1:Skp1 complex with a Glycan Docked PuGat1 homodimer Structure. Overlay of a 2:1 Gat1:Skp1 complex generated by AlphaFold2 with the PuGat1 crystal structure with a docked tetrasaccharide as reported by [45]. Skp1's CTR is positioned in such a way as to allow its tetrasaccharide to bind into the active site of Gat1. Skp1 is shown as green with Pro154 of Skp1 shown in red. *Pythium ultimum* Gat1 Subunit1 is shown as blue with its Gat1 Subunit2 shown in orange. The tetrasaccharide docks into the active site of the opposite dimer subunit allowing for the addition of the terminal Gal moiety of the Skp1 pentasaccharide.

Figure 3.S10 Per-Residue MMGBSA Scores with a Folded Skp1-CTR. MMGBSA scores for each residue from the Gat1:Skp1 complex. Scores for Gat1 are the sum of energetic contributions from each homodimer subunit. Skp1's disordered N-terminus, and the disordered internal loops of both Skp1 and Gat1 are highlighted. Subsites A and B of the Skp1 homodimer are indicated. Coloring of the predicted energetic contributions and standard error of the mean across all 5 simulations are as indicated.

Figure 3.S11 Per-Residue MMGBSA Scores with a Disordered Skp1-CTR. MMGBSA scores for each residue from the Gat1:Skp1 complex. Scores for Gat1 are the sum of energetic contributions from each homodimer subunit. Skp1's disordered N-terminus, and the disordered internal loops of both Skp1 and Gat1 are highlighted. Subsites A and B of the Skp1 homodimer are indicated. Coloring of the predicted energetic contributions and standard error of the mean across all 5 simulations are as indicated.

Figure 3.S12 Predicted Change in Binding Energy for Each Cluster with a Folded Skp1 CTR. Predicted complex ΔΔG for each point mutation in each cluster are indicated. The weighted average of the lowest 3 scoring clusters was used as the final predicted ΔΔG for each point mutation.

Figure 3.S13 Predicted Change in Binding Energy for Each Cluster with a Disordered Skp1 CTR. Predicted complex ΔΔG for each point mutation in each cluster are indicated. The weighted average of the lowest 3 scoring clusters was used as the final predicted ΔΔG for each point mutation.

Figure 3.S14 Predicted Change in Stability for Each Cluster with a Gat1 Homodimer. Predicted Gat1 ΔΔG for each point mutation in each cluster are indicated. The weighted average of the lowest 3 scoring clusters was used as the final predicted ΔΔG for each point mutation.

Figure 3.S15 pLDDT Scores for the 2:1 Gat1(Y18K):Skp1 Complex. Average per-residue pLDDT score for each AlphaFold3 model for the 2:1 Gat1(Y18K):Skp1 complex. These scores were averaged across all 5 structures generated by AlphaFold3 and plotted onto the top scoring model.

Figure 3.S16 pLDDT Scores for the 2:1 Gat1(A51K):Skp1 Complex. Average per-residue pLDDT score for each AlphaFold3 model for the 2:1 Gat1(A51K):Skp1 complex. These scores were averaged across all 5 structures generated by AlphaFold3 and plotted onto the top scoring model.

Figure 3.S17 pLDDT Scores for the 2:1 Gat1(Y18K/A51K):Skp1 Complex. Average per-residue pLDDT score for each AlphaFold3 model for the 2:1 Gat1(Y18K/A51K):Skp1 complex. These scores were averaged across all 5 structures generated by AlphaFold3 and plotted onto the top scoring model.

Figure 3.S18 Distances Between Oppositely Charged Residues Between Skp1 and Gat1. Distances between oppositely charged residues with pairwise interaction energies ≤ -1 kcal/mol are shown. A total of 146 such interactions were observed across all 10 simulations. Productively contributing distances between charged functional groups (<8 Å) are highlighted.

Figure 3.S19 Residuals and c(s) Distributions for Skp1ΔCTR Homodimerization with Gat1. c(s) distributions and associated sedimentation data used in modeling the apparent affinity of the Skp1ΔCTR homodimer with a 1:10 ratio of Gat1:Skp1 present.

Figure 3.1

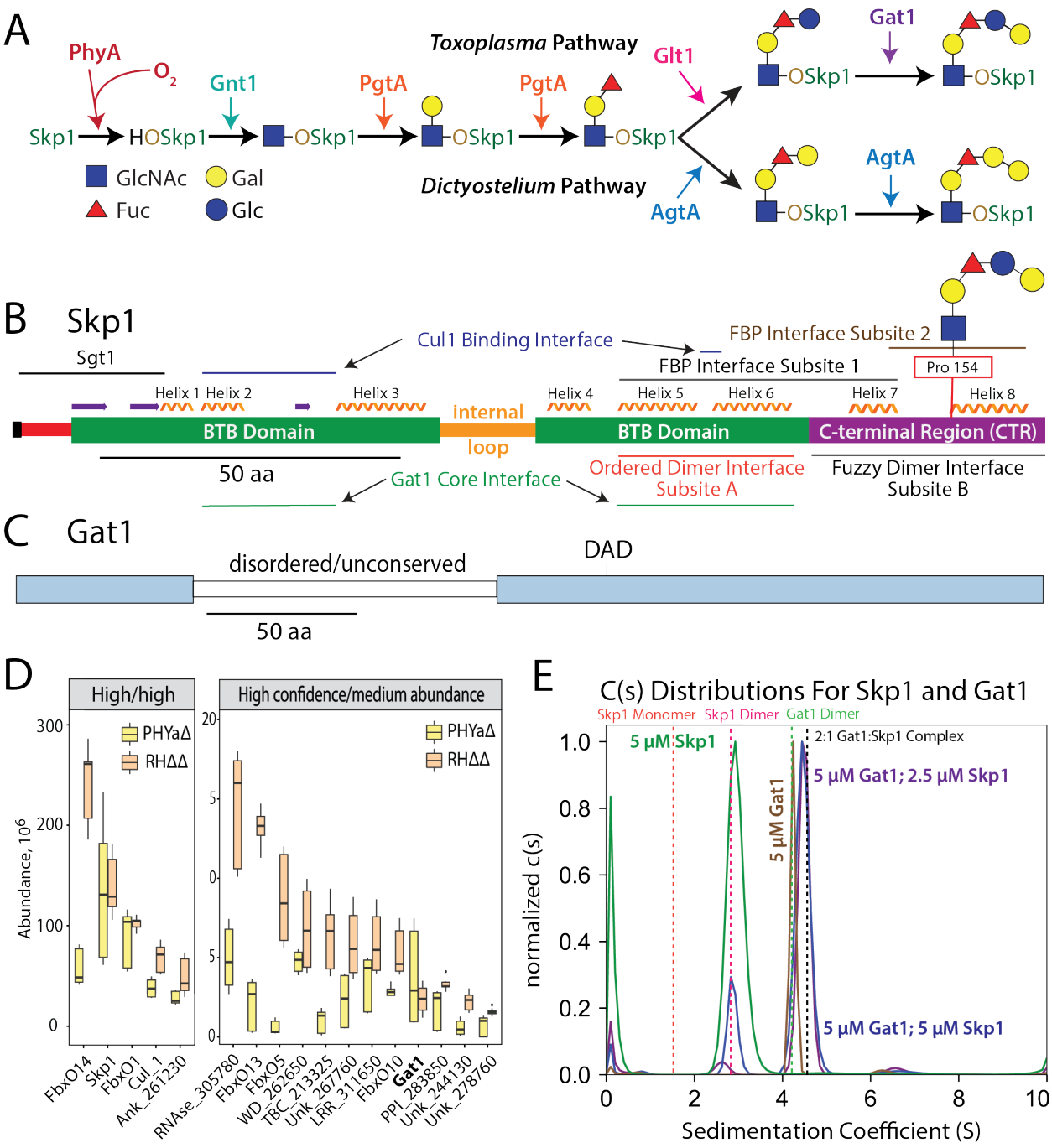

A
PhyA
O2
Gnt1
PgtA
PgtA
Glt1
Gat1
AgtA
AgtA
Skp1
HOSkp1
OSkp1
OSkp1
OSkp1
OSkp1
OSkp1
OSkp1
Toxoplasma Pathway
Dictyostelium Pathway
GlcNAc
Gal
Fuc
Glc
B Skp1
Sgt1
Cul1 Binding Interface
FBP Interface Subsite 2
FBP Interface Subsite 1
Pro 154
Helix 1
Helix 2
Helix 3
Helix 4
Helix 5
Helix 6
Helix 7
Helix 8
BTB Domain
internal loop
BTB Domain
C-terminal Region (CTR)
50 aa
Gat1 Core Interface
Ordered Dimer Interface Subsite A
Fuzzy Dimer Interface Subsite B
C Gat1
disordered/unconserved
DAD
50 aa
D
High/high
High confidence/medium abundance
PHYaΔ
RHΔΔ
Abundance, 10^6
300
200
100
0
20
5
0
5
0
FbxO14
Skp1
FbxO1
Cul_1
Ank_261230
RNAse_305780
FbxO13
FbxO5
WD_262650
TBC_213325
Unk_267760
LRR_311650
FbxO10
Gat1
PPI_283850
Unk_244130
Unk_278760
E
C(s) Distributions For Skp1 and Gat1
Skp1 Monomer
Skp1 Dimer
Gat1 Dimer
5 μM Skp1
2:1 Gat1:Skp1 Complex
5 μM Gat1; 2.5 μM Skp1
5 μM Gat1
5 μM Gat1; 5 μM Skp1
normalized c(s)
1.0
0.8
0.6
0.4
0.2
0.0
0
2
4
6
8
10
Sedimentation Coefficient (S)

Figure 3.2

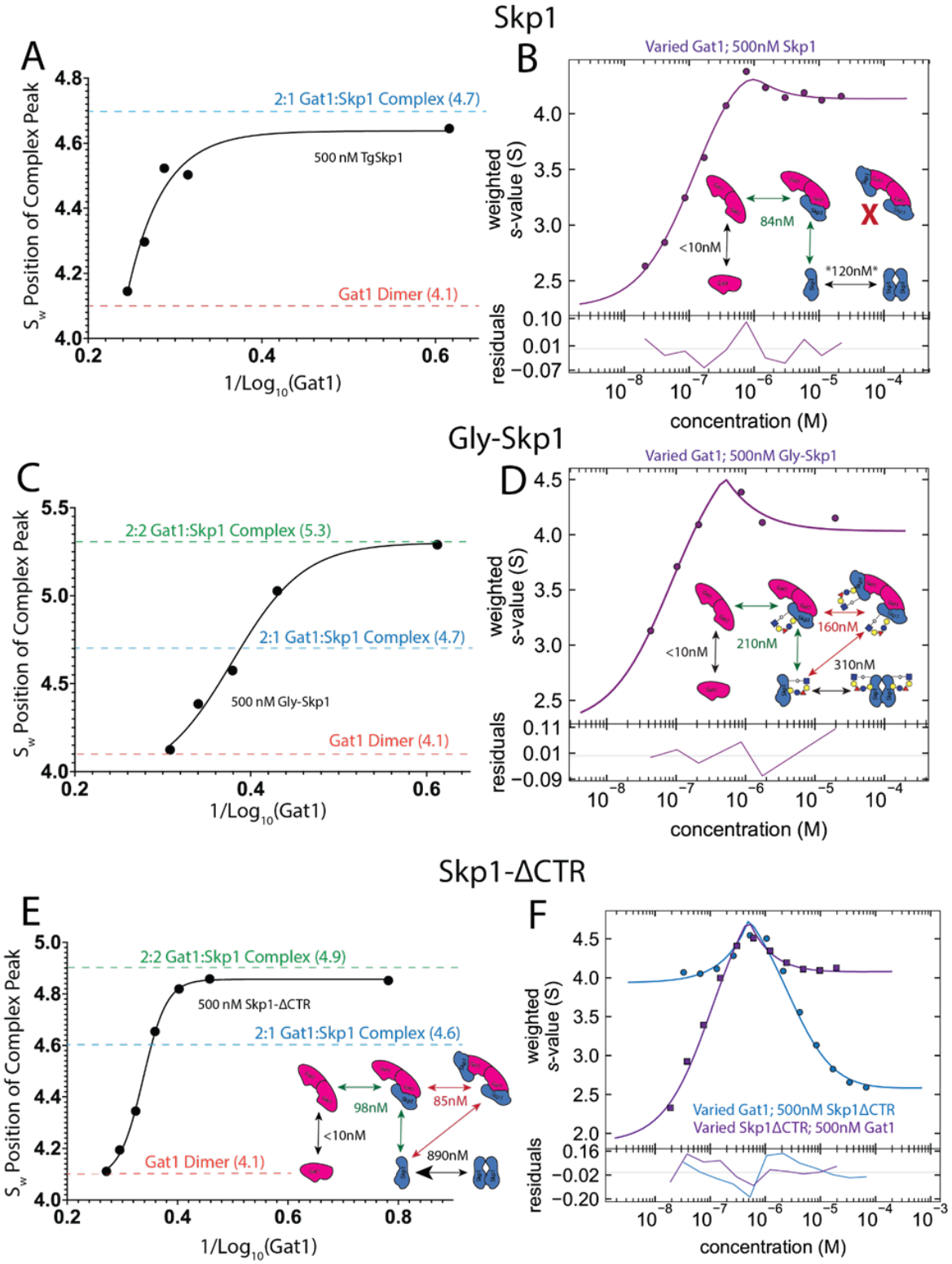

Skp1
A
B
Varied Gat1; 500nM Skp1
2:1 Gat1:Skp1 Complex (4.7)
500 nM TgSkp1
Gat1 Dimer (4.1)
S_w Position of Complex Peak
1/Log10(Gat1)
weighted s-value (S)
residuals
84nM
<10nM
120nM
concentration (M)
Gly-Skp1
C
D
Varied Gat1; 500nM Gly-Skp1
2:2 Gat1:Skp1 Complex (5.3)
2:1 Gat1:Skp1 Complex (4.7)
500 nM Gly-Skp1
Gat1 Dimer (4.1)
210nM
160nM
310nM
Skp1-ΔCTR
E
F
2:2 Gat1:Skp1 Complex (4.9)
500 nM Skp1-ΔCTR
2:1 Gat1:Skp1 Complex (4.6)
98nM
85nM
890nM
Varied Gat1; 500nM Skp1ΔCTR
Varied Skp1ΔCTR; 500nM Gat1

Figure 3.3

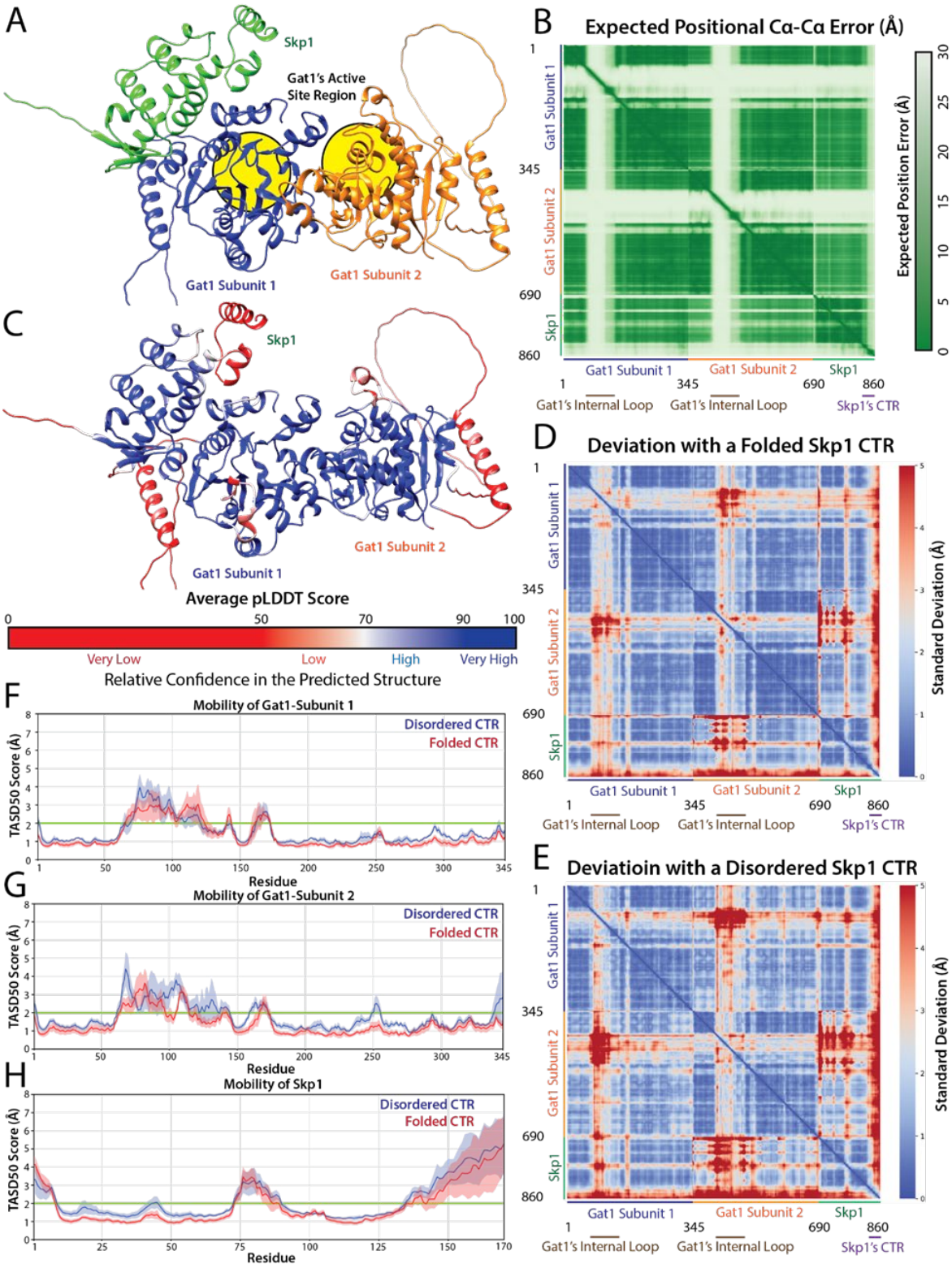

A
Skp1
Gat1's Active Site Region
Gat1 Subunit 1
Gat1 Subunit 2
B
Expected Positional Cα-Cα Error (Å)
Gat1 Subunit 1
Gat1 Subunit 2
Skp1
Expected Position Error (Å)
Gat1's Internal Loop
Gat1's Internal Loop
Skp1's CTR
C
Skp1
Gat1 Subunit 2
Gat1 Subunit 1
Average pLDDT Score
Very Low
Low
High
Very High
D
Deviation with a Folded Skp1 CTR
Standard Deviation (Å)
E
Deviatioin with a Disordered Skp1 CTR
Relative Confidence in the Predicted Structure
F
Mobility of Gat1-Subunit 1
Disordered CTR
Folded CTR
TASD50 Score (Å)
Residue
G
Mobility of Gat1-Subunit 2
H
Mobility of Skp1

Figure 3.4

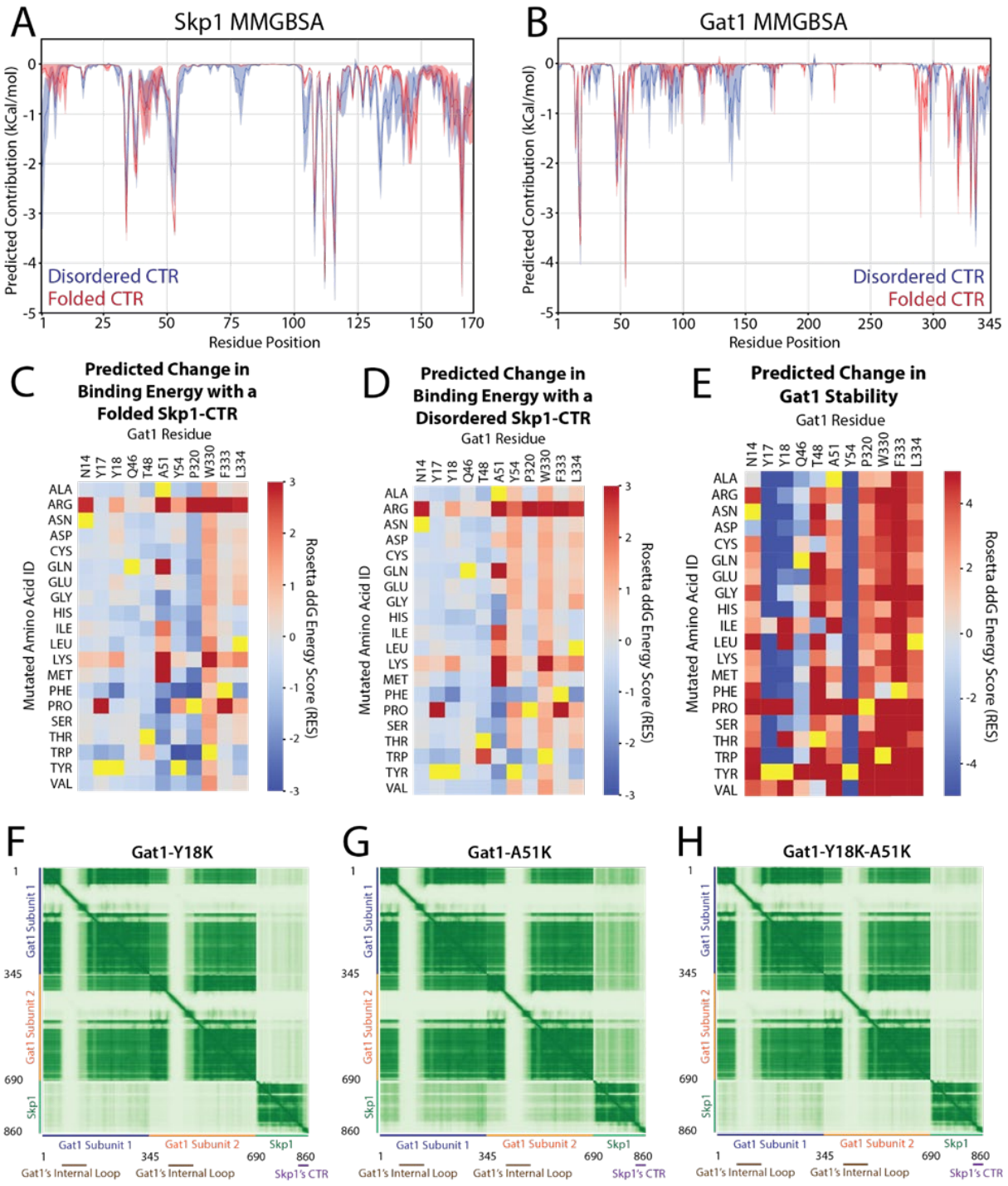

A
Skp1 MMGBSA
Predicted Contribution (kCal/mol)
Residue Position
Disordered CTR
Folded CTR
B
Gat1 MMGBSA
Predicted Contribution (kCal/mol)
Residue Position
Disordered CTR
Folded CTR
C
Predicted Change in Binding Energy with a Folded Skp1-CTR
Gat1 Residue
Mutated Amino Acid ID
Rosetta ddG Energy Score (RES)
D
Predicted Change in Binding Energy with a Disordered Skp1-CTR
Gat1 Residue
Mutated Amino Acid ID
Rosetta ddG Energy Score (RES)
E
Predicted Change in Gat1 Stability
Gat1 Residue
Mutated Amino Acid ID
Rosetta ddG Energy Score (RES)
F
Gat1-Y18K
G
Gat1-A51K
H
Gat1-Y18K-A51K
Gat1 Subunit 1
Gat1 Subunit 2
Skp1
Gat1's Internal Loop
Gat1's Internal Loop
Skp1's CTR

Figure 3.5

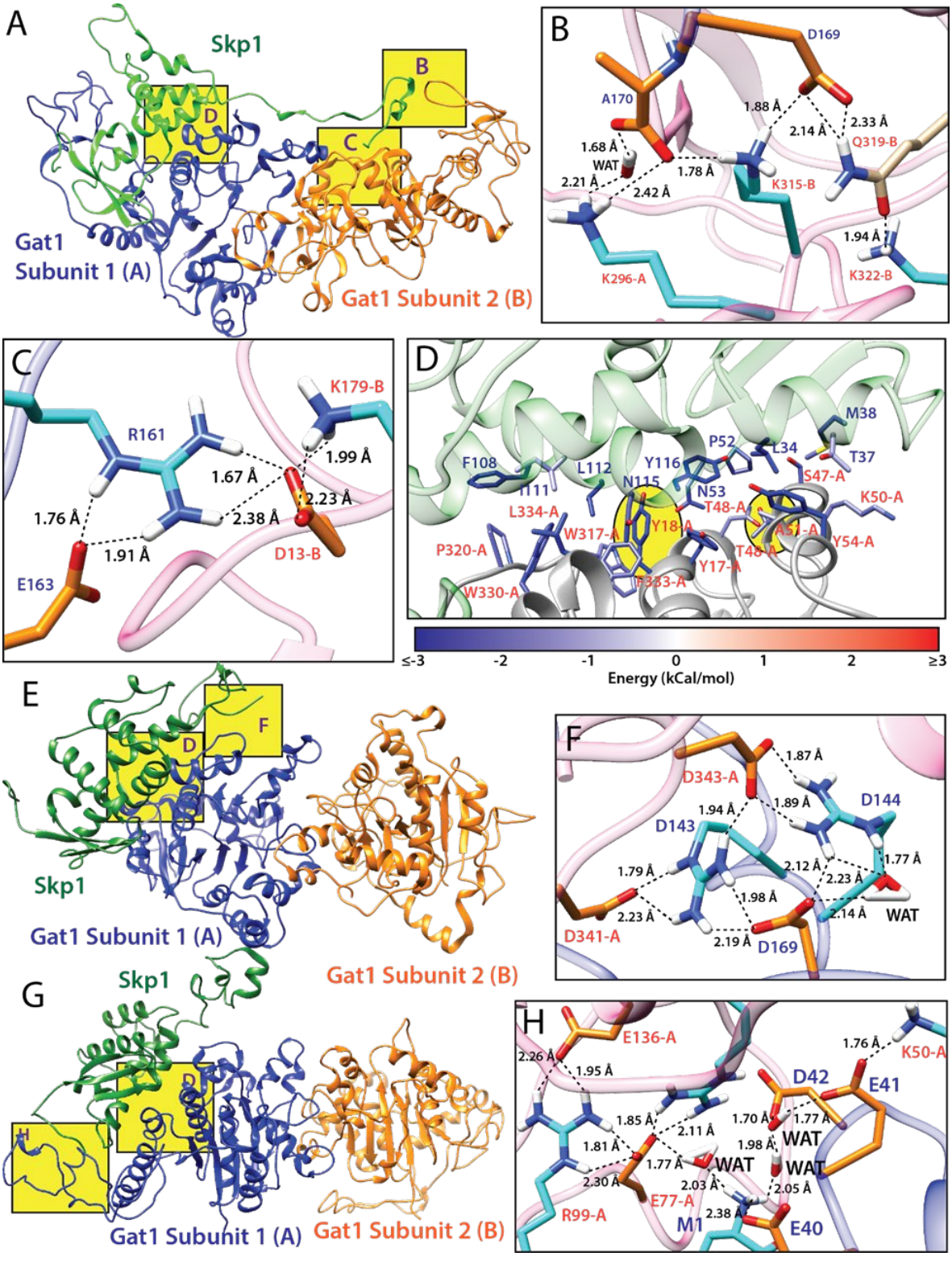

A
Skp1
B
D
C
Gat1
Subunit 1 (A)
Gat1 Subunit 2 (B)
B
D169
A170
1.88 Å
2.14 Å
2.33 Å
Q319-B
1.68 Å
WAT
2.21 Å
2.42 Å
1.78 Å
K315-B
1.94 Å
K296-A
K322-B
C
K179-B
R161
1.99 Å
1.67 Å
2.23 Å
1.76 Å
2.38 Å
1.91 Å
D13-B
E163
D
M38
P52
L34
T37
F108
L112
Y116
S47-A
I111
N115
N53
K50-A
T48-A
L334-A
W317-A
Y18-A
A51-A
Y54-A
P320-A
T48-A
Y17-A
W330-A
F333-A
≤-3
-2
-1
0
1
2
≥3
Energy (kCal/mol)
E
F
D
Skp1
Gat1 Subunit 1 (A)
Gat1 Subunit 2 (B)
F
1.87 Å
D343-A
1.89 Å
D144
1.94 Å
D143
1.79 Å
2.12 Å
1.77 Å
2.23 Å
1.98 Å
2.23 Å
2.14 Å
WAT
D341-A
2.19 Å
D169
G
Skp1
H
Gat1 Subunit 1 (A)
Gat1 Subunit 2 (B)
H
E136-A
2.26 Å
1.95 Å
1.76 Å
K50-A
D42
E41
1.85 Å
2.11 Å
1.70 Å
1.77 Å
1.81 Å
1.98 Å
WAT
1.77 Å
WAT
WAT
2.30 Å
2.03 Å
2.05 Å
E77-A
R99-A
2.38 Å
M1
E40

Figure 3.6

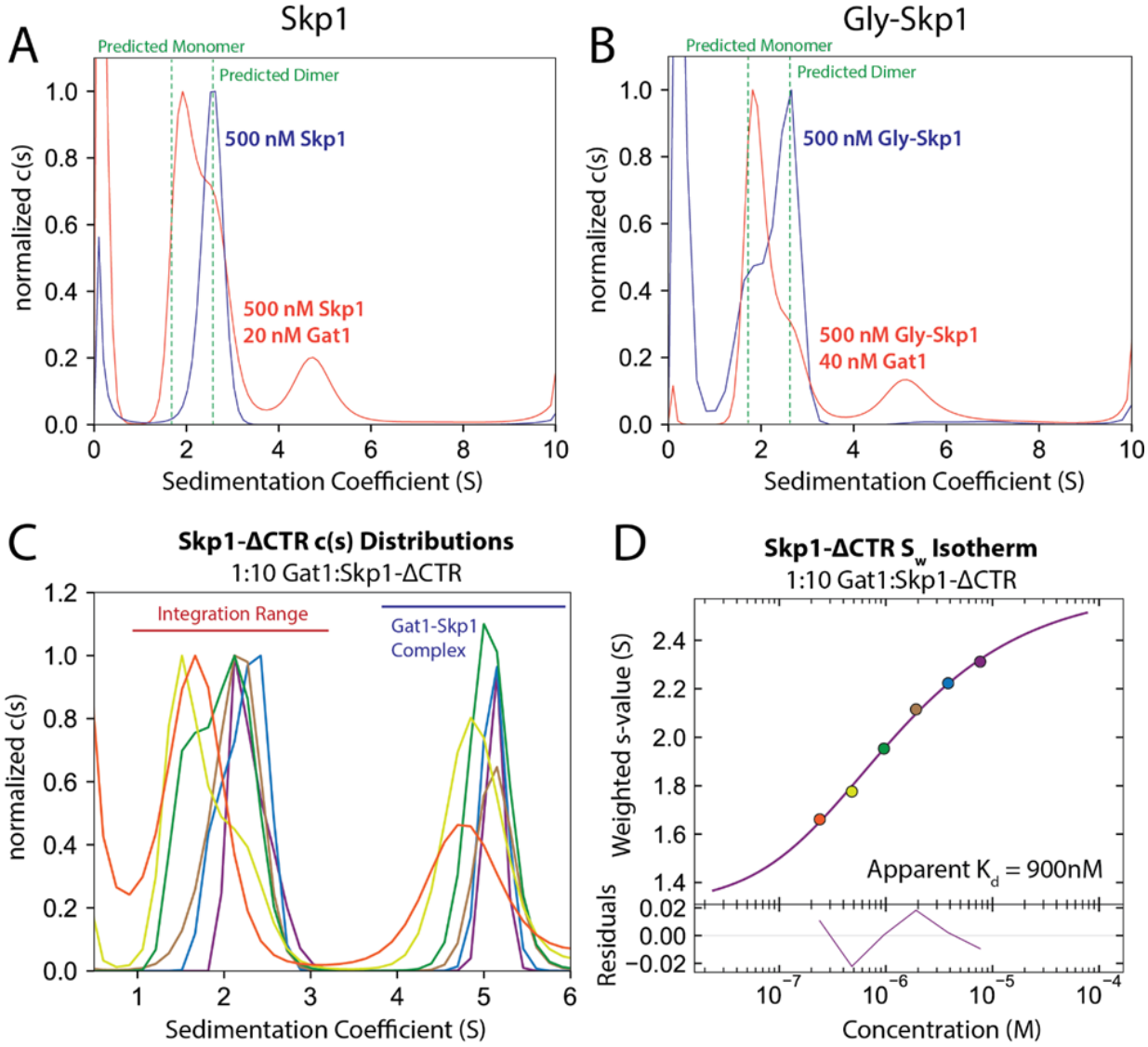

A
Skp1
Predicted Monomer
Predicted Dimer
500 nM Skp1
500 nM Skp1
20 nM Gat1
normalized c(s)
Sedimentation Coefficient (S)
B
Gly-Skp1
Predicted Monomer
Predicted Dimer
500 nM Gly-Skp1
500 nM Gly-Skp1
40 nM Gat1
normalized c(s)
Sedimentation Coefficient (S)
C
Skp1-ΔCTR c(s) Distributions
1:10 Gat1:Skp1-ΔCTR
Integration Range
Gat1-Skp1
Complex
normalized c(s)
Sedimentation Coefficient (S)
D
Skp1-ΔCTR S_w Isotherm
1:10 Gat1:Skp1-ΔCTR
Weighted s-value (S)
Apparent K_d = 900nM
Residuals
Concentration (M)

Figure 3.7

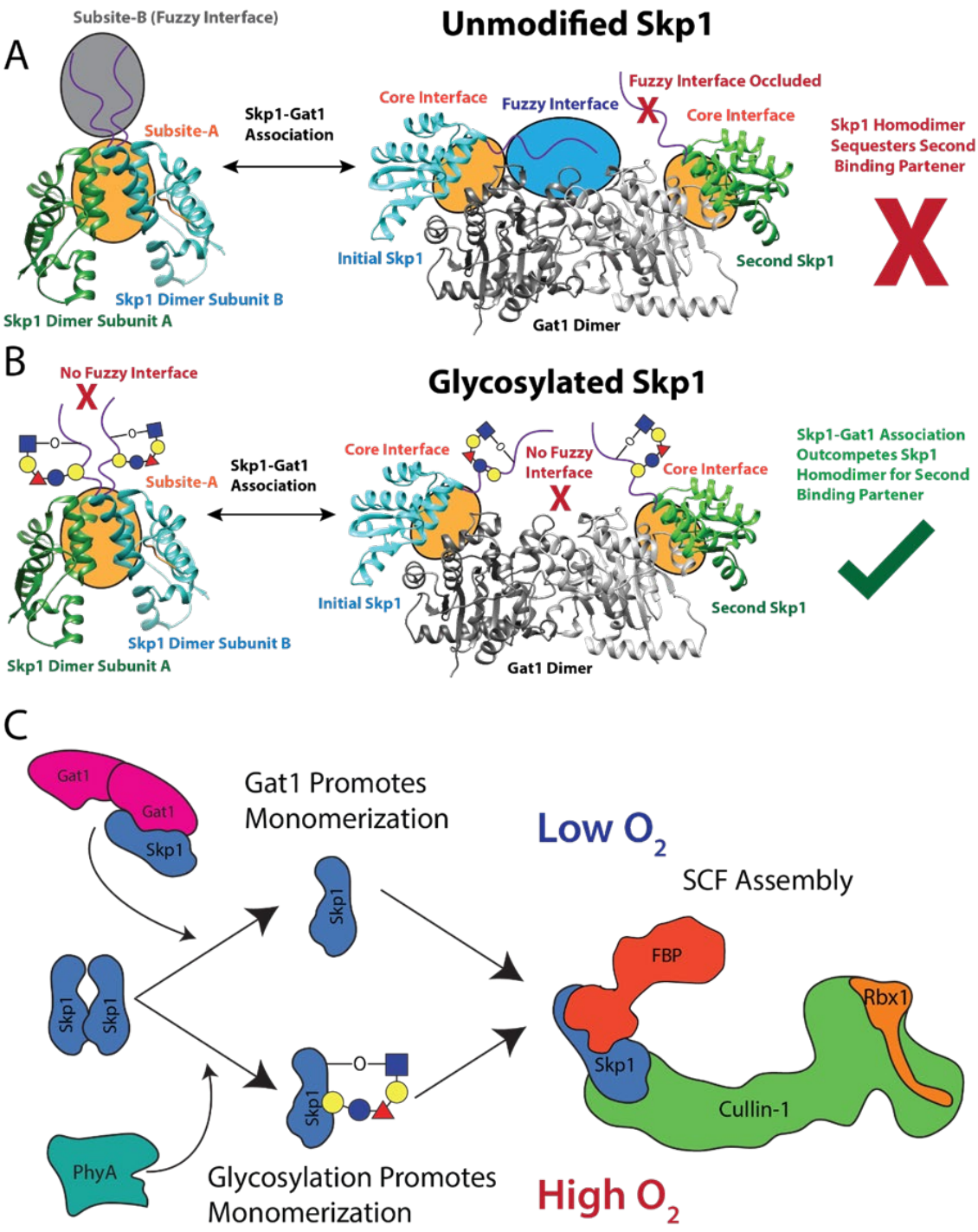
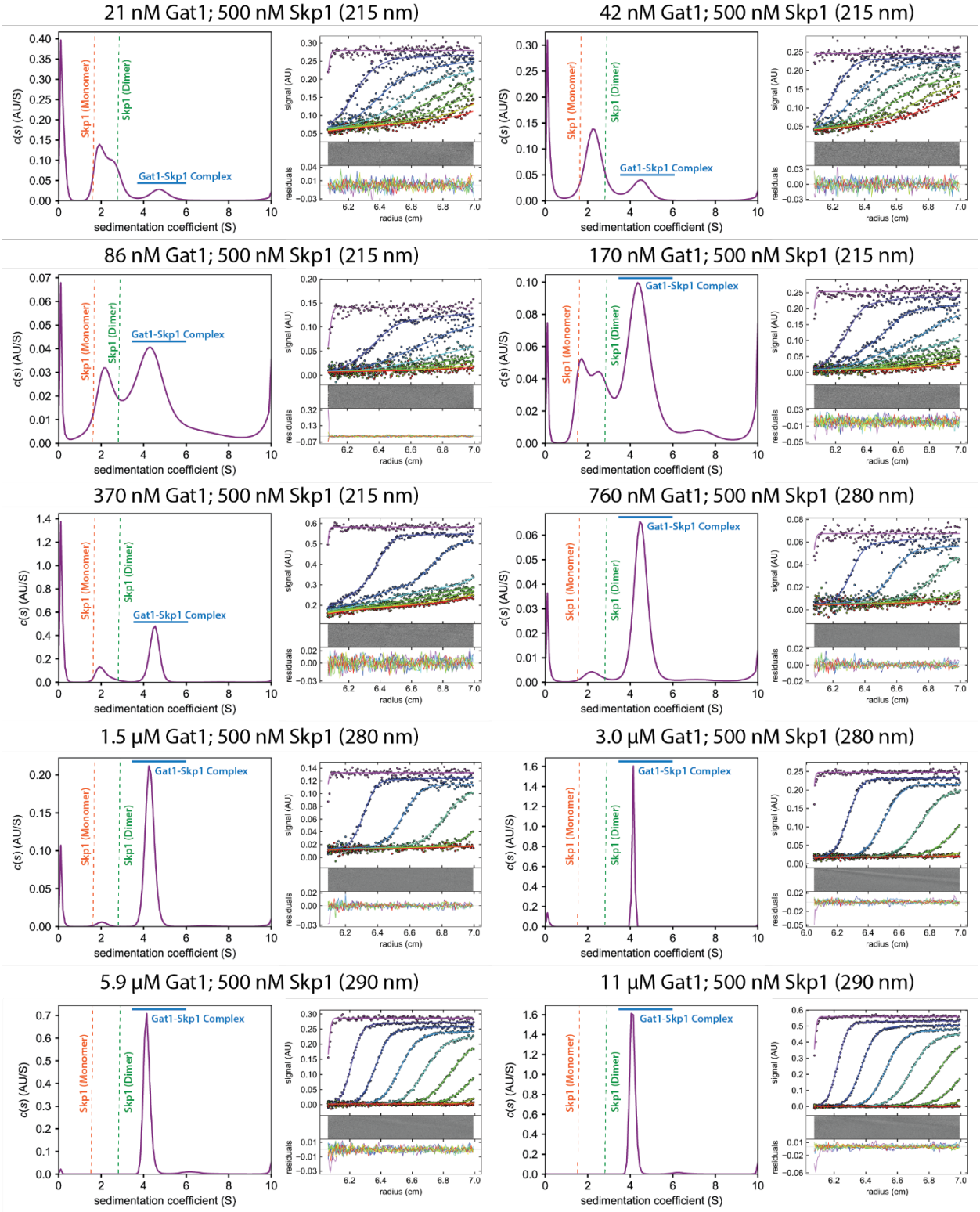

A
Subsite-B (Fuzzy Interface)
Unmodified Skp1
Subsite-A
Skp1-Gat1 Association
Core Interface
Fuzzy Interface
Fuzzy Interface Occluded
Core Interface
Skp1 Homodimer Sequesters Second Binding Partener
Initial Skp1
Second Skp1
Skp1 Dimer Subunit B
Skp1 Dimer Subunit A
Gat1 Dimer
B
No Fuzzy Interface
Glycosylated Skp1
Subsite-A
Skp1-Gat1 Association
Core Interface
No Fuzzy Interface
Core Interface
Skp1-Gat1 Association Outcompetes Skp1 Homodimer for Second Binding Partener
Initial Skp1
Second Skp1
Skp1 Dimer Subunit B
Skp1 Dimer Subunit A
Gat1 Dimer
C
Gat1
Gat1
Skp1
Gat1 Promotes Monomerization
Low O2
SCF Assembly
Skp1
Skp1
Skp1
FBP
Rbx1
Skp1
Cullin-1
PhyA
Glycosylation Promotes Monomerization
High O2

Figure 3.S1


21 nM Gat1; 500 nM Skp1 (215 nm)
42 nM Gat1; 500 nM Skp1 (215 nm)
86 nM Gat1; 500 nM Skp1 (215 nm)
170 nM Gat1; 500 nM Skp1 (215 nm)
370 nM Gat1; 500 nM Skp1 (215 nm)
760 nM Gat1; 500 nM Skp1 (280 nm)
1.5 µM Gat1; 500 nM Skp1 (280 nm)
3.0 µM Gat1; 500 nM Skp1 (280 nm)
5.9 µM Gat1; 500 nM Skp1 (290 nm)
11 µM Gat1; 500 nM Skp1 (290 nm)
Skp1 (Monomer)
Skp1 (Dimer)
Gat1-Skp1 Complex
c(s) (AU/S)
sedimentation coefficient (S)
signal (AU)
residuals
radius (cm)

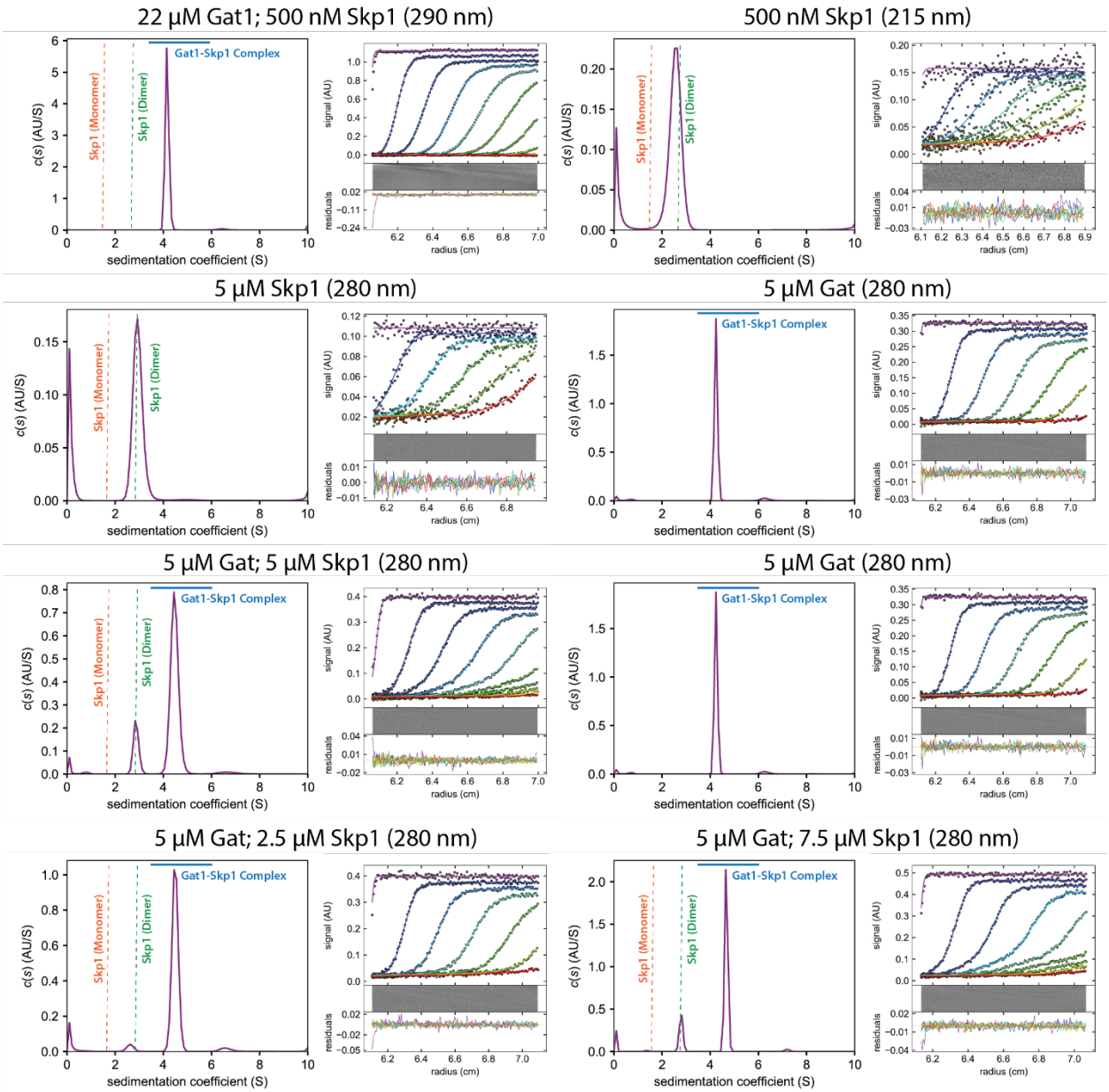

22 µM Gat1; 500 nM Skp1 (290 nm)
500 nM Skp1 (215 nm)
5 µM Skp1 (280 nm)
5 µM Gat (280 nm)
5 µM Gat; 5 µM Skp1 (280 nm)
5 µM Gat (280 nm)
5 µM Gat; 2.5 µM Skp1 (280 nm)
5 µM Gat; 7.5 µM Skp1 (280 nm)
Gat1-Skp1 Complex
Skp1 (Monomer)
Skp1 (Dimer)
c(s) (AU/S)
sedimentation coefficient (S)
signal (AU)
residuals
radius (cm)

Figure 3.S2

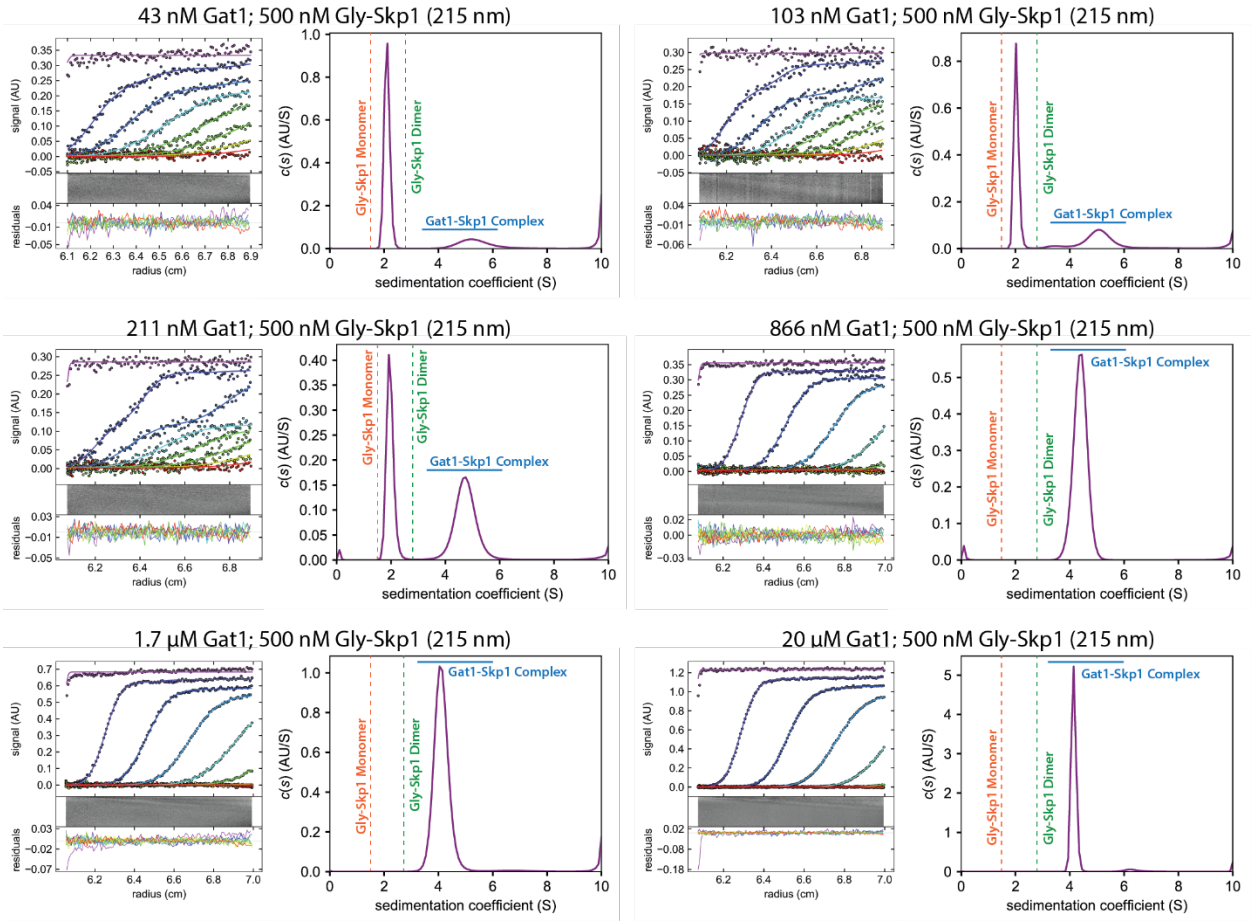
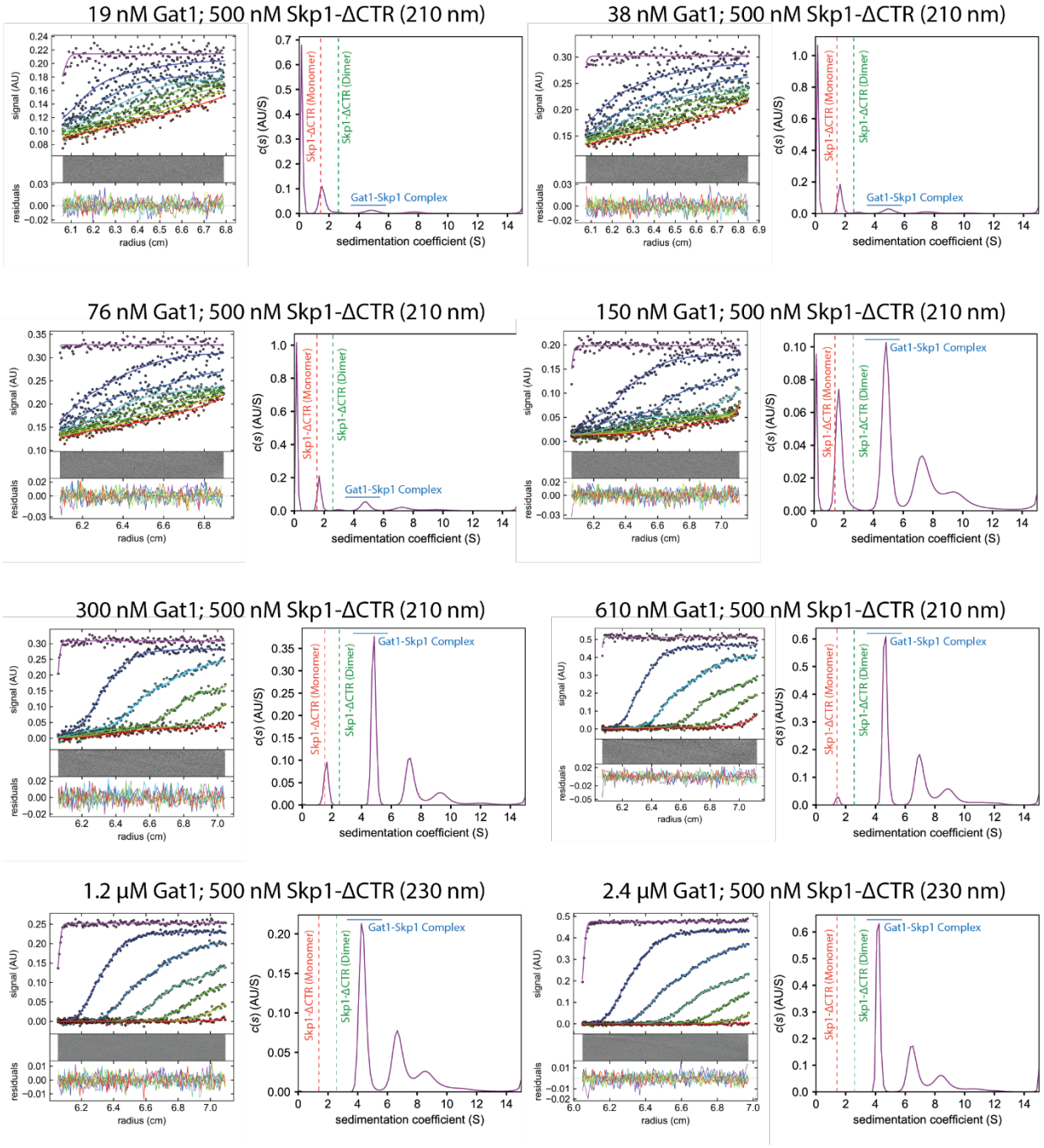
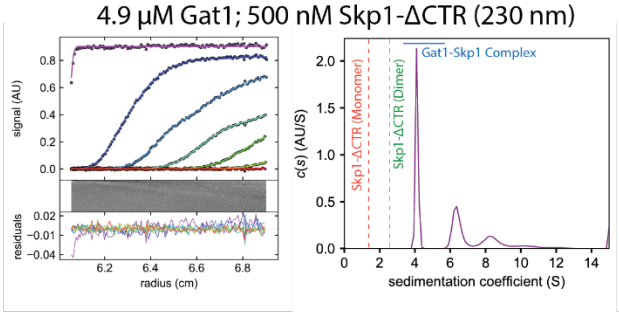

43 nM Gat1; 500 nM Gly-Skp1 (215 nm)
103 nM Gat1; 500 nM Gly-Skp1 (215 nm)
211 nM Gat1; 500 nM Gly-Skp1 (215 nm)
866 nM Gat1; 500 nM Gly-Skp1 (215 nm)
1.7 µM Gat1; 500 nM Gly-Skp1 (215 nm)
20 µM Gat1; 500 nM Gly-Skp1 (215 nm)
signal (AU)
residuals
radius (cm)
c(s) (AU/S)
sedimentation coefficient (S)
Gly-Skp1 Monomer
Gly-Skp1 Dimer
Gat1-Skp1 Complex

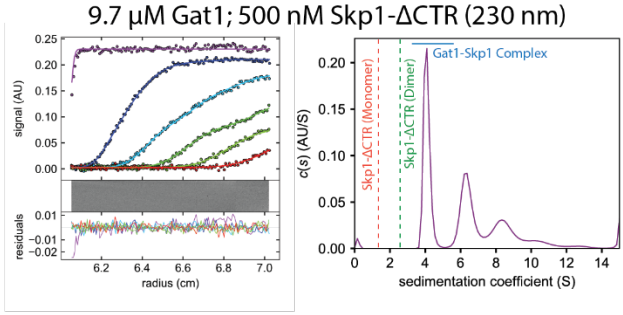
Figure 3.S3


19 nM Gat1; 500 nM Skp1-ΔCTR (210 nm)
38 nM Gat1; 500 nM Skp1-ΔCTR (210 nm)
76 nM Gat1; 500 nM Skp1-ΔCTR (210 nm)
150 nM Gat1; 500 nM Skp1-ΔCTR (210 nm)
300 nM Gat1; 500 nM Skp1-ΔCTR (210 nm)
610 nM Gat1; 500 nM Skp1-ΔCTR (210 nm)
1.2 μM Gat1; 500 nM Skp1-ΔCTR (230 nm)
2.4 μM Gat1; 500 nM Skp1-ΔCTR (230 nm)
signal (AU)
residuals
radius (cm)
c(s) (AU/S)
sedimentation coefficient (S)
Skp1-ΔCTR (Monomer)
Skp1-ΔCTR (Dimer)
Gat1-Skp1 Complex

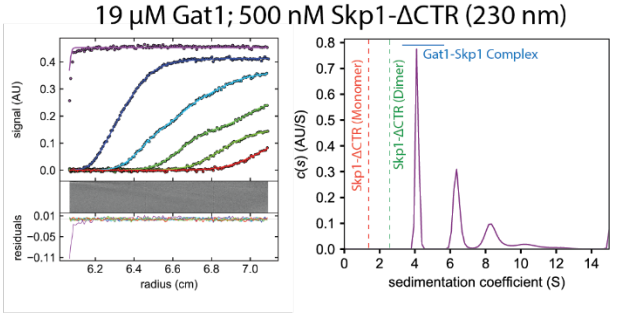
4.9 μM Gat1; 500 nM Skp1-ΔCTR (230 nm)



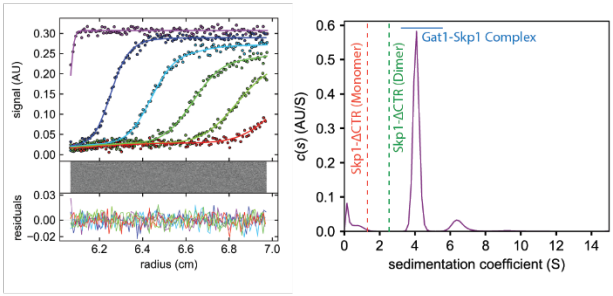
9.7 μM Gat1; 500 nM Skp1-ΔCTR (230 nm)



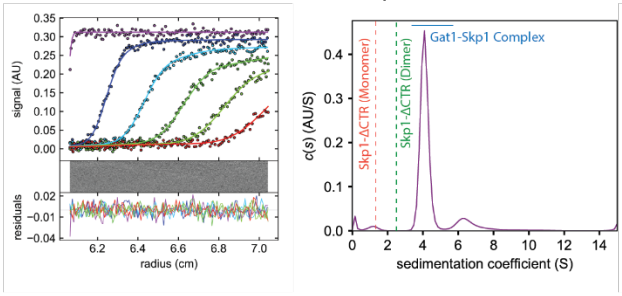
19 μM Gat1; 500 nM Skp1-ΔCTR (230 nm)



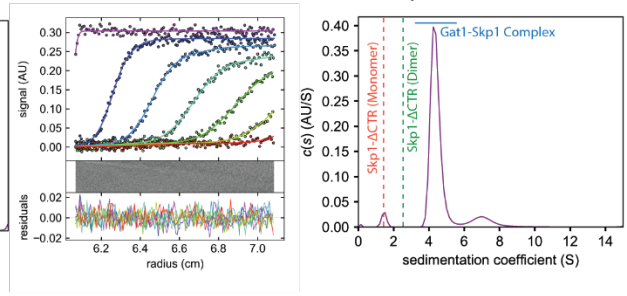
500 nM Gat1; 33 nM Skp1-ΔCTR (215 nm)



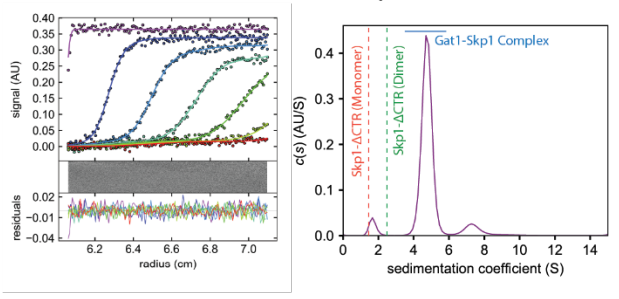
500 nM Gat1; 66 nM Skp1-ΔCTR (215 nm)



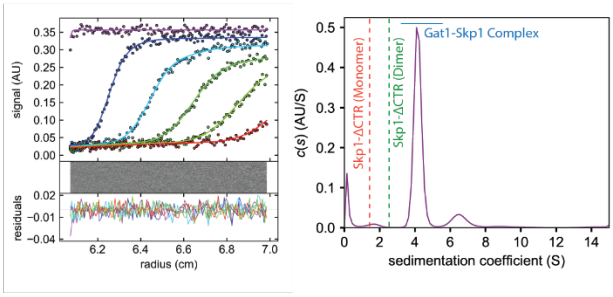
500 nM Gat1; 260 nM Skp1-ΔCTR (215 nm)



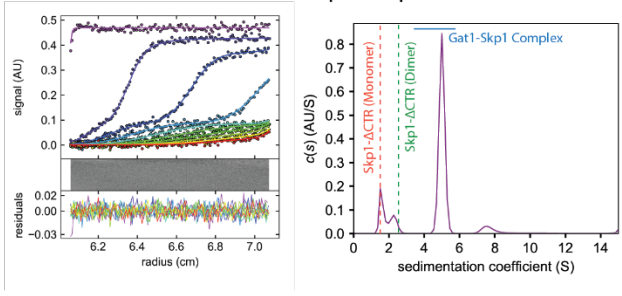
500 nM Gat1; 530 nM Skp1-ΔCTR (215 nm)



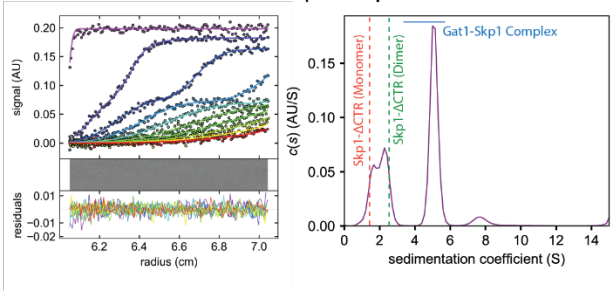
500 nM Gat1; 130 nM Skp1-ΔCTR (215 nm)



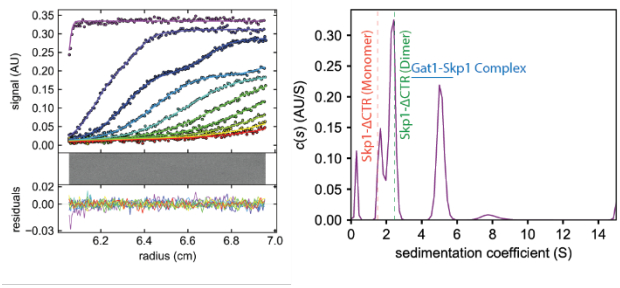
500 nM Gat1; 1.1 μM Skp1-ΔCTR (215 nm)



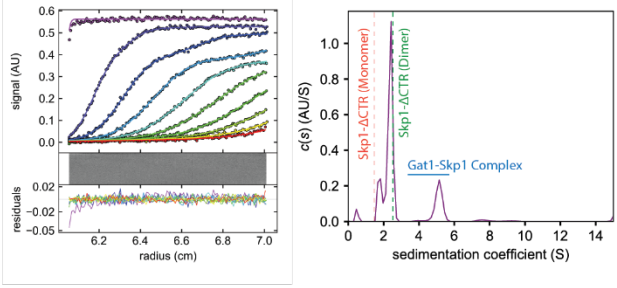
500 nM Gat1; 2.1 μM Skp1-ΔCTR (215 nm)



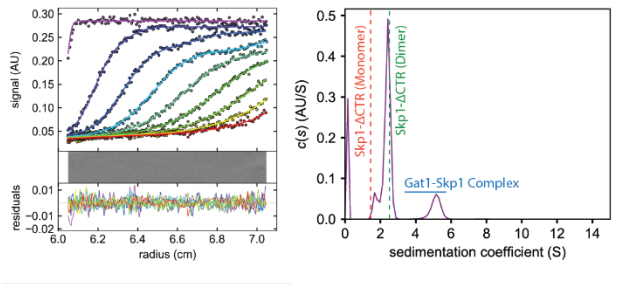
500 nM Gat1; 4.2 µM Skp1-ΔCTR (215 nm)



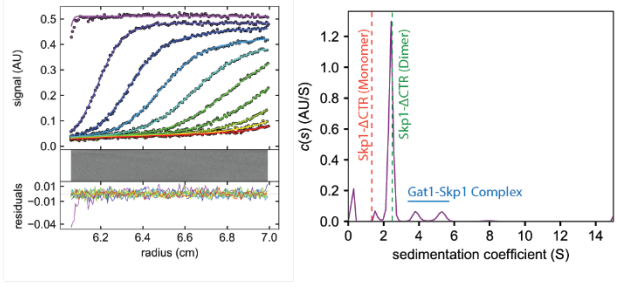
500 nM Gat1; 8.4 µM Skp1-ΔCTR (215 nm)



500 nM Gat1; 17 µM Skp1-ΔCTR (280 nm)



500 nM Gat1; 34 µM Skp1-ΔCTR (280 nm)



500 nM Gat1; 68 µM Skp1-ΔCTR (280 nm)

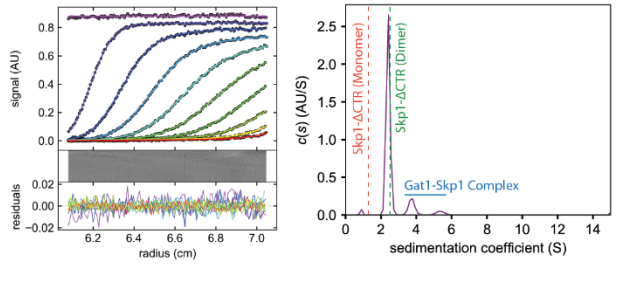


Figure 3.S4

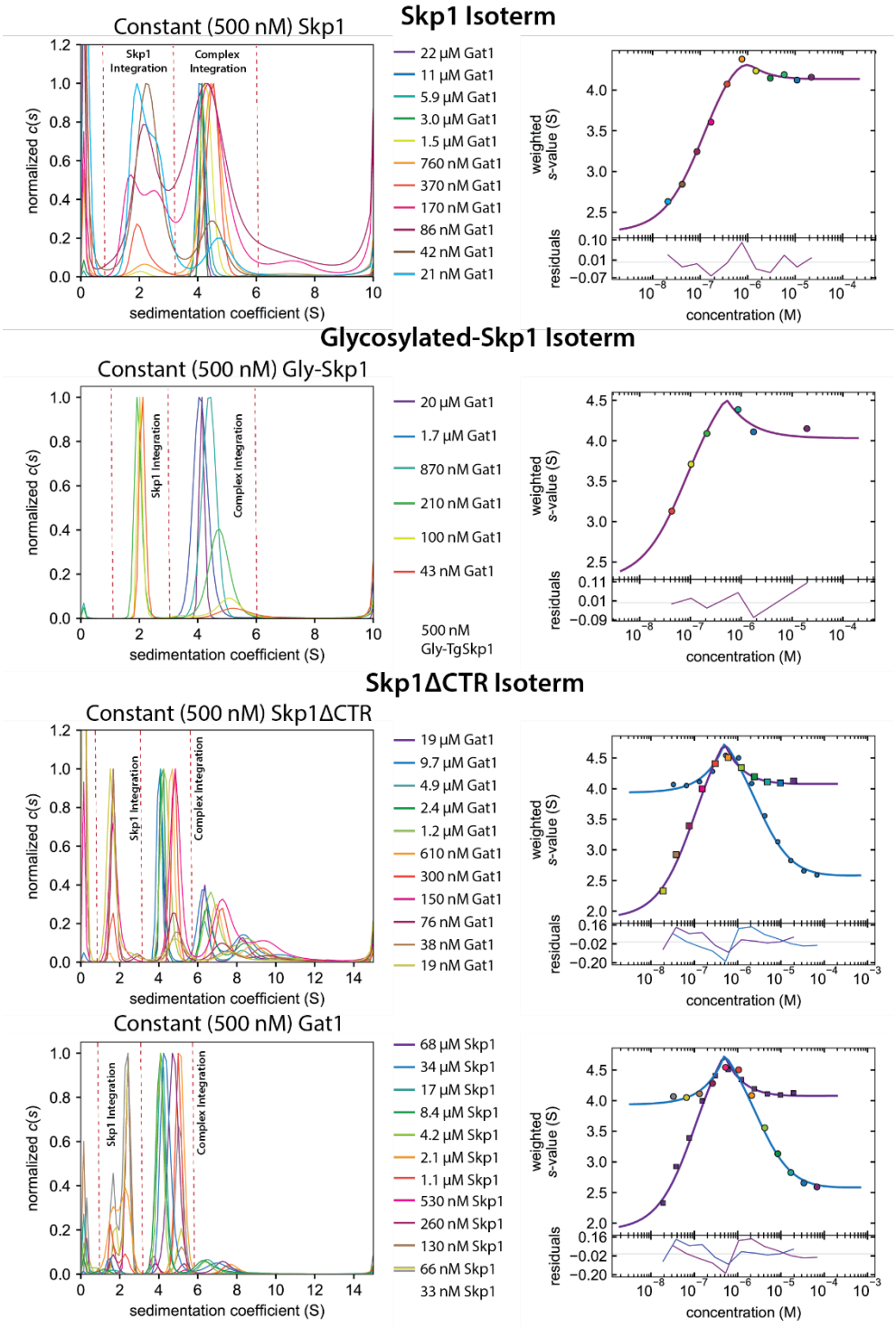

Skp1 Isoterm
Constant (500 nM) Skp1
Skp1 Integration
Complex Integration
normalized c(s)
sedimentation coefficient (S)
22 μM Gat1
11 μM Gat1
5.9 μM Gat1
3.0 μM Gat1
1.5 μM Gat1
760 nM Gat1
370 nM Gat1
170 nM Gat1
86 nM Gat1
42 nM Gat1
21 nM Gat1
weighted s-value (S)
residuals
concentration (M)
Glycosylated-Skp1 Isoterm
Constant (500 nM) Gly-Skp1
20 μM Gat1
1.7 μM Gat1
870 nM Gat1
210 nM Gat1
100 nM Gat1
43 nM Gat1
500 nM Gly-TgSkp1
Skp1ΔCTR Isoterm
Constant (500 nM) Skp1ΔCTR
19 μM Gat1
9.7 μM Gat1
4.9 μM Gat1
2.4 μM Gat1
1.2 μM Gat1
610 nM Gat1
300 nM Gat1
150 nM Gat1
76 nM Gat1
38 nM Gat1
19 nM Gat1
Constant (500 nM) Gat1
68 μM Skp1
34 μM Skp1
17 μM Skp1
8.4 μM Skp1
4.2 μM Skp1
2.1 μM Skp1
1.1 μM Skp1
530 nM Skp1
260 nM Skp1
130 nM Skp1
66 nM Skp1
33 nM Skp1

Figure 3.S5

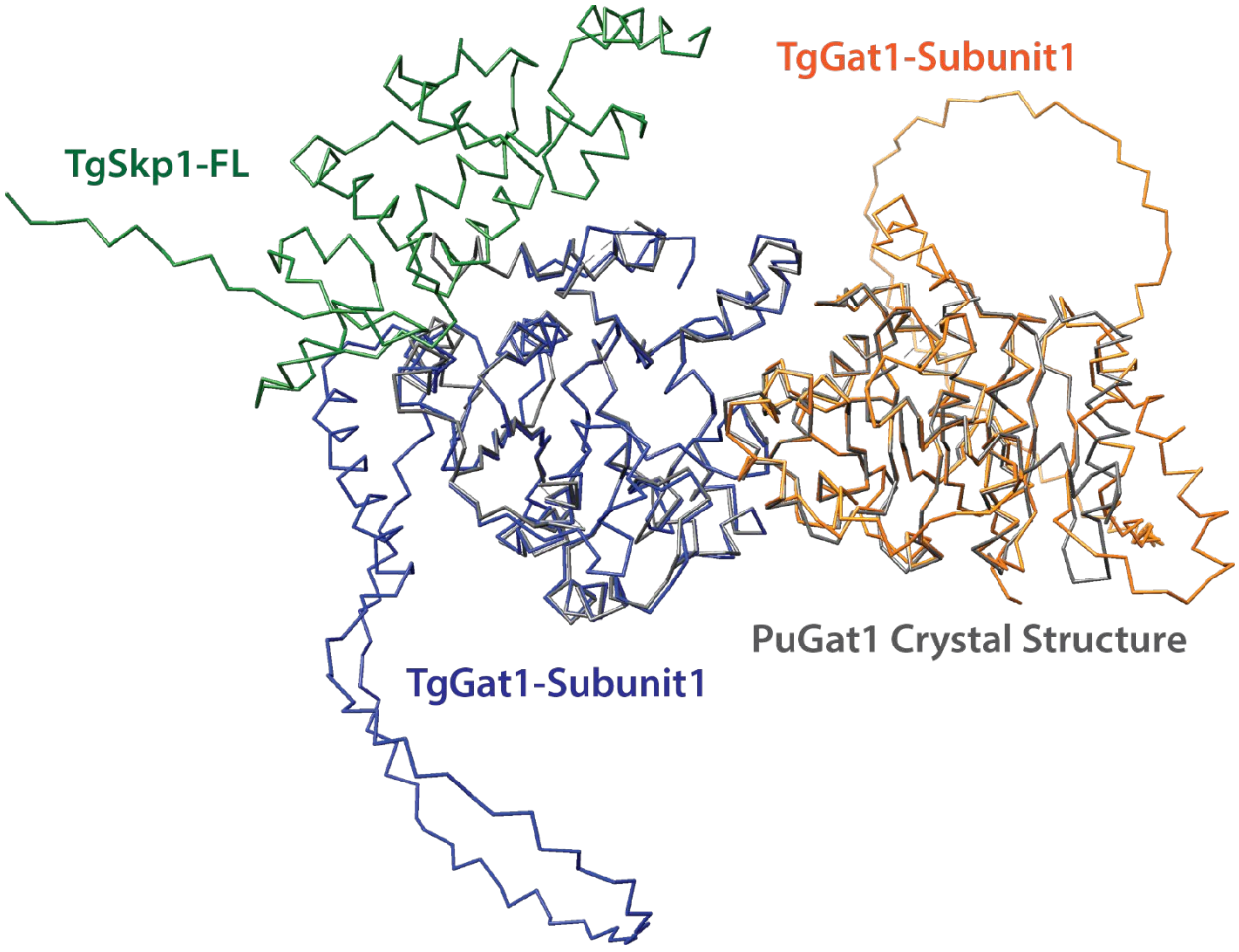

TgGat1-Subunit1
TgSkp1-FL
PuGat1 Crystal Structure
TgGat1-Subunit1

Figure 3.S6

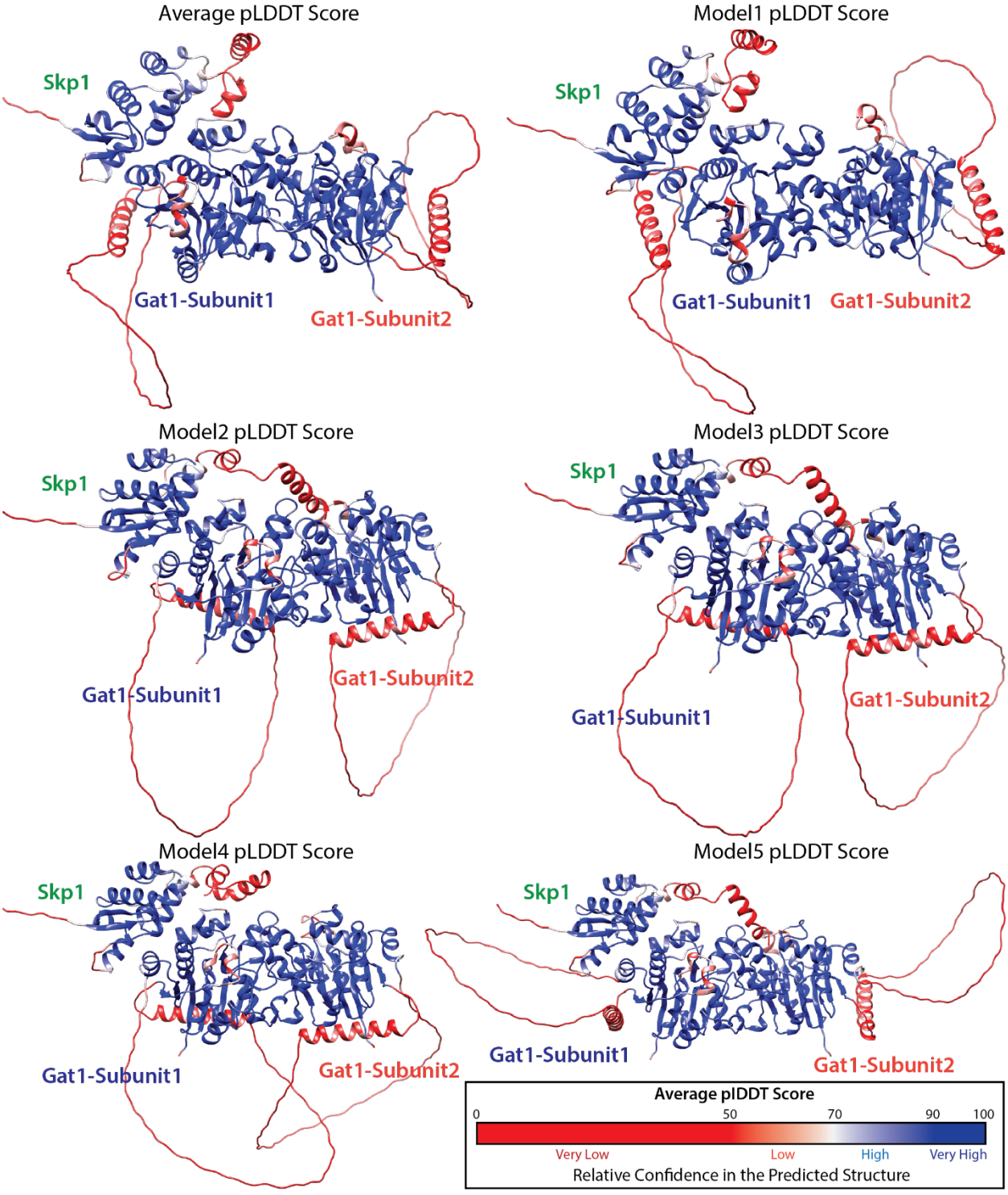

Average pLDDT Score
Skp1
Gat1-Subunit1
Gat1-Subunit2
Model1 pLDDT Score
Skp1
Gat1-Subunit1
Gat1-Subunit2
Model2 pLDDT Score
Skp1
Gat1-Subunit1
Gat1-Subunit2
Model3 pLDDT Score
Skp1
Gat1-Subunit1
Gat1-Subunit2
Model4 pLDDT Score
Skp1
Gat1-Subunit1
Gat1-Subunit2
Model5 pLDDT Score
Skp1
Gat1-Subunit1
Gat1-Subunit2
Average plDDT Score
0
50
70
90
100
Very Low
Low
High
Very High
Relative Confidence in the Predicted Structure

Figure 3.S7

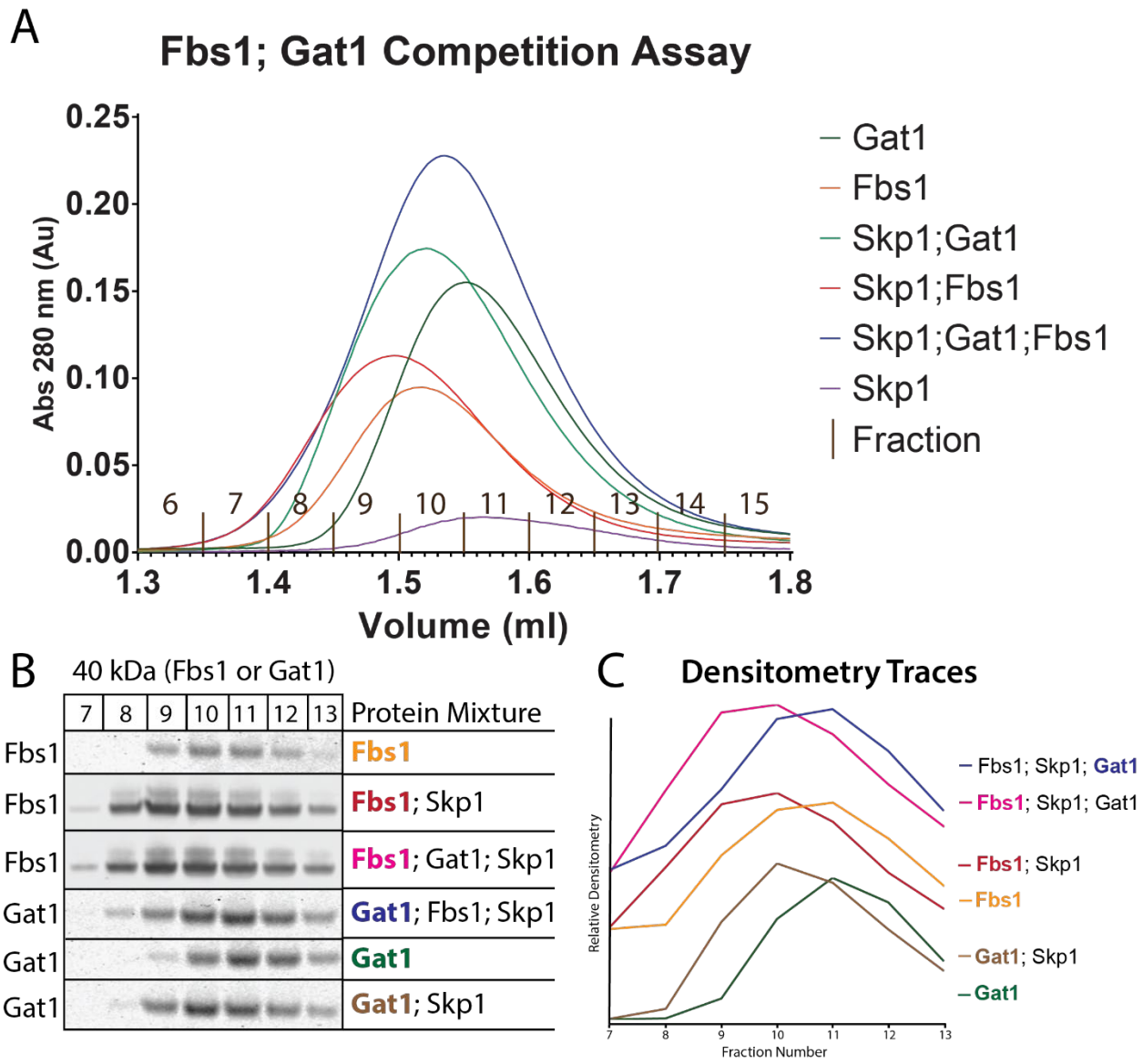

A
Fbs1; Gat1 Competition Assay
Abs 280 nm (Au)
0.25
0.20
0.15
0.10
0.05
0.00
1.3
1.4
1.5
1.6
1.7
1.8
Volume (ml)
6
7
8
9
10
11
12
13
14
15
Gat1
Fbs1
Skp1;Gat1
Skp1;Fbs1
Skp1;Gat1;Fbs1
Skp1
Fraction
B
40 kDa (Fbs1 or Gat1)
7
8
9
10
11
12
13
Protein Mixture
Fbs1
Fbs1
Fbs1; Skp1
Fbs1
Fbs1; Gat1; Skp1
Gat1
Gat1; Fbs1; Skp1
Gat1
Gat1
Gat1
Gat1; Skp1
C
Densitometry Traces
Relative Densitometry
Fraction Number
Fbs1; Skp1; Gat1
Fbs1; Skp1; Gat1
Fbs1; Skp1
Fbs1
Gat1; Skp1
Gat1

Figure 3.S8

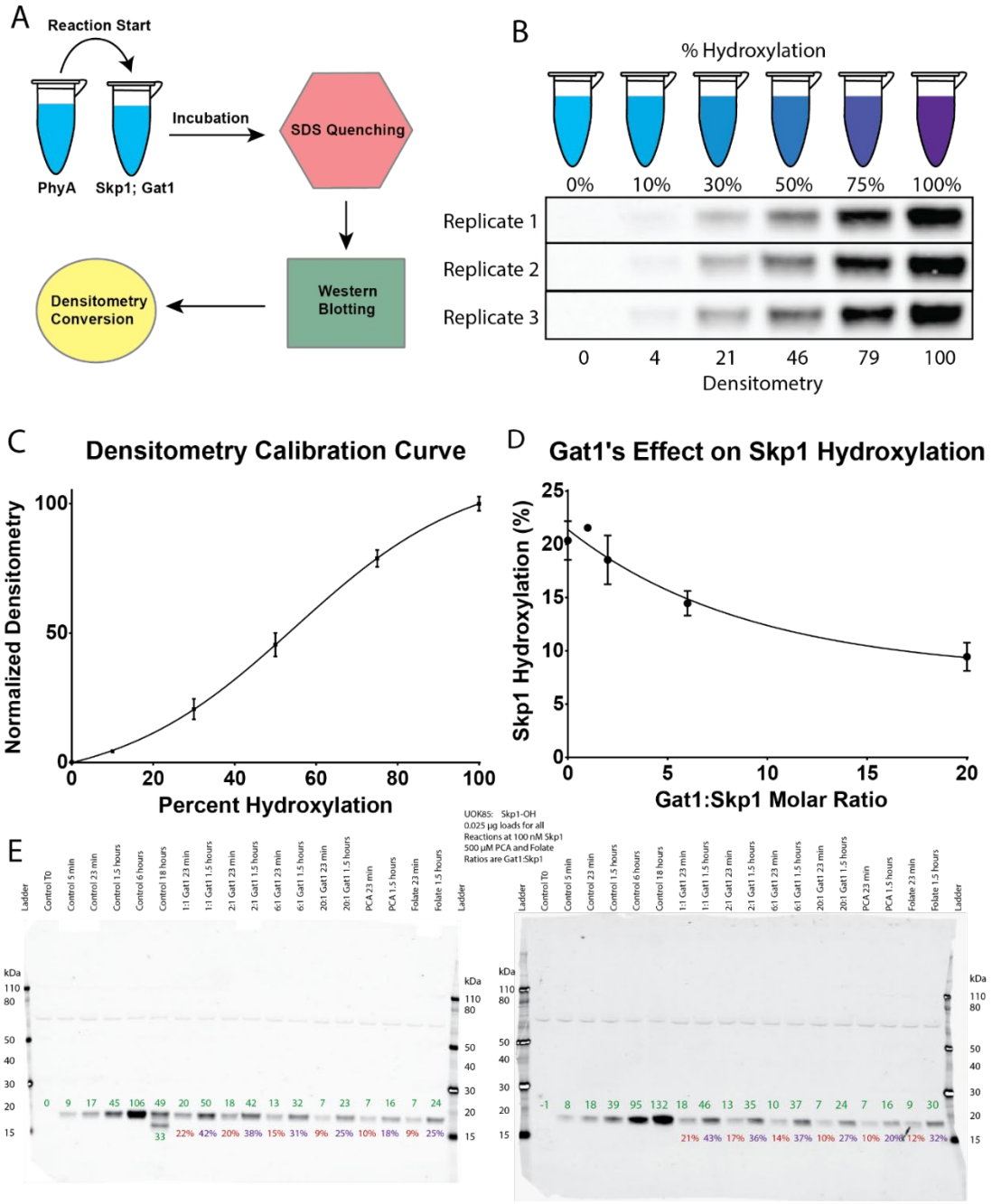

A
Reaction Start
Incubation
SDS Quenching
PhyA
Skp1; Gat1
Western Blotting
Densitometry Conversion
B
% Hydroxylation
0%
10%
30%
50%
75%
100%
Replicate 1
Replicate 2
Replicate 3
0
4
21
46
79
100
Densitometry
C
Densitometry Calibration Curve
Normalized Densitometry
Percent Hydroxylation
D
Gat1's Effect on Skp1 Hydroxylation
Skp1 Hydroxylation (%)
Gat1:Skp1 Molar Ratio
E
UOK85: Skp1-OH
0.025 µg loads for all
Reactions at 100 nM Skp1
500 µM PCA and Folate
Ratios are Gat1:Skp1

Figure 3.S9

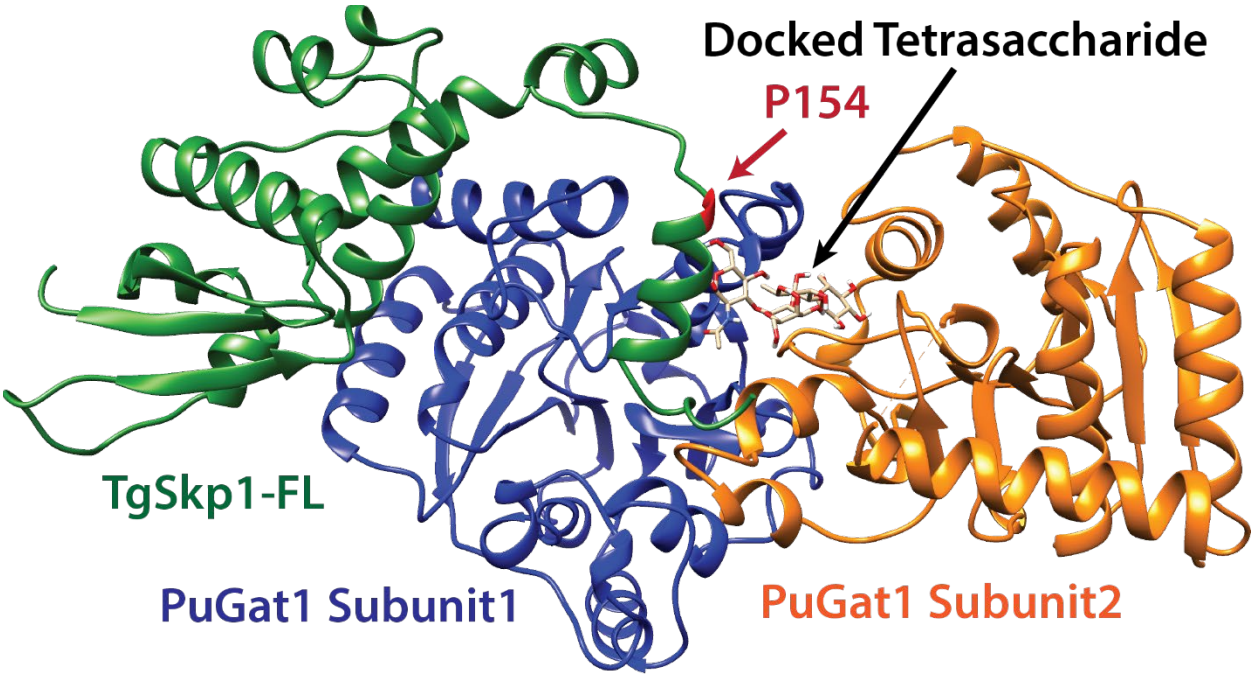

Docked Tetrasaccharide
P154
TgSkp1-FL
PuGat1 Subunit1
PuGat1 Subunit2

Figure 3.S10

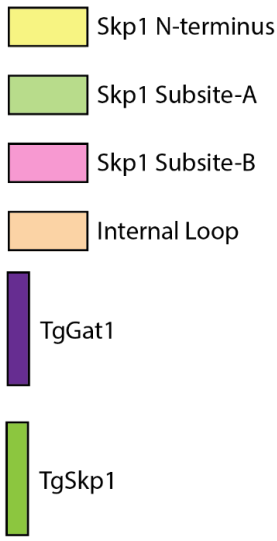
Residue	Average	SEM
MET 1	-0.00106	0.000486
SER 2	-0.00066	0.000122
PRO 3	-0.00074	6.1E-05
ARG 4	-0.00145	0.000179
TYR 5	-0.00167	8.5E-05
ALA 6	-0.00166	9.77E-05
THR 7	-0.00674	0.000303
ALA 8	-0.0036	0.000333
THR 9	-0.0116	0.001099
LEU 10	-0.01811	0.004453
LEU 11	-0.07396	0.00231
THR 12	-0.03034	0.005057
ASP 13	-0.15052	0.00599
ASN 14	-1.6954	0.034257
SER 15	-0.58487	0.022496
PHE 16	-0.23522	0.059564
TYR 17	-3.06288	0.065122
TYR 18	-3.63071	0.025482
GLY 19	-0.05146	0.001431
VAL 20	-0.06525	0.002061
GLU 21	-0.4532	0.035999
ALA 22	-0.06637	0.001903
LEU 23	-0.02841	0.001239
LEU 24	-0.04392	0.001441
LYS 25	-0.33496	0.026527
SER 26	-0.01637	0.000534
LEU 27	-0.01198	0.000348
GLU 28	-0.02641	0.001623
ALA 29	-0.00987	0.001115
THR 30	-0.00575	0.000385
LYS 31	-0.00746	0.000603
THR 32	-0.00379	0.000145
PRO 33	-0.00243	8.51E-05
TYR 34	-0.00346	0.000147
PRO 35	-0.00412	0.00021
VAL 36	-0.00902	0.000394
LEU 37	-0.00682	0.000294
LEU 38	-0.02879	0.000914
LEU 39	-0.01082	0.00059
HIE 40	-0.03289	0.002562
THR 41	-0.01965	0.001173
SER 42	-0.02164	0.002225
ASP 43	-0.06203	0.004901
VAL 44	-0.16643	0.010725
SER 45	-1.05091	0.058603
GLN 46	-0.9626	0.209597
SER 47	-2.46474	0.197269
THR 48	-1.45556	0.089157
ILE 49	-0.23629	0.018024
LYS 50	-2.0932	0.15647
ALA 51	-1.54406	0.073606
LEU 52	-0.27772	0.013741
VAL 53	-0.16486	0.016882
TYR 54	-4.28948	0.180898
GLN 55	-0.83496	0.216228
ARG 56	-0.13819	0.017794
ARG 57	-0.08404	0.062968
LYS 58	-0.11419	0.071579
ALA 59	-0.29373	0.287226
PRO 60	-0.50561	0.501453
ALA 61	-0.05662	0.054303
SER 62	-0.04797	0.046276
GLU 63	-0.06144	0.058996
ASP 64	-0.03724	0.038469
ALA 65	-0.00756	0.006546
GLY 66	-0.00273	0.001915
THR 67	-0.00343	0.002041
THR 68	-0.00532	0.003557
GLY 69	-0.00376	0.002396
LYS 70	-0.02235	0.01871
GLU 71	-0.00739	0.004306
MET 72	-0.00977	0.00582
LYS 73	-0.01301	0.011297
THR 74	-0.00231	0.002209
GLY 75	-0.00155	0.001034
GLN 76	-0.00489	0.004014
GLU 77	-0.00373	0.002831
VAL 78	-0.00574	0.005213
ILE 79	-0.0074	0.0067
PRO 80	-0.00918	0.008838
SER 81	-0.00334	0.003078
SER 82	-0.05577	0.055496
GLN 83	-0.26142	0.261094
CYS 84	-0.15693	0.156673
PRO 85	-0.11255	0.112242
GLU 86	-0.32202	0.321714
HIE 87	-0.13306	0.132629
THR 88	-0.20533	0.205077
PRO 89	-0.12783	0.127542
GLY 90	-0.17943	0.179316
ARG 91	-0.40712	0.406787
ASN 92	-0.14986	0.149612
LEU 93	-0.06356	0.063501
HIE 94	-0.04035	0.040044
SER 95	-0.02218	0.021965
PRO 96	-0.06277	0.062451
ILE 97	-0.1788	0.178242
GLY 98	-0.05925	0.058887
ARG 99	-0.60687	0.60609
LYS 100	-0.23987	0.239338
GLY 101	-0.01048	0.010318
VAL 102	-0.00851	0.008191
ASN 103	-0.03405	0.033567
PRO 104	-0.01692	0.016469
VAL 105	-0.01115	0.010125
SER 106	-0.00493	0.004397
CYS 107	-0.0029	0.002276
SER 108	-0.00475	0.004379
VAL 109	-0.00556	0.005161
THR 110	-0.02099	0.020696
GLN 111	-0.08916	0.088698
ASP 112	-0.03906	0.038752
GLU 113	-0.33414	0.33357
THR 114	-0.04383	0.043487
ARG 115	-0.17957	0.178945

Residue	Average	SEM
VAL 116	-0.07965	0.079192
ARG 117	-0.62069	0.619471
THR 118	-0.05294	0.052419
ASP 119	-0.12482	0.124113
SER 120	-0.01096	0.01041
ASP 121	-0.0127	0.011806
ILE 122	-0.22117	0.21862
LEU 123	-0.02115	0.019342
GLU 124	-0.00603	0.004382
GLU 125	-0.03475	0.029182
ALA 126	-0.01305	0.009429
GLU 127	-0.00599	0.00296
ARG 128	-0.01167	0.007141
ARG 129	0.018913	0.130397
ALA 130	-0.01238	0.009353
SER 131	-0.0087	0.00698
ALA 132	-0.07791	0.076363
ARG 133	-0.17298	0.167384
THR 134	-0.01842	0.016282
SER 135	-0.01861	0.017431
GLU 136	-0.3022	0.300258
ARG 137	-0.12307	0.11947
ALA 138	-0.02345	0.022151
ARG 139	-0.11947	0.117343
ALA 140	-0.12526	0.123742
GLY 141	-0.04645	0.045275
GLY 142	-0.03367	0.032353
THR 143	-0.02282	0.019566
GLU 144	-0.01678	0.011143
GLU 145	-0.01015	0.002207
GLN 146	-0.02035	0.008024
GLY 147	-0.00826	0.001756
ILE 148	-0.0174	0.001167
CYS 149	-0.00883	0.000684
VAL 150	-0.02249	0.001395
ILE 151	-0.01123	0.000559
PRO 152	-0.02415	0.001484
ARG 153	-0.01049	0.000672
LEU 154	-0.01478	0.002006
VAL 155	-0.00626	0.000426
GLY 156	-0.00235	0.000129
SER 157	-0.00386	0.000394
VAL 158	-0.00381	0.000836
ALA 159	-0.00266	0.000736
TYR 160	-0.02787	0.0171
PRO 161	-0.00654	0.002891
LYS 162	-0.00436	0.001746
ALA 163	-0.0033	0.001066
GLU 164	-0.01817	0.009792
ARG 165	-0.00878	0.003051
ASP 166	-0.00531	0.002257
THR 167	-0.00858	0.0033
CYS 168	-0.01794	0.012228
PRO 169	-0.05152	0.045424
VAL 170	-0.10353	0.094556
GLU 171	-0.01647	0.009135
GLY 172	-0.03684	0.030515
TRP 173	-0.53672	0.490468
LYS 174	-0.02118	0.011658
ASP 175	-0.01675	0.007767
CYS 176	-0.10408	0.093922
PHE 177	-0.01724	0.012038
THR 178	-0.00666	0.002148
LYS 179	-0.03082	0.024425
LEU 180	-0.00353	0.001238
ARG 181	-0.004	0.000478
VAL 182	-0.00271	0.000412
TRP 183	-0.0027	0.000527
GLU 184	-0.00173	0.000132
GLN 185	-0.00249	0.00015
VAL 186	-0.00093	5.02E-05
ASP 187	-0.00137	6.38E-05
PHE 188	-0.00232	0.000111
ASP 189	-0.0007	4.33E-05
VAL 190	-0.00101	7.81E-05
ILE 191	-0.00221	0.0002
VAL 192	-0.00261	0.000252
TYR 193	-0.01044	0.003828
VAL 194	-0.00813	0.001704
ASP 195	-0.06425	0.052413
ALA 196	-0.02563	0.008085
ASP 197	-0.15914	0.128487
CYS 198	-0.01548	0.003562
ILE 199	-0.02712	0.009597
VAL 200	-0.00941	0.000318
LEU 201	-0.01373	0.001304
ARG 202	-0.00876	0.001551
PRO 203	-0.00315	0.000187
VAL 204	-0.00276	0.00017
ASP 205	-0.00176	8.25E-05
GLU 206	-0.00143	0.000103
LEU 207	-0.00187	0.000222
PHE 208	-0.00184	0.000127
LEU 209	-0.00077	5.36E-05
ARG 210	-0.00131	0.000188
GLN 211	-0.00055	6.37E-05
PRO 212	-0.00051	7.87E-05
LEU 213	-0.00085	0.000122
PRO 214	-0.001	0.000212
ALA 215	-0.00098	0.000227
PHE 216	-0.00347	0.001134
ALA 217	-0.00299	0.001073
PRO 218	-0.00603	0.002375
ASP 219	-0.04151	0.021859
ILE 220	-0.09962	0.049564
PHE 221	-0.53921	0.253877
PRO 222	-0.02173	0.01029
PRO 223	-0.01161	0.004903
ASP 224	-0.0044	0.001581
LYS 225	-0.00838	0.003536
PHE 226	-0.00777	0.003617
ASN 227	-0.02507	0.013604
ALA 228	-0.0194	0.014257
GLY 229	-0.00954	0.005768
VAL 230	-0.00574	0.001912

Residue	Average	SEM
ALA 231	-0.0021	0.000588
VAL 232	-0.00157	0.000265
LEU 233	-0.00172	0.000269
LYS 234	-0.00085	9.37E-05
PRO 235	-0.00095	7.78E-05
ASP 236	-0.00061	6.63E-05
LEU 237	-0.0008	6.07E-05
GLY 238	-0.00024	2.31E-05
GLU 239	-0.00076	0.000111
TYR 240	-0.00176	0.000242
GLY 241	-0.00033	3.86E-05
ASN 242	-0.00058	8.25E-05
MET 243	-0.00145	0.000352
VAL 244	-0.00107	0.000192
ALA 245	-0.00048	7.27E-05
ALA 246	-0.00067	0.00014
VAL 247	-0.00177	0.00054
GLU 248	-0.00122	0.000246
ARG 249	-0.00123	0.000177
LEU 250	-0.00177	0.000371
PRO 251	-0.00236	0.000458
SER 252	-0.00428	0.001197
TYR 253	-0.01823	0.007412
ASP 254	-0.05974	0.031396
GLY 255	-0.00779	0.00342
GLY 256	-0.01469	0.009017
ASP 257	-0.0827	0.072427
THR 258	-0.03612	0.025887
GLY 259	-0.00608	0.003425
PHE 260	-0.00506	0.00224
LEU 261	-0.00541	0.002774
ASN 262	-0.00486	0.002192
ALA 263	-0.00143	0.00046
TYR 264	-0.0017	0.000448
PHE 265	-0.00188	0.000537
SER 266	-0.00095	0.000237
SER 267	-0.00066	0.000142
TRP 268	-0.00325	0.001009
TYR 269	-0.00263	0.00075
GLU 270	-0.00091	0.000171
ASN 271	-0.0007	0.000136
ALA 272	-0.0004	7.4E-05
ALA 273	-0.00052	0.000103
GLY 274	-0.00039	6.67E-05
ALA 275	-0.00067	0.000149
ARG 276	-0.0019	0.000478
LEU 277	-0.00233	0.000558
PRO 278	-0.00227	0.000561
PHE 279	-0.01351	0.005104
ARG 280	-0.0053	0.000946
TYR 281	-0.0046	0.000899
ASN 282	-0.01017	0.003752
ALA 283	-0.00908	0.002571
LEU 284	-0.05778	0.02678
ARG 285	-0.18188	0.096737
THR 286	-0.52716	0.326156
LEU 287	-0.10805	0.0528
TYR 288	-0.17402	0.051885
HIE 289	-1.30715	0.762955
MET 290	-1.95841	1.123759
THR 291	-0.36009	0.216437
TYR 292	-0.69454	0.303756
SER 293	-0.8874	0.476226
SER 294	-0.68475	0.360907
ARG 295	-0.86185	0.509257
LYS 296	-0.11521	0.04812
GLY 297	-0.02032	0.009735
TYR 298	-0.38212	0.186359
TRP 299	-0.04368	0.011509
ASP 300	-0.01494	0.004817
ALA 301	-0.00592	0.001896
VAL 302	-0.00837	0.002281
LYS 303	-0.01463	0.005381
PRO 304	-0.00419	0.000785
ILE 305	-0.00914	0.001055
LYS 306	-0.00476	0.000346
ILE 307	-0.00789	0.001062
LEU 308	-0.0202	0.002984
HIE 309	-0.06026	0.033377
PHE 310	-0.06716	0.030905
CYS 311	-0.26507	0.14667
SER 312	-1.06803	0.628579
SER 313	-0.92364	0.617233
PRO 314	-0.4461	0.272267
LYS 315	-0.10663	0.08969
PRO 316	-0.21914	0.022003
TRP 317	-1.32846	0.025742
GLU 318	-0.54049	0.06127
GLN 319	-1.06145	0.31383
PRO 320	-2.66675	0.354462
ALA 321	-1.10528	0.173965
LYS 322	-1.59556	0.450248
THR 323	-0.49613	0.131412
ASP 324	-0.18652	0.04814
LEU 325	-0.08557	0.008728
GLU 326	-0.201	0.027766
GLU 327	-0.77679	0.204828
LEU 328	-0.11403	0.028505
TRP 329	-0.41263	0.017697
TRP 330	-3.09108	0.133209
LYS 331	-0.83727	0.411958
VAL 332	-0.10621	0.014445
PHE 333	-2.23015	0.040596
LEU 334	-2.91819	0.207752
THR 335	-0.53511	0.178529
GLY 336	-0.05499	0.005697
THR 337	-0.11591	0.063788
VAL 338	-0.04023	0.012773
PRO 339	-0.11973	0.052727
THR 340	-0.05418	0.024845
ASP 341	-0.23827	0.133897
SER 342	-0.24549	0.153157
ASP 343	-0.10747	0.074775
ILE 344	-0.13957	0.101802
VAL 345	-0.02154	0.006405

Residue	Average	SEM
MET 1	-0.10792	0.085717
SER 2	-0.07843	0.072016
LYS 3	-0.21856	0.212369
GLU 4	-0.28126	0.277676
ARG 5	-0.1573	0.150223
MET 6	-0.41447	0.411671
GLY 7	-0.25949	0.258432
ASP 8	-0.38445	0.382262
ALA 9	-0.15258	0.150651
ARG 10	-0.5033	0.495463
LYS 11	-0.02817	0.021936
VAL 12	-0.03209	0.012666
THR 13	-0.02574	0.006803
LEU 14	-0.0551	0.005286
VAL 15	-0.07745	0.002806
SER 16	-0.056	0.001545
GLN 17	-0.28945	0.02177
GLU 18	-0.04947	0.002027
GLY 19	-0.01846	0.000693
ASP 20	-0.01664	0.000456
GLU 21	-0.01527	0.001553
PHE 22	-0.01634	0.001626
ASP 23	-0.00896	0.002924
VAL 24	-0.01387	0.004286
ASP 25	-0.01683	0.011129
ILE 26	-0.07439	0.059672
GLU 27	-0.07471	0.066696
VAL 28	-0.01607	0.007315
ALA 29	-0.02107	0.003768
SER 30	-0.034	0.009589
MET 31	-0.03683	0.003653
SER 32	-0.12419	0.003055
ALA 33	-0.79167	0.088479
LEU 34	-3.3882	0.168228
ILE 35	-0.23867	0.013679
LYS 36	-0.22506	0.067232
THR 37	-1.79952	0.307685
MET 38	-2.18833	0.131121
VAL 39	-0.32108	0.232359
GLU 40	-0.73363	0.47537
GLU 41	-1.02785	0.599275
ASP 42	-0.75075	0.442514
SER 43	-0.92346	0.565152
ASP 44	-0.47008	0.300642
CYS 45	-0.19101	0.08268
GLN 46	-0.55688	0.485094
GLU 47	-0.27724	0.244396
SER 48	-0.08235	0.030651
ILE 49	-0.48452	0.068628
PRO 50	-0.66416	0.045197
LEU 51	-0.72476	0.030089
PRO 52	-2.73825	0.033702
ASN 53	-3.37462	0.057982
VAL 54	-0.26369	0.007294
ASP 55	-0.0788	0.00295
THR 56	-0.02086	0.000401
CYS 57	-0.01576	0.000442
ILE 58	-0.06377	0.000963
LEU 59	-0.04235	0.000712
LYS 60	-0.01194	0.00028
LYS 61	-0.01655	0.000421
ILE 62	-0.04046	0.000553
ILE 63	-0.01474	0.000773
GLU 64	-0.00657	0.000504
TYR 65	-0.01825	0.001255
CYS 66	-0.01079	0.000993
GLU 67	-0.00563	0.001499
HIE 68	-0.00548	0.001021
HIE 69	-0.01116	0.003273
HIE 70	-0.02161	0.016891
ASN 71	-0.00489	0.002875
ASN 72	-0.00356	0.001462
PRO 73	-0.00568	0.003401
PRO 74	-0.00549	0.00194
GLU 75	-0.00491	0.001427
GLU 76	-0.00871	0.002728
ILE 77	-0.01197	0.003388
PRO 78	-0.00719	0.001812
LYS 79	-0.0393	0.012794
PRO 80	-0.01964	0.006622
LEU 81	-0.02074	0.006584
LYS 82	-0.00934	0.002385
SER 83	-0.00531	0.000953
SER 84	-0.00675	0.001559
ASN 85	-0.00509	0.000821
LEU 86	-0.01141	0.001628
ALA 87	-0.00267	0.000411
GLU 88	-0.00465	0.0013
VAL 89	-0.00753	0.001053
VAL 90	-0.00694	0.000781
SER 91	-0.0027	0.000214
GLU 92	-0.00235	0.000176
TRP 93	-0.0053	0.000338
ASP 94	-0.00599	0.000377
TYR 95	-0.00701	0.000768
GLN 96	-0.00359	0.000175
PHE 97	-0.01223	0.000723
ILE 98	-0.01919	0.001527
ASN 99	-0.00646	0.000372
GLU 100	-0.00626	0.000385
ASN 101	-0.01572	0.001258
SER 102	-0.01622	0.001844
ASP 103	-0.0359	0.003727
GLN 104	-0.39591	0.099665
LYS 105	-0.28248	0.050727
ILE 106	-0.07313	0.003181
LEU 107	-0.16624	0.009442
PHE 108	-3.13569	0.251723
ALA 109	-0.27268	0.00643
LEU 110	-0.1376	0.002768
ILE 111	-1.41631	0.047696
LEU 112	-4.3082	0.952041
ALA 113	-0.37257	0.004709
ALA 114	-0.19213	0.008908
ASN 115	-2.74699	0.095156

Residue	Average	SEM
TYR 116	-3.8025	0.250277
LEU 117	-0.44109	0.010643
ASN 118	-0.90876	0.081393
ILE 119	-0.10436	0.003115
LYS 120	-0.14673	0.020841
PRO 121	-0.03017	0.001847
LEU 122	-0.05851	0.004682
LEU 123	-0.6855	0.055189
ASP 124	-0.09047	0.008645
LEU 125	-0.03931	0.005045
SER 126	-0.1832	0.060938
VAL 127	-0.73574	0.141556
ALA 128	-0.04279	0.00721
LYS 129	-0.05662	0.012223
VAL 130	-0.44976	0.131362
ALA 131	-0.09173	0.025898
THR 132	-0.02788	0.00545
MET 133	-0.11426	0.060568
ILE 134	-0.4097	0.166152
LYS 135	-0.06193	0.011543
ALA 136	-0.03399	0.017997
LYS 137	-0.07706	0.051584
THR 138	-0.04673	0.008699
PRO 139	-0.27183	0.133915
GLU 140	-0.14812	0.047029
GLU 141	-0.20683	0.096845
ILE 142	-0.32122	0.114478
ARG 143	-0.99342	0.416283
ARG 144	-0.40699	0.197384
ILE 145	-1.18896	0.805267
PHE 146	-1.72129	0.288045
ASN 147	-0.95373	0.261047
ILE 148	-1.20286	0.533491
VAL 149	-0.32823	0.171378
ASN 150	-0.13413	0.041238
ASP 151	-0.13196	0.09644
PHE 152	-0.21596	0.10283
THR 153	-0.18361	0.149265
PRO 154	-0.13107	0.09441
GLU 155	-0.27091	0.245147
GLU 156	-0.17165	0.150261
GLU 157	-0.09879	0.048667
ALA 158	-0.21357	0.187895
GLN 159	-0.76468	0.689255
VAL 160	-0.22266	0.12124
ARG 161	-0.56847	0.351372
GLU 162	-0.86976	0.737256
GLU 163	-0.71774	0.498932
ASN 164	-0.71309	0.541864
LYS 165	-1.32579	0.688372
TRP 166	-3.14146	1.521767
CYS 167	-0.8527	0.420009
GLU 168	-0.92742	0.474387
ASP 169	-1.05121	0.568271
ALA 170	-0.92796	0.642168





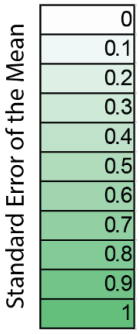


Figure 3.S11

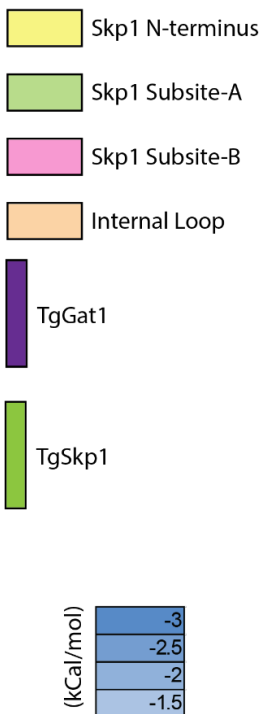
Residue	Average	SEM
MET 1	-0.06864	0.067817
SER 2	-0.05873	0.058029
PRO 3	-0.01143	0.010502
ARG 4	-0.00591	0.003646
TYR 5	-0.00689	0.005054
ALA 6	-0.00315	0.001535
TYR 7	-0.01378	0.00817
ALA 8	-0.00382	0.0004
THR 9	-0.01035	0.000787
LEU 10	-0.01692	0.00626
LEU 11	-0.05575	0.011445
THR 12	-0.07058	0.051303
ASP 13	-0.1381	0.035916
ASN 14	-1.43001	0.372171
SER 15	-0.72017	0.234303
PHE 16	-1.18623	1.030298
TYR 17	-2.52978	0.421657
TYR 18	-3.28761	0.752679
GLY 19	-0.13538	0.088504
VAL 20	-0.09459	0.03411
GLU 21	-0.51254	0.120013
ALA 22	-0.2136	0.13487
LEU 23	-0.0958	0.063988
LEU 24	-0.06187	0.010414
LYS 25	-0.57053	0.281725
SER 26	-0.11723	0.083695
LEU 27	-0.04312	0.018788
GLU 28	-0.12247	0.089798
ALA 29	-0.20287	0.167935
THR 30	-0.22799	0.199205
LYS 31	-0.39085	0.351107
THR 32	-0.09236	0.086079
PRO 33	-0.2196	0.215143
TYR 34	-0.03672	0.034754
PRO 35	-0.0129	0.008573
VAL 36	-0.01133	0.003236
LEU 37	-0.00929	0.00187
LEU 38	-0.02365	0.00292
LEU 39	-0.02968	0.020776
HIE 40	-0.04164	0.015972
THR 41	-0.02734	0.012972
SER 42	-0.0347	0.018979
ASP 43	-0.04747	0.011027
VAL 44	-0.21193	0.103885
SER 45	-0.68361	0.195111
GLN 46	-1.4113	0.696683
SER 47	-1.8959	0.520243
THR 48	-1.71978	0.641524
ILE 49	-0.59905	0.407682
LYS 50	-1.42091	0.411532
ALA 51	-1.2453	0.193318
LEU 52	-0.88152	0.631606
VAL 53	-0.26952	0.111643
TYR 54	-3.52478	0.800895
GLN 55	-1.66094	0.708771
ARG 56	-0.58585	0.352445
ARG 57	-0.26438	0.213282
LYS 58	-0.18498	0.080207
ALA 59	-0.02603	0.013233
PRO 60	-0.03952	0.022572
ALA 61	-0.16282	0.169828
PHE 177	-0.20801	0.055693
GLU 63	-0.01955	0.009621
ASP 64	-0.03407	0.030704
ALA 65	-0.03634	0.032488
GLY 66	0.017523	0.034446
THR 67	-0.47102	0.43475
THR 68	-0.33778	0.316392
GLY 69	-0.35607	0.3467
LYS 70	-0.16274	0.112372
GLU 71	-0.45304	0.410402
MET 72	-0.29618	0.28068
LYS 73	-0.85756	0.847842
THR 74	-0.22367	0.205344
GLY 75	-0.03616	0.022158
GLN 76	-0.37591	0.252987
GLU 77	-0.45968	0.286532
VAL 78	-0.20176	0.188336
ILE 79	-0.1698	0.158105
PRO 80	-0.03541	0.032114
SER 81	-0.09877	0.094911
SER 82	-0.3315	0.329528
GLN 83	-0.1963	0.194342
CYS 84	-0.00722	0.005763
PRO 85	-0.16656	0.164643
GLU 86	-0.31998	0.310608
HIE 87	-0.15452	0.138083
THR 88	-0.20373	0.162133
PRO 89	-0.71947	0.648592
GLY 90	-0.4324	0.389646
ARG 91	-0.79486	0.628613
ASN 92	-0.41855	0.335721
LEU 93	-0.09024	0.057133
HIE 94	-0.70167	0.563159
SER 95	-0.27316	0.246574
PRO 96	-0.61168	0.371098
ILE 97	-0.44681	0.307454
GLY 98	-0.08062	0.04982
ARG 99	-0.28174	0.236282
LYS 100	-0.07829	0.055271
GLY 101	-0.01522	0.008334
VAL 102	-0.04402	0.021902
ASN 103	-0.01533	0.007027
PRO 104	-0.03152	0.022597
VAL 105	-0.02732	0.012974
SER 106	-0.00902	0.004001
CYS 107	-0.01489	0.007937
SER 108	-0.01367	0.009628
VAL 109	-0.06443	0.059596
THR 110	-0.06565	0.061749
GLN 111	-0.07595	0.073521
ASP 112	-0.1907	0.188876
GLU 113	-0.22237	0.22093
THR 114	-0.29553	0.294814
ARG 115	-0.6136	0.611293

Residue	Average	SEM
VAL 116	-0.57631	0.575344
ARG 117	-0.09455	0.091488
THR 118	-0.2387	0.236064
ASP 119	-0.05496	0.051681
SER 120	-0.08249	0.076826
ASP 121	-0.01417	0.009072
HIE 122	-0.04108	0.021565
ILE 123	-0.0557	0.026436
GLU 124	-0.02205	0.009509
GLU 125	-0.04324	0.032486
ALA 126	-0.08953	0.040313
GLU 127	-0.20938	0.190849
ARG 128	-0.03941	0.025947
ARG 129	-0.19067	0.150711
ALA 130	-0.25153	0.205549
SER 131	-0.20001	0.190078
ALA 132	-0.05571	0.043007
ARG 133	-0.40697	0.260043
THR 134	-0.57526	0.553124
SER 135	-0.23621	0.233598
GLU 136	-0.31244	0.296126
ARG 137	-1.00287	0.985274
ALA 138	-0.68332	0.677869
ARG 139	-1.18386	1.17687
ALA 140	-0.7456	0.73797
GLY 141	-0.43444	0.429538
GLY 142	-0.304	0.296999
THR 143	-0.60511	0.588277
GLU 144	-0.73025	0.704821
GLU 145	-0.77557	0.765644
GLN 146	-0.29729	0.273393
GLY 147	-0.06121	0.050172
ILE 148	-0.09047	0.045509
CYS 149	-0.05718	0.030436
VAL 150	-0.03038	0.00519
ILE 151	-0.01976	0.006007
PRO 152	-0.02134	0.002268
ARG 153	-0.03041	0.020552
LEU 154	-0.01249	0.001956
VAL 155	-0.00655	0.001691
GLY 156	-0.00263	0.000952
SER 157	-0.00275	0.000571
VAL 158	-0.00224	0.000631
ALA 159	-0.0013	0.000415
TYR 160	-0.00351	0.001472
PRO 161	-0.00355	0.002616
LYS 162	-0.01351	0.011832
ALA 163	-0.00989	0.008436
GLU 164	-0.06384	0.062233
ARG 165	-0.08705	0.084969
ASP 166	-0.04038	0.036409
THR 167	-0.085	0.078812
CYS 168	-0.09175	0.08797
PRO 169	-0.05763	0.059696
VAL 170	-0.43117	0.42619
GLU 171	-0.48955	0.479244
GLY 172	-0.07757	0.072895
TRP 173	-0.19545	0.179854
LYS 174	-0.04971	0.042226
ASP 175	-0.0535	0.047687
CYS 176	-0.01588	0.012522
THR 178	-0.00795	0.004759
LYS 179	-0.05047	0.047017
LEU 180	-0.00392	0.002304
ARG 181	-0.00443	0.001529
VAL 182	-0.00371	0.001642
TRP 183	-0.00668	0.004793
GLU 184	-0.00178	0.000296
GLN 185	-0.00259	0.000212
VAL 186	-0.0015	0.000479
ASP 187	-0.00192	0.000448
PHE 188	-0.00404	0.00159
ASP 189	-0.00153	0.000637
VAL 190	-0.00185	0.000836
ILE 191	-0.00267	0.000715
VAL 192	-0.00394	0.001378
TYR 193	-0.00567	0.000154
VAL 194	-0.00661	0.000518
ASP 195	-0.00796	0.000355
ALA 196	-0.01233	0.002852
ASP 197	-0.01387	0.001865
CYS 198	-0.00698	0.0008
ILE 199	-0.028	0.005424
VAL 200	-0.02424	0.01259
LEU 201	-0.07652	0.057611
ARG 202	-0.26843	0.216072
PRO 203	-0.38092	0.37159
VAL 204	-0.03131	0.024719
ASP 205	0.008402	0.001856
GLU 206	-0.04184	0.038718
LEU 207	-0.00636	0.004195
PHE 208	-0.00849	0.005616
LEU 209	-0.00529	0.003872
ARG 210	-0.00333	0.001536
GLN 211	-0.00118	0.000387
PRO 212	-0.00073	0.000168
LEU 213	-0.00106	0.000288
PRO 214	-0.00078	0.000113
ALA 215	-0.0008	0.000168
PHE 216	-0.00187	0.000237
ALA 217	-0.00124	0.00016
PRO 218	-0.00189	0.000381
ASP 219	-0.00215	0.000443
ILE 220	-0.00371	0.001074
PHE 221	-0.00431	0.001166
PRO 222	-0.00335	0.001246
PRO 223	-0.0048	0.002547
ASP 224	-0.00256	0.000958
LYS 225	-0.00244	0.000759
PHE 226	-0.01449	0.012798
ASN 227	-0.00362	0.001515
ALA 228	-0.00479	0.003239
GLY 229	-0.00428	0.002539
VAL 230	-0.00735	0.004082

Residue	Average	SEM
ALA 231	-0.00244	0.001023
VAL 232	-0.00293	0.001165
LEU 233	-0.00205	0.000509
LYS 234	-0.00142	0.000429
PRO 235	-0.0011	0.000185
ASP 236	-0.00083	7.72E-05
LEU 237	-0.00073	3.21E-05
GLY 238	-0.00023	1.8E-05
GLU 239	-0.00058	3.48E-05
TYR 240	-0.00122	5.55E-05
GLY 241	-0.00028	3.68E-05
ASN 242	-0.00095	0.000202
MET 243	-0.00126	0.000433
VAL 244	-0.00118	0.000522
ALA 245	-0.00051	0.000163
ALA 246	-0.00092	0.000197
VAL 247	-0.00145	0.000987
GLU 248	-0.00119	0.00051
ARG 249	-0.00189	0.00087
LEU 250	-0.00172	0.00068
PRO 251	-0.00324	0.001741
SER 252	-0.003	0.001556
TYR 253	-0.0094	0.007112
ASP 254	-0.01428	0.009718
GLY 255	-0.00848	0.005362
GLY 256	-0.00798	0.006936
ASP 257	-0.02932	0.027411
THR 258	-0.07503	0.073465
GLY 259	-0.00593	0.005223
PHE 260	-0.00501	0.003667
LEU 261	-0.00502	0.003751
ASN 262	-0.00323	0.002097
ALA 263	-0.00138	0.000706
TYR 264	-0.00171	0.000749
PHE 265	-0.00197	0.000977
SER 266	-0.00095	0.000325
SER 267	-0.00089	0.000298
TRP 268	-0.00192	0.000411
TYR 269	-0.00372	0.00228
GLU 270	-0.00186	0.000946
ASN 271	-0.00071	0.000163
ALA 272	-0.0005	0.000104
ALA 273	-0.00059	0.000142
GLY 274	-0.0006	0.000158
ALA 275	-0.00071	0.000146
ARG 276	-0.00192	0.000451
LEU 277	-0.00266	0.00068
PRO 278	-0.00581	0.003003
PHE 279	-0.00529	0.001267
ARG 280	-0.01618	0.005834
TYR 281	-0.01942	0.009782
ASN 282	-0.00783	0.004167
ALA 283	-0.00566	0.001838
LEU 284	-0.02474	0.019728
ARG 285	-0.02372	0.004796
THR 286	-0.01905	0.013602
LEU 287	-0.01868	0.013042
TYR 288	-0.04192	0.014651
HIE 289	-0.11201	0.076302
MET 290	-0.0388	0.030804
THR 291	-0.01361	0.005544
TYR 292	-0.12229	0.08509
SER 293	-0.07024	0.038152
SER 294	-0.0637	0.040961
ARG 295	-0.08284	0.053208
LYS 296	-0.27175	0.163727
GLY 297	-0.14973	0.124456
TYR 298	-1.1385	1.121497
TRP 299	-0.06626	0.036263
ASP 300	0.015008	0.061028
ALA 301	-0.1074	0.095765
VAL 302	-0.36584	0.387199
LYS 303	-0.18241	0.122633
PRO 304	-0.2458	0.201356
ILE 305	-0.06714	0.046673
LYS 306	-0.0796	0.046173
ILE 307	-0.01321	0.004044
LEU 308	-0.01559	0.002216
HIE 309	-0.01362	0.004793
PHE 310	-0.02841	0.005344
CYS 311	-0.00813	0.002
SER 312	-0.01199	0.004655
SER 313	-0.02086	0.006317
PRO 314	-0.07441	0.025062
LYS 315	-0.10623	0.040135
PRO 316	-0.39084	0.225235
TRP 317	-1.46767	0.450037
GLU 318	-0.69254	0.269163
GLN 319	-0.63395	0.247477
PRO 320	-1.68424	0.739062
ALA 321	-0.64368	0.316871
LYS 322	-0.57165	0.224045
THR 323	-0.19851	0.063307
ASP 324	-0.45312	0.358854
LEU 325	-0.23524	0.181329
GLU 326	-0.16312	0.050576
GLU 327	-0.9623	0.36964
LEU 328	-0.96098	0.825795
TRP 329	-0.39234	0.078921
TRP 330	-2.36934	0.904458
LYS 331	-1.36258	0.527736
VAL 332	-0.51512	0.366042
PHE 333	-1.86617	0.398451
LEU 334	-3.35655	0.320711
THR 335	-1.58984	0.602785
GLY 336	-0.20384	0.086355
THR 337	-0.74821	0.437235
VAL 338	-0.66921	0.35672
PRO 339	-0.67516	0.264112
THR 340	-0.78357	0.434286
ASP 341	-0.92384	0.518908
SER 342	-0.64583	0.371553
ASP 343	-0.45942	0.299355
ILE 344	-0.52566	0.448989
VAL 345	-0.2649	0.114653

Residue	Average	SEM
MET 1	-2.05332	1.289112
SER 2	-1.04404	0.773047
LYS 3	-0.90106	0.571718
GLU 4	-0.29177	0.225568
ARG 5	-0.15229	0.10508
MET 6	-0.9757	0.830205
GLY 7	-0.27574	0.250968
ASP 8	-0.05931	0.044141
ALA 9	-0.03364	0.0275
ARG 10	-0.03315	0.017077
LYS 11	-0.07317	0.065274
VAL 12	-0.02396	0.006264
THR 13	-0.02689	0.008781
LEU 14	-0.05401	0.014075
VAL 15	-0.06882	0.014108
SER 16	-0.07643	0.021606
GLN 17	-0.4883	0.210899
GLU 18	-0.1422	0.061276
GLY 19	-0.04577	0.026908
ASP 20	-0.06522	0.045131
GLU 21	-0.0254	0.012002
PHE 22	-0.0428	0.02882
ASP 23	-0.00969	0.003566
VAL 24	-0.01072	0.002334
ASP 25	-0.03077	0.003049
ILE 26	-0.02202	0.009596
GLU 27	0.007582	0.013617
VAL 28	-0.01738	0.009134
ALA 29	-0.02439	0.010468
SER 30	-0.12146	0.099149
MET 31	-0.23962	0.211973
SER 32	-0.09515	0.022963
ALA 33	-0.55177	0.190272
LEU 34	-2.64398	0.687453
ILE 35	-0.67818	0.517178
LYS 36	-0.15263	0.046739
THR 37	-1.18529	0.313198
MET 38	-1.9048	0.586436
VAL 39	-0.32108	0.196956
GLU 40	-0.29018	0.168209
GLU 41	-0.67971	0.332086
ASP 42	-0.88037	0.566837
SER 43	-0.44085	0.306846
ASP 44	-0.3145	0.19328
CYS 45	-0.42963	0.265982
GLN 46	-0.7069	0.4339
GLU 47	-0.27883	0.170342
SER 48	-0.26243	0.185665
ILE 49	-0.47188	0.147371
PRO 50	-0.85417	0.292404
LEU 51	-1.28476	0.771919
PRO 52	-2.01803	0.592283
ASN 53	-2.19167	0.654619
VAL 54	-1.11142	0.704133
ASP 55	-0.38899	0.246505
THR 56	-0.3016	0.259863
CYS 57	-0.0867	0.056147
ILE 58	-0.15466	0.057623
LEU 59	-0.10374	0.061495
LYS 60	-0.02418	0.010774
LYS 61	-0.02288	0.003299
ILE 62	-0.04615	0.007487
ILE 63	-0.03647	0.023789
GLU 64	-0.01436	0.007816
TYR 65	-0.02055	0.003726
CYS 66	-0.02128	0.012659
GLU 67	-0.10967	0.105309
HIE 68	-0.01225	0.007775
HIE 69	-0.01779	0.010598
HIE 70	-0.08239	0.076475
ASN 71	-0.01322	0.010633
ASN 72	-0.0104	0.006594
PRO 73	-0.01072	0.006198
PRO 74	-0.04298	0.027808
GLU 75	-0.04074	0.028189
GLU 76	-0.05694	0.030738
ILE 77	-0.28893	0.273634
PRO 78	-0.30357	0.288854
LYS 79	-0.64288	0.582015
PRO 80	-0.34637	0.314625
LEU 81	-0.07909	0.052296
LYS 82	-0.13187	0.114546
SER 83	-0.0226	0.012501
SER 84	-0.01754	0.005132
ASN 85	-0.01734	0.006624
LEU 86	-0.03143	0.012686
ALA 87	-0.00495	0.001318
GLU 88	-0.00969	0.001421
VAL 89	-0.00931	0.001426
VAL 90	-0.0078	0.001137
SER 91	-0.00317	0.00027
GLU 92	-0.00351	0.000689
TRP 93	-0.00612	0.000603
ASP 94	-0.0073	0.000599
TYR 95	-0.01243	0.002205
GLN 96	-0.00628	0.001314
PHE 97	-0.01745	0.002757
ILE 98	-0.03132	0.00443
ASN 99	-0.01424	0.004289
GLU 100	-0.01221	0.003403
ASN 101	-0.02901	0.00625
SER 102	-0.05756	0.033044
ASP 103	-0.12087	0.058087
GLN 104	-1.39748	0.775209
LYS 105	-1.26843	0.582263
ILE 106	-0.56543	0.407562
LEU 107	-0.25789	0.049371
PHE 108	-3.28858	0.597252
ALA 109	-1.09902	0.497593
LEU 110	-0.33305	0.158
ILE 111	-1.23102	0.267017
LEU 112	-4.37578	0.140265
ALA 113	-0.59021	0.186238
ALA 114	-0.1861	0.024619
ASN 115	-2.15467	0.437791

Residue	Average	SEM
TYR 116	-3.76017	0.984188
LEU 117	-0.63624	0.296177
ASN 118	-0.74998	0.19957
ILE 119	-0.57704	0.492276
LYS 120	-0.5399	0.438967
PRO 121	-0.27606	0.262705
LEU 122	-0.10742	0.04644
LEU 123	-0.59039	0.128547
ASP 124	0.008341	0.100371
LEU 125	-0.08307	0.034925
SER 126	-0.2633	0.113201
VAL 127	-0.86827	0.205373
ALA 128	-0.20249	0.145088
LYS 129	-0.11913	0.021861
VAL 130	-0.86503	0.263826
ALA 131	-0.37395	0.227801
THR 132	-0.20973	0.122559
MET 133	-1.21083	0.55667
ILE 134	-2.14599	0.571011
LYS 135	-0.90839	0.279694
ALA 136	-0.69097	0.30768
LYS 137	-1.11354	0.488229
THR 138	-0.80614	0.576144
PRO 139	-0.25537	0.139244
GLU 140	-0.7998	0.57488
GLU 141	-0.62023	0.509825
ILE 142	-0.62117	0.396378
ARG 143	-1.42564	0.620587
ARG 144	-0.7497	0.390007
ILE 145	-0.67748	0.547044
PHE 146	-1.06579	0.8811
ASN 147	-0.25531	0.204679
ILE 148	-0.64204	0.408493
VAL 149	-0.42219	0.248277
ASN 150	-0.21957	0.163406
ASP 151	-0.05361	0.035199
PHE 152	-0.16126	0.130657
THR 153	-0.11842	0.103168
PRO 154	-0.11182	0.080063
GLU 155	-0.44839	0.267236
GLU 156	-0.17325	0.103753
GLU 157	-0.46614	0.362042
ALA 158	-0.24213	0.117802
GLN 159	-0.77853	0.397164
VAL 160	-0.64505	0.358523
ARG 161	-1.2895	0.58066
GLU 162	-0.27057	0.177241
GLU 163	-1.22016	0.49551
ASN 164	-0.91622	0.457696
LYS 165	-0.92024	0.634109
TRP 166	-2.89177	1.603855
CYS 167	-1.08289	0.410643
GLU 168	-0.97775	0.613081
ASP 169	-0.7047	0.296398
ALA 170	-0.48901	0.248246





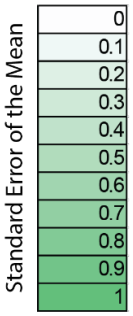


Figure 3.S12

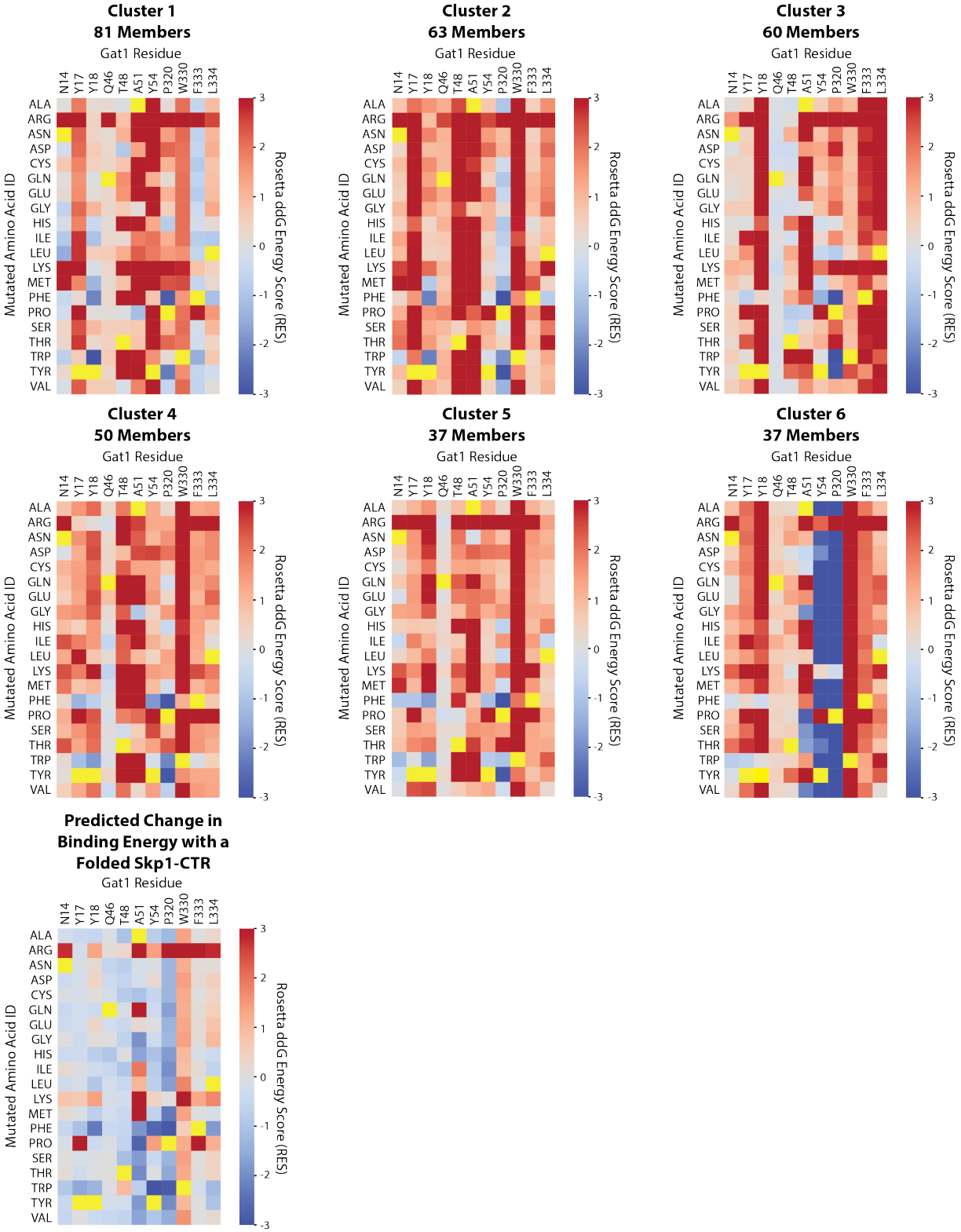

Cluster 1
81 Members
Cluster 2
63 Members
Cluster 3
60 Members
Cluster 4
50 Members
Cluster 5
37 Members
Cluster 6
37 Members
Predicted Change in Binding Energy with a Folded Skp1-CTR
Gat1 Residue
N14 Y17 Y18 Q46 T48 A51 Y54 P320 W330 F333 L334
Mutated Amino Acid ID
ALA ARG ASN ASP CYS GLN GLU GLY HIS ILE LEU LYS MET PHE PRO SER THR TRP TYR VAL
Rosetta ddG Energy Score (RES)
3 2 1 0 -1 -2 -3

Figure 3.S13

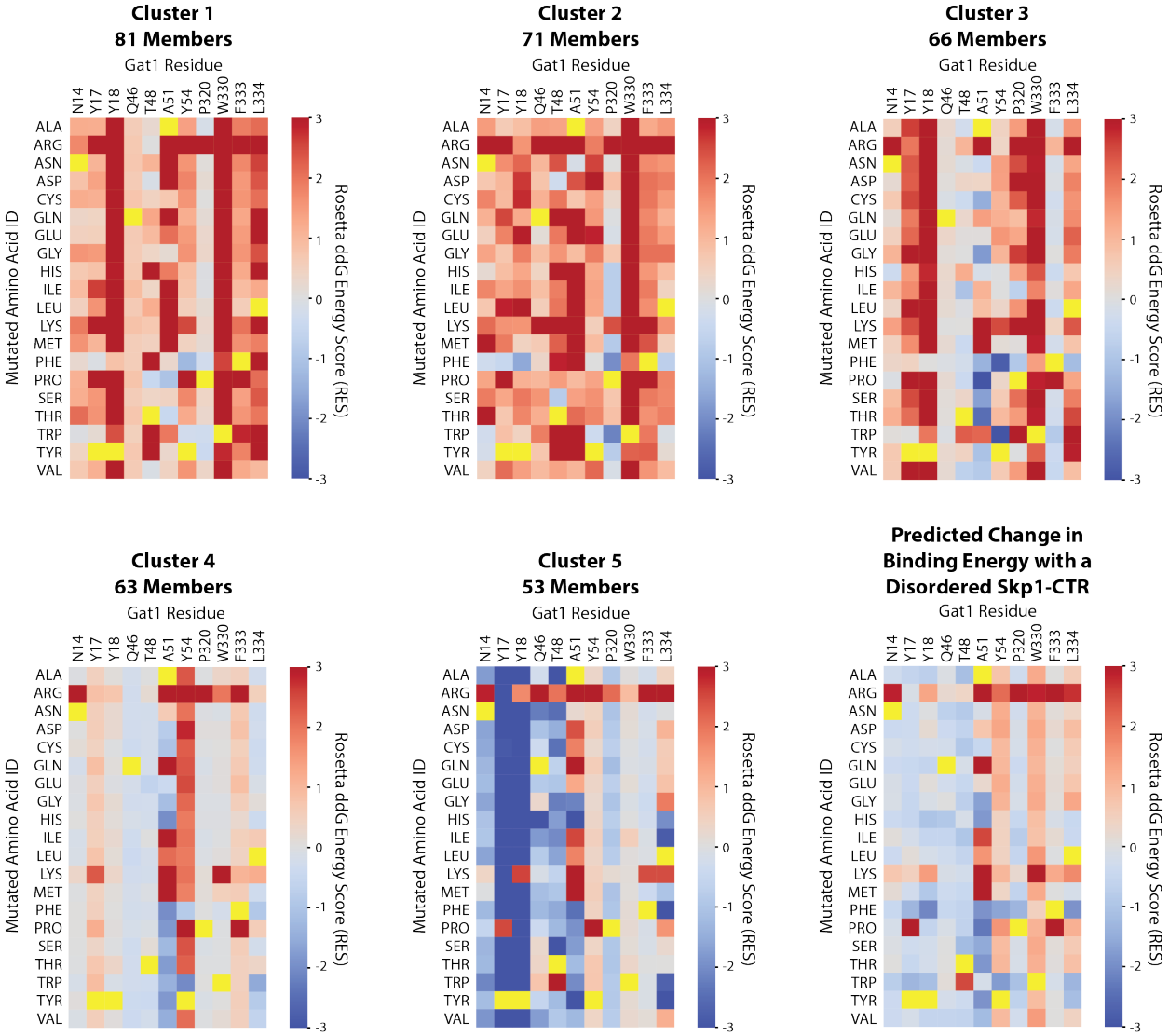

Cluster 1
81 Members
Cluster 2
71 Members
Cluster 3
66 Members
Cluster 4
63 Members
Cluster 5
53 Members
Predicted Change in Binding Energy with a Disordered Skp1-CTR
Gat1 Residue
N14 Y17 Y18 Q46 T48 A51 Y54 P320 W330 F333 L334
Mutated Amino Acid ID
ALA ARG ASN ASP CYS GLN GLU GLY HIS ILE LEU LYS MET PHE PRO SER THR TRP TYR VAL
Rosetta ddG Energy Score (RES)
3 2 1 0 -1 -2 -3

Figure 3.S14

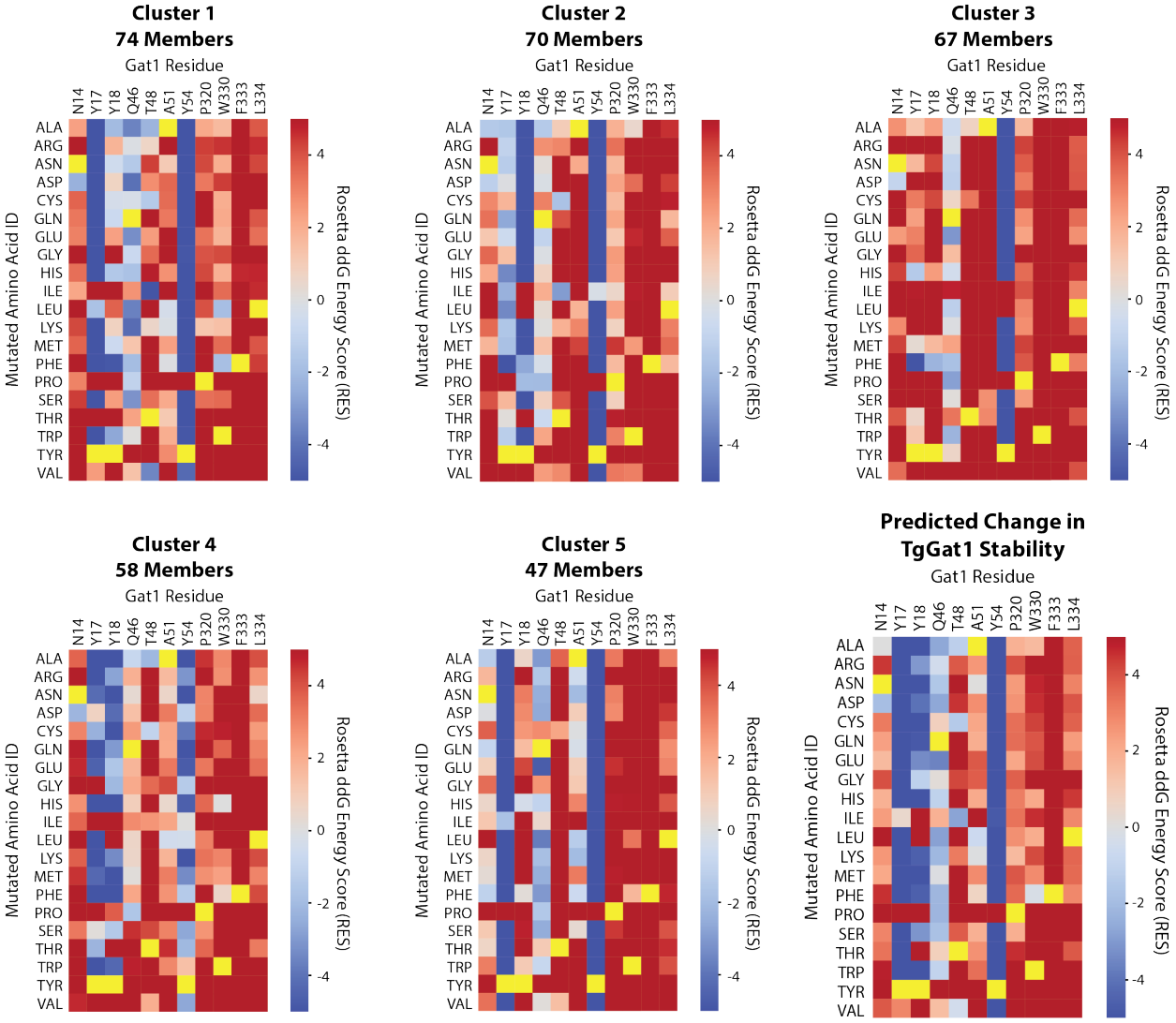

Cluster 1
74 Members
Cluster 2
70 Members
Cluster 3
67 Members
Cluster 4
58 Members
Cluster 5
47 Members
Predicted Change in
TgGat1 Stability
Gat1 Residue
N14 Y17 Y18 Q46 T48 A51 Y54 P320 W330 F333 L334
Mutated Amino Acid ID
ALA ARG ASN ASP CYS GLN GLU GLY HIS ILE LEU LYS MET PHE PRO SER THR TRP TYR VAL
Rosetta ddG Energy Score (RES)
4 2 0 -2 -4

Figure 3.S15

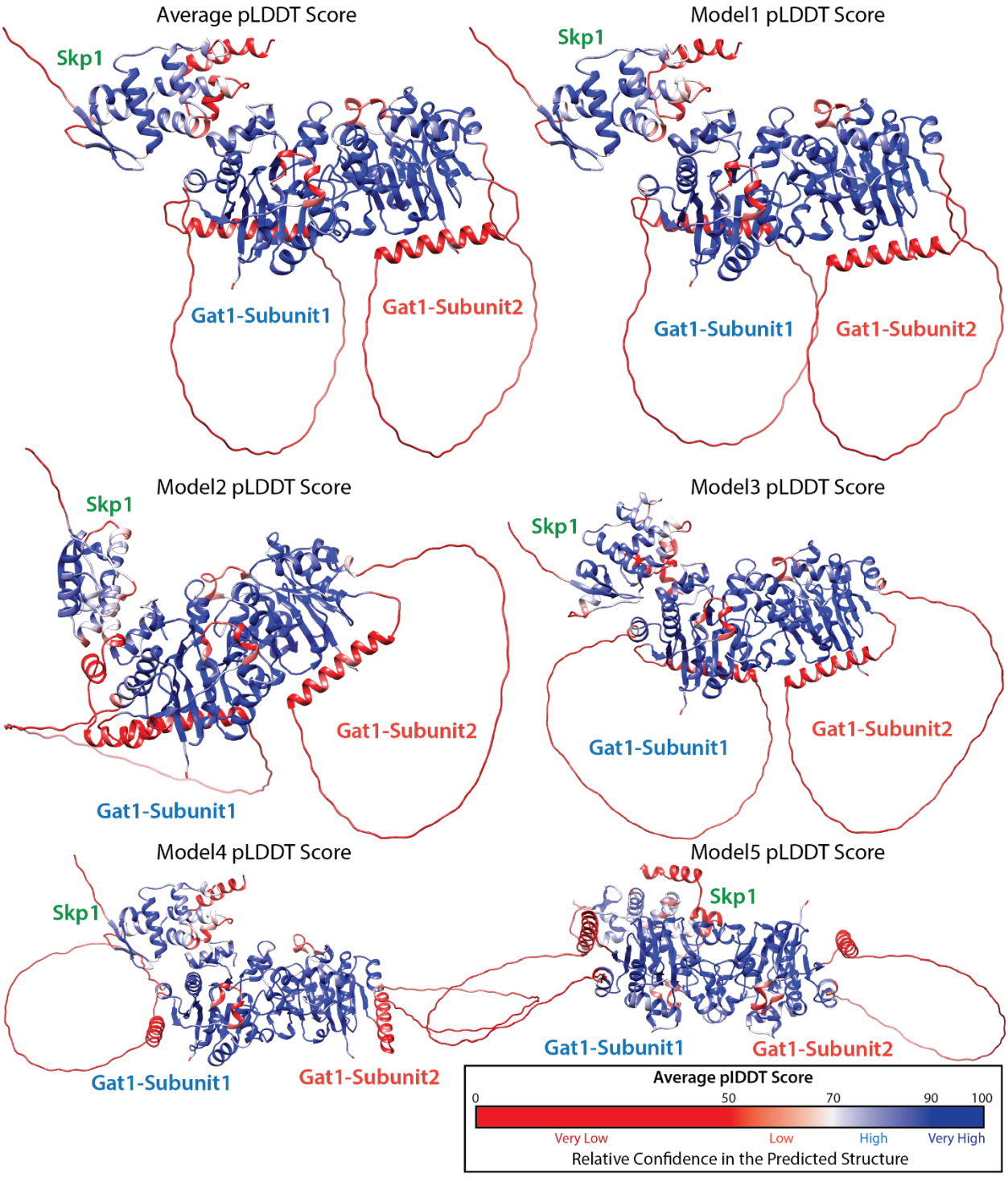

Average pLDDT Score
Skp1
Gat1-Subunit1
Gat1-Subunit2
Model1 pLDDT Score
Skp1
Gat1-Subunit1
Gat1-Subunit2
Model2 pLDDT Score
Skp1
Gat1-Subunit2
Gat1-Subunit1
Model3 pLDDT Score
Skp1
Gat1-Subunit1
Gat1-Subunit2
Model4 pLDDT Score
Skp1
Gat1-Subunit1
Gat1-Subunit2
Model5 pLDDT Score
Skp1
Gat1-Subunit1
Gat1-Subunit2
Average pIDDT Score
0
50
70
90
100
Very Low
Low
High
Very High
Relative Confidence in the Predicted Structure

Figure 3.S16

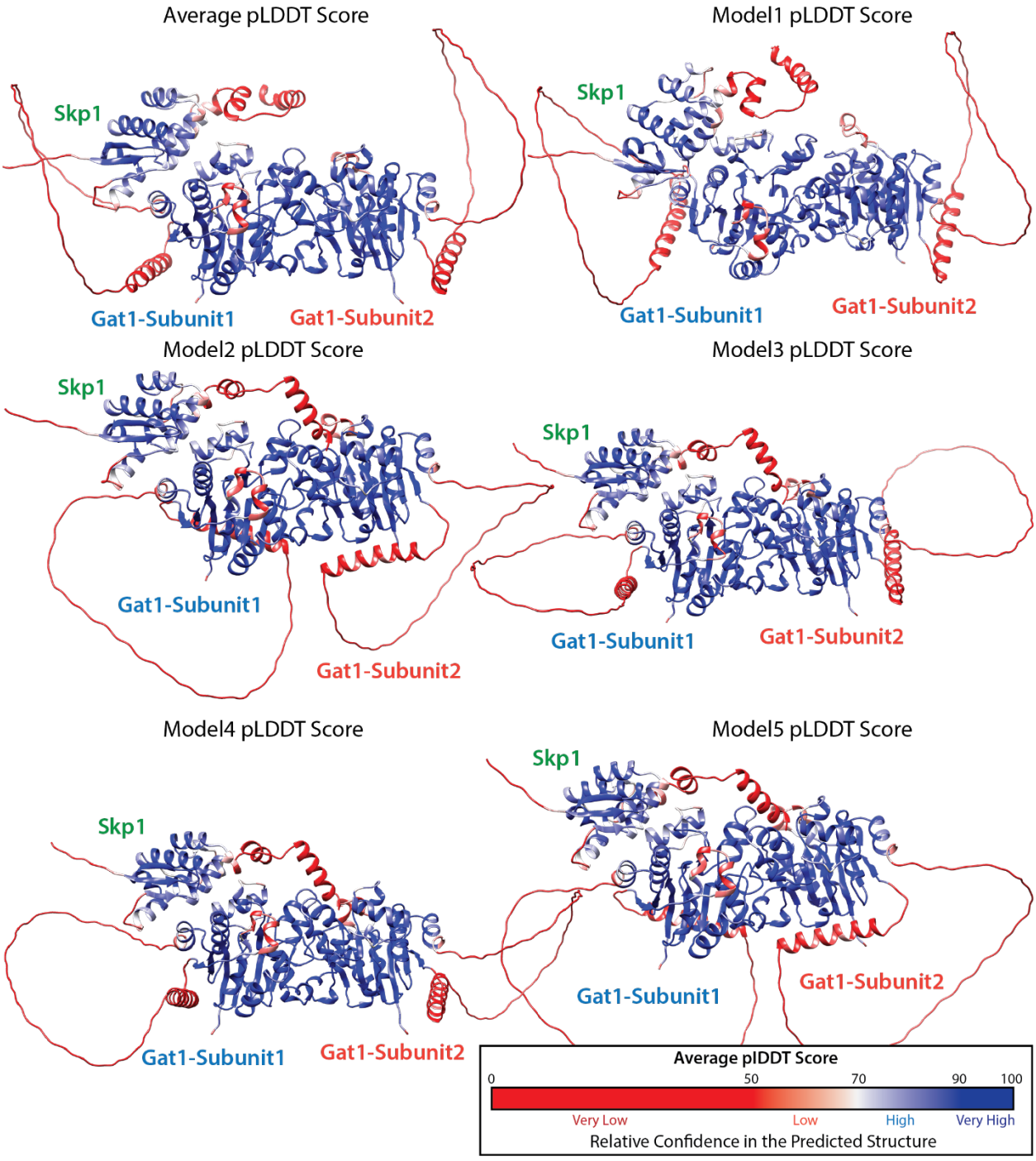

Average pLDDT Score
Skp1
Gat1-Subunit1
Gat1-Subunit2
Model1 pLDDT Score
Skp1
Gat1-Subunit1
Gat1-Subunit2
Model2 pLDDT Score
Skp1
Gat1-Subunit1
Gat1-Subunit2
Model3 pLDDT Score
Skp1
Gat1-Subunit1
Gat1-Subunit2
Model4 pLDDT Score
Skp1
Gat1-Subunit1
Gat1-Subunit2
Model5 pLDDT Score
Skp1
Gat1-Subunit1
Gat1-Subunit2
Average plDDT Score
0
50
70
90
100
Very Low
Low
High
Very High
Relative Confidence in the Predicted Structure

Figure 3.S17

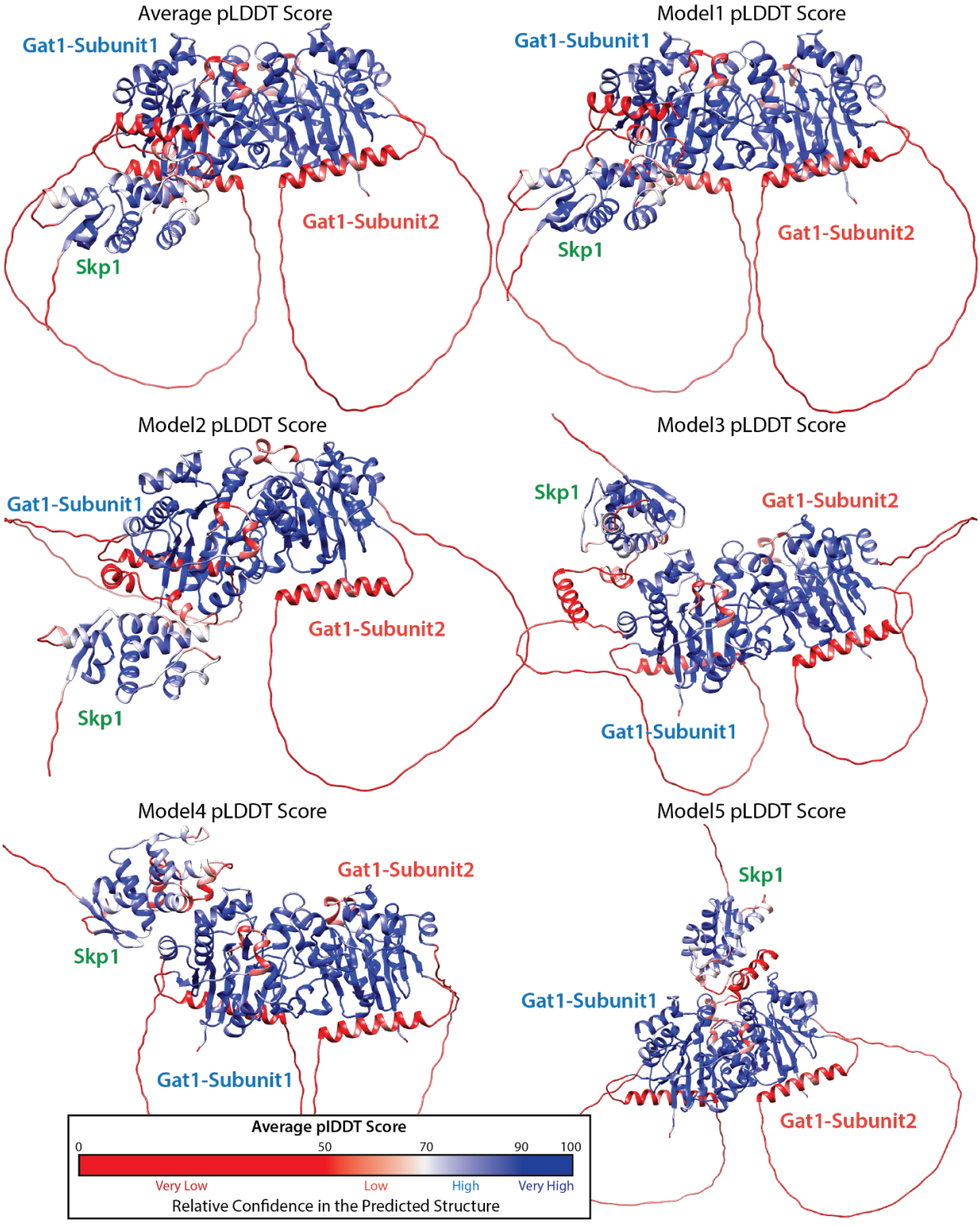
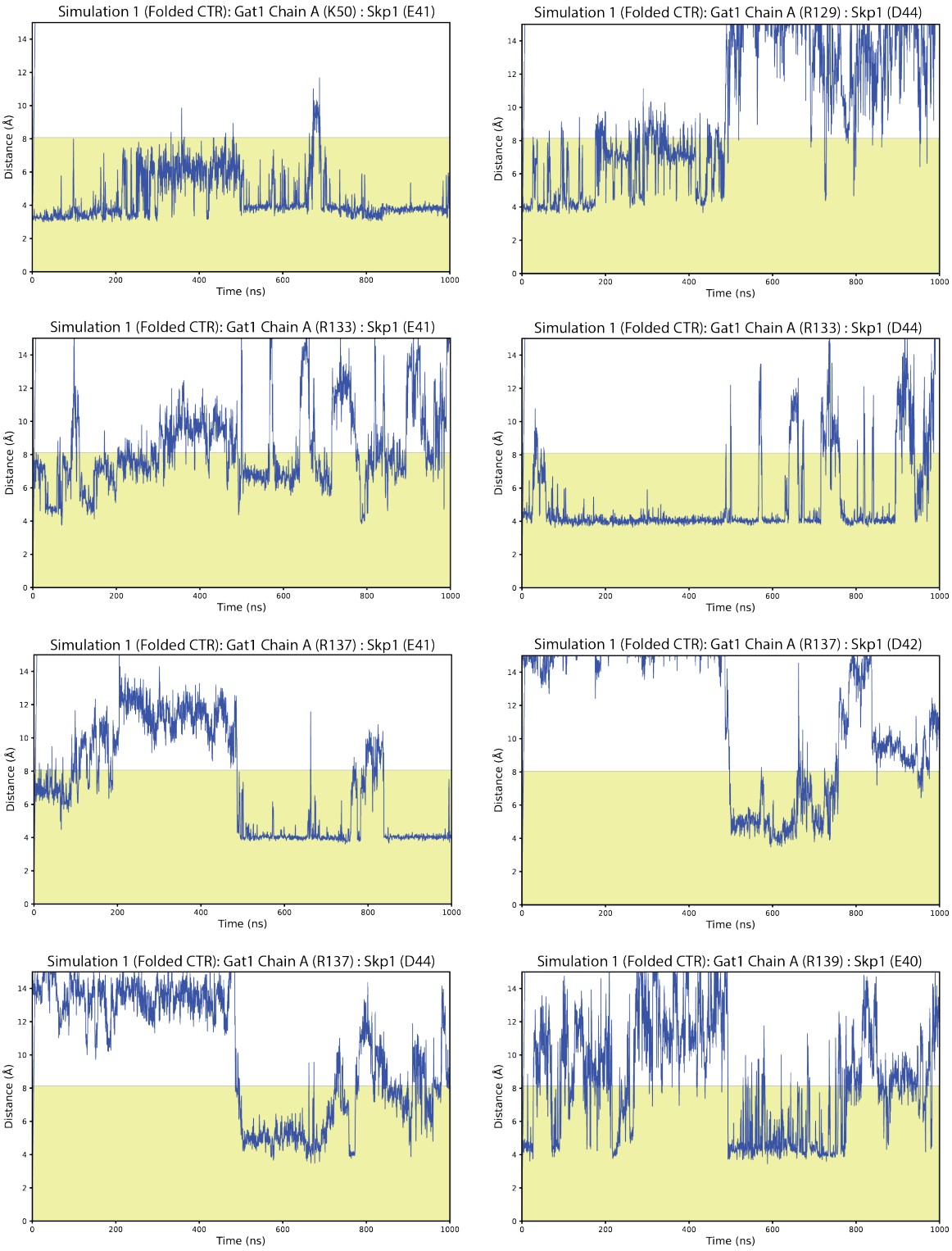
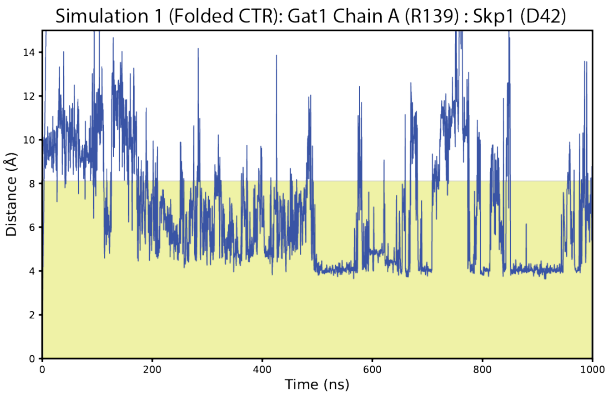
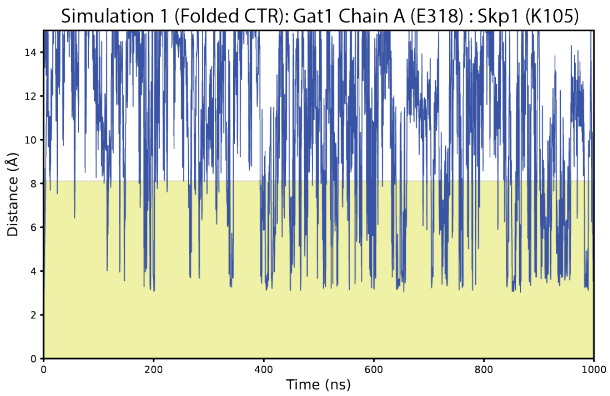
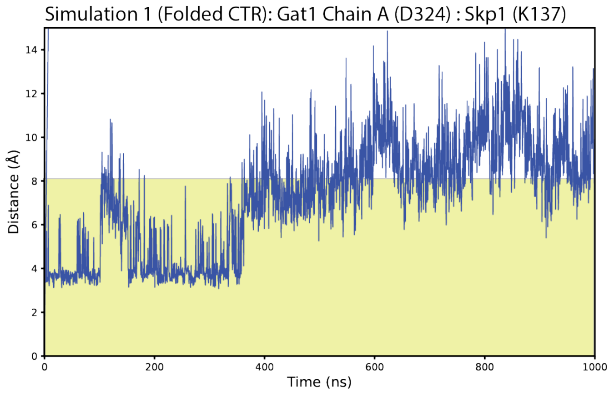

Average pLDDT Score
Gat1-Subunit1
Gat1-Subunit2
Skp1
Model1 pLDDT Score
Gat1-Subunit1
Skp1
Gat1-Subunit2
Model2 pLDDT Score
Gat1-Subunit1
Gat1-Subunit2
Skp1
Model3 pLDDT Score
Skp1
Gat1-Subunit2
Gat1-Subunit1
Model4 pLDDT Score
Gat1-Subunit2
Skp1
Gat1-Subunit1
Model5 pLDDT Score
Skp1
Gat1-Subunit1
Gat1-Subunit2
Average pIDDT Score
0
50
70
90
100
Very Low
Low
High
Very High
Relative Confidence in the Predicted Structure

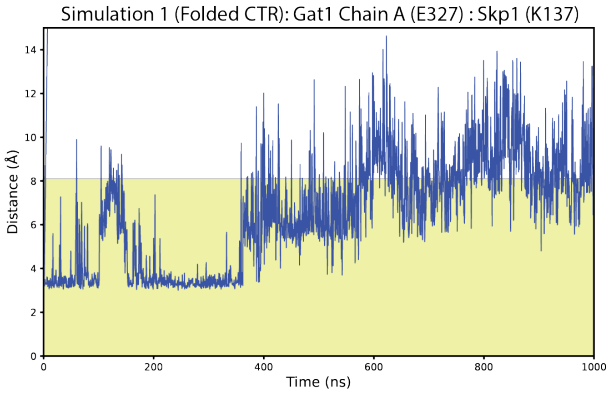
Figure 3.S18

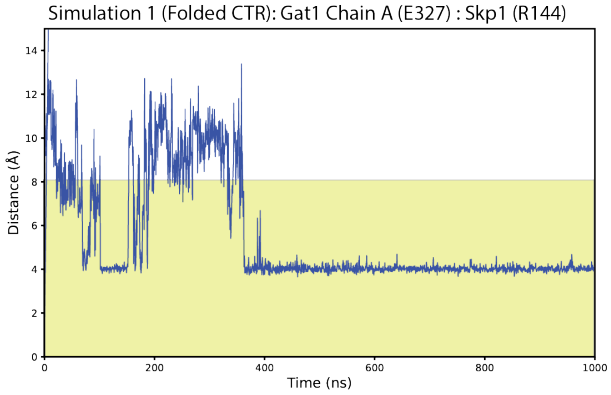

Simulation 1 (Folded CTR): Gat1 Chain A (K50) : Skp1 (E41)
Simulation 1 (Folded CTR): Gat1 Chain A (R129) : Skp1 (D44)
Simulation 1 (Folded CTR): Gat1 Chain A (R133) : Skp1 (E41)
Simulation 1 (Folded CTR): Gat1 Chain A (R133) : Skp1 (D44)
Simulation 1 (Folded CTR): Gat1 Chain A (R137) : Skp1 (E41)
Simulation 1 (Folded CTR): Gat1 Chain A (R137) : Skp1 (D42)
Simulation 1 (Folded CTR): Gat1 Chain A (R137) : Skp1 (D44)
Simulation 1 (Folded CTR): Gat1 Chain A (R139) : Skp1 (E40)
Distance (Å)
Time (ns)

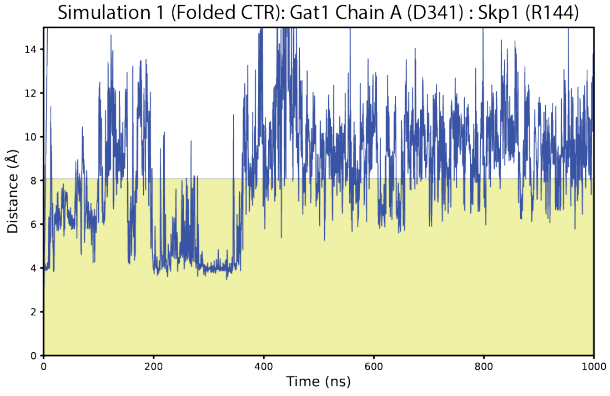

Simulation 1 (Folded CTR): Gat1 Chain A (R139) : Skp1 (D42)
Distance (Å)
Time (ns)

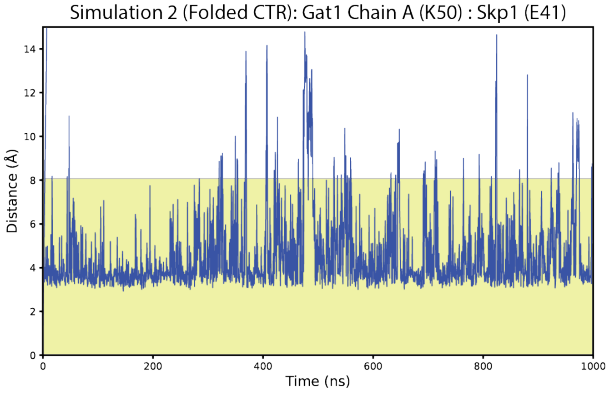

Simulation 1 (Folded CTR): Gat1 Chain A (E318) : Skp1 (K105)
Distance (Å)
Time (ns)

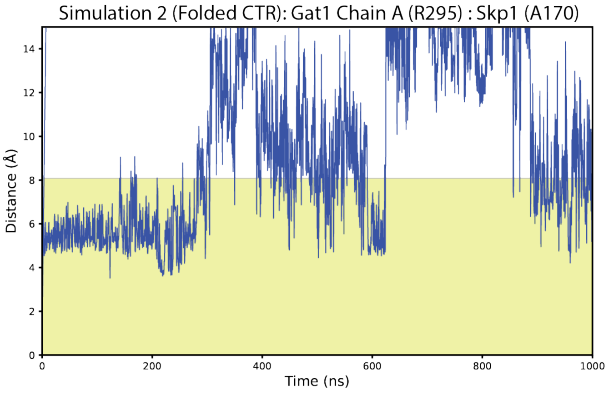

Simulation 1 (Folded CTR): Gat1 Chain A (D324) : Skp1 (K137)
Distance (Å)
Time (ns)

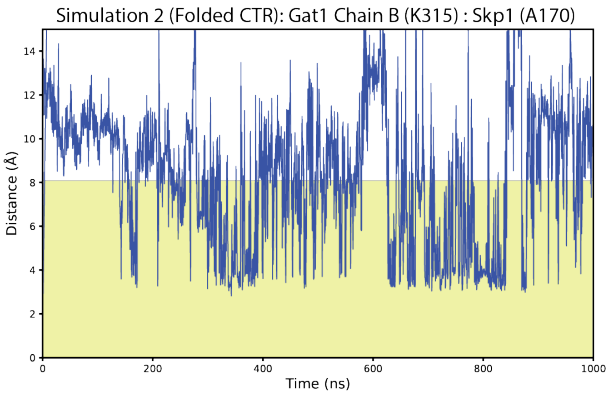

Simulation 1 (Folded CTR): Gat1 Chain A (E327) : Skp1 (K137)
Distance (Å)
Time (ns)

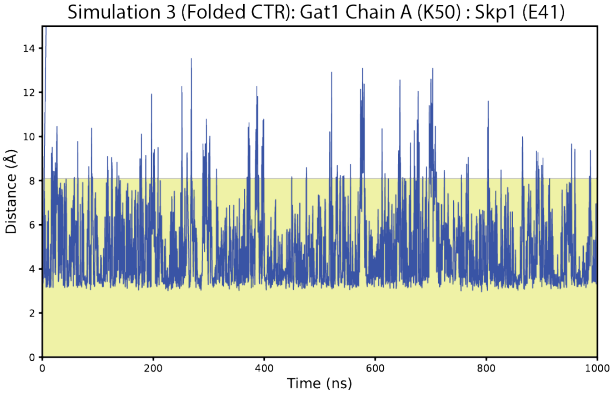

Simulation 1 (Folded CTR): Gat1 Chain A (E327) : Skp1 (R144)
Distance (Å)
Time (ns)

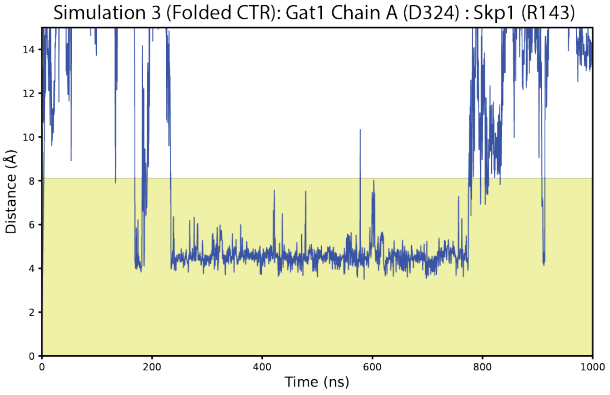

Simulation 1 (Folded CTR): Gat1 Chain A (D341) : Skp1 (R144)
Distance (Å)
Time (ns)

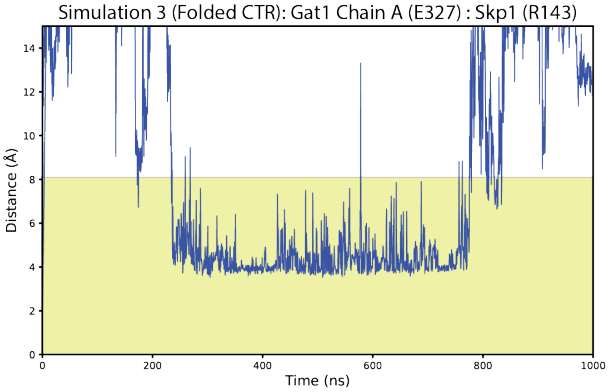

Simulation 2 (Folded CTR): Gat1 Chain A (K50) : Skp1 (E41)
Distance (Å)
Time (ns)

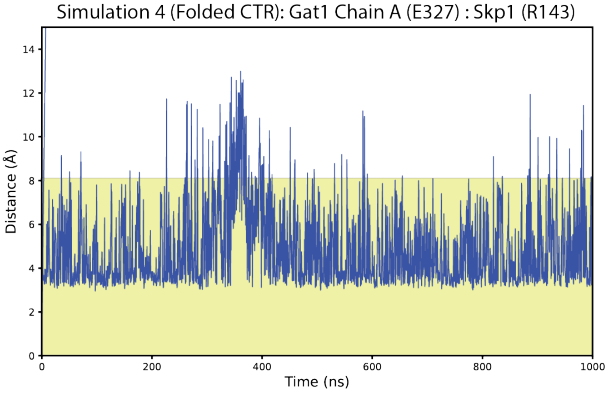

Simulation 2 (Folded CTR): Gat1 Chain A (R295) : Skp1 (A170)
Distance (Å)
Time (ns)

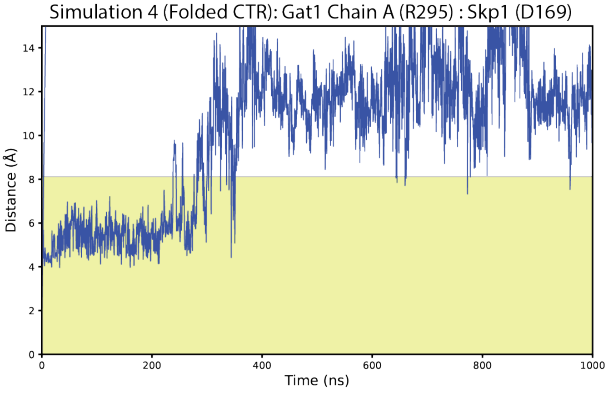

Simulation 2 (Folded CTR): Gat1 Chain B (K315) : Skp1 (A170)
Distance (Å)
Time (ns)

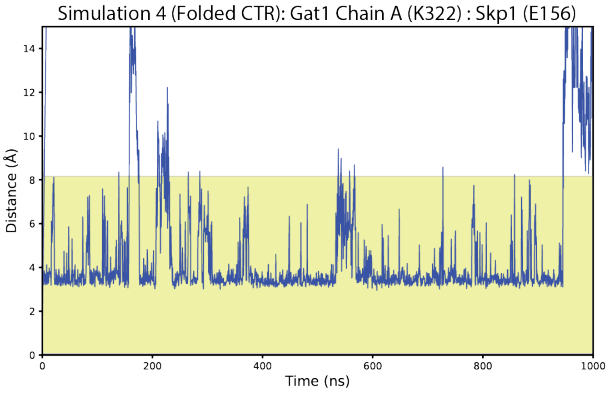

Simulation 3 (Folded CTR): Gat1 Chain A (K50) : Skp1 (E41)
Distance (Å)
Time (ns)

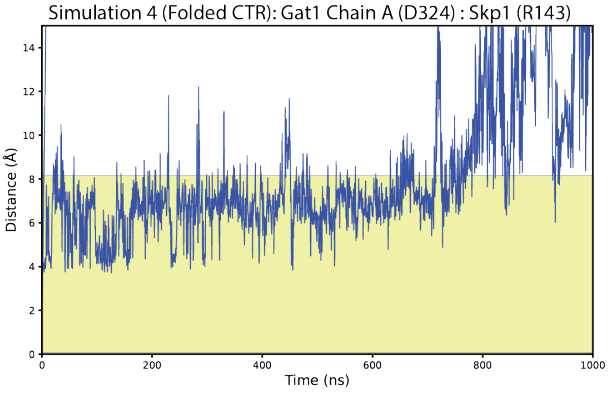

Simulation 3 (Folded CTR): Gat1 Chain A (D324) : Skp1 (R143)
Distance (Å)
Time (ns)

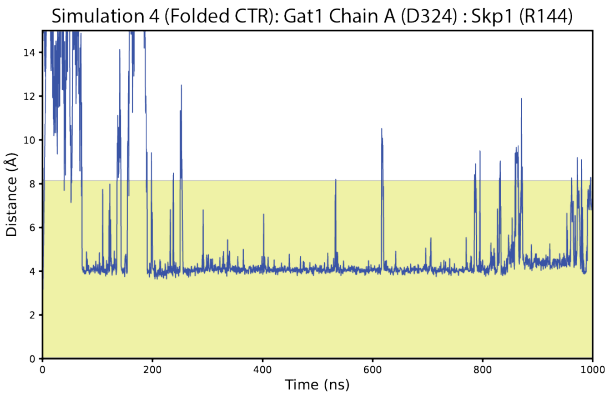

Simulation 3 (Folded CTR): Gat1 Chain A (E327) : Skp1 (R143)
Distance (Å)
Time (ns)

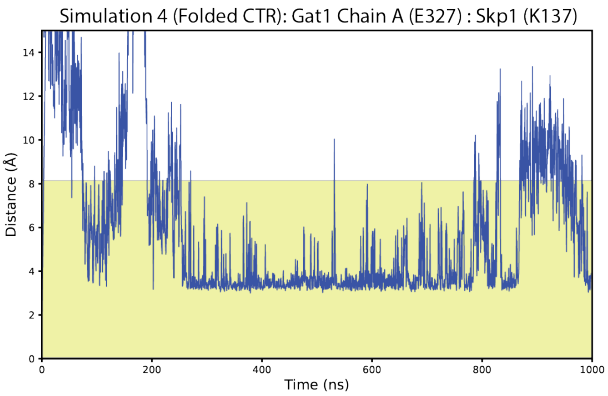

Simulation 4 (Folded CTR): Gat1 Chain A (E327) : Skp1 (R143)
Distance (Å)
Time (ns)

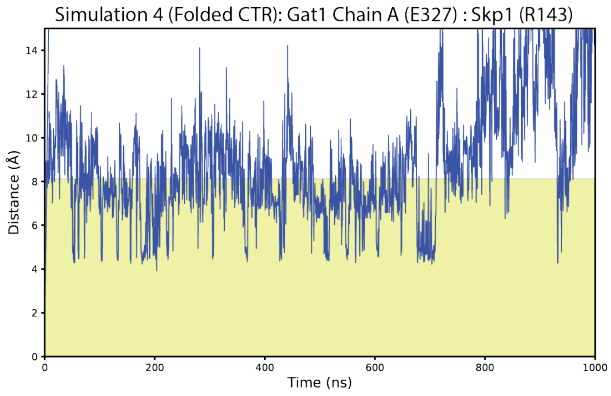

Simulation 4 (Folded CTR): Gat1 Chain A (R295) : Skp1 (D169)
Distance (Å)
Time (ns)

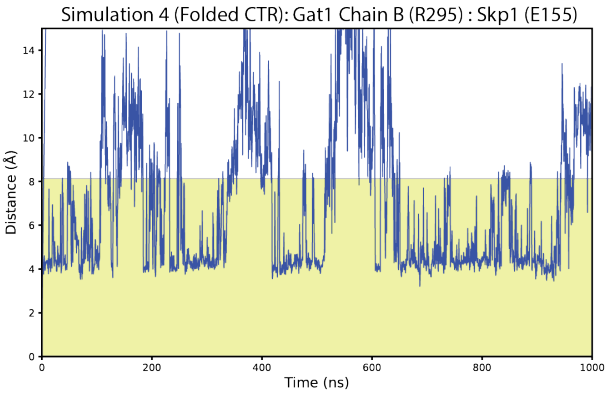

Simulation 4 (Folded CTR): Gat1 Chain A (K322) : Skp1 (E156)
Distance (Å)
Time (ns)

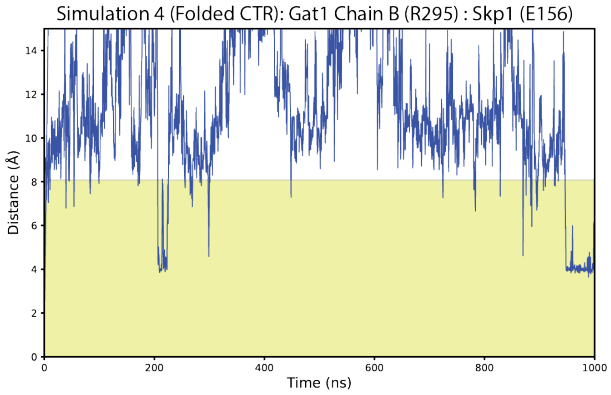

Simulation 4 (Folded CTR): Gat1 Chain A (D324) : Skp1 (R143)
Distance (Å)
Time (ns)

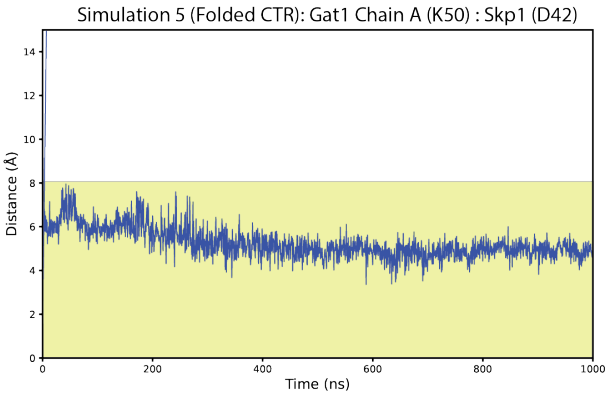

Simulation 4 (Folded CTR): Gat1 Chain A (D324) : Skp1 (R144)
Distance (Å)
Time (ns)

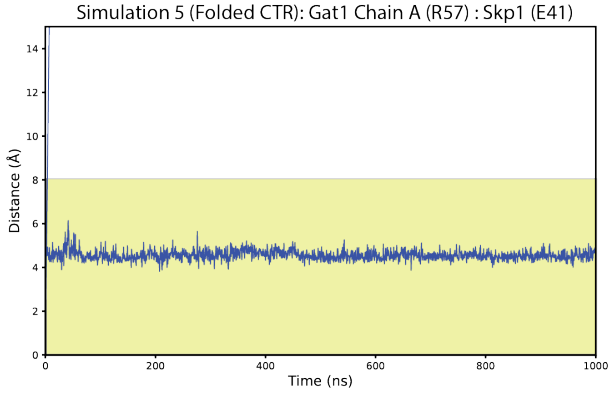

Simulation 4 (Folded CTR): Gat1 Chain A (E327) : Skp1 (K137)
Distance (Å)
Time (ns)

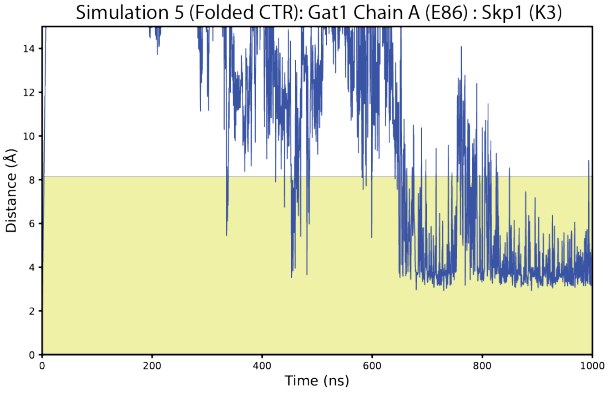

Simulation 4 (Folded CTR): Gat1 Chain A (E327) : Skp1 (R143)
Distance (Å)
Time (ns)

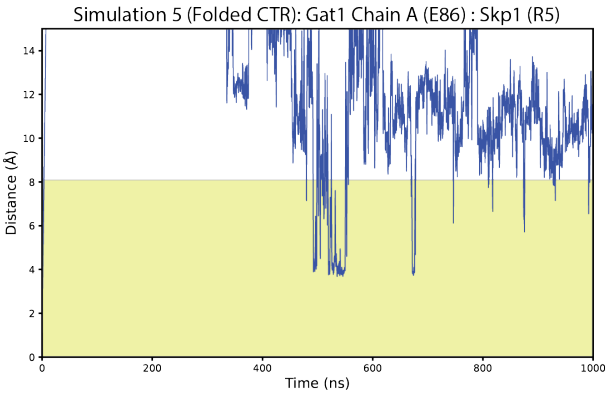

Simulation 4 (Folded CTR): Gat1 Chain B (R295) : Skp1 (E155)
Distance (Å)
Time (ns)

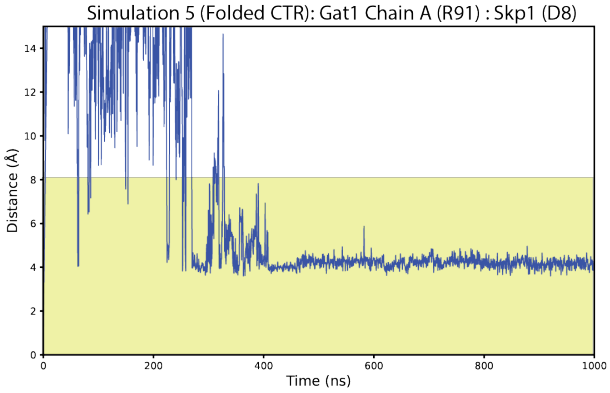

Simulation 4 (Folded CTR): Gat1 Chain B (R295) : Skp1 (E156)
Distance (Å)
Time (ns)

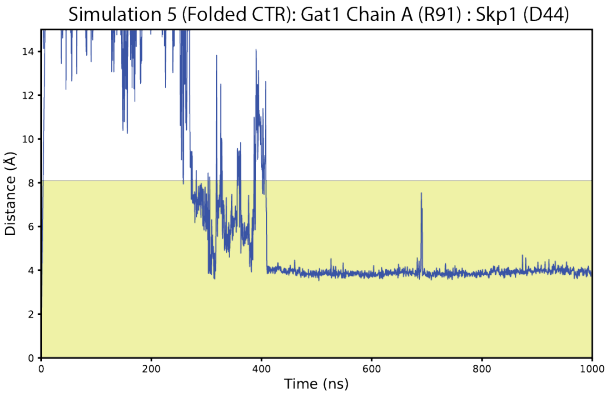

Simulation 5 (Folded CTR): Gat1 Chain A (K50) : Skp1 (D42)
Distance (Å)
Time (ns)

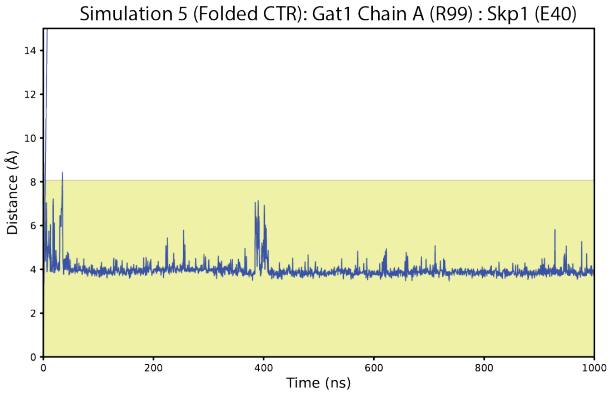

Simulation 5 (Folded CTR): Gat1 Chain A (R57) : Skp1 (E41)
Distance (Å)
Time (ns)

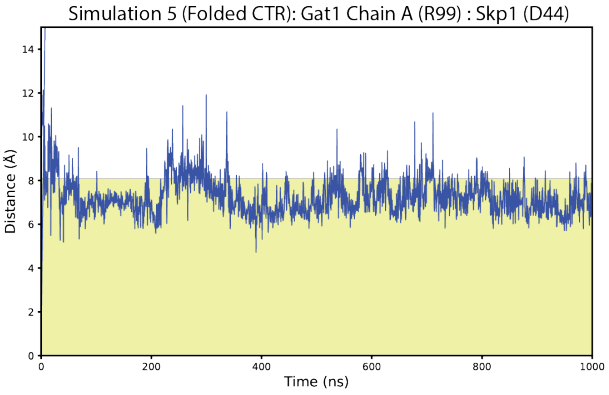

Simulation 5 (Folded CTR): Gat1 Chain A (E86) : Skp1 (K3)
Distance (Å)
Time (ns)

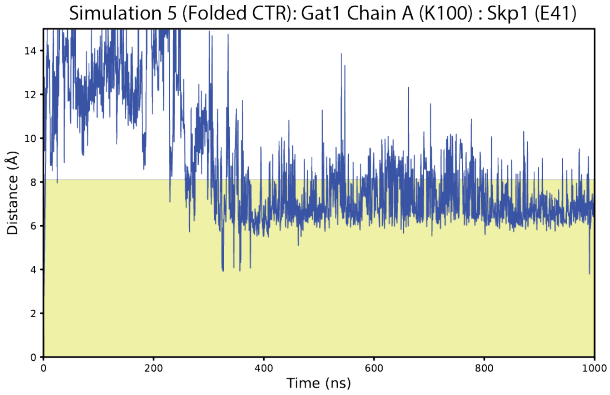

Simulation 5 (Folded CTR): Gat1 Chain A (E86) : Skp1 (R5)
Distance (Å)
Time (ns)

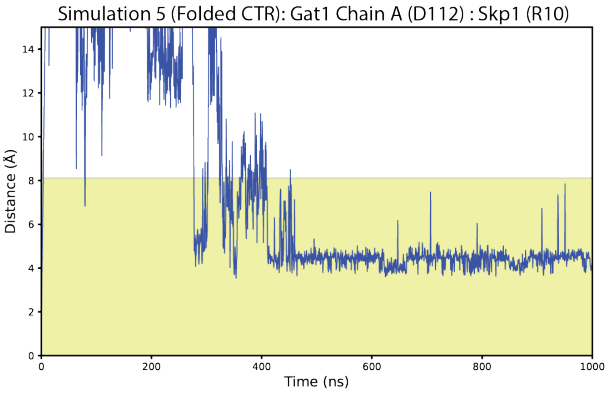

Simulation 5 (Folded CTR): Gat1 Chain A (R91) : Skp1 (D8)
Distance (Å)
Time (ns)

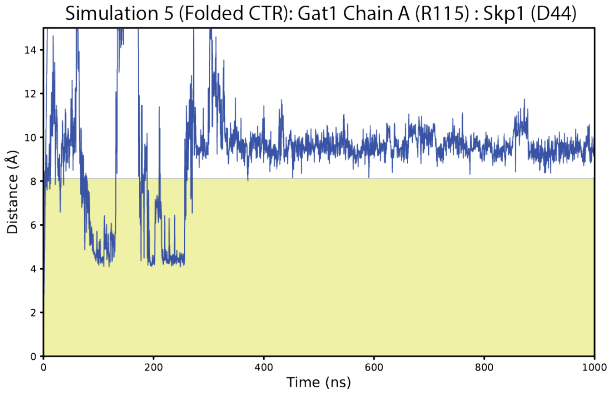

Simulation 5 (Folded CTR): Gat1 Chain A (R91) : Skp1 (D44)
Distance (Å)
Time (ns)

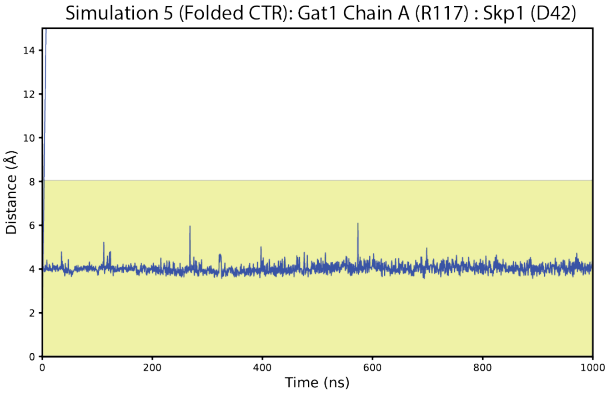

Simulation 5 (Folded CTR): Gat1 Chain A (R99) : Skp1 (E40)
Distance (Å)
Time (ns)

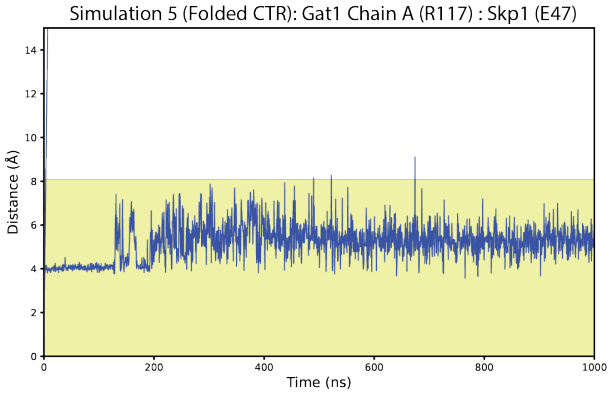

Simulation 5 (Folded CTR): Gat1 Chain A (R99) : Skp1 (D44)
Distance (Å)
Time (ns)

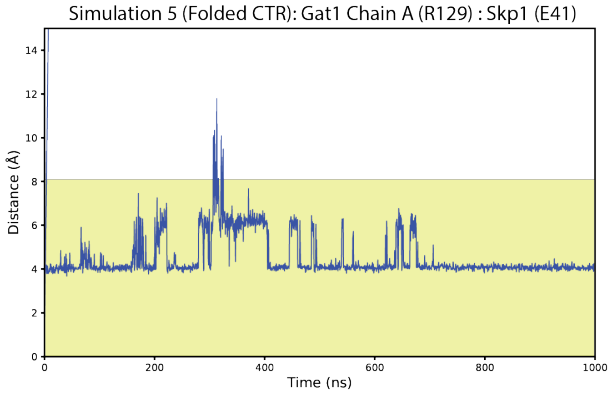

Simulation 5 (Folded CTR): Gat1 Chain A (K100) : Skp1 (E41)
Distance (Å)
Time (ns)

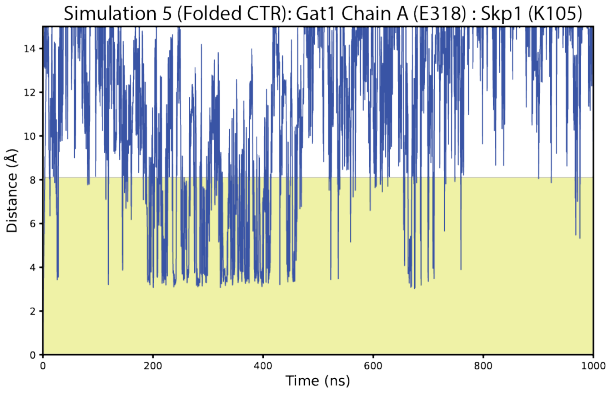

Simulation 5 (Folded CTR): Gat1 Chain A (D112) : Skp1 (R10)
Distance (Å)
Time (ns)

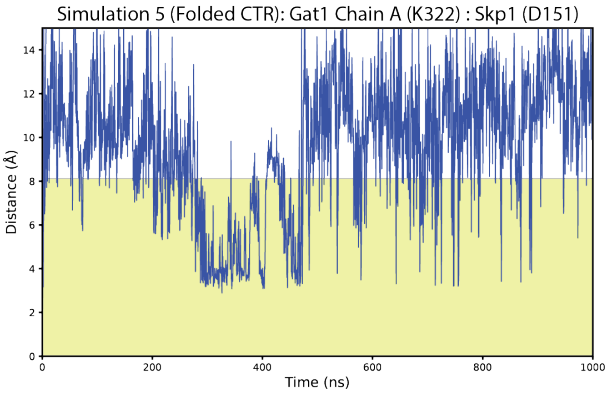

Simulation 5 (Folded CTR): Gat1 Chain A (R115) : Skp1 (D44)
Distance (Å)
Time (ns)

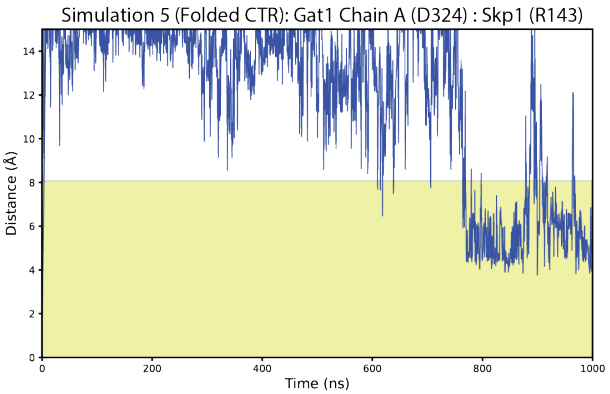

Simulation 5 (Folded CTR): Gat1 Chain A (R117) : Skp1 (D42)
Distance (Å)
Time (ns)

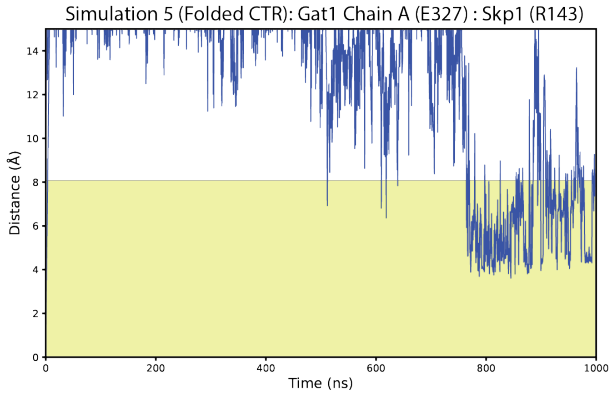

Simulation 5 (Folded CTR): Gat1 Chain A (R117) : Skp1 (E47)
Distance (Å)
Time (ns)

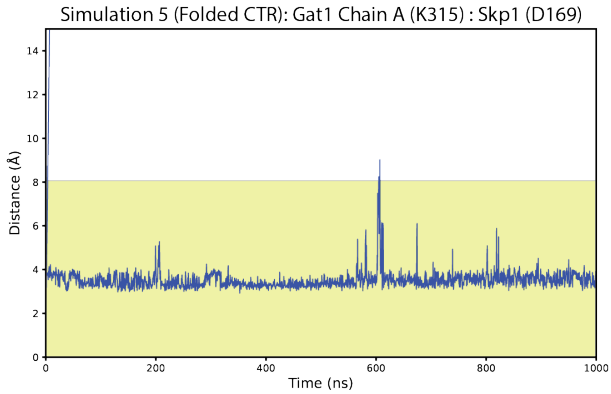

Simulation 5 (Folded CTR): Gat1 Chain A (R129) : Skp1 (E41)
Distance (Å)
Time (ns)

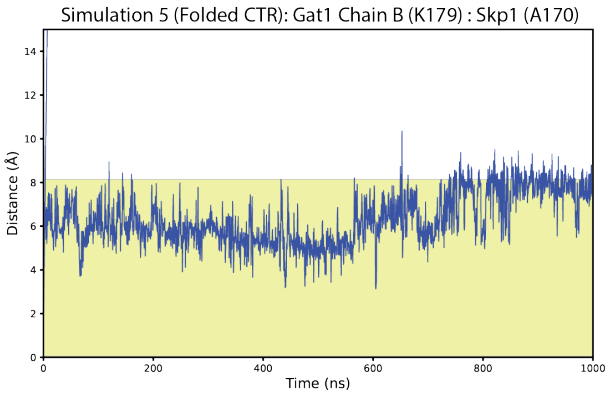

Simulation 5 (Folded CTR): Gat1 Chain A (E318) : Skp1 (K105)
Distance (Å)
Time (ns)

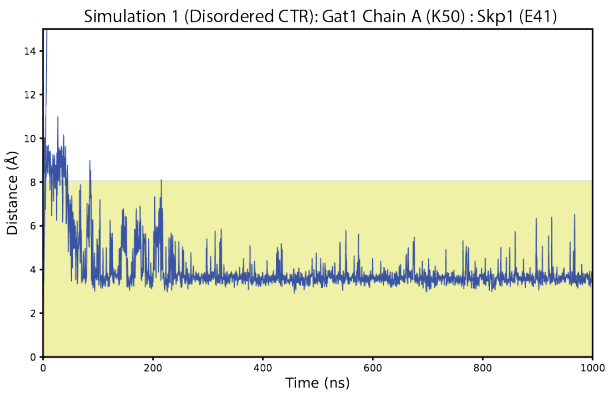

Simulation 5 (Folded CTR): Gat1 Chain A (K322) : Skp1 (D151)
Distance (Å)
Time (ns)

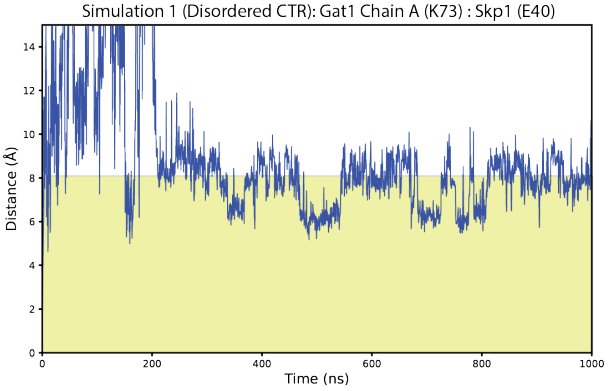

Simulation 5 (Folded CTR): Gat1 Chain A (D324) : Skp1 (R143)
Distance (Å)
Time (ns)

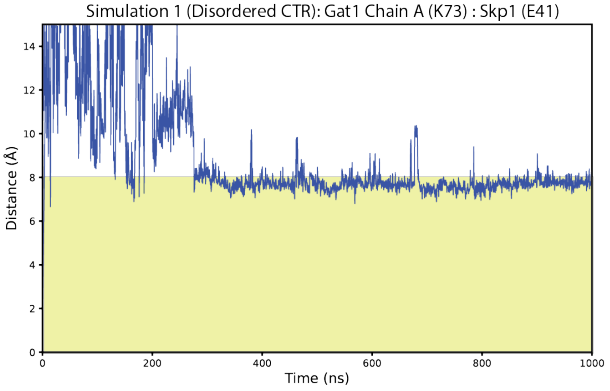

Simulation 5 (Folded CTR): Gat1 Chain A (E327) : Skp1 (R143)
Distance (Å)
Time (ns)

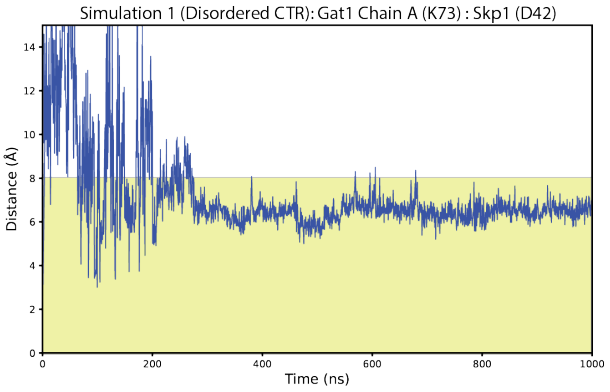

Simulation 5 (Folded CTR): Gat1 Chain A (K315) : Skp1 (D169)
Distance (Å)
Time (ns)

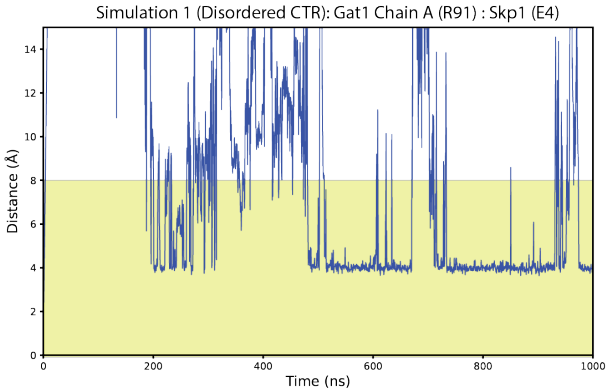

Simulation 5 (Folded CTR): Gat1 Chain B (K179) : Skp1 (A170)
Distance (Å)
Time (ns)

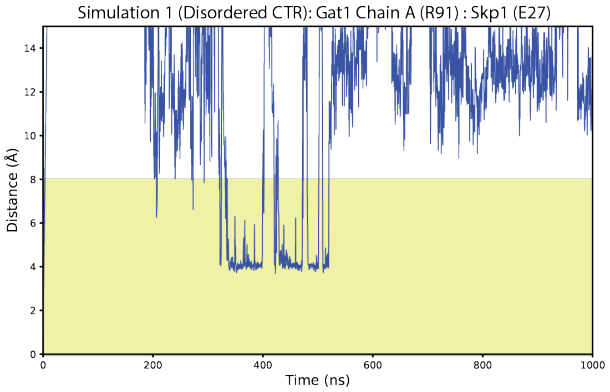

Simulation 1 (Disordered CTR): Gat1 Chain A (K50) : Skp1 (E41)
Distance (Å)
Time (ns)

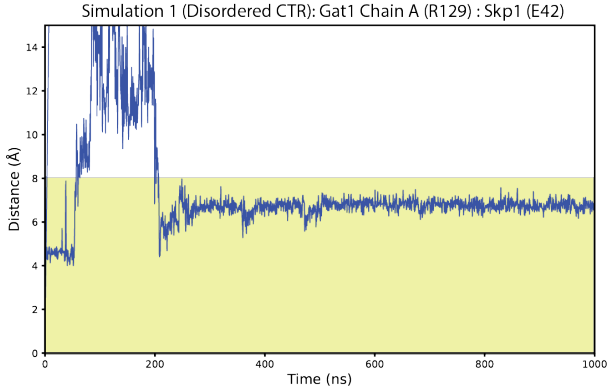

Simulation 1 (Disordered CTR): Gat1 Chain A (K73) : Skp1 (E40)
Distance (Å)
Time (ns)

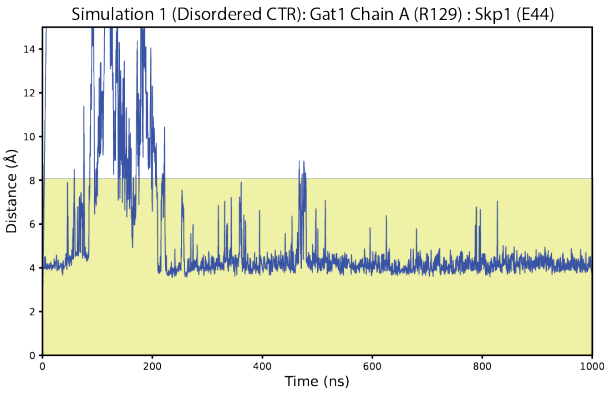

Simulation 1 (Disordered CTR): Gat1 Chain A (K73) : Skp1 (E41)
Distance (Å)
Time (ns)

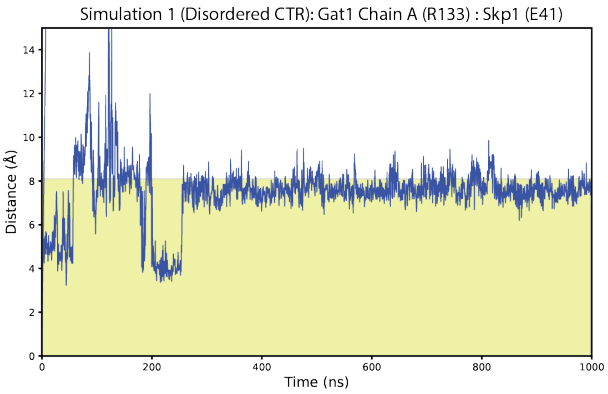

Simulation 1 (Disordered CTR): Gat1 Chain A (K73) : Skp1 (D42)
Distance (Å)
Time (ns)

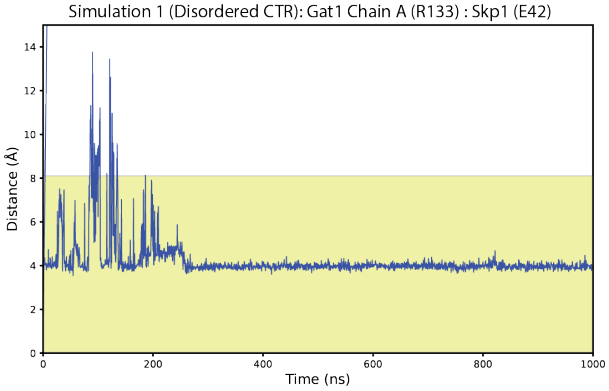

Simulation 1 (Disordered CTR): Gat1 Chain A (R91) : Skp1 (E4)
Distance (Å)
Time (ns)

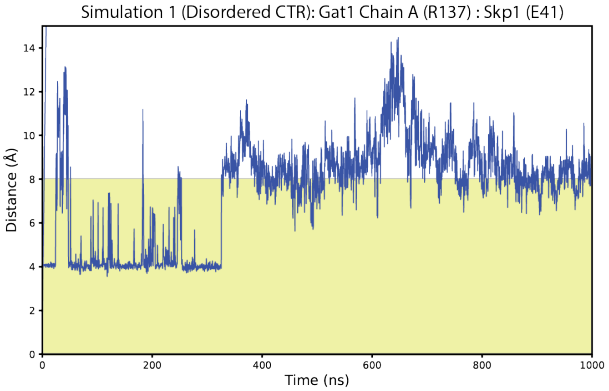

Simulation 1 (Disordered CTR): Gat1 Chain A (R91) : Skp1 (E27)
Distance (Å)
Time (ns)

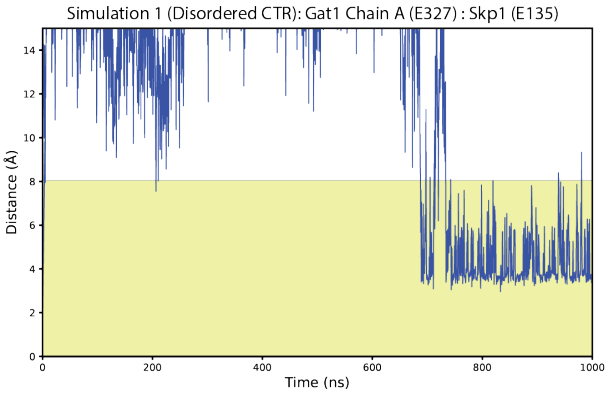

Simulation 1 (Disordered CTR): Gat1 Chain A (R129) : Skp1 (E42)
Distance (Å)
Time (ns)

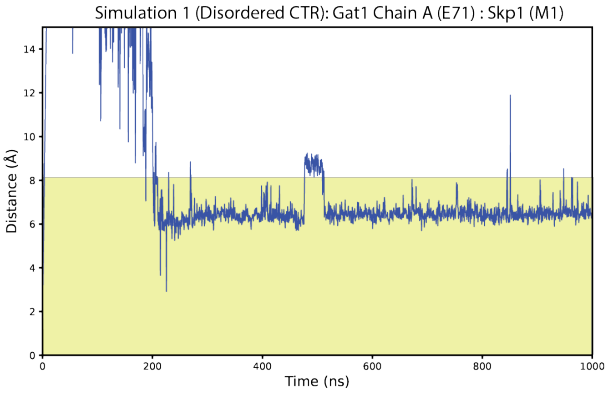

Simulation 1 (Disordered CTR): Gat1 Chain A (R129) : Skp1 (E44)
Distance (Å)
Time (ns)

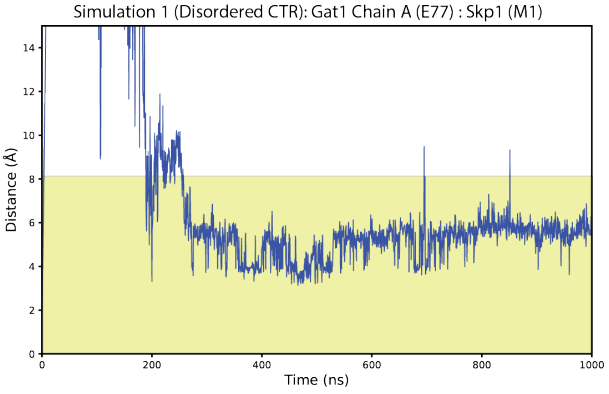

Simulation 1 (Disordered CTR): Gat1 Chain A (R133) : Skp1 (E41)
Distance (Å)
Time (ns)

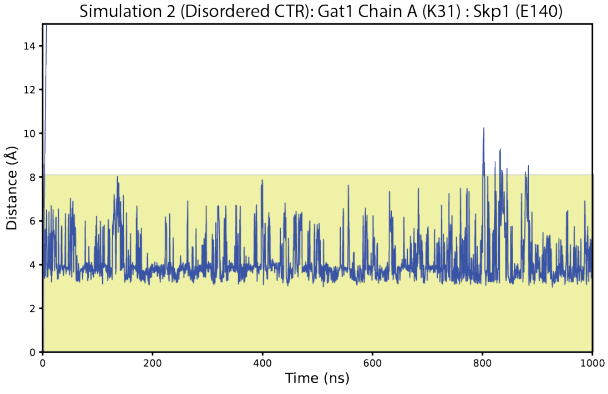

Simulation 1 (Disordered CTR): Gat1 Chain A (R133) : Skp1 (E42)
Distance (Å)
Time (ns)

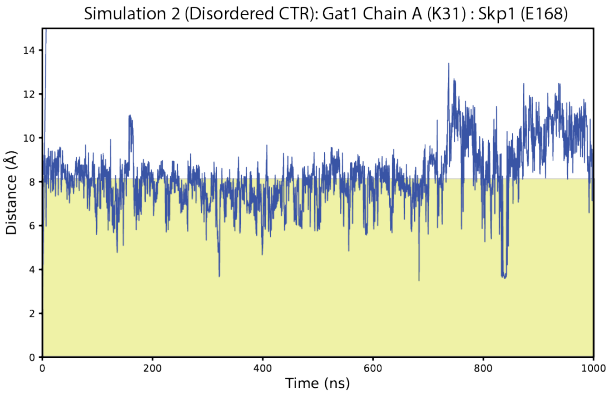

Simulation 1 (Disordered CTR): Gat1 Chain A (R137) : Skp1 (E41)
Distance (Å)
Time (ns)

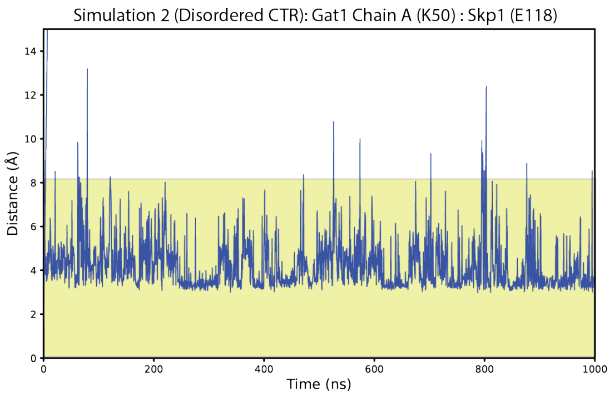

Simulation 1 (Disordered CTR): Gat1 Chain A (E327) : Skp1 (E135)
Distance (Å)
Time (ns)

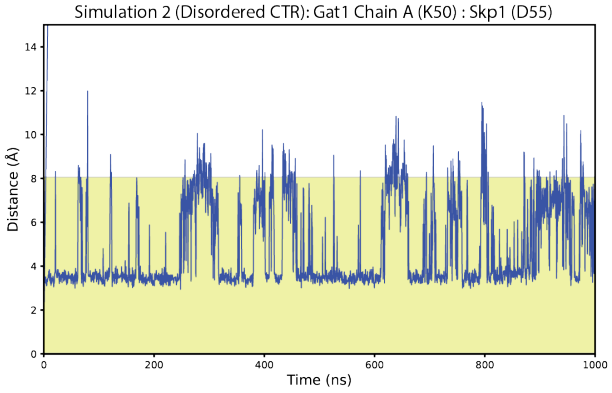

Simulation 1 (Disordered CTR): Gat1 Chain A (E71) : Skp1 (M1)
Distance (Å)
Time (ns)

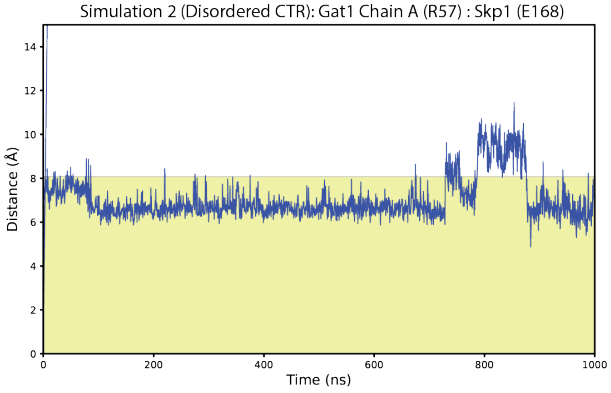

Simulation 1 (Disordered CTR): Gat1 Chain A (E77) : Skp1 (M1)
Distance (Å)
Time (ns)

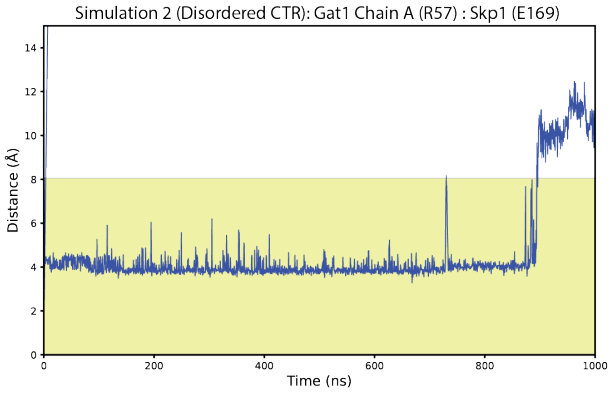

Simulation 2 (Disordered CTR): Gat1 Chain A (K31) : Skp1 (E140)
Distance (Å)
Time (ns)

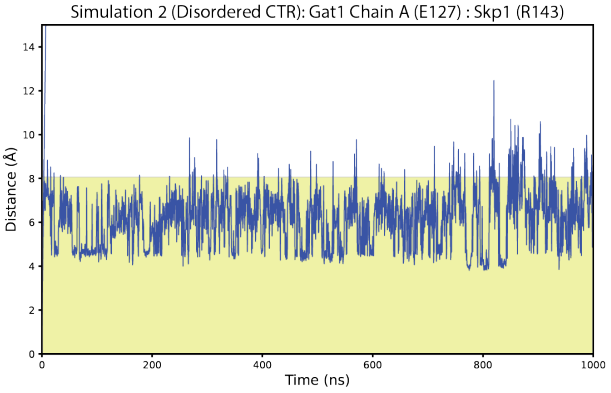

Simulation 2 (Disordered CTR): Gat1 Chain A (K31) : Skp1 (E168)
Distance (Å)
Time (ns)

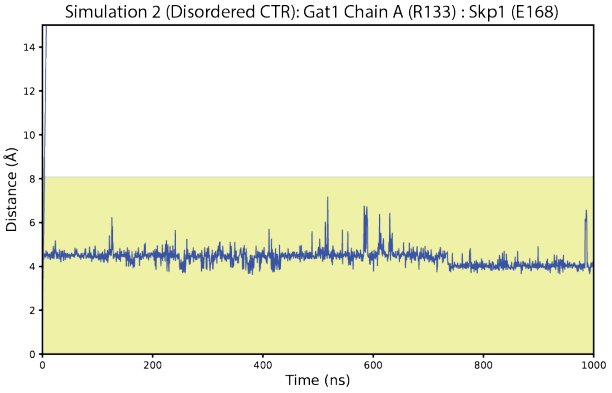

Simulation 2 (Disordered CTR): Gat1 Chain A (K50) : Skp1 (E118)
Distance (Å)
Time (ns)

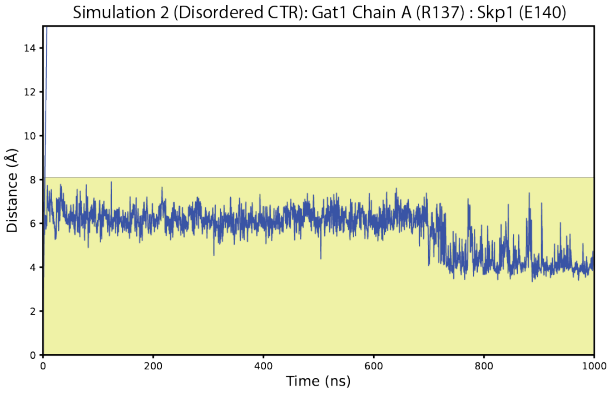

Simulation 2 (Disordered CTR): Gat1 Chain A (K50) : Skp1 (D55)
Distance (Å)
Time (ns)

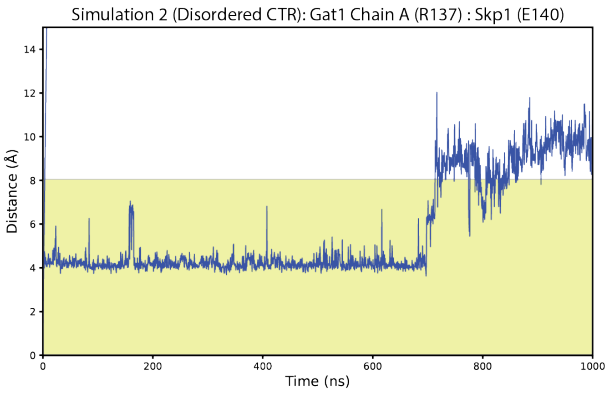

Simulation 2 (Disordered CTR): Gat1 Chain A (R57) : Skp1 (E168)
Distance (Å)
Time (ns)

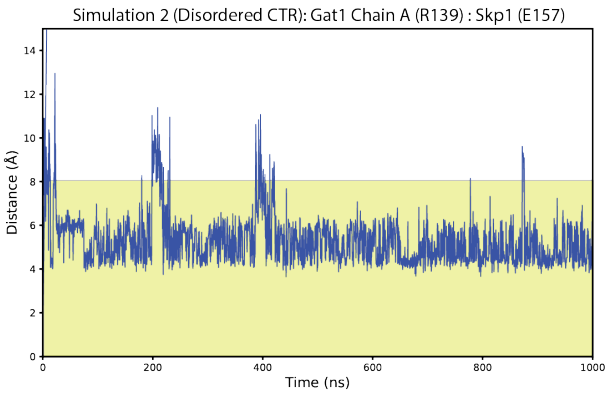

Simulation 2 (Disordered CTR): Gat1 Chain A (R57) : Skp1 (E169)
Distance (Å)
Time (ns)

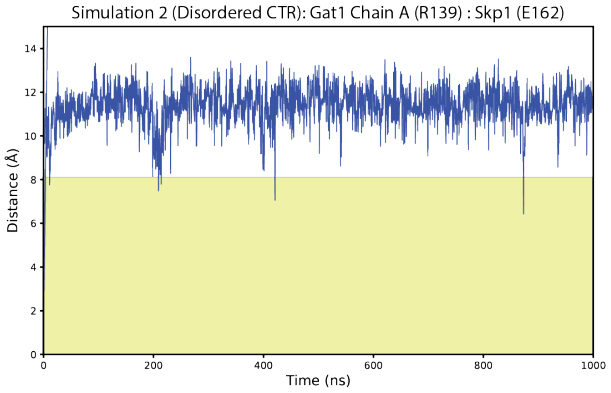

Simulation 2 (Disordered CTR): Gat1 Chain A (E127) : Skp1 (R143)
Distance (Å)
Time (ns)

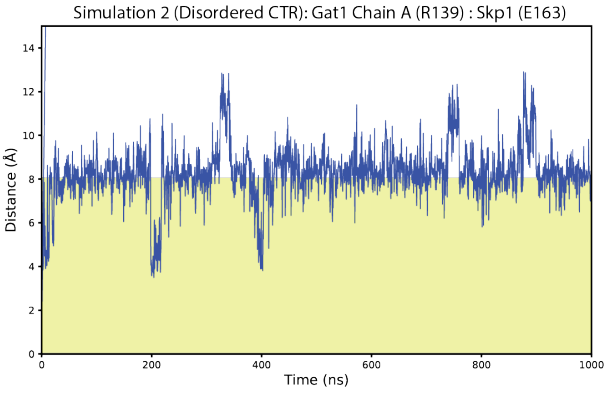

Simulation 2 (Disordered CTR): Gat1 Chain A (R133) : Skp1 (E168)
Distance (Å)
Time (ns)

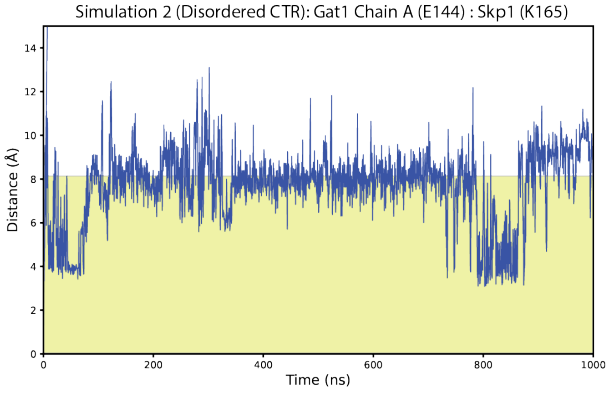

Simulation 2 (Disordered CTR): Gat1 Chain A (R137) : Skp1 (E140)
Distance (Å)
Time (ns)

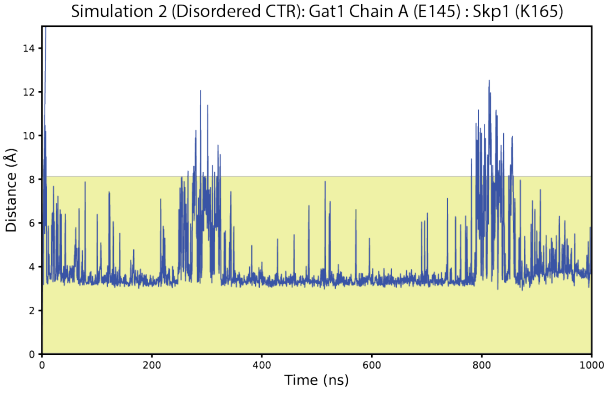

Simulation 2 (Disordered CTR): Gat1 Chain A (R137) : Skp1 (E140)
Distance (Å)
Time (ns)

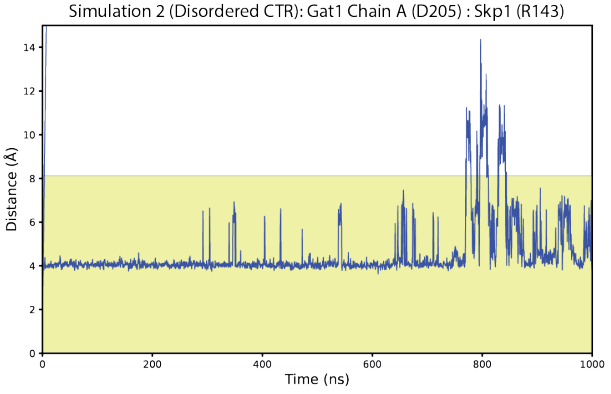

Simulation 2 (Disordered CTR): Gat1 Chain A (R139) : Skp1 (E157)
Distance (Å)
Time (ns)

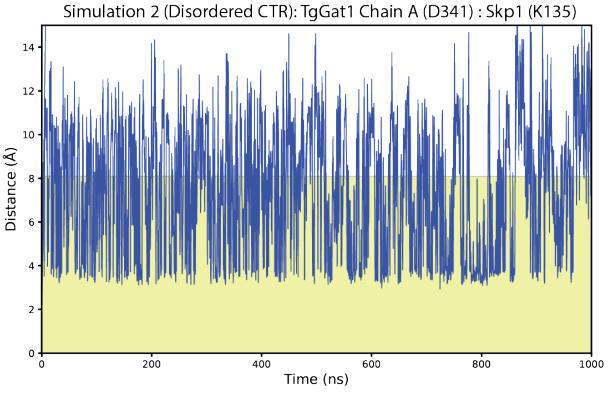

Simulation 2 (Disordered CTR): Gat1 Chain A (R139) : Skp1 (E162)
Distance (Å)
Time (ns)

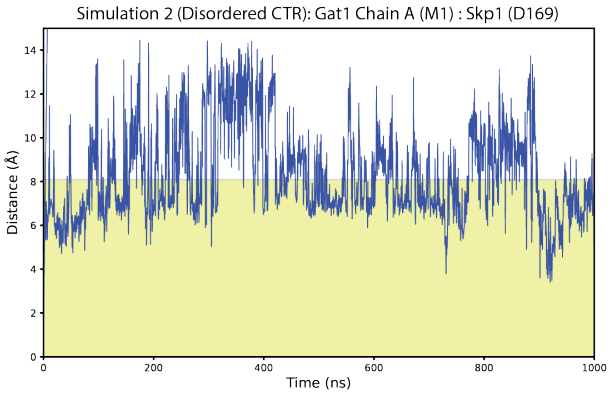

Simulation 2 (Disordered CTR): Gat1 Chain A (R139) : Skp1 (E163)
Distance (Å)
Time (ns)

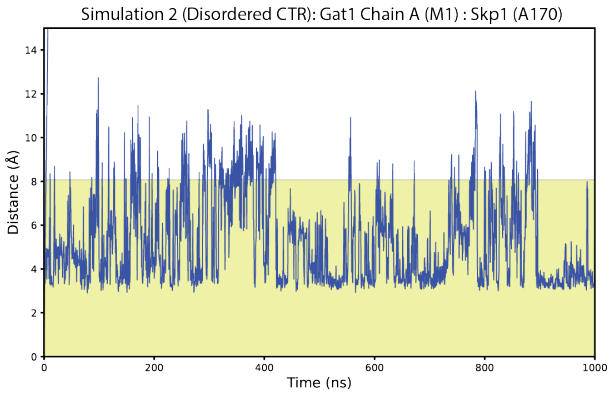

Simulation 2 (Disordered CTR): Gat1 Chain A (E144) : Skp1 (K165)
Distance (Å)
Time (ns)

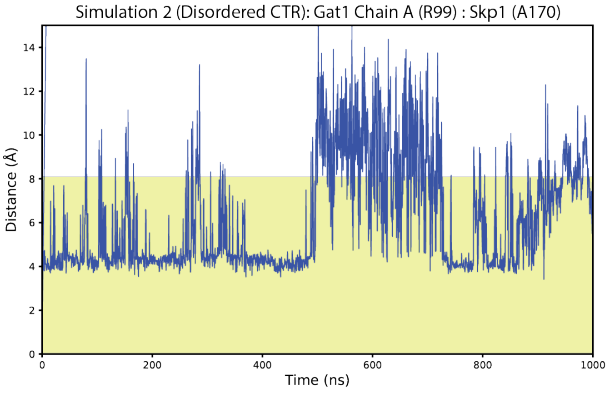

Simulation 2 (Disordered CTR): Gat1 Chain A (E145) : Skp1 (K165)
Distance (Å)
Time (ns)

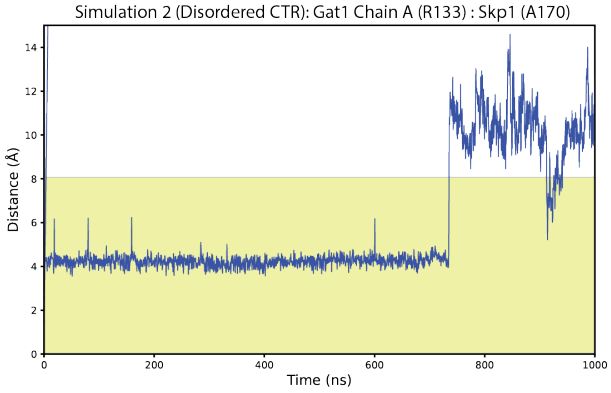

Simulation 2 (Disordered CTR): Gat1 Chain A (D205) : Skp1 (R143)
Distance (Å)
Time (ns)

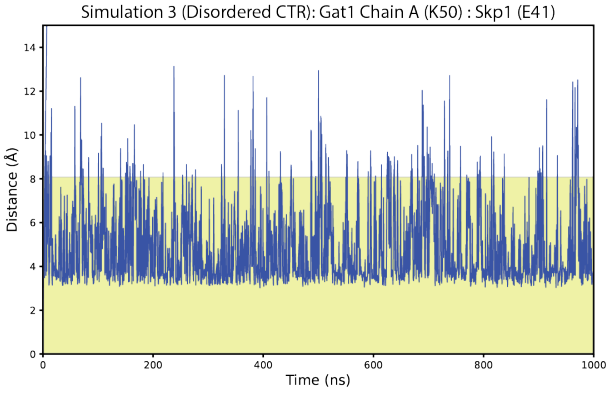

Simulation 2 (Disordered CTR): TgGat1 Chain A (D341) : Skp1 (K135)
Distance (Å)
Time (ns)

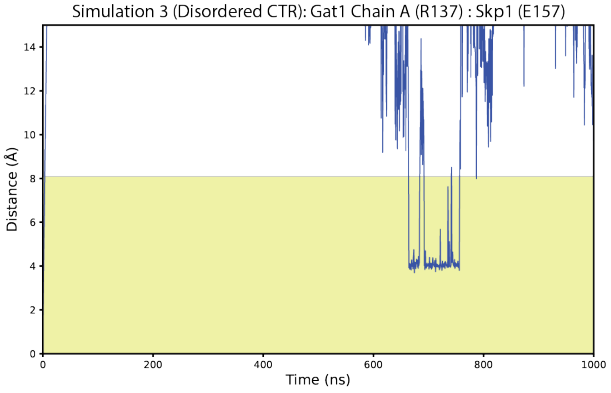

Simulation 2 (Disordered CTR): Gat1 Chain A (M1) : Skp1 (D169)
Distance (Å)
Time (ns)

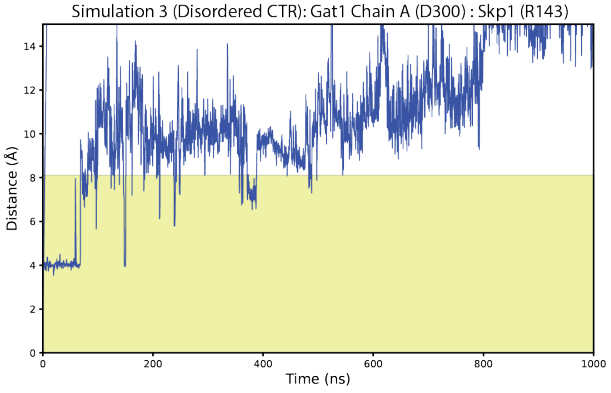

Simulation 2 (Disordered CTR): Gat1 Chain A (M1) : Skp1 (A170)
Distance (Å)
Time (ns)

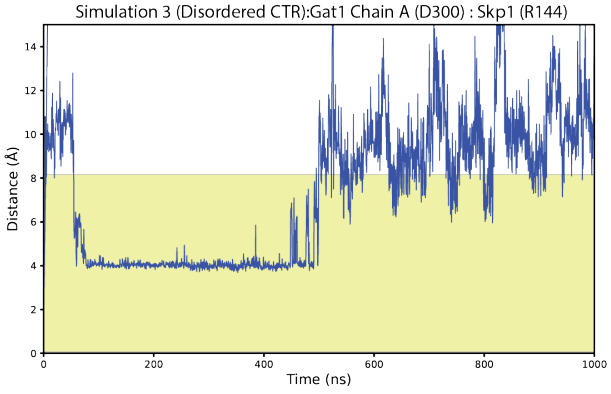

Simulation 2 (Disordered CTR): Gat1 Chain A (R99) : Skp1 (A170)
Distance (Å)
Time (ns)

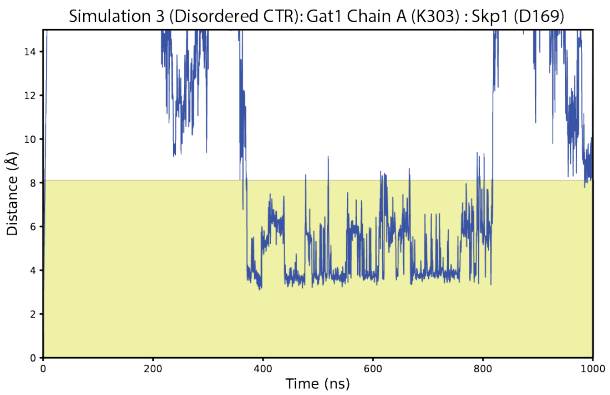

Simulation 2 (Disordered CTR): Gat1 Chain A (R133) : Skp1 (A170)
Distance (Å)
Time (ns)

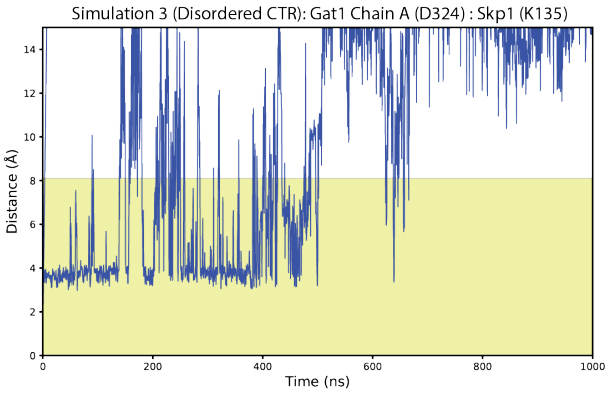

Simulation 3 (Disordered CTR): Gat1 Chain A (K50) : Skp1 (E41)
Distance (Å)
Time (ns)

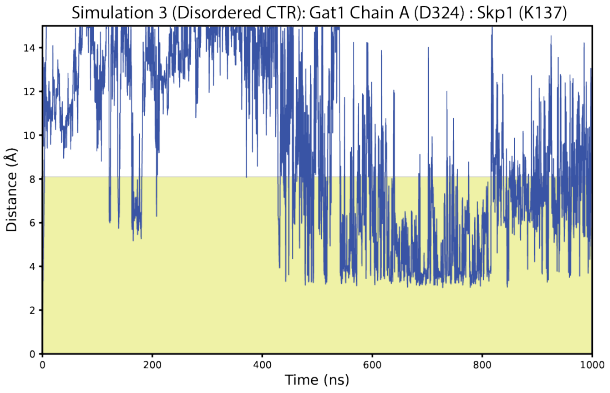

Simulation 3 (Disordered CTR): Gat1 Chain A (R137) : Skp1 (E157)
Distance (Å)
Time (ns)

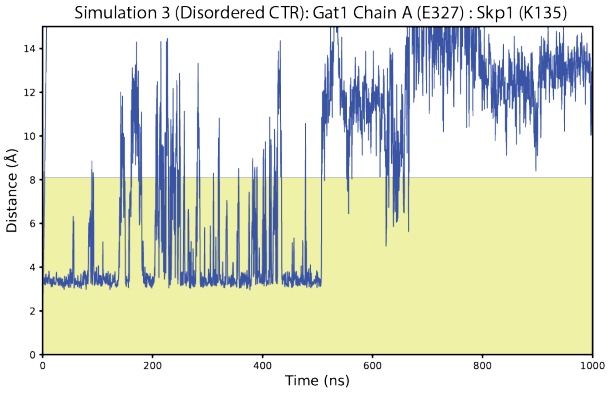

Simulation 3 (Disordered CTR): Gat1 Chain A (D300) : Skp1 (R143)
Distance (Å)
Time (ns)

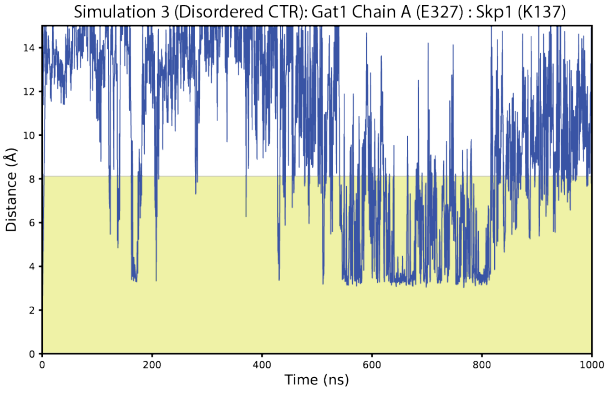

Simulation 3 (Disordered CTR):Gat1 Chain A (D300) : Skp1 (R144)
Distance (Å)
Time (ns)

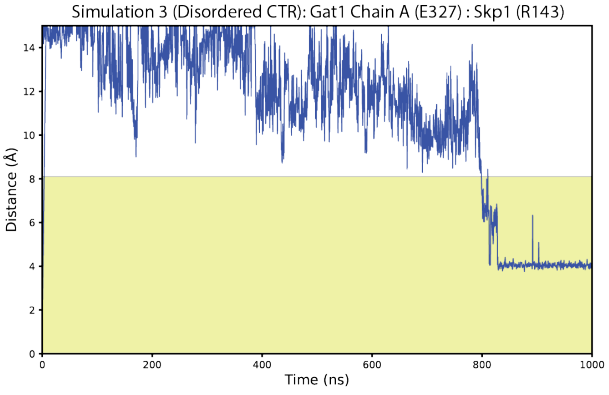

Simulation 3 (Disordered CTR): Gat1 Chain A (K303) : Skp1 (D169)
Distance (Å)
Time (ns)

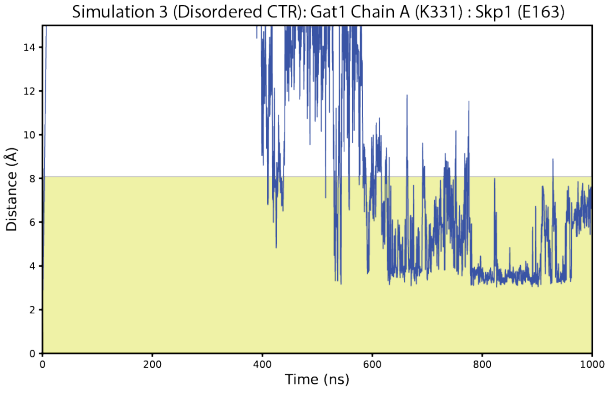

Simulation 3 (Disordered CTR): Gat1 Chain A (D324) : Skp1 (K135)
Distance (Å)
Time (ns)

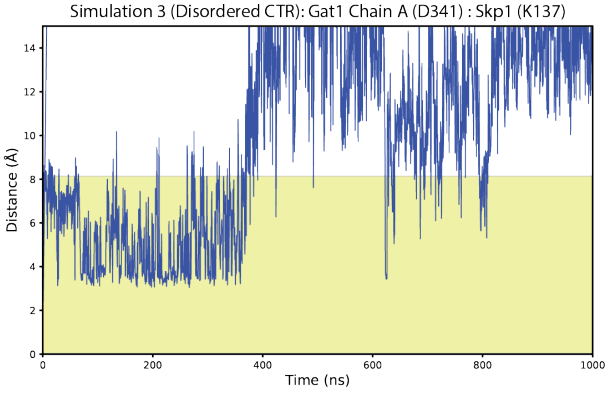

Simulation 3 (Disordered CTR): Gat1 Chain A (D324) : Skp1 (K137)
Distance (Å)
Time (ns)

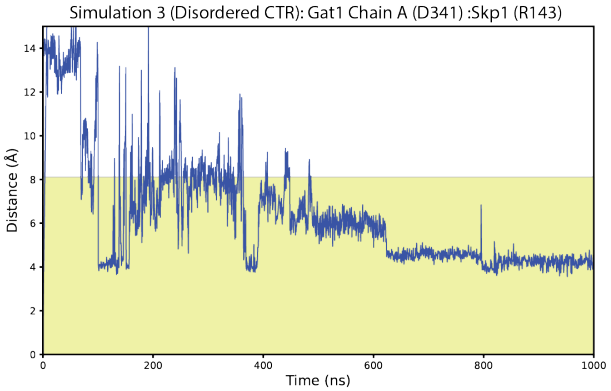

Simulation 3 (Disordered CTR): Gat1 Chain A (E327) : Skp1 (K135)
Distance (Å)
Time (ns)

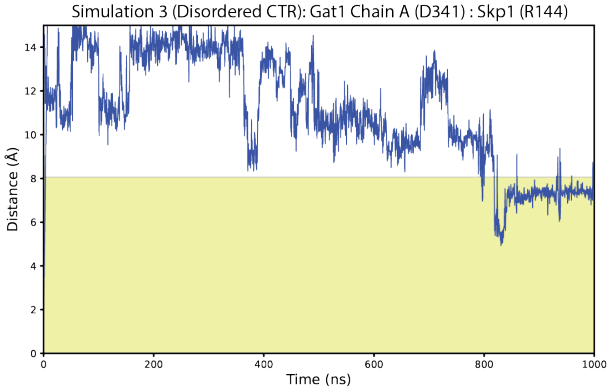

Simulation 3 (Disordered CTR): Gat1 Chain A (E327) : Skp1 (K137)
Distance (Å)
Time (ns)

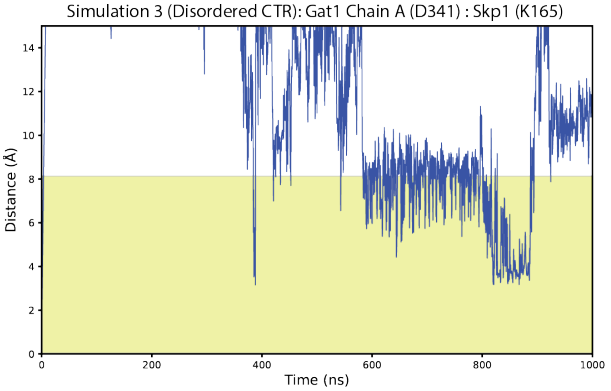

Simulation 3 (Disordered CTR): Gat1 Chain A (E327) : Skp1 (R143)
Distance (Å)
Time (ns)

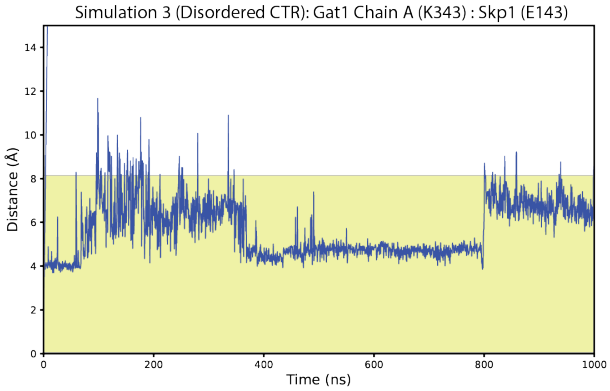

Simulation 3 (Disordered CTR): Gat1 Chain A (K331) : Skp1 (E163)
Distance (Å)
Time (ns)

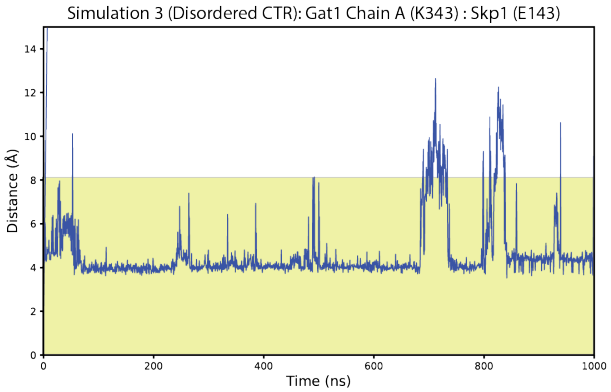

Simulation 3 (Disordered CTR): Gat1 Chain A (D341) : Skp1 (K137)
Distance (Å)
Time (ns)

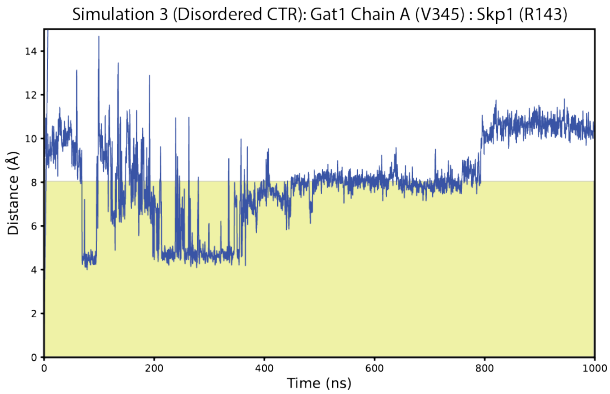

Simulation 3 (Disordered CTR): Gat1 Chain A (D341) :Skp1 (R143)
Distance (Å)
Time (ns)

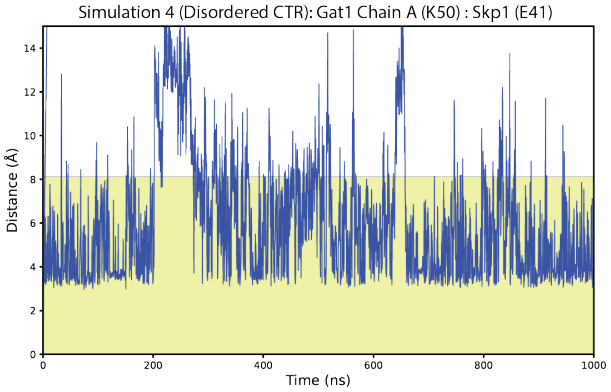

Simulation 3 (Disordered CTR): Gat1 Chain A (D341) : Skp1 (R144)
Distance (Å)
Time (ns)

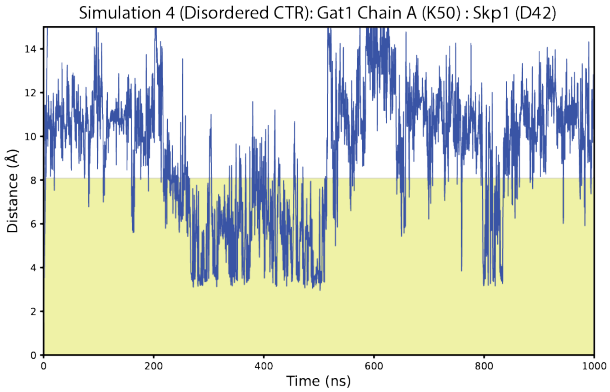

Simulation 3 (Disordered CTR): Gat1 Chain A (D341) : Skp1 (K165)
Distance (Å)
Time (ns)

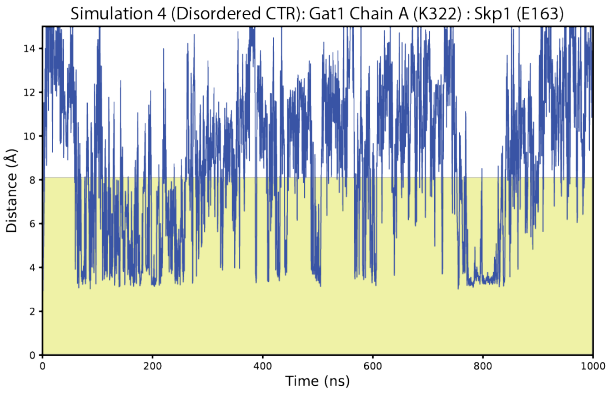

Simulation 3 (Disordered CTR): Gat1 Chain A (K343) : Skp1 (E143)
Distance (Å)
Time (ns)

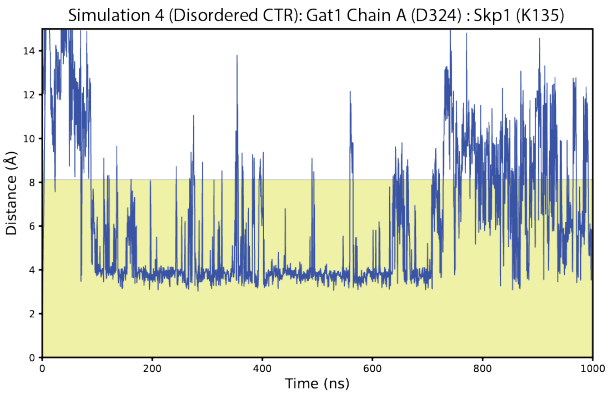

Simulation 3 (Disordered CTR): Gat1 Chain A (K343) : Skp1 (E143)
Distance (Å)
Time (ns)

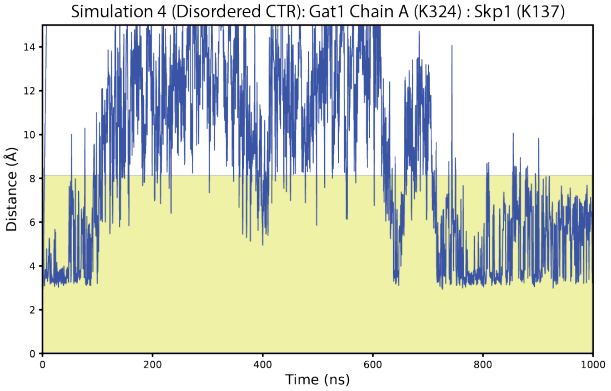

Simulation 3 (Disordered CTR): Gat1 Chain A (V345) : Skp1 (R143)
Distance (Å)
Time (ns)

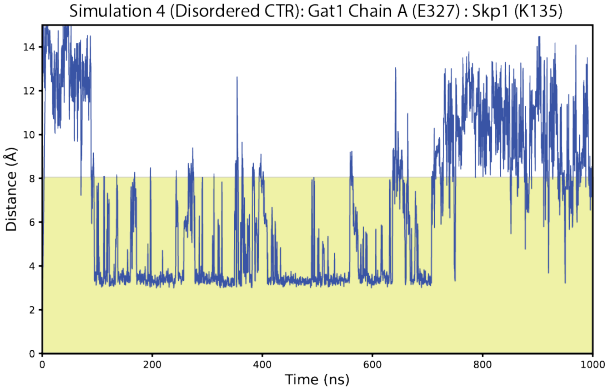

Simulation 4 (Disordered CTR): Gat1 Chain A (K50) : Skp1 (E41)
Distance (Å)
Time (ns)

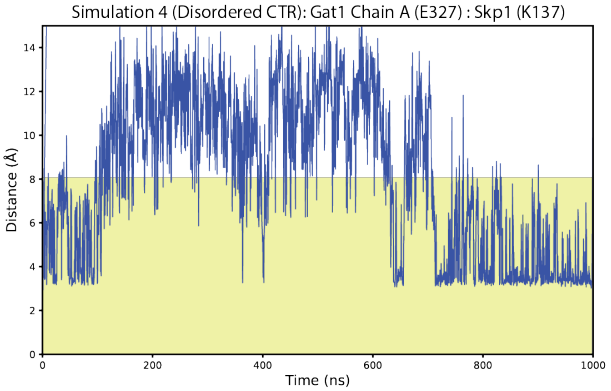

Simulation 4 (Disordered CTR): Gat1 Chain A (K50) : Skp1 (D42)
Distance (Å)
Time (ns)

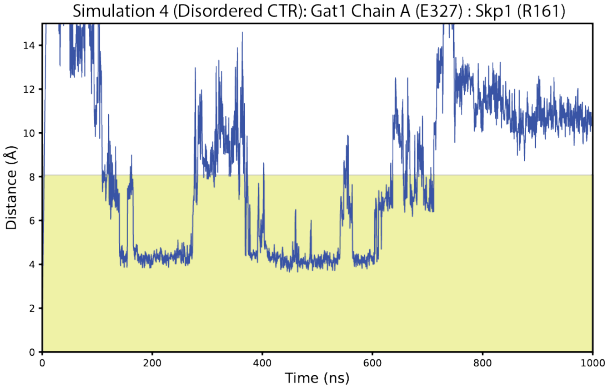

Simulation 4 (Disordered CTR): Gat1 Chain A (K322) : Skp1 (E163)
Distance (Å)
Time (ns)

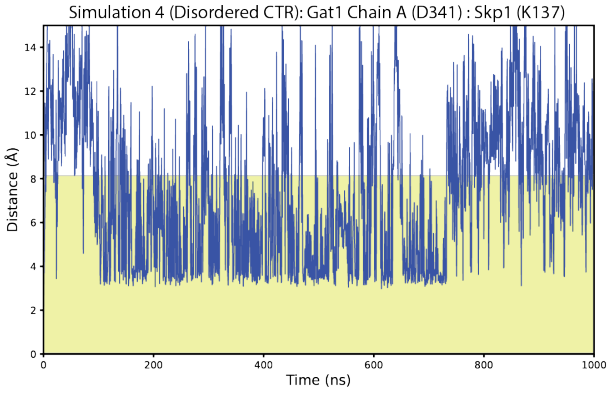

Simulation 4 (Disordered CTR): Gat1 Chain A (D324) : Skp1 (K135)
Distance (Å)
Time (ns)

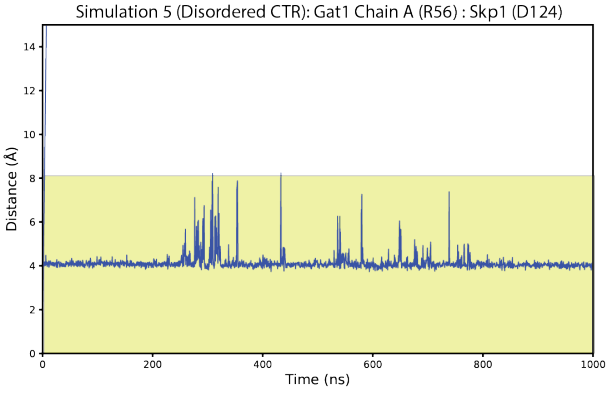

Simulation 4 (Disordered CTR): Gat1 Chain A (K324) : Skp1 (K137)
Distance (Å)
Time (ns)

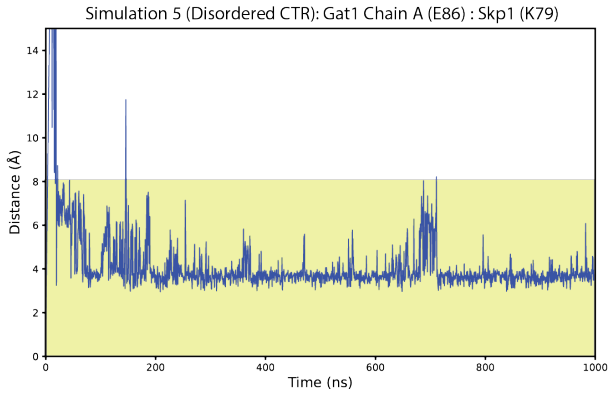

Simulation 4 (Disordered CTR): Gat1 Chain A (E327) : Skp1 (K135)
Distance (Å)
Time (ns)

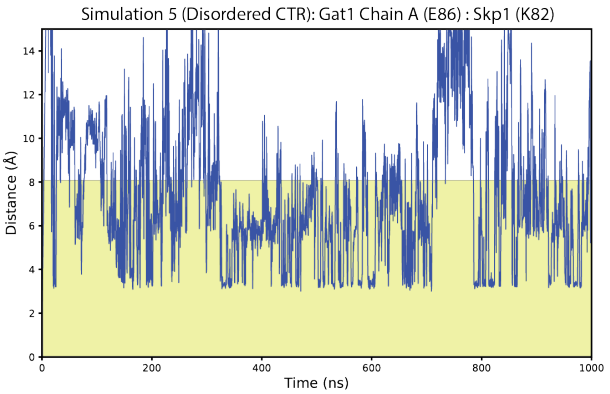

Simulation 4 (Disordered CTR): Gat1 Chain A (E327) : Skp1 (K137)
Distance (Å)
Time (ns)

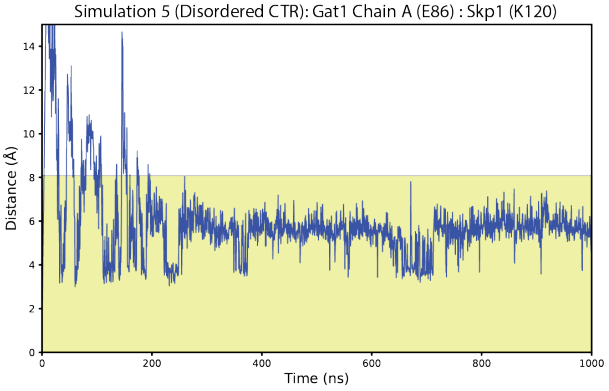

Simulation 4 (Disordered CTR): Gat1 Chain A (E327) : Skp1 (R161)
Distance (Å)
Time (ns)

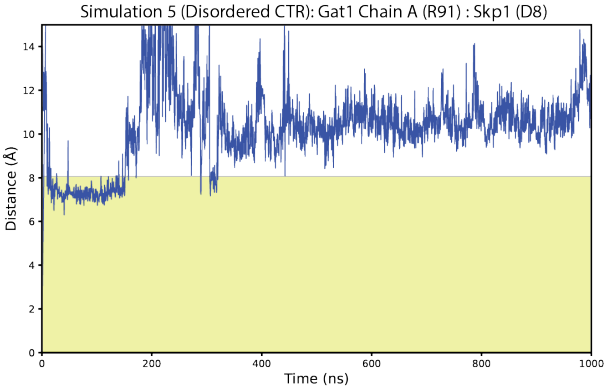

Simulation 4 (Disordered CTR): Gat1 Chain A (D341) : Skp1 (K137)
Distance (Å)
Time (ns)

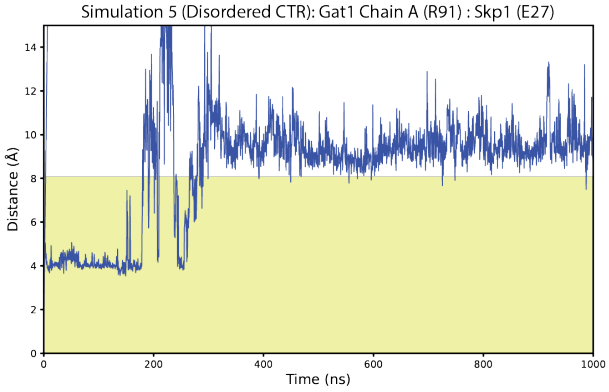

Simulation 5 (Disordered CTR): Gat1 Chain A (R56) : Skp1 (D124)
Distance (Å)
Time (ns)

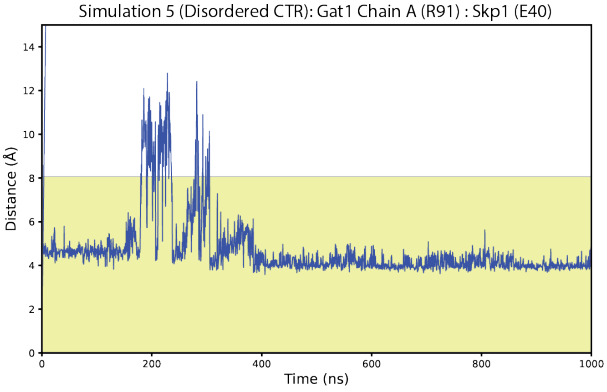

Simulation 5 (Disordered CTR): Gat1 Chain A (E86) : Skp1 (K79)
Distance (Å)
Time (ns)

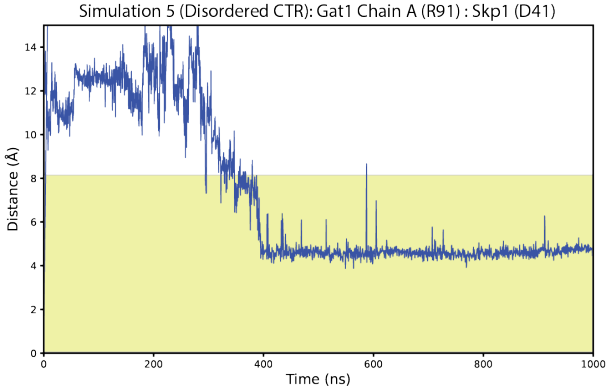

Simulation 5 (Disordered CTR): Gat1 Chain A (E86) : Skp1 (K82)
Distance (Å)
Time (ns)

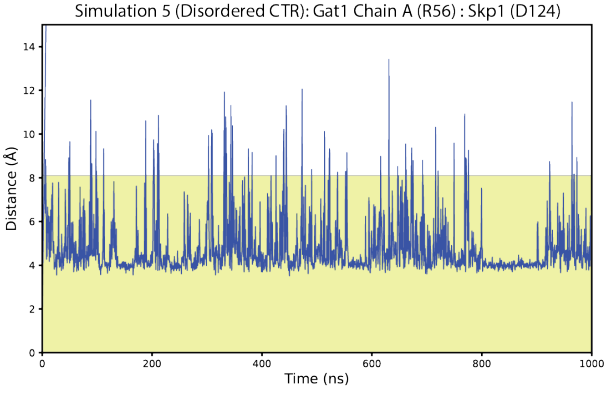

Simulation 5 (Disordered CTR): Gat1 Chain A (E86) : Skp1 (K120)
Distance (Å)
Time (ns)

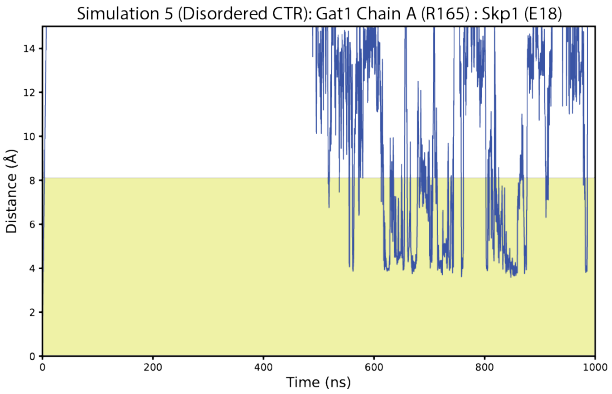

Simulation 5 (Disordered CTR): Gat1 Chain A (R91) : Skp1 (D8)
Distance (Å)
Time (ns)

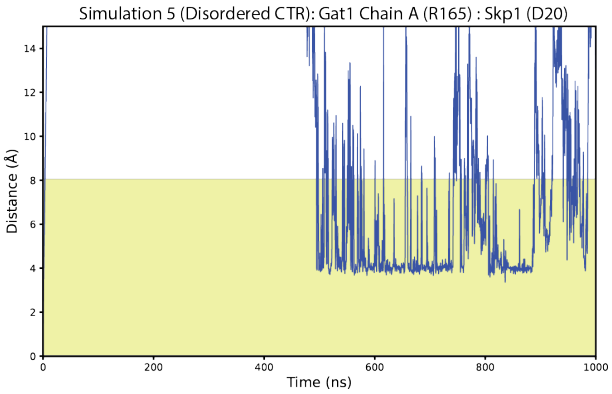

Simulation 5 (Disordered CTR): Gat1 Chain A (R91) : Skp1 (E27)
Distance (Å)
Time (ns)

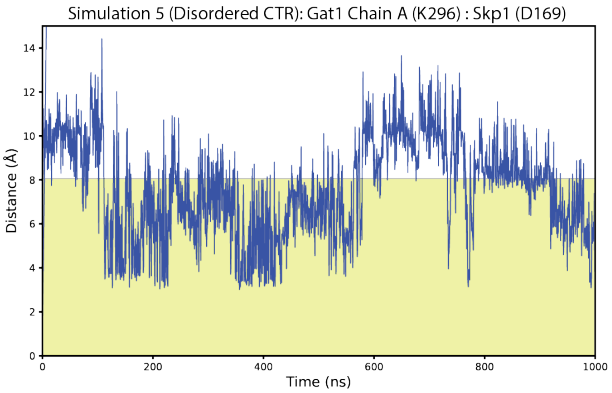

Simulation 5 (Disordered CTR): Gat1 Chain A (R91) : Skp1 (E40)
Distance (Å)
Time (ns)

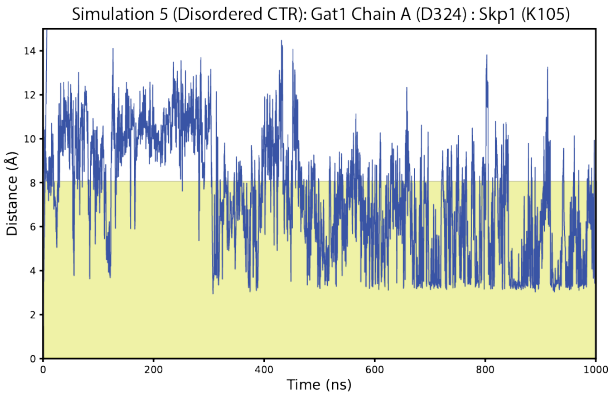

Simulation 5 (Disordered CTR): Gat1 Chain A (R91) : Skp1 (D41)
Distance (Å)
Time (ns)

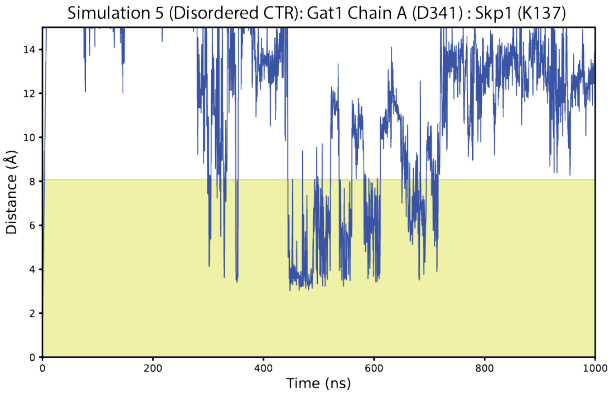

Simulation 5 (Disordered CTR): Gat1 Chain A (R56) : Skp1 (D124)
Distance (Å)
Time (ns)

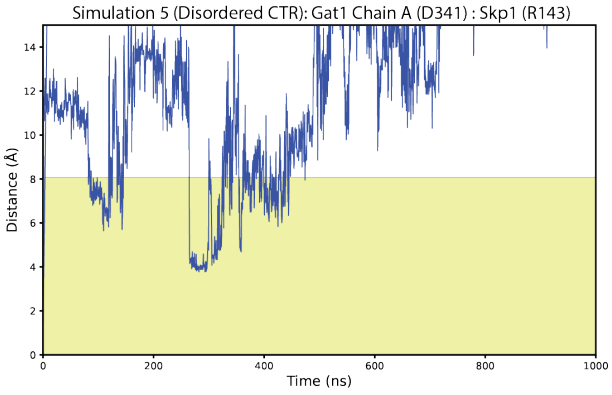

Simulation 5 (Disordered CTR): Gat1 Chain A (R165) : Skp1 (E18)
Distance (Å)
Time (ns)

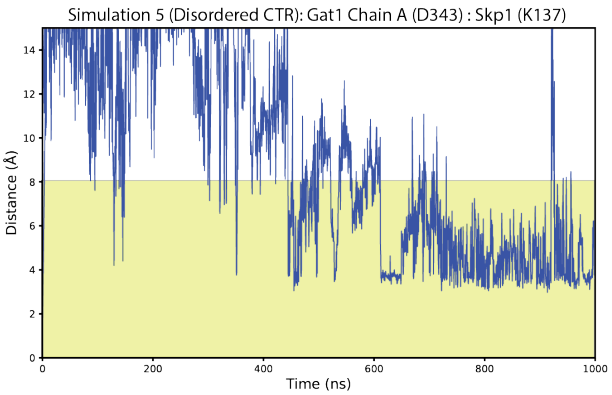

Simulation 5 (Disordered CTR): Gat1 Chain A (R165) : Skp1 (D20)
Distance (Å)
Time (ns)

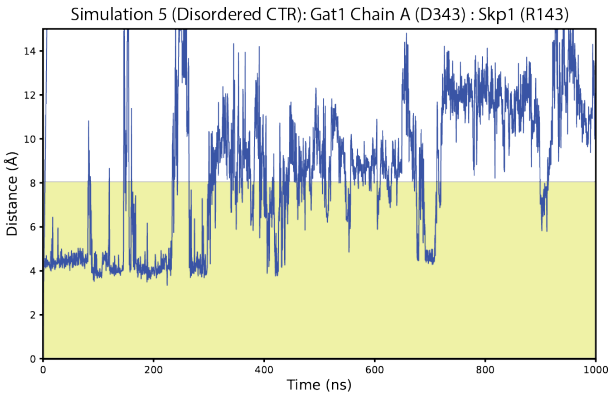

Simulation 5 (Disordered CTR): Gat1 Chain A (K296) : Skp1 (D169)
Distance (Å)
Time (ns)

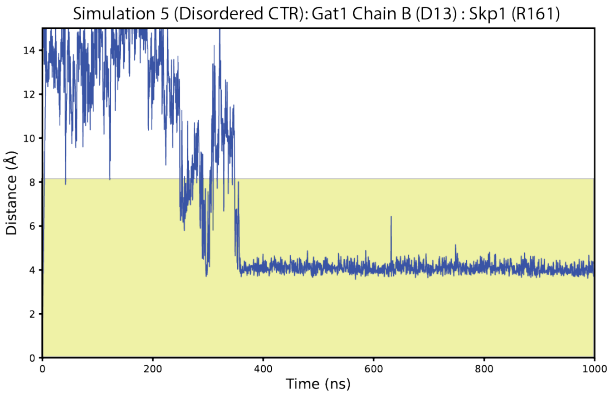

Simulation 5 (Disordered CTR): Gat1 Chain A (D324) : Skp1 (K105)
Distance (Å)
Time (ns)

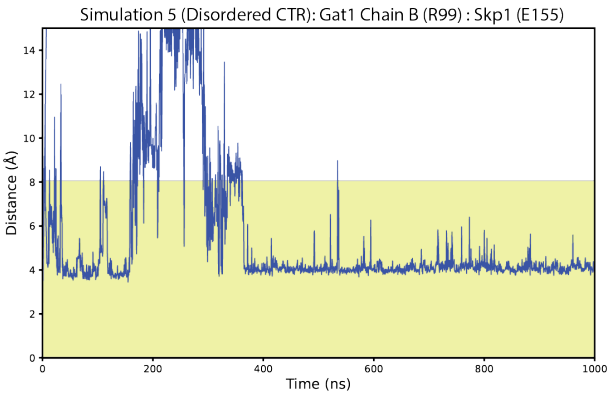

Simulation 5 (Disordered CTR): Gat1 Chain A (D341) : Skp1 (K137)
Distance (Å)
Time (ns)

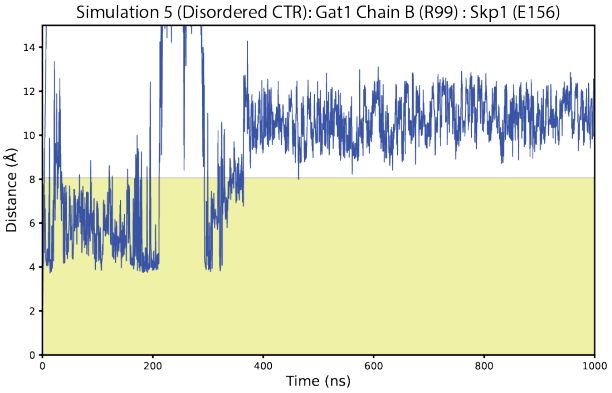

Simulation 5 (Disordered CTR): Gat1 Chain A (D341) : Skp1 (R143)
Distance (Å)
Time (ns)

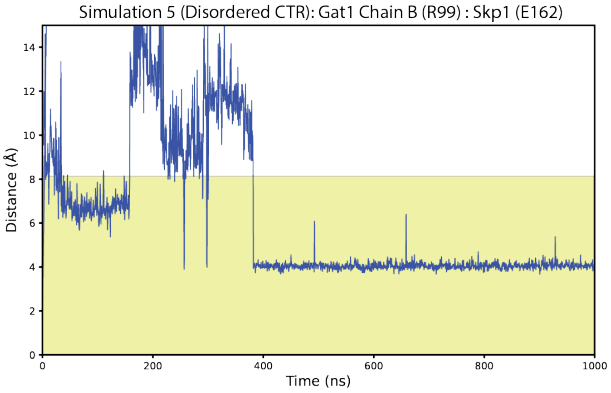

Simulation 5 (Disordered CTR): Gat1 Chain A (D343) : Skp1 (K137)
Distance (Å)
Time (ns)

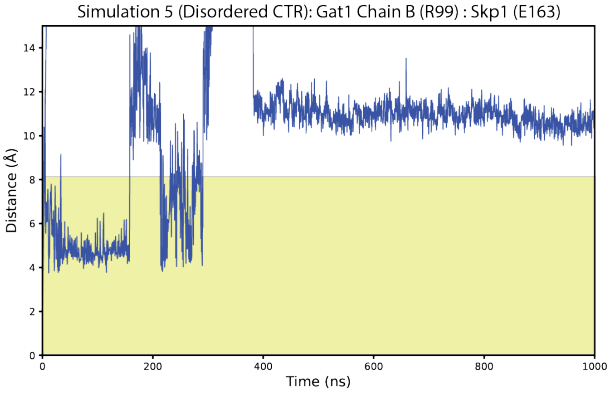

Simulation 5 (Disordered CTR): Gat1 Chain A (D343) : Skp1 (R143)
Distance (Å)
Time (ns)

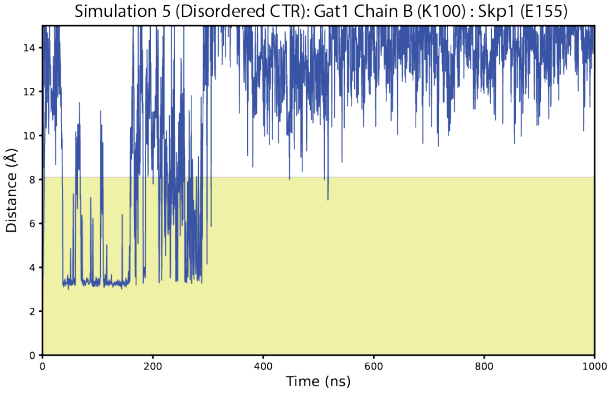

Simulation 5 (Disordered CTR): Gat1 Chain B (D13) : Skp1 (R161)
Distance (Å)
Time (ns)

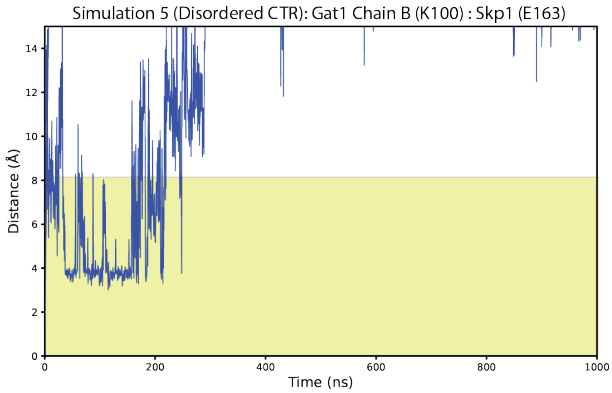

Simulation 5 (Disordered CTR): Gat1 Chain B (R99) : Skp1 (E155)
Distance (Å)
Time (ns)

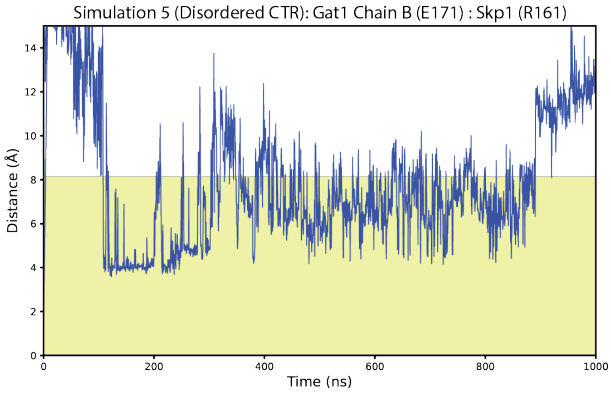

Simulation 5 (Disordered CTR): Gat1 Chain B (R99) : Skp1 (E156)
Distance (Å)
Time (ns)

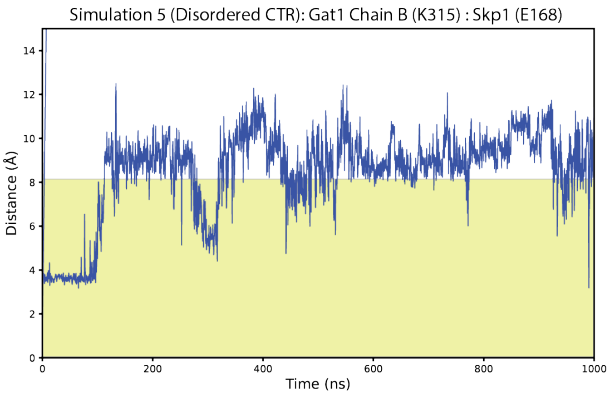

Simulation 5 (Disordered CTR): Gat1 Chain B (R99) : Skp1 (E162)
Distance (Å)
Time (ns)

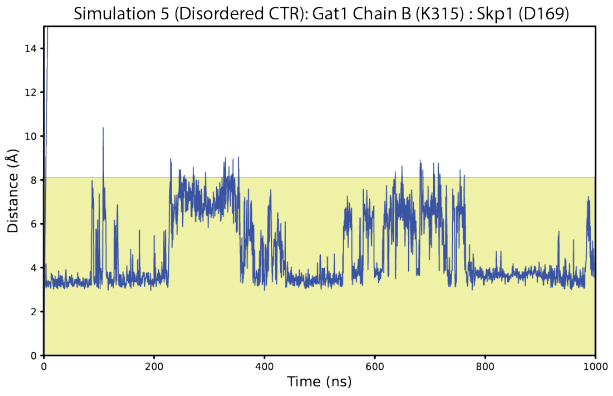

Simulation 5 (Disordered CTR): Gat1 Chain B (R99) : Skp1 (E163)
Distance (Å)
Time (ns)

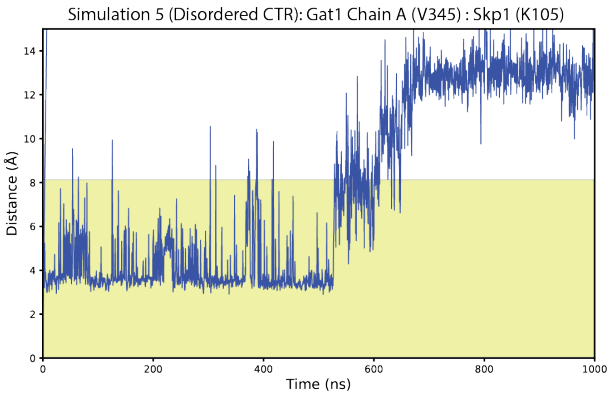

Simulation 5 (Disordered CTR): Gat1 Chain B (K100) : Skp1 (E155)
Distance (Å)
Time (ns)

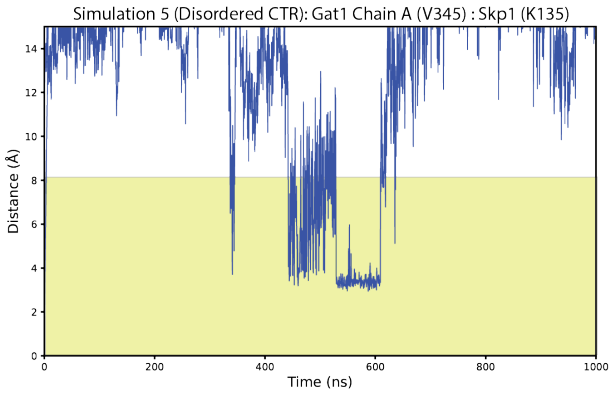

Simulation 5 (Disordered CTR): Gat1 Chain B (K100) : Skp1 (E163)
Distance (Å)
Time (ns)

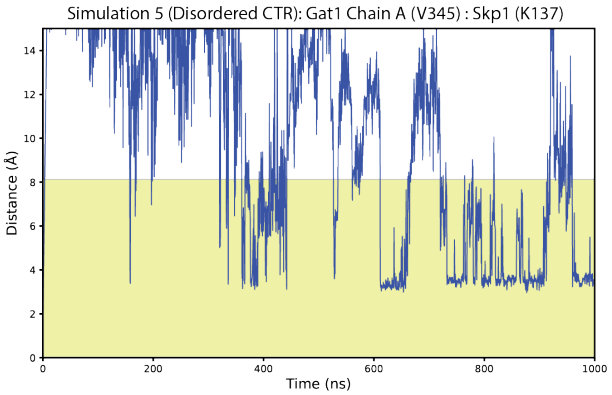

Simulation 5 (Disordered CTR): Gat1 Chain B (E171) : Skp1 (R161)
Distance (Å)
Time (ns)

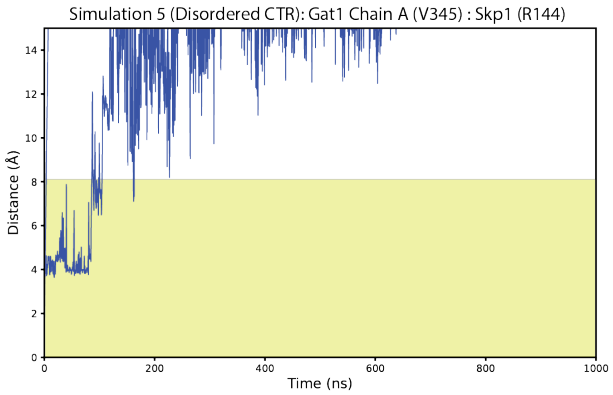

Simulation 5 (Disordered CTR): Gat1 Chain B (K315) : Skp1 (E168)
Distance (Å)
Time (ns)

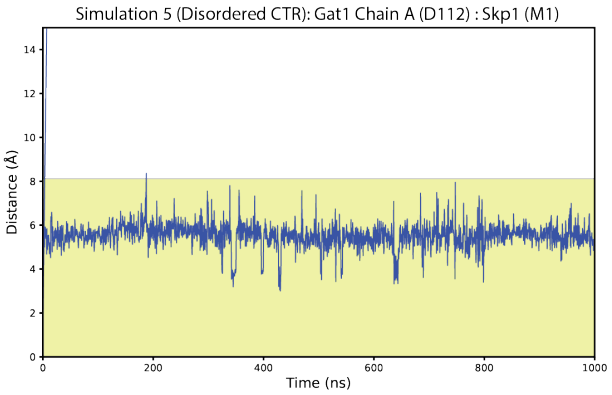

Simulation 5 (Disordered CTR): Gat1 Chain B (K315) : Skp1 (D169)
Distance (Å)
Time (ns)

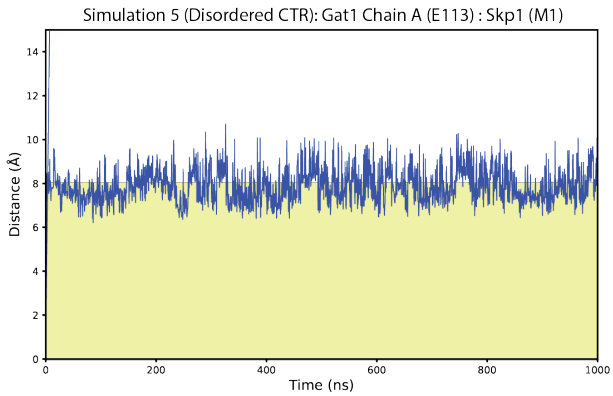

Simulation 5 (Disordered CTR): Gat1 Chain A (V345) : Skp1 (K105)
Distance (Å)
Time (ns)

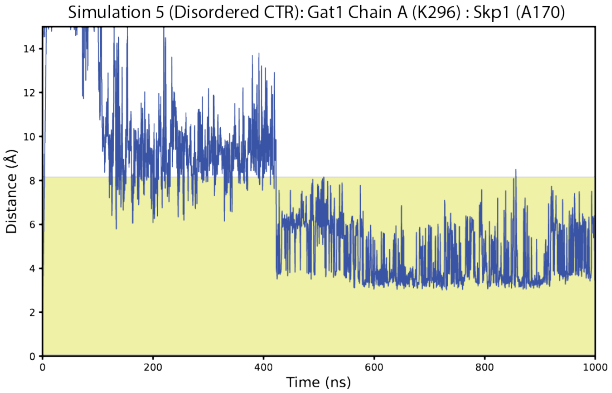

Simulation 5 (Disordered CTR): Gat1 Chain A (V345) : Skp1 (K135)
Distance (Å)
Time (ns)


Simulation 5 (Disordered CTR): Gat1 Chain A (V345) : Skp1 (K137)
Distance (Å)
Time (ns)


Simulation 5 (Disordered CTR): Gat1 Chain A (V345) : Skp1 (R144)
Distance (Å)
Time (ns)


Simulation 5 (Disordered CTR): Gat1 Chain A (D112) : Skp1 (M1)
Distance (Å)
Time (ns)


Simulation 5 (Disordered CTR): Gat1 Chain A (E113) : Skp1 (M1)
Distance (Å)
Time (ns)


Simulation 5 (Disordered CTR): Gat1 Chain A (K296) : Skp1 (A170)
Distance (Å)
Time (ns)
0
2
4
6
8
10
12
14
0
200
400
600
800
1000

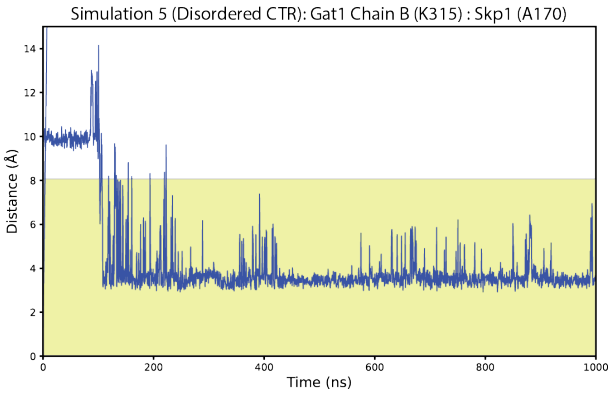
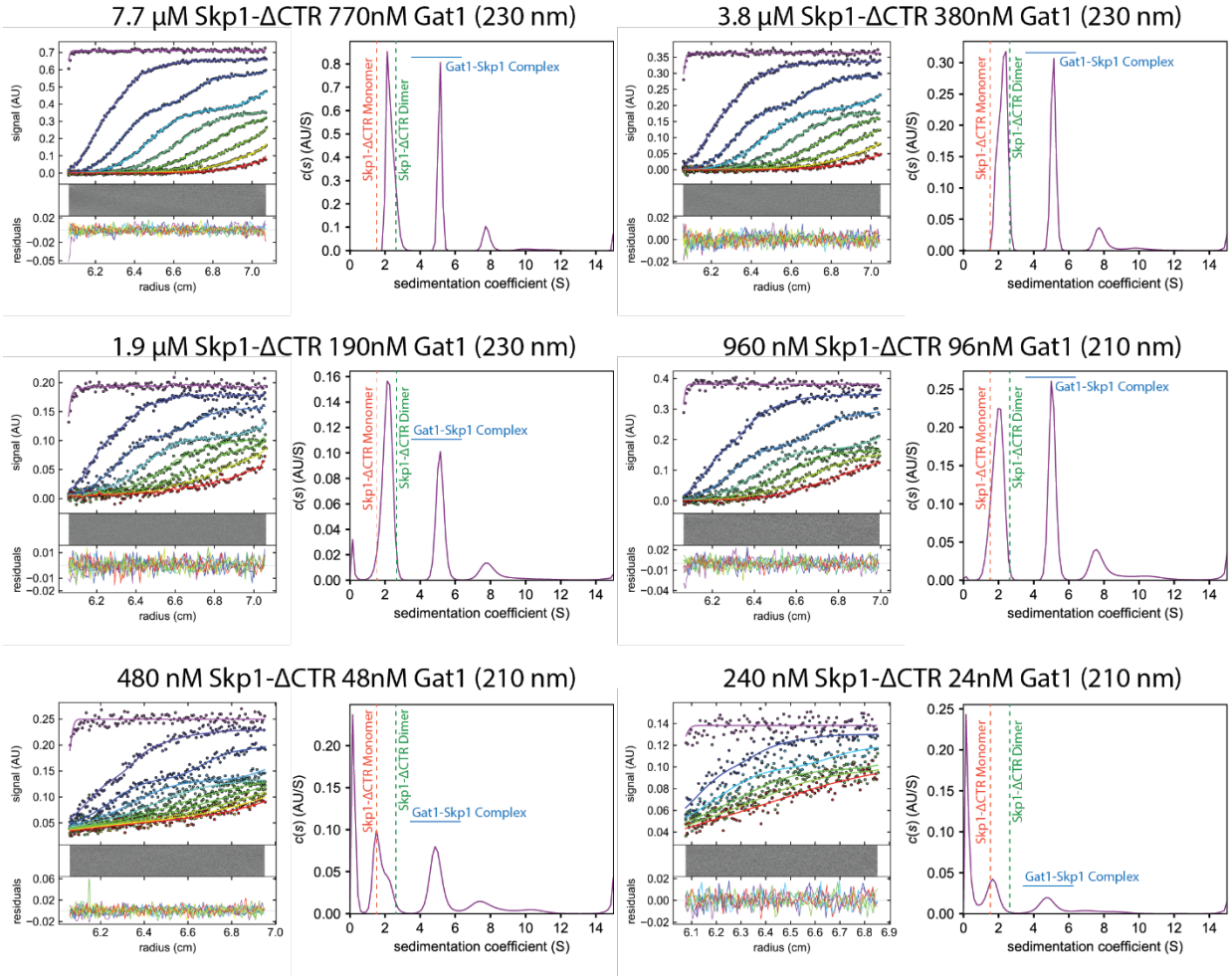

Simulation 5 (Disordered CTR): Gat1 Chain B (K315) : Skp1 (A170)
Distance (Å)
Time (ns)
0
2
4
6
8
10
12
14
0
200
400
600
800
1000

Figure 3.S19


7.7 μM Skp1-ΔCTR 770nM Gat1 (230 nm)
3.8 μM Skp1-ΔCTR 380nM Gat1 (230 nm)
1.9 μM Skp1-ΔCTR 190nM Gat1 (230 nm)
960 nM Skp1-ΔCTR 96nM Gat1 (210 nm)
480 nM Skp1-ΔCTR 48nM Gat1 (210 nm)
240 nM Skp1-ΔCTR 24nM Gat1 (210 nm)
signal (AU)
residuals
radius (cm)
c(s) (AU/S)
sedimentation coefficient (S)
Skp1-ΔCTR Monomer
Skp1-ΔCTR Dimer
Gat1-Skp1 Complex

REFERENCES

(1) Centers for Disease Control and Prevention. (2018). *People at Increased Risk for Toxoplasmosis*. In *Parasites – Toxoplasmosis (Toxoplasma infection)*; U.S. Department of Health and Human Services, Centers for Disease Control and Prevention. https://www.cdc.gov/toxoplasmosis/risk-factors/index.html

(2) Attias, M., Teixeira, D. E., Benchimol, M., Vommaro, R. C., Crepaldi, P. H., and De Souza, W. (2020) The life-cycle of *Toxoplasma gondii* reviewed using animations, Parasites & Vectors 13, 588.

(3) Centers for Disease Control and Prevention (CDC). *Toxoplasmosis*. In *Parasites*; Centers for Disease Control and Prevention: Atlanta, GA, 2024. https://www.cdc.gov/parasites/toxoplasmosis/

(4) Skariah, S., McIntyre, M. K., and Mordue, D. G. (2010) *Toxoplasma gondii*: determinants of tachyzoite to bradyzoite conversion, Parasitology Research 107, 253-260.

(5) Wang, Z.-D., Liu, H.-H., Ma, Z.-X., Ma, H.-Y., Li, Z.-Y., Yang, Z.-B., Zhu, X.-Q., Xu, B., Wei, F., and Liu, Q. (2017) *Toxoplasma gondii* Infection in Immunocompromised Patients: A Systematic Review and Meta-Analysis, Frontiers in Microbiology 8, 389.

(6) Rostami, A., Riahi, S. M., Contopoulos-Ioannidis, D. G., Gamble, H. R., Fakhri, Y., Shiadeh, M. N., Foroutan, M., Behniafar, H., Taghipour, A., Maldonado, Y. A., Mokdad, A. H., and Gasser, R. B. (2019) Acute *Toxoplasma* infection in pregnant women worldwide: A systematic review and meta-analysis, PLOS Neglected Tropical Diseases 13, e0007807.

(7) Molan, A., Nosaka, K., Hunter, M., and Wang, W. (2019) Global status of *Toxoplasma gondii* infection: systematic review and prevalence snapshots, Trop Biomed.;36(4), 898-925.

(8) West, C. M., and Blader, I. J. (2015) Oxygen sensing by protozoans: how they catch their breath, Current Opinion in Microbiology 26, 41-47.

(9) van der Wel, H., Ercan, A., and West, C. M. (2005) The Skp1 Prolyl Hydroxylase from *Dictyostelium* Is Related to the Hypoxia-inducible Factor-α Class of Animal Prolyl 4-Hydroxylases, Journal of Biological Chemistry 280, 14645-14655.

(10) Xu, Y., Brown, K. M., Wang, Z. A., van der Wel, H., Teygong, C., Zhang, D., Blader, I. J., and West, C. M. (2012) The Skp1 Protein from *Toxoplasma* Is Modified by a Cytoplasmic Prolyl 4-Hydroxylase Associated with Oxygen Sensing in the Social Amoeba *Dictyostelium*, Journal of Biological Chemistry 287, 25098-25110.

(11) Semenza, G. L. (2007) Hypoxia-Inducible Factor 1 (HIF-1) Pathway, Science's STKE 2007(407), cm8.

(12) Cordonnier, C., Mandalasi, M., Gigley, J., Wohlfert, E. A., West, C. M., and Blader, I. J. (2024) The *Toxoplasma* oxygen-sensing protein, TgPhyA, is required for resistance to interferon gamma-mediated nutritional immunity in mice, PLOS Biology 22, e3002690.

(13) Zheng, N., Schulman, B. A., Song, L., Miller, J. J., Jeffrey, P. D., Wang, P., Chu, C., Koepp, D. M., Elledge, S. J., Pagano, M., Conaway, R. C., Conaway, J. W., Harper, J. W., and Pavletich, N. P. (2002) Structure of the Cul1–Rbx1–Skp1–F box^{Skp2} SCF ubiquitin ligase complex, Nature 416, 703-709.

(14) Bai, C., Sen, P., Hofmann, K., Ma, L., Goebl, M., Harper, J. W., and Elledge, S. J. (1996) SKP1 Connects Cell Cycle Regulators to the Ubiquitin Proteolysis Machinery through a Novel Motif, the F-Box, Cell 86, 263-274.

(15) Winston, J. T., Koepp, D. M., Zhu, C., Elledge, S. J., and Harper, J. W. (1999) A family of mammalian F-box proteins, Current Biology 9, 1180-S1183.

(16) Hua, Z., Zou, C., Shiu, S.-H., and Vierstra, R. D. (2011) Phylogenetic Comparison of F-Box (FBX) Gene Superfamily within the Plant Kingdom Reveals Divergent Evolutionary Histories Indicative of Genomic Drift, PLOS ONE 6, e16219.

(17) Lee, J. E., Sweredoski, M. J., Graham, R. L. J., Kolawa, N. J., Smith, G. T., Hess, S., and Deshaies, R. J. (2011) The Steady-State Repertoire of Human SCF Ubiquitin Ligase Complexes Does Not Require Ongoing Nedd8 Conjugation, Molecular & Cellular Proteomics 10, M110.006460.

(18) Finley, D., Ulrich, H. D., Sommer, T., and Kaiser, P. (2012) The Ubiquitin–Proteasome System of *Saccharomyces cerevisiae*, Genetics 192, 319-360.

(19) Sarikaya Bayram, Ö., Bayram, Ö., Karahoda, B., Meister, C., Köhler, A. M., Thieme, S., Elramli, N., Frawley, D., McGowan, J., Fitzpatrick, D. A., Schmitt, K., de Assis, L. J., Valerius, O., Goldman, G. H., and Braus, G. H. (2022) F-box receptor mediated control of substrate stability and subcellular location organizes cellular development of *Aspergillus nidulans*, PLOS Genetics 18, e1010502.

(20) Mandalasi, M. N., Gas-Pascual, E., Baptista, C. G., Deng, B., van der Wel, H., Kruijtzer, J. A. W., Boons, G.-J., Blader, I. J., and West, C. M. (2024) Oxygen-dependent regulation of F-box proteins in *Toxoplasma gondii* is mediated by Skp1 glycosylation, Journal of Biological Chemistry 300, 107801.

(21) Boland, A. W., Gas-Pascual, E., Nottingham, B. L., van der Wel, H., Daniel, N. G., Sheikh, M. O., Schafer, C. M., and West, C. M. (2022) Oxygen-dependent regulation of E3(SCF)ubiquitin ligases and a Skp1-associated JmjD6 homolog in development of the social amoeba *Dictyostelium*, Journal of Biological Chemistry 298, 102305.

(22) Skowyra, D., Craig, K. L., Tyers, M., Elledge, S. J., and Harper, J. W. (1997) F-Box Proteins Are Receptors that Recruit Phosphorylated Substrates to the SCF Ubiquitin-Ligase Complex, Cell 91, 209-219.

(23) Liu, J., and Nussinov, R. (2009) The Mechanism of Ubiquitination in the Cullin-RING E3 Ligase Machinery: Conformational Control of Substrate Orientation, PLOS Computational Biology 5, e1000527.

(24) Hershko, A., Heller, H., Elias, S., and Ciechanover, A. (1983) Components of ubiquitin-protein ligase system. Resolution, affinity purification, and role in protein breakdown, Journal of Biological Chemistry 258, 8206-8214.

(25) Pierce, N. W., Kleiger, G., Shan, S.-o., and Deshaies, R. J. (2009) Detection of sequential polyubiquitylation on a millisecond timescale, Nature 462, 615-619.

(26) Ciechanover, A., Heller, H., Elias, S., Haas, A. L., and Hershko, A. (1980) ATP-dependent conjugation of reticulocyte proteins with the polypeptide required for protein degradation, Proceedings of the National Academy of Sciences 77, 1365-1368.

(27) Hershko, A., Ciechanover, A., Heller, H., Haas, A. L., and Rose, I. A. (1980) Proposed role of ATP in protein breakdown: conjugation of protein with multiple chains of the polypeptide of ATP-dependent proteolysis, Proceedings of the National Academy of Sciences 77, 1783-1786.

(28) Grice, G. L., and Nathan, J. A. (2016) The recognition of ubiquitinated proteins by the proteasome, Cellular and Molecular Life Sciences 73, 3497-3506.

(29) Sheikh, M. O., Xu, Y., van der Wel, H., Walden, P., Hartson, S. D., and West, C. M. (2015) Glycosylation of Skp1 Promotes Formation of Skp1–Cullin-1–F-box Protein Complexes in *Dictyostelium*, Molecular & Cellular Proteomics 14, 66-80.

(30) Sheikh, M. O., Schafer, C. M., Powell, J. T., Rodgers, K. K., Mooers, B. H. M., and West, C. M. (2014) Glycosylation of Skp1 Affects Its Conformation and Promotes Binding to a Model F-Box Protein, Biochemistry 53, 1657-1669.

(31) Sheikh, M. O., Thieker, D., Chalmers, G., Schafer, C. M., Ishihara, M., Azadi, P., Woods, R. J., Glushka, J. N., Bendiak, B., Prestegard, J. H., and West, C. M. (2017) O_2 sensing–associated glycosylation exposes the F-box–combining site of the *Dictyostelium* Skp1 subunit in E3 ubiquitin ligases, Journal of Biological Chemistry 292, 18897-18915.

(32) Xu, X., Eletsky, A., Sheikh, M. O., Prestegard, J. H., and West, C. M. (2018) Glycosylation Promotes the Random Coil to Helix Transition in a Region of a Protist Skp1 Associated with F-Box Binding, Biochemistry 57, 511-515.

(33) Kim, H. W., Eletsky, A., Gonzalez, K. J., van der Wel, H., Strauch, E.-M., Prestegard, J. H., and West, C. M. (2020) Skp1 Dimerization Conceals Its F-Box Protein Binding Site, Biochemistry 59, 1527-1536.

(34) Henzl, M. T., Thalmann, I., and Thalmann, R. (1998) OCP2 exists as a dimer in the organ of Corti, Hearing Research 126, 37-46.

(35) Cantrell, D. A., Urbauer, R. J. B., Kim, H. W., Woods, R. J., Urbauer, J. L., Wood, Z. A., and West, C. M. (2025) Glycosylation Weakens Skp1 Homodimerization in *Toxoplasma gondii* by Interrupting a Fuzzy Interaction, Biochemistry 64(10):2262-2279.

(36) Tan, A., Tanner, J. J., and Henzl, M. T. (2008) Energetics of OCP1–OCP2 complex formation, Biophysical Chemistry 134, 64-71.

(37) Borgia, A., Borgia, M. B., Bugge, K., Kissling, V. M., Heidarsson, P. O., Fernandes, C. B., Sottini, A., Soranno, A., Buholzer, K. J., Nettels, D., Kragelund, B. B., Best, R. B., and Schuler, B. (2018) Extreme disorder in an ultrahigh-affinity protein complex, Nature 555, 61-66.

(38) Sottini, A., Borgia, A., Borgia, M. B., Bugge, K., Nettels, D., Chowdhury, A., Heidarsson, P. O., Zosel, F., Best, R. B., Kragelund, B. B., and Schuler, B. (2020) Polyelectrolyte interactions enable rapid association and dissociation in high-affinity disordered protein complexes, Nature Communications 11, 5736.

(39) Heidarsson, P. O., Mercadante, D., Sottini, A., Nettels, D., Borgia, M. B., Borgia, A., Kilic, S., Fierz, B., Best, R. B., and Schuler, B. (2022) Release of linker histone from the nucleosome driven by polyelectrolyte competition with a disordered protein, Nature Chemistry 14, 224-231.

(40) Williamson, M. P. (2023) Protein Binding: A Fuzzy Concept, Life (Basel), 13(4), 855.

(41) West, C. M., van der Wel, H., Sassi, S., and Gaucher, E. A. (2004) Cytoplasmic glycosylation of protein-hydroxyproline and its relationship to other glycosylation pathways, Biochimica et Biophysica Acta (BBA) - General Subjects 1673, 29-44.

(42) Wang, F., Metcalf, T., van der Wel, H., and West, C. M. (2003) Initiation of Mucin-type O-Glycosylation in *Dictyostelium* Is Homologous to the Corresponding Step in Animals and Is Important for Spore Coat Function, Journal of Biological Chemistry 278, 51395-51407.

(43) Ercan, A., Panico, M., Sutton-Smith, M., Dell, A., Morris, H. R., Matta, K. L., Gay, D. F., and West, C. M. (2006) Molecular Characterization of a Novel UDP-galactose:Fucoside α3-Galactosyltransferase That Modifies Skp1 in the Cytoplasm of *Dictyostelium*, Journal of Biological Chemistry 281, 12713-12721.

(44) West, C. M., Wang, Z. A., and van der Wel, H. (2010) A cytoplasmic prolyl hydroxylation and glycosylation pathway modifies Skp1 and regulates O_2-dependent development in *Dictyostelium*, Biochimica et Biophysica Acta (BBA) - General Subjects 1800, 160-171.

(45) Mandalasi, M., Kim, H. W., Thieker, D., Sheikh, M. O., Gas-Pascual, E., Rahman, K., Zhao, P., Daniel, N. G., van der Wel, H., Ichikawa, H. T., Glushka, J. N., Wells, L., Woods, R. J., Wood,

Z. A., and West, C. M. (2020) A terminal α3-galactose modification regulates an E3 ubiquitin ligase subunit in *Toxoplasma gondii*, Journal of Biological Chemistry 295, 9223-9243.

(46) van der Wel, H., Fisher, S. Z., and West, C. M. (2002) A Bifunctional Diglycosyltransferase Forms the Fucα1,2Galβ1,3-Disaccharide on Skp1 in the Cytoplasm of *Dictyostelium*, Journal of Biological Chemistry 277, 46527-46534.

(47) Rahman, K., Zhao, P., Mandalasi, M., van der Wel, H., Wells, L., Blader, I. J., and West, C. M. (2016) The E3 Ubiquitin Ligase Adaptor Protein Skp1 Is Glycosylated by an Evolutionarily Conserved Pathway That Regulates Protist Growth and Development, Journal of Biological Chemistry 291, 4268-4280.

(48) Rahman, K., Mandalasi, M., Zhao, P., Sheikh, M. O., Taujale, R., Kim, H. W., van der Wel, H., Matta, K., Kannan, N., Glushka, J. N., Wells, L., and West, C. M. (2017) Characterization of a cytoplasmic glucosyltransferase that extends the core trisaccharide of the *Toxoplasma* Skp1 E3 ubiquitin ligase subunit, Journal of Biological Chemistry 292, 18644-18659.

(49) Schafer, C. M., Sheikh, M. O., Zhang, D., and West, C. M. (2014) Novel Regulation of Skp1 by the *Dictyostelium* AgtA α-Galactosyltransferase Involves the Skp1-binding Activity of Its WD40 Repeat Domain, Journal of Biological Chemistry 289, 9076-9088.

(50) Ketcham, C., Wang, F., Fisher, S. Z., Ercan, A., van der Wel, H., Locke, R. D., Sirajud-Doulah, K., Matta, K. L., and West, C. M. (2004) Specificity of a Soluble UDP-Galactose:Fucoside α1,3-Galactosyltransferase That Modifies the Cytoplasmic Glycoprotein Skp1 in *Dictyostelium*, Journal of Biological Chemistry 279, 29050-29059.

(51) Baptista, C. G., Lis, A., Deng, B., Gas-Pascual, E., Dittmar, A., Sigurdson, W., West, C. M., and Blader, I. J. (2019) *Toxoplasma* F-box protein 1 is required for daughter cell scaffold function during parasite replication, PLOS Pathogens 15, e1007946.

(52) Wang, Z. A., van der Wel, H., Vohra, Y., Buskas, T., Boons, G.-J., and West, C. M. (2009) Role of a Cytoplasmic Dual-function Glycosyltransferase in O_2 Regulation of Development in *Dictyostelium*, Journal of Biological Chemistry 284, 28896-28904.

(53) Thomas M. Laue, B. S., Teresa M. Ridgeway, S. L. Pelletier. (1992) Computer-aided Interpretation of Sedimentation Data for Proteins, In Analytical ultracentrifugation in biochemistry and polymer science (S. E. Harding, J. C. H., A. J. Rowe, Ed.), pp 90-125, Royal Society of Chemistry, Cambridge, UK.

(54) Schuck, P. (2000) Size-Distribution Analysis of Macromolecules by Sedimentation Velocity Ultracentrifugation and Lamm Equation Modeling, Biophysical Journal 78, 1606-1619.

(55) Brautigam, C. A. (2015) Chapter Five - Calculations and Publication-Quality Illustrations for Analytical Ultracentrifugation Data, In Methods in Enzymology (Cole, J. L., Ed.), pp 109-133, Academic Press.

(56) Wilkins, M. R., Gasteiger, E., Bairoch, A., Sanchez, J.-C., Williams, K. L., Appel, R. D., and Hochstrasser, D. F. (1999) Protein Identification and Analysis Tools in the ExPASy Server, In 2-D Proteome Analysis Protocols (Link, A. J., Ed.), pp 531-552, Humana Press, Totowa, NJ.

(57) Schuck, P. (2003) On the analysis of protein self-association by sedimentation velocity analytical ultracentrifugation, Analytical Biochemistry 320, 104-124.

(58) Ortega, A., Amorós, D., and García de la Torre, J. (2011) Prediction of Hydrodynamic and Other Solution Properties of Rigid Proteins from Atomic- and Residue-Level Models, Biophysical Journal 101, 892-898.

(59) Abramson, J., Adler, J., Dunger, J., Evans, R., Green, T., Pritzel, A., Ronneberger, O., Willmore, L., Ballard, A. J., Bambrick, J., Bodenstein, S. W., Evans, D. A., Hung, C.-C., O'Neill, M., Reiman, D., Tunyasuvunakool, K., Wu, Z., Žemgulytė, A., Arvaniti, E., Beattie, C., Bertolli, O., Bridgland, A., Cherepanov, A., Congreve, M., Cowen-Rivers, A. I., Cowie, A., Figurnov, M., Fuchs, F. B., Gladman, H., Jain, R., Khan, Y. A., Low, C. M. R., Perlin, K., Potapenko, A., Savy, P., Singh, S., Stecula, A., Thillaisundaram, A., Tong, C., Yakneen, S., Zhong, E. D., Zielinski, M., Žídek, A., Bapst, V., Kohli, P., Jaderberg, M., Hassabis, D., and Jumper, J. M. (2024) Accurate structure prediction of biomolecular interactions with AlphaFold 3, Nature 630, 493-500.

(60) Case, D. A., Aktulga, H. M., Belfon, K., Cerutti, D. S., Cisneros, G. A., Cruzeiro, V. W. D., Forouzesh, N., Giese, T. J., Götz, A. W., Gohlke, H., Izadi, S., Kasavajhala, K., Kaymak, M. C., King, E., Kurtzman, T., Lee, T.-S., Li, P., Liu, J., Luchko, T., Luo, R., Manathunga, M., Machado, M. R., Nguyen, H. M., O'Hearn, K. A., Onufriev, A. V., Pan, F., Pantano, S., Qi, R., Rahnamoun, A., Risheh, A., Schott-Verdugo, S., Shajan, A., Swails, J., Wang, J., Wei, H., Wu, X., Wu, Y., Zhang, S., Zhao, S., Zhu, Q., Cheatham, T. E., III, Roe, D. R., Roitberg, A., Simmerling, C., York, D. M., Nagan, M. C., and Merz, K. M., Jr. (2023) AmberTools, Journal of Chemical Information and Modeling 63, 6183-6191.

(61) Maier, J. A., Martinez, C., Kasavajhala, K., Wickstrom, L., Hauser, K. E., and Simmerling, C. (2015) ff14SB: Improving the Accuracy of Protein Side Chain and Backbone Parameters from ff99SB, Journal of Chemical Theory and Computation 11, 3696-3713.

(62) Kirschner, K. N., Yongye, A. B., Tschampel, S. M., González-Outeiriño, J., Daniels, C. R., Foley, B. L., and Woods, R. J. (2008) GLYCAM06: A generalizable biomolecular force field. Carbohydrates, Journal of Computational Chemistry 29, 622-655.

(63) Jorgensen, W. L., Chandrasekhar, J., Madura, J. D., Impey, R. W., and Klein, M. L. (1983) Comparison of simple potential functions for simulating liquid water, The Journal of Chemical Physics 79, 926-935.

(64) Joung, I. S., and Cheatham, T. E., III. (2008) Determination of Alkali and Halide Monovalent Ion Parameters for Use in Explicitly Solvated Biomolecular Simulations, The Journal of Physical Chemistry B 112, 9020-9041.

(65) Darden, T., York, D., and Pedersen, L. (1993) Particle mesh Ewald: An N·log(N) method for Ewald sums in large systems, The Journal of Chemical Physics 98, 10089-10092.

(66) Webb, B., and Sali, A. (2016) Comparative Protein Structure Modeling Using MODELLER, Current Protocols in Bioinformatics 54, 5.6.1-5.6.37.

(67) Woods, R. J. (2014) GLYCAM-Web, glycam.
Kirschner KN, Yongye AB, Tschampel SM, González-Outeiriño J, Daniels CR, Foley BL, Woods RJ (2008) GLYCAM06: a generalizable biomolecular force field. Carbohydrates, J Comput Chem. 29(4), 622-655.

(68) Pettersen, E. F., Goddard, T. D., Huang, C. C., Couch, G. S., Greenblatt, D. M., Meng, E. C., and Ferrin, T. E. (2004) UCSF Chimera—A visualization system for exploratory research and analysis, Journal of Computational Chemistry 25, 1605-1612.

(69) Miller, B. R., III, McGee, T. D., Jr., Swails, J. M., Homeyer, N., Gohlke, H., and Roitberg, A. E. (2012) MMPBSA.py: An Efficient Program for End-State Free Energy Calculations, Journal of Chemical Theory and Computation 8, 3314-3321.

(70) McKay, K., Hamilton, N. B., Remington, J. M., Schneebeli, S. T., and Li, J. (2022) Essential Dynamics Ensemble Docking for Structure-Based GPCR Drug Discovery, Frontiers in Molecular Biosciences 9, 879212.

(71) Kelley, L. A., Gardner, S. P., and Sutcliffe, M. J. (1996) An automated approach for clustering an ensemble of NMR-derived protein structures into conformationally related subfamilies, Protein Engineering, Design and Selection 9, 1063-1065.

(72) Mitternacht, S. (2016) FreeSASA: An open-source C library for solvent accessible surface area calculations, F1000Research 5, 189.

(73) Lee, B., and Richards, F. M. (1971) The interpretation of protein structures: Estimation of static accessibility, Journal of Molecular Biology 55, 379-IN374.

(74) Shrake, A., and Rupley, J. A. (1973) Environment and exposure to solvent of protein atoms. Lysozyme and insulin, Journal of Molecular Biology 79, 351-371.

(75) Martínez, L. (2015) Automatic Identification of Mobile and Rigid Substructures in Molecular Dynamics Simulations and Fractional Structural Fluctuation Analysis, PLOS ONE 10, e0119264.

(76) Tyka, M. D., Keedy, D. A., André, I., DiMaio, F., Song, Y., Richardson, D. C., Richardson, J. S., and Baker, D. (2011) Alternate States of Proteins Revealed by Detailed Energy Landscape Mapping, Journal of Molecular Biology 405, 607-618.

(77) Das, R., and Baker, D. (2008) Macromolecular Modeling with Rosetta, Annual Review of Biochemistry 77, 363-382.

(78) Barlow, K. A., Ó Conchúir, S., Thompson, S., Suresh, P., Lucas, J. E., Heinonen, M., and Kortemme, T. (2018) Flex ddG: Rosetta Ensemble-Based Estimation of Changes in Protein–Protein Binding Affinity upon Mutation, The Journal of Physical Chemistry B 122, 5389-5399.

(79) Fleishman, S. J., Leaver-Fay, A., Corn, J. E., Strauch, E.-M., Khare, S. D., Koga, N., Ashworth, J., Murphy, P., Richter, F., Lemmon, G., Meiler, J., and Baker, D. (2011) RosettaScripts: A Scripting Language Interface to the Rosetta Macromolecular Modeling Suite, PLOS ONE 6, e20161.

(80) Smith, C. A., and Kortemme, T. (2008) Backrub-Like Backbone Simulation Recapitulates Natural Protein Conformational Variability and Improves Mutant Side-Chain Prediction, Journal of Molecular Biology 380, 742-756.

(81) Kellogg, E. H., Leaver-Fay, A., and Baker, D. (2011) Role of conformational sampling in computing mutation-induced changes in protein structure and stability, Proteins: Structure, Function, and Bioinformatics 79, 830-838.

(82) West, C. M., van der Wel, H., Chinoy, Z., Boons, G.-J., Gauthier, T. J., Taylor, C. M., and Xu, Y. (2015) Generating Isoform-Specific Antibodies: Lessons from Nucleocytoplasmic Glycoprotein Skp1, In Glycoscience: Biology and Medicine (Taniguchi, N., and Endo, T., and Hart, G. W., and Seeberger, P. H., and Wong, C.-H., Eds.), pp 927-934, Springer Japan, Tokyo.

(83) Swanson, C. J., and Sivaramakrishnan, S. (2014) Harnessing the Unique Structural Properties of Isolated α-Helices, Journal of Biological Chemistry 289, 25460-25467.

(84) Sivaramakrishnan, S., Spink, B. J., Sim, A. Y. L., Doniach, S., and Spudich, J. A. (2008) Dynamic charge interactions create surprising rigidity in the ER/K α-helical protein motif, Proceedings of the National Academy of Sciences 105, 13356-13361.

(85) Sommese, R. F., Sivaramakrishnan, S., Baldwin, R. L., and Spudich, J. A. (2010) Helicity of short E-R/K peptides, Protein Science 19, 2001-2005.

(86) Baker, E. G., Bartlett, G. J., Crump, M. P., Sessions, R. B., Linden, N., Faul, C. F. J., and Woolfson, D. N. (2015) Local and macroscopic electrostatic interactions in single α-helices, Nature Chemical Biology 11, 221-228.

(87) van der Wel, H., Johnson, J. M., Xu, Y., Karunaratne, C. V., Wilson, K. D., Vohra, Y., Boons, G.-J., Taylor, C. M., Bendiak, B., and West, C. M. (2011) Requirements for Skp1 Processing by Cytosolic Prolyl 4(trans)-Hydroxylase and α-N-Acetylglucosaminyltransferase Enzymes Involved in O_2 Signaling in *Dictyostelium*, Biochemistry 50, 1700-1713.

(88) Kozarov, E., van der Wel, H., Field, M., Gritzali, M., Brown, R. D., and West, C. M. (1995) Characterization of FP21, a Cytosolic Glycoprotein from *Dictyostelium*, Journal of Biological Chemistry 270, 3022-3030.

(89) Simonetta, K. R., Taygerly, J., Boyle, K., Basham, S. E., Padovani, C., Lou, Y., Cummins, T. J., Yung, S. L., von Soly, S. K., Kayser, F., Kuriyan, J., Rape, M., Cardozo, M., Gallop, M. A., Bence, N. F., Barsanti, P. A., and Saha, A. (2019) Prospective discovery of small molecule enhancers of an E3 ligase-substrate interaction, Nature Communications 10, 1402.

(90) Tan, X., Calderon-Villalobos, L. I. A., Sharon, M., Zheng, C., Robinson, C. V., Estelle, M., and Zheng, N. (2007) Mechanism of auxin perception by the TIR1 ubiquitin ligase, Nature 446, 640-645.

(91) Nishio, K., Kawarasaki, T., Sugiura, Y., Matsumoto, S., Konoshima, A., Takano, Y., Hayashi, M., Okumura, F., Kamura, T., Mizushima, T., and Nakatsukasa, K. (2023) Defective import of mitochondrial metabolic enzyme elicits ectopic metabolic stress, Science Advances 9, eadf1956.

(92) He, X.-h., Li, J.-r., Shen, S.-y., and Xu, H. E. (2025) AlphaFold3 versus experimental structures: assessment of the accuracy in ligand-bound G protein-coupled receptors, Acta Pharmacologica Sinica 46, 1111-1122.

(93) Strom, J. M., and Luck, K. (2025) Bias in, bias out – AlphaFold-Multimer and the structural complexity of protein interfaces, Current Opinion in Structural Biology 91, 103002.

(94) Zonta, F., and Pantano, S. (2024) From sequence to mechanobiology? Promises and challenges for AlphaFold 3, Mechanobiology in Medicine 2, 100083.

(95) Wee, J., and Wei, G.-W. (2024) Evaluation of AlphaFold 3's Protein–Protein Complexes for Predicting Binding Free Energy Changes upon Mutation, Journal of Chemical Information and Modeling 64, 6676-6683.

CHAPTER 4

ENGINEERING RECOMBINANT EXPRESSION SYSTEMS FOR SOLUBLE SCF COMPONENTS FROM PROTISTS

Cantrell, D. A., Wilson, T., and West, C. M. (2025) Engineering Recombinant Expression Systems for Soluble SCF Components from Protists.
To be submitted to a peer-reviewed journal.

ABSTRACT

The Skp1/Cullin1/F-Box (SCF) complex is an E3 ubiquitin ligase responsible for proteomic control in a wide variety of eukaryotes including protists. Substrate specificity is dictated by the specific F-Box protein (FBP) bound into the complex. The Skp1 adaptor protein binds a large variety of FBPs and is responsible for linking them to Cullin1 of the complex. Within many protists, oxygen sensing is carried out via hydroxylation and subsequent glycosylation of the Skp1 protein. This results in a change in the FBP binding repertoire of Skp1 likely changing which substrates are polyubiquitinated. Several models have been proposed to explain the change in Skp1's FBP binding repertoire. Despite this, biophysical characterization of these interactions has been hampered by the insolubility of endogenous FBPs in the absence of Skp1. Here, we demonstrate the construction and purification of a library of soluble endogenous FBPs from *E. coli*. First, we show that the relatively weak DdSkp1A homodimer affinity minimally changes upon glycosylation, reducing the convoluting factors in characterizing FBP/Skp1 interactions. Thus, we built a library of *Dictyostelium* FBPs fused to maltose binding protein (MBP) and screened them for soluble protein production. Finally, we demonstrated the effectiveness of a dual affinity purification system in purifying full-length MBP-FBP constructs from a heterogenous mixture of construct fragments and *E. coli* proteins. Pulldown assays are currently undergoing optimization to compare binding of purified MBP-FBPs to different Skp1 glycoforms. Engineered constructs will be valuable for developing assays to characterize the effects of glycosylation on SCF ubiquitin-ligase activity.

INTRODUCTION

Oxygen sensing is a vital component of environmental sensing in organisms. Within animals including humans, oxygen sensing is mediated by the prolyl hydroxylase PHD2 [1]. Under normoxic conditions, PHD2 targets the protein HIF1α with the hydroxylation of multiple Pro residues. The resulting hydroxyproline generates a degron on HIF1α allowing for its recognition by the von Hipple Lindau E3 ubiquitin ligase. The von Hipple Lindau E3 ubiquitin ligase polyubiquitinates HIF1α leading to its recognition and subsequent degradation by the 26S proteosome. Under hypoxic conditions, HIF1α is stabilized allowing for it to signal expression of hypoxia related genes [1]. Within protists, oxygen sensing is mediated by the widely dispersed PHD2 homologue PhyA which targets the Skp1 adaptor protein of the Skp1/Cullin1/F-Box (SCF) E3 ubiquitin ligase complex [2]. PhyA, which is likely ancestral to PHD2, hydroxylates a Pro conserved within protist Skp1 proteins [3]. Skp1 acts as a core junction within the SCF complex and mediates the association of tens to hundreds of F-Box Proteins (FBPs) [4, 5]. These FBPs represent the substrate recognition portion of the SCF complex [6-13].

Hydroxylation of Skp1 results in the formation of a hydroxyproline which acts as the attachment site for subsequent glycosylation [2]. Skp1 glycosylation is mediated by a series of cytoplasmic glycosyltransferases which show absolute specificity for Skp1. The action of these glycosyltransferases results in the construction of a homogeneous, linear pentasaccharide on the C-terminal partially disordered region (CTR) of Skp1. Organisms which contain this glycosylation pathway include the parasites *Toxoplasma gondii* and *Pythium ultimum* along with the social amoeba *Dictyostelium discoideum* [2]. Evidence suggests that glycosylation alters Skp1's FBP binding repertoire which likely changes the substrates targeted for degradation by the SCF complex [11, 12, 14]. Glycosylation also appears to influence the stability of FBPs themselves [11,

12]. There additionally seems to be a greater association between proteasomal subunits and the SCF complex upon glycosylation [11, 12, 14]. This offers an alternative mechanism by which an oxygen sensitive prolyl hydroxylase controls the cellular proteome.

Several mechanisms have been proposed for how glycosylation controls its FBP binding repertoire. These mechanisms primarily center around an expected disorder to order transition that has been proposed to occur in Skp1's CTR upon glycosylation [15-17]. Recent data suggests that glycosylation of Skp1 in *Toxoplasma* results in the weakening of its strong (apparent K_d ~50 nM) Skp1 homodimer to a much weaker 400 nM K_d homodimer [18]. The strong TgSkp1 homodimer is on par with the 25 nM apparent K_d previously determined for Fbs1 and Skp1 in the mammalian system [19]. If visualized as an affinity hierarchy, TgSkp1's ~50 nM homodimer affinity would be expected to exert differential inhibitory effects dependent upon the affinity of each specific FBP-Skp1 interaction. A direct effect of Skp1 glycosylation on FBP binding has also been proposed [15, 17, 20]. In this model, the disorder to order transition in Skp1's CTR promotes a conformational ensemble more favorable to FBP binding. This may be due in large part to the reduced entropic penalty of binding a conformationally restrained Skp1 CTR. In fact, a large entropic penalty has been observed for the binding between Skp1 and Fbs1 in the mammalian system [19]. Fbs1 represents the only known FBP that can be expressed as a soluble construct in the absence of Skp1. A limited *in vitro* study investigated the role of glycosylation in binding Fbs1 which correlated with changes in secondary structure [20]. However, biophysical analysis of this process has been severely hampered by the lack of soluble, endogenous FBPs with which to perform experiments.

Here, we demonstrate that *Dictyostelium* represents an effective model system for investigating the role of glycosylation in influencing the direct interaction of FBPs and Skp1. Sedimentation Velocity (SV) experiments suggest that along with forming a much weaker

homodimer as compared to TgSkp1, DdSkp1A has a minimal shift in homodimerization upon glycosylation. These effects show a reduction in confounding variables in FBP-Skp1 binding studies as compared to TgSkp1. We then design and utilize a system where we generate a library of endogenous FBPs solubilized via an MBP solubility tag. Despite the heavy fragmentation of these MBP-FBP fusion proteins during production, we demonstrate effective purification of soluble, full-length proteins. This is done through the use of a two-step affinity purification technique utilizing both N and C-terminal affinity tags. Our engineered system shows significant potential in our efforts to elucidate the mechanisms driving differential binding of Skp1's glycoforms to their FBP binding partners.

METHODS

Cloning of Purification DdSkp1A Constructs.

Deletion of DdSkp1A's CTR was conducted as previously described for TgSkp1 [18]. The pNIC28-HisTEV-DdSkp1A-FL plasmid was utilized as the template [21]. Primers were designed against the template to exclude amplification of Skp1's CTR with a 16 bp overlap on their 5' ends **(Fig 4.S11)**. This overlap allowed homologous end joining once transformed into *Escherichia coli* resulting in a plasmid lacking Skp1's CTR **(Fig 4.S12)**. The PCR reaction utilized the GXL PrimeStar Polymerase from TaKaRa. Clones were initially screened using colony PCR with Taq Polymerase (NEB) followed by Sanger Sequencing. DdSkp1A constructs containing an equal length PolySer and Scrambled (Scrambled4) replacement of its CTR were synthesized by GenScript and inserted into the pNIC28 backbone resulting in the pNIC28-HisTEV-DdSkp1A-PolySer and pNIC28-HisTEV-DdSkp1A-Scrambled4 plasmids **(Fig 4.S13)**. DdSkp1A constructs were purified as previously described for TgSkp1 [18].

Purification of Skp1 Glycosylation Enzymes and Fbs1.

DdAgtA [22], DdPgtA [23], and GpFbs1 (OCP1) [19] were purified as previously described. GpFbs1 was not treated with Thrombin.

Glycosylation of DdSkp1A.

His-DdSkp1A was expressed in *E. coli* in the presence of expressed DdPhyA and Chimeric Gnt1 and purified as previously described for TgSkp1 [18]. The PgtA reaction was conducted overnight (~16-18 h) at room temperature by incubating 93 µM Gn-(His-DdSkp1A) in the presence of (75 mM HEPES-NaOH (pH 7.5), 75 mM NaCl, 1 mM DTT, 5 mM $MgCl_2$, 2 mM $MnCl_2$, 0.1% (v/v) Tween-20, 5 mM benzamidine, 10 µg/ml leupeptin, 10 µg/ml aprotinin, 0.01 Units/µl Calf Intestinal Alkaline Phosphatase, 186 µM UDP-Gal (2× molar excess), 186 µM GDP-Fuc (2× molar excess), and 370 nM DdPgtA (1:250 Skp1:PgtA)). The reaction was then dialyzed against Q-Column Buffer A (50 mM Tris-HCl (pH 7.5), 1 mM EDTA, and 5 mM $MgCl_2$) at 4°C overnight. FGGn-(His-DdSkp1A) was then loaded onto a 5 ml Hi-Binding Q-Column (Cytiva) before purification using a salt gradient between Q-Column Buffer A and Buffer B (50 mM Tris-HCl (pH 7.5), 1 mM EDTA, 5 mM $MgCl_2$, and 1 M NaCl). FGGn-(HisDdSkp1A) was then concentrated and buffer exchanged using a 10 kDa Cutoff centrifugal ultrafiltration device (Millipore). The AgtA reaction was then conducted overnight (~16-18 h) at room temperature by incubating 140 µM FGGn-(His-DdSkp1A) in (75 mM HEPES-NaOH (pH 7.5), 75 mM NaCl, 1 mM DTT, 1 mM PMSF, 5 mM benzamidine, 10 µg/ml aprotinin, 10 µg/ml leupeptin, 0.5 mM $MgCl_2$, 0.01 Units/µl Calf Intestinal Alkaline Phosphatase, 550 µM UDP-Gal (4× molar excess), and 2.8 µM DdAgtA (1:50 Skp1:AgtA)). Completion of each reaction was confirmed using Matrix

Assisted Laser Desorption-Time of Flight (MALDI-TOF) mass spectroscopy. The reaction was then buffer exchanged using the same 10 kDa filter into Wash Buffer (50 mM Na/K phosphate (pH 7.4), 300 mM NaCl) and was repurified using the same His-Tag purification protocol as other Skp1 variants.

Sedimentation Velocity Analysis of DdSkp1A Constructs.

Sedimentation Velocity experiments were conducted for DdSkp1A constructs as previously done for TgSkp1 constructs [18]. Buffer and protein parameters were calculated using SedNTerp [24]. Distributions were modeled using SedFit [25] and overlayed and integrated in Gussi [26]. S_w values were then plotted in SedPhat where a Monomer-Dimer self-association model was used to model each SV isotherm. Expected sedimentation values were previously determined for DdSkp1A [27] using HYDROPRO [28].

Building Cullin Constructs.

An expression strategy was utilized as previously described for full-length HsCul3 [29]. Coding seuqences for DdCulE (Uniprot ID: Q54XF7) and DdRbx1 (Uniprot ID: Q54K33) were codon optimized and cloned into the pET-Duet1 expression vector by Genscript **(Fig 4.S14)**. For TgCul1 (Uniprot ID: B9QE00), a long unconserved and likely disordered stretch at the N-terminus of the protein was replaced by the equivalent sequence from the Cul1 in the apicomplexan *Sarcocystis neurona*. The final sequences for TgCul1 and TgRbx1 (Uniprot ID: A0A125YHW3) were then codon optimized and cloned into the pET-Duet1 expression vector by Genscript **(Fig 4.S15)**. A StrepII-tag and TEV cleavage site were appended to the N-terminus of TgRbx1 using primers designed to generate non-homologous blunt ends **(Fig 4.S11)**. The new plasmid was PCR

generated using PrimeStar GXL polymerase (TaKaRa) and was treated with the KLD (Kinase, Ligase, and DpnI) mix from NEB before transformation. The added StrepII-tag and TEV cleavage site were then utilized to extend the StrepII-tag into a full-sized SF-tag on TgRbx1. Primers containing 5' homology regions were designed to amplify the SF (Twin StrepII + FLAG) tag from the pSF-TAP-SKP1-CAT plasmid [11] with the TgCul1 and TgRbx1 containing backbone **(Fig 4.S11)**. These fragments were then assembled using the HiFi Assembly Master Mix from NEB to give the final plasmid shown in **(Fig 4.S15)**.

Building His-MBP-FBP Constructs.

For initial cloning, primers were designed against the pET28-HisMBP-HsFbxO3 plasmid to generate a common backbone for all FBPs **(Fig 4.S11)**. Primers containing a 5' homology region with the common plasmid backbone were designed against the coding regions of each FBP target. A codon optimized sequence for a previously designed DdJcdI-Short-H319A construct was used as the template for DdJcdI [12]. The coding sequence for TgFbxO13 (Uniprot ID: V4Z4Z1) was codon optimized and synthesized by Genscript before being placed in the pET-Duet1 plasmid with TgSkp1 (Uniprot ID: A0A0F7UNE6) **(Fig 4.S16)**. This plasmid was used as the template for TgFbxO13. The pET15b-His-TgFbxO1 plasmid [30] was used as the template for TgFbxO1. Genomic *Toxoplasma gondii* DNA which was purified as previously described [11] and was used as the template for TgFbxO14 given its expected lack of introns. All other *Dictyostelium discoideum* FBPs utilized were amplified from a total cDNA library which was generated as previously described [12]. PCR amplifications from templates were carried out using either Platinum SuperFi 2X Green Master Mix (Fisher) or GXL PrimeStar Polymerase (TaKaRa). For cDNA sequences amplified using GXL PrimeStar Polymerase, a ratio of 3:1 (AT):(CG) bases were

used while maintaining the recommended final dNTP concentration due to the AT rich nature of *Dictyostelium* DNA. PCR amplifications that showed multiple bands were purified through gel purification using the NEB Gel Extraction Kit while PCR reactions showing a single discrete product were utilized directly for assembly reactions. Assembly reactions were carried out using the HiFi Assembly Master Mix (NEB). A representative final plasmid sequence for DdFbxF is given in **(Fig 4.S17)**. Inserted FBP sequences for other plasmid assemblies are given in **(Figs 4.S18-4.S29)**. Multiple attempts to clone DdFbxA failed due to repeated missense mutations at different sites in the plasmid. An intact sequence for DdFbxA from a plasmid with a missense mutation in the MBP is given in **(Fig 4.S30)**. During initial plasmid construction, a sequence consistent with (Dictybase ID: DDB_G0273011_ps) was amplified from cDNA for DdFbxK rather than the closely related target (Dictybase ID: DDB_G0273009) **(Fig 4.S22)**. Each protein was renamed DdFbxK-1 and DdFbxK-2 respectively. Despite being annotated as a pseudogene, amplification of the DdFbxK-1 coding sequence from cDNA strongly supported its active expression. Additionally, our sequence diverged from that in Dictybase in such a way that it would be expected to produce a complete FBP very similar to DdFbxK-2. Although our coding sequence diverged from that predicted in Dictybase, the EST (DDB0299438) was a perfect match for our sequence.

Dictyostelium FBPs that passed the initial solubility screens and *Toxoplasma* FBPs had a thrombin cleavable C-terminal SF (Twin-StrepII + FLAG) tag added to facilitate dual affinity purification. Primers were designed to amplify a common SF-tag sequence from the pSF-TAP-SKP1-CAT plasmid [11] **(Fig 4.S11)**. The MBP-FBP construct containing backbone was also amplified by utilizing a common forward primer paired with a variable FBP specific reverse primer. Each primer set contained a common 5’ homology region to facilitate assembly of the

plasmid fragments. Fragments PCR amplified using the Platinum Superfi Polymerase 2X Master Mix (Fisher) and gel purified utilizing the Gel Extraction Kit from NEB. Plasmid assembly was conducted using the HiFi Assembly Master Mix from NEB before transformation. Clones were initially screened using colony PCR followed by whole plasmid nanopore sequencing. An example of a final plasmid sequence is shown in **(Fig 4.S31)** with the C-terminal SF-tag appended to the end of the DdFbxN sequence.

Expression and Solubility Screening of His-MBP-FBP Constructs.

Constructs containing the desired HisMBP-FBP constructs (before SF addition) were transformed into Rosetta E3 *E. coli* cells. Rosetta E3 cells contain the chloramphenicol resistant pRARE plasmid that enhances expression of non-codon optimized sequences. Clonal populations were then grown at 37°C rotating at 180 RPM in 6 ml (TB + 35 µg/ml chloramphenicol + 50 µg/ml kanamycin) starter cultures until reaching an OD_{600} of approximately 0.5 AU. 5 ml of each starter culture were then added to 100 ml of the same medium for induction. Cultures continued to grow until reaching an OD_{600} (1 cm pathlength) of approximately 1.2 AU and then brought down to 20°C for 30 min before taking a T0 timepoint sample and inducing with 500 µM IPTG. Two 10-ml samples were additionally collected at 1.5 h, 3 h, 6 h, and 17.5 h. Cultures were pelleted in 15 ml centrifuge tubes at 3200 × g for 15 min at 4°C, resuspended in 1 ml of LB on ice, transferred to 1.5 ml centrifuge tubes, and pelleted at 15,000 × g for 1 min at 4°C before freezing at -80°C. HisDdCulE + DdRbx1 cultures were treated similarly but grown in ER2566 *E. coli* cells and in the presence of (TB + 100 µg/ml ampicillin).

Expression levels over the time courses were screened as follows. *E. coli* pellets were resuspended in 1 ml of 0.2% SDS in water and vortexed (10-20 min each). Aliquots were then

diluted in a 3:1 (Sample: Loading Buffer) ratio with a 4× gel loading buffer (final: 62 mM Tris-HCl (pH 6.8), 10% (v/v) glycerol, 2% SDS, 20 mM DTT, and bromophenol blue) before loading 5 µl onto premade Midi Gels (Invitrogen). These were run in MOPS Running Buffer (50 mM MOPS, 50 mM Tris, 3.5 mM SDS, and 1 mM EDTA (final pH 7.7)) before blotting using an I-Blot gel blotting device (Invitrogen). Known concentrations of the soluble FBP Fbs1 were loaded onto each gel for normalization and estimation of yields. Timepoints for FBPs that passed the initial expression screen were then screened for solubility. This was done by first resuspending frozen pellets from each timepoint in 1 ml of Super Lysis Buffer (100 mM Na/K Phosphate (pH 7.4), 150 mM NaCl, 0.5 M D-sorbitol, 1 M glycine betaine, 0.7 M trehalose, 5 mM benzamidine, 10 µg/ml leupeptin, 10 µg/ml aprotinin, 0.5 µg/ml pepstatin A, and 0.5 mM PMSF) supplemented with 1 mg/ml Lysozyme, 5 mM $MgCl_2$, 50 µg/ml RNaseA, and 10 µg/ml DNase1. Lysis was aided by sonication using a 1/8-inch sonication probe for 4 min at 30% amplitude for 1 sec on, 3 sec off on ice totaling 1 min of sonication time per sample. Samples were then centrifuged at 21,000 × g for 1 h at 4°C. Clarified supernatants were transferred to a new 1.5 ml centrifuge tube, while pellets were resuspended in 1 ml of 0.2% SDS. Aliquots were then diluted in gel loading buffer and run on a western blot as done before. 10 µl loads were used for DdFbxM, DdFbxD, DdFbxI, DdDlrA, and DdCulE while 5 µl loads were used for all other samples. A similar screening protocol was used for the *Toxoplasma* FBPs, but growth was tested at both 20°C and 37°C. 10 µl loads were utilized for subsequent solubility screens. SF-tagged constructs were used for TgFBP solubility screens.

Solubility Screening of TgCul1 and TgGlt1.

E. coli strains containing HisTgCul1 + TgRbx1 **(Fig 4.S15; No SF tag on TgRbx1)** in ER2566 and HisTgGlt1 in Gold [31] were grown in 50 ml (TB + 100 µg/ml ampicillin) at 37°C and 180 RPM until reaching an OD_{600} of ~0.5 AU. 120 ml TB induction cultures (TB + 100 µg/ml ampicillin) and autoinduction (AI) cultures ((Final pH: 7.2), 64 mM Na/K Phosphate (pH 7.2), 2% (w/v) Tryptone, 0.5% (w/v) Bacto Yeast Extract, 86 mM NaCl, 0.8% glycerol (v/v), 0.052% (w/v) dextrose (glucose), 0.21% (w/v) lactose, and 100 µg/ml ampicillin) were then inoculated with 8 ml of starter culture. In addition to the base TB and AI cultures, each type of growth media was supplemented with Sorbitol (300 mM D-sorbitol + 2.5 mM glycine-betaine), Ethanol (3% (v/v) ethanol), or All (300 mM D-sorbitol + 2.5 mM glycine-betaine + 3% ethanol). Induction cultures were grown to an OD_{600} of ~1 AU at 37°C and 180 RPM before shifting growth conditions to 16°C for 30 min. At this point a T0 was collected as was done in the DdFBP expression screen. Timepoints were additionally collected at 6h, 20h, 40h, and 70h for TB inductions and 20h, 40h, 70h, and 80h for AI inductions. Timepoints were collected as was done in the DdFBP expression screen.

A solubility screen was conducted on all timepoints according to the following protocol. Pellets were resuspended in 1 ml of Super Lysis Buffer supplemented with 1 mg/ml lysozyme, 5 mM $MgCl_2$, 1 mg/ml RNaseA, and 10 µg/ml DNase1. Suspended pellets were then lysed and pelleted according to the DdFBP solubility screen. Aliquots were then diluted in a 3:1 (Sample: Loading Buffer) ratio with a 4X Reduction and Alkylation Buffer (Final: 225 mM Tris-HCl (pH 8.45), 6% glycerol (v/v), 2% SDS, 0.0025% (w/v) phenol red, 0.0025% (w/v) Coomassie-G, and 50 mM DTT) before loading 10 µl onto an SDS-PAGE gel followed by western blotting with anti-His Ab. These blots were run according to the protocol for the DdFBP solubility screen. The P21

(pellet) and S21 (supernatant) of T0 were run in the same well for a total load volume of 20 µl for T0.

Purification of His-MBP-FBP Constructs.

Cultures were prepared as described above for the expression screen, and induction of HisMBP-FBPs was performed according to conditions determined to be optimal in the solubility screen: 6 h IPTG induction at 20°C for DdJcdI, DdFbxF, DdJcdH, and TgFbxO14, and 18 h IPTG induction at 20°C for DdFbxN, DdDlrA, and TgFbxO13. Cells were then pelleted at 5,000 × *g* for 15 min at 4°C and being frozen at -80°C for later use.

Pellets were resuspended on ice in Super Lysis Buffer in a ratio of ~3:1 Buffer: Pellet. Cells were lysed via 3 passes through a French pressure cell before pelleting at 27,000 × *g* for 45 min at 4°C. Supernatants from the 27,000 × *g* spin (S27) were then centrifuged at 100,000 × *g* for 70 min at 4°C while the pellets (P27) were resuspended in 0.2% SDS for analysis. The S100 was then loaded onto a column packed with 10 ml of His-60 Ni Superflow Resin (TaKaRa) and minimally washed with FBP Wash Buffer (100 mM Na/K phosphate (pH 7.4), 150 mM NaCl, 0.5 M D-sorbitol, 1 M glycine-betaine, 20% (w/v) D-sucrose, 0.2% Tween-20, and 0.05% (w/v) NaN_3) to bind the N-terminal His-tag. The large, high-capacity column and minimal washing were necessary to capture FBPs due to a blocking effect observed for the smaller and higher-affinity fragments. The wash and flow-through fractions from this step (Ni-FT) were saved for future analyses and purifications. Bound FBPs and their fragments were eluted directly onto a 5 ml StrepTactin-XT 4Flow high capacity FPLC column (IBA Lifesciences) using FBP Wash Buffer supplemented with 500 mM imidazole. This allowed the capture of full-length proteins containing the C-terminal twin-strep tag. The flow through from this step (Strep-FT / Ni Elution) was retained for further

analysis. The StrepTactin-XT column was then washed with 6 column volumes of FBP Strep Binding Buffer (100 mM Tris-HCl (pH 8.0), 150 mM NaCl, 1 mM EDTA, 10% (w/v) D-sucrose, 10% (w/v) D-sorbitol, 750 mM glycine-betaine, 0.2% Tween-20, and 0.05% (w/v) NaN_3). The wash (Strep-Wash) was retained for future analysis. Finally, the bound FBP constructs were eluted using FBP Strep-Elution Buffer (FBP Strep Binding Buffer + 50 mM D-biotin) to yield purified protein. Collected aliquots of P27, S27, P100, S100, Ni-FL, Strep-FT, Strep-Wash, and Strep-Elution were run on an SDS-PAGE gel as was done for the DdFBP solubility screens, and gels were stained in Coomassie Brilliant Blue. Constant percentages were loaded with a target load of ~1 µg of protein in the Strep-Elution. Typical yields for initial protein purifications utilizing this protocol are around 1 mg of full-length, intact protein per liter of growth culture.

Pull Down of DdJcdI-Short-H319A.

Purified proteins were loaded onto an S75 (16/600) or S200 (16/600) column and exchanged into AUC buffer as previously described [18]. Peak fractions were taken for pull down experiments. Proteins were divided into 5 conditions of 80 µl each which had the following compositions, all in Pull-down Buffer (50 mM K phosphate (pH 7.4), 150 mM KCl, 1 mg/ml bovine serum albumin (BSA), 0.2% (v/v) Tween-20, 10 µg/ml aprotinin, 10 µg/ml leupeptin). Conditions 1+2: 40 nM HisMBP-DdJcdI-Short-H319A-SF and 250 nM Gly-DdSkp1A-FL. Condition 3: No FBP and 250 nM Gly-DdSkp1A-FL. Condition 4: 40 nM HisMBP-DdJcdI-Short-H319A-SF and 500 nM DdSkp1A-FL. Condition 5: 40 nM HisMBP-DdJcdI-Short-H319A-SF and 500 nM Gly-DdSkp1A-FL). Mixtures were incubated for 1 h before transferring 40 µl to a microtube containing 5 µl of 5% MagStrep StrepTactin-XT beads (IBA Lifesciences) washed in

PBS. Beads were incubated for 1 h on a mixing roller before washing 3 times in 100 µl of PBS and eluting with FBP Strep-Elution Buffer.

Disulfide bonds were reduced by adding 8 µl of 100 mM DTT and 20 µl of 4x Reduction and Alkylation Buffer to 40 µl of sample and incubating at 60°C for 1 h. Alkylation was performed by adding 8 µl of 250 mM iodoacetamide in water and 4 µl of water to the samples and incubation at room temperature in the dark for 1 h. Samples were subjected to SDS-PAGE run in MOPS Running Buffer (Invitrogen) followed by Western blotting using anti-His to visualize DdJcdI with a 12.5% load for all samples excluding the 10% load for Wash 1. Skp1 was probed by Western blotting with UOK77 (All Skp1 glycoforms) and UOK87 (unmodified Skp1 only) after SDS-PAGE run in MES Running Buffer (50 mM MES, 50 mM Tris, 3.5 mM SDS, and 1 mM EDTA (final pH 7.3)). 1.88% of each sample was loaded for the initial incubation, unbound, and initial wash. 12.5% and 18.8% loads were used to visualize the unbound and elution fractions respectively due to the large molar excess of Skp1 over JcdI.

RESULTS AND DISCUSSION

The Skp1 Protein in *Dictyostelium* is Amenable to Glycostate Specific Binding Studies.

Skp1 from *Toxoplasma* forms a high affinity (~50 nM K_d) homodimer which is expected to compete with FBPs for available Skp1 [18]; this is similar to the apparent affinity for the Skp1-Fbs1 (FBP) interaction previously measured in the Guinea pig system [19]. Glycosylation modulates this competitive homodimer by disrupting a fuzzy interface (Subsite-B) and weakening homodimerization by an estimated order of magnitude to a K_d of 400 nM [18]. Skp1 from *Dictyostelium* also forms a homodimer with a competitive interface, however the strength of this homodimer is substantially weaker at around 2.5 µM [27]. To confirm that this difference is not an

artifact of the purification method used, DdSkp1A-FL was purified using a TEV cleavable N-terminal His-tag. As seen in **(Fig 4.1A)**, a closely matching homodimer affinity of 2.9 μM was determined for this construct. The significance of glycosylation was investigated using DdSkp1A with its native glycan. Surprisingly, a minimal effect on DdSkp1A homodimerization was observed upon glycosylation **(Fig 4.1B)**. For reasons that are unexplained, this contrasts with previous gel filtration experiments which suggested weaker homodimerization of Gly-DdSkp1A as compared to unmodified DdSkp1A [20]. These results indicate that glycosylation acts by a mechanism other than Skp1 homodimerization to regulate FBP association with Skp1 in *Dictyostelium*. Additionally, the overall weaker DdSkp1A homodimer and reduced differences in homodimer K_d between glycoforms reduces the number of confounding variables when analyzing Skp1/FBP association.

An extremely high degree of sequence conservation is observed between DdSkp1A and TgSkp1 [18]. Therefore, it stands to reason that Skp1's homodimer Subsite-B present in *Toxoplasma* would also be present in *Dictyostelium*. A CTR deletion analogous to that used in *Toxoplasma* [18] or previous NMR studies [27] was generated and subjected to SV analysis. As shown in **(Fig 4.1C)**, deletion of Skp1's CTR results in an approximate 4-fold weakening of Skp1 homodimerization. Although not as significant as the effect observed in *Toxoplasma*, this result suggests that DdSkp1A maintains a fuzzy Subsite-B. The lesser effect of DdSkp1A's Subsite-B as compared to TgSkp1 may be related to the overall weaker DdSkp1A homodimer. Another difference is the use of a Lys instead of an Arg in DdSkp1A's positive charge patch (R132-K133). Arg residues have been shown to more readily facilitate transient interactions as compared to Lys residues [32-38]. The importance of DdSkp1A's positive charge patch is reinforced by the weakened DdSkp1A homodimer observed when a scrambled variant lacking paired positively

charged residues is analyzed **(Fig 4.1D)**. Overall, despite a weaker homodimer and reduced effects of glycosylation, DdSkp1A's overall homodimer architecture is likely similar to TgSkp1.

Engineering FBPs for Soluble Protein Expression.

Preliminary data from Peter Kaiser's lab suggested that FBPs could be solubilized using an N-terminal MBP solubility tag (Peter Kaiser (UC Irvine, personal communication)). To generate an FBP library for downstream analysis, we opted for a high throughput method of generating and testing HisMBP-FBP fusion constructs **(Fig 4.2A)**. For this approach, we generated a common HisMBP plasmid backbone. A library of FBPs from primarily cDNA and other sources was also generated using PCR and primers with 5' homology regions to the common backbone. This allowed assembly of a library of HisMBP-FBP expression plasmids. These plasmids were then used for expression and solubility screening to identify FBPs and growth conditions that would allow expression of soluble HisMBP-FBP constructs. Identified optimal growth conditions were then used in designing a protein purification protocol for soluble constructs. Given the large number of predicted DdFBPs (~50), FBPs targeted for analysis were chosen based on previous Co-IP pull down data [12, 14] **(Fig 4.2B)**. Group1 FBPs were selected based on consistent and similar representation in Skp1's FBP repertoire regardless of Skp1's glycosylation status. These FBPs were expected to have minimal differences in Skp1 binding affinity between Skp1 glycostates. This would allow for biophysical comparison of Skp1 binding with Group2 FBPs. Group2 FBPs were selected based on consistent and large differences in their binding profile with Skp1 in Wild Type (glycosylated) and *phyA*- (unmodified) *Dictyostelium* strains. These FBPs were expected to have potentially large differences in Skp1 binding affinity between Skp1 glycostates. This would allow biophysical characterization of how glycosylation controls FBP-Skp1 complex

formation. Despite inconsistent results between experiments, a JcdI construct (DdJcdI-Short-H319A) was also included due to the presence of previous research on this FBP [12, 14] and its homology to TgFbxO13 [11]. The DdJcdI-Short-H319A variant was chosen based on its reduced propensity to be proteolyzed (unpublished data) [12]. Several well characterized FBPs from *Toxoplasma* were also chosen for screening including the Group1 FBP TgFbxO1 [11, 30], and Group2 FBPs TgFbxO13 and TgFbxO14 [11].

Solubility screens indicated soluble expression of the Group1 *Dictyostelium* FBPs DdDlrA and DdFbxF along with the Group2 *Dictyostelium* FBPs DdFbxN and DdJcdH **(Fig 4.2D)**. Soluble expression was also observed for DdJcdI-Short-H319A **(Fig 4.2D)**, TgFbxO13, and TgFbxO14 **(Figs 4.S7-4.S8)**. Although DdCulE failed to produce soluble protein under the tested conditions **(Fig 4.2D)**, TgCul1 produced soluble protein under several tested conditions **(Fig 4.S5)**. Despite additives such as ethanol or sorbitol failing to improve soluble protein expression for TgCul1, ethanol proved helpful in promoting soluble TgGlt1 expression under certain conditions **(Fig 4.S6)**. Heavy fragmentation of soluble HisMBP-FBP constructs was observed under almost all tested conditions **(Fig 4.2D)**. This means that a simple one-step affinity purification would fail to isolate pure, full-length protein. Because of this, we opted to add a Thrombin cleavable SF tag which includes a twin-Strep tag to the C-terminus of the soluble protein constructs. This would complement the N-terminal His-tag allowing for IMAC purification. An example of this construct using DdFbxN is depicted in **(Fig 4.2C)**. This would allow purification of full-length protein away from its protein fragments through a two-step affinity purification **(Fig 4.3A)**.

Purification of FBPs via a Two-Step Affinity Purification.

A protein purification protocol was necessary to purify soluble, expressed protein while removing contaminating protein fragments. To this end we utilized constructs similar to that shown in **(Fig 4.2C)** for a purification protocol outlined in **(Fig 4.3A)**. First, clarified *E. coli* lysates were loaded onto high-capacity Ni column allowing for binding of N-terminally tagged constructs and fragments. The high capacity of the column reduced blocking effects caused by smaller fragments in preliminary studies while allowing a higher capture rate of the weaker binding, full-length constructs. This blocking effect is easily explainable through other studies which indicate that protein size can significantly influence its retention on an IMAC column [39]. This results in the compounding effects of weakening column binding for the full-length constructs while introducing higher affinity, competing interactions via protein fragmentation. The Ni column was then eluted directly onto a StrepTactin-XT column allowing for the capture of C-terminally tagged, full-length constructs with the Twin-Strep tag. Protein fragments, which at this point would only contain the N-terminal His-tag, would be allowed to flow through the column. Washing and eluting the StrepTactin-XT column would result in the purification of full-length constructs isolated from the far more abundant protein fragments. The success of this method has been demonstrated with DdJcdH **(Fig 4.3B)**, DdFbxF **(Fig 4.3C)**, DdFbxN **(Fig 4.3D)**, DdJcdI-Short-H319A **(Fig 4.3E)**, TgFbxO14 **(Fig 4.3F)** and TgFbxO13 **(Fig 4.3G)**.

Although these FBPs can be effectively purified to homogeneity in their soluble forms, preliminary FBP-Skp1 pulldown experiments using DdJcdI-Short-H319A demonstrate further optimization is necessary. In these pulldown experiments, DdJcdI fails to effectively pull down Skp1 despite itself effectively binding to the utilized StrepTactin-XT magnetic beads **(Fig 4.S10)**. There are several potential reasons for this. The first is that the concentration of DdJcdI is relatively

low at 40 nM in these experiments. This may may hamper binding if its affinity for Skp1 is significantly weaker than the 25 nM affinity observed for Fbs1 and Skp1 [19]. In this case, an increase in protein concentration will be necessary for effective binding. Another and potentially more likely explanation is that the F-Box domain may fail to properly fold in solution, even in the presence of a binding partner. This is somewhat related to a third potential explanation that chaperones may be necessary for effective Skp1-FBP complex formation. This explanation is supported by the moderating role chaperones have been proposed to play in the FBP-Skp1 interaction and assembly of other E3 ligases [40-44]. In either case, mixtures of FBPs with each Skp1 glycoform can be supplemented with *Dictyostelium* lysates in addition to ATP to promote chaperone activity.

ACKNOWLEDGMENTS

We are grateful for the assistance of Dr. Peter Kaiser and Dr. Linda Lauinger (University of California, Irvine) for materials and advice. They provided the pET28-HisMBP-FbxO3 plasmid which was used to generate the common backbone for our initial FBP library. Second, their accounts of previous successes and failures of the HisMBP-FBP constructs in their lab was instrumental in several aspects of our study design. Their accounts aided in deciding how many FBPs would give us the best probability of success and were useful in setting initial growth conditions in our FBP expression screens. We would also like to thank John Kim, Elisabet Gas-Pascual, and Msano Mandalasi for their provision of several materials used in this study, and Tania Wilson for performing many of the experiments.

FIGURE LEGENDS

Figure 4.1 SV-Isotherms of DdSkp1A Constructs. S_w isotherms and associated c(s) distributions used to determine the homodimer affinities of **(A)** DdSkp1A-FL, **(B)** Gly-DdSkp1A-FL, **(C)** DdSkp1A-CTR, and **(D)** DdSkp1A-Scrambled4. Affinities are given in the lower right corner of each isotherm. Data points are colored according to their associated c(s) distribution below. The integration range used to generate the S_w isotherm is given with a solid red line above the overlayed distributions. Individual distributions are shown in **(Figs 4.S1-4.S4)**.

Figure 4.2 Generation of Soluble FBP Constructs. (A) Schematic for generating and screening initial MBP-FBP constructs. (1-A) A common backbone plasmid was amplified from a HisMBP-FbxO3 plasmid previously generated in Peter Kaiser's lab. (1-B) Targeted FBPs were amplified from a total cDNA library generated against different timepoints in *Dictyostelium* development. Primers were designed against the 5' (Start codon) and 3' (Stop codon) ends of each FBP's coding sequence. Each FBP targeting primer contained a homology region with the backbone plasmid to allow insertion into a common site in the plasmid. (2) A Gibson Assembly based approach was utilized to insert each successfully amplified FBP into the common plasmid backbone. (3) FBP constructs were subjected to expression screening where production of the desired FBP constructs was analyzed. Time points allowing expression of FBP constructs were further subjected to solubility screening to identify constructs fit for purification. (4) Constructs that successfully produced soluble protein were subjected to purification. **(B)** Two groups of FBPs were selected for screening based on a high likelihood for desired behavior between different DdSkp1A glycoforms based on previous co-IP data [12, 14]. Group 1 FBPs were expected to have minimal differences in binding between different Skp1 glycoforms. Group 2 FBPs were expected to have differential

binding between different Skp1 glycoforms. Dictybase IDs, FBP names, substrate binding domains, native FBP sizes, and the presence of other identifiable domains are indicated. **(C)** A domain diagram of the final purified construct of HisMBP-DdFbxN-SF which is representative of other purified FBP constructs. **(D)** Solubility screens of successfully expressed FBPs and DdCulE. The Soluble (S21) and insoluble (P21) fractions are indicated for each construct. The molecular weights of each tested full-length construct are given. Successfully solubilized constructs with their optimal expression times are indicated. Expression screens used to choose conditions for DdFBP solubility screening are shown in **(Fig 4.S9)**.

Figure 4.3 Purification of FBP Constructs. (A) Schematic of each final FBP construct purification. *Escherichia coli* lysates were centrifuged at 27,000g followed by 100,000g to remove insoluble particles. Step 1. The final supernatant (S100) was then loaded onto a 10 ml His-60 Ni column and washed. This captured full-length constructs and fragments containing the N-terminal His-tag. Step 2. The His-60 Ni column was eluted using 500 mM Imidazole directly onto a 5 ml StrepTactin-XT High-Capacity column before subsequent washing. This column captured full-length constructs while allowing fragments lacking the SF/Twin-Strep tag to flow through. Step 3. Full-length constructs were eluted from the StrepTactinXT column using 50 mM Biotin yielding highly purified full-length HisMBP-FBP-SF constructs. Coomassie Brilian Blue gels depicting the purification of **(B)** DdJcdH, **(C)** DdFbxF, **(D)** DdFbxN, **(E)** DdJcdI-Short-H319A, **(F)** TgFbxO14, and **(G)** TgFbxO13. The construct name, molecular weight, gel loading amount, and level scanned are indicated above each gel. Samples are labeled (P27) for the pellet of the 27,000 g spin; (S27) supernatant of the 27,000 g spin; (P100) pellet of the 100,000 g spin; (S100) supernatant of the 100,000g spin; (Ni-FT) flow through from the 10 ml His-60 Ni column; (Strep-FT) flow through

from the 5 ml SrepTactin-XT column or elution from the 10 ml His-60 Ni column; (Strep-Wash) washing from the StrepTactin-XT column; and (Strep-Elution) elution from the StrepTactin-XT column utilizing 50 mM Biotin. The Strep-Wash and Strep-Elution of the TgFbxo13 **(H)** purification are burned in to allow greater visibility of the eluted protein.

SUPPLEMENTAL FIGURE LEGENDS

Figure 4.S1 Sedimentation Velocity Distributions for DdSkp1A-FL. Individual sedimentation datasets for each DdSkp1A-FL concentration with their associated c(s) distributions.

Figure 4.S2 Sedimentation Velocity Distributions for Fully Glycosylated Gly-DdSkp1A-FL. Individual sedimentation datasets for each Gly-DdSkp1A-FL concentration with their associated c(s) distributions.

Figure 4.S3 Sedimentation Velocity Distributions for DdSkp1A-ΔCTR. Individual sedimentation datasets for each DdSkp1A-ΔCTR concentration with their associated c(s) distributions.

Figure 4.S4 Sedimentation Velocity Distributions for DdSkp1A-Scrambled4. Individual sedimentation datasets for each DdSkp1A-Scrambled4 concentration with their associated c(s) distributions.

Figure 4.S5 TgCul1 Solubility Screening Gels. Anti-His Western Blots from solubility screens of TgCul1 under different growth conditions. The growth conditions, timepoints, soluble fractions (S21), insoluble fractions (P21), and molecular weights are indicated. TgCul1 has an expected molecular weight of 104.9 kDa while the untagged TgRbx1 has an expected molecular weight of 13.9 kDa.

Figure 4.S6 TgGlt1 Solubility Screening Gels. Anti-His Western Blots from solubility screens of TgGlt1 under different growth conditions. The growth conditions, timepoints, soluble fractions (S21), insoluble fractions (P21), and molecular weights are indicated. TgGlt1 has an expected molecular weight of 70.2 kDa.

Figure 4.S7 TgFBP Expression Screening Gels. Whole-cell lysates from each timepoint and each condition were loaded onto an Anti-His Western Blot. Growth temperatures, FBPs, timepoints, and molecular weights are indicated. Expected molecular weights are 137.1 kDa for TgFbxO1, 130.9 kDa for TgFbxO13, and 166.6 kDa for TgFbxO14.

Figure 4.S8 TgFBP Solubility Screen. Fractionated lysates from each timepoint and each condition were loaded onto an Anti-His Western Blot. Growth temperatures, FBPs, timepoints, soluble fractions (S21), insoluble fractions (P21), and molecular weights are indicated. Expected molecular weights are 137.1 kDa for TgFbxO1, 130.9 kDa for TgFbxO13, and 166.6 kDa for TgFbxO14.

Figure 4.S9 Expression Screen of DdFBPs. Whole-cell lysates from each timepoint and each condition were loaded onto an Anti-His Western Blot. Growth temperatures, FBPs, timepoints, and molecular weights are indicated. Expected molecular weights for each construct are given next to each gel. His-Fbs1 is given as a known reference of loaded protein.

Figure 4.S10 Preliminary DdJcdI Pulldown. Anti-His (DdJcdI), UOK77 (All Skp1), and UOK87 (Unmodified Skp1) Western Blots are shown. Loads are given under each Western Blot Label. Conditions are given and color coded. Molecular weight markers are given. Expected molecular weights are 94.4 kDa for DdJcdI and 18.8 kDa for DdSkp1A.

Figure 4.S11 Primers Utilized in this Study. Primers used for the initial FBP plasmid assemblies, SF-tagging the soluble constructs, and other utilized primers are indicated. Initial assembly primers used for DdFbxG, DdFbxJ, and DdFbxL that failed to amplify from cDNA are also given.

Figure 4.S12 Sequences for DdSkp1A-FL and DdSkp1A-ΔCTR. The portion of the pNIC28 plasmid containing the initial DdSkp1A sequence and the derived DdSkp1A-ΔCTR sequences are indicated. The resulting DdSkp1A-ΔCTR sequence is colored purple.

Figure 4.S13 Sequences for Synthesized DdSkp1A Constructs. The portion of the pNIC28 plasmid containing the Genscript synthesized DdSkp1A constructs is given and divergent portions of the sequence are color coded.

Figure 4.S14 Sequence for the Synthesized His-DdCulE + DdRbx1 Construct. The portion of the pETDuet sequence containing the final His-DdCulE + DdRbx1 codon optimized constructs are given. The His-tag and TEV cleavage sites are indicated.

Figure 4.S15 Sequence for the Final His-TgCul1 + SF-TgRbx1 Construct. The portion of the pETDuet sequence containing the final His-TgCul1 + SF-TgRbx1 codon optimized constructs are given. The His-tag, TEV cleavage sites, StrepII-tag, and FLAG tag are indicated. The sequence contributed by *S. neurona* is colored purple, while the later added SF tag is colored red. The original plasmid sequence is identical to that shown but lacked the red sequence.

Figure 4.S16 Sequence for the Synthesized His-TgFbxO13 + TgSkp1 Construct. The portion of the pETDuet sequence containing the codon optimized His-TgFbxO13 + TgSkp1 genes is given. The His-tag and TEV cleavage sites are indicated.

Figure 4.S17 Plasmid Map for the Representative His-MBP-DdFbxF Construct. Representative sequence of a His-MBP-FBP plasmid using DdFbxF. The His-tag, MBP-tag, Factor Xa cleavage site, and TEV cleavage site are indicated. The protein sequence contributed by the

common plasmid backbone is colored purple, while that of the inserted DdFbxF sequence is colored red.

Figure 4.S18 FBP Sequence for DdDlrA. Sequence for DdDlrA cloned into the pET28-HisMBP-DdDlrA plasmid.

Figure 4.S19 FBP Sequence for DdFbxD. Sequence for DdFbxD cloned into the pET28-HisMBP-DdFbxD plasmid.

Figure 4.S20 FBP Sequence for DdFbxH. Sequence for DdFbxH cloned into the pET28-HisMBP-DdFbxH plasmid.

Figure 4.S21 FBP Sequence for DdFbxI. Sequence for DdFbxI cloned into the pET28-HisMBP-DdFbxI plasmid.

Figure 4.S22 FBP Sequence for DdFbxK-1. Sequence for DdFbxK-1 cloned into the pET28-HisMBP-DdFbxK-1 plasmid. The region where our sequence differs from that in Dictybase is indicated. Our sequence was supported by the EST (DDB0299438).

Figure 4.S23 FBP Sequence for DdFbxM. Sequence for DdFbxM cloned into the pET28-HisMBP-DdFbxM plasmid.

Figure 4.S24 FBP Sequence for DdFbxN. Sequence for DdFbxN cloned into the pET28-HisMBP-DdFbxN plasmid.

Figure 4.S25 FBP Sequence for DdJcdH. Sequence for DdJcdH cloned into the pET28-HisMBP-DdJcdH plasmid. The predicted JmjC domain is indicated.

Figure 4.S26 FBP Sequence for DdJcdI-Short-H319A. Sequence for DdJcdI-Short-H319A cloned into the pET28-HisMBP-DdJcdI-Short-H319A plasmid. The predicted F-Box domain and H319A point mutation are indicated.

Figure 4.S27 FBP Sequence for TgFbxO1. Sequence for TgFbxO1 cloned into the pET28-HisMBP-TgFbxO1 plasmid. The predicted F-Box domain is indicated.

Figure 4.S28 FBP Sequence for TgFbxO13. Sequence for TgFbxO13 cloned into the pET28-HisMBP-TgFbxO13 plasmid. The predicted F-Box and JmjC domains are indicated.

Figure 4.S29 FBP Sequence for TgFbxO14. Sequence for TgFbxO14 cloned into the pET28-HisMBP-TgFbxO14 plasmid. The predicted F-Box domain is highlighted.

Figure 4.30 FBP Sequence for DdFbxA. Coding sequence of DdFbxA with its respective protein sequence.

Figure 4.S31 Representative His-MBP-DdFbxN-SF Construct. A representative construct sequence of a HisMBP-FBP-SF using DdFbxN. The FLAG-tag, StrepII-tag, Thrombin cleavage site, His-tag, MBP-tag, Factor Xa cleavage site, and TEV cleavage site are indicated. The DdFbxN sequence is colored red, while the newly added SF-tag is colored blue.

Figure 4.1

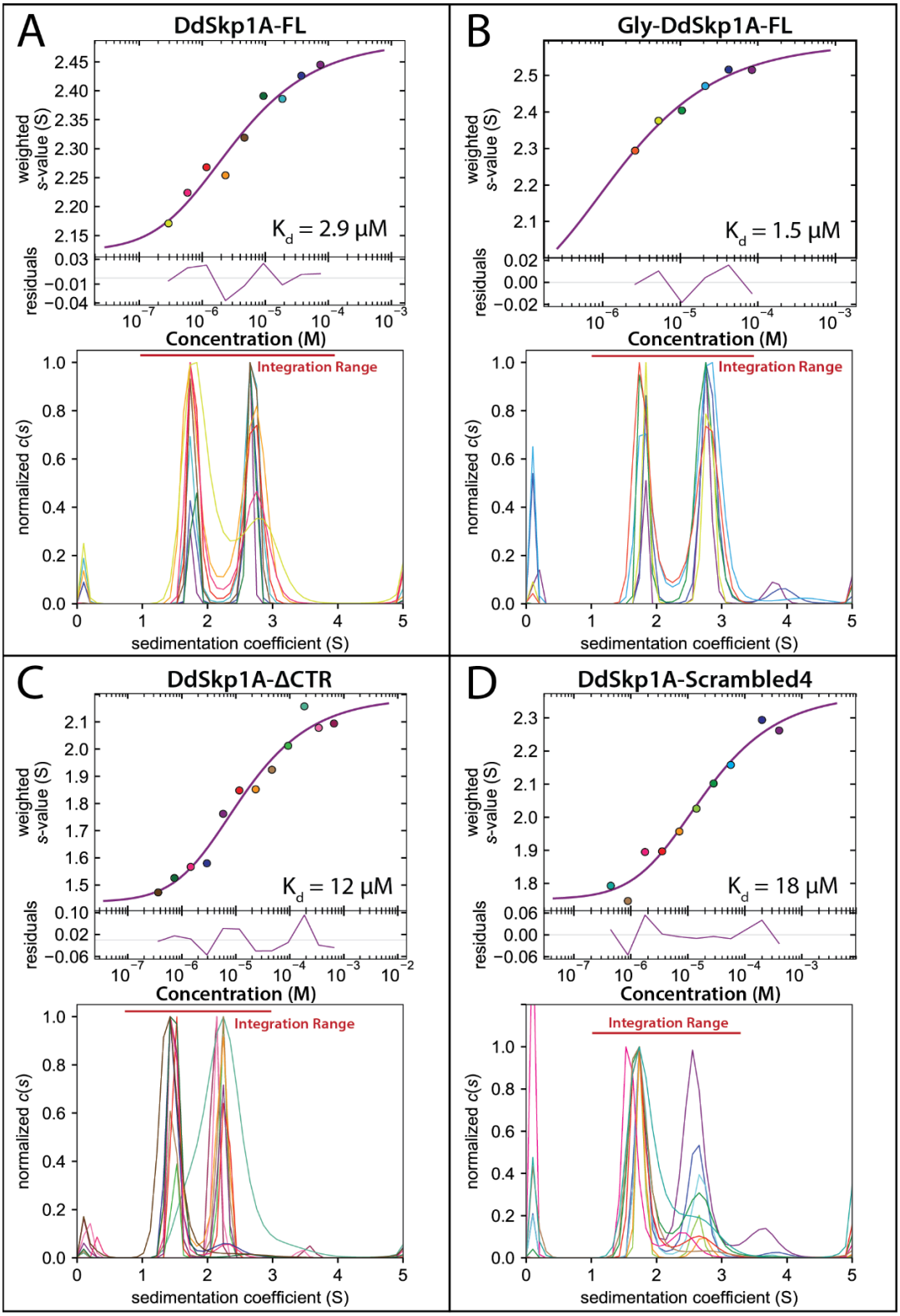

A
DdSkp1A-FL
weighted s-value (S)
residuals
K_d = 2.9 µM
Concentration (M)
Integration Range
normalized c(s)
sedimentation coefficient (S)
B
Gly-DdSkp1A-FL
K_d = 1.5 µM
C
DdSkp1A-ΔCTR
K_d = 12 µM
D
DdSkp1A-Scrambled4
K_d = 18 µM

Figure 4.2

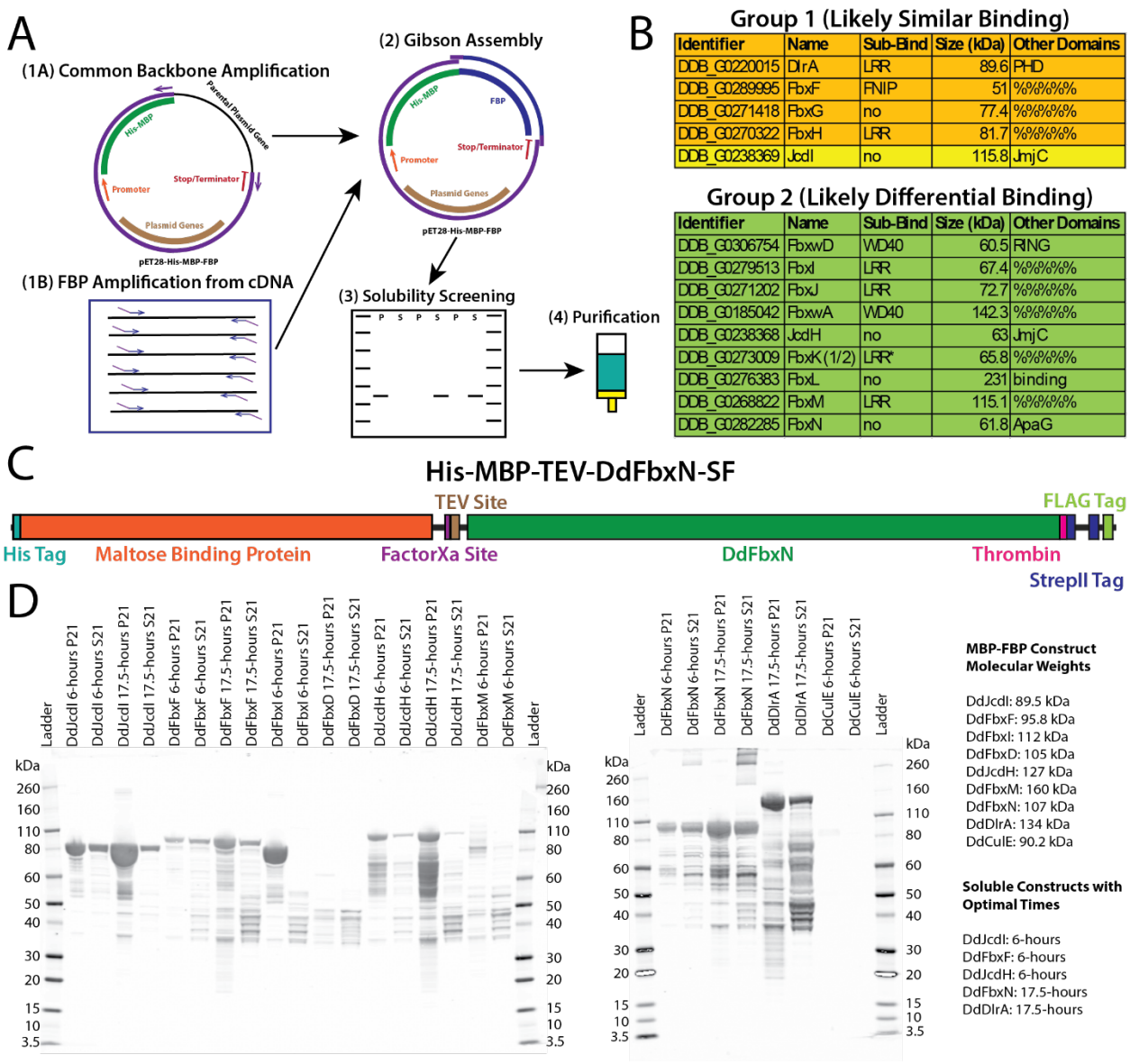

A
(1A) Common Backbone Amplification
Parental Plasmid Gene
His-MBP
Promoter
Stop/Terminator
Plasmid Genes
pET28-His-MBP-FBP
(2) Gibson Assembly
FBP
(1B) FBP Amplification from cDNA
(3) Solubility Screening
P S P S P S
(4) Purification
B
Group 1 (Likely Similar Binding)
Identifier | Name | Sub-Bind | Size (kDa) | Other Domains
DDB_G0220015 | DlrA | LRR | 89.6 | PHD
DDB_G0289995 | FbxF | FNIP | 51 | %%%%%
DDB_G0271418 | FbxG | no | 77.4 | %%%%%
DDB_G0270322 | FbxH | LRR | 81.7 | %%%%%
DDB_G0238369 | JcdI | no | 115.8 | JmjC
Group 2 (Likely Differential Binding)
Identifier | Name | Sub-Bind | Size (kDa) | Other Domains
DDB_G0306754 | FbxwD | WD40 | 60.5 | RING
DDB_G0279513 | FbxI | LRR | 67.4 | %%%%%
DDB_G0271202 | FbxJ | LRR | 72.7 | %%%%%
DDB_G0185042 | FbxwA | WD40 | 142.3 | %%%%%
DDB_G0238368 | JcdH | no | 63 | JmjC
DDB_G0273009 | FbxK (1/2) | LRR* | 65.8 | %%%%%
DDB_G0276383 | FbxL | no | 231 | binding
DDB_G0268822 | FbxM | LRR | 115.1 | %%%%%
DDB_G0282285 | FbxN | no | 61.8 | ApaG
C
His-MBP-TEV-DdFbxN-SF
TEV Site
FLAG Tag
His Tag
Maltose Binding Protein
FactorXa Site
DdFbxN
Thrombin
StrepII Tag
D
Ladder
DdJcdI 6-hours P21
DdJcdI 6-hours S21
DdJcdI 17.5-hours P21
DdJcdI 17.5-hours S21
DdFbxF 6-hours P21
DdFbxF 6-hours S21
DdFbxF 17.5-hours P21
DdFbxF 17.5-hours S21
DdFbxI 6-hours P21
DdFbxI 6-hours S21
DdFbxD 17.5-hours P21
DdFbxD 17.5-hours S21
DdJcdH 6-hours P21
DdJcdH 6-hours S21
DdJcdH 17.5-hours P21
DdJcdH 17.5-hours S21
DdFbxM 6-hours P21
DdFbxM 6-hours S21
DdFbxN 6-hours P21
DdFbxN 6-hours S21
DdFbxN 17.5-hours P21
DdFbxN 17.5-hours S21
DdDlrA 17.5-hours P21
DdDlrA 17.5-hours S21
DdCulE 6-hours P21
DdCulE 6-hours S21
kDa
260
160
110
80
60
50
40
30
20
15
10
3.5
MBP-FBP Construct Molecular Weights
DdJcdI: 89.5 kDa
DdFbxF: 95.8 kDa
DdFbxI: 112 kDa
DdFbxD: 105 kDa
DdJcdH: 127 kDa
DdFbxM: 160 kDa
DdFbxN: 107 kDa
DdDlrA: 134 kDa
DdCulE: 90.2 kDa
Soluble Constructs with Optimal Times
DdJcdI: 6-hours
DdFbxF: 6-hours
DdJcdH: 6-hours
DdFbxN: 17.5-hours
DdDlrA: 17.5-hours

Figure 4.3

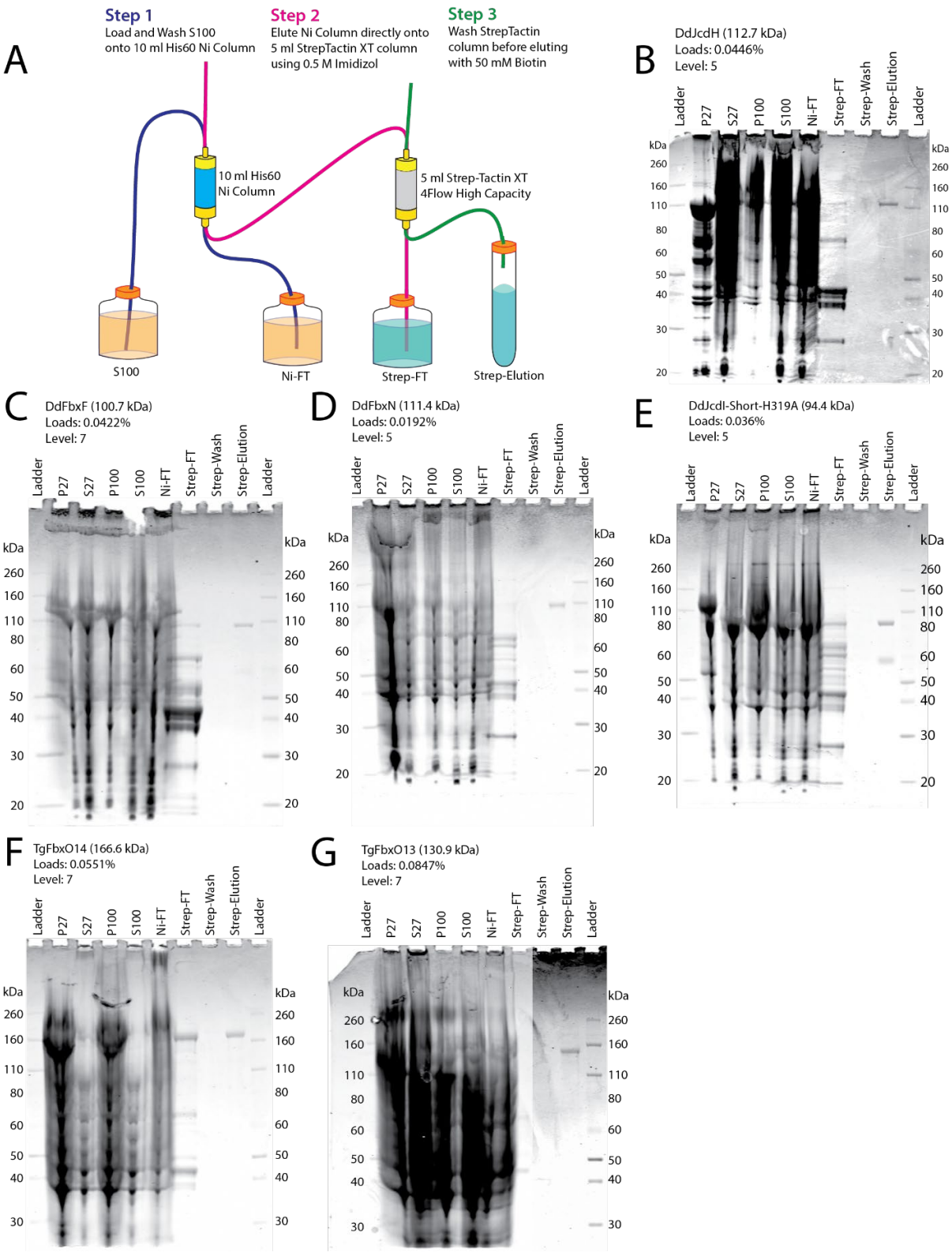

A
Step 1
Load and Wash S100
onto 10 ml His60 Ni Column
Step 2
Elute Ni Column directly onto
5 ml StrepTactin XT column
using 0.5 M Imidizol
Step 3
Wash StrepTactin
column before eluting
with 50 mM Biotin
10 ml His60
Ni Column
5 ml Strep-Tactin XT
4Flow High Capacity
S100
Ni-FT
Strep-FT
Strep-Elution
B
DdJcdH (112.7 kDa)
Loads: 0.0446%
Level: 5
C
DdFbxF (100.7 kDa)
Loads: 0.0422%
Level: 7
D
DdFbxN (111.4 kDa)
Loads: 0.0192%
Level: 5
E
DdJcdI-Short-H319A (94.4 kDa)
Loads: 0.036%
Level: 5
F
TgFbxO14 (166.6 kDa)
Loads: 0.0551%
Level: 7
G
TgFbxO13 (130.9 kDa)
Loads: 0.0847%
Level: 7
Ladder
P27
S27
P100
S100
Ni-FT
Strep-FT
Strep-Wash
Strep-Elution
Ladder
kDa

Figure 4.S1

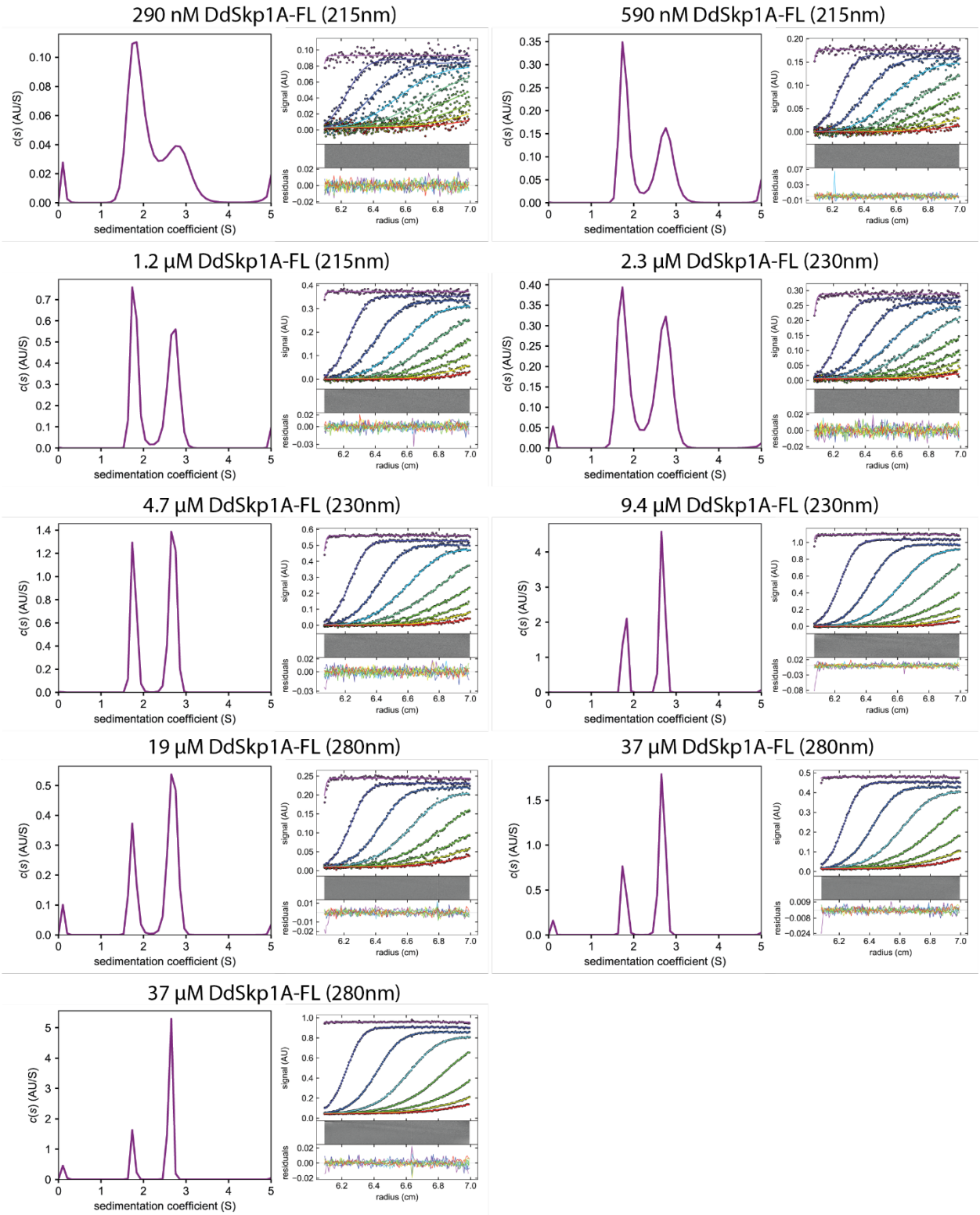

290 nM DdSkp1A-FL (215nm)
590 nM DdSkp1A-FL (215nm)
1.2 µM DdSkp1A-FL (215nm)
2.3 µM DdSkp1A-FL (230nm)
4.7 µM DdSkp1A-FL (230nm)
9.4 µM DdSkp1A-FL (230nm)
19 µM DdSkp1A-FL (280nm)
37 µM DdSkp1A-FL (280nm)
37 µM DdSkp1A-FL (280nm)
c(s) (AU/S)
sedimentation coefficient (S)
signal (AU)
residuals
radius (cm)

Figure 4.S2

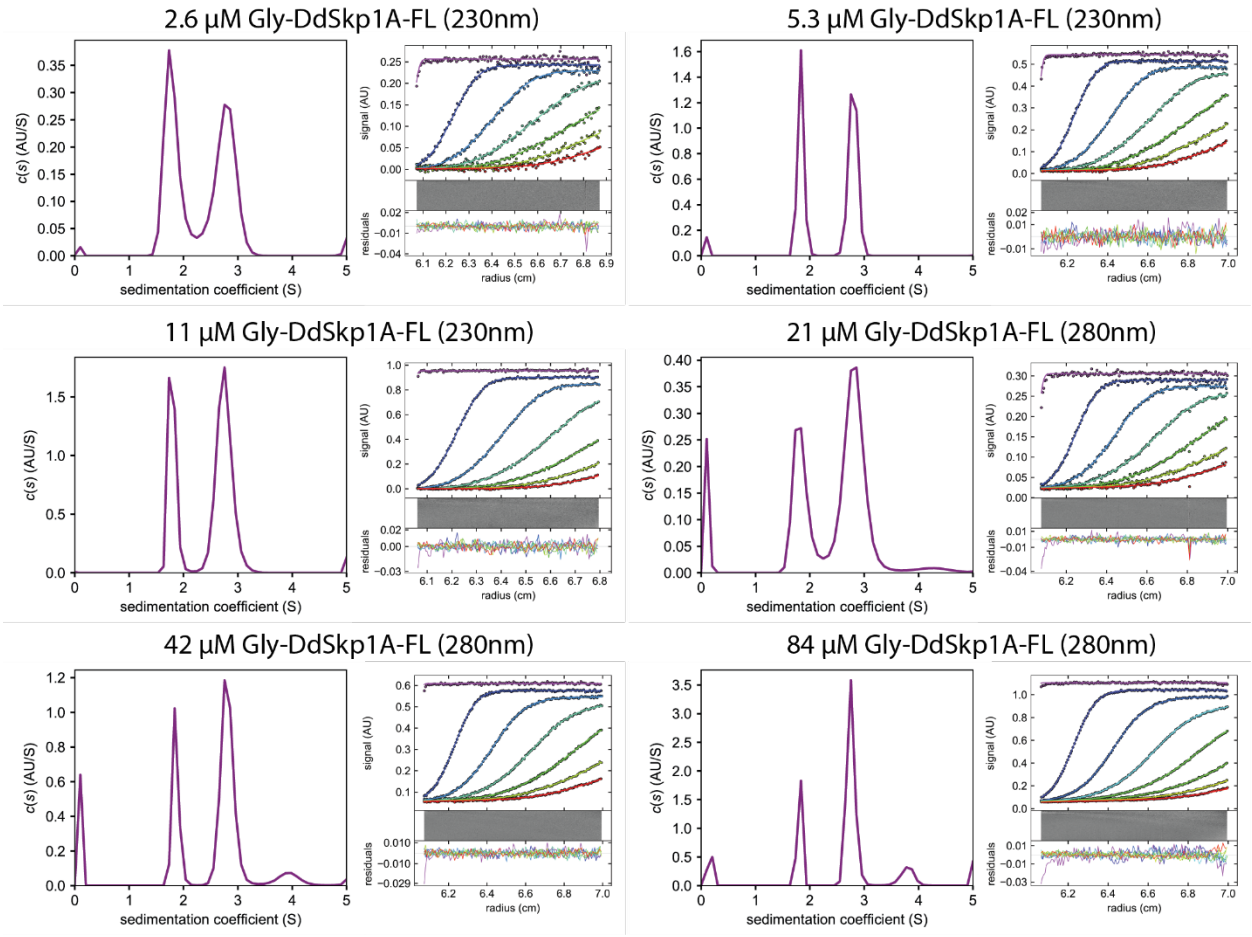
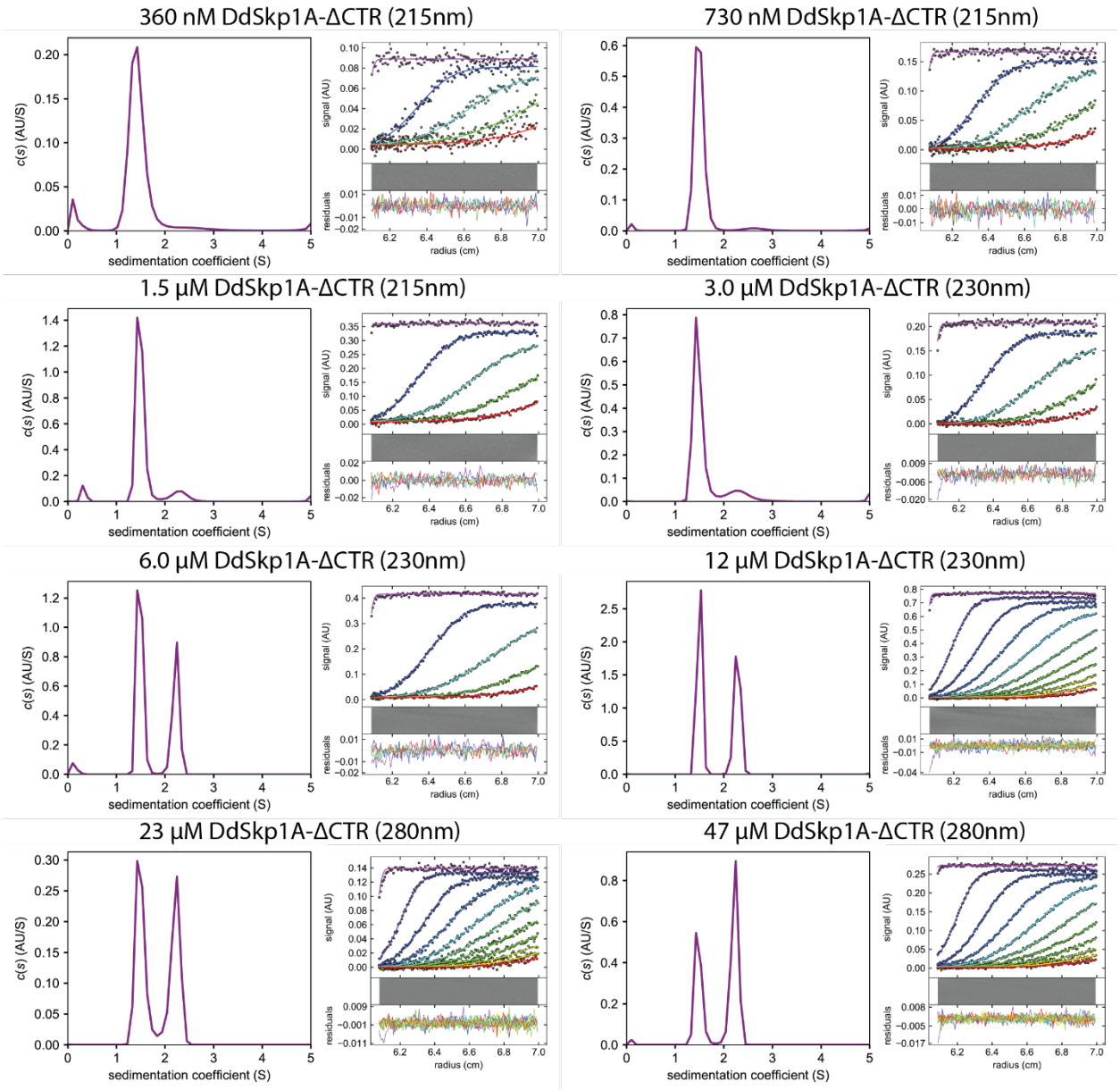

2.6 µM Gly-DdSkp1A-FL (230nm)
5.3 µM Gly-DdSkp1A-FL (230nm)
11 µM Gly-DdSkp1A-FL (230nm)
21 µM Gly-DdSkp1A-FL (280nm)
42 µM Gly-DdSkp1A-FL (280nm)
84 µM Gly-DdSkp1A-FL (280nm)
c(s) (AU/S)
sedimentation coefficient (S)
signal (AU)
residuals
radius (cm)

Figure 4.S3


360 nM DdSkp1A-ΔCTR (215nm)
730 nM DdSkp1A-ΔCTR (215nm)
1.5 μM DdSkp1A-ΔCTR (215nm)
3.0 μM DdSkp1A-ΔCTR (230nm)
6.0 μM DdSkp1A-ΔCTR (230nm)
12 μM DdSkp1A-ΔCTR (230nm)
23 μM DdSkp1A-ΔCTR (280nm)
47 μM DdSkp1A-ΔCTR (280nm)
c(s) (AU/S)
sedimentation coefficient (S)
signal (AU)
residuals
radius (cm)

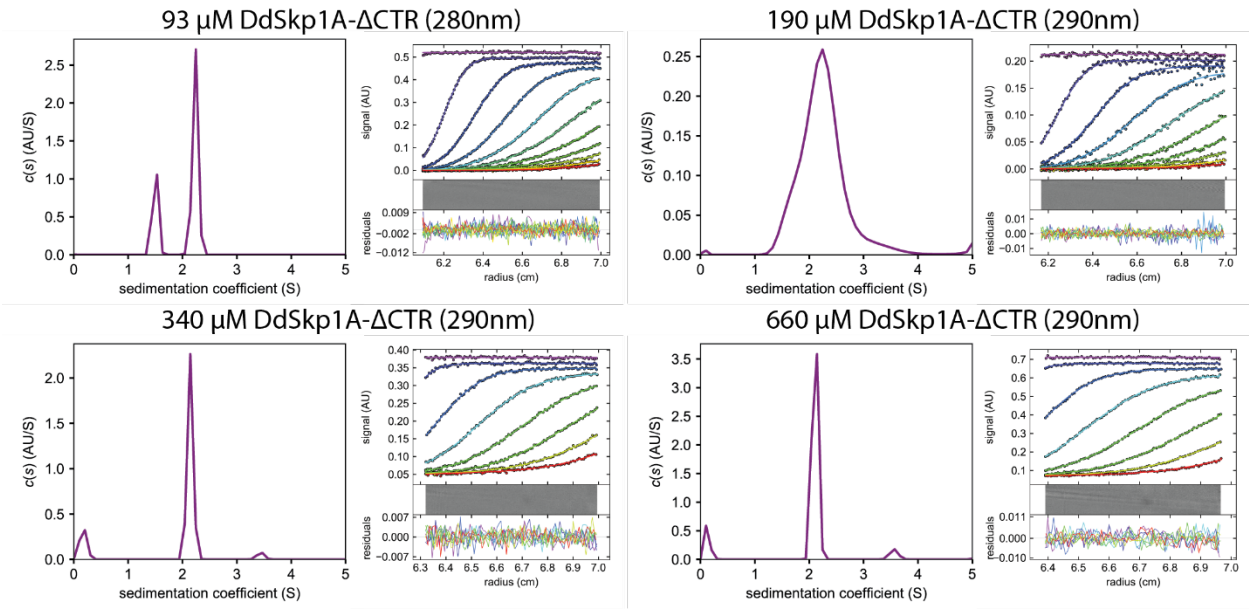

93 µM DdSkp1A-ΔCTR (280nm)
190 µM DdSkp1A-ΔCTR (290nm)
340 µM DdSkp1A-ΔCTR (290nm)
660 µM DdSkp1A-ΔCTR (290nm)
c(s) (AU/S)
sedimentation coefficient (S)
signal (AU)
residuals
radius (cm)

Figure 4.S4

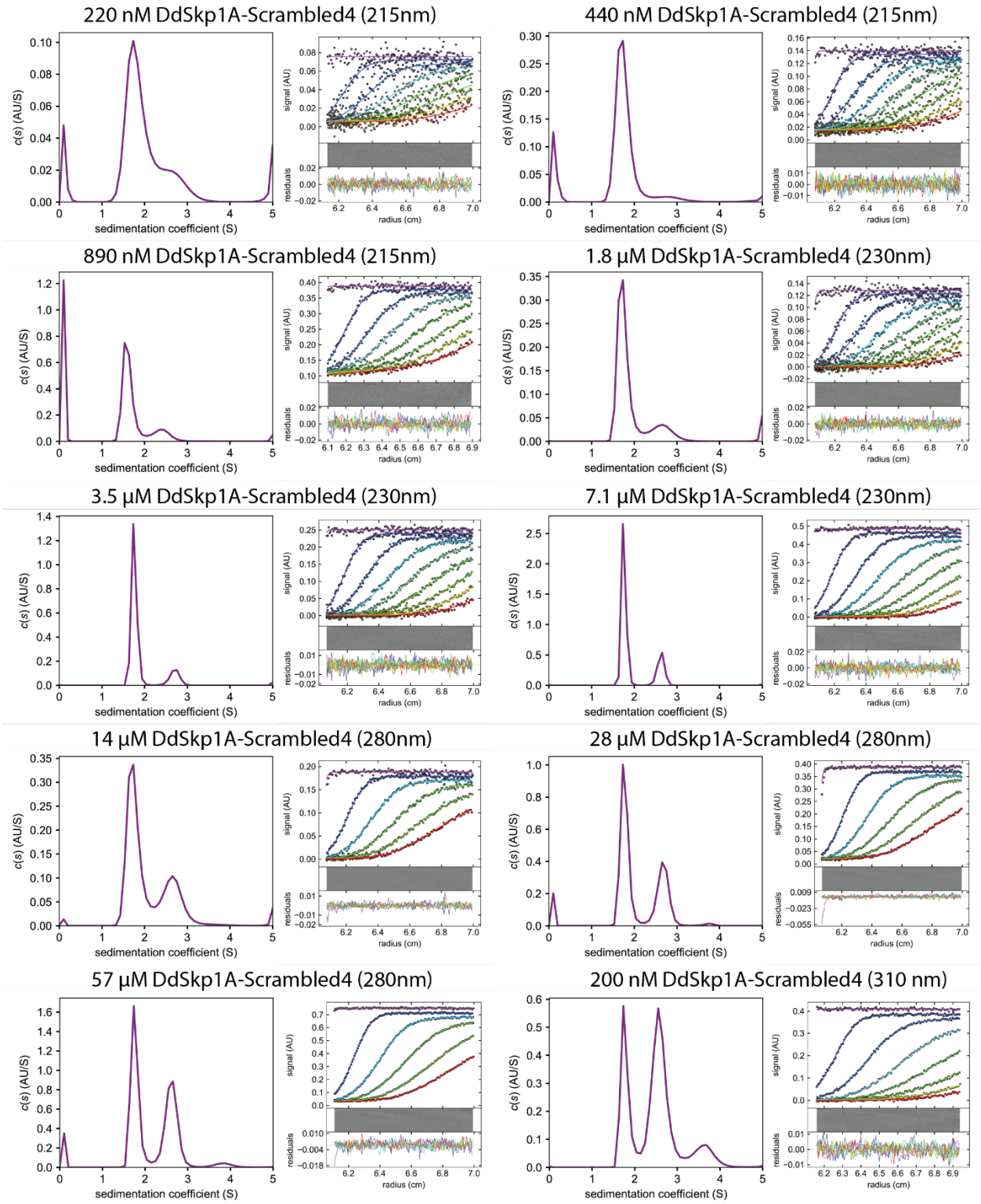
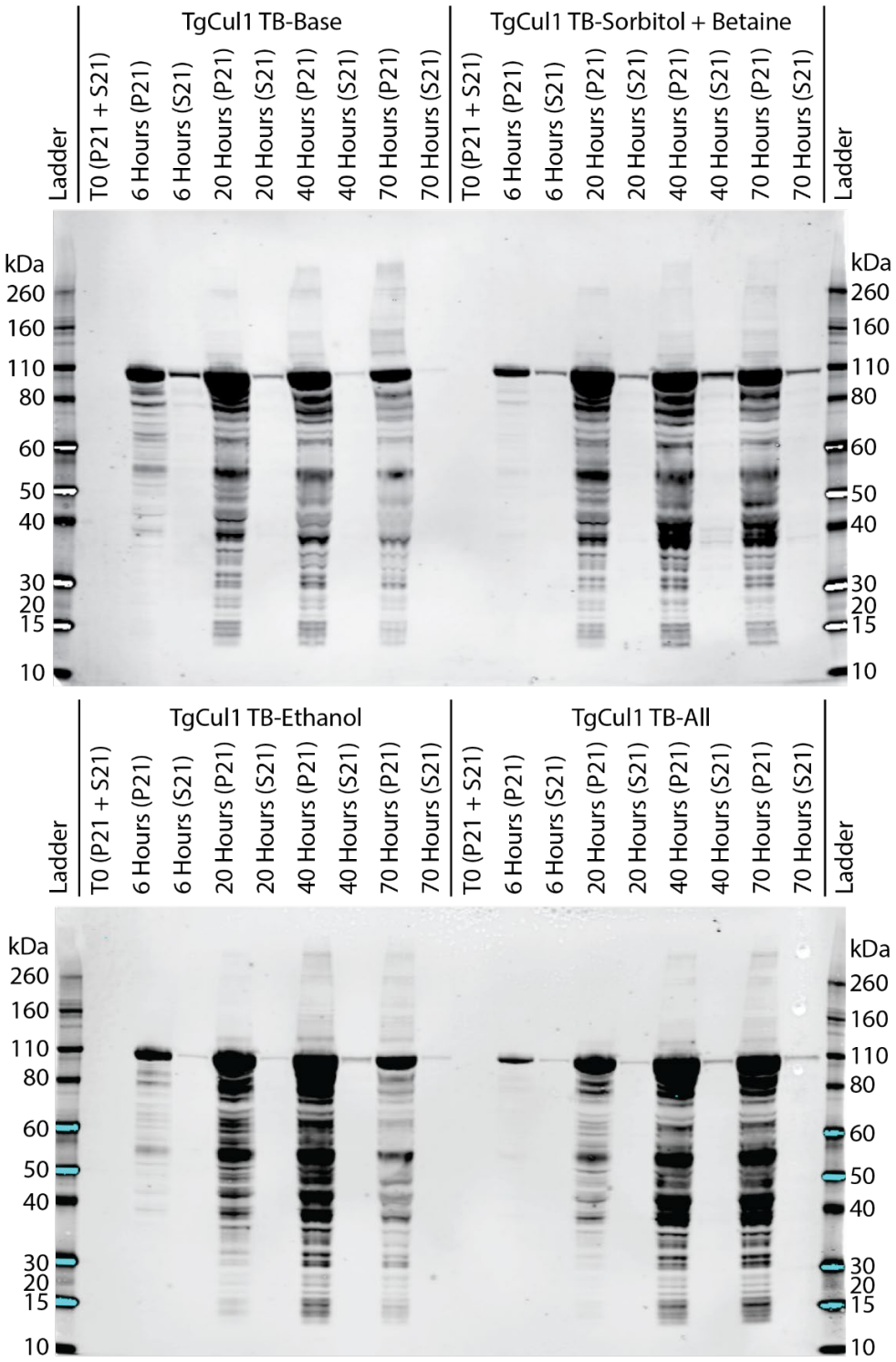

220 nM DdSkp1A-Scrambled4 (215nm)
440 nM DdSkp1A-Scrambled4 (215nm)
890 nM DdSkp1A-Scrambled4 (215nm)
1.8 µM DdSkp1A-Scrambled4 (230nm)
3.5 µM DdSkp1A-Scrambled4 (230nm)
7.1 µM DdSkp1A-Scrambled4 (230nm)
14 µM DdSkp1A-Scrambled4 (280nm)
28 µM DdSkp1A-Scrambled4 (280nm)
57 µM DdSkp1A-Scrambled4 (280nm)
200 nM DdSkp1A-Scrambled4 (310 nm)
c(s) (AU/S)
sedimentation coefficient (S)
signal (AU)
residuals
radius (cm)

Figure 4.S5


TgCul1 TB-Base
TgCul1 TB-Sorbitol + Betaine
TgCul1 TB-Ethanol
TgCul1 TB-All
Ladder
T0 (P21 + S21)
6 Hours (P21)
6 Hours (S21)
20 Hours (P21)
20 Hours (S21)
40 Hours (P21)
40 Hours (S21)
70 Hours (P21)
70 Hours (S21)
kDa
260
160
110
80
60
50
40
30
20
15
10

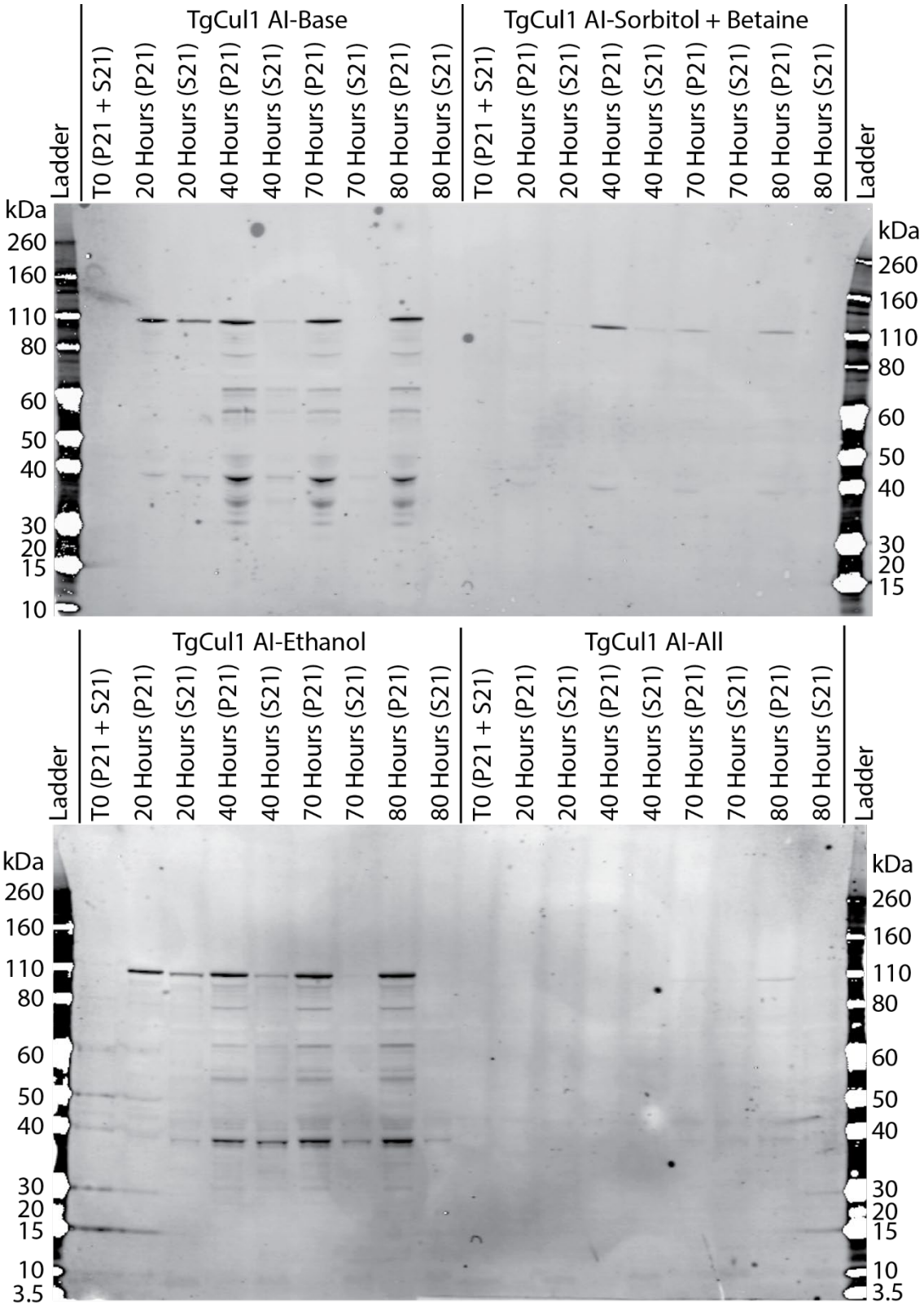
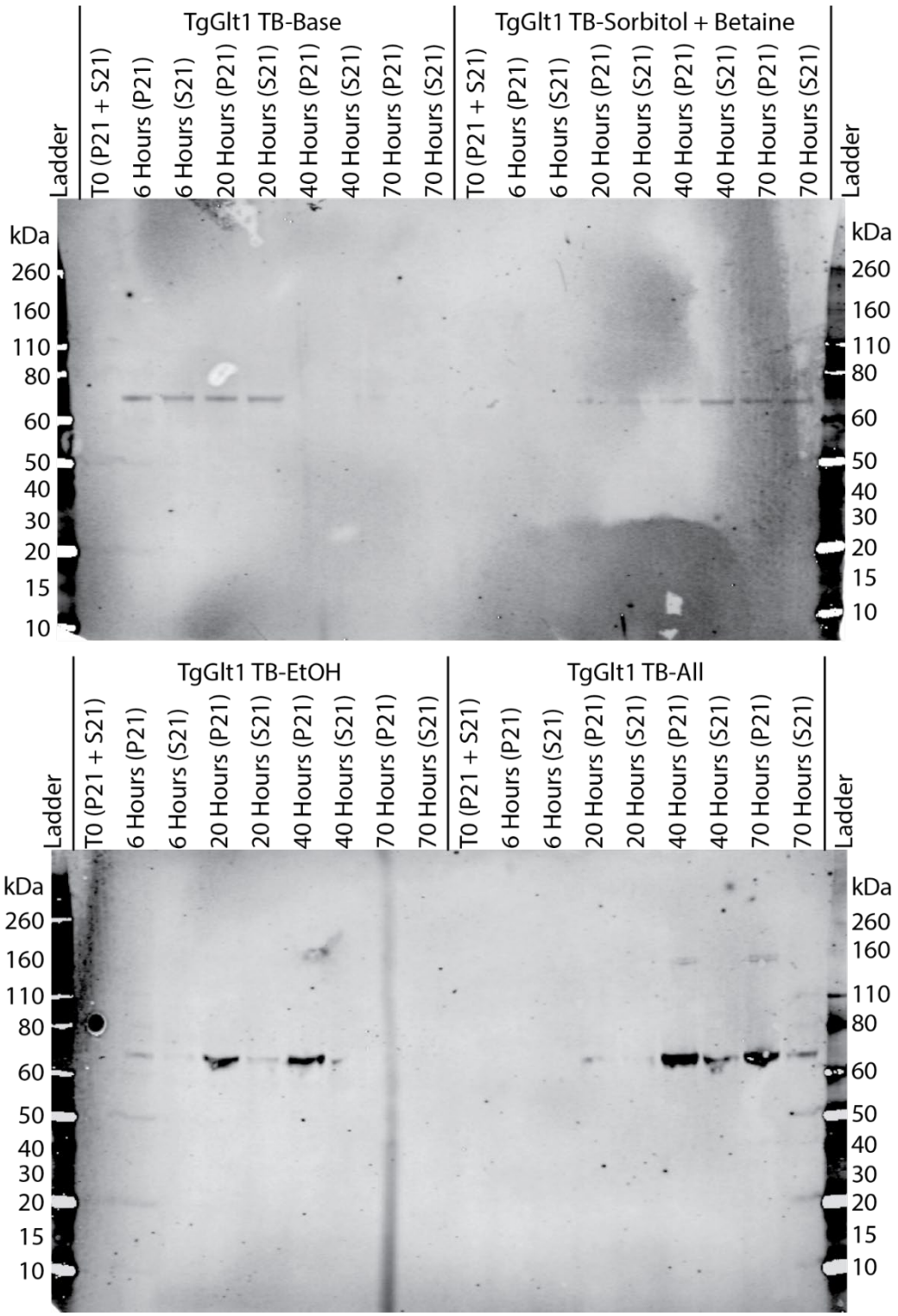

TgCul1 AI-Base
TgCul1 AI-Sorbitol + Betaine
TgCul1 AI-Ethanol
TgCul1 AI-All
Ladder
T0 (P21 + S21)
20 Hours (P21)
20 Hours (S21)
40 Hours (P21)
40 Hours (S21)
70 Hours (P21)
70 Hours (S21)
80 Hours (P21)
80 Hours (S21)
kDa
260
160
110
80
60
50
40
30
20
15
10
3.5

Figure 4.S6


TgGlt1 TB-Base
TgGlt1 TB-Sorbitol + Betaine
TgGlt1 TB-EtOH
TgGlt1 TB-All
Ladder
T0 (P21 + S21)
6 Hours (P21)
6 Hours (S21)
20 Hours (P21)
20 Hours (S21)
40 Hours (P21)
40 Hours (S21)
70 Hours (P21)
70 Hours (S21)
kDa
260
160
110
80
60
50
40
30
20
15
10

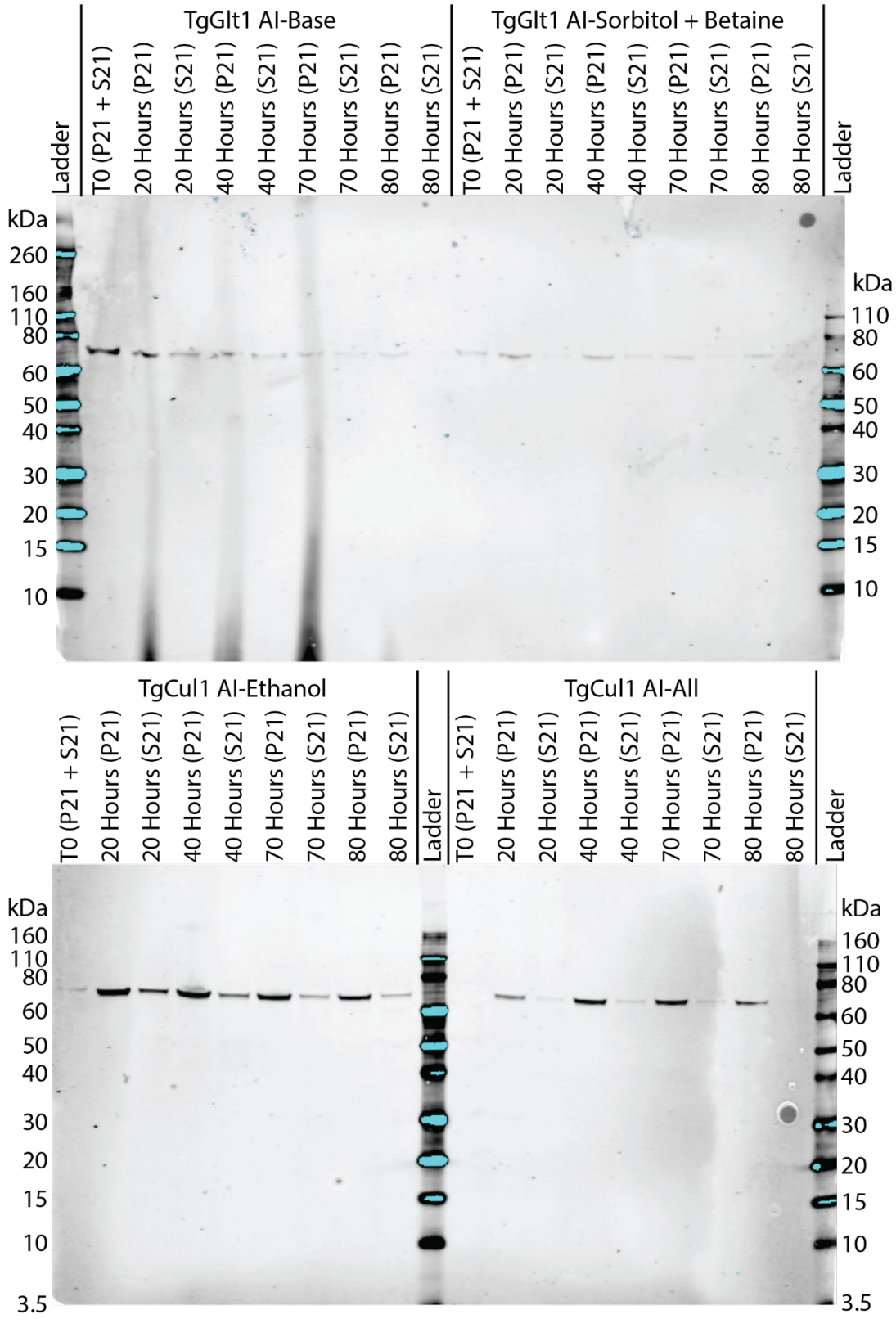

TgGlt1 AI-Base
TgGlt1 AI-Sorbitol + Betaine
Ladder
T0 (P21 + S21)
20 Hours (P21)
20 Hours (S21)
40 Hours (P21)
40 Hours (S21)
70 Hours (P21)
70 Hours (S21)
80 Hours (P21)
80 Hours (S21)
kDa
260
160
110
80
60
50
40
30
20
15
10
TgCul1 AI-Ethanol
TgCul1 AI-All
3.5

Figure 4.S7

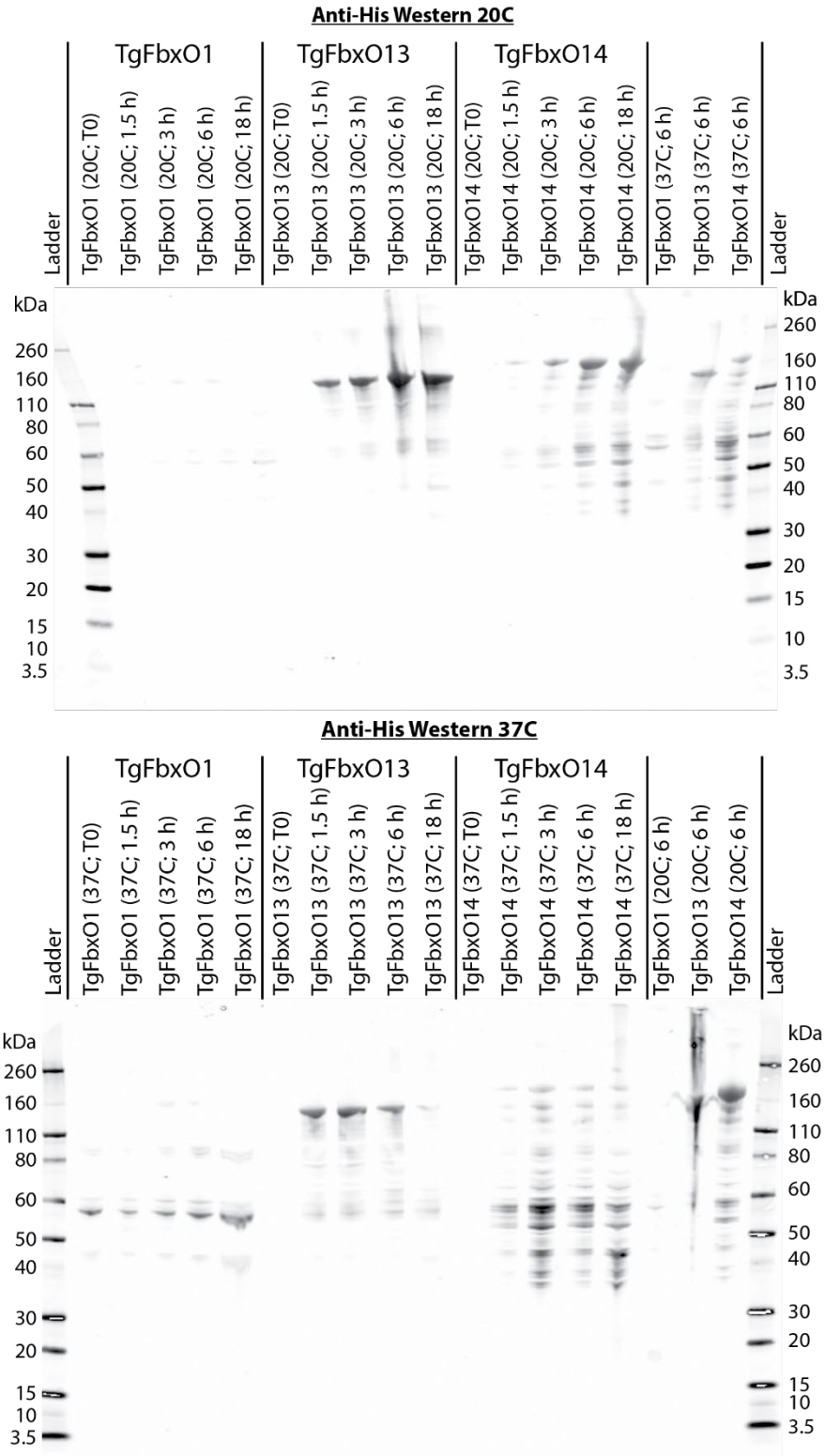

Anti-His Western 20C
TgFbxO1
TgFbxO13
TgFbxO14
Ladder
TgFbxO1 (20C; T0)
TgFbxO1 (20C; 1.5 h)
TgFbxO1 (20C; 3 h)
TgFbxO1 (20C; 6 h)
TgFbxO1 (20C; 18 h)
TgFbxO13 (20C; T0)
TgFbxO13 (20C; 1.5 h)
TgFbxO13 (20C; 3 h)
TgFbxO13 (20C; 6 h)
TgFbxO13 (20C; 18 h)
TgFbxO14 (20C; T0)
TgFbxO14 (20C; 1.5 h)
TgFbxO14 (20C; 3 h)
TgFbxO14 (20C; 6 h)
TgFbxO14 (20C; 18 h)
TgFbxO1 (37C; 6 h)
TgFbxO13 (37C; 6 h)
TgFbxO14 (37C; 6 h)
Ladder
kDa
260
160
110
80
60
50
40
30
20
15
10
3.5
Anti-His Western 37C
TgFbxO1
TgFbxO13
TgFbxO14
Ladder
TgFbxO1 (37C; T0)
TgFbxO1 (37C; 1.5 h)
TgFbxO1 (37C; 3 h)
TgFbxO1 (37C; 6 h)
TgFbxO1 (37C; 18 h)
TgFbxO13 (37C; T0)
TgFbxO13 (37C; 1.5 h)
TgFbxO13 (37C; 3 h)
TgFbxO13 (37C; 6 h)
TgFbxO13 (37C; 18 h)
TgFbxO14 (37C; T0)
TgFbxO14 (37C; 1.5 h)
TgFbxO14 (37C; 3 h)
TgFbxO14 (37C; 6 h)
TgFbxO14 (37C; 18 h)
TgFbxO1 (20C; 6 h)
TgFbxO13 (20C; 6 h)
TgFbxO14 (20C; 6 h)
Ladder
kDa
260
160
110
80
60
50
40
30
20
15
10
3.5

Figure 4.S8

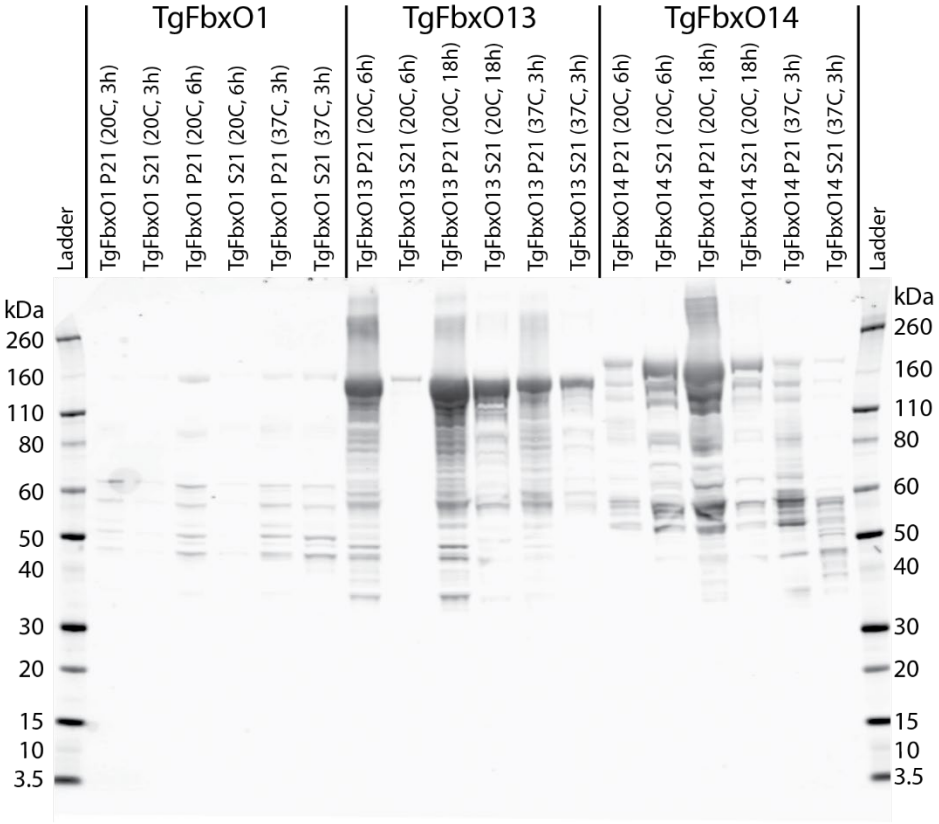
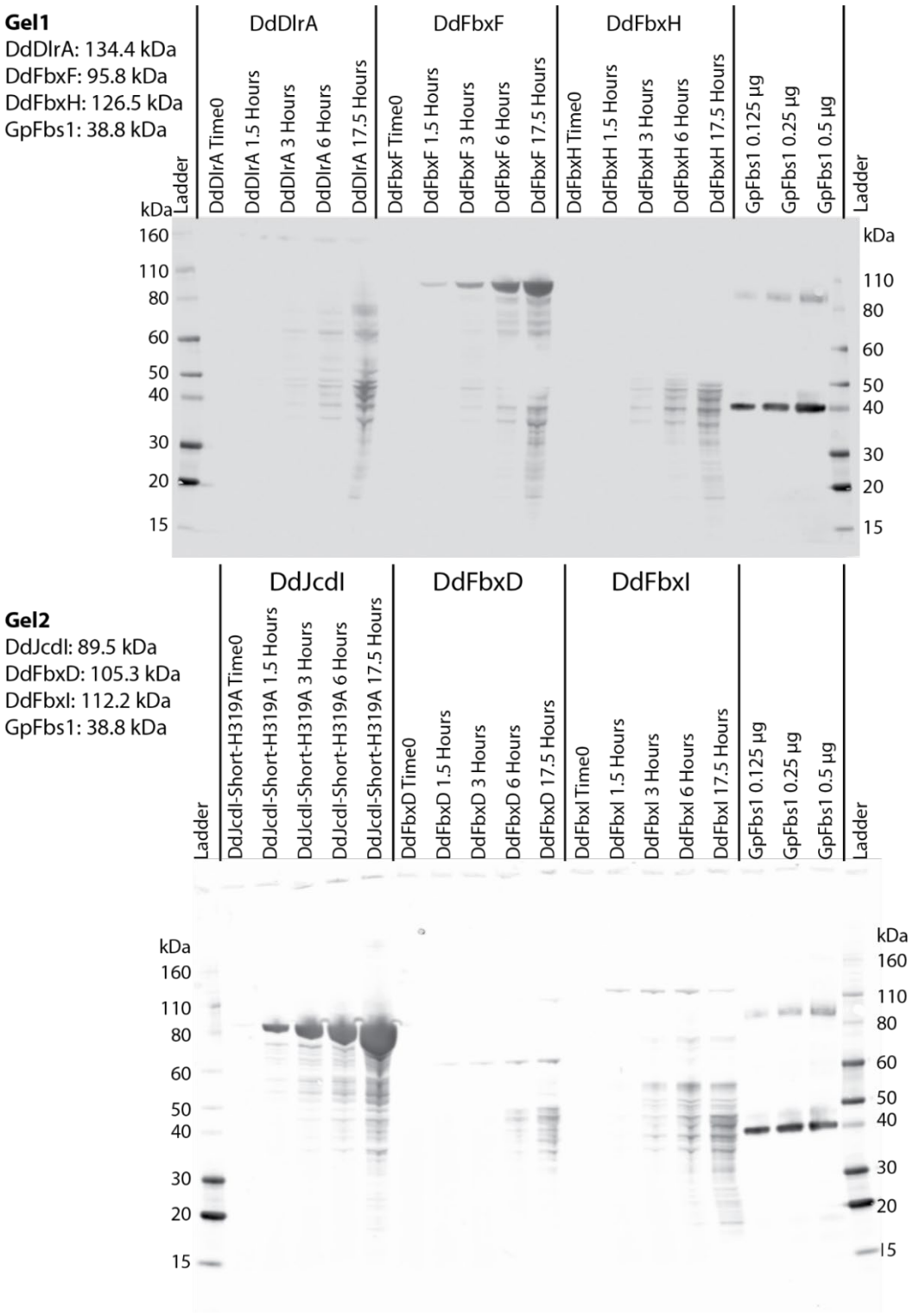
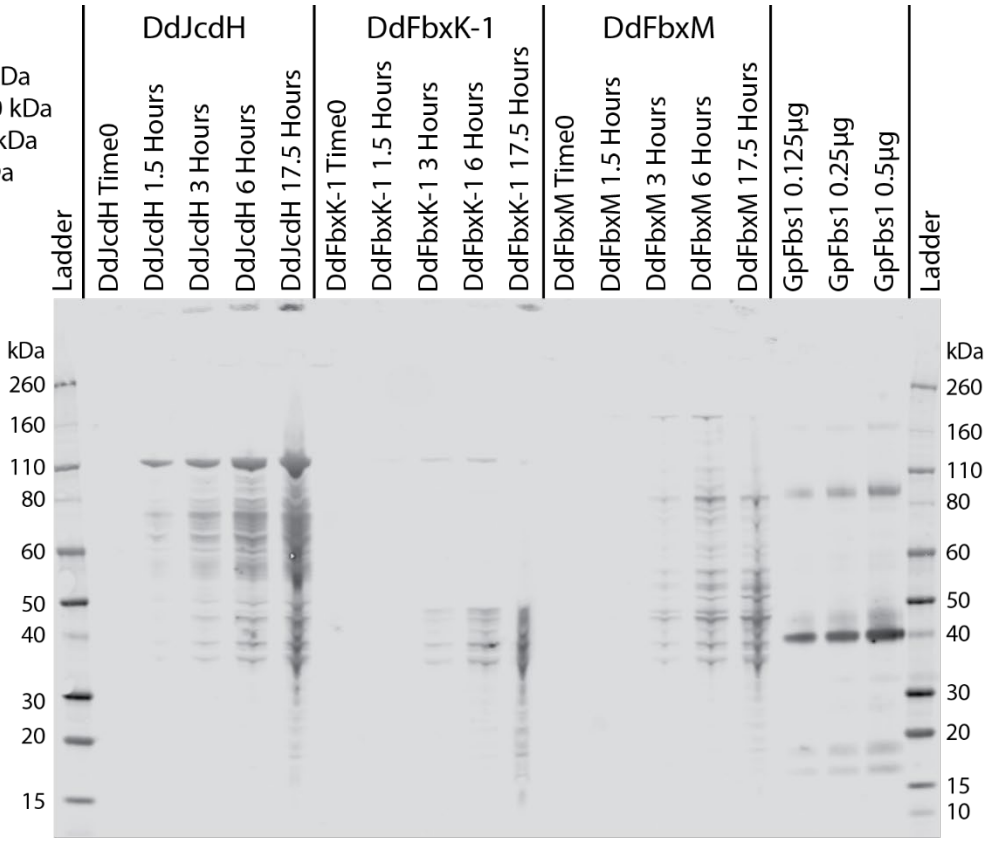

TgFbxO1
TgFbxO13
TgFbxO14
Ladder
TgFbxO1 P21 (20C, 3h)
TgFbxO1 S21 (20C, 3h)
TgFbxO1 P21 (20C, 6h)
TgFbxO1 S21 (20C, 6h)
TgFbxO1 P21 (37C, 3h)
TgFbxO1 S21 (37C, 3h)
TgFbxO13 P21 (20C, 6h)
TgFbxO13 S21 (20C, 6h)
TgFbxO13 P21 (20C, 18h)
TgFbxO13 S21 (20C, 18h)
TgFbxO13 P21 (37C, 3h)
TgFbxO13 S21 (37C, 3h)
TgFbxO14 P21 (20C, 6h)
TgFbxO14 S21 (20C, 6h)
TgFbxO14 P21 (20C, 18h)
TgFbxO14 S21 (20C, 18h)
TgFbxO14 P21 (37C, 3h)
TgFbxO14 S21 (37C, 3h)
Ladder
kDa
260
160
110
80
60
50
40
30
20
15
10
3.5

Figure 4.S9


Gel1
DdDlrA: 134.4 kDa
DdFbxF: 95.8 kDa
DdFbxH: 126.5 kDa
GpFbs1: 38.8 kDa
DdDlrA
DdFbxF
DdFbxH
Ladder
DdDlrA Time0
DdDlrA 1.5 Hours
DdDlrA 3 Hours
DdDlrA 6 Hours
DdDlrA 17.5 Hours
DdFbxF Time0
DdFbxF 1.5 Hours
DdFbxF 3 Hours
DdFbxF 6 Hours
DdFbxF 17.5 Hours
DdFbxH Time0
DdFbxH 1.5 Hours
DdFbxH 3 Hours
DdFbxH 6 Hours
DdFbxH 17.5 Hours
GpFbs1 0.125 µg
GpFbs1 0.25 µg
GpFbs1 0.5 µg
Ladder
kDa
160
110
80
60
50
40
30
20
15
Gel2
DdJcdI: 89.5 kDa
DdFbxD: 105.3 kDa
DdFbxI: 112.2 kDa
GpFbs1: 38.8 kDa
DdJcdI
DdFbxD
DdFbxI
Ladder
DdJcdI-Short-H319A Time0
DdJcdI-Short-H319A 1.5 Hours
DdJcdI-Short-H319A 3 Hours
DdJcdI-Short-H319A 6 Hours
DdJcdI-Short-H319A 17.5 Hours
DdFbxD Time0
DdFbxD 1.5 Hours
DdFbxD 3 Hours
DdFbxD 6 Hours
DdFbxD 17.5 Hours
DdFbxI Time0
DdFbxI 1.5 Hours
DdFbxI 3 Hours
DdFbxI 6 Hours
DdFbxI 17.5 Hours
GpFbs1 0.125 µg
GpFbs1 0.25 µg
GpFbs1 0.5 µg
Ladder
kDa
160
110
80
60
50
40
30
20
15

Gel3
DdJcdH: 107.8 kDa
DdFbxK-1: 107.0 kDa
DdFbxM: 160.0 kDa
GpFbs1: 38.8 kDa



Gel4
DdFbxN: 106.6 kDa
DdCulE: 90.2 kDa
(DdRbx1: 12.1 kDa)
GpFbs1: 38.8 kDa

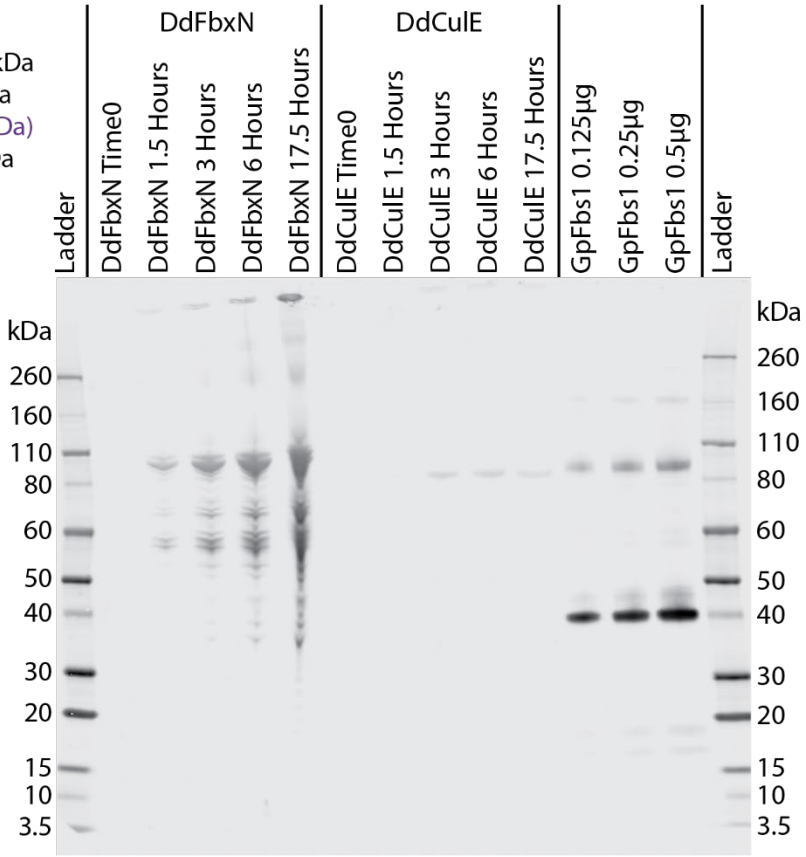


Figure 4.S10

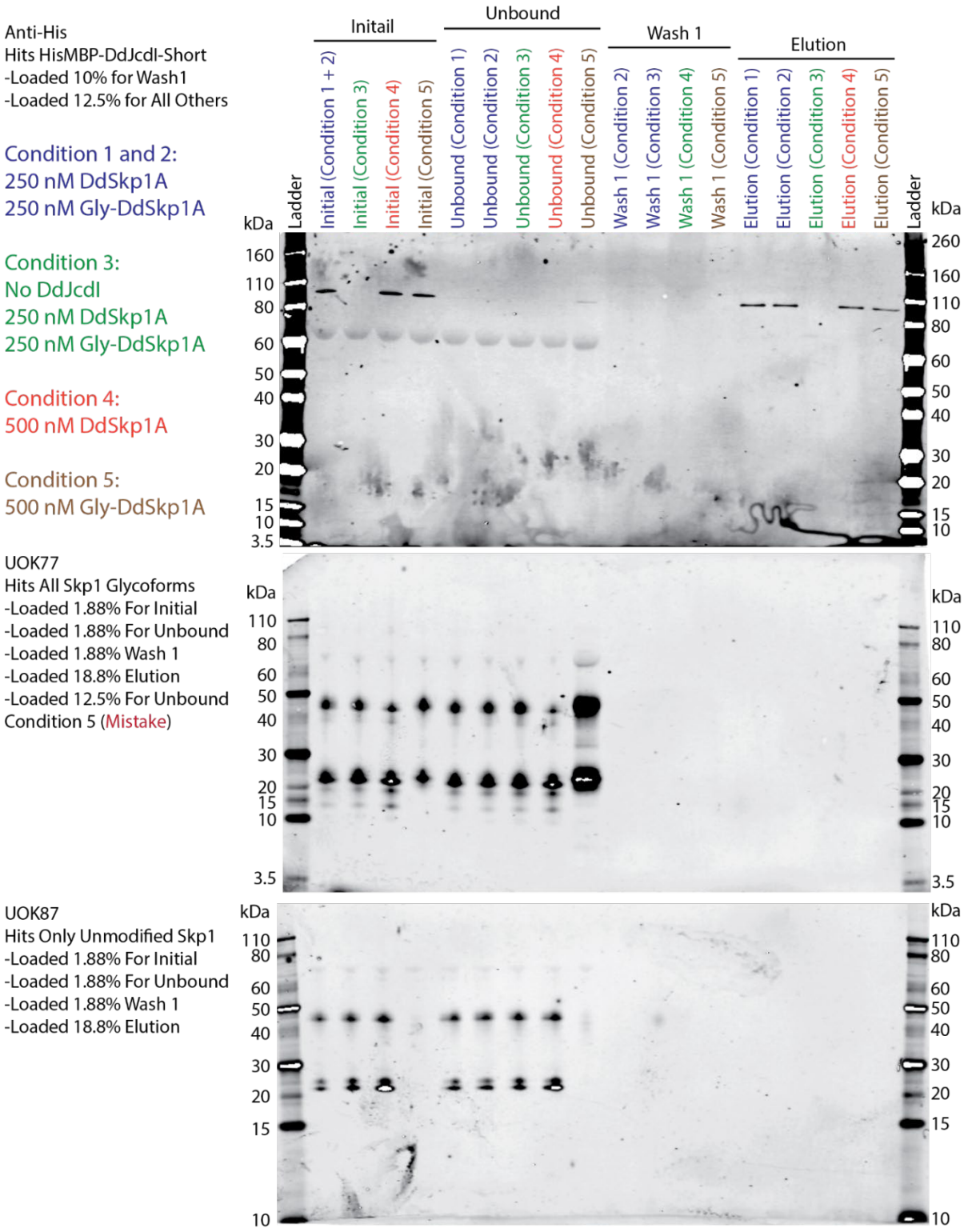

Anti-His
Hits HisMBP-DdJcdI-Short
-Loaded 10% for Wash1
-Loaded 12.5% for All Others
Condition 1 and 2:
250 nM DdSkp1A
250 nM Gly-DdSkp1A
Condition 3:
No DdJcdI
250 nM DdSkp1A
250 nM Gly-DdSkp1A
Condition 4:
500 nM DdSkp1A
Condition 5:
500 nM Gly-DdSkp1A
Initail
Unbound
Wash 1
Elution
Ladder
Initial (Condition 1 + 2)
Initial (Condition 3)
Initial (Condition 4)
Initial (Condition 5)
Unbound (Condition 1)
Unbound (Condition 2)
Unbound (Condition 3)
Unbound (Condition 4)
Unbound (Condition 5)
Wash 1 (Condition 2)
Wash 1 (Condition 3)
Wash 1 (Condition 4)
Wash 1 (Condition 5)
Elution (Condition 1)
Elution (Condition 2)
Elution (Condition 3)
Elution (Condition 4)
Elution (Condition 5)
Ladder
kDa
160
110
80
60
50
40
30
20
15
10
3.5
260
UOK77
Hits All Skp1 Glycoforms
-Loaded 1.88% For Initial
-Loaded 1.88% For Unbound
-Loaded 1.88% Wash 1
-Loaded 18.8% Elution
-Loaded 12.5% For Unbound
Condition 5 (Mistake)
UOK87
Hits Only Unmodified Skp1
-Loaded 1.88% For Initial
-Loaded 1.88% For Unbound
-Loaded 1.88% Wash 1
-Loaded 18.8% Elution

Figure 4.S11

Initial FBP Plasmid Assembly Primers

Primer Name	Primer Sequence
Common Backbone Forward	GCGGCCGCGATCCGGCT
Common Backbone Reverse	CATTGGCCACATATGAGTAATATCACCTTG
DdDlrA Forward	TGATATTACTCATATGTGGCCAATGATGCAAAATCACCAGAATCAAATGAATGTT
DdDlrA Reverse	CCGGATCGCGGCCGCTTATACAATAATACGAAGATTTGTATTAAGATTATTATTTCTATTATTAGAACC
DdFbxF Forward	TGATATTACTCATATGTGGCCAATGATGGGATTATTTGGTAAAATTTTTAAAAAGAAAACAAATGG
DdFbxF Reverse	CCGGATCGCGGCCGCTTAATTTTTTTCATTAACTTTTAAAATATGTTTTGGAATATCATAAGAAATTAAAG
DdJcdI-Short- H319A Forward	TGATATTACTCATATGTGGCCAATGTCTAAAGGCGTGAAAGTGGTTATTGG
DdJcdI-Short- H319A Reverse	CCGGATCGCGGCCGCTTAGTTCTGTGAATTGCAAAAGTTTTGCG
DdFbxD Forward	TGATATTACTCATATGTGGCCAATGATGTCATATGACTATAACTGTTGGGTTTGC
DdFbxD Reverse	CCGGATCGCGGCCGCTTAATCTAAATTAAAATTATATAATCTAACTAAATTATTGAAAACACCAATAATACG
DdFbxI Forward	TGATATTACTCATATGTGGCCAATGATGATGACAAATATCAATGAATTACCAATACCAG
DdFbxI Reverse	CCGGATCGCGGCCGCTTAAATTTCTTCAACTAAATCATAATAATAAATTGATTTATTTTGTTGAATTG
DdFbxA Forward	TGATATTACTCATATGTGGCCAATGATGCAATACGTTAATGGTAATGATATTTCAAGTC
DdFbxA Reverse	CCGGATCGCGGCCGCTTAAAAGTCCCATCTCAAAACCAATCCAT
DdJcdH Forward	TGATATTACTCATATGTGGCCAATGATGTCAAAATATAATGAAGAAAACTTAAATGAAGATGTTG
DdJcdH Reverse	CCGGATCGCGGCCGCTTAATTATCACTTAAATCATCACCAAAAGAGAATGAAAATG
DdFbxK Forward	TGATATTACTCATATGTGGCCAATGATGGTTGTGTTATTACCATTATATATTCAAAAATATATAATTAAAATTTTATGTAG
DdFbxK Reverse	CCGGATCGCGGCCGCTTATTTTTTATAATCCAATAAAATTACTGGATTGAAATTTTCAGTTTCAT
DdFbxM Forward	TGATATTACTCATATGTGGCCAATGATGTCGCACAGTGTGGTTAGTTCT
DdFbxM Reverse	CCGGATCGCGGCCGCTTAATGTTTATTACATTGAAATTGTTGATTAAAATAATTTGATAATTTTGATCTATG
DdFbxN Forward	TGATATTACTCATATGTGGCCAATGATGGAAGATGAAGATAATCAACAACAACAACC
DdFbxN Reverse	CCGGATCGCGGCCGCTTAACTTTGAATTGTTGTTAAAAAAAAAGTTGGAACTG
DdFbxH Forward	TGATATTACTCATATGTGGCCAATGATGAAAACAAATTTCACACCACCATCAAAA
DdFbxH Reverse	CCGGATCGCGGCCGCTTAATAAATTACATTACAACGCAAAGCAGAAGTTTGA
TgFbxO1 Forward	TGATATTACTCATATGTGGCCAATGATGGGCAACACGGAATCCACG
TgFbxO1 Reverse	CCGGATCGCGGCCGCTCACGCATTGGCTCCGCCC
TgFbxO13 Forward	TGATATTACTCATATGTGGCCAATGATGGAAGTTGACGAACGTCAACAAAC
TgFbxO13 Reverse	CCGGATCGCGGCCGCTTACGCGACCGCCTGGC
TgFbxO14 Forward	TGATATTACTCATATGTGGCCAATGATGGAATTTTTGGACCAGGCTACTTTG
TgFbxO14 Reverse	CCGGATCGCGGCCGCTCACAGCACATCTCGTTTAATCCATATG
DdFbxG Forward	TGATATTACTCATATGTGGCCAATGATGTCAACAAAAAAAAAAATTAAAACAGATAATAATAATAAAATATTTCAAG
DdFbxG Reverse	CCGGATCGCGGCCGCTTAATATGGGCTATTCTTTATTGTTGTTTTGAAATATGG
DdFbxJ Forward	TGATATTACTCATATGTGGCCAATGATGTCAACAAATAAAAAAATAAAAACAGATAATAATAAAAAAATATTTCAAG
DdFbxJ Reverse	CCGGATCGCGGCCGCTTAGGTTATTTTCTTTATTAATGTTGTGGTGAAATATGG
DdFbxL Forward	TGATATTACTCATATGTGGCCAATGATGACAGATAACCAGGGTTTAAAAAAAGAAG
DdFbxL Reverse	CCGGATCGCGGCCGCTTAAATTAAAAGATATTTTTTACAAATTTTTCTAACATATGGAATATTAATTGGG

FBP-SF Assembly Primers

Primer Name	Primer Sequence
Common SF-Tag Forward	CTGGTGCCGCGAGGGTCCTGGTCTCATCCTCAGTTTGAAAAAGG
Common SF-Tag Reverse	CCGGATCGCGGCCGCTTATTTATCGTCGTCGTCTTTGTAATCCTC
Common (SF-Tag) Backbone Forward	GCGGCCGCGATCCGGCT
DdFbxN Reverse	GGACCCTCGCGGCACCAGACTTTGAATTGTTGTTAAAAAAAAAGTTGGAACTG
DdFbxF Reverse	GGACCCTCGCGGCACCAGATTTTTTTCATTAACTTTTAAAATATGTTTTGGAATATCATAAGAAATTAAAG
DdDlrA Reverse	GGACCCTCGCGGCACCAGTACAATAATACGAAGATTTGTATTAAGATTATTATTTCTATTATTAGAACCAC
DdJcdH Reverse	GGACCCTCGCGGCACCAGATTATCACTTAAATCATCACCAAAAGAGAATGAAAATG
DdJcdI-Short-H319A Reverse	GGACCCTCGCGGCACCAGGTTCTGTGAATTGCAAAAGTTTTGCGTAA
TgFbx01 Reverse	GGACCCTCGCGGCACCAGCGCATTGGCTCCGCCC
TgFbx013 Reverse	GGACCCTCGCGGCACCAGCGCGACCGCCTGGCT
TgFbx014 Reverse	GGACCCTCGCGGCACCAGCAGCACATCTCGTTTAATCCATATGTACAC

Other Utilized Primers

Primer Name	Primer Sequence
pNIC28 ColonyPCR Forward	CGGGGCCTGCCACCATACCCACG
pNIC28 ColonyPCR Reverse	GTGGTGGTGGTGGTGCTCGAGTGCGG
pET28-MBP ColoyPCR Forward	CGCCAGCGGTCGTCAG
pET28-MBP ColoyPCR Reverse	CCAATCCGGATATAGTTCCTCCTTTC
DdSkp1A-ΔCTR Forward	TCAGAGGTTAACAGTAAAGGTGGATACGGATCCGA
DdSkp1A-ΔCTR Reverse	TACTGTTAACCTCTGATCATATTGGCAACAGTTTTACA
TgRbx1 Fragment SF Tagging Forward	CGACGATAAATCTGGTGTAGATCTGGGTAC
TgRbx1 Fragment SF Tagging Reverse	GATGAGACCACGCAGACATATGTATATCTCC
SF Fragment for TgRbx1 Forward	TATGTCTGCGTGGTCTCATCCTCAGTTTG
SF Fragment for TgRbx1 Reverse	CTACACCAGATTTATCGTCGTCGTCTTTG
TgRbx1 ColonyPCR Forward	CGTATTGTACACGGCCGCATAATC
TgRbx1 ColonyPCR Reverse	CGCTGGCAAGTGTAGCGG
TgRbx1 StrepII-Tag Addition Forward	GGTGTAGATCTGGGTACCGAGAACCTGTACTTCCAATCAGGAGCTGAAGATCCAAC
TgRbx1 StrepII-Tag Addition Reverse	AGAAGATTTTTCAAACTGCGGATGGCTCCACGCAGACATATGTATATCTCCTTCTTATACTTAAC

Figure 4.S12

>pNIC28-HisTEV-DdSkp1A-FL
TEV Site

```
TAATACGACTCACTATAGGGGAATTGTGAGCGGATAACAATTCCCCTCTAGAAATAATTTTGTT
TAACTTTAAGAAGGAGATATACAT
M  H  H  H  H  H  H  S  S  G  V  D  L  G  T  E  N  L  Y  F
ATGCACCATCATCATCATCATTCTTCTGGTGTAGATCTGGGTACCGAGAACCTGTACTTC
Q><S  M  S  L  V  K  L  E  S  S  D  E  K  V  F  E  I  E  K
CAATCCATGTCTTTAGTTAAATTAGAATCTTCAGATGAAAAAGTCTTTGAAATTGAAAAA
E  I  A  C  M  S  V  T  I  K  N  M  I  E  D  I  G  E  S  D
GAAATCGCTTGTATGTCAGTTACAATCAAGAATATGATTGAAGATATTGGTGAATCAGAT
S  P  I  P  L  P  N  V  T  S  T  I  L  E  K  V  L  D  Y  C
AGTCCAATTCCATTACCAAATGTTACTAGCACTATTTTAGAGAAAGTTCTTGACTATTGC
R  H  H  H  Q  H  P  S  P  Q  G  D  D  K  K  D  E  K  R  L
AGACATCACCATCAACATCCATCACCACAAGGTGACGATAAAAAGGATGAAAAGAGATTA
D  D  I  P  P  Y  D  R  D  F  C  K  V  D  Q  P  T  L  F  E
GATGATATCCCACCATATGATAGAGATTTCTGTAAAGTCGATCAACCAACCTTATTCGAA
L  I  L  A  A  N  Y  L  D  I  K  P  L  L  D  V  T  C  K  T
TTAATCTTGGCAGCCAATTATTTGGATATCAAACCATTATTAGATGTTACCTGTAAAACT
V  A  N  M  I  R  G  K  T  P  E  E  I  R  K  I  F  N  I  K
GTTGCCAATATGATCAGAGGTAAAACCCCAGAAGAAATCAGAAAAATCTTCAACATCAAG
V  A  N  M  I  R  G  -  -  -  -  -  -  -  -  -  -  -  -  -  ΔCTR
GTTGCCAATATGATCAGAGGT----------------------------------------
N  D  F  T  P  E  E  E  E  Q  I  R  K  E  N  E  W  C  E  D
AACGACTTTACTCCAGAAGAAGAAGAACAAATCAGAAAAGAAAATGAATGGTGTGAAGAT
-  -  -  -  -  -  -  -  -  -  -  -  -  -  -  -  -  -  -  -  -  ΔCTR
--------------------------------------------------------------
K  G  G  N  *
AAAGGTGGAAACTAACAGTAAAGGTGGATACGGATCCGAATTCGAGCTCCGTCGACAAGC
-  -  -  -  *                                                  ΔCTR
------------TAACAGTAAAGGTGGATACGGATCCGAATTCGAGCTCCGTCGACAAGC
TTGCGGCCGCACTCGAGCACCACCACCACCACCACTGAGATCCGGCTGCTAACAAAGCCCGAAA
GGAAGCTGAGTTGGCTGCTGCCACCGCTGAGCAATAACTAGCATAACCCCTTGGGGCCTCTAAA
CGGGTCTTGAGGGGTTTTTTGCTGAAAGGAGGAACTATATCCGGATTGGCGAATGGGACGCGCC
CTGTAGCGGCGCATTAAGCGCGGCGGGTGTGGTGGTTACGCGCAGCGTGACCGCTACACTTGCC
AGCGCCCTAGCGCCCGCTCCTTTCGCTTTCTTCCCTTCCTTTCTCGCCACGTTCGCCGGCTTTC
CCCGTCAAGCTCTAAATCGGGGGCTCCCTTTAGGGTTCCGATTTAGTGCTTTACGGCACCTCGA
```

Figure 4.S13

>pNIC28-HisTEV-DdSkp1A-Scrambled4/PolySer
Scramble4 (Scr4)
PolySer (PolS)

TAATACGACTCACTATAGGGGAATTGTGAGCGGATAACAATTCCCCTCTAGAAATAATTTTGTT
TAACTTTAAGAAGGAGATATACAT
M H H H H H H S S G V D L G T E N L Y F
ATGCACCATCATCATCATCATTCTTCTGGTGTAGATCTGGGTACCGAGAACCTGTACTTC
Q S M S L V K L E S S D E K V F E I E K
CAATCCATGTCTTTAGTTAAATTAGAATCTTCAGATGAAAAAGTCTTTGAAATTGAAAAA
E I A C M S V T I K N M I E D I G E S D
GAAATCGCTTGTATGTCAGTTACAATCAAGAATATGATTGAAGATATTGGTGAATCAGAT
S P I P L P N V T S T I L E K V L D Y C
AGTCCAATTCCATTACCAAATGTTACTAGCACTATTTTAGAGAAAGTTCTTGACTATTGC
R H H H Q H P S P Q G D D K K D E K R L
AGACATCACCATCAACATCCATCACCACAAGGTGACGATAAAAAGGATGAAAAGAGATTA
D D I P P Y D R D F C K V D Q P T L F E
GATGATATCCCACCATATGATAGAGATTTCTGTAAAGTCGATCAACCAACCTTATTCGAA
L I L A A N Y L D I K P L L D V T C K T
TTAATCTTGGCAGCCAATTATTTGGATATCAAACCATTATTAGATGTTACCTGTAAAACT
V A N M I R G K I K K G G E W D R N T E Scr4
GTTGCCAATATGATCAGAGGTAAAATAAAGAAAGGGGGAGAATGGGATAGGAACACCGAA
V A N M I R G S S S S S S S S S S S S S PolS
GTTGCCAATATGATCAGAGGTTCAAGTTCTTCCTCAAGCAGTTCATCGTCTTCGAGCTCC
E E F E I N I T R Q K N I C E E E K P F Scr4
GAGGAGTTCGAGATCAATATTACGCGTCAGAAGAACATCTGCGAAGAGGAAAAACCGTTT
S S S S S S S S S S S S S S S S S S S PolS
AGCTCCTCTAGCAGCTCGTCGAGCAGCTCTTCCAGCAGCTCCTCTAGCAGCAGCAGCAGC
N D E P * Scr4
AACGACGAACCGTAAGGATCCGAATTCGAGCTCCGTCGACAAGCTTGCGGCCGCACTCGA
S S S S * PolS
AGTTCCTCATCTTAAGGATCCGAATTCGAGCTCCGTCGACAAGCTTGCGGCCGCACTCGA
GCACCACCACCACCACCACTGAGATCCGGCTGCTAACAAAGCCCGAAAGGAAGCTGAGTTGGCT
GCTGCCACCGCTGAGCAATAACTAGCATAACCCCTTGGGGCCTCTAAACGGGTCTTGAGGGGTT

Figure 4.S14

>pETDuet1-HisDdCulE-DdRbx1
DdCulE
(Uniprot ID: Q54XF7) (Dictybase ID: DDB_G0278991)

DdRbx1
(Uniprot ID: Q54K33) (Dictybase ID: DDB_G0287629)

His Tag
TEV Site

GGGGAATTGTGAGCGGATAACAATTCCCCTCTAGAAATAATTTTGTTTAACTTTAAGAAGGAGA
TATACC
M G S S H H H H H H S Q D P N S S S E N
ATGGGCAGCAGCCATCACCATCATCACCACAGCCAGGATCCGAATTCGAGCTCGGAAAAT
L Y F Q><S V D M S D Q I T V D E L W A E
CTATATTTTCAATCAGTCGACATGTCTGATCAAATCACCGTCGACGAGCTGTGGGCAGAG
C E Q T F E D L F L N L K K G L S R K R
TGCGAACAGACCTTCGAAGATTTGTTCCTCAACTTGAAGAAAGGTCTGTCTCGTAAGCGC
Y M E I Y T K I Y N Y C S S A N E K A L
TATATGGAAATCTACACCAAAATCTACAATTACTGCAGCTCCGCTAACGAGAAGGCGCTG
I D F Y I P K V K V L V A Q K A V E I M
ATCGACTTCTATATCCCGAAGGTTAAAGTTTTGGTGGCCCAAAAAGCGGTTGAGATCATG
S R S E S Y P N D A L L L F F R N Q W N
TCTAGAAGCGAGAGCTATCCGAATGACGCCCTGCTGTTGTTCTTTCGTAATCAGTGGAAC
E W K M S S N V L K N L L S P V N K I H
GAGTGGAAAATGAGCAGCAATGTACTGAAGAACCTGCTGAGTCCGGTTAATAAAATCCAC
S S D K K T T S S S A N Q N E S V V Y S
AGCTCGGACAAGAAAACCACCAGCAGCTCGGCGAATCAAAACGAAAGCGTCGTGTATAGC
D T L N S W R E T A F N P L K N K L S V
GACACCCTAAACAGCTGGCGTGAAACCGCGTTTAACCCGTTGAAGAACAAATTATCTGTT
S L L Q I I K N D R T G F S T N L Q V L
AGCTTGCTTCAGATAATTAAAAACGATCGTACCGGTTTTTCCACCAACTTGCAAGTGTTG
S D S L E C Y V Q L G P E K N K L E I Y
TCCGACAGCCTGGAATGCTACGTCCAGCTGGGTCCGGAAAAAAATAAGTTGGAAATTTAC
Q S C F E Q Q F L Q E T E T F Y K A E S
CAGTCTTGTTTTGAGCAACAATTCCTCCAAGAAACCGAAACATTTTACAAAGCGGAATCC
A D F I E K N G V C E Y M R H V Y N R I
GCCGATTTCATAGAGAAGAACGGTGTTTGCGAGTACATGCGTCACGTGTATAACCGTATC
E Q E T N R V N Q Y M P I S T L E K L T
GAGCAAGAGACCAACCGCGTAAACCAGTACATGCCGATTAGCACCTTGGAAAAACTCACT
K I L N N V L I S N Y K E Q F A S K F L
AAGATCCTGAACAACGTTCTGATCTCTAACTACAAAGAACAATTCGCCTCAAAGTTCCTG
D I L I E D K S S D L V M M Y S L L S R
GATATCCTTATCGAGGACAAGAGCAGCGATCTGGTTATGATGTATTCCCTTCTATCACGC

V N H L T P L K N I F S D F I K S E G L
GTTAACCATCTGACGCCGCTGAAGAACATTTTCAGCGACTTCATCAAATCCGAAGGTCTC
K E I E S N L K E A Q E K P Q V L I S I
AAAGAGATCGAGTCTAACTTGAAGGAGGCTCAGGAGAAGCCGCAGGTTCTCATTAGCATT
L L K I Y S R F N I M I K E C Y G N D T
CTGCTGAAGATCTACAGCCGCTTCAACATCATGATTAAGGAGTGCTATGGTAATGACACC
D F T T A M D K S F S I L V N E N P A S
GACTTCACCACGGCTATGGATAAGAGCTTCAGCATCCTCGTCAACGAGAACCCGGCAAGC
Y D P K K K E S N I P V V L S K F C D Q
TACGACCCGAAGAAAAAGGAAAGCAACATCCCGGTGGTGCTGTCTAAATTCTGCGATCAG
I L R K G P H H I S D E A E L E K K L T
ATTCTGCGTAAAGGTCCGCATCACATTTCTGACGAAGCGGAACTGGAAAAGAAGTTAACC
E A V C L F K Y L P D K D I F M L N Y Q
GAAGCGGTGTGCCTGTTTAAGTATCTGCCAGATAAGGACATCTTTATGCTGAATTACCAA
K M L S K R L V E D L S A S E D A E T L
AAAATGCTGAGCAAGCGTTTAGTTGAGGACTTGTCGGCGAGCGAGGATGCGGAAACCCTG
M I N K L K N Y Q G F D Y C T K L T R M
ATGATCAACAAGCTGAAAAACTACCAAGGCTTCGATTACTGCACCAAGTTGACTCGCATG
I T D M R L C K D I N I N F Q N H L N E
ATCACTGATATGCGCCTGTGTAAAGATATTAACATCAACTTTCAGAACCACCTGAATGAG
K S L T L P Y Q F N F Y V L T N G S W T
AAGTCCTTGACTCTGCCCTATCAATTTAATTTTTACGTGTTGACGAACGGCTCATGGACC
L T N K Q T A T P F K P P S E M L S S I
CTGACCAACAAGCAAACCGCTACTCCATTTAAACCGCCTAGTGAGATGCTGAGCAGCATC
T Y F E S F Y K K S Y Q G R V L T F L Y
ACCTACTTCGAGAGCTTTTATAAAAAGTCCTATCAAGGCCGTGTTCTGACATTTCTGTAT
D F S R A D V D S R Q A K G K I Y K L T
GATTTTAGCCGTGCGGACGTGGATAGCCGCCAGGCGAAAGGCAAAATCTACAAATTAACC
T T A Y Q M A I L L M F N G A D K I T R
ACGACTGCGTATCAAATGGCAATTCTGCTTATGTTTAACGGCGCAGACAAGATCACCCGT
F L I N D T I G L D E T S I R L P L L A
TTTCTGATCAACGACACGATCGGTCTGGATGAAACCTCCATCCGCCTGCCGCTGCTGGCA
L I K T G I I E C S E P S F K N W N N D
CTCATTAAAACCGGTATTATTGAATGTAGCGAACCGTCGTTCAAGAATTGGAATAATGAC
T E F T V N S K F S S K K M K V S C N I
ACCGAGTTCACGGTGAATAGCAAATTCAGCTCTAAGAAAATGAAGGTGTCCTGTAATATT
A V Q I G E T K Q S E G Q Q T V S E Q E
GCAGTGCAGATCGGCGAAACGAAACAGTCCGAGGGCCAGCAGACTGTCAGCGAGCAGGAG
I E K E R F F K L Q A A I V R I M K S K
ATTGAGAAAGAACGTTTCTTCAAACTGCAAGCGGCGATCGTTCGTATTATGAAGAGCAAG
K T M T H N D L T V E T T T Q V S K W F
AAAACCATGACCCATAATGACCTGACGGTCGAAACGACCACCCAGGTTTCCAAGTGGTTT
T P K I T A I K K A I E Y L I D Q E Y I
ACCCCGAAAATCACCGCTATTAAAAAGGCGATCGAGTATTTGATTGACCAGGAATATATT
R R T T D D N P S A R K Y E Y M A *
CGTCGTACCACCGATGATAATCCGTCAGCGCGTAAATACGAATACATGGCTTAAAAGCTT

GCGGCCGCATAATGCTTAAGTCGAACAGAAAGTAATCGTATTGTACACGGCCGCATAATCGAAA
TTAATACGACTCACTATAGGGGAATTGTGAGCGGATAACAATTCCCCATCTTAGTATATTAGTT
AAGTATAAGAAGGAGATATACAT

M A D V E A S S S A S K T P K K K F E V

ATGGCTGATGTAGAAGCGTCAAGTAGCGCATCTAAGACGCCGAAGAAAAAGTTCGAGGTG

K R W N A V A L W I W D I V V D N C A I

AAGCGCTGGAACGCTGTGGCGCTGTGGATCTGGGACATCGTCGTGGACAACTGTGCCATC

C R N H I M D L C I E C Q A N Q A S N T

TGCCGTAATCACATTATGGATTTGTGCATCGAGTGCCAAGCGAACCAGGCAAGCAATACC

S E E C T V A W G I C N H A F H F H C I

TCCGAAGAGTGCACCGTTGCGTGGGGTATTTGTAATCATGCGTTTCACTTTCATTGCATT

S R W L K S R Q V C P L D N R D W E F Q

TCTCGTTGGCTGAAAAGCCGCCAAGTTTGTCCGCTGGATAACCGTGACTGGGAATTCCAG

K Y G R *

AAATACGGCCGTTAACCTAGGCTGCTGCCACCGCTGAGCAATAACTAGCATAACCCCTTG
GGGCCTCTAAACGGGTCTTGAGGGGTTTTTTGCTGAAAGGAGGAACTATATCCGGATTGGCGAA
TGGGACGCGCCCTGTAGCGGCGCATTAAGCGCGGCGGGTGTGGTGGTTACGCGCAGCGTGACCG
CTACACTTGCCAGCGCCCTAGCGCCCGCTCCTTTCGCTTTCTTCCCTTCCTT

Figure 4.S15

>pETDuet1-HisTgCul1-TgRbx1

TgCul1 (Uniprot ID: B9QE00) (ToxoDB ID: TGGT1_289310)

TgRbx1 (Uniprot ID: A0A125YHW3) (ToxoDB ID: TGGT1_213690)

His Tag
TEV Site
StrepII Tag
Flag Tag
Sarcocystis neurona Cul1 portion
Added SF Tag

TAATACGACTCACTATAGGGGAATTGTGAGCGGATAACAATTCCCCTCTAGAAATAATTTTGTT
TAACTTTAAGAAGGAGATATACC
M G S S H H H H H H S Q D P N S S S E N
ATGGGCAGCAGCCATCACCATCATCACCACAGCCAGGATCCGAATTCGAGCTCGGAAAAT
L Y F Q><S V D M A S H P R A S A A S P A
CTATATTTTCAATCAGTCGACATGGCCAGCCATCCGCGTGCGTCTGCGGCTTCGCCGGCC
G A A A T D R M P P A M G V A R A M G G
GGTGCGGCAGCGACCGATCGTATGCCGCCGGCGATGGGCGTGGCCCGTGCAATGGGTGGT
P Q G V V D L E A G W A M L R D C A I R
CCGCAAGGCGTGGTCGACCTGGAGGCGGGCTGGGCAATGCTGCGCGATTGTGCAATTCGA
R L E H F L R T G E A L G R R K D G K L
CGACTGGAACATTTTTTGCGTACCGGCGAAGCCCTGGGGCGTCGTAAGGATGGTAAGTTA
C I F T R K E Y S D M Y T T V Y N M C T
TGCATTTTCACGCGTAAAGAGTATAGCGACATGTACACCACCGTTTATAACATGTGCACC
Q R Y P N N W S A Q L Y Q R Y G E A L A
CAGCGTTACCCGAACAACTGGTCCGCGCAACTGTACCAGAGGTACGGCGAGGCACTAGCT
S Y V N R E V V P R L E G L T E E E L L
AGTTATGTGAACCGCGAAGTTGTGCCGCGTCTGGAGGGCCTGACTGAAGAGGAGTTGCTG
R E L L H R W K N H K I Y V S W L E R F
CGTGAATTGTTGCACCGCTGGAAAAATCACAAAATCTATGTGAGCTGGCTGGAGAGATTT
F V Y L D R Y Y V K L Q S E E P L H H K
TTTGTCTATTTGGATCGTTACTACGTTAAACTTCAGAGCGAAGAGCCACTGCACCACAAA
G I L I F K E L V F N R V R I P L R E A
GGTATTCTAATCTTCAAAGAACTGGTGTTTAACCGTGTGCGTATTCCGCTGCGGGAAGCG
I L R A I Q R Q R E G E R V D E E L L G
ATCCTCCGTGCAATCCAACGTCAACGTGAGGGTGAACGTGTTGACGAAGAGCTGCTGGGT
D V V F M Y I G L D A N G L S L Y Q R E
GACGTTGTGTTCATGTATATCGGCCTGGACGCTAATGGTCTGTCGTTGTACCAACGAGAG
L E D Y L L P E S R D Y Y A R V S A S W
CTAGAGGACTACCTGTTACCGGAGAGCAGAGACTATTACGCCCGTGTGTCCGCAAGCTGG
V V N L S F T D Y M H H A Q E A L L A E
GTTGTTAACCTGAGCTTCACCGATTACATGCATCATGCACAAGAGGCTCTACTAGCAGAG

Q N R C A M I L H R S T K L K L Q A V V
CAGAATCGTTGCGCCATGATTTTGCACCGTAGCACCAAACTGAAGCTGCAGGCGGTTGTG
F D A L L S A R Q D Q L L E K N T A I E
TTTGATGCGCTGTTGTCTGCACGCCAGGATCAGCTGCTTGAGAAAAACACCGCGATCGAA
F L L A R D R R Q E L R L A H R L F T Y
TTTTTGCTCGCACGAGACCGCCGTCAAGAGCTGCGTCTGGCTCACCGTCTGTTTACGTAC
V D G G V E A I A L T F K N F V T S Q G
GTAGACGGGGGTGTGGAAGCCATCGCCTTAACCTTTAAGAACTTTGTCACCAGCCAGGGT
N K I V D Q R L A Q L E S A S S P P S A
AATAAAATCGTAGACCAAAGACTGGCTCAACTGGAGAGCGCTAGCAGCCCACCGTCGGCT
S P P A S P S P A S R P S G S A S I A E
TCACCACCGGCGTCTCCGAGCCCGGCGTCTCGACCGTCCGGTAGCGCTAGCATTGCGGAA
A Q Q T D A A F V Q Q L L D L H E R S K
GCGCAGCAGACGGACGCGGCATTTGTTCAGCAACTGCTAGACCTGCATGAACGTAGCAAA
K V L E E C F L L S S P A S S S R S L L
AAAGTTCTGGAGGAGTGCTTTTTACTCTCGAGTCCGGCCAGCTCCTCTCGCTCTCTGCTG
G V S P Q Q K L F R P C E E T P W S D A
GGCGTGTCTCCGCAACAAAAGCTGTTTCGTCCGTGTGAAGAAACCCCGTGGAGCGACGCG
G R D S G A L S S A P D P L F Q K S L K
GGCCGTGATAGCGGTGCGCTCTCGAGTGCACCGGATCCGCTGTTCCAGAAGAGCCTGAAA
E A F E H F V N R D M G R Q S F A H L L
GAGGCGTTCGAGCACTTCGTGAACCGTGATATGGGTCGTCAGTCGTTCGCACACCTGTTG
A I F C D R L L K K T S E K R S E E Q I
GCCATCTTCTGCGACCGCCTCTTGAAGAAGACCAGCGAAAAGCGTTCCGAAGAGCAAATT
E S M L V R V V E M F N Y V T E K D V F
GAGTCCATGTTAGTTCGTGTCGTTGAGATGTTCAACTATGTTACCGAAAAGGACGTGTTC
A E C Y R S Q L A R R L L H E T S A S E
GCAGAGTGCTATCGGTCCCAACTGGCCCGTCGCCTGCTGCACGAAACCAGCGCATCTGAA
D L E K S V I G K L K L K C G A H F T S
GATCTGGAGAAGAGTGTTATTGGCAAATTGAAGCTGAAGTGCGGTGCACACTTCACCAGC
K L E G M L H D L N G A A D T Y R K F L
AAATTGGAGGGTATGCTGCACGATCTGAACGGTGCGGCTGATACCTACCGCAAGTTCCTG
A W I S E E K Q K R P A E A E A G E A Q
GCATGGATTAGCGAGGAGAAACAGAAGCGCCCGGCTGAAGCGGAGGCTGGCGAGGCCCAA
A S V S G E N E E K T V E K L L E R V S
GCGTCCGTGAGCGGTGAAAATGAAGAAAAGACCGTCGAAAAGCTGCTGGAGCGCGTGAGC
V S S A S A H M Q T G A T G H G V A F V
GTTTCGAGCGCATCTGCGCACATGCAAACGGGCGCGACCGGTCATGGTGTTGCGTTTGTA
D G I E F S V Q I L T T G Y W P T Y P T
GACGGCATCGAGTTCAGCGTCCAGATCCTGACGACCGGCTATTGGCCTACATACCCGACC
A P V N L P A S M Q L C Q T V F E K F Y
GCGCCAGTTAACCTGCCGGCGTCAATGCAACTTTGCCAGACCGTATTCGAAAAGTTTTAT
A S Q T Q H R R V T W I P A L G T A S V
GCGTCCCAGACGCAGCATCGCCGTGTTACCTGGATTCCAGCACTGGGCACCGCGAGCGTG
S A M F Q K R H D F I C N T Y Q A C V L
AGCGCTATGTTTCAGAAGCGCCACGACTTCATCTGTAATACTTACCAGGCATGTGTTCTG
L L F N W E S A H Q R S E A E Q N G P R

TTGTTATTCAATTGGGAAAGCGCTCACCAGCGTTCGGAAGCGGAACAGAACGGCCCACGA
V D P Q L S L S T I T A A L G L D D A T
GTAGACCCGCAGCTGAGCCTATCGACCATTACCGCGGCTCTTGGCCTGGACGATGCCACT
A K K M L A S F F L G R F K I I K K L S
GCGAAAAAGATGCTGGCGTCCTTCTTCCTGGGTCGTTTTAAAATTATCAAAAAACTGTCT
D D A Y A V N S G F T C L N R K I K I P
GACGATGCGTATGCAGTTAACAGCGGCTTTACGTGCCTGAATCGCAAGATCAAGATCCCG
T P V Q E E V Q S R E R V E E D R S I A
ACCCCGGTTCAAGAAGAGGTTCAAAGCAGGGAGCGCGTCGAGGAAGACCGTTCGATCGCT
I E A A I V R I M K A R K T M Q H Q Q L
ATCGAGGCGGCAATCGTGCGCATTATGAAAGCAAGAAAGACCATGCAACATCAGCAGTTG
L A E V L S Q L S F F K P N P K L I K K
CTGGCGGAGGTGTTGAGCCAGCTGAGCTTTTTCAAACCGAATCCGAAACTGATTAAAAAG
R L E H L I E R E F L E R D A E N T N L
CGCCTGGAACACCTGATCGAACGGGAATTCCTAGAGCGTGATGCGGAGAACACGAACCTT
Y R Y V A *
TACCGTTACGTGGCCTAAAAGCTTGCGGCCGCATAATGCTTAAGTCGAACAGAAAGTAAT
CGTATTGTACACGGCCGCATAATCGAAATTAATACGACTCACTATAGGGGAATTGTGAGCGGAT
AACAATTCCCCATCTTAGTATATTAGTTAAGTATAAGAAGGAGATATACAT
M S A W S H P Q F E K G G G S G G G S G
ATGTCTGCGTGGTCTCATCCTCAGTTTGAAAAAGGTGGTGGTTCTGGTGGTGGTTCCGGT
G G S W S H P Q F E K G A S G E D Y K D
GGTGGTTCTTGGTCTCATCCGCAATTCGAAAAGGGCGCCTCTGGTGAGGATTACAAAGAC
D D D K S G V D L G T E N L Y F Q><S G A
GACGACGATAAATCTGGTGTAGATCTGGGTACCGAGAACCTGTACTTCCAATCAGGAGCT
E D P T S P M D V S A P P P S A S S S G
GAAGATCCAACAAGTCCCATGGACGTTAGCGCTCCGCCACCGAGCGCGAGCAGCTCCGGC
S G A A A D A S S S E V P V R R F E V K
TCTGGCGCAGCTGCCGATGCGAGCAGCTCCGAGGTGCCGGTGCGCCGTTTTGAAGTCAAA
K W S A V A L W S W D I V V D N C A I C
AAGTGGTCAGCTGTGGCCCTGTGGAGCTGGGATATTGTTGTTGATAACTGCGCGATTTGT
R N H I M D L C I E C Q A S Q G G S S S
CGTAATCACATCATGGACCTTTGCATCGAGTGCCAAGCGAGCCAAGGTGGTAGCTCTTCT
E E C T V A W G V C N H A F H F H C I S
GAGGAATGCACGGTGGCGTGGGGTGTCTGTAACCATGCATTTCATTTCCACTGCATCAGC
R W L K T R Q V C P L D N A D W E F Q K
CGCTGGCTGAAGACCCGTCAGGTTTGTCCGTTGGACAACGCGGACTGGGAATTCCAGAAA
Y G R *
TACGGCCGTTAACCTAGGCTGCTGCCACCGCTGAGCAATAACTAGCATAACCCCTTGGGG
CCTCTAAACGGGTCTTGAGGGGTTTTTTGCTGAAAGGAGGAACTATATCCGGATTGGCGA
ATGGGACGCGCCCTGTAGCGGCGCATTAAGCGCGGCGGGTGTGGTGGTTACGCGCAGCGT
GACCGCTACACTTGCCAGCGCCCTAGCGCCCGCTCCTTTCGCTTTCTTCCCTTCCTTTCT

Figure 4.S16

>pET-Duet1-HisTgFbxO13-TgSkp1

TgFbxO13 (JMJD6b) (Uniprot ID: V4Z4Z1) (ToxoDB ID: TGGT1_283890)

TgSkp1 (Uniprot ID: A0A0F7UNE6) (ToxoDB ID: TGGT1_207680)

His Tag
TEV Site

GGGGAATTGTGAGCGGATAACAATTCCCCTCTAGAAATAATTTTGTTTAACTTTAAGAAGGAGA
TATACC
M G S S H H H H H H S Q D P S E N L Y F
ATGGGCAGCAGCCATCACCATCATCACCACAGCCAGGATCCGTCAGAAAATTTATATTTT
Q><S E L M E V D E R Q Q T R V A F D P G
CAAAGTGAGCTCATGGAAGTTGACGAACGTCAACAAACCCGTGTAGCGTTCGACCCGGGT
R K K N L K K K K P R L L L T K H P F G
CGCAAAAAGAACCTGAAGAAGAAGAAACCGCGTCTGCTTTTAACCAAACATCCGTTTGGT
L L P S G N A L F V S S G G S T V V D R
CTGCTGCCGAGTGGCAACGCATTGTTCGTGTCCTCCGGCGGCTCTACCGTTGTGGACCGT
S A S L G S F A A L D D A A F L A F L S
AGCGCTTCTCTGGGCAGCTTCGCCGCGCTGGACGACGCTGCGTTTCTGGCGTTCCTTAGC
T L A E F V P L S A L L S L S C A S K F
ACCCTGGCGGAGTTCGTGCCTCTGAGCGCTTTGCTGTCCCTGAGCTGTGCGAGCAAGTTT
L L A A L L D E E L W Q S L L L S R Q Q
CTGTTGGCGGCGTTGTTGGACGAAGAGCTGTGGCAGTCCCTGTTGTTGAGCCGCCAACAA
R R V G R E E S G A R G L G A R E H G E
AGACGCGTGGGTCGTGAGGAAAGCGGTGCGCGCGGACTGGGCGCGCGTGAGCACGGCGAG
Q G T R K N G E T L L G T A D P L L L S
CAGGGAACCCGTAAAAACGGTGAGACTCTGTTAGGTACGGCCGACCCCCTGTTGCTGTCT
D S A S P S A P S P P S L S S S F S A C
GACAGCGCCAGCCCGTCAGCTCCGTCTCCGCCGTCCCTGTCATCGTCGTTCAGCGCGTGC
S E E G E T P T K D E T S E S T D F T W
AGCGAAGAGGGTGAAACTCCGACCAAAGATGAAACTTCAGAAAGCACCGATTTTACCTGG
R G S W K K T Y L F A E R E R L T R Q R
CGTGGCTCCTGGAAAAAGACCTATCTGTTCGCGGAGCGTGAGCGTCTGACCCGCCAGCGT
T A R A S S S S S S S A C S T Q E E R S
ACCGCTCGCGCATCTTCTTCCTCCTCCAGCTCAGCGTGTAGCACGCAAGAAGAGCGTAGC
A D T C L D T A G D S V D R Q S L P V L
GCGGATACGTGCCTGGATACTGCGGGTGATAGCGTAGATCGCCAAAGCCTGCCTGTTCTG
R G V C S D T F Y Q R W L C A T V D I S
CGTGGTGTTTGCAGTGATACCTTTTACCAGCGTTGGCTGTGCGCTACCGTTGACATCAGC
S L F F R H Y D N L E R V S A S A L S V
AGCTTGTTCTTTCGCCACTACGACAACCTTGAACGCGTCTCAGCGAGCGCGTTAAGTGTC
D A F V E L Y E K P N K P V V I T D L V
GACGCGTTCGTCGAACTCTACGAAAAGCCGAACAAACCGGTCGTTATCACCGACCTGGTG

P K W A A F G K W N G E Y F R R H F G G
CCGAAATGGGCAGCGTTCGGCAAATGGAATGGCGAATATTTCAGACGTCACTTTGGCGGT
V R F N A G A A S N I Q L E T F Y Q Y A
GTTCGTTTTAACGCCGGTGCTGCCTCTAACATTCAGCTGGAAACCTTCTACCAGTATGCA
D S N F D E A P L F I F D P R F A E S T
GATAGCAACTTCGACGAGGCGCCACTGTTTATTTTTGACCCGCGTTTTGCCGAGTCGACC
R E A L S S S S A L S S P S S S S P V N
CGTGAGGCATTAAGCTCTTCCAGTGCCCTAAGCTCGCCGAGCAGCAGTAGCCCAGTTAAT
V P P A S R E I G E Q G D C R R E T T G
GTTCCGCCGGCAAGCCGTGAGATCGGCGAGCAGGGCGACTGTCGTAGGGAGACCACCGGC
A Q A S A E E R R H H E L G D R V C S L
GCGCAAGCAAGCGCGGAGGAGCGTAGACACCATGAATTGGGCGACCGTGTCTGCTCCTTA
A E D Y E V P P Y F S D S R D L F A C L
GCTGAGGATTATGAAGTGCCACCGTACTTTAGCGATAGCCGTGATCTGTTCGCATGCCTG
G E R R P N F R W L L V G N C R S G S K
GGCGAACGTCGCCCAAATTTCCGCTGGCTGCTGGTTGGTAATTGTAGGTCCGGTAGCAAG
W H V D P N Q T S A W N A V V R G A K R
TGGCATGTTGACCCCAACCAGACCAGCGCGTGGAATGCCGTGGTGCGTGGTGCGAAACGT
W I L L P P T V C P P G V F P S H D G G
TGGATTCTGCTGCCGCCAACGGTGTGCCCGCCGGGTGTGTTTCCGAGCCATGATGGTGGC
E V T Q P T A L V E W L M N Y Y F D A L
GAGGTGACCCAGCCGACCGCGCTCGTGGAGTGGCTGATGAACTATTACTTCGATGCGTTG
H A P G Y P Y T G G I A P I E G S V R E
CACGCACCGGGTTATCCGTACACCGGTGGTATTGCACCTATCGAAGGCAGCGTTCGGGAG
G E L I F V P Q G W W H C V L N E E D D
GGCGAACTCATCTTCGTGCCGCAAGGCTGGTGGCACTGCGTTTTGAATGAGGAGGATGAT
T I A V T Q N F V S P V I L Q N V R S F
ACGATTGCTGTTACCCAAAACTTTGTGAGCCCGGTCATCCTGCAGAACGTTCGCTCCTTC
L H Y K K D Q I S G L C A Q G R H E T F
CTGCACTACAAAAAGGACCAGATTAGCGGCCTTTGCGCCCAGGGCCGTCACGAAACCTTT
A S E F D A A V G A S Y P E L L P L V S
GCAAGCGAATTTGATGCGGCAGTGGGCGCCAGCTACCCGGAATTGTTGCCGCTCGTTAGC
S P P P P C P S S S P S S P S P V S R T
TCTCCGCCGCCACCGTGCCCGTCTTCGTCCCCGTCGAGCCCATCGCCGGTTAGTCGCACC
A L R S S R P K E T C G E E Q K G V E R
GCGCTCCGCAGCTCTAGACCGAAAGAAACATGCGGTGAGGAACAAAAAGGTGTCGAACGT
G G G Q C G E P Q D I R E Q T D G E G R
GGTGGTGGTCAGTGTGGTGAACCGCAAGATATCCGCGAGCAGACCGATGGTGAGGGCCGT
E G T K R N Q E P Q D S G S F W E W L K
GAAGGTACGAAGCGTAATCAGGAGCCGCAAGATAGCGGTTCCTTCTGGGAATGGCTGAAG
K R R R P V V L R R H A D G E T P T S Q
AAGCGAAGGCGTCCGGTGGTACTACGTCGTCATGCTGACGGCGAGACGCCGACGAGCCAG
A V A *
GCGGTCGCGTAAAAGCTTGCGGCCGCATAATGCTTAAGTCGAACAGAAAGTAATCGTATT
GTACACGGCCGCATAATCGAAATTAATACGACTCACTATAGGGGAATTGTGAGCGGATAACAAT
TCCCCATCTTAGTATATTAGTTAAGTATAAGAAGGAGATATACAT
M S K E R M G D A R K V T L V S Q E G D

ATGTCAAAAGAAAGAATGGGAGATGCCCGGAAGGTCACTCTCGTCTCGCAAGAGGGAGAC
E F D V D I E V A S M S A L I K T M V E
GAGTTTGATGTTGACATCGAGGTCGCCTCCATGAGTGCGTTGATAAAGACAATGGTGGAA
E D S D C Q E S I P L P N V D T C I L K
GAAGACAGCGACTGCCAAGAGAGCATTCCTCTTCCCAACGTGGATACATGCATTCTGAAG
K I I E Y C E H H H N N P P E E I P K P
AAAATCATCGAGTATTGTGAACATCACCACAACAACCCACCCGAAGAAATCCCCAAGCCT
L K S S N L A E V V S E W D Y Q F I N E
CTAAAGTCGTCCAACCTTGCTGAAGTGGTCAGCGAGTGGGACTACCAATTCATCAACGAA
N S D Q K I L F A L I L A A N Y L N I K
AACAGCGACCAGAAGATTTTGTTTGCTTTGATTTTGGCGGCTAACTACCTCAACATCAAG
P L L D L S V A K V A T M I K A K T P E
CCGCTGCTGGATCTGAGCGTCGCGAAAGTGGCGACAATGATCAAAGCCAAGACGCCGGAA
E I R R I F N I V N D F T P E E E A Q V
GAAATCCGACGCATTTTCAACATCGTCAATGACTTCACTCCTGAGGAAGAAGCTCAGGTG
R E E N K W C E D A *
CGCGAGGAGAACAAGTGGTGCGAAGATGCATGACCTAGGCTGCTGCCACCGCTGAGCAAT
AACTAGCATAACCCCTTGGGGCCTCTAAACGGGTCTTGAGGGGTTTTTTGCTGAAAGGAGGAAC
TATATCCGGATTGGCGAATGGGACGCGCCCTGTAGCGGCGCATTAAGCGCGGCGGGTGTGGTGG
TTACGCGCAGCGTGACCGCTACACTTGCCAGCGCCCTAGCGCCCGCTCCTTTCGCTTTCTTCCC
TTCCTTTCTCGCCACGTTCGCCGGCTTTCCCCGTCAAGCTCTAAATCG

Figure 4.S17

>pET28-His-MBP-DdFbxF (Uniprot ID: Q54GQ5)
(Dictybase ID: DDB_G0289995)
His Tag
MBP Tag
Factor Xa Site (Cleavage Position Designated as ><)
TEV Site (Cleavage Position Designated as ><)
Protein sequence contributed by the common plasmid backbone.
Inserted FBP Sequence.

TAATACGACTCACTATAGGGGAATTGTGAGCGGATAACAATTCCCCTCTAGAAATAATTTTGTT
TAACTTTAAGAAGGAGATATACC
M D H H H H H H I E E G K L V I W I N G
ATGGATCATCATCATCATCATCATATCGAAGAAGGTAAACTGGTAATCTGGATTAACGGC
D K G Y N G L A E V G K K F E K D T G I
GATAAAGGCTATAACGGTCTCGCTGAAGTCGGTAAGAAATTCGAGAAAGATACCGGAATT
K V T V E H P D K L E E K F P Q V A A T
AAAGTCACCGTTGAGCATCCGGATAAACTGGAAGAGAAATTCCCACAGGTTGCGGCAACT
G D G P D I I F W A H D R F G G Y A Q S
GGCGATGGCCCTGACATTATCTTCTGGGCACACGACCGCTTTGGTGGCTACGCTCAATCT
G L L A E I T P D K A F Q D K L Y P F T
GGCCTGTTGGCTGAAATCACCCCGGACAAAGCGTTCCAGGACAAGCTGTATCCGTTTACC
W D A V R Y N G K L I A Y P I A V E A L
TGGGATGCCGTACGTTACAACGGCAAGCTGATTGCTTACCCGATCGCTGTTGAAGCGTTA
S L I Y N K D L L P N P P K T W E E I P
TCGCTGATTTATAACAAAGATCTGCTGCCGAACCCGCCAAAAACCTGGGAAGAGATCCCG
A L D K E L K A K G K S A L M F N L Q E
GCGCTGGATAAAGAACTGAAAGCGAAAGGTAAGAGCGCGCTGATGTTCAACCTGCAAGAA
P Y F T W P L I A A D G G Y A F K Y E N
CCGTACTTCACCTGGCCGCTGATTGCTGCTGACGGGGGTTATGCGTTCAAGTATGAAAAC
G K Y D I K D V G V D N A G A K A G L T
GGCAAGTACGACATTAAAGACGTGGGCGTGGATAACGCTGGCGCGAAAGCGGGTCTGACC
F L V D L I K N K H M N A D T D Y S I A
TTCCTGGTTGACCTGATTAAAAACAAACACATGAATGCAGACACCGATTACTCCATCGCA
E A A F N K G E T A M T I N G P W A W S
GAAGCTGCCTTTAATAAAGGCGAAACAGCGATGACCATCAACGGCCCGTGGGCATGGTCC
N I D T S K V N Y G V T V L P T F K G Q
AACATCGACACCAGCAAAGTGAATTATGGTGTAACGGTACTGCCGACCTTCAAGGGTCAA
P S K P F V G V L S A G I N A A S P N K
CCATCCAAACCGTTCGTTGGCGTGCTGAGCGCAGGTATTAACGCCGCCAGTCCGAACAAA
E L A K E F L E N Y L L T D E G L E A V
GAGCTGGCAAAAGAGTTCCTCGAAAACTATCTGCTGACTGATGAAGGTCTGGAAGCGGTT
N K D K P L G A V A L K S Y E E E L A K
AATAAAGACAAACCGCTGGGTGCCGTAGCGCTGAAGTCTTACGAGGAAGAGTTGGCGAAA
D P R I A A T M E N A Q K G E I M P N I
GATCCACGTATTGCCGCCACAATGGAAAACGCCCAGAAAGGTGAAATCATGCCGAACATC

P Q M S A F W Y A V R T V V I N A A S G
CCGCAGATGTCCGCTTTCTGGTATGCCGTGCGTACTGTGGTGATCAACGCCGCCAGCGGT
R Q T V D E A L K D A Q T N S S S D Y D
CGTCAGACTGTCGATGAAGCCCTGAAAGACGCGCAGACTAATTCGAGCTCAGATTATGAT
I P T T G I E G R><G E N L Y F><Q G D I T
ATTCCGACCACCGGGATCGAGGGAAGGGGAGAAAATCTTTATTTTCAAGGTGATATTACT
H M W P M M G L F G K I F K K T N G E
CATATGTGGCCAATGATGGGATTATTTGGTAAAATTTTTAAAAAGAAAACAAATGGTGAA
K E E N F N D D D K D L S K I K Q E S S
AAAGAAGAAAATTTTAATGATGATGATAAAGATTTAAGTAAAATTAAACAAGAAAGTTCA
K D L S K I K Q G S S K D L G K I K Q G
AAAGATTTAAGTAAAATTAAACAAGGTAGTTCAAAAGATTTAGGTAAAATTAAACAAGGT
S S K D L S K I K Q G S S K D L S S Q S
AGTTCAAAAGATTTAAGTAAAATTAAACAAGGTAGTTCAAAAGATTTATCATCACAATCA
I Y I D S E E I I L N N I V I D N F F L
ATTTATATAGATAGTGAAGAGATTATATTGAATAATATTGTGATTGATAATTTCTTTTTA
L D N S V R F N V F N E S H C D D K S N
TTAGATAATAGTGTAAGATTCAATGTATTCAATGAATCACATTGTGATGATAAATCAAAT
I F Y K V W R T Q A I I Q V I F K H Y V
ATATTTTATAAAGTATGGAGAACTCAAGCTATAATTCAAGTGATTTTCAAACATTATGTA
I K S I P T Q S T V I T I T D L F N K K
ATTAAATCAATTCCAACTCAAAGTACAGTGATCACAATAACAGATTTATTCAATAAGAAG
L T T G F I P D T T K S V T F G R K F N
CTAACTACAGGTTTCATACCAGACACTACTAAATCCGTTACATTTGGTAGAAAATTCAAT
Q S L E V G S I P E S V T Y L K F G D E
CAGAGTTTAGAGGTTGGTTCAATTCCAGAGAGTGTCACCTATTTGAAATTTGGTGATGAA
F S P I S L P L N V L P S N L K T L I F
TTCTCACCAATTTCACTACCACTGAATGTATTGCCATCAAATTTGAAAACACTTATTTTC
G Q Y F H T A F K M V N I P P S V E I L
GGACAATATTTTCACACTGCTTTTAAAATGGTGAATATCCCCCCATCAGTGGAGATATTG
R L A R C N T E L L A E K L P K N V Q D
CGTTTGGCAAGATGTAATACTGAATTATTGGCTGAAAAGTTGCCAAAGAATGTACAAGAT
L N L G E V N G R T L T I G D I P E S V
TTAAATTTGGGTGAAGTTAATGGTCGTACATTAACCATTGGTGACATTCCAGAATCGGTG
T T L S L D Q S F T N K N P I L E V G S
ACAACGCTATCACTTGATCAAAGTTTTACAAATAAAAACCCAATTCTTGAAGTTGGTTCA
I P S T V K T L I L G P N Y N Q L P P I
ATTCCAAGTACTGTTAAAACCCTTATTTTAGGCCCAAACTATAATCAATTGCCACCGATT
N S I P D S V A S L T F G D S F N Q P L
AATAGTATACCAGATTCAGTTGCTTCATTAACATTTGGTGACTCATTCAATCAACCTTTA
S P G L I G N S V G M L V F G E A F N Q
TCACCTGGTTTAATTGGTAATTCAGTTGGTATGTTAGTATTTGGTGAAGCATTTAATCAA
I I S P G C L P D C V N I L E F S N Y N
ATCATTTCACCAGGTTGTTTACCAGATTGTGTTAATATTTTAGAATTTTCAAATTATAAT
K P F V Y G A L P N S I I Y L D L G K S
AAACCATTTGTTTATGGTGCACTTCCAAATTCAATCATTTATTTAGATCTTGGAAAAAGT
Y N L P L S N L P E N L R S L K L G R S

TATAATTTACCTTTATCAAATTTACCAGAGAATTTAAGATCACTAAAACTTGGTCGTTCA
F K Q Q L T M D T L P P S I T E I Y L V
TTTAAACAACAATTAACAATGGATACTTTACCACCTTCAATAACTGAAATTTATTTAGTT
P N F D K T L I S Y D I P K H I L K V N
CCAAATTTTGATAAAACTTTAATTTCTTATGATATTCCAAAACATATTTTAAAAGTTAAT
E K N *
GAAAAAAATTAAGCGGCCGCGATCCGGCTGCTAACAAAGCCCGAAAGGAAGCTGAGTTGG
CTGCTGCCACCGCTGAGCAATAACTAGCATAACCCCTTGGGGCCTCTAAACGGGTCTTGAGGGG
TTTTTTGCTGAAAGGAGGAACTATATCCGGATTGGCGAATGGGACGCGCCCTGTAGCGGCGCAT
TAAGCGCGGCGGGTGTGGTGGTTACGCGCAGCGTGACCGCTACACTTGCCAGCGCCCTAGCGCC
CGCTCCTTTCGCTTTCTTCCCTTCCTTTCTCGCCACGTTCGCCGGCTTTCCCCGTCAAGCTCTA
AATCGGGGGCTCCCTTTAGGGTTCCGATTTAGTGCTTTACGGCACCTCGACCCCAAAAAACTTG
ATTAGGGTGATGGTTCACGTAGTGGGCCATCGCCCTGATAGACGGTTTTTCGCCCTTTGACGTT
GGAGTCCACGTTCTTTAATAGTGGACTCTTGTTCCAAACTGGAACAACACTCAACCCTATCTCG
GTCTATTCTTTTGATTTATAAGGGATTTTGCCGATTTCGGCCTATTGGTTAAAAAATGAGCTGA
TTTAACAAAAATTTAACGCGAATTTTAACAAAATATTAACGCTTACAATTTAGGTGGCACTTTT
CGGGGAAATGTGCGCGGAACCCCTATTTGTTTATTTTTCTAAATACATTCAAATATGTATCCGC
TCATGAATTAATTCTTAGAAAAACTCATCGAGCATCAAATGAAACTGCAATTTATTCATATCAG
GATTATCAATACCATATTTTTGAAAAAGCCGTTTCTGTAATGAAGGAGAAAACTCACCGAGGCA
GTTCCATAGGATGGCAAGATCCTGGTATCGGTCTGCGATTCCGACTCGTCCAACATCAATACAA
CCTATTAATTTCCCCTCGTCAAAAATAAGGTTATCAAGTGAGAAATCACCATGAGTGACGACTG
AATCCGGTGAGAATGGCAAAAGTTTATGCATTTCTTTCCAGACTTGTTCAACAGGCCAGCCATT
ACGCTCGTCATCAAAATCACTCGCATCAACCAAACCGTTATTCATTCGTGATTGCGCCTGAGCG
AGACGAAATACGCGATCGCTGTTAAAAGGACAATTACAAACAGGAATCGAATGCAACCGGCGCA
GGAACACTGCCAGCGCATCAACAATATTTTCACCTGAATCAGGATATTCTTCTAATACCTGGAA
TGCTGTTTTCCCGGGGATCGCAGTGGTGAGTAACCATGCATCATCAGGAGTACGGATAAAATGC
TTGATGGTCGGAAGAGGCATAAATTCCGTCAGCCAGTTTAGTCTGACCATCTCATCTGTAACAT
CATTGGCAACGCTACCTTTGCCATGTTTCAGAAACAACTCTGGCGCATCGGGCTTCCCATACAA
TCGATAGATTGTCGCACCTGATTGCCCGACATTATCGCGAGCCCATTTATACCCATATAAATCA
GCATCCATGTTGGAATTTAATCGCGGCCTAGAGCAAGACGTTTCCCGTTGAATATGGCTCATAA
CACCCCTTGTATTACTGTTTATGTAAGCAGACAGTTTTATTGTTCATGACCAAAATCCCTTAAC
GTGAGTTTTCGTTCCACTGAGCGTCAGACCCCGTAGAAAAGATCAAAGGATCTTCTTGAGATCC
TTTTTTTTCTGCGCGTAATCTGCTGCTTGCAAACAAAAAAACCACCGCTACCAGCGGTGGTTTG
TTTGCCGGATCAAGAGCTACCAACTCTTTTTCCGAAGGTAACTGGCTTCAGCAGAGCGCAGATA
CCAAATACTGTCCTTCTAGTGTAGCCGTAGTTAGGCCACCACTTCAAGAACTCTGTAGCACCGC
CTACATACCTCGCTCTGCTAATCCTGTTACCAGTGGCTGCTGCCAGTGGCGATAAGTCGTGTCT
TACCGGGTTGGACTCAAGACGATAGTTACCGGATAAGGCGCAGCGGTCGGGCTGAACGGGGGGT
TCGTGCACACAGCCCAGCTTGGAGCGAACGACCTACACCGAACTGAGATACCTACAGCGTGAGC
TATGAGAAAGCGCCACGCTTCCCGAAGGGAGAAAGGCGGACAGGTATCCGGTAAGCGGCAGGGT
CGGAACAGGAGAGCGCACGAGGGAGCTTCCAGGGGGAAACGCCTGGTATCTTTATAGTCCTGTC
GGGTTTCGCCACCTCTGACTTGAGCGTCGATTTTTGTGATGCTCGTCAGGGGGGCGGAGCCTAT
GGAAAAACGCCAGCAACGCGGCCTTTTTACGGTTCCTGGCCTTTTGCTGGCCTTTTGCTCACAT
GTTCTTTCCTGCGTTATCCCCTGATTCTGTGGATAACCGTATTACCGCCTTTGAGTGAGCTGAT
ACCGCTCGCCGCAGCCGAACGACCGAGCGCAGCGAGTCAGTGAGCGAGGAAGCGGAAGAGCGCC
TGATGCGGTATTTTCTCCTTACGCATCTGTGCGGTATTTCACACCGCAATGGTGCACTCTCAGT
ACAATCTGCTCTGATGCCGCATAGTTAAGCCAGTATACACTCCGCTATCGCTACGTGACTGGGT
CATGGCTGCGCCCCGACACCCGCCAACACCCGCTGACGCGCCCTGACGGGCTTGTCTGCTCCCG

GCATCCGCTTACAGACAAGCTGTGACCGTCTCCGGGAGCTGCATGTGTCAGAGGTTTTCACCGT
CATCACCGAAACGCGCGAGGCAGCTGCGGTAAAGCTCATCAGCGTGGTCGTGAAGCGATTCACA
GATGTCTGCCTGTTCATCCGCGTCCAGCTCGTTGAGTTTCTCCAGAAGCGTTAATGTCTGGCTT
CTGATAAAGCGGGCCATGTTAAGGGCGGTTTTTTCCTGTTTGGTCACTGATGCCTCCGTGTAAG
GGGGATTTCTGTTCATGGGGGTAATGATACCGATGAAACGAGAGAGGATGCTCACGATACGGGT
TACTGATGATGAACATGCCCGGTTACTGGAACGTTGTGAGGGTAAACAACTGGCGGTATGGATG
CGGCGGGACCAGAGAAAAATCACTCAGGGTCAATGCCAGCGCTTCGTTAATACAGATGTAGGTG
TTCCACAGGGTAGCCAGCAGCATCCTGCGATGCAGATCCGGAACATAATGGTGCAGGGCGCTGA
CTTCCGCGTTTCCAGACTTTACGAAACACGGAAACCGAAGACCATTCATGTTGTTGCTCAGGTC
GCAGACGTTTTGCAGCAGCAGTCGCTTCACGTTCGCTCGCGTATCGGTGATTCATTCTGCTAAC
CAGTAAGGCAACCCCGCCAGCCTAGCCGGGTCCTCAACGACAGGAGCACGATCATGCGCACCCG
TGGGGCCGCCATGCCGGCGATAATGGCCTGCTTCTCGCCGAAACGTTTGGTGGCGGGACCAGTG
ACGAAGGCTTGAGCGAGGGCGTGCAAGATTCCGAATACCGCAAGCGACAGGCCGATCATCGTCG
CGCTCCAGCGAAAGCGGTCCTCGCCGAAAATGACCCAGAGCGCTGCCGGCACCTGTCCTACGAG
TTGCATGATAAAGAAGACAGTCATAAGTGCGGCGACGATAGTCATGCCCCGCGCCCACCGGAAG
GAGCTGACTGGGTTGAAGGCTCTCAAGGGCATCGGTCGAGATCCCGGTGCCTAATGAGTGAGCT
AACTTACATTAATTGCGTTGCGCTCACTGCCCGCTTTCCAGTCGGGAAACCTGTCGTGCCAGCT
GCATTAATGAATCGGCCAACGCGCGGGGAGAGGCGGTTTGCGTATTGGGCGCCAGGGTGGTTTT
TCTTTTCACCAGTGAGACGGGCAACAGCTGATTGCCCTTCACCGCCTGGCCCTGAGAGAGTTGC
AGCAAGCGGTCCACGCTGGTTTGCCCCAGCAGGCGAAAATCCTGTTTGATGGTGGTTAACGGCG
GGATATAACATGAGCTGTCTTCGGTATCGTCGTATCCCACTACCGAGATATCCGCACCAACGCG
CAGCCCGGACTCGGTAATGGCGCGCATTGCGCCCAGCGCCATCTGATCGTTGGCAACCAGCATC
GCAGTGGGAACGATGCCCTCATTCAGCATTTGCATGGTTTGTTGAAAACCGGACATGGCACTCC
AGTCGCCTTCCCGTTCCGCTATCGGCTGAATTTGATTGCGAGTGAGATATTTATGCCAGCCAGC
CAGACGCAGACGCGCCGAGACAGAACTTAATGGGCCCGCTAACAGCGCGATTTGCTGGTGACCC
AATGCGACCAGATGCTCCACGCCCAGTCGCGTACCGTCTTCATGGGAGAAAATAATACTGTTGA
TGGGTGTCTGGTCAGAGACATCAAGAAATAACGCCGGAACATTAGTGCAGGCAGCTTCCACAGC
AATGGCATCCTGGTCATCCAGCGGATAGTTAATGATCAGCCCACTGACGCGTTGCGCGAGAAGA
TTGTGCACCGCCGCTTTACAGGCTTCGACGCCGCTTCGTTCTACCATCGACACCACCACGCTGG
CACCCAGTTGATCGGCGCGAGATTTAATCGCCGCGACAATTTGCGACGGCGCGTGCAGGGCCAG
ACTGGAGGTGGCAACGCCAATCAGCAACGACTGTTTGCCCGCCAGTTGTTGTGCCACGCGGTTG
GGAATGTAATTCAGCTCCGCCATCGCCGCTTCCACTTTTTCCCGCGTTTTCGCAGAAACGTGGC
TGGCCTGGTTCACCACGCGGGAAACGGTCTGATAAGAGACACCGGCATACTCTGCGACATCGTA
TAACGTTACTGGTTTCACATTCACCACCCTGAATTGACTCTCTTCCGGGCGCTATCATGCCATA
CCGCGAAAGGTTTTGCGCCATTCGATGGTGTCCGGGATCTCGACGCTCTCCCTTATGCGACTCC
TGCATTAGGAAGCAGCCCAGTAGTAGGTTGAGGCCGTTGAGCACCGCCGCCGCAAGGAATGGTG
CATGCAAGGAGATGGCGCCCAACAGTCCCCCGGCCACGGGGCCTGCCACCATACCCACGCCGAA
ACAAGCGCTCATGAGCCCGAAGTGGCGAGCCCGATCTTCCCCATCGGTGATGTCGGCGATATAG
GCGCCAGCAACCGCACCTGTGGCGCCGGTGATGCCGGCCACGATGCGTCCGGCGTAGAGGATCG
AGATCTCGATCCCGCGAAAT

Figure 4.S18

>DdDlrA (Uniprot ID: Q54FR1) (Dictybase ID: DDB_G0290485)

M Q N H Q N Q M N V D H Q F Y F I S G Q
ATGCAAAATCACCAGAATCAAATGAATGTTGATCATCAATTTTATTTTATATCAGGACAA
D Q S N N L E T Q I K K E D I D I S D Q
GATCAATCAAACAATTTAGAGACGCAAATAAAAAAAGAGGATATAGATATTTCAGATCAA
A S Y H Q P G L D K N N N N N N N N N S
GCATCATATCACCAACCTGGTTTGGATAAAAATAATAATAATAATAATAATAATAGT
N S N S N S N S N S N S N S N S N N N N
AATAGTAATAGTAATAGTAATAGTAATAGTAATAGTAATAGTAATAGTAATAATAATAAC
N N N N N N N N N N S N N N N N N S N
AATAATAACAATAATAATAATAATAATAATAGTAATAATAACAACAATAATAATAGTAAT
N N S N N N N I N N S N N N N S N N N N
AATAATAGTAATAATAATAATATTAATAATAGTAATAATAATAATAGTAATAACAATAAT
H P I N H M Q Q H H I H Q H L Q N Y H F
CACCCAATAAATCATATGCAACAACACCATATTCATCAACATTTACAAAATTATCATTTC
Q S N N N S N N N N N N N N N N N N N N
CAATCAAATAATAATAGTAATAATAACAATAATAATAATAATAATAATAATAATAATAAT
N N S N N N N S N N Y N N H N N N Q G N
AATAATAGTAATAATAATAATAGCAATAATTATAATAACCACAATAATAACCAAGGGAAT
G N Q Q E P T S S P Q I S H H N N N N F
GGTAATCAACAAGAACCAACATCATCGCCACAAATAAGTCACCATAATAACAATAATTTT
N K N D N S I T N L T N S D S I E E S T
AATAAAAACGATAATTCAATAACAAATTTAACAAATTCAGATTCGATTGAGGAGTCGACA
S S S S S N L M A G S G S S A S N Q S P
TCATCATCATCAAGTAATTTAATGGCAGGAAGTGGAAGTAGTGCATCAAACCAATCACCA
R V T S S T T P P N N N N N N N N N Q S A
CGGGTTACATCATCAACCACTCCGCCTAATAATAATAATAATAATAATAATCAATCAGCA
P N N I T Y E T P E I L L K P G E R P P
CCAAATAATATAACATATGAAACACCAGAAATATTATTAAAACCAGGAGAAAGACCACCA
F I G S L A D I I I S N I L G K A H K D
TTTATTGGATCATTAGCAGATATTATTATTTCCAATATTTTGGGTAAAGCACATAAAGAT
E P N S Q N F T N I C S V C S K W R K I
GAACCAAATTCACAAAATTTTACAAACATATGTAGTGTATGTAGTAAATGGAGAAAGATA
S V G R L V N Y T Y Q L P P D R S I T N
TCAGTTGGAAGATTAGTTAATTATACCTATCAATTACCACCAGATCGTAGTATTACCAAT
L F R N L S N N V Y P N L I N L Q L K V
TTATTTCGTAATCTTTCAAATAATGTATATCCAAATTTAATAAACCTTCAACTAAAGGTA
S T P T L F D V S S F V R M L L T K N T
TCAACACCTACCCTTTTCGATGTATCAAGTTTTGTTAGGATGTTATTAACCAAAAATACC
T I T T L E L S Q N G I G N K A A H C I
ACAATCACGACATTGGAACTCTCACAAAATGGTATTGGAAATAAAGCAGCACATTGTATT
G E C L L A N K T I T H L N L S F N S I
GGTGAATGTTTGTTGGCAAATAAAACCATCACTCATTTGAATTTGAGTTTTAATTCCATT
G N E G A E E I S K A I L V N T T L I N

GGTAATGAGGGTGCCGAAGAGATCTCCAAAGCGATATTGGTAAATACCACCCTAATCAAT
L D L S Q N C I G L K G S K A L G Q A L
TTGGATCTTTCACAAAATTGTATTGGTCTCAAAGGCTCAAAAGCATTGGGTCAAGCACTT
Q S T T I L Q T I N L S K N R F G A K G
CAATCCACTACGATCCTACAAACCATTAATCTCTCTAAAAATAGATTCGGCGCCAAAGGT
I D F I V E S I G K N S S L T E V D F S
ATCGATTTCATCGTGGAATCCATTGGTAAGAATAGTTCACTAACAGAGGTTGACTTTTCA
K N D L N E K S S K Y V G E A I R K H P
AAGAATGATCTCAATGAAAAGAGTTCGAAATACGTTGGTGAAGCCATTAGAAAACATCCT
C L A S V N L C D T K L S P E S M K Y I
TGTCTTGCTTCTGTAAATTTATGTGATACTAAACTATCACCCGAAAGTATGAAATATATC
S E G I Q A S Q T I A Y L D M S R N E F
TCCGAAGGTATTCAAGCCAGTCAAACGATTGCCTATCTCGATATGTCAAGAAACGAATTC
N Y K G L K P L A A A L S M C Q S I T Y
AATTACAAAGGTTTAAAACCATTGGCTGCCGCTTTATCCATGTGTCAATCTATAACCTAT
L D L T G D S I G D K G A V Q L G D A L
CTCGATTTGACCGGTGATTCAATCGGTGATAAAGGTGCCGTTCAATTGGGGGATGCTCTA
A Q N H S I I N L S L A F N N I G A S G
GCTCAAAATCATTCAATCATTAATTTATCATTGGCTTTCAATAATATTGGTGCAAGCGGT
A T S L G N A L K T N R S L E I L N L S
GCCACTTCACTTGGTAATGCTTTGAAAACAAATAGATCTTTAGAGATACTAAATCTCTCA
I N P E I G H L G A I H I A E G L A M N
ATCAATCCTGAAATTGGTCACCTTGGTGCAATTCATATAGCTGAGGGTTTAGCAATGAAT
K K I S K L S M C T N G L G P I G A K R
AAGAAAATCTCAAAACTTTCAATGTGTACCAATGGATTGGGTCCAATTGGTGCAAAACGT
L G E A L R Q N S T I T D L Q L R G N E
TTGGGTGAAGCATTACGTCAAAATTCAACAATCACCGATCTTCAATTACGTGGAAATGAA
I G D E G C R A L S D S L K Q N Q S I T
ATTGGTGATGAAGGTTGTAGAGCTCTAAGTGATTCATTAAAACAAAATCAATCAATCACT
E L N L S G N G I T N D G A K A L C E A
GAATTAAACCTTTCTGGTAATGGTATCACAAATGATGGTGCTAAAGCCTTATGTGAAGCT
L W Y N Q S L A S I Q L N H N N I N T Q
CTATGGTACAATCAATCATTGGCTTCAATACAATTAAACCATAACAATATCAATACTCAA
G V Q F M K E L L L R S Y L V N L D S Y
GGTGTACAGTTCATGAAAGAGTTATTGCTTCGTAGTTATTTGGTTAATTTAGATTCTTAT
F Y P P T S T T I V S V L Y V T R G R N
TTTTACCCTCCAACCTCAACAACTATTGTATCAGTCTTATATGTAACTAGAGGTCGTAAT
R G S N N R N N N L N T N L R I I V *
CGTGGTTCTAATAATAGAAATAATAATCTTAATACAAATCTTCGTATTATTGTATAA

Figure 4.S19

>DdFbxD (Uniprot ID: Q54DE4) (Dictybase ID: DDB_G0292312)

M S Y D Y N C W V C F E L F T E P V T L
ATGTCATATGACTATAACTGTTGGGTTTGCTTTGAATTGTTCACTGAACCAGTGACATTA
Y C S H S F C K E C I E K S Y H I E Q L
TATTGTTCACATTCATTTTGTAAAGAATGTATAGAGAAATCATATCATATCGAACAATTA
C P F C R K E I Q M P L P P I D K E L N
TGTCCATTTTGCAGAAAAGAAATTCAAATGCCACTACCACCAATTGATAAAGAATTGAAT
K K I L K L K G F D V D E N N N N T N N
AAAAAAATTTTAAAACTTAAAGGTTTTGATGTTGATGAAAATAATAATAACACAAATAAC
N N N N N N N T S N N N N N R D V V M E
AATAATAACAACAACAACAACACAAGTAATAATAATAATAATAGAGATGTAGTTATGGAA
E S Q P I K K I T Y G I L N L P S T I Y
GAATCTCAACCAATTAAAAAAATTACATATGGTATTTTAAATTTACCAAGTACAATTTAT
A Q I F S E F P V K E I L K F S L V C K
GCACAAATTTTTTCAGAATTTCCAGTTAAAGAGATATTAAAATTCTCATTAGTTTGTAAA
E F N K A I N H K F L W K I K L F Q F I
GAATTTAATAAAGCAATTAATCATAAATTCTTATGGAAGATTAAATTATTCCAATTTATT
E F F N T E K Y E Y D Y K K C F K I C Y
GAATTTTTTAATACAGAAAAATATGAATATGATTATAAAAAATGTTTTAAAATTTGTTAT
Q N E K N E N K G A A G T F K M V P F R
CAAAATGAAAAGAATGAGAATAAAGGAGCAGCAGGTACATTTAAGATGGTACCATTTAGA
G H S Q P I T S I Q H I G N V M C T G S
GGACATTCACAACCTATTACATCCATTCAGCATATTGGTAATGTAATGTGTACTGGTAGT
V D S T V K V W D L S S K K G T N T Q T
GTTGATTCAACGGTAAAGGTATGGGATTTGTCATCGAAAAAAGGTACAAACACTCAAACA
F T G H S G S V T C I K Q R Q Y S V I S
TTTACAGGACATAGTGGAAGTGTTACATGTATTAAACAACGTCAATATTCAGTTATATCA
G S D D C S V R V W D F E K G V E S N C
GGTAGTGATGATTGTTCAGTTAGAGTTTGGGATTTTGAGAAAGGTGTGGAATCAAATTGT
L K T E S P I L S I D Y N V N I G G D G
TTGAAAACTGAATCACCAATTCTATCAATTGATTATAATGTGAATATCGGGGGTGACGGT
Q I I A T N K D T I Q I W D H R D K Q S
CAAATAATTGCAACTAATAAAGACACAATCCAAATTTGGGATCATAGGGATAAACAAAGT
G D G M V G I S G E V F S S K F H S N G
GGTGATGGTATGGTTGGGATTAGTGGTGAGGTGTTTTCCTCAAAGTTTCACTCAAACGGT
H L F V H T S D Y L D S W D L R R F D R
CACCTATTCGTCCACACTAGTGATTATTTAGATTCATGGGATTTAAGAAGATTCGATAGA
P I L R L P S P Q W Y Q P T K D F V Y V
CCAATACTCAGATTACCAAGCCCACAATGGTATCAACCAACTAAAGATTTCGTTTACGTT
F S N N R S I L K Y N I L N G K L M G S
TTCTCAAATAATCGTAGTATTTTAAAATATAATATTTTAAATGGAAAGTTAATGGGATCA
K S L S N H F S I A G G H Q L F S A T N
AAATCATTATCAAATCATTTCTCAATTGCTGGCGGCCACCAATTATTCTCGGCCACCAAC
D N V A Y N I G D F N V H L L D S N L N

GATAACGTAGCTTACAATATTGGTGATTTTAATGTCCATCTTTTAGATTCAAATTTAAAT
P L L V L S N H T N Q I N S I T I D N K
CCACTTCTTGTACTCTCAAATCATACAAATCAAATTAATAGTATCACAATTGATAATAAA
K I L T G S K D N T I K V W D K Q S G N
AAGATTTTAACAGGTTCAAAAGATAATACTATCAAAGTATGGGATAAACAATCTGGAAAT
R L Y S L L G G S N I V N P S D P I P L
CGTTTATATTCATTACTTGGTGGTTCAAATATCGTTAATCCATCCGATCCAATTCCATTA
T P G C S L V N Y D R S R I I G V F N N
ACTCCTGGCTGTAGTTTAGTAAATTATGATAGATCTCGTATTATTGGTGTTTTCAATAAT
L V R L Y N F N L D *
TTAGTTAGATTATATAATTTTAATTTAGATTAA

Figure 4.S20

>DdFbxH (Uniprot ID: Q55BX4) (Dictybase ID: DDB_G0270322)

M K T N F T P P S K I I K K N I F D L T
ATGAAAACAAATTTCACACCACCATCAAAAATAATTAAAAAGAATATATTTGATTTAACA
F T I N S L P T H L I R K I L S Y Y Y N
TTTACAATTAATAGTTTACCAACACATTTAATTAGAAAGATATTATCATATTATTATAAT
H C L S M Y E Y I E K S K G S Q F S G Y
CACTGTTTATCAATGTATGAGTATATTGAAAAGAGTAAAGGTAGTCAATTCTCAGGATAT
K L R F R W M D L C L V C K F W M E M V
AAATTAAGATTTCGTTGGATGGATTTATGTTTAGTTTGTAAATTTTGGATGGAAATGGTT
M P Y L P N T F Y F M D S Q Q K L E T Y
ATGCCGTACCTACCGAATACATTCTATTTTATGGATTCTCAGCAAAAGTTGGAAACCTAT
L N L C E Y G G T F P R R Y L K Q T V L
TTAAATCTATGTGAATATGGTGGCACGTTTCCAAGACGTTATTTAAAGCAAACTGTACTT
R V S K P P A S I K K Y P F H I N S L A
CGTGTATCAAAACCACCAGCTTCAATAAAGAAATACCCATTCCACATAAACTCGCTAGCA
I Y I N R Y Q M P N H Y Q P D T I I P E
ATTTATATCAATCGTTATCAAATGCCAAATCATTATCAGCCAGATACAATCATACCAGAA
F I Y Q Q I L K I S P D L K N L K F Q T
TTTATCTATCAACAAATCTTAAAGATATCACCAGACTTGAAGAATCTTAAATTTCAAACT
A K T E K D L Y Y L L K S I N E S I T Q
GCAAAAACTGAAAAAGATTTATACTACCTATTGAAATCAATTAATGAATCTATAACTCAA
S I T P L L S S L N F D Y S I F S A S M
TCGATTACACCATTACTATCATCATTGAATTTCGATTATTCAATATTTTCAGCCTCAATG
L Y Q L C K I I E S P N C T I T N L S L
CTTTATCAACTTTGTAAAATAATAGAATCACCAAATTGTACTATTACAAATCTATCATTA
N N C T L S T N S L G E F S D G I I D D
AACAATTGCACTTTGTCAACCAATTCATTAGGTGAATTTAGTGATGGCATCATTGATGAT
G D D D T K V S F I T S F K K N K S I T
GGTGATGATGATACAAAAGTTTCATTCATTACATCATTTAAAAAGAATAAATCAATTACA
T L K M N E N N F F T N S K S S K N R I
ACTTTAAAAATGAATGAAAATAATTTCTTTACAAATTCAAAATCATCAAAGAATAGAATT
L M G G T I L Q F L K L V L V D S T S I
TTAATGGGTGGCACAATTTTACAATTTTTAAAATTGGTTTTAGTAGATTCAACTTCAATT
S N F Q F N G S E I F L D E L N N E C N
TCAAATTTTCAATTCAATGGTAGTGAAATATTTTTAGATGAATTAAATAATGAATGTAAT
K I N Y L T P M Q S S F E K L S L S L L
AAAATCAATTATCTAACACCAATGCAATCATCATTTGAAAAACTATCATTATCCCTATTG
N I D S F L P Y L E Y L I T S S S N S I
AATATTGATAGTTTCTTACCATATTTAGAATATTTAATCACTAGTTCAAGTAATAGTATT
K E L D L S H S R F S N Y S N L N N L L
AAAGAATTGGATCTTTCTCATTCAAGATTTTCAAATTATTCAAATTTAAATAATTTATTA
I S I Q H C Q S L L K L N L S S S S F N
ATTTCAATTCAACATTGTCAATCATTATTAAAATTAAATTTATCATCTTCTTCATTTAAT
I I E N S N N N N N N V G F I Q H P Q P

ATAATTGAAAATTCAAATAATAATAATAATAATGTTGGTTTTATTCAACATCCTCAACCA
Q Q P P L P P Q Q Q Q D F N G N G G D D
CAACAACCACCATTACCACCACAACAACAACAAGATTTTAATGGAAATGGTGGTGATGAT
D E F F D E N G G G G F G G N N F D A N
GATGAATTTTTTGATGAAAATGGTGGTGGTGGTTTTGGTGGTAATAATTTTGATGCAAAT
S T N A F N E N F N D Q T L F N R S P I
TCAACAAATGCTTTTAATGAAAATTTTAATGATCAAACTTTATTTAATAGATCACCAATT
G W E R F S F L Y G T Q S L I S I N L S
GGTTGGGAAAGATTTAGTTTTTTATATGGTACACAATCGTTGATTTCAATTAATTTATCA
S I R M R D E K E M N S L F Q S L C G S
TCGATTAGAATGAGAGATGAAAAAGAGATGAACTCATTATTTCAATCATTGTGTGGTTCA
P Q I Q Q L Y L N R C G L T S G C L T Q
CCTCAAATTCAACAACTATATTTGAATAGATGTGGTTTAACAAGTGGTTGTTTAACTCAA
L T N F I R Q P N S K L E L L H I G S N
TTAACCAATTTCATTAGACAACCAAATTCAAAGTTAGAGCTATTACATATTGGTAGTAAT
G L G G G G S S I Q I L L M A F Q L N K
GGATTGGGTGGTGGTGGCTCGTCAATTCAAATTCTATTAATGGCATTTCAATTAAATAAA
S L S D I D L S Y N S M T D I E G Y H I
TCATTAAGTGATATCGATTTATCCTATAATAGTATGACTGATATAGAGGGTTATCATATT
A N F L K S N V Y G D K Q Q I R H L N L
GCAAACTTTTTAAAATCAAATGTATATGGTGATAAACAACAAATTAGACATTTAAATCTT
S G S S F K L G A I N Q L G H A L M T N
TCTGGTAGTAGTTTTAAATTGGGTGCAATCAATCAATTGGGTCATGCTCTAATGACCAAT
N S L V S L N L S N I Q M G M L E I T Y
AATTCTTTGGTCTCTTTAAACCTTTCAAATATTCAAATGGGTATGTTGGAAATTACCTAT
I F D A L V S H P T I S L L N L S N V G
ATCTTTGATGCTTTGGTCTCTCATCCAACTATCTCTTTATTAAATCTTTCAAATGTTGGT
S N E M I T S L V Q T S A L R C N V I Y
TCAAATGAAATGATTACTTCTTTAGTTCAAACTTCTGCTTTGCGTTGTAATGTAATTTAT
*****
TAA

Figure 4.S21

>DdFbxI (Uniprot ID: Q54WP6) (Dictybase ID: DDB_G0279513)

M M T N I N E L P I P V L I K L F G F V
ATGATGACAAATATCAATGAATTACCAATACCAGTTTTAATTAAATTATTTGGATTTGTA
N K I N S S S Y W F V N Y T L V C K L W
AATAAAATTAATAGCTCAAGTTATTGGTTTGTAAATTATACATTAGTATGTAAATTATGG
T T Q I L P T A W N E M T I A T S Q P A
ACAACCCAAATTTTACCAACAGCATGGAATGAAATGACCATTGCAACCAGTCAACCAGCT
E P L I E Y S E D G I L S Q F P S T T S
GAACCATTAATTGAATACAGTGAAGATGGTATATTATCACAATTTCCAAGTACAACATCA
E P Y K F N K L V M R V G K V S E Y I D
GAACCATATAAATTTAATAAATTAGTGATGAGAGTTGGTAAAGTTAGTGAATATATTGAC
K I K S L T T I D L R N N S S T N Y V I
AAGATTAAATCTTTGACAACTATTGATTTAAGAAATAATTCATCAACCAATTATGTAATT
D R L A E A L K S N K T L T Y L N L Y N
GATAGATTAGCCGAAGCATTAAAGTCCAATAAAACTTTAACCTATTTAAATCTTTACAAC
N R L M Q K G G T S I A N A M K K N Q S
AATAGATTAATGCAAAAGGGTGGTACATCAATTGCAAATGCAATGAAAAAGAATCAATCG
I T H L D L G L N L L G A N G G N A I A
ATTACTCATTTAGATTTAGGTTTAAATTTATTGGGTGCAAATGGTGGTAATGCAATTGCC
D A L K V N N T L V H L D L S S N Q L G
GATGCATTAAAAGTTAATAATACTTTGGTACATTTAGATCTCTCAAGTAATCAATTAGGT
L R G A G P V V E A L K I N K S I K Y L
CTTCGTGGTGCTGGACCAGTTGTTGAAGCTTTAAAAATCAATAAATCCATTAAATATTTA
I L N S N Q L R D E C S L P L A D I L R
ATATTAAATTCAAATCAATTACGTGATGAATGTTCATTACCATTGGCCGATATTTTACGT
S N I G F I E L A L N D N E I G S K G G
TCAAACATTGGTTTCATTGAATTGGCATTGAATGATAATGAAATTGGTTCAAAAGGTGGT
I A L A K M L K S S K V L T K L E F G K
ATTGCCTTGGCAAAAATGTTAAAATCTTCAAAAGTTTTAACAAAGTTAGAGTTTGGTAAG
N E L G D D G G L A M A D V L K N N K N
AATGAATTAGGTGATGATGGTGGTTTAGCAATGGCCGATGTGTTAAAGAATAATAAAAAT
I K V V R L N W N K L G V K A I K A L S
ATTAAAGTCGTCAGATTAAATTGGAATAAATTGGGTGTGAAAGCAATTAAAGCCCTCTCT
E S F K T N S T I I Q L D L S F N N F G
GAATCATTTAAAACCAATTCAACCATCATCCAATTGGATCTTAGTTTTAATAATTTCGGT
D E G L V C L S E S F K Q N K S I L S L
GATGAAGGTTTAGTTTGTCTCTCTGAATCATTCAAACAAAATAAATCAATTCTTTCATTG
D L S R V A S G L V G H K A L A D S L R
GATCTCAGTAGAGTTGCCTCTGGTTTGGTAGGTCATAAAGCATTGGCTGATTCATTACGT
V N N T I Q T L D L T N C K I T N E G G
GTTAATAATACCATCCAAACATTAGATTTAACAAATTGTAAAATTACAAATGAAGGTGGT
V E L A K S L V D N K S I S T L I L N N
GTCGAATTGGCAAAATCTTTAGTTGACAATAAATCAATTTCAACTTTAATCTTAAATAAT
N T F S K D T V S E L A K T L E S N S T

AATACTTTCTCAAAAGATACCGTTTCAGAATTAGCTAAAACTCTTGAATCAAATTCAACC
I T S L S L V H N Q L T I D G V E D L F
ATTACTTCACTCTCCTTAGTTCATAATCAATTAACTATTGACGGTGTTGAAGATTTATTC
K S L S T S T N K S L Q T L D L T N N L
AAATCTTTATCCACTTCCACTAATAAATCCTTACAAACTTTGGATTTAACTAATAATCTT
L G S D G G N I I A Q H L T K S N L S E
TTGGGTTCTGATGGTGGTAATATCATTGCTCAACATTTAACAAAATCAAATCTCTCTGAA
L I L T N N Q L S S Q G A S S I L N V L
CTTATCCTTACAAATAATCAATTATCATCTCAAGGTGCCTCCTCAATCTTAAATGTATTA
P Q S N L Q T L D I S N N S I E P D V A
CCACAATCTAATTTACAAACTTTAGATATCTCTAATAATTCTATTGAACCTGATGTTGCC
T S L C S A I S N S Q I L K L N I S T N
ACTTCATTATGTTCTGCAATTTCAAATAGTCAAATTTTGAAGTTAAATATCTCTACAAAT
K L D D T V I P P L I Q A I Q T N Q S L
AAACTCGACGATACTGTTATCCCACCTTTAATTCAAGCAATTCAAACTAATCAATCACTC
I S I Q I S A N Q F S K E S N N K L L Y
ATTAGCATTCAAATCTCTGCAAATCAATTTTCAAAAGAATCAAATAATAAATTATTATAT
S I Q Q N K S I Y Y Y D L V E E I *
TCAATTCAACAAAATAAATCAATTTATTATTATGATTTAGTTGAAGAAATTTAA

Figure 4.S22

>DdFbxK-1 (Uniprot ID: Q558V8) (Dictybase ID: DDB_G0273011_ps)
The initial target for amplification was FbxK-2: (Dictybase ID: DDB_G0273009).
Our sequence differs from that in Dictybase in the region highlighted in Green. Our sequence is supported by the EST in Dictybase (DDB0299438).

M V V L L P L Y I Q K Y I I K I L C R Y
ATGGTTGTGTTATTACCATTATATATTCAAAAATATATAATTAAAATTTTATGTAGATAT
I D K N N K S I D Y V G G D Y R G N E S
ATAGATAAAAATAATAAATCAATTGATTATGTTGGTGGTGACTATAGAGGGAATGAAAGT
Q I K R L M L T L A L V S Q D W F K T L
CAAATTAAAAGATTAATGTTAACATTGGCATTAGTATCTCAAGATTGGTTTAAAACTTTA
S N N L T V S V D F N Y T N L N H N K N
TCAAATAATTTAACTGTATCAGTTGATTTTAATTATACAAATTTAAATCATAATAAAAAT
N N N N N N N K N D I D L K Y S I I K K
AATAATAATAATAATAATAATAAAAATGACATTGATTTAAAATATTCAATAATTAAAAAA
E N L K T L K L H F D H Q G S F F Y I K
GAGAATTTAAAAACATTGAAATTACATTTCGATCATCAAGGTTCATTCTTTTATATTAAA
D I S I Y E K D K K Q S P K D N D I F D
GATATTAGTATTTATGAAAAAGATAAAAAACAATCACCAAAAGATAATGATATTTTTGAT
D D K S D E K I I E L D I V N K E L E K
GACGATAAATCTGATGAAAAAATAATAGAATTGGATATAGTTAATAAAGAATTAGAAAAA
L S K L K T T I P S T L S L L E N Q K Q
TTATCAAAATTAAAAACAACCATACCATCAACTTTATCATTATTAGAAAATCAAAAACAA
Q Q Q Q Q T I I F K N L I L R N I S S S
CAACAACAACAACAAACAATTATATTTAAAAACTTAATATTAAGAAATATATCATCATCA
N E T E D T D I L Q S L Y R C E A T D G
AACGAGACTGAAGATACTGATATTTTACAATCACTTTATCGATGTGAAGCGACTGATGGT
N I H L L E L D L N P I F T F K S L N K
AATATTCATCTATTAGAATTAGATTTAAATCCAATTTTTACATTTAAATCTTTAAATAAA
I K K H V K K V F T L K I N S C F D N E
ATAAAAAAACATGTTAAAAAGGTATTTACTTTGAAAATTAATTCATGTTTTGATAATGAA
L I I E S F K Q Y K N S I A Q L F I I K
CTCATTATCGAATCATTTAAACAATATAAAAATTCAATTGCTCAATTATTCATTATAAAA
Y T S Q Q D K M Q L F P I L A G I I P F
TATACTTCTCAACAAGATAAAATGCAATTATTTCCAATATTAGCTGGTATTATACCTTTT
N N N N N E E N K K Y N E K I N Y L E N
AATAATAATAATAATGAAGAAAATAAGAAATATAATGAAAAAATTAATTATTTAGAAAAT
I E F L K I F S M E V S L K D L E L I L
ATAGAATTTTTAAAAATATTTTCAATGGAAGTTTCATTAAAAGATTTAGAATTAATTTTA
N Y S K K V S Q L V I S I C F N N L I Y
AATTATTCAAAGAAAGTAAGTCAGCTTGTAATTAGTATTTGTTTTAATAATTTAATATAT
Y L S T K T E R K K S K I K K C N C D S
TATTTATCGACAAAAACTGAAAGAAAGAAATCAAAAATTAAAAAATGTAATTGTGATAGT

V I R N P S N S M E V N E E F N K N W D
GTAATTAGAAATCCTTCAAATTCAATGGAAGTGAATGAGGAATTCAATAAAAATTGGGAC
S L K E A L K N N K T L K S L E F F H E
TCTTTAAAAGAAGCCTTGAAAAATAATAAAACCCTAAAAAGTTTAGAATTCTTTCATGAA
C Y A S Q I L L C K Q S P S K T F I E R
TGTTATGCATCTCAAATACTACTATGTAAACAATCACCATCAAAAACATTTATTGAAAGA
F S S L I S S S T S M E S F G T G I N C
TTTTCATCACTAATTTCATCAAGCACATCAATGGAATCATTTGGTACAGGTATTAACTGT
P Q L I E R I L E Q N K T I T D F S V S
CCACAATTAATAGAGAGAATTTTAGAACAAAATAAAACTATCACTGATTTTTCTGTCAGT
I V E V N G R P D M I Q P Y Q S L I D K
ATAGTTGAAGTTAATGGTAGACCCGATATGATTCAACCGTATCAATCATTAATCGATAAA
N K Q H L N S L K L V K F V F N Y E T E
AATAAGCAACATCTAAATAGTTTAAAATTAGTTAAATTTGTTTTCAATTATGAAACTGAA
N F N P V I L L D Y K K *
AATTTCAATCCAGTAATTTTATTGGATTATAAAAAATAA

Figure 4.S23

>DdFbxM (Uniprot ID: Q55EM8) (Dictybase ID: DDB_G0268822)

M S H S V V S S P T I I S Q L L P F S T
ATGTCGCACAGTGTGGTTAGTTCTCCAACTATAATTTCTCAACTTCTTCCTTTTTCGACA
D S S N N N N S N T G S S N N N N S G N
GATAGCAGTAATAACAACAATAGCAATACTGGTAGTAGTAATAACAACAATAGCGGCAAT
L N N T E S N N S G G S R S R G N S G S
TTAAACAATACCGAAAGTAATAATAGTGGTGGTAGTAGAAGTAGAGGAAATAGTGGATCA
N N Y R I N T V L H S G N T S N N N S P
AATAATTATAGAATAAACACAGTTTTACACAGTGGTAATACTAGTAATAATAACTCTCCA
N S L N Y N N N N S P L S N G V V T G R
AATTCACTCAACTATAATAATAATAACTCTCCATTGTCCAATGGAGTCGTCACAGGTAGA
K R S H S D L T A S I L E A Q S S M D F
AAGAGATCTCACTCTGATTTAACAGCTTCTATCCTTGAAGCACAATCATCAATGGATTTT
M N N N N N N N N N N N N N N N N I N N
ATGAATAATAATAATAACAATAACAACAACAATAACAATAACAATAATAATATTAATAAT
N N N N N S Y H S S N N N N S Y S N N N
AATAATAATAACAATAGTTATCATAGTAGTAATAATAATAATAGTTATAGTAATAATAAT
T S P S S S S S L S C H D M M I Q Y K S
ACATCACCATCGTCATCATCATCATTATCTTGTCATGACATGATGATTCAATATAAGTCA
L L P P I P F I P L S P N K S N N S G N
TTATTACCACCAATACCATTCATTCCATTATCTCCAAATAAAAGTAATAATAGTGGCAAT
N N S T I S Y T S I V N D E M F K F N T
AATAATTCAACTATTAGTTATACATCAATTGTTAATGACGAAATGTTTAAATTTAATACA
G I D C S N K K E D S S I N N N N N N N
GGTATTGATTGTAGTAATAAAAAAGAAGATAGTAGTATTAATAATAATAATAATAATAAT
N N N N N N N N N N I E E I Y L P I D V
AATAATAATAACAACAATAACAATAATAATATAGAGGAAATTTATTTACCGATTGATGTG
L D L I F S Q L S F I D R C I C A S V C
TTAGATTTAATATTTTCACAATTATCATTTATAGATAGATGTATTTGTGCATCAGTATGT
S S W R N V L I M Q P H P L L E N C F V
AGTTCATGGAGAAATGTATTAATAATGCAGCCACATCCATTGTTGGAGAATTGTTTTGTA
S L H N Q P P I Q S V P I I T P F L L N
TCACTTCATAATCAACCACCAATTCAATCGGTACCAATTATAACACCATTTTTATTAAAT
N F N I T I S P C S C Y K C Y Y T N P T
AACTTCAATATAACTATATCACCATGTTCATGTTATAAATGTTATTATACAAATCCAACC
Y K Y L S N W M E Y L K P F Y S V V K L
TATAAATATTTATCAAACTGGATGGAATACTTAAAACCATTCTATTCAGTTGTTAAATTA
N K L V F R V F Q N S T D M S T S S S S
AATAAATTGGTTTTTAGAGTATTTCAAAATTCAACTGATATGTCTACCTCTTCTTCTTCT
S P S S P S S N T T T T T T T T T T S
TCACCTTCTTCACCTTCATCAAATACAACAACAACAACAACCACCACCACAACTACCTCT
S S S S A G G T N N N N H N N D G L L S
TCTTCATCTTCTGCTGGTGGTACAAATAATAACAATCATAATAATGATGGTTTACTTTCT
P F P S S P M P T F P E F S I S Q I N N

CCATTCCCTTCATCACCAATGCCAACTTTCCCAGAGTTTAGTATAAGCCAAATTAATAAT
N N N N N N N N N S N N N N N N N N N
AACAATAATAATAATAACAATAATAACTCTAATAATAATAATAATAATAATAATAATAAT
N N N N N N N N N N N N N N N N G R T N
AATAATAATAATAATAATAATAATAATAATAATAATAATAATAATAATGGTAGAACAAAT
H F L H Q S P F L T G L R N S G E H Q H
CACTTTTTACATCAAAGTCCATTTTTAACTGGATTACGTAATAGTGGTGAACATCAACAT
I H N H Y L H N H Y N Q Q Q Q Q T Q Q Q
ATTCATAATCATTATCTTCATAATCATTATAACCAACAACAACAACAAACACAACAACAA
Q Q Q Q Q Q L L Q T P Q P Q H S P L V S
CAACAACAACAACAACAATTGTTACAAACTCCACAACCACAACATTCACCATTGGTATCA
I S S P S S A S L A A S S I Q Y N G G G
ATATCATCACCATCTAGTGCATCATTAGCTGCATCTTCAATTCAATACAATGGAGGAGGA
G A G A G G V G G D Q Q L E L L S N C E
GGAGCAGGAGCAGGAGGAGTAGGAGGAGATCAACAATTAGAATTATTATCAAATTGTGAA
C H E K V S K E S M L H G D D S F D G N
TGCCATGAAAAGGTTTCAAAAGAATCAATGTTACATGGTGATGATAGTTTTGATGGTAAT
N G G N Y S Q W C L D L E K P I T L P L
AATGGTGGAAACTATTCACAATGGTGTTTAGATTTAGAGAAACCAATAACATTACCATTA
K D R S A S I P L S T F I K V L D N S E
AAAGATAGAAGTGCATCAATACCATTAAGCACATTTATTAAAGTTTTAGATAATAGTGAA
M V E R I K M R V C I D L P W S K T K E
ATGGTTGAAAGAATAAAGATGAGAGTTTGTATAGATTTACCATGGTCAAAAACTAAAGAG
F S L F K P I K N A E K L T E I G L L N
TTTTCACTTTTTAAGCCAATAAAAAATGCAGAGAAATTAACAGAGATTGGTTTATTAAAT
H D P F D T S M S S A Q T T T S N I N S
CATGACCCATTCGATACTAGTATGAGTTCAGCTCAAACTACAACCTCAAATATCAATTCA
L I F S T L F S N A S S F V N L K R L Y
TTGATTTTCTCAACCCTATTTTCAAATGCATCAAGTTTTGTAAATTTAAAAAGACTCTAT
L I T T N I D H K F L Y N L K L H L P S
TTAATTACCACCAACATCGATCATAAATTTCTTTACAATTTAAAACTTCATTTACCATCG
V T G L H L S V W N V N V L G L F E M I
GTTACAGGACTTCATTTATCAGTTTGGAATGTTAATGTACTTGGTTTATTTGAAATGATC
T S V Y G D S L K E L S I R F T T C L G
ACATCGGTCTATGGTGATTCATTAAAGGAACTTTCCATTAGATTTACAACTTGTTTAGGT
I K Y K P F S H T E Y K L D D S I V E L
ATAAAGTATAAACCATTCTCTCATACCGAATATAAATTGGATGATTCAATCGTGGAGTTA
L V N K C P N L Q H F S F E G W L S N I
TTGGTTAACAAATGCCCAAATTTACAACATTTCTCATTCGAGGGTTGGTTATCAAATATA
S S K S F Q L L S K L T L K H L V L K N
TCTTCGAAATCATTTCAACTCTTATCAAAATTAACCTTAAAACATTTGGTATTAAAGAAT
G P Y S Q T S C K P I W A R V K M E S T
GGTCCATATTCTCAAACTTCATGTAAACCAATTTGGGCAAGAGTTAAAATGGAATCAACA
E N P Y Q S L L V S E Q E I K D F V R S
GAGAATCCTTATCAATCATTATTGGTTTCTGAACAAGAAATTAAAGATTTTGTTAGATCT
Q R N L K V F E I F T P Q I D K F T S K
CAAAGAAATTTAAAAGTATTTGAAATTTTTACACCACAAATCGATAAATTCACTTCAAAA

D F L N N L E I L D I N Q G S T G G S S
GACTTTTTAAATAATTTAGAAATTTTAGATATTAATCAAGGTTCAACTGGTGGTAGTAGT
S N S T S L T I I N N N N N I N N N N N
AGTAATTCTACTTCATTAACAATAATTAATAATAATAATAATATAAATAATAATAATAAT
S P D L P F E C D S L N S Y L T N L Q N
TCACCAGATTTACCATTTGAATGTGATAGTTTAAATAGTTATTTAACCAATTTACAAAAC
L Q K H V A F S H Q E S L N S L S D D L
CTTCAAAAACATGTAGCATTTAGTCATCAAGAGAGTTTGAATAGTTTATCAGATGATCTT
I T N F V E S G P N L K Y L K I V D R L
ATCACCAATTTCGTTGAATCTGGTCCAAATTTAAAATATTTAAAGATTGTTGATAGATTA
N F R S H I K G G N R N K Y H R S K L S
AACTTTCGTTCTCACATTAAAGGTGGTAATAGAAATAAATATCATAGATCAAAATTATCA
N Y F N Q Q F Q C N K H *
AATTATTTTAATCAACAATTTCAATGTAATAAACATTAA

Figure 4.S24

>DdFbxN (Uniprot ID: B0G139) (Dictybase ID: DDB_G0282285)

M E D E D N Q Q Q Q P C Y I L N I P F E
ATGGAAGATGAAGATAATCAACAACAACAACCATGTTACATTTTAAATATACCATTTGAA
N L L I I L Q N L H T K S L L E L S Q V
AATTTATTAATTATATTACAAAATTTACATACAAAATCACTTTTAGAATTATCTCAAGTT
N L Y F N Q I I S N S S I S N M I W N D
AATTTATATTTTAACCAAATCATTTCAAATTCTTCAATTTCAAATATGATTTGGAATGAT
I I Q K D F L L S T D N A I I K Y K L N
ATTATTCAAAAAGATTTCTTATTATCAACTGATAATGCAATTATCAAATATAAATTAAAT
I N N E E V E N N V N T N N E E E E D N
ATTAATAATGAAGAAGTAGAAAATAATGTTAATACTAATAATGAGGAGGAGGAGGATAAT
K D E E N E D E K E E Y D E E Y D E E Y
AAAGATGAAGAAAATGAAGATGAAAAAGAAGAGTATGATGAAGAGTATGATGAAGAGTAT
D E D D E D E D N D D D D D D I N E E A
GATGAAGATGATGAAGATGAAGATAATGATGACGATGACGATGATATTAATGAAGAAGCA
N Y L K E L R K S Y K S Q N K N K N E H
AATTATTTAAAAGAATTAAGAAAATCATATAAAAGTCAAAATAAAAATAAAAATGAACAT
L D L E R E Q N E I I E K E K L T P I I
TTAGATTTAGAAAGAGAACAAAATGAAATAATAGAAAAAGAAAAATTAACACCAATTATT
V N K L L H Q R F N S N I I H H Y K T M
GTAAATAAATTATTACATCAAAGATTTAATTCAAATATAATTCATCATTATAAAACAATG
R Y I W D R F E N W M D L N S M D S M K
AGATACATTTGGGATAGATTTGAAAATTGGATGGATTTAAATTCAATGGATTCAATGAAA
K S F H S I S H T K L Y K L I S T I K F
AAATCTTTTCATTCGATTTCTCATACTAAATTATATAAATTAATTTCAACTATTAAATTT
V N N S S N N S S N N V V N N D N N I K
GTAAATAATAGTTCAAATAATAGTTCAAATAATGTTGTTAATAATGATAATAATATAAAA
L P A D Y L C S M L I H N G Q K E F T R
TTACCAGCTGATTATTTATGTTCAATGTTAATTCATAATGGACAAAAAGAATTTACAAGA
Y G L L G T V E A Y E S K T N I F L L S
TATGGTTTATTAGGTACAGTTGAAGCATATGAATCAAAAACAAATATATTTTTATTATCA
L E K T I S L Y K K T R N M Q S F Q H V
CTTGAAAAGACGATATCGTTATATAAAAAGACTAGAAATATGCAATCATTTCAACATGTT
L F V A C S A S R R Y Y I M A L R D F K
TTATTTGTAGCATGTTCTGCCTCTAGAAGATATTATATAATGGCATTGCGGGATTTTAAA
I E E K S F K K D Q I L L I A P G S P M
ATTGAAGAAAAGAGTTTTAAAAAGGACCAAATCTTATTAATTGCTCCGGGTAGTCCAATG
I V A N S F W E F L Y L H A F A L E K G
ATTGTTGCAAATAGTTTTTGGGAATTTTTATATTTACATGCTTTTGCATTAGAGAAAGGT
V F T T R R K I L Y R Y P E F S P Y N G
GTATTCACAACTAGAAGGAAAATACTCTATAGATATCCAGAGTTTTCACCTTACAATGGT
D E V V T Q G V K I K C S A V Y I P E D
GATGAGGTTGTAACTCAAGGTGTTAAAATAAAATGTAGTGCAGTTTATATACCAGAGGAT
E N S Y T F F Y R V T I S M D K D E D P

GAAAATTCTTATACCTTCTTTTATAGAGTAACTATCTCAATGGATAAAGATGAAGATCCA
K N A C Q L T H R F W I I S T I D G S S
AAAAATGCTTGTCAATTAACTCATCGTTTTTGGATAATATCAACAATTGATGGTTCTTCA
N V N G P G V I G K F P I I K P G V T F
AATGTAAATGGTCCTGGTGTAATTGGTAAATTTCCAATTATAAAACCTGGTGTAACTTTT
E Y C S R C E I E R S Q G H M G G Y F T
GAATATTGTAGTAGGTGTGAGATTGAACGTTCTCAGGGTCATATGGGAGGTTATTTTACA
M V K L N N R D Y S F R A T V P T F F L
ATGGTTAAATTAAATAATAGAGATTATTCATTCCGTGCAACAGTTCCAACTTTTTTTTTA
T T I Q S *
ACAACAATTCAAAGTTAA

Figure 4.S25

>DdJcdH (Uniprot ID: Q54VA7) (Dictybase ID: DDB_G0280485)

JmjC Domain

M S K Y N E E N L N E D V E L Y I P H P
ATGTCAAAATATAATGAAGAAAACTTAAATGAAGATGTTGAATTATATATTCCACATCCA
F G V K P K G N F Y F D S F N K D F V D
TTTGGTGTAAAACCAAAAGGAAATTTTTATTTTGATTCATTTAATAAAGATTTTGTTGAT
S R K L G L G L F S V F E D N F I I D S
AGTAGAAAATTAGGATTAGGATTATTTTCAGTATTTGAAGATAATTTTATAATTGATTCA
I L D L L S A E E L T K T M N L V S K T
ATTTTAGATTTATTAAGTGCAGAAGAATTAACTAAAACAATGAATTTAGTTAGTAAAACA
F Y I Y V Q E E E Q W K M R S I N K F S
TTTTATATTTATGTTCAAGAGGAGGAACAGTGGAAAATGAGATCAATTAATAAATTTTCA
D G E F K Y Q H S W Q Y T Y K S N C D K
GATGGTGAATTTAAATATCAACATAGTTGGCAATATACATATAAATCAAATTGTGATAAA
S F S K E P I P I Q V K Y F Y S D Y L F
TCATTTTCAAAGGAACCAATACCAATCCAAGTGAAATATTTCTATTCCGATTATTTATTT
H I H R C A T V D L K Q F E H G D S I D
CATATTCATAGATGTGCAACAGTTGATCTTAAACAATTTGAACATGGTGATTCAATTGAT
R R T N L T F E E F T R E Y L I P N K P
AGACGTACCAATTTAACATTTGAAGAGTTTACAAGAGAATATTTAATACCAAATAAACCA
V I I S D A C K D W A A S K N W T R E T
GTGATCATATCTGATGCATGTAAAGATTGGGCAGCTTCAAAAAATTGGACAAGGGAAACC
L A E K C G D V K L Y I N A G V F M N V
TTGGCAGAGAAATGCGGTGATGTTAAACTTTACATTAATGCAGGTGTATTTATGAATGTA
K D F F Y Y S E H C K E E M P M Y L F D
AAAGATTTCTTTTACTATAGTGAGCATTGTAAAGAAGAAATGCCAATGTATTTATTCGAC
H Y Y G E K V P S L L E D Y S A D A Y F
CATTATTATGGTGAAAAAGTACCATCACTTTTGGAGGATTATTCAGCAGATGCTTATTTC
K E D L F N V L G D K R P S F R W L L A
AAAGAGGATTTATTCAATGTATTAGGTGATAAAAGACCATCATTTAGATGGTTATTAGCA
G P P R S G A S F H K D P N H T S A W N
GGTCCACCAAGATCAGGTGCTTCATTTCATAAAGATCCAAACCATACATCCGCTTGGAAT
A V I T G R K K W I M Y P P H V V P P G
GCTGTAATCACTGGTCGTAAGAAATGGATAATGTATCCACCACATGTTGTACCACCAGGT
V Y P S D D G L E I T A P S S I I E W F
GTTTACCCATCTGATGATGGTTTAGAAATTACTGCACCAAGTTCAATAATTGAATGGTTT
I N F Y E K P D N D H D E K D K D S L E
ATTAACTTTTATGAAAAACCTGATAATGATCATGATGAAAAAGACAAAGATAGTTTAGAA
Q Q Q Q Q K E N D K K N T R F K L K D K
CAACAACAACAACAAAAAGAAAATGATAAAAAAAATACAAGATTTAAATTAAAAGATAAA
K V N N I N N N Q Q K Q N N N N E N D N E I
AAAGTTAATATTAATAATCAACAAAAACAAAATAATAACAATGAAAATGATAATGAAATT
E T Y E T V K P L E G I L H A G E M I F

GAAACTTATGAAACAGTTAAACCATTAGAAGGTATTTTACATGCTGGTGAAATGATATTT
V P S G W Y H S V L N L E E S I A I T H
GTGCCATCTGGTTGGTATCATAGTGTTTTAAATTTAGAGGAATCAATTGCAATCACTCAT
N F I D S N N L L K V V D F M A T K K K
AATTTCATTGACTCAAATAATCTATTAAAAGTTGTTGATTTTATGGCAACAAAGAAAAAG
K D L Y N E F T N K I E Q A Y P G K L E
AAAGATTTATATAACGAATTTACAAATAAAATTGAACAAGCTTATCCAGGTAAATTAGAG
S L R N A E K Q K Q E E I K R K E E E R
TCACTTAGAAATGCTGAAAAACAAAAACAAGAAGAAATTAAAAGAAAAGAAGAAGAAAGA
L K N K K K S I W E T T T N D S N N V P
TTAAAAAATAAGAAAAAATCAATTTGGGAAACTACAACTAATGATTCAAATAATGTACCA
T S K S F S F S F G D D L S D N *
ACTTCAAAATCATTTTCATTCTCTTTTGGTGATGATTTAAGTGATAATTAA

Figure 4.S26

>DdJcdI-Short-H319A (Derived from Dictybase ID: DDB_G0270006) (Derived from Uniprot ID: Q55CL5)
The H319A point mutation is indicated by a green highlight.
The F-Box domain is indicated by a blue highlight.

M S K G V K V V I G E T D L R T K S L G
ATGTCTAAAGGCGTGAAAGTGGTTATTGGTGAAACCGATCTGCGTACGAAATCCCTAGGC
A L S I L E D Q I L L N V V F N E F T C
GCCCTGAGCATTCTGGAAGATCAAATCCTGCTGAATGTCGTGTTTAACGAATTCACCTGC
S E L L K Y Q C V S P A F Y I L L G D D
AGCGAACTGCTGAAATATCAGTGTGTGAGCCCGGCGTTTTACATCCTCCTAGGCGATGAC
R L W K D A F L R E I K G R K E F V K Y
CGTCTGTGGAAAGATGCCTTTCTGCGTGAAATCAAAGGTCGTAAAGAATTCGTTAAATAC
I E N W K I S A L S Y L Y P N S F N K F
ATCGAAAACTGGAAAATCAGCGCACTGAGCTACCTGTACCCGAACTCATTCAACAAATTC
K K P Y I P L H F P D F Y S H E V Y T R
AAAAAACCGTACATCCCGCTGCATTTTCCGGATTTCTATTCGCACGAAGTTTACACCCGT
W L R R H M K V K D Y G V D F G H V K H
TGGCTGCGTCGTCACATGAAAGTCAAAGACTATGGCGTGGATTTCGGTCATGTTAAACAC
I E S D E L T V E E F Q R E Y E I P S I
ATTGAATCAGATGAACTGACCGTGGAAGAATTTCAACGTGAATACGAAATCCCGTCGATT
P V I F K N A Q R G T P M M E K N E W S
CCGGTTATCTTCAAAAATGCGCAGCGTGGCACGCCGATGATGGAGAAAAACGAATGGAGC
E E R L I E R C G D V V F K I S H Q D N
GAAGAACGTCTGATCGAACGTTGCGGTGATGTTGTCTTTAAAATTAGCCACCAGGACAAT
K R I Q M T F R D Y C Q Y M K T Q T D E
AAACGTATCCAAATGACCTTCCGTGATTATTGTCAGTACATGAAAACCCAAACGGATGAA
E P L Y V F D Q A F G E K V P S L L D D
GAACCGCTGTATGTGTTTGACCAGGCATTCGGCGAAAAAGTTCCGAGTCTGCTGGATGAC
Y N I P K F F P E D L F K Y N G E E H R
TATAATATTCCGAAATTTTTCCCGGAAGACCTGTTTAAATACAACGGTGAAGAACATCGT
P H F R W I V I G P E R S G A S W A I D
CCGCACTTCCGTTGGATCGTGATTGGCCCGGAACGTAGTGGTGCTTCCTGGGCGATCGAT
P A G T S A W N S L I S G R K R W L M Y
CCGGCAGGCACGAGTGCTTGGAATTCACTGATCTCGGGTCGTAAACGTTGGCTGATGTAT
P P N F T P Y T V E S D E V V D K I Y G
CCGCCGAACTTTACCCCGTACACGGTCGAATCCGACGAAGTGGTTGATAAAATTTATGGT
S P P S L L W L L E V Y P Y L P P D Y R
AGCCCGCCGAGCCTGCTGTGGCTGCTGGAAGTTTATCCGTACCTGCCGCCGGATTACCGT
P I E C I Q E P G E T I F V P G G W W H
CCGATTGAATGCATCCAGGAACCGGGTGAAACCATCTTTGTTCCGGGCGGTTGGTGGCAC
M V L N M E Q S I A V T Q N F C N S Q N
ATGGTCCTGAATATGGAACAGAGCATTGCAGTTACGCAAAACTTTTGCAATTCACAGAAC
*****
TAA

Figure 4.S27

>TgFbxO1 (Uniprot ID: B6KAF9) (ToxoDB ID: TGGT1_262530)
F-box Domain

M G N T E S T A A E L H D N Y L A V L K
ATGGGCAACACGGAATCCACGGCCGCTGAGTTGCACGACAACTACTTGGCGGTTCTTAAA
S V E G R L G Q Y P S R T L S P R S Q S
AGCGTCGAGGGTCGGTTGGGACAGTACCCAAGCCGAACGCTCTCCCCTCGGTCGCAGTCA
S G V D R S R A R V R P E E A Y R D P G
AGCGGTGTGGATCGGTCTCGCGCGAGGGTACGCCCCGAGGAGGCGTACCGGGATCCTGGA
K R G A G N R P R N L P S K G E K P S R
AAACGGGGTGCTGGAAACCGCCCTCGCAACTTGCCATCCAAAGGCGAGAAGCCCTCTCGG
S A H K S G S T S S V D Q F N N G P G A
TCTGCGCACAAGTCGGGATCCACTTCCTCAGTGGACCAGTTCAACAACGGGCCTGGTGCG
N R K H G K D S V Q R R D D A P P Q A D
AACCGGAAACACGGAAAGGACAGCGTCCAGCGGCGCGATGATGCCCCGCCACAAGCAGAT
Q E H S S L Q P A D G K R R P A A K G E
CAGGAACACTCTTCGCTTCAACCAGCTGACGGCAAGCGCCGGCCTGCCGCGAAAGGAGAG
T P N V E S T A T G S D W G D S A V N D
ACTCCCAATGTGGAGTCGACTGCGACAGGATCCGACTGGGGAGACTCCGCTGTCAACGAT
F A E E D S C A V E S P A H F K L Q T K
TTTGCTGAAGAGGATAGCTGCGCCGTTGAGAGTCCAGCACACTTTAAGCTTCAGACGAAG
E S G V K A P S P R L F P C E T L Y E V
GAGTCGGGTGTCAAGGCACCTTCGCCGCGCCTCTTCCCCTGTGAAACGCTGTATGAGGTC
T S Q I D L A D E K T Q V E D G E L S S
ACTTCGCAGATAGACCTCGCGGATGAGAAAACGCAAGTCGAAGACGGAGAGCTCAGCTCT
L P S S P T A S A E V A T D K P G E G R
CTCCCGAGTTCCCCCACGGCCTCTGCAGAGGTCGCGACGGACAAGCCCGGGGAGGGACGG
T A T R E D T R T G R S A E G D R G P C
ACGGCGACGCGGGAAGACACGCGGACTGGTCGGTCAGCTGAGGGAGACAGAGGGCCTTGC
H T E N Q V D G A D A K E N E S D N S H
CATACAGAGAATCAGGTCGACGGAGCAGACGCGAAGGAGAATGAGTCAGACAACTCACAC
G E S D Q D L R R R S D G R G A S S Q R
GGCGAGTCAGACCAAGACCTGCGACGTCGGAGCGACGGCCGCGGTGCATCCTCCCAGAGA
S R D E A S N S G E P P S Q S K P S Q L
TCCAGGGACGAGGCCTCGAACAGTGGCGAGCCTCCGTCACAGTCGAAACCGTCGCAGCTT
S K Q I R K K E L A P E P L R A A D I D
TCAAAGCAAATACGGAAGAAAGAACTCGCCCCGGAGCCTCTCCGCGCAGCAGATATCGAC
L S S D V R V G A S L K G G K G G K G D
CTTTCCTCAGATGTCCGTGTCGGAGCCTCGTTGAAGGGGGGGAAGGGAGGGAAGGGAGAC
A E G D N V A D L T A G F E G F S P Y S
GCTGAGGGTGATAATGTCGCCGACCTCACAGCTGGATTCGAGGGATTTTCGCCGTACTCG
P S Y S L G F S Q P S S K K A A K T T A
CCCTCCTACTCTCTTGGCTTCAGTCAGCCGTCGTCGAAGAAGGCTGCAAAAACGACAGCT
E N S K A H L P G G T R G S G N N T A V
GAAAACTCCAAAGCACACCTACCAGGAGGAACCCGCGGCAGCGGCAACAACACTGCTGTC

```
D  R  D  A  C  I  Y  G  N  K  K  N  H  F  P  F  L  D  E  P
GACCGGGACGCGTGCATCTACGGAAACAAGAAAAACCACTTTCCCTTCCTCGACGAACCT
A  L  S  L  L  V  P  F  L  F  G  R  S  L  A  T  C  M  T  V
GCCTTGTCACTGCTTGTACCATTTCTCTTCGGCAGAAGCCTCGCGACTTGCATGACCGTC
C  P  H  W  F  M  K  I  N  R  A  M  E  R  M  C  G  P  A  T
TGTCCACACTGGTTCATGAAAATCAATCGGGCTATGGAACGCATGTGTGGGCCTGCCACA
K  G  F  Q  Q  M  Y  S  K  Y  L  E  V  W  G  S  A  V  K  L
AAAGGTTTCCAGCAAATGTACTCAAAATACTTGGAAGTCTGGGGAAGCGCTGTCAAACTT
Q  P  L  Q  T  V  G  D  G  G  V  R  V  D  W  V  I  F  A  K
CAGCCTCTCCAGACAGTTGGCGATGGCGGAGTCCGCGTGGACTGGGTGATTTTTGCCAAG
V  L  P  E  C  E  G  H  I  L  D  I  S  Y  T  Y  S  Y  I  S
GTCCTCCCGGAATGTGAAGGTCACATCCTTGACATATCGTATACCTATTCCTACATTTCC
E  S  S  S  S  T  A  R  P  V  D  E  A  D  K  P  A  A  G  G
GAAAGTTCGAGTTCGACTGCTCGTCCGGTGGACGAAGCGGACAAGCCCGCGGCGGGTGGG
K  R  D  R  G  R  Q  G  E  K  R  R  S  L  S  A  N  F  D  E
AAGAGAGATCGCGGACGGCAAGGAGAAAAAAGGCGATCCCTTTCTGCCAACTTCGACGAA
G  V  I  L  S  P  C  G  Q  P  C  P  T  N  M  P  S  R  V  F
GGCGTCATTCTCTCTCCGTGCGGACAGCCTTGCCCGACCAACATGCCTTCGCGCGTGTTC
T  V  S  Y  S  L  A  A  G  A  A  K  S  S  R  T  L  W  M  H
ACGGTGTCTTACTCGCTGGCGGCGGGTGCGGCGAAGAGCAGCCGAACGCTTTGGATGCAC
R  D  L  C  R  F  H  G  D  E  T  G  V  A  A  M  G  S  V  S
CGAGACTTGTGCCGGTTCCACGGAGACGAGACTGGGGTCGCTGCCATGGGCTCCGTCTCA
S  V  C  V  G  D  F  V  E  V  A  V  T  V  Y  N  G  G  G  R
AGTGTCTGCGTAGGAGACTTCGTGGAAGTCGCTGTCACTGTGTACAACGGAGGCGGGCGC
V  A  L  D  K  V  K  W  L  P  A  R  V  E  W  R  R  E  A  V
GTTGCTCTGGACAAAGTCAAGTGGCTGCCTGCGCGAGTCGAGTGGAGACGGGAGGCTGTT
S  T  R  G  V  F  N  R  E  I  C  P  L  E  R  C  S  P  D  W
TCGACTCGCGGCGTCTTCAACAGAGAAATCTGTCCTCTCGAACGCTGCTCTCCCGACTGG
L  P  A  D  Q  F  R  I  M  T  T  E  R  L  K  A  P  E  D  F
CTTCCTGCAGACCAGTTCCGCATCATGACTACGGAACGCCTGAAGGCTCCAGAGGACTTC
S  P  C  L  K  H  V  K  T  E  F  S  G  M  D  V  A  V  R  K
TCGCCGTGTTTGAAACATGTCAAGACAGAATTTTCCGGAATGGATGTCGCCGTTCGCAAA
S  T  Y  R  A  V  R  Q  G  S  L  G  S  A  A  C  R  S  W  G
TCAACATATCGAGCAGTCCGCCAAGGGTCGCTGGGATCAGCAGCGTGCCGGTCTTGGGGG
F  P  C  E  I  L  P  Q  G  V  P  V  V  C  S  L  T  R  W  G
TTCCCTTGTGAGATCCTTCCTCAAGGCGTCCCTGTTGTTTGCTCCCTGACGCGCTGGGGA
L  Q  H  D  R  F  L  S  V  Q  L  R  E  G  D  I  I  D  Y  Y
CTCCAGCATGATCGATTCCTCTCCGTTCAGCTGCGCGAGGGCGACATAATCGATTACTAC
M  S  Q  G  G  A  N  A  *
ATGAGTCAGGGCGGAGCCAATGCGTGA
```

Figure 4.S28

>TgFbxO13 (JMJD6b) (Uniprot ID: V4Z4Z1)
(ToxoDB ID: TGGT1_283890)
Predicted F-Box Domain
JmjC Domain

M E V D E R Q Q T R V A F D P G R K K N
ATGGAAGTTGACGAACGTCAACAAACCCGTGTAGCGTTCGACCCGGGTCGCAAAAAGAAC
L K K K K P R L L L T K H P F G L L P S
CTGAAGAAGAAGAAACCGCGTCTGCTTTTAACCAAACATCCGTTTGGTCTGCTGCCGAGT
G N A L F V S S G G S T V V D R S A S L
GGCAACGCATTGTTCGTGTCCTCCGGCGGCTCTACCGTTGTGGACCGTAGCGCTTCTCTG
G S F A A L D D A A F L A F L S T L A E
GGCAGCTTCGCCGCGCTGGACGACGCTGCGTTTCTGGCGTTCCTTAGCACCCTGGCGGAG
F V P L S A L L S L S C A S K F L L A A
TTCGTGCCTCTGAGCGCTTTGCTGTCCCTGAGCTGTGCGAGCAAGTTTCTGTTGGCGGCG
L L D E E L W Q S L L L S R Q Q R R V G
TTGTTGGACGAAGAGCTGTGGCAGTCCCTGTTGTTGAGCCGCCAACAAAGACGCGTGGGT
R E E S G A R G L G A R E H G E Q G T R
CGTGAGGAAAGCGGTGCGCGCGGACTGGGCGCGCGTGAGCACGGCGAGCAGGGAACCCGT
K N G E T L L G T A D P L L L S D S A S
AAAAACGGTGAGACTCTGTTAGGTACGGCCGACCCCCTGTTGCTGTCTGACAGCGCCAGC
P S A P S P P S L S S S F S A C S E E G
CCGTCAGCTCCGTCTCCGCCGTCCCTGTCATCGTCGTTCAGCGCGTGCAGCGAAGAGGGT
E T P T K D E T S E S T D F T W R G S W
GAAACTCCGACCAAAGATGAAACTTCAGAAAGCACCGATTTTACCTGGCGTGGCTCCTGG
K K T Y L F A E R E R L T R Q R T A R A
AAAAAGACCTATCTGTTCGCGGAGCGTGAGCGTCTGACCCGCCAGCGTACCGCTCGCGCA
S S S S S S S A C S T Q E E R S A D T C
TCTTCTTCCTCCTCCAGCTCAGCGTGTAGCACGCAAGAAGAGCGTAGCGCGGATACGTGC
L D T A G D S V D R Q S L P V L R G V C
CTGGATACTGCGGGTGATAGCGTAGATCGCCAAAGCCTGCCTGTTCTGCGTGGTGTTTGC
S D T F Y Q R W L C A T V D I S S L F F
AGTGATACCTTTTACCAGCGTTGGCTGTGCGCTACCGTTGACATCAGCAGCTTGTTCTTT
R H Y D N L E R V S A S A L S V D A F V
CGCCACTACGACAACCTTGAACGCGTCTCAGCGAGCGCGTTAAGTGTCGACGCGTTCGTC
E L Y E K P N K P V V I T D L V P K W A
GAACTCTACGAAAAGCCGAACAAACCGGTCGTTATCACCGACCTGGTGCCGAAATGGGCA
A F G K W N G E Y F R R H F G G V R F N
GCGTTCGGCAAATGGAATGGCGAATATTTCAGACGTCACTTTGGCGGTGTTCGTTTTAAC
A G A A S N I Q L E T F Y Q Y A D S N F
GCCGGTGCTGCCTCTAACATTCAGCTGGAAACCTTCTACCAGTATGCAGATAGCAACTTC
D E A P L F I F D P R F A E S T R E A L
GACGAGGCGCCACTGTTTATTTTTGACCCGCGTTTTGCCGAGTCGACCCGTGAGGCATTA
S S S S A L S S P S S S S P V N V P P A
AGCTCTTCCAGTGCCCTAAGCTCGCCGAGCAGCAGTAGCCCAGTTAATGTTCCGCCGGCA

S R E I G E Q G D C R R E T T G A Q A S
AGCCGTGAGATCGGCGAGCAGGGCGACTGTCGTAGGGAGACCACCGGCGCGCAAGCAAGC
A E E R R H H E L G D R V C S L A E D Y
GCGGAGGAGCGTAGACACCATGAATTGGGCGACCGTGTCTGCTCCTTAGCTGAGGATTAT
E V P P Y F S D S R D L F A C L G E R R
GAAGTGCCACCGTACTTTAGCGATAGCCGTGATCTGTTCGCATGCCTGGGCGAACGTCGC
P N F R W L L V G N C R S G S K W H V D
CCAAATTTCCGCTGGCTGCTGGTTGGTAATTGTAGGTCCGGTAGCAAGTGGCATGTTGAC
P N Q T S A W N A V V R G A K R W I L L
CCCAACCAGACCAGCGCGTGGAATGCCGTGGTGCGTGGTGCGAAACGTTGGATTCTGCTG
P P T V C P P G V F P S H D G G E V T Q
CCGCCAACGGTGTGCCCGCCGGGTGTGTTTCCGAGCCATGATGGTGGCGAGGTGACCCAG
P T A L V E W L M N Y Y F D A L H A P G
CCGACCGCGCTCGTGGAGTGGCTGATGAACTATTACTTCGATGCGTTGCACGCACCGGGT
Y P Y T G G I A P I E G S V R E G E L I
TATCCGTACACCGGTGGTATTGCACCTATCGAAGGCAGCGTTCGGGAGGGCGAACTCATC
F V P Q G W W H C V L N E E D D T I A V
TTCGTGCCGCAAGGCTGGTGGCACTGCGTTTTGAATGAGGAGGATGATACGATTGCTGTT
T Q N F V S P V I L Q N V R S F L H Y K
ACCCAAAACTTTGTGAGCCCGGTCATCCTGCAGAACGTTCGCTCCTTCCTGCACTACAAA
K D Q I S G L C A Q G R H E T F A S E F
AAGGACCAGATTAGCGGCCTTTGCGCCCAGGGCCGTCACGAAACCTTTGCAAGCGAATTT
D A A V G A S Y P E L L P L V S S P P P
GATGCGGCAGTGGGCGCCAGCTACCCGGAATTGTTGCCGCTCGTTAGCTCTCCGCCGCCA
P C P S S S P S S P S P V S R T A L R S
CCGTGCCCGTCTTCGTCCCCGTCGAGCCCATCGCCGGTTAGTCGCACCGCGCTCCGCAGC
S R P K E T C G E E Q K G V E R G G G Q
TCTAGACCGAAAGAAACATGCGGTGAGGAACAAAAAGGTGTCGAACGTGGTGGTGGTCAG
C G E P Q D I R E Q T D G E G R E G T K
TGTGGTGAACCGCAAGATATCCGCGAGCAGACCGATGGTGAGGGCCGTGAAGGTACGAAG
R N Q E P Q D S G S F W E W L K K R R R
CGTAATCAGGAGCCGCAAGATAGCGGTTCCTTCTGGGAATGGCTGAAGAAGCGAAGGCGT
P V V L R R H A D G E T P T S Q A V A *
CCGGTGGTACTACGTCGTCATGCTGACGGCGAGACGCCGACGAGCCAGGCGGTCGCGTAA

Figure 4.S29

>TgFbxO14 (Uniprot ID: B9QB88) (ToxoDB ID: TGGT1_259880)
F-Box Domain

M E F L D Q A T L A T L A T F L L S N E
ATGGAATTTTTGGACCAGGCTACTTTGGCCACCCTGGCCACCTTTCTTCTTTCCAATGAG
L P K L R L L S K A L N G R L F P V D S
CTGCCCAAGCTCCGGCTTCTCTCTAAAGCACTCAATGGTCGTCTTTTCCCCGTTGACTCG
F R R L I R E P R S L V F P A E W G Q E
TTTCGGCGGCTTATACGAGAGCCGCGATCGCTGGTCTTTCCAGCCGAATGGGGACAAGAG
K L E S V K N R S K R E Q L F E E G S Q
AAACTGGAAAGCGTGAAGAATCGCAGCAAGCGTGAGCAGCTTTTCGAGGAAGGAAGCCAA
R A Q G G A V P E A S E V H S V T A S P
AGAGCGCAAGGCGGTGCTGTGCCAGAGGCGTCGGAGGTCCACAGCGTGACTGCGTCCCCG
P V S L D I P V S S V A P S R R D F N Y
CCGGTTTCCCTGGACATACCGGTTTCATCAGTTGCCCCTTCCAGACGAGATTTTAACTAC
L R V L V N L P P P P P H L L H L T L H
CTTCGGGTTCTGGTGAACTTACCCCCCCCACCGCCGCATTTGCTGCACCTGACTCTTCAC
I P E N L R T V T R S W L R T Y H Q L L
ATCCCGGAGAATTTACGCACAGTAACGCGTTCGTGGCTGCGAACCTACCATCAGCTTCTG
C V A A P H L E T L Q L V E F F S A R L
TGTGTGGCGGCTCCTCACCTGGAAACTCTGCAGCTCGTCGAGTTTTTCTCAGCTCGTCTG
R K D L M V R D G A V H A E D K N G D A
CGGAAGGACCTCATGGTACGCGATGGGGCCGTTCATGCTGAAGACAAAAACGGTGACGCC
S C S A D T S N P R E S I P E S D A V A
TCGTGCTCAGCAGACACTTCGAATCCACGAGAGTCGATTCCGGAAAGTGACGCAGTCGCC
P E N Q E N R Q E E A P V C S C P W R A
CCGGAGAATCAGGAGAACCGTCAAGAAGAGGCTCCAGTTTGCTCGTGTCCGTGGAGAGCT
P K K H E A L P L P A F P R L R F L A V
CCTAAAAAGCACGAAGCTCTGCCGCTTCCCGCCTTTCCGCGACTCCGTTTTCTGGCAGTG
R N R G G W S V R P P L P C A F T Y L F
CGCAACCGCGGCGGGTGGTCTGTCCGTCCACCTCTGCCGTGTGCCTTTACTTACCTATTC
L G D L Q T G D S S R E S C W A S S E S
CTCGGGGATTTGCAGACCGGCGATTCTTCTCGTGAGTCCTGTTGGGCCTCCTCGGAGTCC
T T P S E A F P V L K D I R F L E F T T
ACAACGCCTTCTGAAGCGTTTCCTGTCTTGAAAGACATCCGATTTCTCGAGTTCACCACC
I G L D L F R Q F L V K H N V T S A E H
ATAGGTTTGGATTTGTTCAGGCAGTTTCTAGTCAAACACAACGTGACGTCTGCGGAGCAC
I A I G M W H M S P L Q D F L L F L V R
ATTGCGATAGGCATGTGGCACATGAGTCCGTTGCAGGACTTCTTGTTGTTTTTGGTGCGC
E N S K P K R R F H K L R S L D V H G A
GAGAATTCGAAGCCAAAACGGCGATTCCACAAGCTGAGGAGTCTAGACGTGCACGGAGCG
R F I W P P D E F W Y F F W R S W C D F
AGATTCATATGGCCACCAGACGAGTTCTGGTATTTCTTTTGGCGAAGTTGGTGTGACTTC
T Q I W K E S F L Q R S S D S D R G D A
ACGCAAATCTGGAAGGAAAGCTTTCTTCAGCGCAGCTCAGACAGCGACCGGGGAGACGCG

R R R A S A L C D D H W T S C P K D W S
CGACGACGAGCTTCTGCTCTGTGTGACGACCACTGGACGTCTTGCCCCAAAGATTGGTCT
T C P D Q W G T D N D P L L R V S D G D
ACGTGCCCTGACCAATGGGGAACAGACAACGACCCGCTACTACGAGTTAGCGACGGTGAC
C E P Q D E D L V E E G G S I N D E F L
TGCGAACCACAAGACGAAGATTTGGTGGAAGAAGGTGGCTCAATCAATGACGAATTCCTG
S D A G E D E G K D R E S I V R M L K R
TCGGATGCGGGAGAGGATGAGGGGAAAGACCGCGAGAGTATCGTGCGCATGCTGAAAAGG
L P C L R R V L L S G F V G T F V A E E
CTTCCCTGCCTTCGCCGTGTTCTTTTGTCAGGTTTTGTGGGCACATTTGTAGCCGAGGAA
A D E A I R F F E D I F P Q A V V D V E
GCAGACGAGGCCATTCGCTTTTTCGAGGATATATTCCCCCAAGCAGTTGTGGACGTGGAG
G E I I V S T N A L L E A V V Q A T A H
GGCGAGATCATCGTCAGCACGAATGCTCTCCTGGAGGCCGTTGTCCAAGCGACTGCGCAT
P G W A S R L D S F M A R K R E H R A Q
CCTGGGTGGGCGTCCCGACTTGATTCGTTTATGGCTCGAAAAAGGGAGCACCGCGCGCAA
V T Q A T G S R A S P W T E D F D R S G
GTGACTCAGGCGACAGGGTCACGAGCAAGCCCATGGACAGAAGATTTTGATCGAAGTGGA
V T A A A V G A P N S E V S T S N A E L
GTGACTGCGGCCGCCGTGGGAGCACCAAACAGTGAAGTCTCAACCTCTAACGCCGAGCTA
E R D D E S E H L A L E G R R Y D E R N
GAACGGGATGACGAGAGTGAGCATCTTGCACTCGAAGGTCGTCGGTACGATGAGCGGAAC
W E A L D G V F L S E R G K E N F G R W
TGGGAAGCGTTAGATGGAGTCTTCCTGTCTGAACGAGGAAAAGAGAATTTCGGTCGGTGG
L A L G V I E D V Y I E V S N P T Y P K
CTGGCTCTGGGCGTCATCGAGGACGTTTACATAGAAGTGAGTAATCCAACATATCCAAAA
V H L Q I N A F H R Y C V S T Y F K C L
GTGCATTTGCAAATCAATGCATTTCATCGATATTGCGTGTCTACATATTTTAAATGTTTG
E L P A T K M E D P V G Q D W G L P S V
GAACTGCCAGCAACCAAGATGGAGGATCCCGTAGGGCAAGACTGGGGTCTTCCATCAGTG
T V R H V V Q W G T K Y V Q D F L D I V
ACTGTCCGTCACGTGGTGCAGTGGGGTACGAAGTATGTTCAGGATTTTTTAGATATTGTT
S T F R H V I L N L N Y I F W T D R G E
TCCACCTTCCGGCACGTCATTCTCAATTTGAATTACATCTTCTGGACAGACCGGGGAGAA
Y V D A N A E R C L G S E A G E A C R T
TATGTAGACGCAAACGCTGAGAGATGCCTCGGATCTGAAGCGGGCGAAGCATGTAGGACA
P S E G N L I Q S D A P C A R T D G R A
CCGTCAGAGGGAAATCTTATACAGAGCGACGCGCCATGCGCGCGCACAGACGGTCGGGCT
Q D V H D V A K A D F S V D Q E S G E T
CAGGATGTCCATGACGTGGCAAAAGCAGATTTCTCCGTAGATCAGGAGTCTGGTGAGACG
D A E P P P V V S A D T R F L Q C S E S
GACGCGGAGCCCCCGCCGGTTGTATCGGCTGACACGCGCTTTCTCCAGTGCTCCGAAAGT
A S P A D G A S I R S S D A G D E R L V
GCCAGCCCTGCCGACGGGGCCAGTATCAGAAGCAGCGACGCCGGTGACGAACGGTTGGTG
A S D R T A H Q G S K E V V R L G E F D
GCTTCGGATAGAACGGCTCACCAAGGGAGCAAGGAGGTTGTTCGTTTGGGTGAATTTGAC
G H F P N V V G L L L P L Y W M D D A T

GGTCATTTCCCGAACGTTGTTGGGCTTCTCCTGCCCCTGTACTGGATGGATGATGCAACA
W S T D E I A R I A E K Y R S Q T Q V V
TGGTCCACTGATGAGATAGCGCGAATTGCGGAGAAGTACAGAAGCCAAACGCAGGTCGTA
R I K N L F P I M G E Y A T V D D P V S
CGTATCAAAAACCTTTTTCCAATCATGGGGGAATACGCCACGGTAGACGATCCAGTGTCA
L M A R D F E I V T R I C K D T M R V I
CTGATGGCTCGAGATTTCGAAATTGTGACACGCATCTGTAAAGACACAATGCGTGTAATT
D Y R V Y S F F S W K D E L G L D E N T
GATTATCGAGTTTACAGCTTTTTCTCGTGGAAGGATGAGCTCGGCCTCGATGAGAACACG
L I P Q F L K E F V S N N P E F T L A K
TTGATACCTCAGTTCTTGAAGGAGTTTGTATCAAACAATCCTGAATTTACTTTGGCTAAG
R L D S P S M T Q T G V V T V G Q E A L
CGCCTCGACTCTCCTTCGATGACGCAGACAGGTGTGGTGACTGTCGGACAAGAAGCGCTT
C Q L R V Y I W I K R D V L *
TGTCAATTGCGCGTGTACATATGGATTAAACGAGATGTGCTGTGA

Figure 4.S30

>DdFbxA (Uniprot ID: Q9Y0T2) (Dictybase ID: DDB_G0276887)

M Q Y V N G N D I S S Q S I H E V L E L
ATGCAATACGTTAATGGTAATGATATTTCAAGTCAAAGTATTCATGAAGTTTTAGAACTT
A F S T K I P W T K L E Y E S S E K H I
GCATTTTCAACAAAAATCCCATGGACAAAATTAGAATATGAATCAAGTGAAAAACATATA
I H S Y S S H E R G I Y L S K G V A E F
ATACATTCCTATTCATCACATGAAAGAGGTATTTATTTAAGTAAAGGTGTTGCAGAATTT
N I S P E N M Y E L L L D I S S R S K W
AATATTTCACCAGAAAATATGTATGAACTTTTATTGGATATTTCTTCAAGATCAAAATGG
D F H C R E A H I I E E Y D H L N H I I
GATTTTCATTGTAGAGAAGCACATATTATTGAAGAATATGATCATTTAAATCATATTATT
H L N F T N P L I S N L D M N L Y R S C
CATTTAAATTTTACAAATCCATTAATTAGTAATTTGGATATGAATTTATATAGAAGTTGT
K Y D P Q E R L F V I A M R S I E L E D
AAGTATGATCCACAAGAGAGATTATTTGTAATTGCTATGAGATCAATTGAATTGGAGGAT
G D V D Q F E C S Q N G L V I Q G L R G
GGTGATGTTGATCAATTTGAATGTTCACAAAATGGATTGGTAATTCAAGGTTTAAGAGGA
Q K D K C K M T F V Q Q C D L R D I E L
CAAAAAGATAAATGTAAGATGACATTCGTTCAACAATGTGATCTAAGAGATATAGAACTT
Q R I P G Y K S F N S K E R L E D F Q F
CAACGTATTCCAGGTTATAAATCATTCAATAGTAAAGAGAGACTTGAGGATTTTCAATTT
L T L F P A T V S G R L A K I F E S I E
CTTACATTGTTTCCTGCCACTGTAAGTGGTAGACTTGCAAAGATTTTCGAATCTATAGAA
L Y I S N N V K D I E T K D I R I S I M
CTATACATATCAAACAATGTGAAGGATATTGAAACCAAGGATATTCGTATCTCAATTATG
E K A E K E V N E M F G T T N P D Y G W
GAAAAAGCAGAAAAGGAGGTAAATGAAATGTTTGGTACAACCAATCCAGACTATGGTTGG
K I Y L K K L D M E I L I K K T T S G Y
AAAATTTATTTAAAGAAATTGGATATGGAAATTCTAATTAAAAAGACAACCTCTGGTTAC
Y M I G K G S F S S R Y S P E L L A D V
TATATGATTGGTAAGGGTAGTTTTTCTTCGAGGTATTCACCAGAGTTATTGGCTGATGTA
L Y Q K N P F E W D T F Y D K T K L V E
CTCTATCAGAAGAATCCTTTCGAATGGGATACTTTTTATGATAAAACTAAATTGGTTGAA
S I N S S I R E V E V H Y R M W R N T I
AGTATCAATAGTTCAATCAGAGAGGTCGAGGTTCATTATAGAATGTGGAGAAATACAATC
T M R L L Q S V K K G P G N F S S V H W
ACCATGAGATTGCTACAATCCGTTAAAAAAGGACCTGGTAATTTCTCATCGGTACATTGG
R S I C S P N Y Q V A D G I E V H Y L P
AGAAGTATTTGTTCTCCAAATTATCAAGTGGCTGATGGTATCGAAGTACATTATCTTCCT
T A L L N Y G L G D G S F T S F L A A I
ACTGCACTCTTAAACTATGGTTTAGGTGATGGTAGTTTCACAAGTTTCTTGGCGGCAATC
E V K G Y P T P W E E E M V T K M F A A
GAGGTTAAAGGTTATCCAACTCCTTGGGAGGAAGAGATGGTAACTAAAATGTTTGCTGCT
R I I S N Q N S I I N H V N K L T G G S

AGAATCATTTCAAATCAAAATAGTATCATAAATCATGTAAATAAATTAACAGGTGGTTCA
E M I R E L P V I P S V Q H H C G D V G
GAGATGATAAGAGAATTACCTGTTATTCCTTCAGTTCAACATCATTGTGGTGATGTTGGT
S H I G T P Q V Y N A M V E N F A D I L
TCTCATATTGGTACTCCTCAAGTCTATAATGCAATGGTCGAAAATTTTGCTGATATACTT
L D E G N K D G N V V S S K N K R K R N
TTAGATGAAGGTAATAAAGATGGAAATGTAGTTTCTTCAAAAAATAAAAGAAAAAGAAAT
K N N E N K N N N N D N I I D E E I E Q
AAAAATAATGAAAATAAAAATAATAATAATGATAATATAATTGATGAAGAAATTGAACAA
E E E N I E K D Q Q Q T Q Q Q Q T Q K Q
GAGGAGGAAAATATTGAAAAAGATCAACAACAAACCCAACAACAACAAACTCAAAAACAA
Q Q Q Q Q Q Q Q K T Q Q Q P Q Q Q Q Q Q
CAACAACAACAACAACAACAACAAAAAACACAACAACAACCACAACAGCAACAACAACAA
P Q E Q Q Q N H S Q L K K E I K P T R P
CCACAAGAACAACAACAAAATCACTCACAACTAAAAAAAGAAATCAAACCTACAAGACCA
S I R F T Y L L S N S S S G Q R P I A W
AGTATTCGTTTTACCTATTTATTAAGTAACAGTAGTAGTGGACAACGTCCAATTGCTTGG
Y E S K K Q P F L F L V S D S S E R K G
TATGAATCAAAAAAACAACCATTCTTATTTTTGGTTAGTGATAGTAGTGAGAGAAAAGGA
K I Q R K T Y Y F S N S G F D N L P E E
AAGATTCAAAGAAAGACTTATTATTTCTCAAATTCAGGTTTTGATAATTTACCAGAGGAA
V V Q I I F S N L S A I N I V N L S L V
GTGGTTCAAATTATATTTTCCAATTTATCGGCAATCAATATTGTCAACTTATCATTAGTT
C K R F K M A T D S P I L W K N L Y K S
TGTAAAAGATTTAAAATGGCAACTGATAGTCCAATTCTTTGGAAAAATCTTTATAAAAGT
N P L F H K K T P K R K Q I I H S N L S
AATCCATTATTTCATAAAAAGACACCAAAAAGAAAACAAATCATTCATTCAAATCTAAGT
N D E N K V N S N S G D S A D G S S S Q
AATGATGAAAATAAAGTAAATTCAAATTCTGGTGATTCTGCTGATGGTTCATCAAGCCAA
E E E E Q Q Q Q N Q Q Q N Q Q Q N Q Q Q
GAAGAAGAAGAACAACAACAACAAAATCAACAACAAAATCAACAACAAAATCAACAACAA
Q Q Q Q T F D L S N I N L N D P I S L L
CAACAACAACAAACATTTGACCTTTCAAATATTAATTTAAATGATCCAATATCATTATTA
M V F T N G I I P Q N L S P T E I I N V
ATGGTATTTACAAATGGAATAATTCCTCAAAATTTATCACCAACTGAAATAATAAATGTT
G G I V S Q I D L N D L S N V E T L I Q
GGTGGAATAGTGTCTCAAATTGATTTGAATGATCTTTCAAACGTTGAAACTCTTATTCAA
Q L P H Q V L S L I Q M N T L D A K I Q
CAATTACCTCATCAAGTTTTATCATTGATTCAAATGAATACACTTGATGCAAAGATTCAA
H L S M I S G M P A T I G Q E S P I N K
CATTTATCAATGATTAGTGGAATGCCAGCAACCATTGGTCAAGAATCACCAATCAATAAA
N S S D N P K P N A Y N K R D N N S Y I
AACTCTTCAGATAATCCAAAACCAAATGCATACAATAAAAGAGATAACAACTCTTATATT
P D E E F I N W K S H Y T E K H K Q S K
CCTGATGAAGAGTTTATTAATTGGAAATCACATTACACTGAAAAACATAAGCAATCAAAG
R W V N M E P I R I T P L K G H N R A I
AGATGGGTTAATATGGAACCAATTCGTATCACCCCTCTAAAGGGTCACAATAGGGCAATC

K A V K S E G N S A I T V S T E K K I K
AAAGCTGTAAAGAGTGAGGGTAATTCAGCTATCACCGTATCAACAGAGAAAAAAATCAAA
F W N L N T G Q C I G D Y E G E S G V L
TTTTGGAATTTAAACACTGGTCAATGTATTGGAGACTACGAAGGTGAATCAGGTGTTCTC
S V E Y D H T Q K S S C I W P L S D Y T
TCTGTAGAGTATGATCACACTCAAAAGTCATCTTGTATTTGGCCATTGTCAGATTATACC
K V H I G H K N G T V T M V D F I E Q P
AAAGTCCACATTGGCCATAAGAATGGTACCGTCACTATGGTTGATTTCATTGAACAACCA
I E V I H T S R P T N L A D G F D F T F
ATTGAAGTTATTCATACATCAAGACCAACCAATTTGGCTGATGGTTTCGATTTCACCTTT
P G K Y L I W E H T I I H Y W D V E T S
CCTGGTAAATATTTGATTTGGGAACACACAATCATTCACTATTGGGATGTTGAAACAAGT
T L L W N E L N A H T K K I T Q S K I V
ACACTCTTGTGGAATGAACTAAATGCTCACACAAAGAAAATCACTCAATCAAAGATTGTC
A Q H E L S N K G I V F T T S S D K S A
GCACAACATGAACTTTCTAATAAAGGTATCGTATTCACAACTAGCTCTGATAAATCTGCA
K V W D L T N G T C I N T L V G H S Y A
AAAGTTTGGGATTTAACAAATGGTACTTGTATAAATACTTTGGTTGGCCATTCATATGCC
V N C I E P I G D Y M A L T G S T D K T
GTCAATTGTATTGAACCAATTGGTGACTATATGGCTTTGACAGGTTCCACTGATAAAACT
L K L W D L R Q A S T F I S S Y S T K H
CTTAAACTTTGGGATCTTAGACAAGCCTCAACATTTATATCTAGTTACTCTACTAAACAC
T G P I R C I S Y Q E K N G I V L S G S
ACTGGTCCAATTAGATGTATTTCCTATCAAGAAAAGAATGGTATTGTTTTAAGTGGTAGT
D D G S I I A F N L D N W N L S N I S V
GATGATGGTTCAATCATTGCATTTAACTTGGATAATTGGAATCTTTCAAATATCTCTGTT
V K K P I F N N V I G N I G T T T T T T
GTTAAAAAACCAATCTTTAATAATGTTATTGGTAATATTGGTACAACAACAACAACAACT
T T T T T T T T T T T S T T N N T N V P
ACTACTACCACTACAACTACAACTACTACTACTTCAACTACAAATAATACTAATGTACCA
E I P K I N L G T F K D S K R L H N H E
GAGATTCCAAAGATTAATTTAGGTACTTTTAAGGATTCCAAAAGACTTCATAATCATGAA
S A V T C I E S D E A G F I S G S Q N G
TCTGCTGTAACTTGCATTGAATCTGATGAAGCTGGTTTTATTAGTGGATCACAAAATGGA
L V L R W D F *
TTGGTTTTGAGATGGGACTTTTAA

Figure 4.S31

>Pet28-His-MBP-DdFbxN-SF
Flag Tag
StrepII Tag
Thrombin Site
His Tag
MBP Tag
Factor Xa Site
TEV Site
FbxN
Added SF Tag

TAATACGACTCACTATAGGGGAATTGTGAGCGGATAACAATTCCCCTCTAGAAATAATTTTGTT
TAACTTTAAGAAGGAGATATACC
M D H H H H H H I E E G K L V I W I N G
ATGGATCATCATCATCATCATCATATCGAAGAAGGTAAACTGGTAATCTGGATTAACGGC
D K G Y N G L A E V G K K F E K D T G I
GATAAAGGCTATAACGGTCTCGCTGAAGTCGGTAAGAAATTCGAGAAAGATACCGGAATT
K V T V E H P D K L E E K F P Q V A A T
AAAGTCACCGTTGAGCATCCGGATAAACTGGAAGAGAAATTCCCACAGGTTGCGGCAACT
G D G P D I I F W A H D R F G G Y A Q S
GGCGATGGCCCTGACATTATCTTCTGGGCACACGACCGCTTTGGTGGCTACGCTCAATCT
G L L A E I T P D K A F Q D K L Y P F T
GGCCTGTTGGCTGAAATCACCCCGGACAAAGCGTTCCAGGACAAGCTGTATCCGTTTACC
W D A V R Y N G K L I A Y P I A V E A L
TGGGATGCCGTACGTTACAACGGCAAGCTGATTGCTTACCCGATCGCTGTTGAAGCGTTA
S L I Y N K D L L P N P P K T W E E I P
TCGCTGATTTATAACAAAGATCTGCTGCCGAACCCGCCAAAAACCTGGGAAGAGATCCCG
A L D K E L K A K G K S A L M F N L Q E
GCGCTGGATAAAGAACTGAAAGCGAAAGGTAAGAGCGCGCTGATGTTCAACCTGCAAGAA
P Y F T W P L I A A D G G Y A F K Y E N
CCGTACTTCACCTGGCCGCTGATTGCTGCTGACGGGGGTTATGCGTTCAAGTATGAAAAC
G K Y D I K D V G V D N A G A K A G L T
GGCAAGTACGACATTAAAGACGTGGGCGTGGATAACGCTGGCGCGAAAGCGGGTCTGACC
F L V D L I K N K H M N A D T D Y S I A
TTCCTGGTTGACCTGATTAAAAACAAACACATGAATGCAGACACCGATTACTCCATCGCA
E A A F N K G E T A M T I N G P W A W S
GAAGCTGCCTTTAATAAAGGCGAAACAGCGATGACCATCAACGGCCCGTGGGCATGGTCC
N I D T S K V N Y G V T V L P T F K G Q
AACATCGACACCAGCAAAGTGAATTATGGTGTAACGGTACTGCCGACCTTCAAGGGTCAA
P S K P F V G V L S A G I N A A S P N K
CCATCCAAACCGTTCGTTGGCGTGCTGAGCGCAGGTATTAACGCCGCCAGTCCGAACAAA
E L A K E F L E N Y L L T D E G L E A V
GAGCTGGCAAAAGAGTTCCTCGAAAACTATCTGCTGACTGATGAAGGTCTGGAAGCGGTT
N K D K P L G A V A L K S Y E E E L A K
AATAAAGACAAACCGCTGGGTGCCGTAGCGCTGAAGTCTTACGAGGAAGAGTTGGCGAAA

D P R I A A T M E N A Q K G E I M P N I
GATCCACGTATTGCCGCCACAATGGAAAACGCCCAGAAAGGTGAAATCATGCCGAACATC
P Q M S A F W Y A V R T V V I N A A S G
CCGCAGATGTCCGCTTTCTGGTATGCCGTGCGTACTGTGGTGATCAACGCCGCCAGCGGT
R Q T V D E A L K D A Q T N S S S D Y D
CGTCAGACTGTCGATGAAGCCCTGAAAGACGCGCAGACTAATTCGAGCTCAGATTATGAT
I P T T G I E G R><G E N L Y F Q><G D I T
ATTCCGACCACCGGGATCGAGGGAAGGGGAGAAAATCTTTATTTTCAAGGTGATATTACT
H M W P M M E D E D N Q Q Q Q P C Y I L
CATATGTGGCCAATGATGGAAGATGAAGATAATCAACAACAACAACCATGTTACATTTTA
N I P F E N L L I I L Q N L H T K S L L
AATATACCATTTGAAAATTTATTAATTATATTACAAAATTTACATACAAAATCACTTTTA
E L S Q V N L Y F N Q I I S N S S I S N
GAATTATCTCAAGTTAATTTATATTTTAACCAAATCATTTCAAATTCTTCAATTTCAAAT
M I W N D I I Q K D F L L S T D N A I I
ATGATTTGGAATGATATTATTCAAAAAGATTTCTTATTATCAACTGATAATGCAATTATC
K Y K L N I N N E E V E N N V N T N N E
AAATATAAATTAAATATTAATAATGAAGAAGTAGAAAATAATGTTAATACTAATAATGAG
E E E D N K D E E N E D E K E E Y D E E
GAGGAGGAGGATAATAAAGATGAAGAAAATGAAGATGAAAAAGAAGAGTATGATGAAGAG
Y D E E Y D E D D E D E D N D D D D D D
TATGATGAAGAGTATGATGAAGATGATGAAGATGAAGATAATGATGACGATGACGATGAT
I N E E A N Y L K E L R K S Y K S Q N K
ATTAATGAAGAAGCAAATTATTTAAAAGAATTAAGAAAATCATATAAAAGTCAAAATAAA
N K N E H L D L E R E Q N E I I E K E K
AATAAAAATGAACATTTAGATTTAGAAAGAGAACAAAATGAAATAATAGAAAAAGAAAAA
L T P I I V N K L L H Q R F N S N I I H
TTAACACCAATTATTGTAAATAAATTATTACATCAAAGATTTAATTCAAATATAATTCAT
H Y K T M R Y I W D R F E N W M D L N S
CATTATAAAACAATGAGATACATTTGGGATAGATTTGAAAATTGGATGGATTTAAATTCA
M D S M K K S F H S I S H T K L Y K L I
ATGGATTCAATGAAAAAATCTTTTCATTCGATTTCTCATACTAAATTATATAAATTAATT
S T I K F V N N S S N N S S N N V V N N
TCAACTATTAAATTTGTAAATAATAGTTCAAATAATAGTTCAAATAATGTTGTTAATAAT
D N N I K L P A D Y L C S M L I H N G Q
GATAATAATATAAAATTACCAGCTGATTATTTATGTTCAATGTTAATTCATAATGGACAA
K E F T R Y G L L G T V E A Y E S K T N
AAAGAATTTACAAGATATGGTTTATTAGGTACAGTTGAAGCATATGAATCAAAAACAAAT
I F L L S L E K T I S L Y K K T R N M Q
ATATTTTTATTATCACTTGAAAAGACGATATCGTTATATAAAAAGACTAGAAATATGCAA
S F Q H V L F V A C S A S R R Y Y I M A
TCATTTCAACATGTTTTATTTGTAGCATGTTCTGCCTCTAGAAGATATTATATAATGGCA
L R D F K I E E K S F K K D Q I L L I A
TTGCGGGATTTTAAAATTGAAGAAAAGAGTTTTAAAAAGGACCAAATCTTATTAATTGCT
P G S P M I V A N S F W E F L Y L H A F
CCGGGTAGTCCAATGATTGTTGCAAATAGTTTTTGGGAATTTTTATATTTACATGCTTTT
A L E K G V F T T R R K I L Y R Y P E F

GCATTAGAGAAAGGTGTATTCACAACTAGAAGGAAAATACTCTATAGATATCCAGAGTTT
S P Y N G D E V V T Q G V K I K C S A V
TCACCTTACAATGGTGATGAGGTTGTAACTCAAGGTGTTAAAATAAAATGTAGTGCAGTT
Y I P E D E N S Y T F F Y R V T I S M D
TATATACCAGAGGATGAAAATTCTTATACCTTCTTTTATAGAGTAACTATCTCAATGGAT
K D E D P K N A C Q L T H R F W I I S T
AAAGATGAAGATCCAAAAAATGCTTGTCAATTAACTCATCGTTTTTGGATAATATCAACA
I D G S S N V N G P G V I G K F P I I K
ATTGATGGTTCTTCAAATGTAAATGGTCCTGGTGTAATTGGTAAATTTCCAATTATAAAA
P G V T F E Y C S R C E I E R S Q G H M
CCTGGTGTAACTTTTGAATATTGTAGTAGGTGTGAGATTGAACGTTCTCAGGGTCATATG
G G Y F T M V K L N N R D Y S F R A T V
GGAGGTTATTTTACAATGGTTAAATTAAATAATAGAGATTATTCATTCCGTGCAACAGTT
P T F F L T T I Q S L V P R><G S W S H P
CCAACTTTTTTTTTAACAACAATTCAAAGTCTGGTGCCGCGAGGGTCCTGGTCTCATCCT
Q F E K G G G S G G G S G G G S W S H P
CAGTTTGAAAAAGGTGGTGGTTCTGGTGGTGGTTCCGGTGGTGGTTCTTGGTCTCATCCG
Q F E K G A S G E D Y K D D D D K *
CAATTCGAAAAGGGCGCCTCTGGTGAGGATTACAAAGACGACGACGATAAATAAGCGGCCGCGA
TCCGGCTGCTAACAAAGCCCGAAAGGAAGCTGAGTTGGCTGCTGCCACCGCTGAGC

REFERENCES

(1) Li, L., Shen, S., Bickler, P., Jacobson, M. P., Wu, L. F., and Altschuler, S. J. (2023) Searching for molecular hypoxia sensors among oxygen-dependent enzymes, eLife 12, e87705.

(2) West, C. M., and Blader, I. J. (2015) Oxygen sensing by protozoans: how they catch their breath, Current Opinion in Microbiology 26, 41-47.

(3) van der Wel, H., Ercan, A., and West, C. M. (2005) The Skp1 Prolyl Hydroxylase from *Dictyostelium* Is Related to the Hypoxia-inducible Factor-α Class of Animal Prolyl 4-Hydroxylases, Journal of Biological Chemistry 280, 14645-14655.

(4) Zheng, N., Schulman, B. A., Song, L., Miller, J. J., Jeffrey, P. D., Wang, P., Chu, C., Koepp, D. M., Elledge, S. J., Pagano, M., Conaway, R. C., Conaway, J. W., Harper, J. W., and Pavletich, N. P. (2002) Structure of the Cul1–Rbx1–Skp1–F box^{Skp2} SCF ubiquitin ligase complex, Nature 416, 703-709.

(5) Bai, C., Sen, P., Hofmann, K., Ma, L., Goebl, M., Harper, J. W., and Elledge, S. J. (1996) SKP1 Connects Cell Cycle Regulators to the Ubiquitin Proteolysis Machinery through a Novel Motif, the F-Box, Cell 86, 263-274.

(6) Winston, J. T., Koepp, D. M., Zhu, C., Elledge, S. J., and Harper, J. W. (1999) A family of mammalian F-box proteins, Current Biology 9, 1180-S1183.

(7) Hua, Z., Zou, C., Shiu, S.-H., and Vierstra, R. D. (2011) Phylogenetic Comparison of F-Box (FBX) Gene Superfamily within the Plant Kingdom Reveals Divergent Evolutionary Histories Indicative of Genomic Drift, PLOS ONE 6, e16219.

(8) Lee, J. E., Sweredoski, M. J., Graham, R. L. J., Kolawa, N. J., Smith, G. T., Hess, S., and Deshaies, R. J. (2011) The Steady-State Repertoire of Human SCF Ubiquitin Ligase Complexes Does Not Require Ongoing Nedd8 Conjugation, Molecular & Cellular Proteomics 10, M110.006460.

(9) Finley, D., Ulrich, H. D., Sommer, T., and Kaiser, P. (2012) The Ubiquitin–Proteasome System of *Saccharomyces cerevisiae*, Genetics 192, 319-360.

(10) Sarikaya Bayram, Ö., Bayram, Ö., Karahoda, B., Meister, C., Köhler, A. M., Thieme, S., Elramli, N., Frawley, D., McGowan, J., Fitzpatrick, D. A., Schmitt, K., de Assis, L. J., Valerius, O., Goldman, G. H., and Braus, G. H. (2022) F-box receptor mediated control of substrate stability and subcellular location organizes cellular development of *Aspergillus nidulans*, PLOS Genetics 18, e1010502.

(11) Mandalasi, M. N., Gas-Pascual, E., Baptista, C. G., Deng, B., van der Wel, H., Kruijtzer, J. A. W., Boons, G.-J., Blader, I. J., and West, C. M. (2024) Oxygen-dependent regulation of F-box proteins in *Toxoplasma gondii* is mediated by Skp1 glycosylation, Journal of Biological Chemistry 300, 107801.

(12) Boland, A. W., Gas-Pascual, E., Nottingham, B. L., van der Wel, H., Daniel, N. G., Sheikh, M. O., Schafer, C. M., and West, C. M. (2022) Oxygen-dependent regulation of E3(SCF)ubiquitin ligases and a Skp1-associated JmjD6 homolog in development of the social amoeba *Dictyostelium*, Journal of Biological Chemistry 298, 102305.

(13) Skowyra, D., Craig, K. L., Tyers, M., Elledge, S. J., and Harper, J. W. (1997) F-Box Proteins Are Receptors that Recruit Phosphorylated Substrates to the SCF Ubiquitin-Ligase Complex, Cell 91, 209-219.

(14) Sheikh, M. O., Xu, Y., van der Wel, H., Walden, P., Hartson, S. D., and West, C. M. (2015) Glycosylation of Skp1 Promotes Formation of Skp1–Cullin-1–F-box Protein Complexes in *Dictyostelium*, Molecular & Cellular Proteomics 14, 66-80.

(15) Sheikh, M. O., Thieker, D., Chalmers, G., Schafer, C. M., Ishihara, M., Azadi, P., Woods, R. J., Glushka, J. N., Bendiak, B., Prestegard, J. H., and West, C. M. (2017) O_2 sensing–associated glycosylation exposes the F-box–combining site of the *Dictyostelium* Skp1 subunit in E3 ubiquitin ligases, Journal of Biological Chemistry 292, 18897-18915.

(16) Xu, X., Eletsky, A., Sheikh, M. O., Prestegard, J. H., and West, C. M. (2018) Glycosylation Promotes the Random Coil to Helix Transition in a Region of a Protist Skp1 Associated with F-Box Binding, Biochemistry 57, 511-515.

(17) Mandalasi, M., Kim, H. W., Thieker, D., Sheikh, M. O., Gas-Pascual, E., Rahman, K., Zhao, P., Daniel, N. G., van der Wel, H., Ichikawa, H. T., Glushka, J. N., Wells, L., Woods, R. J., Wood, Z. A., and West, C. M. (2020) A terminal α3-galactose modification regulates an E3 ubiquitin ligase subunit in *Toxoplasma gondii*, Journal of Biological Chemistry 295, 9223-9243.

(18) Cantrell, D. A., Urbauer, R. J. B., Kim, H. W., Woods, R. J., Urbauer, J. L., Wood, Z. A., and West, C. M. (2025) Glycosylation Weakens Skp1 Homodimerization in *Toxoplasma gondii* by Interrupting a Fuzzy Interaction, Biochemistry 64(10), 2262-2279.

(19) Tan, A., Tanner, J. J., and Henzl, M. T. (2008) Energetics of OCP1–OCP2 complex formation, Biophysical Chemistry 134, 64-71.

(20) Sheikh, M. O., Schafer, C. M., Powell, J. T., Rodgers, K. K., Mooers, B. H. M., and West, C. M. (2014) Glycosylation of Skp1 Affects Its Conformation and Promotes Binding to a Model F-Box Protein, Biochemistry 53, 1657-1669.

(21) Liu, T., Abboud, M. I., Chowdhury, R., Tumber, A., Hardy, A. P., Lippl, K., Lohans, C. T., Pires, E., Wickens, J., McDonough, M. A., West, C. M., and Schofield, C. J. (2020) Biochemical and biophysical analyses of hypoxia sensing prolyl hydroxylases from *Dictyostelium discoideum* and *Toxoplasma gondii*, Journal of Biological Chemistry 295, 16545-16561.

(22) Schafer, C. M., Sheikh, M. O., Zhang, D., and West, C. M. (2014) Novel Regulation of Skp1 by the *Dictyostelium* AgtA α-Galactosyltransferase Involves the Skp1-binding Activity of Its WD40 Repeat Domain, Journal of Biological Chemistry 289, 9076-9088.

(23) Wang, Z. A., van der Wel, H., Vohra, Y., Buskas, T., Boons, G.-J., and West, C. M. (2009) Role of a Cytoplasmic Dual-function Glycosyltransferase in O_2 Regulation of Development in *Dictyostelium*, Journal of Biological Chemistry 284, 28896-28904.

(24) Thomas M. Laue, B. S., Teresa M. Ridgeway, S. L. Pelletier. (1992) Computer-aided Interpretation of Sedimentation Data for Proteins, In Analytical ultracentrifugation in biochemistry and polymer science (S. E. Harding, J. C. H., A. J. Rowe, Ed.), pp 90-125, Royal Society of Chemistry, Cambridge, UK.

(25) Schuck, P. (2000) Size-Distribution Analysis of Macromolecules by Sedimentation Velocity Ultracentrifugation and Lamm Equation Modeling, Biophysical Journal 78, 1606-1619.

(26) Brautigam, C. A. (2015) Chapter Five - Calculations and Publication-Quality Illustrations for Analytical Ultracentrifugation Data, In Methods in Enzymology (Cole, J. L., Ed.), pp 109-133, Academic Press.

(27) Kim, H. W., Eletsky, A., Gonzalez, K. J., van der Wel, H., Strauch, E.-M., Prestegard, J. H., and West, C. M. (2020) Skp1 Dimerization Conceals Its F-Box Protein Binding Site, Biochemistry 59, 1527-1536.

(28) Ortega, A., Amorós, D., and García de la Torre, J. (2011) Prediction of Hydrodynamic and Other Solution Properties of Rigid Proteins from Atomic- and Residue-Level Models, Biophysical Journal 101, 892-898.

(29) Small, E., Eggler, A., and Mesecar, A. D. (2010) Development of an efficient *E. coli* expression and purification system for a catalytically active, human Cullin3–RINGBox1 protein complex and elucidation of its quaternary structure with Keap1, Biochemical and Biophysical Research Communications 400, 471-475.

(30) Baptista, C. G., Lis, A., Deng, B., Gas-Pascual, E., Dittmar, A., Sigurdson, W., West, C. M., and Blader, I. J. (2019) *Toxoplasma* F-box protein 1 is required for daughter cell scaffold function during parasite replication, PLOS Pathogens 15, e1007946.

(31) Rahman, K., Mandalasi, M., Zhao, P., Sheikh, M. O., Taujale, R., Kim, H. W., van der Wel, H., Matta, K., Kannan, N., Glushka, J. N., Wells, L., and West, C. M. (2017) Characterization of a cytoplasmic glucosyltransferase that extends the core trisaccharide of the *Toxoplasma* Skp1 E3 ubiquitin ligase subunit, Journal of Biological Chemistry 292, 18644-18659.

(32) Hong, Y., Najafi, S., Casey, T., Shea, J.-E., Han, S.-I., and Hwang, D. S. (2022) Hydrophobicity of arginine leads to reentrant liquid-liquid phase separation behaviors of arginine-rich proteins, Nature Communications 13, 7326.

(33) Vernon, R. M., Chong, P. A., Tsang, B., Kim, T. H., Bah, A., Farber, P., Lin, H., and Forman-Kay, J. D. (2018) Pi-Pi contacts are an overlooked protein feature relevant to phase separation, eLife 7, e31486.

(34) Qamar, S., Wang, G., Randle, S. J., Ruggeri, F. S., Varela, J. A., Lin, J. Q., Phillips, E. C., Miyashita, A., Williams, D., Ströhl, F., Meadows, W., Ferry, R., Dardov, V. J., Tartaglia, G. G., Farrer, L. A., Kaminski Schierle, G. S., Kaminski, C. F., Holt, C. E., Fraser, P. E., Schmitt-Ulms, G., Klenerman, D., Knowles, T., Vendruscolo, M., and St George-Hyslop, P. (2018) FUS Phase Separation Is Modulated by a Molecular Chaperone and Methylation of Arginine Cation-π Interactions, Cell 173, 720-734.e715.

(35) Greig, J. A., Nguyen, T. A., Lee, M., Holehouse, A. S., Posey, A. E., Pappu, R. V., and Jedd, G. (2020) Arginine-Enriched Mixed-Charge Domains Provide Cohesion for Nuclear Speckle Condensation, Molecular Cell 77, 1237-1250.e1234.

(36) Schuster, B. S., Dignon, G. L., Tang, W. S., Kelley, F. M., Ranganath, A. K., Jahnke, C. N., Simpkins, A. G., Regy, R. M., Hammer, D. A., Good, M. C., and Mittal, J. (2020) Identifying sequence perturbations to an intrinsically disordered protein that determine its phase-separation behavior, Proceedings of the National Academy of Sciences 117, 11421-11431.

(37) Wang, J., Choi, J.-M., Holehouse, A. S., Lee, H. O., Zhang, X., Jahnel, M., Maharana, S., Lemaitre, R., Pozniakovsky, A., Drechsel, D., Poser, I., Pappu, R. V., Alberti, S., and Hyman, A. A. (2018) A Molecular Grammar Governing the Driving Forces for Phase Separation of Prion-like RNA Binding Proteins, Cell 174, 688-699.e616.

(38) Fisher, R. S., and Elbaum-Garfinkle, S. (2020) Tunable multiphase dynamics of arginine and lysine liquid condensates, Nature Communications 11, 4628.

(39) Tovar, C. N., and Odunuga, O. O. (2019) Size of Protein is a Major Factor that Affects Retention on Preparative IMAC Columns, The Protein Journal 38, 76-82.

(40) Mathur, R., Yen, J. L., and Kaiser, P. (2015) Skp1 Independent Function of Cdc53/Cul1 in F-box Protein Homeostasis, PLOS Genetics 11, e1005727.

(41) Melville, M. W., McClellan, A. J., Meyer, A. S., Darveau, A., and Frydman, J. (2003) The Hsp70 and TRiC/CCT Chaperone Systems Cooperate *In Vivo* To Assemble the Von Hippel-Lindau Tumor Suppressor Complex, Molecular and Cellular Biology 23, 3141-3151.

(42) Yam, A. Y., Xia, Y., Lin, H.-T. J., Burlingame, A., Gerstein, M., and Frydman, J. (2008) Defining the TRiC/CCT interactome links chaperonin function to stabilization of newly made proteins with complex topologies, Nature Structural & Molecular Biology 15, 1255-1262.

(43) Wang, R., Zhang, Y., Kieffer, M., Yu, H., Kepinski, S., and Estelle, M. (2016) HSP90 regulates temperature-dependent seedling growth in *Arabidopsis* by stabilizing the auxin co-receptor F-box protein TIR1, Nature Communications 7, 10269.

(44) Willhoft, O., Kerr, R., Patel, D., Zhang, W., Al-Jassar, C., Daviter, T., Millson, S. H., Thalassinos, K., and Vaughan, C. K. (2017) The crystal structure of the Sgt1-Skp1 complex: the link between Hsp90 and both SCF E3 ubiquitin ligases and kinetochores, Scientific Reports 7, 41626.

CHAPTER 5

CONCLUSIONS AND FUTURE DIRECTIONS

TgSkp1 Forms a Tight, Competitive Homodimer

In chapter 2, I describe the presence of a high affinity homodimer for Skp1 from *Toxoplasma gondii* **(Fig 2.3A)**. Previous studies into the Skp1 homodimer indicated a homodimerization K_d of 2.5 μM and 1.0 μM in *Dictyostelium discoideum* [1] and guinea pigs [2] respectively. Although interpreted as a monomer, human Skp1 also showed a sedimentation profile consistent with a dimer while in the low μM concentration range [3]. As opposed to studies where a micromolar affinity was determined for DdSkp1, our study failed to extensively dissociate the TgSkp1 homodimer even at a 300 nM concentration. Due to this, it was necessary to extrapolate the homodimer affinity of TgSkp1 by estimating the degree of dissociation at 300 nM. Sedimentation values for both the monomer (1.6) and dimer (2.7) species of other equal-length constructs were observable, and TgSkp1-FL had a homodimer sedimentation profile consistent with these values **(Table 2.1)**. Using a calculated ~18% dissociation at 300 nM based on these values and assuming non-cooperative binding, we estimated a homodimer K_d of ~50 nM for TgSkp1-FL. This strong homodimerization is unlikely to be an artifact of the construct or purification technique used, as indicated by the 2.9 μM affinity DdSkp1A-FL homodimer using the same protocol **(Fig 4.1A)**.

Skp1's C-terminal Region (CTR) contributes Subsite-B to the self-association interface, while Skp1's folded BTB domain contributes Subsite-A. Thus, the large difference in homodimer affinity between TgSkp1-ΔCTR **(Fig 2.4E)** and DdSkp1A-ΔCTR **(Fig 4.1C)** strongly suggests that Skp1's Subsite-A is at least partially responsible for the stronger TgSkp1-FL homodimer affinity. Within DdSkp1A, a C116V variant was predicted by a Rosetta screen to result in a stronger homodimer by contributing an expected -1 kCal/mol based on computational saturation mutagenesis [1]. This amino acid substitution is, in fact, present in the TgSkp1A protein giving a

potential explanation for this difference **(Fig 2.1E)**. The hypothesis that this amino acid substitution is partially responsible for changing Skp1 homodimerization can be easily tested. An isotherm of the appropriate variant in either TgSkp1 or DdSkp1A should yield a homodimer affinity more similar to that of the other protein. Sequence differences also exist with P94K, D107N, and K117A substitutions, though the effects of these variants are expected to be more negligible. Computational saturation mutagenesis in TgSkp1 can be leveraged to reinforce these predictions in *Toxoplasma*. Other potential explanations are less straightforward. Entropic effects have been observed to alter protein function [4, 5] including by changing the affinity for binding partners [5]. The potential for similar effects in Skp1 is exemplified by the identification of two additional intrinsically disordered regions in the free protein [3, 6, 7]. Skp1's major internal loop **(Fig 2.6B; unpublished data)** and Skp1's CTR **(Figs 2.4E, 4.1C)** have both been shown to influence Skp1 homodimerization. Although Skp1's CTR has been shown to engage in a fuzzy self-association **(Fig 2.8)**, the role for the internal loop remains unknown. The highly dynamic nature of Skp1's internal loop has been proposed to allow accommodation of a wider range of protein-protein interactions [3]. Computational modeling of full-length and Δloop variants through all-atom MD could prove useful in generating a model for how Skp1's internal loop influences homodimerization. Skp1's conformational ensemble can be analyzed for changes in internal structure. First, comparison of internal bond angles and packing can give hints to any stability change that can be expected between the variants. This can be paired with thermal melt experiments to measure the thermal stability of each variant. TgSkp1 variants have shown reversible folding behavior **(Fig 2.S4)** allowing for effective measurements of T_m. A computational Distance Variability Matrix analysis such as that done in **(Fig 3.3)** can also be used to measure changes in internal protein dynamics between variants. A comparison of MMGBSA calculations

between each group of simulations could also give hints as to how Skp1's internal loop influences binding interactions in Skp1's Subsite-A.

The interface of the Skp1 homodimer has been shown to overlap with that of the Skp1-FBP interface indicating a competitive interaction [1]. Effective competition of DdSkp1A's 2.5 μM K_d homodimer with FBP-Skp1 complexes is not expected given the comparatively tight Fbs1-Skp1 interaction of 25 nM [8]. This contrasts with the expected tight homodimer of TgSkp1 which has an estimated homodimer affinity just two-fold higher than that for the Fbs1-Skp1 complex. If FBP-Skp1 interactions exist in an affinity hierarchy such as that shown if **(Fig 1.6D)**, differential inhibition of FBP-Skp1 interactions can be expected based on the presence of the Skp1 homodimer. Future work which aims to define affinities for multiple endogenous FBP-Skp1 complexes may be able to probe the presence of such an affinity hierarchy.

The Skp1 Homodimer Contains a Two Component Interface.

The existence of a bipartite homodimer interface in Skp1 was confirmed in Chapter 2. Initial structural studies on the Skp1 homodimer previously revealed only the well-ordered portion of this interface (Subsite-A) [1]. The presence of a more expansive interface was suspected from inhibitory effects observed on Skp1's homodimer when Skp1 is glycosylated on its disordered CTR **(Fig 2.3)**. Deletion of Skp1's CTR was confirmed to play an inhibitory role on Skp1 homodimerization **(Fig 2.4E)**. Previous NMR data [6] and our CD analysis of TgSkp1-FL vs. TgSkp1-ΔCTR **(Fig 2.4B)** suggested that Skp1's CTR functioned to promote homodimerization while existing without stable secondary structure. We initially proposed that this was due to a length dependent entropic effect as has been observed by IDRs in the past [4]. The tighter homodimer affinities observed for TgSkp1-Scrambled5 **(Fig 2.5D)** and TgSkp1-Scrambled6 **(Fig**

2.5C) in comparison to TgSkp1-ΔCTR **(Fig 2.4E)** support this model. The inert nature of the TgSkp1-PolySer CTR, however, disproves it **(Fig 2.5E)**. The presence of charged residue patches in Skp1's CTR then lead us to pursue an alternative model. Patches of charged residues have been previously shown to facilitate transient yet productive contacts between disordered protein regions [9-12]. These interactions typically apply to the association of oppositely charged proteins; we however suspected that positioning of Skp1's CTRs proximal to a strong homodimer interface would allow association based on charge distribution alone. We turned to the TgSkp1-ΔLoop background to test this model given its more easily quantifiable homodimer **(Fig 2.6B)** and its ability to reproduce the effects of deleting Skp1's CTR **(Fig 2.6B,E)**. High salt conditions would be expected to disrupt electrostatic interactions such as those that allow association of charge patches. When Skp1's CTR is deleted, the effects of salt concentration on Skp1 homodimerization are minimal **(Fig 2.6E-F)**. This contrasts with the observation when Skp1's CTR is present where a 200 nM K_d homodimer is weakened to 8.5 μM **(Fig 2.6B-C)**. This is consistent with a model where charge patch associations drive the associative effects of Skp1's CTR.

All atom molecular dynamics simulations were then utilized to visualize the association of these charge patches. These simulations replicated the predicted Subsite-A observed in previous Skp1 homodimer studies **(Fig 2.7A)** [1]. It also showed a concentration of binding energy around a positively charged cluster in Skp1's CTR **(Fig 2.7A)**. There was a noticeable lack of energy association with the negatively charged patches. This is likely due to the net negative charge of the interface (twice as many negative as positive charges) and the reduced per-residue number of productive binding conformations as compared to the positively charged patch. Further breaking contributions into pairwise binding energies showed variable conformations of consistent association events between Skp1's positively charged patch and Skp1's various negatively charged

patches **(Figs 2.7B, 2.S15A, 2.S16A)**. Rapid kinetics were observed for these pairwise interactions **(Fig 2.S17)**, that may be related to what was observed in previous simulations of ProTα and H1 phase separation events [13]. Similar electrostatic interaction networks were also observed **(Figs 2.7C, 2.S15B, 2.S16B)** which dynamically interchanged with each other **(Fig 2.S17)**, similar to the previously mentioned phase separation events [13]. This behavior is interesting as it allows us to visualize Skp1's fuzzy interaction as a microscale phase separation event. The action of solvent shielding modeled through the particle-Mesh Ewald algorithm likely allows these charge patch interactions to dominate despite the net negative charge of the interface [14]. Productive electrostatic contacts were also augmented by transient hydrophobic contacts which became favorable due to the restrained peptide backbone motions **(Figs 2.7D, 2.S15C, 2.S16C)**. This behavior mimics that described for other phase separation events where residues near to primary contacts contribute to auxiliary interactions [15]. In addition to CTR-CTR interactions described here, contributions of CTR-BTB contacts are suspected **(Table 2.3)**. Overall, our MD simulations effectively modeled the association of each Skp1 CTR into a fuzzy interface.

Our studies show the utility of MD simulations in modeling the behavior of Skp1's fuzzy Subsite-B. Future studies could seek to leverage this tool to more finely probe the productive contributions that form Skp1's Subsite-B. MD simulations of different scrambled variants may offer insights into how charge distribution influences CTR self-association. MMGBSA analysis of these simulations would be expected to show a concentration of binding energy around positively charged patches of residues. It is likely that Skp1's positive charge patch is finely balanced with the presence of negatively charged residue patches. By quantifying the association of these patches, we can identify patterns in which negative charge patches are most actively associated with the positive charge patch in Skp1's CTR. This may be aided through the use of accelerated

MD or the use of a larger number of long simulations. The concentration of energy around Skp1's positive charge patch suggests that this patch is vital for forming Skp1's fuzzy interface **(Fig 2.7A)**. This is supported by the presence of paired positively charged residues in the tight TgSkp1-Scrambled6 homodimer **(Fig 2.5B)**. By swapping the position of a positively charged residue in this patch with a neutral or negative residue elsewhere in Skp1's CTR, the importance of this patch can be investigated. A positional swap between two residues on Skp1's CTR would be more appropriate than a simple Arg to Ala or Ser mutation. This would maintain the net charge of Skp1's CTR allowing results to be based on charge distribution rather than net charge effects. A swap such as this would be expected to severely weaken or possibly ablate the formation of Skp1's fuzzy interface. This process can be repeated with Skp1's other scrambled variants to support these results. Simulations using versions of Skp1's CTR where its non-charged residues are mutated may allow us to investigate the role of auxiliary hydrophobic contacts in stabilizing Skp1's fuzzy interface. Ser residues are expected to be relatively inert within Skp1's CTR based on **(Fig 2.5E)**. By mutating all non-charged residues to Ser, the role of these auxiliary contacts can be investigated. This approach can be even more finely tuned by only mutating residues in proximity to the CTR's positively charged patch. MD simulations can be paired with sedimentation velocity isotherms where we would directly measure the influence of each variant on homodimerization. This would allow validation of computational results through experimental means.

The presence of Skp1's fuzzy Subsite-B is important for several reasons. First, it offers a potential mechanism to allow Skp1's modification enzymes to access Skp1's CTR to allow for glycosylation despite TgSkp1's high affinity homodimer. This is supported by evidence that fuzzy protein interfaces are more accessible to enzymes which confer post translational modifications as compared to well-ordered interfaces [10, 16-18]. This interface may also allow for the more ready

exchange with FBPs, an activity that may be aided via a Gat1 exchange factor **(Fig 3.6A)**. Once incorporated into FBPs, the reverse kinetics of this interaction are expected to be slow (unpublished data) and thereby promote the stability of this complex. Another important implication of Skp1's Subsite-B is the potential it opens in understanding other protein-protein interactions. Until now, electrostatically mediated fuzzy protein interactions were understood to be facilitated by net opposite charges with minor contributions from charge distribution. This paradigm is embodied by the fuzzy association of ProTα and H1 [16]. Here, we have demonstrated that in some cases, charge distribution alone can mediate fuzzy protein association, even among identically charged proteins. By understanding the properties that allow this to happen, the presence of similar interactions can be predicted for other protein complexes.

Glycosylation Disrupts Skp1's Subsite-B in *Toxoplasma* Skp1.

As shown in **(Fig 2.3)**, glycosylation weakens the TgSkp1 homodimer. Given the location of Skp1's glycan on P154 of its CTR, the simplest explanation is that glycosylation disrupts Skp1's fuzzy Subsite-B. This is currently thought to happen through a disorder to order transition within Skp1's CTR, in part because of the intrinsic order of the glycan itself [6]. By favoring the formation of a more well organized CTR, it is expected that conformations which allow transient electrostatic contacts in Subsite-B will be disfavored. This expected disorder to order transition can be investigated computationally through MD simulations. The glycan's effects on the conformational stability of Skp1's CTR can be investigated through several means. First, the conformational dynamics of a folded Skp1 CTR can be measured in the presence or absence of Skp1's glycan. This would be similar to approaches already taken in simulations of monomeric Skp1 [19, 20], but would be run for longer periods of time (1 μs). Specifically, we would focus on the mobility of the

region from the start of helix 7 to the end of helix 8 using methods used in **(Fig 3.3)**. According to the current model, Skp1's glycan would be expected to reduce the mobility of this region of the protein as compared to unmodified Skp1. The formation and dissolution of alpha helices can also be examined using distances between hydrogen-bond forming backbone atoms. In addition to P154 in TgSkp1, Skp1's CTR also appears to contain a degenerate E-R/K helix motif at the N-terminus of helix 8 **(Fig 2.1E)** [21-24]. The conformational restraining effects of P154 and glycosylation may work with the degenerate E-R/K helix motif to promote the disorder to order transition in Skp1's CTR. Helical content and conformational flexibility in variants lacking Pro154, the E-R/K helix motif, and glycosylation can be compared. Additionally, a more canonical E-R/K helix motif can be simulated to determine effect on helical content and conformational flexibility. These studies can be combined with circular dichroism (CD) experiments on Skp1's CTR. A single Met residue near the N-terminus of Skp1's CTR should allow for the generation of free Skp1 CTR peptides **(Fig 2.1E)** using CnBr. Previous CD experiments showed changes in secondary structure upon glycosylation [25]. By limiting this analysis to Skp1's CTR, we can be sure that any secondary structural changes between unmodified and glycosylated Skp1 are due to Skp1's CTR alone. Despite previous gel filtration studies that indicated glycosylated Skp1 forms a weaker homodimer [25], sedimentation velocity analysis suggests that there is a minimal change in homodimerization upon glycosylation of DdSkp1A **(Fig 4.1A-B)**. This is in spite of a DdSkp1A-ΔCTR variant supporting the existence of Subsite-B in DdSkp1A **(Fig 4.1C)**. An explanation of this effect awaits further understanding of how glycosylation weakens Subsite-B in *Toxoplasma*.

Stoichiometry of the Gat1:Skp1 Complex is Dictated by Skp1 Glycosylation.

Gat1, the terminal glycosyltransferase for the Skp1 glycan, has been shown to interact with Skp1 *in vivo* **(Fig 3.1D)** [26] and directly *in vitro* **(Fig 3.1E)**. Sedimentation velocity analysis of this interaction at more physiological concentrations indicates that TgSkp1-FL forms a 2:1 Gat1:Skp1 complex **(Fig 3.2A)**. This contrasts with the 2:2 Gat1:Skp1 complex observed for Gly-TgSkp1-FL **(Fig 3.2C)**. In addition, modeling the apparent affinities of each interaction suggests that TgSkp1-FL binds Gat1 at a higher affinity than Gly-TgSkp1-FL **(Fig 3.2B,D)**. This is consistent with TgSkp1-FL forming a more extensive interface with Gat1 than Gly-TgSkp1-FL. This larger interface likely excludes the binding of another Skp1 subunit to Gat1 in the case of TgSkp1-FL. This hypothetical interface is then likely disrupted by glycosylation to allow the formation of a 2:2 Gat1:Skp1 complex. This conclusion is reinforced by the 2:2 Gat1:Skp1 complex formed by the TgSkp1-ΔCTR variant **(Fig 3.2E)**. This indicates that a lectin based binding effect with Gly-TgSkp1-FL is unlikely the reason for the glycosylation dependent shift in Gat1:Skp1 stoichiometry. The TgSkp1-ΔCTR variant has been modeled to form a complex with Gat1 of similar affinity to the TgSkp1-FL variant **(Fig 3.2B,F)**. This effect is not satisfactorily explained by the model but may be the result of reduced excluded volume effects from Skp1's disordered CTR. Skp1's CTR is highly mobile in simulations of the 2:1 Gat1:Skp1 complex **(Fig 3.3)** offering a potential mechanism to generate excluded volume effects. These effects may be compensated for in TgSkp1-FL via transient electrostatic contacts between charge patches on Skp1 and Gat1 **(Fig 3.5)**.

The Gat1:Skp1 Complex Consists of a Core Hydrophobic Interface Augmented by Transient Electrostatic Contacts.

Computational modeling of the 2:1 Gat1:Skp1 complex using AlphaFold3 results in a high scoring placement of TgSkp1 onto a single subunit of the Gat1 homodimer. This occurs in such a way that the acceptor tetrasaccharide would be accessible to the active site **(Fig 3.3B)**. MMGBSA analysis of downstream MD simulations identifies a patch of hydrophobic residues on Gat1 responsible for forming the core interface with Skp1 **(Figs 3.4B, 3.5D)**. This is complemented by a hydrophobic interface on TgSkp1 which utilizes Skp1 residues of the homodimer Subsite-A, FBP binding Subsite-1, and Cullin1 binding interface **(Figs 3.4A, 3.5D)**. This interface architecture explains how a 2:1 Gat1:Skp1 complex can form despite Skp1 existing at concentrations orders of magnitude above its expected homodimer K_d. This and peripheral Gat1-Skp1 interactions are expected to burry approximately 3180-3380 Å2 of solvent accessible surface area. The overlapping Skp1 homodimer and Gat1-Skp1 interfaces on the Skp1 protein would be expected to introduce confounding variables in measuring Gat1-Skp1 association. Given this, we opted to design point mutations targeting Gat1 instead. Computational saturation mutagenesis of important Gat1 interface residues identified several point mutations that would be expected to weaken the Gat1-Skp1 interface while preventing destabilization of Gat1 itself **(Fig 3.4C-E)**. These Y18K and A51K point mutations severely hamper AlphaFold3's ability to predict the Gat1-Skp1 interface **(Fig 3.4F-H)**. Work is currently underway to generate these point mutations in Gat1. Upon successful generation of these variants, proper folding will be checked via sedimentation velocity analysis. Gat1 forms a tight homodimer involving a separate surface to Skp1 binding with a distinct sedimentation profile **(Fig 3.1E)**. A properly folded Gat1 protein should be able to successfully form this homodimer resulting in a matching sedimentation profile. Misfolding of the Gat1 protein

will be indicated by a slower sedimentation profile indicative of several possibilities. The first is that Gat1 is no longer capable of forming its tight homodimer due to an inability to properly fold this portion of the protein. The second possibility is that water has begun to invade the hydrophobic core of Gat1 resulting in its expansion and slower sedimentation profile. Either possibility will render its respective Gat1 variant unsuitable for Skp1 binding studies. The experiments conducted in **(Fig 3.2)** will then be utilized to determine if each Gat1 variant can bind Skp1, and if so, identify the apparent affinities of each interaction. An inability for either Gat1 variant to bind Skp1 despite proper folding will support the computational model generated by AlphaFold3 and refined through MD.

MD analysis also indicates that the core hydrophobic interface of the Gat1-Skp1 complex is supplemented by transient electrostatic contacts. Examples of these contacts are shown in **(Fig 3.5)** while **(Fig 3.S18)** indicates that these contacts occur at high frequency. The ability to form these contacts despite the highly mobile nature of Skp1's CTR **(Fig 3.3H)** is reminiscent of contacts made by Skp1's Subsite-B. In these simulations, charge patch interactions are mediated by both Skp1's CTR **(Fig 3.5B,C,F)** and Gat1's internal loop **(Fig 3.5H)**. Either highly mobile region associates largely with the folded portion of their binding partner, but interactions also occur between a disordered internal loop of Gat1 and the Skp1 CTR **(Fig 3.S18)**. Importantly, some conformations of Skp1's CTR would be expected to inhibit binding of a second Skp1 binding partner **(Fig 3.5A)**. These auxiliary interactions would, therefore, be expected to explain the strict 2:1 Gat1:Skp1 complex. A disorder to order transition upon Skp1 glycosylation would be expected to disrupt these transient electrostatic contacts. As can be seen in **(Fig 3.S18)**, starting a simulation with a pre-folded Skp1 CTR results in an approximately 2-fold decrease in the number of productive electrostatic contacts. It is plausible that stabilizing Skp1's CTR in an ordered state

would further inhibit formation of these contacts. This may explain the reduction in apparent binding affinity for TgSkp1 upon its glycosylation **(Fig 3.2B,D)**. Simulations of the Gat1-Skp1 complex could be used to compare stability of the folded Skp1 CTR state when Skp1 is glycosylated or unmodified. The frequency of productive electrostatic contacts can also be examined between glycosylated and unmodified models. Given the findings in **(Fig 3.S18)**, it is expected that glycosylated Skp1 would result in an increased stability for Skp1s folded CTR accompanied by a decrease in productive electrostatic contacts. Scrambled Skp1 variants can also be leveraged to investigate the nature of Skp1's CTR in the Gat1-Skp1 complex. For example, the TgSkp1-Scrambled6 variant was able to effectively reconstitute Skp1's Subsite-B **(Fig 2.5C)**. Given that similar interactions are expected in the Gat1-Skp1 complex, successfully forming a 2:1 Gat1:Skp1 complex would support the existence of a fuzzy component in this complex. Additionally, the contributions of Gat1's internal loop can be investigated via substitution of residues in its charge patches. Overall, the Gat1-Skp1 complex represents yet another instance of the adaptability of Skp1 in forming a wide range of protein-protein contacts. This instance bears some similarities with the evidence that the terminal glycosyltransferase for DdSkp1, which is an unrelated enzyme, also modulates Skp1 activity via physical association regardless of its glycosylation status [27].

Gat1 Acts as a Skp1 Exchange factor in a CTR Dependent Manner.

Substoichiometric concentrations of Gat1 were observed to promote dissociation of the tight TgSkp1-FL homodimer **(Fig 3.6A)**. A similar but less pronounced effect appears for Gly-TgSkp1-FL **(Fig 3.6B)**. This effect may indicate a moonlighting function for Gat1 as a Skp1 exchange factor **(Fig 3.7C)**. In this model, Gat1 acts to promote association of Skp1 with various

FBPs under hypoxic conditions, which may buffer the competitive effects of the tight Skp1 homodimer under hypoxic conditions. Binding isotherms such as the one depicted in **(Fig 3.7D)** can be generated for TgSkp1-FL and Gly-TgSkp1-FL to quantify the dissociative effects of Gat1 on the Skp1 homodimer. This can be complemented by experiments involving FBPs. According to the exchange factor model, Gat1 would be expected to promote a more rapid association of Skp1 with its respective FBPs. Once binding conditions have been optimized, TgFbxO13 **(Fig 4.3G)** or TgFbxO14 **(Fig 4.3F)** can be used for kinetic binding experiments. SPR or Stopped-flow experiments can then be used to confirm changes in the k_{on} for Skp1-FBP interactions in varying ratios of Gat1 and Skp1. Increased k_{on} rates in the presence of Gat1 would confirm Gat1's role as an exchange factor to promote FBP-Skp1 complex formation.

Interestingly, Gat1's exchange factor effect appears to depend on Skp1's CTR **(Fig 3.7D)**. This may indicate that Gat1 acts by utilizing Skp1's fuzzy Subsite-B to promote exchange of the Skp1 homodimer. This hypothesis could be tested through the use of TgSkp1-Scrambled6 or TgSkp1-Scrambled5 variants. Both variants reconstitute Skp1's Subsite-B to varying degrees **(Fig 2.5C-D)**. If Gat1 is able to utilize these heavily altered Skp1 CTRs to promote exchange of the Skp1 homodimer, it would offer strong support for our model. Such a model would be in line with previously characterized fuzzy interfaces which can readily facilitate post translational modifications or exchange between binding partners [10, 16-18]. This would offer yet another example of how Skp1's fuzzy Subsite-B can leverage the properties of fuzzy protein interfaces for functional roles in an identically charged homodimer.

***Dictyostelium* Skp1 Homodimerization Presents Fewer Confounding Variables in Measuring Glycosylation's Effects on the Skp1-FBP interface.**

TgSkp1 forms a very tight homodimer which is significantly weakened upon glycosylation **(Fig 2.3)**. This offers a facile mechanism for the role of glycosylation in regulating Skp1-FBP interactions. This does, however, introduce several confounding variables when investigating the role of glycosylation in influencing the FBP-Skp1 interface itself. The first is that its high affinity self-association would be expected to compete with Skp1's association with FBPs. If the presence of an affinity hierarchy of FBPs is assumed, some weaker affinity FBP-Skp1 interactions could be significantly inhibited. A second confounding variable is the large change in homodimer affinity upon Skp1 glycosylation. This makes direct comparison of apparent binding affinities between FBP-Skp1 interactions in different glycostates more difficult. Although both problems can be addressed using the competitive binding model, this is less ideal when probing unknown effects on a protein-protein interface. Both confounding variables appear to be less prominent in DdSkp1A **(Fig 4.1A-B)**. DdSkp1 forms a micromolar affinity homodimer which appears to have minimal differences in homodimerization upon glycosylation. This is despite deletion of DdSkp1A's CTR also supporting the existence of Subsite-B in *Dictyostelium* **(Fig 4.1C)**. This information also strongly suggests that glycosylation alters FBP-Skp1 association through a mechanism other than controlling homodimerization in *Dictyostelium*. Our current models suggest that glycosylation promotes a conformational ensemble in Skp1's CTR making it more favorable for FBP binding [6, 19, 20, 25].

Soluble SCF Constructs Can be Expressed and Purified from *E. coli*.

FBPs have expressed well in *E. coli* when co-expressed with Skp1, however, we have only successfully generated GlcNAc-Skp1 by co-expressing PhyA and Gnt1. We have been unable to extend the glycan by attempted co-expression of PgtA or by *ex vivo* extension of the glycan when Skp1 is complexed with an FBP. Therefore, we will attempt to assemble FBP:Gly-Skp1 subcomplexes *in vitro*. Purification of soluble FBPs also leaves open the possibility of direct binding studies. To this end in chapter 4, I describe a relatively high-throughput protocol for generating soluble FBP constructs as outlined in **(Fig 4.2A)**. This protocol was applied to a series of FBPs which were expected to have similar (Group 1) and differential (Group 2) binding to Skp1 based on its glycostate **(Fig 4.2B)**. As can be seen in solubility screens, this protocol was able to effectively generate an FBP library consisting of both Group 1 and 2 FBPs **(Fig 4.2D)**. Given the high degree of apparent breakdown and contamination with *E. coli* proteins, we subsequently incorporated a backbone allowing insertion of a C-terminal SF-tag as seen in **(Fig 4.2C)**. As shown in **(Fig 4.3)**, a two-step affinity purification leveraging both the N-terminal His-tag and C-terminal Twin-Strep tag was effective in isolating full-length constructs from a heterogeneous mixture. Given the success of TgCul1 solubility screens **(Fig 4.S5)**, a similar approach is expected to be successful in purifying His-tagged TgCul1 stably associated with SF-tagged TgRbx1. TgRbx1 associates with the C-terminal domain of Cul1 distal from its His-tagged N-terminus. The successful purification of TgFBPs **(Fig 4.3F-G)** also indicates that this protocol is effective in both *Dictyostelium* and *Toxoplasma* systems. If greater yields of a particular FBP become necessary, a more stringent expression and solubility screening regime can be implemented.

Future Directions in Studying the Skp1-FBP Interface.

The first necessary step will be the optimization of conditions to allow Skp1-FBP binding. As demonstrated in **(Fig 4.S10)**, although FBPs can be effectively purified and captured in pulldown experiments, binding to Skp1 is minimal. This is despite coexpression of Skp1 with various FBPs in *E. coli* resulting in the copurification of Skp1 with the associated FBPs [28](Deng, B. (2020) M.S. thesis, unpublished data). This lack of *in vitro* binding may be due to several factors. The first factor could be the concentration of FBP utilized. If DdJcdI-Short-H319A forms a significantly weaker complex than the 25 nM K_d observed between Fbs1 and Skp1, the 40 nM concentration used in the pulldown may be too low. An easy approach to test this would be to increase the concentration of the FBP. An alternative and potentially more likely explanation is that the relevant F-Box domains fail to properly fold in solution despite the presence of their Skp1 binding partner. A somewhat related explanation is that chaperone action is required for FBP-Skp1 associations. This explanation is supported by evidence that chaperones play a vital role in the assembly of various E3 ubiquitin ligases [29-33]. To address this, cytosolic lysates from *Dictyostelium* and *E. coli* can be added to solutions containing FBPs and Skp1 and supplemented with ATP to promote chaperone activity. *Dictyostelium* lysates would contain native chaperones to facilitate FBP-Skp1 association. Coexpression of FBPs and Skp1 in *E. coli* allows the successful formation of FBP-Skp1 complexes (unpublished data). This indicates that *E. coli* lysates may be successfully used to promote association of FBPs with Skp1. *E. coli* lysates would have the advantage of lacking other SCF components including Skp1 that may further add confounding factors to binding studies. If lysates can effectively allow association of FBPs with Skp1, fluorescence-based techniques may be utilized to allow characterization of these interactions in a complex solution. Although less ideal than using a defined solution, the ability to quantify binding

of FBPs to Skp1 would be a large advancement from current biochemical tools. Microscale thermophoresis offers one potential method for characterizing these interactions. This method utilizes a very small quantity of protein and can be performed in very complex solutions. Skp1 constructs which have been N-terminally tagged with the far-red fluorescent protein mCardinal have already been generated (unpublished data). This far-red fluorescent protein would allow detection via the pico-red laser in an MST instrument while minimizing background fluorescence common for lower wavelengths in complex solutions. If chaperone activity proves to be necessary for FBP-Skp1 complex formation, this may offer an alternative method of regulating Skp1's FBP binding repertoire. In this case, glycosylation might influence the Skp1-chaperone complex in such a way as to selectively influence association with certain FBPs. This hypothetical model, however, remains highly speculative.

The FBP sequences in our current library could be utilized in transient overexpression plasmids in their native environment. A pDM320 transient overexpression plasmid containing a StrepII-tag has proven useful in obtaining milligram quantities of highly purified DdPgtA from *Dictyostelium* (unpublished data). This precedent suggests that homogenous samples of FBPs can be purified from their native organism. Additionally, using *phyA*- and wild type strains, FBPs can be purified with Skp1 in the unmodified and fully glycosylated states respectively. Given that glycosylated Skp1 represents the majority (>95%) of Skp1 in *Dictyostelium* at 21% oxygen [34, 35], these purifications can be expected to be homogenous. This would allow structural characterization via single particle cryo-EM. Structural determination can be aided by using TgCul1 to complete the horseshoe shaped SCF complex. Even using the smallest FBP in our library (DdFbxF), this would result in a ~190 kDa complex. The FBPs DdFbxA, DdFbxD,

DdJcdH, DdJcdI, and DdFbxN represent the likely most important targets for this study due to their previous characterization in *Dictyostelium* and Skp1's interactome.

Another major use of FBPs would be the identification of FBP substrates. These substrates have been difficult to detect using traditional co-immunoprecipitation studies from extracts [26, 36], or by modifying FBPs with Ub-binding domains to trap substrates (unpublished datda). One approach to do this would be to use purified FBPs in pulldown experiments with *Dictyostelium* lysates. Given the high degree of reliance on factors such as post translational modifications discussed in Chapter 1, various conditions would be necessary to effectively screen for substrates. Another approach to this problem could be the use of BioID [37] which biotinylates proteins within 10 nm of the fusion protein [38]. These approaches will benefit from the use of proteasome inhibitors to prevent degradation of the target proteins. The purification of FBPs and Cul1, the identification of FBP substrates, and obtaining commercially available ubiquitin charged E2 enzymes may eventually allow the reconstitution of the SCF complex. This would allow direct measurements of Skp1 glycosylation's effects on SCF activity.

Significance of the Dissertation

In this dissertation, I have characterized the role of glycosylation in regulating several of Skp1's protein-protein interactions. This has not only allowed us to build a novel model for how glycosylation regulates Skp1's interactome but also aided in our understanding of protein-protein interactions as a whole. I have demonstrated that glycosylation disrupts the contribution of Skp1's C-terminal region (CTR) to homodimerization. Through further characterization of Skp1's CTR, I have determined that it forms a fuzzy protein interface (Subsite-B) which complements the previously characterized ordered homodimer interface (Subsite-A). This is particularly significant,

as the preexisting paradigm for electrostatically mediated fuzzy protein interactions was that they are primarily mediated by net opposite charges separately presented by each partner. By demonstrating an electrostatically mediated fuzzy protein interface within a homodimer, I have demonstrated that charge distribution alone can facilitate fuzzy protein interactions. I have also proposed a facile mechanism for how glycosylation can control Skp1's F-Box protein (FBP) binding repertoire in *Toxoplasma*. In this model, glycosylation disrupts Subsite-B of Skp1's homodimer, weakening it from a strong, competitive homodimer to a relatively weak homodimer. This reduces the strength of a major competitive interaction with FBPs allowing greater binding of FBPs to Skp1, especially those with relatively weak FBP-Skp1 interactions. Comparative studies with Skp1 from a highly divergent protist, *Dictyostelium*, indicate that the contribution of the CTR is subject to substantial evolutionary tuning. Additionally, I have identified a potential moonlighting function for the Skp1 glycosyltransferase Gat1 which intersects with this mechanism. Here, I demonstrate that Gat1 forms a complex with Skp1 whose stoichiometry is dictated by Skp1's glycostate. Through computational modeling, I have identified a core hydrophobic interface which is augmented by transient protein interactions similar to those identified in Skp1's Subsite-B. These interactions are likely to dictate complex stoichiometry as well as allow Gat1 to act as a Skp1 exchange factor. This may offer an alternative mechanism by which the high affinity Skp1 homodimer exchanges with and binds to FBPs. Finally, I developed a system whereby we obtained a library of soluble FBPs. This system includes a relatively high throughput method to build, test the solubility of, and purify recombinant FBPs despite apparent proteolysis and the presence of *E. coli* proteins. The work done in this dissertation expands our understanding of protein-protein interactions and allows us to more effectively investigate the roles of glycosylation in controlling Skp1's interactome.

REFERENCES

(1) Kim, H. W., Eletsky, A., Gonzalez, K. J., van der Wel, H., Strauch, E.-M., Prestegard, J. H., and West, C. M. (2020) Skp1 Dimerization Conceals Its F-Box Protein Binding Site, Biochemistry 59, 1527-1536.

(2) Henzl, M. T., Thalmann, I., and Thalmann, R. (1998) OCP2 exists as a dimer in the organ of Corti, Hearing Research 126, 37-46.

(3) Bhattacharya, A., Shukla, V. K., Kachariya, N., Preeti, Sehrawat, P., and Kumar, A. (2022) Disorder in the Human Skp1 Structure is the Key to its Adaptability to Bind Many Different Proteins in the SCF Complex Assembly, Journal of Molecular Biology 434, 167830.

(4) Keul, N. D., Oruganty, K., Schaper Bergman, E. T., Beattie, N. R., McDonald, W. E., Kadirvelraj, R., Gross, M. L., Phillips, R. S., Harvey, S. C., and Wood, Z. A. (2018) The entropic force generated by intrinsically disordered segments tunes protein function, Nature 563, 584-588.

(5) Tzeng, S.-R., and Kalodimos, C. G. (2012) Protein activity regulation by conformational entropy, Nature 488, 236-240.

(6) Xu, X., Eletsky, A., Sheikh, M. O., Prestegard, J. H., and West, C. M. (2018) Glycosylation Promotes the Random Coil to Helix Transition in a Region of a Protist Skp1 Associated with F-Box Binding, Biochemistry 57, 511-515.

(7) Schulman, B. A., Carrano, A. C., Jeffrey, P. D., Bowen, Z., Kinnucan, E. R. E., Finnin, M. S., Elledge, S. J., Harper, J. W., Pagano, M., and Pavletich, N. P. (2000) Insights into SCF ubiquitin ligases from the structure of the Skp1–Skp2 complex, Nature 408, 381-386.

(8) Tan, A., Tanner, J. J., and Henzl, M. T. (2008) Energetics of OCP1–OCP2 complex formation, Biophysical Chemistry 134, 64-71.

(9) Hazra, M. K., and Levy, Y. (2020) Charge pattern affects the structure and dynamics of polyampholyte condensates, Physical Chemistry Chemical Physics 22, 19368-19375.

(10) Sottini, A., Borgia, A., Borgia, M. B., Bugge, K., Nettels, D., Chowdhury, A., Heidarsson, P. O., Zosel, F., Best, R. B., Kragelund, B. B., and Schuler, B. (2020) Polyelectrolyte interactions enable rapid association and dissociation in high-affinity disordered protein complexes, Nature Communications 11, 5736.

(11) Hazra, M. K., and Levy, Y. (2021) Biophysics of Phase Separation of Disordered Proteins Is Governed by Balance between Short- And Long-Range Interactions, The Journal of Physical Chemistry B 125, 2202-2211.

(12) Yamazaki, H., Takagi, M., Kosako, H., Hirano, T., and Yoshimura, S. H. (2022) Cell cycle-specific phase separation regulated by protein charge blockiness, Nature Cell Biology 24, 625-632.

(13) Galvanetto, N., Ivanović, M. T., Chowdhury, A., Sottini, A., Nüesch, M. F., Nettels, D., Best, R. B., and Schuler, B. (2023) Extreme dynamics in a biomolecular condensate, Nature 619, 876-883.

(14) Darden, T., York, D., and Pedersen, L. (1993) Particle mesh Ewald: An N·log(N) method for Ewald sums in large systems, The Journal of Chemical Physics 98, 10089-10092.

(15) Holehouse, A. S., and Kragelund, B. B. (2024) The molecular basis for cellular function of intrinsically disordered protein regions, Nature Reviews Molecular Cell Biology 25, 187-211.

(16) Borgia, A., Borgia, M. B., Bugge, K., Kissling, V. M., Heidarsson, P. O., Fernandes, C. B., Sottini, A., Soranno, A., Buholzer, K. J., Nettels, D., Kragelund, B. B., Best, R. B., and Schuler, B. (2018) Extreme disorder in an ultrahigh-affinity protein complex, Nature 555, 61-66.

(17) Heidarsson, P. O., Mercadante, D., Sottini, A., Nettels, D., Borgia, M. B., Borgia, A., Kilic, S., Fierz, B., Best, R. B., and Schuler, B. (2022) Release of linker histone from the nucleosome driven by polyelectrolyte competition with a disordered protein, Nature Chemistry 14, 224-231.

(18) Williamson, M. P. (2023) Protein Binding: A Fuzzy Concept, Life (Basel), 10(4), 855.

(19) Sheikh, M. O., Thieker, D., Chalmers, G., Schafer, C. M., Ishihara, M., Azadi, P., Woods, R. J., Glushka, J. N., Bendiak, B., Prestegard, J. H., and West, C. M. (2017) O_2 sensing–associated glycosylation exposes the F-box–combining site of the *Dictyostelium* Skp1 subunit in E3 ubiquitin ligases, Journal of Biological Chemistry 292, 18897-18915.

(20) Mandalasi, M., Kim, H. W., Thieker, D., Sheikh, M. O., Gas-Pascual, E., Rahman, K., Zhao, P., Daniel, N. G., van der Wel, H., Ichikawa, H. T., Glushka, J. N., Wells, L., Woods, R. J., Wood, Z. A., and West, C. M. (2020) A terminal α3-galactose modification regulates an E3 ubiquitin ligase subunit in *Toxoplasma gondii*, Journal of Biological Chemistry 295, 9223-9243.

(21) Swanson, C. J., and Sivaramakrishnan, S. (2014) Harnessing the Unique Structural Properties of Isolated α-Helices, Journal of Biological Chemistry 289, 25460-25467.

(22) Sivaramakrishnan, S., Spink, B. J., Sim, A. Y. L., Doniach, S., and Spudich, J. A. (2008) Dynamic charge interactions create surprising rigidity in the ER/K α-helical protein motif, Proceedings of the National Academy of Sciences 105, 13356-13361.

(23) Sommese, R. F., Sivaramakrishnan, S., Baldwin, R. L., and Spudich, J. A. (2010) Helicity of short E-R/K peptides, Protein Science 19, 2001-2005.

(24) Baker, E. G., Bartlett, G. J., Crump, M. P., Sessions, R. B., Linden, N., Faul, C. F. J., and Woolfson, D. N. (2015) Local and macroscopic electrostatic interactions in single α-helices, Nature Chemical Biology 11, 221-228.

(25) Sheikh, M. O., Schafer, C. M., Powell, J. T., Rodgers, K. K., Mooers, B. H. M., and West, C. M. (2014) Glycosylation of Skp1 Affects Its Conformation and Promotes Binding to a Model F-Box Protein, Biochemistry 53, 1657-1669.

(26) Mandalasi, M. N., Gas-Pascual, E., Baptista, C. G., Deng, B., Wel, H. v. d., Kruijtzer, J. A. W., Boons, G.-J., Blader, I. J., and West, C. M. (2024) Oxygen-dependent regulation of F-box proteins in *Toxoplasma gondii* is mediated by Skp1 glycosylation, Journal of Biological Chemistry 300(11), 107801.

(27) Schafer, C. M., Sheikh, M. O., Zhang, D., and West, C. M. (2014) Novel Regulation of Skp1 by the *Dictyostelium* AgtA α-Galactosyltransferase Involves the Skp1-binding Activity of Its WD40 Repeat Domain, Journal of Biological Chemistry 289, 9076-9088.

(28) van der Wel, H., Johnson, J. M., Xu, Y., Karunaratne, C. V., Wilson, K. D., Vohra, Y., Boons, G.-J., Taylor, C. M., Bendiak, B., and West, C. M. (2011) Requirements for Skp1 Processing by Cytosolic Prolyl 4(trans)-Hydroxylase and α-N-Acetylglucosaminyltransferase Enzymes Involved in O_2 Signaling in *Dictyostelium*, Biochemistry 50, 1700-1713.

(29) Mathur, R., Yen, J. L., and Kaiser, P. (2015) Skp1 Independent Function of Cdc53/Cul1 in F-box Protein Homeostasis, PLOS Genetics 11, e1005727.

(30) Melville, M. W., McClellan, A. J., Meyer, A. S., Darveau, A., and Frydman, J. (2003) The Hsp70 and TRiC/CCT Chaperone Systems Cooperate *In Vivo* To Assemble the Von Hippel-Lindau Tumor Suppressor Complex, Molecular and Cellular Biology 23, 3141-3151.

(31) Yam, A. Y., Xia, Y., Lin, H.-T. J., Burlingame, A., Gerstein, M., and Frydman, J. (2008) Defining the TRiC/CCT interactome links chaperonin function to stabilization of newly made proteins with complex topologies, Nature Structural & Molecular Biology 15, 1255-1262.

(32) Wang, R., Zhang, Y., Kieffer, M., Yu, H., Kepinski, S., and Estelle, M. (2016) HSP90 regulates temperature-dependent seedling growth in *Arabidopsis* by stabilizing the auxin co-receptor F-box protein TIR1, Nature Communications 7, 10269.

(33) Willhoft, O., Kerr, R., Patel, D., Zhang, W., Al-Jassar, C., Daviter, T., Millson, S. H., Thalassinos, K., and Vaughan, C. K. (2017) The crystal structure of the Sgt1-Skp1 complex: the link between Hsp90 and both SCF E3 ubiquitin ligases and kinetochores, Scientific Reports 7, 41626.

(34) Sassi, S., Sweetinburgh, M., Erogul, J., Zhang, P., Teng-umnuay, P., and West, C. M. (2001) Analysis of Skp1 glycosylation and nuclear enrichment in *Dictyostelium*, Glycobiology 11, 283-295.

(35) Xu, Y., Wang, Z. A., Green, R. S., and West, C. M. (2012) Role of the Skp1 prolyl-hydroxylation/glycosylation pathway in oxygen dependent submerged development of *Dictyostelium*, BMC Developmental Biology 12, 31.

(36) Boland, A. W., Gas-Pascual, E., Nottingham, B. L., van der Wel, H., Daniel, N. G., Sheikh, M. O., Schafer, C. M., and West, C. M. (2022) Oxygen-dependent regulation of E3(SCF)ubiquitin ligases and a Skp1-associated JmjD6 homolog in development of the social amoeba *Dictyostelium*, Journal of Biological Chemistry 298, 102305.

(37) Roux, K. J., Kim, D. I., Raida, M., and Burke, B. (2012) A promiscuous biotin ligase fusion protein identifies proximal and interacting proteins in mammalian cells, Journal of Cell Biology 196, 801-810.

(38) Kim, D. I., Kc, B., Zhu, W., Motamedchaboki, K., Doye, V., and Roux, K. J. (2014) Probing nuclear pore complex architecture with proximity-dependent biotinylation, Proceedings of the National Academy of Sciences 111, E2453-E2461.